

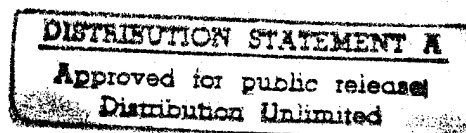
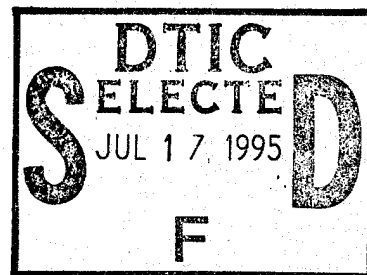
FOR PUBLIC DISTRIBUTION**ONR Grant N00014-90-J-1014: Final Scientific Report - 1995****Title:** Coherent Radiative Control of Chemical Reactions

Principal Investigator: P. Brumer, Professor, Chemical Physics Theory Group, Department of Chemistry, University of Toronto, Toronto, Canada M5S 1A1
(416-978-3569);

Subcontractor: M. Shapiro, Professor, The Weizmann Institute of Science

ONR Scientific Officer: Dr. P. Reynolds

Grant Period: October 1992 - September 1995



19950713 051

DTIC QUALITY INSPECTED 5

FOR PUBLIC DISTRIBUTION

ONR Grant N00014-90-J-1014: Final Scientific Report - 1995

Title: Coherent Radiative Control of Chemical Reactions

Principal Investigator: P. Brumer, Professor, Chemical Physics Theory Group, Department of Chemistry, University of Toronto, Toronto, Canada M5S 1A1
(416-978-3569);

Subcontractor: M. Shapiro, Professor, The Weizmann Institute of Science

ONR Scientific Officer: Dr. P. Reynolds

Grant Period: October 1992 - September 1995

Accession For	
NTIS CRA&I	<input checked="checked" type="checkbox"/>
DTIC TAB	<input type="checkbox"/>
Unannounced	<input type="checkbox"/>
Justification	
By	
Distribution /	
Availability Codes	
Dist	Avail and/or Special
A-1	

Grant-Supported Publications

The following papers describe research supported under this grant. Papers numbered 1-15, as well as a sample conference proceedings review (number 23) are included with this report.

Publications:

A. Refereed Publications:

1. "Weak Field Optimal Control Over Product Yields: The Pump Dump Scenario", M. Shapiro and P. Brumer, Chem. Phys. Lett. **208**, 193 (1993).
2. "Coherence and Laser Control of Chemical Reactions", P. Brumer and M. Shapiro, in "Molecules in Laser Fields", pages 287-348, ed. A. Bandrauk, (Marcel Dekker, 1994)
3. "Two Color Coherent Control with SEP Preparation: Electronic Branching in Na₂ Photodissociation," J. Dods, P. Brumer and M. Shapiro, Can. J. Chem. (Polanyi Honor Issue) **72**, 958 (1994)
4. "Interference Control of Photodissociation Branching Ratios: Two Color Frequency Tuning of Intense Laser Fields", Z. Chen, M. Shapiro and P. Brumer, Chem. Phys. Lett. **228**, 289 (1994)
5. "Relative Laser Phase in the Coherent Control and Interference Control of Photodissociation Branching Ratios", P. Brumer, Z. Chen and M. Shapiro, Israel J. Chem. **34**, 137 (1994)

6. "Coherent and Incoherent Laser Control of Photochemical Reactions", M. Shapiro, and P. Brumer, *International Reviews of Physical Chemistry* **13**, 187 (1994)
7. "Uniform Semiclassical Wavepacket Propagation and Eigenstate Extraction in a Smooth Chaotic System", D. Provost and P. Brumer, *Phys. Rev. Lett.* **74**, 250 (1995)
8. "Laser Control of Molecular Motion", P. Brumer and M. Shapiro, *Scientific American*, **272**, 56 (1995)
9. "Interference Control without Laser Coherence: Molecular Photodissociation", Z. Chen, M. Shapiro and P. Brumer, *J. Chem. Phys.* **102**, 5683 (1995)
10. "Quantum Limitations on Control and Dynamics", M. Shapiro, and P. Brumer, *J. Chem. Phys.* (in press)
11. "Incoherent Interference Control of Photodissociation in the Strong Field Domain" Z. Chen, M. Shapiro and P. Brumer, *Intl. J. Nonlinear Optical Physics*, (in press)
12. "Phase and Intensity Control of Integral and Differential Above Threshold Ionization Rates", R. Blank and M. Shapiro, *Phys. Rev. A* (in press)
13. "Incoherent Interference Control of Two Photon Dissociation" Z. Chen, M. Shapiro and P. Brumer, *Phys. Rev. A* (in press)
14. "Pump-Dump Coherent Control with Partially Coherent Laser Pulses" X-P. Jiang, M. Shapiro and P. Brumer, *J. Chem. Phys.* (submitted)
15. "Electronic Spectra of Diatomics on non-Static Surfaces: IBr on MgO(001)" X-P.

Jiang, M. Shapiro and P. Brumer, J. Chem. Phys. (to be submitted — preliminary version enclosed)

B. Manuscripts in Preparation:

16. "Initial Value Representation for Polyatomic Photofragmentation", G. Campolieti and P. Brumer.
17. "Partial Laser Coherence Effects in 1+3 Photon Coherent Control", X-P. Jiang, M. Shapiro and P. Brumer
18. "Optimal Pulsed Laser Control of Na₂ Photodissociation", J. Paci, M. Shapiro and P. Brumer
19. "Coherent Control of Molecular Processes", P. Brumer and M. Shapiro, (Monograph on Coherent Control)
20. "Experimental Observation of Laser Controlled Branching in the Photodissociation of Na₂ → Na(3s) + Na(3d), Na(3p) , Na(4s)", I. Sofer, A. Shnitman, I. Golub, A. Yogeve, M. Shapiro, Z. Chen and P. Brumer (in preparation)

C. Conference Proceedings

21. " Control of Molecular Photodissociation via Frequency Tuning of Intense Laser Fields", Z. Chen, M. Shapiro, and P. Brumer, in "Laser Techniques for State-Selected and State-to-State Chemistry II", ed. J.W. Hepburn, SPIE-Int. Soc. Opt. Eng. 2124, 60-67 (1994).

22. "Laser Control of Chemical Reactions in a Thermal Environment", Z. Chen, M. Shapiro and P. Brumer, in "Mode-Locked and Solid State Lasers, Amplifiers and Applications", ed. M. Piche and P.W. Pace, SPIE-Int. Soc. Opt. Eng. 2041, 166-172 (1994).

23. "Laser Control of Molecular Processes: Resonant Excitation in a Thermal Environment", by Z. Chen, M. Shapiro, and P. Brumer, in "Multiphoton Processes", ed. D.K. Evans and S.L. Chin, (World Scientific, N.J., 1994) pgs 317-324.

D. Publications previously reported (Final Report - 1992) as submitted, now published

24. "Theory of Resonant Two-Photon Dissociation of Na_2 ", Z. Chen, M. Shapiro and P. Brumer, J. Chem Phys. **98**, 8647 (1993).

25. "Multiproduct Coherent Control of Molecular Photodissociation via 2-Photon vs. 2-Photon Interference", Z. Chen, P. Brumer and M. Shapiro J. Chem. Phys. **98**, 6843 (1993).

26. "Three Dimensional Quantum-Mechanical Computations of the Control of the $\text{H}+\text{OD} \leftarrow \text{DOH} \rightarrow \text{D}+\text{OH}$ Reaction", M. Shapiro and P. Brumer, J. Chem. Phys. **98**, 201 (1993).

27. "Total N -Channel Control in the Weak Field Domain", M. Shapiro and P. Brumer, J. Chem. Phys. **97**, 6259 (1992).

28. "Coherent Radiative Control of Molecular Photodissociation via Resonant 2-Photon plus 2-Photon Interference", Z. Chen, M. Shapiro and P. Brumer, Chem. Phys. Letters **198**, 498 (1992).

29. "Laser Control of Molecular Processes", P. Brumer and M. Shapiro, Annual Reviews of Physical Chemistry, **43**, 257, (1992).

Work In Progress

30. "Semiclassical Propagation of Polyatomic Photofragmentation", (with J. Campolieti).
31. "Quantum Computations of Polyatomic Photofragmentation", (with A. Abrashkevitch).
32. "Pulsed Incoherent Interference Control via Adiabatic Following", (with Z. Chen)
33. "Control of Refractive Indices", (with E. McCullough)
34. "Partial Coherent Laser Effects in the 1-photon plus 3-photon Control Scenario", (with X-P. Jiang)

Research Accomplishments

We continue research on our approach to the coherent radiative control of molecular processes. Our focus remains, as in the past, on extending the general theory and on theoretically designing laboratory scenarios for displaying control. The latter also entails a significant effort to minimize effects which tend to diminish control, such as collisional dephasing, thermal population distributions and partial laser coherence. We have, during the course of this grant period, done several seminal pieces of research which both extend the theory and provide the basis for considerably greater advances in the near future. Particularly notable successes during this research period include (where reference numbers refer to the list above):

- a) analysis of the general role of laser phase in coherent control scenarios⁵. Typical applications include a stimulated-emission-pumping scheme for carrying out two-color coherent control³;
- b) the introduction⁴ and extensive development^{9,11,13} of Incoherent Interference Control, a strong laser field based method of control which is relatively insensitive to the coherence of the laser sources;
- c) extensive and highly successful computational interaction with experimentalists²⁰ to implement, observe and interpret experimental studies of incoherent interference control in Na_2 . Significantly, experiments were carried out with Na_2 in a *bulk thermal environment*;
- d) The development of a new approach to optimal control in the weak field pump-dump coherent control scenario¹;

- e) continuing development of semiclassical propagation methods^{7,30} to allow studies of photodissociation and control in polyatomic systems;
- f) proof of a general theorem on control which provides quantum limitations on the extent of control possible in bound systems¹⁰;
- g) application of the 1-photon plus 3-photon coherent control scenario to control the integral and differential cross sections in above threshold ionization¹²;
- h) the completion of initial steps in the study of control in condensed phases by developing a model of the electronic spectroscopy of molecules adsorbed on a dynamic surface¹⁵.
- i) The use of a realistic model of Na₂ photodissociation, [which forms Na(3s) + Na(4s), Na(3s) + Na(3d) and Na(3s) + Na(3p)] to study the utility of all proposed scenarios. Our results emerge from fully quantum mechanical, state-of-the-art, photodissociation calculations which include seventeen electronic potential energy curves.

In addition, we wrote several invited introductory⁸ and advanced^{2,6,11} review articles, summarizing our increasingly deeper understanding of the principles and range of utility of coherent control.

This report provides a very brief sketch of results obtained during the past three years under ONR support. In particular, we provide some comments to introduce the accompanying preprints and reprints. Details are, however, given in instances where work is in progress and a preprint is not yet available.

In addition to our own work on coherent control it is important to note that significant

progress in coherent control during the past three years has occurred on the experimental front. In particular, we note experiments by Gordon (University of Illinois) which demonstrate control over two product channels in the photoionization of HI using our 1-photon plus 3-photon scenario (M. Shapiro, J. Hepburn and P. Brumer Chem. Phys. Lett. 149, 451, 1988) and the demonstration of control over photocurrents by Corkum (National Research Council, Ottawa), an extension of our original proposal to do so in doped semiconductors (G. Kurizki, M. Shapiro and P. Brumer, Phys. Rev. B 39, 3435 1989). Finally, note the experiment on Na₂ in item (c) above, demonstrating coherent control over multiple products in a bulk thermal environment. These experiments reflect the growing experimental interest in coherent control.

A. The Role of Laser Phase in Coherent Control Scenarios and an SEP Approach to Two Color Coherent Control (Refs. 3 and 5)

Even in our initial paper on coherent control (P. Brumer and M. Shapiro, Chem. Phys. Letters 126, 541, 1986) it was clear that an essential feature of control was the transfer of the laser phase, upon irradiation, to the molecular wavefunction. During the past three years we have systematized the role of the laser in coherent control⁵ which, in conjunction with nonlinear optics techniques, allows the development of various schemes which minimize the role of the coherence of the laser sources in coherent control.

In particular, we noted that absorption of a photon from a CW source with laser phase ϕ_1 contributes a phase of $(-\phi_1)$ to the continuum molecular wavefunction whereas stimulated emission by a CW laser with phase ϕ_2 contributes a phase of ϕ_2 to the wavefunction. Utilizing these simple rules allows us to design and analyze the relative phase associated

with multiple excitation routes to the continuum, upon which coherent control depends. This relative phase analysis⁵ is now a fundamental tool in our approach to designing control scenarios.

As an example we designed a stimulated-emission-pumping approach³ to the preparation of a superposition state, which is subsequently photodissociated in our original two color control scenario (M. Shapiro and P. Brumer, J. Chem. Phys. 84, 4103 1986; Chem. Phys. Letters 126, 541, 1986 and Faraday Disc. Chem. Soc. 82, 177 1987). The particular nonlinear optics based method of preparation of laser frequencies allowed us to design a scheme which was relatively insensitive to the relative laser phase.

B. Incoherent Interference Control (Refs. 4,9,11,13)

At the start of this granting period there were only two experimental demonstrations of coherent control (S.M. Park, S-P. Lu, and R.J. Gordon, J. Chem. Phys. 94, 8622, 1991 and C. Chen, Y-Y. Yin, and D.S. Elliott, Phys. Rev. Lett. **64**, 507 (1990); Phys. Rev. Lett. **65**, 1737 (1990)) both of which showed control in systems with a single controlled product channel and both of which utilized collision-free molecular beam conditions. During the course of this granting period we focused heavily on the important goal of developing a control approach which would be useful in realistic environments, where both collisional and thermal effects cause loss of phase coherence, reducing the extent of control.

We reached this goal by introducing a new high field control scenario⁴ which displays a number of desirable features. Specifically, consider dissociating a molecule by irradiating it with frequencies ω_1 and ω_2 . The frequencies are chosen such that ω_1 dissociates a populated bound state $|E_1\rangle$ by raising it to energy E and ω_2 couples an unpopulated

bound state $|E_2\rangle$ to the same continuum at energy E . The strong field nature of the two fields induce multiple excitation pathways to the continuum which interfere with one another. An analysis of the laser phases imparted to molecules, assuming coherent light sources throughout, shows that they are the same for all pathways. This result has two consequences: (1) that the scenario is relatively insensitive to the coherence of each of the lasers and (2) that the phases of the lasers can not be used as control parameters in this scenario. However, the frequencies of each of the lasers serve as useful control parameters, with control effective over a range proportional to the power broadening of the bound levels. Since this approach does not rely upon laser phases and since it is inherently less sensitive to laser coherence we termed this approach "incoherent interference control".

Further studies^{9,11,13} of incoherent interference control in Na_2 showed that extensive control over all atomic photodissociation products results from this approach, and that the addition of an initial resonant excitation step (where $2\omega_1$ provides sufficient energy for dissociation and where ω_1 is resonant with a bound-bound transition) provides an effective means of doing incoherent interference control in a thermally populated molecular sample.

C. Theoretical Support in the Incoherent Interference Control of Na_2 in the Laboratory (Ref. 20)

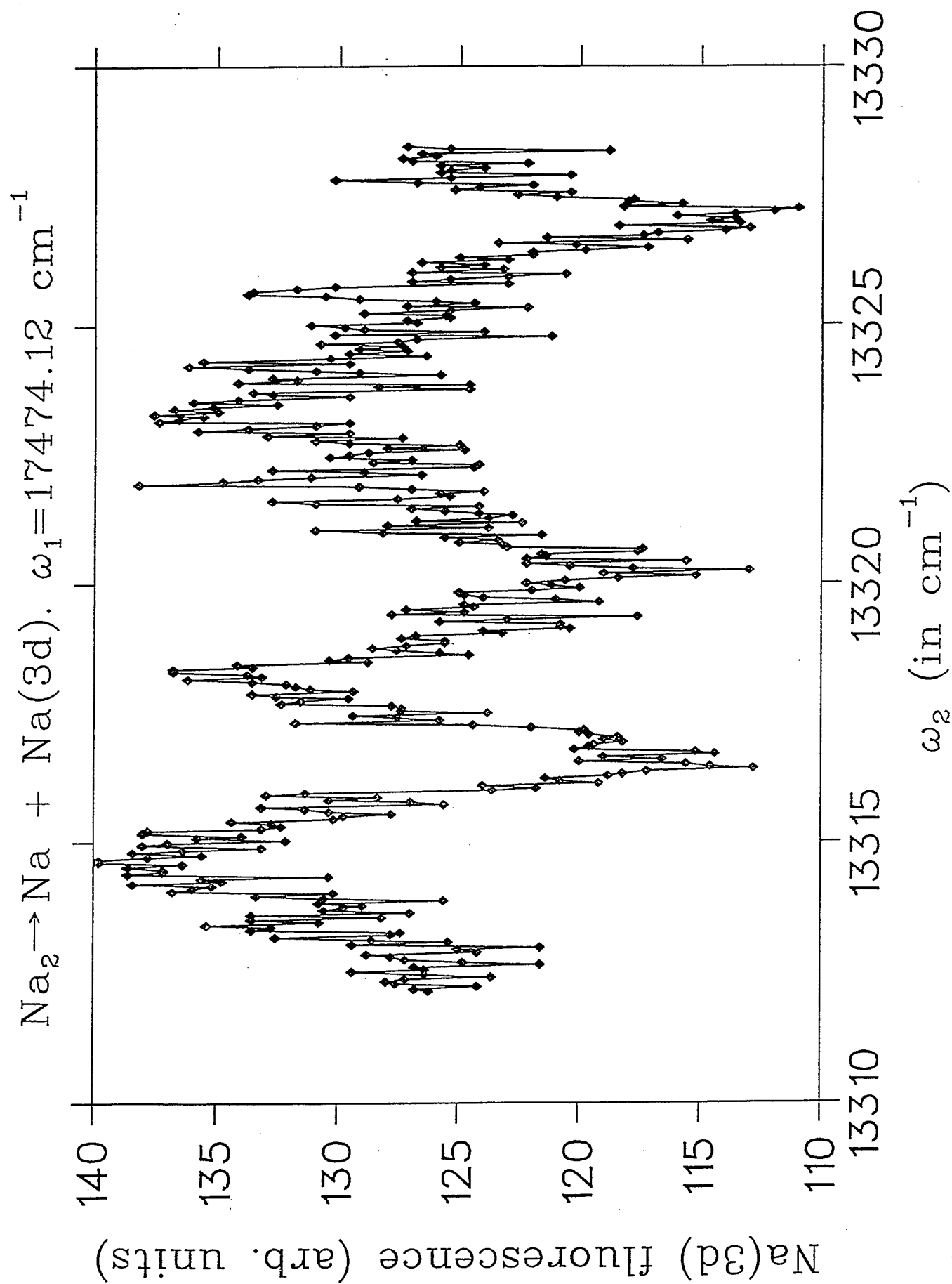
The possibility of carrying out incoherent interference control on Na_2 in a thermal sample with conventional lasers motivated an experimental study by I. Sofer, A. Shnitman, I. Golub, A. Yogev and M. Shapiro at the Weizmann Institute, carried out in conjunction with theoretical studies by Chen and Brumer at the University of Toronto. A theoretical-experimental interactive approach was adopted, with experiment guiding theory and vice-

versa, until a frequency region displaying significant control was identified.

In the experiment, Na_2 , in thermal equilibrium in a heat pipe at $T=370^\circ\text{C}$, was photodissociated with two ordinary nanosecond lasers. One laser was fixed at 17474.12 cm^{-1} while the second was tuned between $13,312\text{ cm}^{-1}$ and $13,328\text{ cm}^{-1}$. Products of Na_2 photodissociation are the atomic pairs $\text{Na}(3s) + \text{Na}(4s)$, $\text{Na}(3s) + \text{Na}(3d)$ and $\text{Na}(3s) + \text{Na}(3p)$. Spontaneous emission from the excited Na atomic products were dispersed in a spectrometer and a detector with a narrow bandpass filter and served to measure the product yields. A typical Na(3d) signal is shown in Fig. 1, where three broad deep minima in the Na(3d) yield are seen as a function of ω_2 . Also shown are numerous reproducible narrow features which we believe arise from hyperfine splittings. A theoretical result showing photodissociation out of a single initially populated state ($J=3/2, v=0$) is shown in Fig. 2. The large scale dips seen in the experimental results are clearly visible in the computational result. Although it is not possible to fully model photodissociation out of a thermal ensemble, adding the results of photodissociation out of a number of initial states adds considerable structure to the theoretical curve, bringing it closer to the experimental results.

Considering the large amount of uncertainty associated with the potentials and with the assignment of initial state from which photodissociation primarily occurs, the agreement in the values of the frequencies at which the deep minima occur is remarkable. Current experimental work is aimed at observing the theoretically predicted increase in the $\text{Na}(3s) + \text{Na}(3p)$ yield at those ω_2 frequencies where minima in $\text{Na}(3s) + \text{Na}(3d)$ are observed.

D. Optimal Control in the Pump-Dump Coherent Control Scenario (Ref. 1)



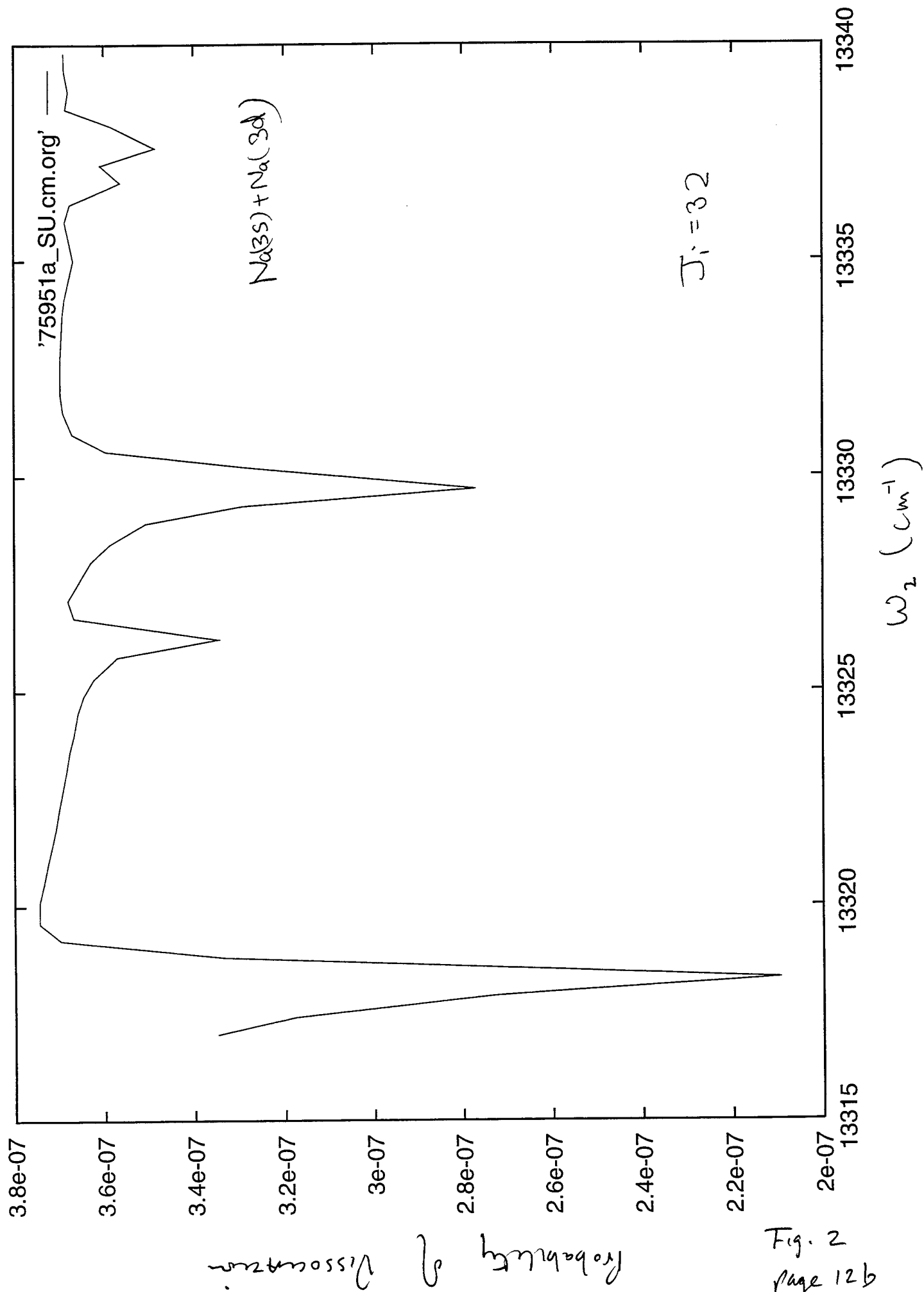


Fig. 2
page 12b

Much of our work runs counter to pulse shaping optimal control methods, where the suggestion is that vast increases in the yield of desired processes would result from highly sophisticated laser pulse shaping. Our experience, based upon large numbers of results, is that highly selective control can be achieved by using relatively simple pulses, e.g. Gaussian or CW. Nonetheless, in order to investigate the utility of pulse shaping in the weak field pump-dump scenario we designed a useful numerical approach to the control of pulse shapes and time delays. Specifically¹ we expanded both laser pulses in harmonic bases. Optimization of the yield difference then requires the solution to a simple set of linear equations. This leads to a highly effective method of optimizing the difference in yield between product channels. This method is now being applied to photodissociation of both Na_2 and to a number of model problems¹⁸.

E. Semiclassical Propagation (Ref. 7)

Since quantum mechanics will, in the foreseeable future, be limited to small molecules, we began to examine possible classical and semiclassical methods for treating laser controlled photodissociation.

Classical methods have been highly successful in providing both qualitative and quantitative results on unimolecular and bimolecular heavy particle reactions. Our interest is in light-induced reactions and simple classical trajectory methods have also been applied in such cases, e.g. to compute photodissociation cross sections. However, the methods which have been developed are not directly applicable to control since simple photodissociation calculations only require the computation of probabilities, rather than the required photodissociation amplitudes. We have begun to develop semiclassical methods which avoid

the difficult two-point boundary value problem (i.e., trajectory root-searches) associated with standard semiclassical approaches, to compute these amplitudes. Computations on the photodissociation of HOD based on one such approach¹⁶, the initial value representation of the Moller Wave Operator, are currently in progress and are discussed in detail in our proposal for future ONR support.

During the course of this research grant we investigated a second approach to semiclassical propagation, with the ultimate intent of applying the method to photodissociation. Specifically, we implemented Klauder's uniform semiclassical approximation to the quantum propagator (J.R. Klauder, Phys. Rev. Lett. 56, 897, 1986). This approach is also in the spirit of an initial value propagator insofar as it is based upon trajectories which carry phases and which therefore can interfere with one another. No stationary phase approximation or root search procedure is required.

We modified Klauder's method and applied it to a relatively complex problem, the dynamics of a system which is classically chaotic. The results⁷, which required propagating well beyond the so-called log time which limits van-Vleck type propagators, showed excellent agreement with the exact quantum results. Clearly such propagators contain the essential physics and offer the possibility of computations on larger molecules. As a consequence we propose further studies on such semiclassical propagators.

F. Quantum Limitations on Control in Bound Systems (Ref. 10)

In addition to direct applications of coherent control to molecular processes, developing general control theorems which define the range over which processes can be controlled quantum mechanically is an important goal. In a recent paper¹⁰ we considered the case of

dynamics emanating from an initial Hilbert space \mathcal{H}_0 and terminating in \mathcal{H}_1 and \mathcal{H}_2 . The dimensions of these Hilbert spaces are M_0, M_1 and M_2 , respectively. A typical control goal would be to move population from \mathcal{H}_0 to \mathcal{H}_1 without populating \mathcal{H}_2 . There are two possible means by which this may occur: (1) there are natural processes or external fields which can cause this transition or, if there are not, then (2) it is possible to linearly combine states in \mathcal{H}_0 such that this goal can be achieved. We showed, in a concise theorem¹⁰, that the latter is virtually impossible if $M_2 > M_0$, but achievable if $M_2 < M_0$. Of particular interest is that this theorem (1) applies directly to individual systems, i.e. is not a statistical result, and (2) that it is a purely quantum mechanical result. That is, classical mechanics permits control under all circumstances.

G. Control of Above Threshold Ionization (Ref. 12)

Above threshold ionization (ATI) is a process of considerable recent interest. We have shown¹² that the phase and intensity variations in the 1-photon plus 3-photon scenario provides a powerful means of controlling both partial and total ionization rates as well as differential quantities such as the angular alignment of the each kinetic energy peak. Indeed studies on ATI in hydrogen show that proper combinations of phase and intensity ratios allow for extensive control.

H. Dephasing in Condensed Phases: Electronic Spectroscopy of Adsorbates (Ref. 15)

Dephasing processes are generally detrimental to control. For example, in the gas phase collisional and thermal broadening effects tend to diminish control and must be overcome by explicit design (see, e.g. M. Shapiro and P. Brumer, J. Chem. Phys. 90, 6179, 1989 and Ref. 23). For systems in the condensed phase (e.g., molecules in solution or on surfaces)

it is coupling to the environment which results in the loss of phase information necessary to coherent control.

We have begun to examine the question of control of molecules on surfaces and to investigate the nature of the molecule-surface coupling. In particular, we have designed a model theoretical and computational approach to the electronic spectroscopy of molecules on surfaces. To do so we generalized the Caldiera-Leggett approach and derived¹⁵ a useful model for the electronic spectrum of a molecule on a non-static surface, suitably averaged over surface modes. Applications to IBr on MgO(001) allow a phenomenological treatment of the decreasing sharpness of spectra with increasing surface-molecule coupling. The resultant model should allow studies of coherent control of photodissociation of molecules on surfaces.

Additional Work in Progress

In addition, major studies have been initiated, on the effect of partial laser coherence in the 1+3 control scenario¹⁷, on incoherent interference control using laser pulses³², and on an initial value representation based approach to propagation in polyatomic systems¹⁶. These topics form components of the research which we propose in our request for renewal of this grant. They are therefore discussed in detail in the proposal.

Weak field optimal control over product yields. The pump-dump scenario

Moshe Shapiro

Chemical Physics Department, The Weizmann Institute of Science, Rehovot 76100, Israel

and

Paul Brumer

Chemical Physics Theory Group, Department of Chemistry, University of Toronto, Toronto, Ontario, Canada M5S 1A1

Received 2 February 1993

It is demonstrated, with specific application to pump-dump control, that optimal control problems are substantially simplified by focusing on the regime of weak laser fields. Under such circumstances complex nonlinear problems of strong field optimal control are replaced by far simpler numerical tasks.

Laser control over the ratio of product yields in chemical reactions has been the subject of considerable interest over the past few years (for a recent review, see ref. [1]), with two principal approaches dominant. The first, coherent radiative control of chemical reactions, relies on defining two or more coherent optical pathways to the energy at which products are formed. Such multiple pathways introduce quantum interference effects which lead to constructive enhancement and destructive depletion of particular products. By proposing specific laser-based scenarios with well defined control parameters, the coherent control approach provides the experimentalist with specific laboratory parameters which are to be varied in order to control product yields. In addition, coherent control theory has been applied to many computational examples showing a vast range of control, over the product ratio, resulting from this technique (for recent computations, see ref. [2]). Such computations, and the formalism of coherent control theory have, thus far, focused on weak laser fields where quantum interference effects are readily proposed and understood.

The second route which has received considerable attention is that of optimal control theory (OCT),

in which laser pulse shapes and sequences are designed, through optimal control theory, to achieve specific objectives [1,3-6]. For the case of control over reactive yields most attention has been focused on simple model systems as efforts continue to solve major computational technique problems associated with the optimal control problems set up by this approach. OCT studies have tended to focus on the use of high fields. Thus, coherent control, as applied thus far, is a theory which is linear in the laser fields and in which one maximizes the long-time reactive probabilities using weak fields; optimal control theory is a non-linear theory involving strong laser pulses in which one attempts to attain general objectives.

The purpose of this Letter is to demonstrate that examining optimal control in the weak field regime where perturbation theory is valid provides an important new direction which allows the rapid and efficient design of pulses. These results follow upon a previous demonstration [7,8] that perturbation theory provides a powerful contribution to control optimization. Specifically, we showed [7] that an exact solution for the problem of obtaining *total yield control* is achievable in the weak field regime. That result was, however, restricted to molecules with spe-

cific resonance characteristics and required a sufficient number of available, phase related, independent laser frequencies.

The advantages of examining weak fields in optimal control results, as shown below, from the fact that optimal pulse shapes can be obtained without the need for a tedious nonlinear optimization procedure. This advantage, which we formulate below for the pump-dump scenario [3,9]^{*1}, is readily extended to the host of other scenarios. In this Letter, we focus upon the theory; computational studies on a variety of systems are in progress.

Consider a sequence of two pulses, one serving to excite a molecule to a set of intermediate bound states with wavefunction ψ_i and energy E_i , and the second to dissociate these states. We denote the two pulses ($k=1, 2$) by

$$\begin{aligned}\epsilon^{(k)}(t) &= \int d\omega \{ \epsilon^{(k)}(\omega) \exp[-i\omega(t-z/c)] + \text{c.c.} \} \\ &= \int d\omega [\bar{\epsilon}^{(k)}(\omega) \exp(-i\omega t) + \text{c.c.}],\end{aligned}\quad (1)$$

where $\bar{\epsilon}^{(k)}(\omega) \equiv \epsilon^{(k)}(\omega) \exp(i\omega z/c)$, with z being the propagation direction. The wavepacket formed during the action of this pulse on some initial state ψ_g is given, in first-order perturbation theory [11,12] as

$$\begin{aligned}\psi^{(1)}(t) &= (i/\hbar) \sum_i \bar{\epsilon}^{(1)}(\omega_i) \mu_{i,g} c_i(t) \psi_i \\ &\times \exp(-iE_i t/\hbar),\end{aligned}\quad (2)$$

where

$$\mu_{i,g} \equiv \langle \psi_i | \mu | \psi_g \rangle. \quad (3)$$

The coefficients $c_i(t)$ are "universal" preparation coefficients, related to $\epsilon^{(1)}(t)$ by

$$\begin{aligned}c_i(t) &\equiv \frac{1}{\bar{\epsilon}^{(1)}(\omega_i)} \int_{-\infty}^t dt' \epsilon^{(1)}(t') \exp(i\omega_i t') \\ &= \frac{1}{\bar{\epsilon}^{(1)}(\omega_i)} \int d\omega \bar{\epsilon}^{(1)}(\omega) \frac{\exp[i(\omega_i - \omega)t]}{i(\omega_i - \omega)},\end{aligned}\quad (4)$$

^{*1} For the use of pump-dump schemes in the context of coherent radiative control, see ref. [10].

with $\omega_i \equiv (E_i - E_g)/\hbar$.

The c_i coefficients describe the buildup of each level during the pulse. They are given by [11,12]

$$\begin{aligned}c_i(t) &\rightarrow 0, \quad \text{for } t \rightarrow -\infty \\ &\text{and} \\ c_i(t) &\rightarrow 2\pi, \quad \text{for } t \rightarrow \infty.\end{aligned}\quad (5)$$

Consider now the effect of the second pulse, $\epsilon^{(2)}(t)$, on this bound superposition. Using eq. (5), we can write the wavepacket formed as a result of the combined action of the two pulses, at the end of the dissociation pulse, as

$$\begin{aligned}\psi^{(2)}(t) &= -2\pi/\hbar^2 \int dE \sum_{v,q} \bar{\epsilon}^{(1)}(\omega_i) c_i(\tau) \mu_{i,g} \\ &\times \exp(-iE_i \tau/\hbar) \bar{\epsilon}^{(2)}(\omega_{E,i}) \mu_i^{(q,v)}(E) \psi_{q,v}^-(E) \\ &\times \exp(-iEt/\hbar),\end{aligned}\quad (6)$$

where $\omega_{E,i} = (E - E_i)/\hbar$, $\psi_{q,v}^-(E)$ are the incoming scattering eigenstates of the field-free Hamiltonian, and

$$\mu_i^{(q,v)}(E) \equiv \langle \psi_{q,v}^-(E) | \mu | \psi_i \rangle \quad (7)$$

is a transition-dipole matrix element between the i th intermediate state and the scattering states.

The probability of observing a given product channel labeled by arrangement quantum label q at infinite time, irrespective of the value of the other (v, E) quantum numbers, is given, using the long-time properties of the incoming scattering states [13] as

$$\begin{aligned}P^{(q)} &= \int dE \sum_v P_v^{(q)}(E) \\ &= 4\pi^2/\hbar^4 \int dE \sum_v \left| \sum_i \bar{\epsilon}^{(1)}(\omega_i) \mu_{i,g} c_i(\tau) \right. \\ &\quad \left. \times \exp(-iE_i \tau/\hbar) \bar{\epsilon}^{(2)}(\omega_{E,i}) \mu_i^{(q,v)}(E) \right|^2.\end{aligned}\quad (8)$$

Eq. (8) can be conveniently rewritten as

$$P^{(q)} = \sum_{i,j} d_{ij}^{(q)} \epsilon_{i,j} c_i(\tau) c_j^*(\tau) \exp(-i\omega_{i,j} \tau), \quad (9)$$

where

$$\omega_{i,j} = (E_i - E_j)/\hbar,$$

$$d_{ij}^{(q)} \equiv 4\pi^2/\hbar^4 \int dE \sum_v \bar{\epsilon}^{(2)}(\omega_{E,i}) \bar{\epsilon}^{(2)*}(\omega_{E,j}) \times \mu_i^{(q,v)}(E) \mu_j^{(q,v)*}(E), \quad (10)$$

and

$$\epsilon_{ij} \equiv \bar{\epsilon}^{(1)}(\omega_i) \bar{\epsilon}^{(1)*}(\omega_j) \mu_{i,g} \mu_{j,g}^*. \quad (11)$$

Here we consider maximizing either probability in a single channel, i.e. $P^{(q)}$, or the selectivity of one channel in preference to another, i.e. $P^{(q_1)} - P^{(q_2)}$. Optimization is carried out subject to the constraint of fixed average pulse power, i.e. ($k=1, 2$)

$$J^{(k)} \equiv \int d\omega \epsilon^{(k)}(\omega) \epsilon^{(k)*}(\omega) = I^{(k)}. \quad (12)$$

Thus we wish to maximize either

$$D^{(q)} \equiv P^{(q)} - \lambda_1 J^{(1)} - \lambda_2 J^{(2)}, \quad (13)$$

or

$$D^{(q_1, q_2)} \equiv P^{(q_1)} - P^{(q_2)} - \lambda_1 J^{(1)} - \lambda_2 J^{(2)}, \quad (14)$$

or where λ_i , $i=1, 2$ are Lagrange multipliers.

Solving these problems is conveniently carried out by expanding each field in an orthonormal basis set $\{u_n(\omega, x)\}$ (e.g. harmonic oscillator eigenfunctions),

$$\begin{aligned} \bar{\epsilon}^{(1)}(\omega) &= \sum_m a_m u_m(\omega, x_1), \\ \bar{\epsilon}^{(2)}(\omega) &= \sum_n b_n u_n(\omega, x_2), \end{aligned} \quad (15)$$

where efforts are now directed at obtaining the optimizing a_m , b_n .

The optimization problem can now be reduced to the iterative solution to a set of linear equations in the following way. Defining

$$U_{mm',ij} \equiv u_m(\omega_i, x_1) u_{m'}(\omega_j, x_1) \mu_{i,g} \mu_{j,g}^*, \quad (16)$$

and

$$\begin{aligned} X_{nn',ij}^{(q)} &\equiv 4\pi^2/\hbar^4 \\ &\times \sum_v \int dE u_n(\omega_{E,i}, x_2) u_{n'}(\omega_{E,j}, x_2) \\ &\times \mu_i^{(q,v)}(E) \mu_{j,g}^{(q,v)*}(E), \end{aligned} \quad (17)$$

we have that

$$\epsilon_{ij} = \sum_{mm'} a_m a_{m'}^* U_{mm',ij} \quad (18)$$

and

$$d_{ij}^{(q)} = \sum_{nn'} b_n b_{n'}^* X_{nn',ij}^{(q)}. \quad (19)$$

Using eqs. (9), (18) and (19), we can write $P^{(q)}$ as a double bilinear form in the a_m and b_n coefficients,

$$P^{(q)} = \sum_{m,m'} a_m a_{m'}^* \sum_{n,n'} b_n b_{n'}^* Y_{mm',nn'}^{(q)}(\tau), \quad (20)$$

where

$$\begin{aligned} Y_{mm',nn'}^{(q)}(\tau) &\equiv \sum_{ij} U_{mm',ij} X_{nn',ij}^{(q)} \\ &\times c_i(\tau) c_j^*(\tau) \exp(-i\omega_{ij}\tau). \end{aligned} \quad (21)$$

With the availability of powerful time-independent computational techniques [14,15] for both the bound-bound $\mu_{i,g}$ and bound-free $\mu_j^{(q,v)*}(E)$ matrix elements, the $U_{mm',ij} X_{nn',ij}^{(q)}$ and hence $Y_{mm',nn'}^{(q)}(\tau)$ matrices are calculable for many realistic systems.

The extrema of eqs. (13) or (14), obtained via the relations

$$\begin{aligned} \frac{\partial D^{(q)}}{\partial a_m} &= \sum_{m'} a_{m'}^* \left(\sum_{n,n'} b_n b_{n'}^* Y_{mm',nn'}^{(q)}(\tau) \right. \\ &\quad \left. - \lambda_1 \delta_{m,m'} \right) = 0, \end{aligned} \quad (22)$$

$$\begin{aligned} \frac{\partial D^{(q)}}{\partial b_n} &= \sum_{n'} b_{n'}^* \left(\sum_{m,m'} a_m a_{m'}^* Y_{mm',nn'}^{(q)}(\tau) \right. \\ &\quad \left. - \lambda_2 \delta_{n,n'} \right) = 0, \end{aligned} \quad (23)$$

result in a set of nonlinear equations in the field coefficients a_m , b_n . These equations can be solved iteratively as a set of linear equations by first defining

$$B_{m,m'} \equiv \sum_{n,n'} b_n b_{n'}^* Y_{mm',nn'}^{(q)}(\tau), \quad (24)$$

$$A_{n,n'} \equiv \sum_{m,m'} a_m a_{m'}^* Y_{mm',nn'}^{(q)}(\tau). \quad (25)$$

The iteration proceeds by assuming that

$$b = b^0 \quad (26)$$

where b (a) is a row vector composed of the b_n (a_m) coefficients.

Eq. (26) reduces eq. (22) to a set of algebraic-eigenvalue equations,

$$a(b^0 Y_{m,m'}^{(q)}(\tau) b^{0\dagger} - \lambda_1 I) = 0, \quad (27)$$

where I is the identity matrix, $Y_{m,m'}^{(q)}(\tau)$ - the $Y_{mm',nn'}^{(q)}(\tau)$ matrix, in the b space. These equations are solved for the a matrix, out of which the a row of coefficients corresponding to the λ_1 eigenvalue which maximizes $D^{(q)}$ is chosen. These coefficients are used to update the A matrix of eq. (25), and solve the eigenvalue equation for the b coefficients,

$$b(A - \lambda_2 I) = 0. \quad (28)$$

The b row corresponding to the λ_2 eigenvalue which maximizes the $D^{(q)}$ objective is chosen to update B . The process is repeated until convergence.

The fields thus generated are still a function of the delay time τ , which is treated here as a nonlinear parameter. It is possible to solve the above set of equations for every value of τ and to obtain the optimal value of the time delay between the pulses as the one corresponding to the global maximum of $P^{(q)}(\tau)$.

The discussion, as well as our previous N -level theorem [7] for total control in a particular scenario, shows that the weak field regime constitutes an important area for consideration in optimal control theory. It offers the opportunity to obtain optimal pulse shapes via comparatively simple numerical approaches. In addition, contrary to popular expectation, one can produce substantial product using weak fields. Specifically, numerical studies [16] indicate that fully 20% of the ground state may be dissociated while the system remains in the perturbation theory limit. Thus, adequate total yields may also be achieved in this regime.

Further studies are in progress [17] applying this approach to a number of specific molecular systems.

We acknowledge support from the US Office of Naval Research under contract No. N00014-90-J-1014.

References

- [1] P. Brumer and M. Shapiro, *Ann. Rev. Phys. Chem.* 43 (1992) 257; *Accounts Chem. Res.* 22 (1989) 407.
- [2] Z. Chen, P. Brumer and M. Shapiro, *Chem. Phys. Letters* 198 (1992) 498; M. Shapiro and P. Brumer, *J. Chem. Phys.* 98 (1993) 201.
- [3] D.J. Tannor and S.A. Rice, *J. Chem. Phys.* 83 (1985) 5013; R. Kosloff, S.A. Rice, P. Gaspard, S. Tersigni and D.J. Tannor, *Chem. Phys.* 139 (1989) 201; S. Tersigni, P. Gaspard and S.A. Rice, *J. Chem. Phys.* 93 (1990) 1670.
- [4] S. Shi, A. Woody and H. Rabitz, *J. Chem. Phys.* 88 (1988) 6870; S. Shi and H. Rabitz, *Chem. Phys.* 139 (1989) 185.
- [5] R.S. Judson, K.K. Lehmann, H. Rabitz and W.S. Warren, *J. Mol. Struct.* 223 (1990) 425.
- [6] Y.J. Yan, R. Gillilan, R.M. Whittell, K.R. Wilson and S. Mukamel, *J. Phys. Chem.*, in press.
- [7] M. Shapiro and P. Brumer, *J. Chem. Phys.* 97 (1992) 6259.
- [8] I. Averbukh and M. Shapiro, *Phys. Rev. A*, submitted for publication.
- [9] A.H. Zewail, *Science* 242 (1988) 1645.
- [10] T. Seideman, M. Shapiro and P. Brumer, *J. Chem. Phys.* 90 (1989) 7132; I. Levy, M. Shapiro and P. Brumer, *J. Chem. Phys.* 93 (1990) 2493.
- [11] M. Shapiro, *Theory of Continuum-Raman Spectroscopy with Pulses*, *J. Chem. Phys.*, submitted for publication; R.D. Taylor and P. Brumer, *Discussions Faraday Soc.* 75 (1983) 117.
- [12] P. Brumer and M. Shapiro, in: *Mode-selective chemistry*, eds. J. Jortner, R.D. Levine and B. Pullman (Kluwer, Dordrecht, 1991) p. 323.
- [13] R.D. Levine, *Quantum mechanics of molecular rate processes* (Oxford Univ. Press, Oxford, 1969).
- [14] M. Shapiro, *J. Chem. Phys.* 56 (1972) 2582; M. Shapiro and R. Bersohn, *Ann. Rev. Phys. Chem.* 33 (1982) 409.
- [15] R. Schinke, *Photodissociation dynamics* (Cambridge Univ. Press, Cambridge, 1992).
- [16] P. Brumer and M. Shapiro, unpublished.
- [17] P. Brumer, M. Shapiro and J. Paci, work in progress.

Coherence and Laser Control of Chemical Reactions

Paul Brumer

University of Toronto, Toronto, Ontario, Canada

Moshe Shapiro

The Weizmann Institute of Science, Rehovot, Israel

6.1 INTRODUCTION

Manipulating the yield of chemical reactions is the essence of chemistry and the capability to control reactions using lasers has been a goal for decades. We have previously demonstrated [1–19] how this goal could be achieved. An appreciation of this approach, termed *coherent control* of chemical reactions, opens up new avenues in chemistry by introducing chemical control concepts based upon previously unutilized quantum effects.

The purpose of this chapter is to provide an introduction to the concepts [20] underlying coherent control of chemical reactions and to review its current status. The paper is organized along the following lines. Section 6.1 provides an introduction to the basics of coherent control, followed by a detailed discussion of two control scenarios in Section 6.2. Some specific topics are dealt with in Section 6.3 where we discuss the issue of control in the presence of incoherence effects and the role of selection rules in designing

control scenarios. Finally, Section 6.4 describes two interesting applications: control of symmetry breaking and the production of photocurrents in semiconductors. In all cases we provide meaningful examples to demonstrate the wide range of control possible. In most cases these results are obtained via fully quantum mechanical photodissociation calculations on reliable potential energy surfaces.

A. Aspects of Scattering Theory and Reaction Dynamics

We shall focus on unimolecular reactions where decomposition into more than one product is possible,



and remark as well on branching bimolecular reactions



where A, B, C are atoms or groups of atoms and n, n' denote the vibrational, rotational, etc., states of the reactant or product pair. Both inelastic (Equation 6.2a) and reactive scattering (Equation 6.2b) are indicated.

Treating the dynamics of a chemical reaction requires solving the Schrödinger Equation

$$H\Psi(t) = i\hbar\partial\Psi(t)/\partial t \quad (6.3)$$

for the wavefunction $|\Psi(t)\rangle$ associated with specific initial reactant conditions (i.e., $\Psi(0)$). The wavefunction at long times (i.e., when the products are well separated), then provides the probabilities of forming the products. The time-dependent Schrödinger equation is conveniently solved in two steps, first obtaining the stationary eigenfunctions ψ_i as solutions to the time-independent Schrödinger equation $H\psi_i = E_i\psi_i$, and then by building the time dependence in as a superposition of time-independent eigenfunctions.

Consider then the nature of the time-independent eigenfunctions. We focus attention on the system at a fixed energy E in the continuum where,

as we shall show, the essence of controlling reactions is manifest. The system requires, at such an energy, an independent wavefunction to describe each of the possible outcomes that can be observed in the product regions [21]. As a consequence, one expects substantial degeneracy at energy E . Further, the fact that this set of degenerate wavefunctions of the separated products exists, implies [22] that a related set of degenerate eigenfunctions of the total Hamiltonian exists.

This requirement, that total system eigenfunctions correlate with specific asymptotic product state eigenfunctions, may be included as a boundary condition on the total system wavefunctions and serves to considerably simplify the understanding of the dynamics of unimolecular decay, which will serve subsequently as our primary example. Specifically, say we distinguish the different possible chemical product arrangements of the decay of ABC by the numerical value of an index q , (e.g., $q = 1$ denotes $A + BC$ in Equation 6.1, etc.) and m denotes all additional identifying state labels (e.g., $j', v',$ scattering angle, etc.). Then we can define the set of Hamiltonian continuum eigenstates $|E, m, q\rangle$ via the Schrödinger equation $HE, m, q\rangle = HE, m, q\rangle$ and via the requirement that this eigenstate describes, at large distances, the state of the separated products, denoted $|E, m, q\rangle_0$, which is of energy E , arrangement q , and remaining quantum numbers m . The "minus" superscript serves to indicate this choice of boundary condition.

Imposition of such boundary conditions and the description of the system in terms of $|E, m, q\rangle$ has a number of important simplifying consequences. For example, if one sets up (either experimentally or conceptually) a state at $t = 0$, at energy E , consisting of $|E, m, 1\rangle$ then the probability of observing the product in the $q = 1$ arrangement, and with quantum numbers m , is unity since $|E, m, 1\rangle$ uniquely correlates with that particular product state. Similarly, if we set up the system in a linear combination of states:

$$|\psi(0)\rangle = \sum_m [c_{1m}|E, m, 1\rangle + c_{2m}|E, m, 2\rangle] \quad (6.4)$$

Then the probability of observing one of the arrangements (e.g., $q = 1$) is

$$\sum_m |c_{1m}|^2$$

This apparently simple discussion allows us to make a few crucial statements:

1. The product yield (i.e., the probability of obtaining a particular chemical product at long-time, is solely determined by the state created at $t = 0$). Furthermore, our choice of "minus states" $|E, m, q\rangle$ allows expression of this fact in a relatively simple way (i.e., the coefficients in the $t = 0$ superposition state are identical and equal to the coefficients at long-time whose squares are the product probabilities). The fact that the long-time state is predetermined by the initially created state is, admittedly, intuitively obvious. However, consequences of this feature are often misunderstood. For example it makes clear that arguments such as "intramolecular energy scrambling makes reaction control difficult", are misleading. Viewed from the proper perspective (i.e., the minus states) there simply is no time-evolving scrambling on the way to product. We have discussed these issues and their role in understanding control of reactions in detail in [15].
2. Since product probabilities are predetermined by the composition of the prepared ($t = 0$) superposition state, the route to controlling a chemical reaction is to control the content of the initially prepared superposition state.
3. The branching of the reaction probabilities into various product channels occurs at a fixed energy E . As such, a continuum wave packet built of states over a range of energies and its associated time dependence need not be introduced in order to consider control over reaction yields.

Next, we demonstrate that the key to laser control of chemical reactions is to use the lasers to alter the nature of the prepared superposition state and hence to alter the product probabilities. That this strategy is the essence of controlling chemical reactions should be clear from the above discussion. First, however, we discuss preparation of states from the viewpoint of perturbation theory.

B. Perturbation Theory, System Preparation, and Coherence

In preparation for a discussion of laser induced unimolecular dissociation consider the effect of an electric field on a molecule. Consider an isolated molecule with Hamiltonian H_M in an eigenstate $|\varphi_g\rangle$ which is subjected to a perturbing incident radiation field. The overall Hamiltonian is then given by:

$$H = H_M - \mathbf{d}[\bar{\epsilon}(t) + \bar{\epsilon}^*(t)] \quad (6.5)$$

where H_M is the molecular Hamiltonian and \mathbf{d} is the component of the dipole moment along the electric field, $\bar{\epsilon}(t)$.

To ascertain the effect of the field on the molecule requires that we solve the time-dependent Schrödinger equation for the given Hamiltonian, including the perturbation. To do so we invoke time-dependent perturbation theory and expand the solution $\Psi(t)$ in solutions to the problem in the absence of the perturbation

$$H_M \varphi_i = E_i \varphi_i \quad (6.6)$$

Specifically, writing the full wavefunction $\Psi(t)$ as:

$$\Psi(t) = \sum_i c_i(t) \varphi_i e^{-iE_i t/\hbar} \quad (6.7)$$

with the $c_i(t)$ as yet to be determined expresses the solution precisely in terms we want physically (i.e., $|c_i(t)|^2$ gives the probability of being in the molecular state $|\varphi_i\rangle$ at time t).

Inserting Equation 6.7 into the Schrödinger Equation yields a set of ordinary differential equations for $c_i(t)$ that may be solved numerically [23]. For weak fields this is not necessary and a simple perturbation theory solution for the long-time (i.e., when the electric field is off) behavior can be obtained as:

$$c_i(t \rightarrow \infty) = \frac{\sqrt{2\pi}}{i\hbar} \epsilon(\omega_{E_i, E_g}) \langle \varphi_i | \mathbf{d} | \varphi_g \rangle \quad (6.8)$$

with

$$\epsilon(\omega) = \frac{1}{\sqrt{2\pi}} \int_{-\infty}^{\infty} e^{i\omega t} \bar{\epsilon}(t) dt \quad (6.9)$$

In this case

$$\omega = \omega_{E_i E_g} = (E_i - E_g)/\hbar$$

Note that the object which is created by the effect of the incident electric field on the bound state is a pure state (i.e., it can be described by a wavefunction $\Psi(t)$). The fact that a well defined electric field produces a pure state (and hence a state which is phase-coherent) is essential to the subsequent discussion.

Consider now laser-induced photodissociation where we excite a molecule in an eigenstate $|\varphi_g\rangle$ with an electric field which provides enough energy to dissociate the molecule. Our interest is in ascertaining the probability of forming particular products. With the product of the electric field and dipole moment assumed to be small enough to allow the use of first-order perturbation theory [24] we proceed in the standard fashion [25] and expand the wavefunction in eigenstates of the molecular Hamiltonian. Since the photon lifts the system into the continuum, our expansion is in terms of the eigenstates $|E, m, q\rangle$,

$$|\Psi(t)\rangle = c_g |\varphi_g\rangle e^{-iE_g t/\hbar} + \sum_{m,q} \int dE c_{E,m,q}(t) |E, m, q\rangle e^{-iEt/\hbar} \quad (6.10)$$

Following through with standard perturbation theory gives, for the probability $P(E, q)$ of forming product in arrangement q :

$$P(E, q) = \lim_{t \rightarrow \infty} \sum_m |c_{E,m,q}(t)|^2 = \frac{2\pi}{\hbar^2} \sum_m |\epsilon(\omega_{E,E_g}) \langle \varphi_g | d | E, m, q \rangle|^2 \quad (6.11)$$

The ratio $R(1,2;E)$ of products in channel $q = 1$ to $q = 2$ at energy E is:

$$R(1,2;E) = \frac{\sum_m |\langle \varphi_g | d | E, m, 1 \rangle|^2}{\sum_m |\langle \varphi_g | d | E, m, 2 \rangle|^2} \quad (6.12)$$

An understanding of the qualitative structure of this yield ratio (see Section 6.2.C) is crucial to recognizing the difficulties associated with experimental

attempts to alter the yield in a traditional unimolecular decay experiment. It also motivates the specific control approach which we advocate.

C. Coherent Radiative Control of Chemical Reactions

Our primary goal is to experimentally alter the yield ratio R so as to control the product distribution. Equation (6.12) makes clear that this can not be achieved, for example, by moderately altering the laser power, which cancels out in forming the ratio R . Hence this, and any quantity which appears in a similar form in both the numerator and denominator, can not serve as a handle on yield control. An alternate possibility for controlling the reaction yield is to vary the frequency of excitation $[(E - E_g)/\hbar]$ and see the effect on the ratio. However, such a procedure is not systematic and its success, if any, is based solely upon a *chance* occurrence of a desirable result with variations in the laser frequency.

There is, however, an alternate possibility. Specifically, note the form of Equation 6.12, which has the square of an amplitude in both the numerator and the denominator. If we could manage to experimentally alter the quantity within the square then the effect on the numerator and the denominator might differ and we would have experimental control over the ratio. Our coherent radiative control approach reflects this philosophy and is coupled with the recognition that quantum interference phenomena alter the amplitude within the square in a particularly useful fashion.

As a pedagogical example, consider starting with a molecule prepared in a superposition $c_1 |\varphi_1\rangle + c_2 |\varphi_2\rangle$ of molecular eigenstates $|\varphi_i\rangle$ (Figure 6.1). The c_1 and c_2 coefficients, which are determined by the method of preparation, have phases and magnitudes which are functions of the *experimentally controllable* parameters.

This bound superposition state is subjected to an electric field which contains frequency components that can independently transform both of these states to a state of energy E ; for example, excitation with two CW sources

$$\vec{E}(t) = \epsilon_1 e^{-i\omega_1 t + i\chi_1} + \epsilon_2 e^{-i\omega_2 t + i\chi_2}$$

where $\hbar\omega_i = E - E_i$. We then ask for the yield ratio R under these circumstances. A straightforward computation [1] gives the result:

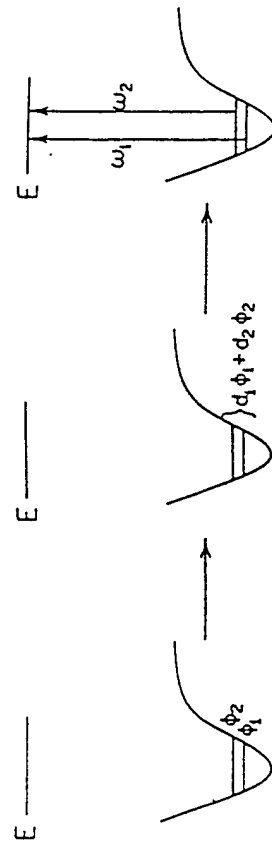


Figure 6.1 A general two step scheme for inducing controllable quantum interference effects into the continuum state at energy E . The two bound states ϕ_1, ϕ_2 belong to a lower electronic state whereas the level at energy E is that of an excited electronic state. Coherence introduced in the first step is carried into the continuum. Source: from [12].

$$R(1,2;E) = \frac{\sum_m |\tilde{\epsilon}_1 c_1 \phi_1 + \tilde{\epsilon}_2 c_2 \phi_2| d|E, m, 1\rangle|^2}{\sum_m |\tilde{\epsilon}_1 c_1 \phi_1 + \tilde{\epsilon}_2 c_2 \phi_2| d|E, m, 2\rangle|^2} \quad (6.13a)$$

where $\tilde{\epsilon}_j = \epsilon_j \exp(i\chi_j)$. Expanding the square gives:

$$R(1,2;E) = \frac{\sum_m [|\tilde{\epsilon}_1 c_1|^2 \langle \phi_1 | d | E, m, 1 \rangle|^2 + |\tilde{\epsilon}_2 c_2|^2 \langle \phi_2 | d | E, m, 1 \rangle|^2 + 2 \operatorname{Re}[c_1^* c_2 \tilde{\epsilon}_1^* \tilde{\epsilon}_2 \langle \phi_1 | d | E, m, 1 \rangle \langle \phi_2 | d | E, m, 1 \rangle]}{\sum_m [|\tilde{\epsilon}_1 c_1|^2 \langle \phi_1 | d | E, m, 2 \rangle|^2 + |\tilde{\epsilon}_2 c_2|^2 \langle \phi_2 | d | E, m, 2 \rangle|^2 + 2 \operatorname{Re}[c_1^* c_2 \tilde{\epsilon}_1^* \tilde{\epsilon}_2 \langle \phi_1 | d | E, m, 2 \rangle \langle \phi_2 | d | E, m, 2 \rangle]} \quad (6.13b)$$

The result of this computation is qualitatively straightforward. Specifically, the superposition state $[c_1 \phi_1 + c_2 \phi_2]$ has replaced the initial state ϕ_g of Equation 6.12 and the two electric fields, which now remain in this expression, are those which raise each of the individual levels to the excited state.

The structure of each of the numerator and denominator of Equation 6.13 is clearly of the type desired (i.e., each has two terms associated with the two different independent excitations of levels at energies E_1 and E_2 and

set of terms corresponding to the interference between these two processes). The interference term can either constructively enhance or destructively cancel out contributions to either product channel. What makes Equation 6.13 so important in practice is that the interference terms have coefficients whose magnitude and sign depend upon *experimentally controllable* parameters. Thus the experimentalist can manipulate laboratory parameters and, in doing so, directly alter the reaction product yield by varying the magnitude of the interference term. In the case of Equation 6.13 the experimental parameters which alter the yield [1] are the absolute magnitude and phase of the quantity

$$A = \frac{\tilde{\epsilon}_2 c_2}{\tilde{\epsilon}_1 c_1}$$

Results of a specific computational example based upon Equation 6.13 are shown in Figure 6.2. Here we consider control over the relative probability of forming $^2P_{3/2}$ versus $^2P_{1/2}$ atomic iodine, denoted I and I^* , in the dissociation of methyl iodide:



Although this reaction is an example of electronic branching of products, the same principles of control apply. Note that computations were carried out with realistic potential surfaces within the framework of a fully quantum computational photodissociation method.

Figure 6.2 shows a typical plot of the yield of I^* as a function of A , where

$$S = \frac{A^2}{(1 + A^2)}$$

and

$$\theta_1 - \theta_2 = \arg(A)$$

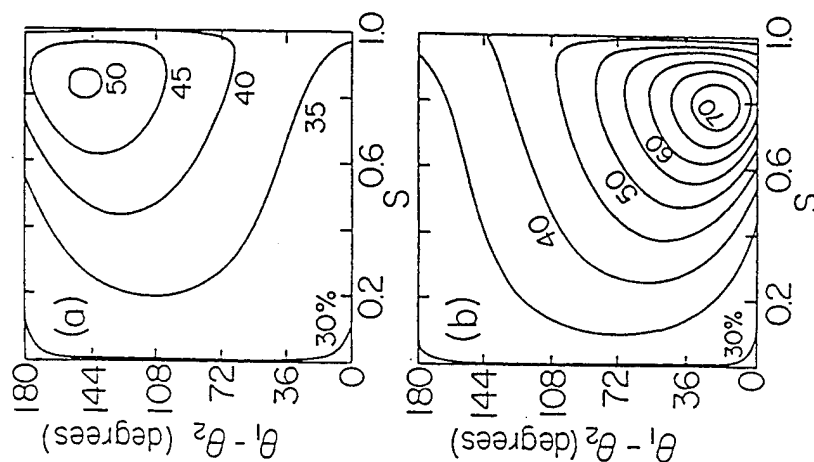


Figure 6.2 Contour plot of the yield of I^* (i.e., fraction of I^* as product) in the photodissociation of CH_3I from a superposition state comprised of (a) $(v_1, J_1, M_1) = (0,0,0) + (v_2, J_2, M_2) = (0,1,0)$ and (b) $(0,0,0) + (0,2,0)$. Here v_i, J_i, M_i are the vibrational, rotational and rotational projection quantum numbers of the i^{th} bound state. Source: from [1].

With this choice, $S = 0$ corresponds to $\tilde{\epsilon}_1 = 0$ (i.e., laser 1 off), whereas $S = 1$ corresponds to $\tilde{\epsilon}_2 = 0$ (i.e., laser 2 off). Note the large range of control with variation in S and $\theta_1 - \theta_2$ (i.e., the yield varies from 30–70% I). Higher and lower ratios can also be achieved [27] with different choices of the initial pair of states $|\phi_1\rangle$ and $|\phi_2\rangle$.

This scenario assumes starting with a superposition of two bound states. Experimental possibilities for creating such an initial state include pulsed excitation with an electromagnetic field whose frequency width spans the two levels [9–11] or stimulated emission pumping through an intermediate electronic state [19]. A coherent control scenario, in which the superposition state preparation is followed by a second pulse, as distinct from photodissociation with CW sources, is discussed in detail in Section 6.2.B below. Furthermore, a theoretical scheme, in which there are N product channels and the initial superposition is comprised of N levels, is discussed elsewhere [16]. In this case we have shown that under certain conditions one can control the product yields *completely*. That is, one may specify a desired product distribution and analytically determine the N electromagnetic fields required to attain this product distribution.

D. The Essential Principle

The two step approach of Figures 6.1 and 6.2 is but one particular implementation of the principle of coherent control. That is, the essence of control is in the content of the superposition state at energy E where dissociation into various products is possible. Numerous other scenarios may be designed which rely upon the same essential principle: that coherently driving a pure state through multiple optical excitation routes to the same final state allows for the possibility of control. This procedure has a well-known analogy: the interference between paths as a beam of either particles or of light passes through a double slit. In that case interference between two coherent beams leads to interference, manifest as patterns of enhanced or reduced probabilities on an observation screen. In the case of coherent control the overall coherence of a pure state plus laser source allows for the constructive or destructive manipulation of probabilities in product channels.

The coherence of the laser and the knowledge of the molecular phase are essential elements of control. It is easy to see that, for example, total laser incoherence leads to loss of control. That is, laser incoherence implies

that the phases of \tilde{E}_1 and \tilde{E}_2 in Equation 6.13 are random. Doing an ensemble average over these phases results in the disappearance of the interference term. Nonetheless, we have also shown that control does persist in the presence of *partial* laser incoherence [14] and when the initial state is described by a (nondiagonal) density matrix [7], so some degree of phase incoherence can be tolerated without total loss of phase control.

6.2 REPRESENTATIVE CONTROL SCENARIOS

A. Interference Between N-Photon and M-Photon Routes

As a second example of a useful experimental implementation of coherent control consider Equation 6.12 once again. There we introduced quantum interference by modifying the initial state prior to excitation into the continuum. An alternative method readily suggests itself. Specifically, consider adding a second, multiphoton, optical route to energy E . The simultaneous one and multiphoton excitation then lead to controllable interference contributions and thus to yield control.

As the simplest example, we examine one photon plus three photon absorption. (The approach generalizes in a straightforward fashion to the case of two or more excitation routes with N and M photons as long as the choice of fields obeys requisite selection rules; see Section 6.3.A). Let H_g and H_e be the nuclear Hamiltonians for the ground and excited states, respectively, and $|E_g\rangle$ be the ground eigenstate (i.e., $H_g|E_g\rangle = E_g|E_g\rangle$). The kets $|E, n, q\rangle$ are continuum eigenstates of H_e with incoming boundary conditions as discussed earlier.

The molecule, initially in $|E_g\rangle$, is subjected to two electric fields (Figure 6.3) given by

$$\mathcal{E}(t) = \mathcal{E}_1 \cos(\omega_1 t + \mathbf{k}_1 \cdot \mathbf{R} + \theta_1) + \mathcal{E}_3 \cos(\omega_3 t + \mathbf{k}_3 \cdot \mathbf{R} + \theta_3) \quad (6.15)$$

Here $\omega_3 = 3\omega_1$, $\mathcal{E}_l = \hat{\epsilon}_l \hat{\epsilon}_l$, $l = 1, 3$; $\hat{\epsilon}_l$ is the magnitude and $\hat{\epsilon}_l$ is the polarization of the electric fields. The two fields are chosen parallel, with $\mathbf{k}_3 = 3\mathbf{k}_1$. The probability $P(E, q; E_g)$ of producing product with energy E in arrangement q from a state $|E_g\rangle$ is given by

$$P(E, q; E_g) = P_3(E, q; E_g) + P_{13}(E, q; E_g) + P_1(E, q; E_g) \quad (6.16)$$

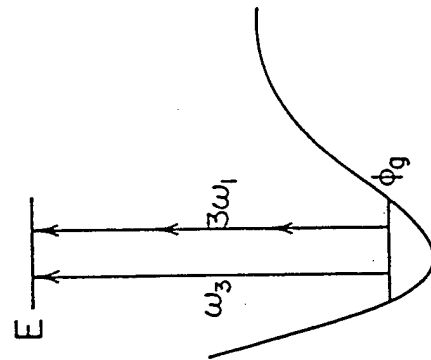


Figure 6.3 A multiple optical-route scheme to inducing controllable quantum interference effects into the continuum state at energy E . Here the level Φ_g is a bound state of a lower electronic state and that at E is a continuum state of the excited electronic state. Simultaneous application of frequencies ω_1 and $\omega_3 = 3\omega_1$ leads to interference in the continuum state. *Source:* from [12].

where $P_1(E, q; E_g)$ and $P_3(E, q; E_g)$ are the probabilities of dissociation due to the ω_1 and ω_3 excitation, and $P_{13}(E, q; E_g)$ is the term due to interference between the two excitation routes.

In the weak field limit, $P_3(E, q; E_g)$ is given by

$$P_3(E, q; E_g) = \left(\frac{\pi}{h} \right)^2 \mathcal{E}_3^2 \sum_n |\langle E, n, q | (\hat{\epsilon}_3 \cdot \mathbf{d})_e | E_g \rangle|^2 \quad (6.17)$$

Here \mathbf{d} is the electric dipole operator and

$$(\hat{\epsilon}_3 \cdot \mathbf{d})_{e,g} = \langle e | \hat{\epsilon}_3 \cdot \mathbf{d} | g \rangle \quad (6.18)$$

where $|g\rangle$ and $|e\rangle$ are the ground and excited electronic state wavefunctions, respectively. Assuming also that $E_g + 2\hbar\omega_1$ is below the dissociation threshold, with dissociation occurring from the excited electronic state, $P_1(E, q; E_g)$ is given in third-order perturbation theory by [6]

$$P_1(E, q; E_i) = \left(\frac{\pi}{\hbar} \right)^2 \varepsilon_1^6 \sum_n | \langle E, n, q | \nabla E_i \rangle |^2 \quad (6.19)$$

with

$$T = (\hat{\varepsilon}_1 \cdot \mathbf{d})_{e,g} (E_i - H_g + 2\hbar\omega_1)^{-1} (\hat{\varepsilon}_1 \cdot \mathbf{d})_{g,e} (E_i - H_e + \hbar\omega_1)^{-1} (\hat{\varepsilon}_1 \cdot \mathbf{d})_{e,g} \quad (6.20)$$

A similar derivation [6] gives the cross-term in Equation 6.16 as

$$P_{13}(E, q; E_i) = -2 \left(\frac{\pi}{\hbar} \right)^2 \varepsilon_3 \varepsilon_1^3 \cos(\theta_3 - 3\theta_1 + \delta\{3\}) F\{3\} \quad (6.21)$$

with the amplitude $|F\{3\}|$ and phase $\delta\{3\}$ defined by

$$|F\{3\}| \exp(i\delta\{3\}) = \sum_n \langle E_i | \nabla E, n, q \rangle \langle E, n, q | (\hat{\varepsilon}_3 \cdot \mathbf{d})_{e,g} | E_i \rangle \quad (6.22)$$

The branching ratio $R_{qq'}$ for channels q and q' , can then be written as

$$\begin{aligned} R_{qq'} &= \frac{P(E, q; E_i)}{P(E, q'; E_i)} \\ &= \frac{\varepsilon_3^2 F\{q\} - 2\varepsilon_3 \varepsilon_1^3 \cos(\theta_3 - 3\theta_1 + \delta\{q\}) |F\{q\}| + \varepsilon_1^6 F\{q\}}{\varepsilon_3^2 F\{q'\} - 2\varepsilon_3 \varepsilon_1^3 \cos(\theta_3 - 3\theta_1 + \delta\{q'\}) |F\{q'\}| + \varepsilon_1^6 F\{q'\}} \end{aligned} \quad (6.23)$$

where

$$\begin{aligned} F\{3\} &= \left(\frac{\hbar}{\pi \varepsilon_3} \right)^2 P_3(E, q; E_i) \\ F\{1\} &= \left(\frac{\hbar}{\pi \varepsilon_1} \right)^2 P_1(E, q; E_i) \end{aligned} \quad (6.24)$$

with $F\{q\}$ and $F\{q'\}$ defined similarly. Next, we rewrite Equation 6.23 in a more convenient form. We define a dimensionless parameter $\bar{\varepsilon}_i$ and a parameter x as follows:

$$\varepsilon_i = \bar{\varepsilon}_i \varepsilon_0; \quad x = \frac{\bar{\varepsilon}_1^3}{\bar{\varepsilon}_3} \quad (6.25)$$

for $l = 1, 3$. The quantity ε_0 essentially carries the unit for the electric fields; variations of the magnitude of ε_0 can also be used to account for unknown transition dipole moments. Utilizing these parameters, Equation 6.23 becomes

$$R_{qq'} = \frac{F\{q\} - 2x \cos(\theta_3 - 3\theta_1 + \delta\{q\}) \bar{\varepsilon}_0^2 |F\{q\}| + x^2 \varepsilon_0^4 F\{q\}}{F\{q'\} - 2x \cos(\theta_3 - 3\theta_1 + \delta\{q'\}) \bar{\varepsilon}_0^2 |F\{q'\}| + x^2 \varepsilon_0^4 F\{q'\}} \quad (6.26)$$

The numerator and denominator of Equation 6.26 each display what may be regarded as the canonical form for coherent control: of independent contributions from more than one route, modulated by an interference term. Since the interference term is controllable through variation of laboratory parameters, so too is the product ratio $R_{qq'}$. Thus the principle upon which this control scenario is based is the same as in the first example but the interference is introduced in an entirely different way.

Experimental control over $R_{qq'}$ is obtained by varying the difference $(\theta_3 - 3\theta_1)$ and the parameter x . The former is the phase difference between the ω_3 and the ω_1 laser fields and the latter, via Equation 6.25, incorporates the ratio of the two lasers amplitudes. Experimentally, one envisions using tripling to produce ω_3 from ω_1 , the subsequent variation of the phase of one of these beams provides a straightforward method of altering $\theta_3 - 3\theta_1$. Indeed, generating ω_3 from ω_1 allows for compensation of any phase jumps in the two laser sources. Thus the relative phase $\omega_3 - 3\omega_1$ is well defined. Were it not (e.g., as in the case of incoherent sources), then the cross-term and control would vanish.

With the qualitative principle of interfering pathways established, it remains to determine the quantitative extent to which coherent control alters the yield ratio in a realistic system. To this end we consider an application to one photon versus three photon photodissociation of IBr. In particular, we focus on the energy regime where IBr dissociates to both $I(^2P_{3/2}) +$

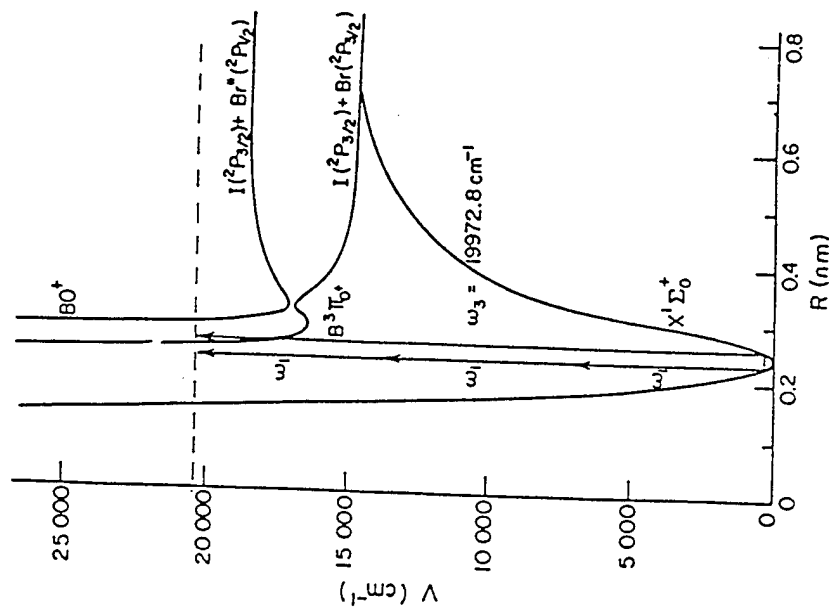


Figure 6.4 IBr potential curves relevant in the one-plus-three photon induced dissociation. *Source:* from [13].

$\text{Br}(\text{}^2P_{3/2})$ and $\text{I}(\text{}^2P_{3/2}) + \text{Br}(\text{}^2P_{1/2})$. The IBr potential curves used in the calculation are shown in Figure 6.4.

A complete IBR computation requires inclusion of angular momentum. Thus the notation $|E_i\rangle$ is replaced by $|E_i, J_i, M_i\rangle$, where J_i is the angular momentum, M_i is its z projection, and the ket is of energy E_i , whose value incorporates specification of the vibrational quantum number v . Where no confusion arises, we continue to use $|E_i\rangle$ for simplicity.

The primary quantity required in the control calculation is the photodissociation amplitude $\langle E, n, q | (\hat{\epsilon}_1 \cdot \mathbf{d}) | E, n, q \rangle$ where the quantum number n in the continuum state $|E, n, q\rangle$ denotes the scattering angles $\hat{\mathbf{k}} = \varphi_k \hat{\theta}_k$ and $q = 1, 2$ labels either the $\text{Br}(\text{}^2P_{3/2})$ or $\text{Br}(\text{}^2P_{1/2})$ channel. In terms of this notation, the one-photon photodissociation amplitude is given by

$$\langle E, \hat{\mathbf{k}}, \hat{q}^{-1}(\hat{\mathbf{e}}_1 \cdot \mathbf{d})_{e,g} | E_i J_i M_i \rangle = \frac{(2J+1)^{1/2}}{\hbar} \sum_J (2J+1)^{1/2} \begin{pmatrix} J & 1 & J_i \\ -M_1 & 0 & M_i \end{pmatrix} D_{0,M_i}^J(\varphi_i, \theta_i, -\theta_i) (E_i J_i M_i | J_i) \quad (6.27)$$

Here μ is the reduced mass of IBr, k is the relative momentum of the dissociated particles, D'_{0M_i} is the rotation matrix element, and

$$\begin{pmatrix} j_1 & j_2 & j_3 \\ M_1 & M_2 & M_3 \end{pmatrix}$$

is the Wigner $3 - j$ symbol and $\iota(E, J, q | E_r, J_r)$ is the (M_r -independent) reduced amplitude, containing the essential dynamics of the photodissociation process [28]. Equation (27) follows from the usual procedure of expanding $\langle E, \hat{\mathbf{k}}, q | \varphi_{\mathbf{k}}, \theta_r, r \rangle$, where r is the I-Br distance, in partial waves labeled by angular momentum J and its z projection M . The angular integration of the resulting expression follows from the Wigner-Eckart theorem and the r integration is incorporated in $\iota(E, J, q | E_r, J_r)$. We have calculated these $\iota(E, J, q | E_r, J_r)$ exactly [13] using the potential curves and coupling strengths given by Child [26].

As shown here, the required P_i and P_{13} (Equation 6.16) are conveniently expressed in terms of the primary quantities $\mathbf{d}^{(q)}(E_i, J_i, M_i; E_i, J_i, M_i; E)$, where

$$\begin{aligned}
& \mathbf{d}^{(q)}(E_j, J_p, M_j; E_i, J_i, M_i; E) \\
&= \int d\hat{\mathbf{k}} \langle E_j, J_p, M_j | \hat{\mathbf{e}}_i \cdot \mathbf{d} \rangle_{e,g} |E_i, \hat{\mathbf{k}}, q\rangle \langle E_i, \hat{\mathbf{k}}, q | \hat{\mathbf{e}}_i \cdot \mathbf{d} \rangle_{e,g} |E_i, J_i, M_i\rangle \\
&= \frac{8\pi\mu k}{\hbar^2} \sum_J \begin{pmatrix} J & 1 & J_i \\ -M_i & 0 & M_j \end{pmatrix} \begin{pmatrix} J & 1 & J_j \\ -M_j & 0 & M_i \end{pmatrix} \delta_{M_i M_j} \mathbf{d}^{(q)*}(E_i, J_i, M_i; E) \mathbf{d}^{(q)}(E_j, J_j, M_j; E)
\end{aligned} \quad (6.28)$$

The integration over the scattering angles $\hat{\mathbf{k}}$ corresponds to the n -summation in Equations 6.17 and 6.19 and the Kronecker delta $\delta_{M_i M_j}$ arises from the fact that the laser-molecule interaction does not depend on the azimuthal angle for the case of linearly polarized light.

The probability P_3 is given, from the definition (Equation 6.17) of $\mathbf{d}^{(q)}$, by

$$P_3(E, q; E_i, J_i, M_i) = \left(\frac{\pi}{\hbar} \right)^2 \epsilon_3^2 \mathbf{d}^{(q)}(E_i, J_i, M_i; E_i, J_i, M_i; E) \quad (6.29)$$

The terms P_{13} and P_1 can also be written in terms of the $\mathbf{d}^{(q)}$. To do so we express $\langle E, n, q | \mathbf{I} | E_i \rangle$ in Equation 6.20 explicitly in terms of $\langle E, n, q | \hat{\mathbf{e}}_i \cdot \mathbf{d} \rangle_{e,g} |E_i\rangle$ by inserting appropriate resolutions of the identity:

$$\begin{aligned}
\langle E, n, q | \mathbf{I} | E_i \rangle &= \sum_{j, n', q'} \int dE' \times \\
& \frac{\langle E, n, q | \hat{\mathbf{e}}_i \cdot \mathbf{d} \rangle_{e,g} |E_i\rangle \langle E_j | \hat{\mathbf{e}}_i \cdot \mathbf{d} \rangle_{g,e} |E', n', q'\rangle \langle E', n', q' | \hat{\mathbf{e}}_i \cdot \mathbf{d} \rangle_{e,g} |E_i\rangle}{(E_j - E_i - 2\hbar\omega_1)(E' - E_i - \hbar\omega_1)}
\end{aligned} \quad (6.30)$$

Here, as noted previously, $|E_i\rangle$ denotes all of $|E_i, J_i, M_i\rangle$ and the j -summation indicates a sum over all bound states $|E_j\rangle$ of the ground $X^1\Sigma_0^+$ potential surface. Computationally, of all the bound eigenstates of $X^1\Sigma_0^+$, the contribution to $\langle E, n, q | \mathbf{I} | E_i \rangle$ is dominated by those states with energy E_j satisfying the near two-photon resonance condition

$$E_j \approx E_i + 2\hbar\omega_1 \quad (6.31)$$

From Equation 6.30 and the definition of $\mathbf{d}^{(q)}$, $|\mathbf{F}^{(q)}| \exp(i\delta^{(q)})$ in the cross-term P_{13} , is given by

$$\begin{aligned}
|\mathbf{F}^{(q)}| \exp(i\delta^{(q)}) &= \sum_{E_j, J_j, q'} \int dE' \times \\
& \frac{\mathbf{d}^{(q)}(E_i, J_i, M_i; E_i, J_i, M_i; E) \mathbf{d}^{(q)*}(E_j, J_j, M_j; E_i, J_i, M_i; E')}{(E_j - E_i - 2\hbar\omega_1)(E' - E_i - \hbar\omega_1)}
\end{aligned} \quad (6.32)$$

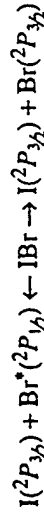
where the J_j and the E_j summation indicates a summation over all bound eigenstates of the $X^1\Sigma_0^+$ state.

Similarly, using Equations 6.19 and 6.30, the probability for the three-photon process is given by

$$\begin{aligned}
P_1(E, q; E_i, J_i, M_i) &= \sum_{E_j, E_i, J_j, \bar{J}, \bar{q}, q'} \int dE' \int d\bar{E} \times \\
& \frac{\mathbf{d}^{(q)}(E_i, J_i, M_i; E_i, J_i, M_i; E) \mathbf{d}^{(q')}(E_j, J_j, M_j; E_i, J_i, M_i; E') \mathbf{d}^{(\bar{q})*}(E_j, \bar{J}, \bar{M}; E_i, \bar{J}, \bar{M}; \bar{E})}{(E_j - E_i - 2\hbar\omega_1)(E_i - E_j - 2\hbar\omega_1)(E' - E_i - \hbar\omega_1)(\bar{E} - E_i - \hbar\omega_1)}
\end{aligned} \quad (6.33)$$

These expressions are quite complex and simple qualitative rules for tabulating the terms are provided elsewhere [13]. Given these results, the quantities $F_3^{(q)}$ and $F^{(q)}$ in the branching ratio ($R_{qq'}$) expression of Equation 6.26 are then written easily in terms of $\mathbf{d}^{(q)}$ using Equations 6.24, 6.29, 6.32, and 6.33.

Computational results were obtained using this scenario for the case of IBr photodissociation:



Two different cases were examined, those corresponding to fixed initial M_i values and those corresponding to averaging over a random distribution of M_i , for fixed J_i . Results typical of those obtained are shown in Figures 6.5 and 6.6, where we provide a contour plot of the yield of $\text{Br}^*(^2P_{3/2})$ for the case of excitation from $J_i = 1$, $M_i = 0$, and $J_i = 42$ with an average over M_i .

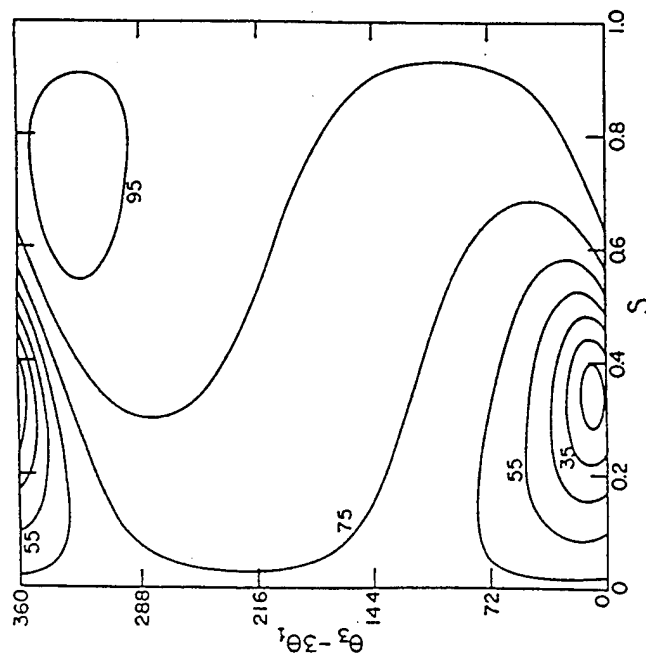


Figure 6.5 Contour plot of the yield of $\text{Br}^*(^2P_{1/2})$ (percentage of Br^* as product) in the photodissociation of IBr from an initial bound state in $X^1\Sigma_g^+$ with $\nu = 0$, $J_1 = 1$, $M_1 = 0$. Results arise from simultaneous (ω_1, ω_3) excitation $(\omega_3 = 3\omega_1)$, with $\omega_1 = 6657.5 \text{ cm}^{-1}$. Source: from [13].

as a function of laser control parameters (relative intensity and phase). The range of control in each case is vast, with no loss of control with averaging over M_J . A related, high field study of two-photon + four-photon control in the photodissociation of Cl_2 has been carried out by Bandrauk et al. [31].

This three-photon + one-photon scenario has now been experimentally implemented [32, 33], in studies of Hg and HCl ionization through a resonant-bound Rydberg state. Specifically, in the work of Gordon et al. [33], HCl is excited to a selected rotational state in the $^3\Sigma^-(\omega^+)$ manifold using $\omega_1 = 336 \text{ nm}$; ω_3 is obtained by third harmonic generation in a Krypton gas cell. The relative phase of the light fields was then varied by passing the beams through a second gas cell and varying the gas pressure. The population of the resultant Rydberg state was interrogated by ionizing to HCl^+ with an

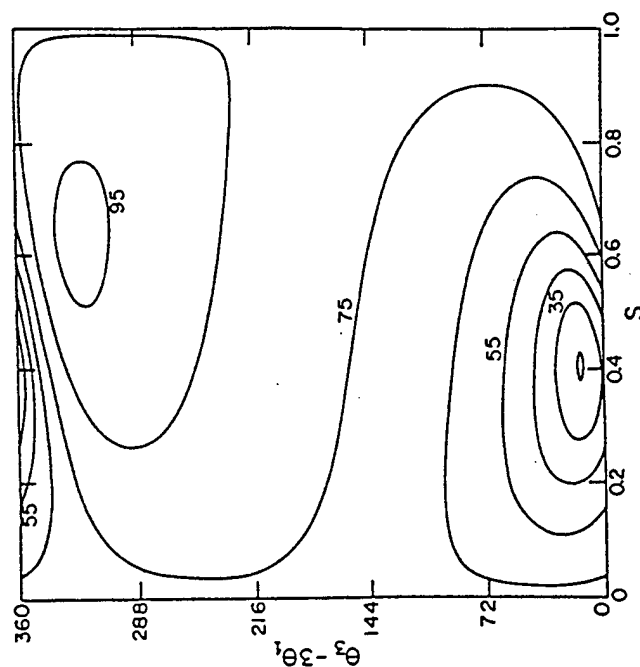


Figure 6.6 As in Figure 6.5 but for $\nu = 0$, $J_1 = 42$, $\omega_1 = 6635.0 \text{ cm}^{-1}$ and M -averaged ($e_0 = 1/8$). Source: from [13].

additional photon. This REMPI-type experiment showed that the HCl^+ ion probability depended upon both the relative phase and intensity of the two exciting lasers, in accord with the theory described here. A similar phase control experiment has been performed on atoms [32], in the simultaneous three-photon + five-photon ionization of Hg . Although the effect of the relative laser intensity was not studied, the Hg^+ ionization probability was shown to be a function of relative phase of the two lasers.

In another laboratory study, photocurrent directionality, which we predicted to be achievable in semiconductors using coherent control techniques with no bias voltage (see Section 6.4.B) has been demonstrated using one-photon + two-photon interferences [34].

These experiments clearly show that coherent control of simple molecular processes through quantum interference of multiple optical excitation routes is both feasible and experimentally observable. Further experimental

studies designed to show control over processes with more than one product channel are in progress by a number of experimental groups.

B. Pump-Dump Scenarios

An important generalization of the scenario outlined in Section 6.2.A arises when the initial superposition of bound states is prepared with a laser pulse and is subsequently dissociated with a laser pulse. The scenario is shown qualitatively in Figure 6.7.

The pump and dump steps are assumed to be temporally separated, with a time delay τ_d between their temporal centers. The analysis here shows that under these circumstances the convenient control parameters are the central frequency of the pump pulse and the time delay between the pulses.

Consider a molecule, initially ($t = 0$) in eigenstate $|E_g\rangle$ of Hamiltonian H_M , which is subjected to two sequential transform-limited light pulses. The total Hamiltonian is of the form:

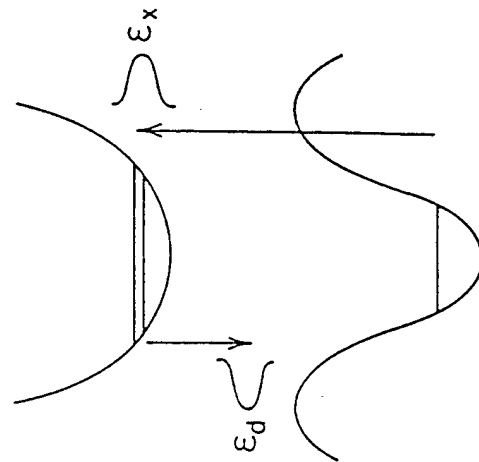


Figure 6.7 Coherent radiative control via a picosecond pulse scheme. In this case a single level is excited with a laser pulse to produce a superposition of two bound states in an excited electronic state. Subsequent deexcitation of this state to the continuum of the ground state allows control over the reaction on the ground state surface. *Source:* from [12].

$$H = H_M + V = H_M - \mathbf{d}[\bar{\epsilon}(t) + \bar{\epsilon}^*(t)] \quad (6.34)$$

where \mathbf{d} is the dipole operator along the electric field direction. The field $\bar{\epsilon}(t)$ consists of two temporally separated pulses $\bar{\epsilon}(t) = \bar{\epsilon}_x(t) + \bar{\epsilon}_d(t)$, with the Fourier transform of $\bar{\epsilon}_x(t)$ denoted $\epsilon_x(\omega)$, etc. For convenience, these are chosen as gaussian pulses peaking at $t = t_x$ and t_d respectively. The $\bar{\epsilon}_x(t)$ pulse induces a transition to a linear combination of two excited, bound, electronic states with nuclear eigenfunctions $|E_1\rangle$ and $|E_2\rangle$, and the $\bar{\epsilon}_d(t)$ pulse dissociates the molecule by further exciting it to the continuous part of the spectrum. Both fields are chosen to be sufficiently weak so that perturbation theory is valid [24].

The superposition state prepared by the $\bar{\epsilon}_x(t)$ pulse, whose width is chosen to encompass just the two E_1 and E_2 levels, is given in first-order perturbation theory as,

$$|\varphi(t)\rangle = |E_g\rangle e^{-iE_g t/\hbar} + c_1 |E_1\rangle e^{-iE_1 t/\hbar} + c_2 |E_2\rangle e^{-iE_2 t/\hbar}$$

where

$$c_k = \frac{\sqrt{2\pi}}{i\hbar} \langle E_k | \mathbf{d} | E_g \rangle \epsilon_x(\omega_{kg}), \quad k = 1, 2, \quad (6.35)$$

with

$$\omega_{kg} \equiv \frac{E_k - E_g}{\hbar}.$$

After a time delay $\tau (= \tau_d - \tau_x)$ the system is subjected to the $\bar{\epsilon}_d(t)$ pulse. Following that pulse the system wavefunction, expanded in a complete set of continuum eigenstates $|E, n, q\rangle$, labeled by energy E , arrangement channel label q and remaining labels n , is then,

$$|\psi(t)\rangle = |\varphi(t)\rangle + \sum_{n,q} \int dE B(E, n, q | t) |E, n, q\rangle e^{-iEt/\hbar} \quad (6.36)$$

Here we are interested in the probability $P(E, q)$ of forming product in arrangement channel q at energy E . However, we require $P(E, m_j, q)$ (i.e.,

the probability of forming product in q , E , and total fragment angular momentum projection m_j along the space fixed axis; see Section 6.4.A). The two probabilities are related by $P(E, q) = \sum_{m_j} P(E, m_j, q)$. Hence we first produce $P(E, m_j, q)$ and subsequently sum to obtain $P(E, q)$.

Using first-order perturbation theory and the rotating wave approximation in conjunction with Equation 6.36, gives:

$$P(E, m_j, q) = \sum_n |B(E, n, q|t = \infty)|^2 \\ = \left(\frac{2\pi}{\hbar^2} \right) \sum_n \left| \sum_{k=1,2} c_k \langle E, n, q | d | E_k \rangle \epsilon_k(\omega_{EE_k}) \right|^2 \quad (6.37)$$

where $\omega_{EE_k} = (E - E_k)/\hbar$, c_k is given by Equation 6.35 and where the prime denotes summation over all quantum numbers n other than m_j .

Expanding the square and using the gaussian pulse shape gives:

$$P(E, m_j, q) =$$

$$\left(\frac{2\pi}{\hbar^2} \right) \left[|c_1|^2 |d_1^{(q)}|^2 |\epsilon_1|^2 + |c_2|^2 |d_2^{(q)}|^2 |\epsilon_2|^2 + 2|c_1 c_2 \epsilon_1 \epsilon_2 d_1^{(q)} d_2^{(q)}| \cos(\omega_{2,1}(t_d - t_r) + \alpha_1^{(q)}(E) + \phi) \right] \quad (6.38)$$

where $\epsilon_i = |E_d(\omega_{EE_i})|$, $\omega_{2,1} = (E_2 - E_1)/\hbar$ and the phases ϕ , $\alpha_1^{(q)}(E)$ are defined by

$$\langle E_1 | d | E_r \rangle \langle E_r | d | E_2 \rangle \equiv \langle E_1 | d | E_r \rangle \langle E_r | d | E_2 \rangle e^{i\phi} \\ d_{1,2}^{(q)}(E) \equiv |d_{1,2}^{(q)}(E)| e^{i\alpha_{1,2}^{(q)}(E)} = \sum_n \langle E, n, q | d | E_r \rangle \langle E_r | d | E, n, q \rangle \quad (6.39)$$

Integrating over E to encompass the width of the second pulse, assumed sufficiently small so that $d_{1,2}^{(q)}(E)$ can be assumed constant, and forming the ratio

$$Y = \frac{\sum_{m_j} P(q, m_j)}{\sum_{m_j, q} P(q, m_j)} \quad (6.40)$$

gives the ratio of products in each of the two arrangement channels (i.e., the quantity we wish to control). Once again it is the sum of two direct photo-dissociation contributions plus an interference term.

Examination of Equation 6.38 makes clear that the product ratio Y can be varied by changing the delay time $\tau = (t_d - t_r)$ or ratio $x = |c_1/c_2|$; the latter is most conveniently done by detuning the initial excitation pulse.

It is enlightening to consider this scenario as applied [9] to a model collinear reaction with masses of D and H,



Typical results (see also [9]) for control are shown in Figure 6.8 where the yield is seen to vary from 16–72% as the time delay and tuning of the initial excitation pulse are varied. This is an extreme range of control, especially in light of the fact that the two product channels differ only by mass factors.

It is highly instructive to examine the nature of the superposition state prepared in the initial excitation (Equation 6.35) and its time evolution during the delay between pulses. An example of such a state is shown in Figure 6.9 where we plot the wavefunction for a collinear model of reaction (40). Specifically, the coordinates are the reaction coordinate S and its orthogonal conjugate x . The wavefunction is shown evolving over one half of its total possible period. Examination of Figure 6.9 shows that de-exciting this superposition state during frame (b) would result in a substantially different product yield than de-exciting at the time of frame (c). However, there is clearly no particular preference of the wavefunction for large positive or large negative S at these particular times, which would be the case if the reaction control were a result of some spatial characteristics of the wavefunction. Rather, the essential control characteristics of the wavefunction are carried in the quantum amplitude and phase of the created superposition state.

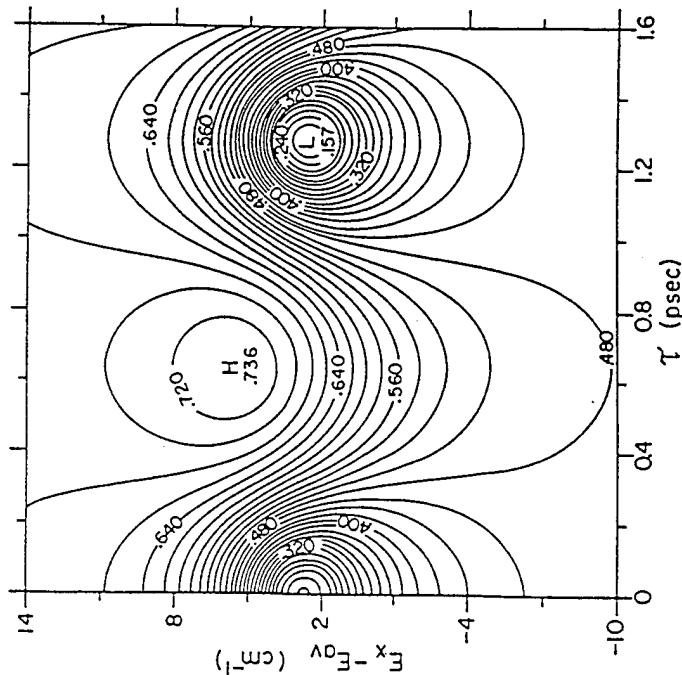
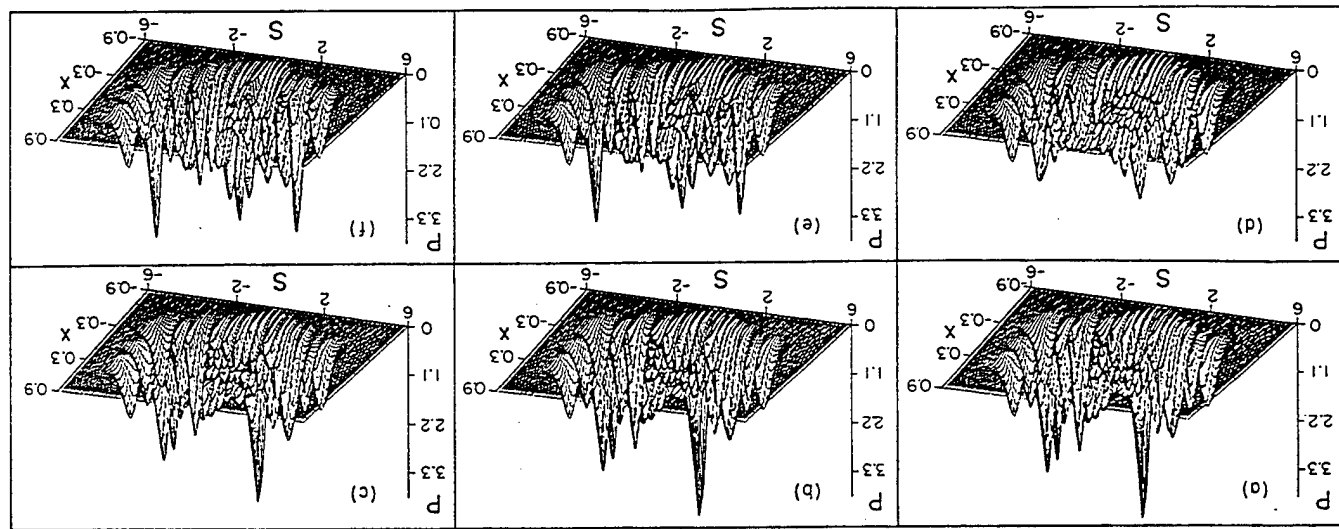


Figure 6.8 Contour plot of the DH yield in the reaction $D + H_2 \leftarrow DH_2 \rightarrow DH + H$. The control parameters are the difference in energy between the excitation pulse center E_x and the average of the energy of the two excited levels E_{av} and the time between the pulses τ . Although the abscissa begins at zero and spans approximately one period, the results are periodic in the delay time. *Source:* from [9].

A second example of pump-dump control [11] is provided by IBBr photodissociation. Specifically, we showed that it is possible to control the Br* versus Br yield in this process by using two conveniently chosen picosecond pulses in the following way. The first pulse prepares a linear superposition of two bound states which arise from mixing of the X and A states. A subsequent pulse pumps this superposition to dissociation where the relative yields of Br and Br* are examined. Results typical of those obtained are shown in Figure 6.10 where the relative yield is shown as a function of the delay between pulses and the detuning of the pump pulse from the energetic center of the two bound states in the initial superposition. The

Figure 6.9 Time evolution of the square of the wavefunction for a superposition state comprised of levels 56 and 57 of the G1 surface of H_3 . The probability is shown as a function of the reaction coordinate S and orthogonal distance x at times (a) 0, (b) 0.0825 psec, (c) 0.165 psec, (d) 0.33 psec, (e) 0.495 psec, (f) 0.66 psec, which correspond to equal fraction of one half the period $2\pi/\omega_{2,1}$. *Source:* from [9].



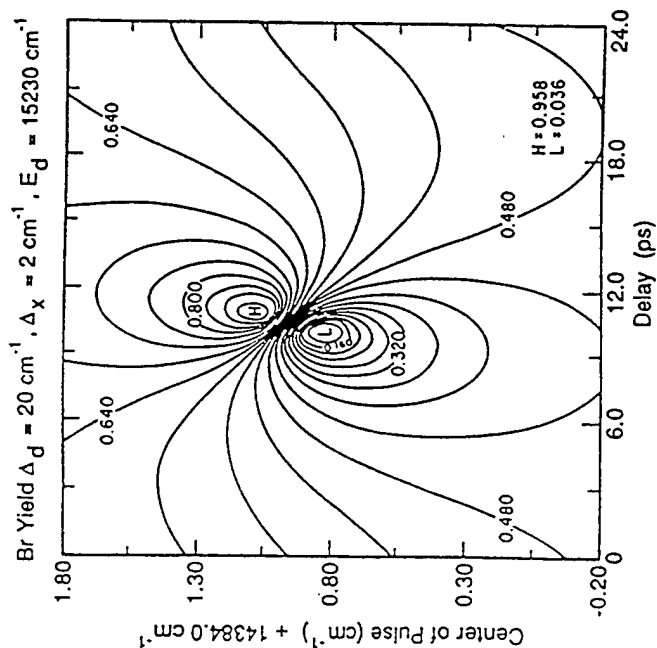


Figure 6.10 Computed control over the Br yield as a function of E_x —the excitation pulse detuning and τ —the time delay between the pulses. Parameters are of Figure 6.6, Ref. [11]. Source: from [11].

results show the vast range of control which is possible with this relatively simple experimental setup. Once again it is worth noting that both the potential energy surfaces and quantum photodissociation computations are state-of-the-art, so that the results should be representative of results expected in the laboratory.

6.3 DESIGNING CONTROL SCENARIOS

Given the general principle established above, one can design numerous scenarios to obtain control over reactions in the laboratory. Such scenarios must, however, properly account for a number of factors which reduce or eliminate control. In this section we briefly note four such features and subsequently discuss two in greater detail.

1. In any proposed scenario it is necessary to minimize extraneous uncontrolled satellites; that is, photoexcitation often results in contributions which are uncontrolled, in addition to the desired controlled contributions. An example is the $J = 3$ state created by three photon absorption in the above scenario. Since there is only one route to $J = 3$ (unlike $J = 1$) photodissociation from the $J = 3$ component is insensitive to the relative phase and intensities of the one and three photon routes. Similar uncontrolled contributions arise in other scenarios as well. Effective control schemes must insure that such contributions are small compared to the controlled component.
2. A successful laboratory scenario must insure properly treated laser spatial dependence and phase jitter. Since the ability to accurately manipulate the laser relative phase is crucial to coherent control, one must account for all laboratory features which affect the phase. For example, scenarios must be designed so as to eliminate effects due to the $k \cdot R$ spatial dependence of the laser phase. Not doing so results in the reduction of control resulting from the variation of this term over the molecule beam-laser beam intersection volume.
3. The laboratory scenario must be designed to compete effectively against effects which tend to destroy coherence (e.g., collisions and laser phase instabilities). The collision and laser incoherence studies [7, 17] (discussed in Section 6.3.A) indicate that control can survive moderate levels of such phase destructive processes or that clever scenarios can overcome their effects.
4. Selection rules play a fundamental role in the nature of the processes which can be controlled. Control requires that the interference term (e.g., $F\{q\}$) between optical routes is nonzero. In general, this is the case only if the various optical excitation routes satisfy specific rules regarding conserved integrals of motion. The importance of the issue of selection rules in designing control scenarios leads us to discuss them in detail.

A. Selection Rules

So far we have not considered the question of *selection rules* in coherent control. In this section we show that indeed there are some strict limitations on the type of processes which can be used to control integral attributes. The term *integral*, in contrast to *differential*, is used here to describe a quantity in which averaging over angles and/or final polarizations takes place in the detection process. It turns out that most of the limitations imposed on the

control of integral quantities do not apply to the control of differential attributes. Naturally, if our main interest is in the *total yield* of a chemical reaction, we must consider processes which control integral quantities. There are, however, many important applications, such as the control of current directionality [8] (see Section 6.4.B), and angular distributions of photo-fragments [5], in which we aim to control the differential attributes.

For example, in order to maintain control over integral attributes in the scenario described in Section 6.1.C we must ensure that the interference term of Equation 6.13b does not vanish when we perform the averaging which defines the particular integral quantity of interest. Thus, if we wish to control integral *cross-sections*, the interference term should survive integration over scattering angles; if we wish to control a *nonpolarized* but otherwise differential quantity we must make sure that the interference term survives the averaging over the appropriate magnetic quantum-numbers.

The discussion below can be summarized in terms of two general selection rules for integral control:

1. The (two) interfering pathways must be able to access continuum states with the same magnetic quantum numbers. This rule holds even when the initial states are *M*-polarized.
2. If the initial state is not *M*-polarized, integral control can only be achieved via interference between continuum states of equal parity. Two pathways which generate states of opposite parity, such as a one-photon and a two-photon absorption, cannot lead to integral control of unpolarized initial states. However, these pathways can [5, 8] and do [34] lead to differential control of unpolarized states or integral control of polarized beams (subject to selection rule 1).

In order to see how these selection rules come about, we use a symmetric-top molecule as a working example and the the superposition-state control scenario outlined in Section 6.1.C. To be more specific, we take CH_3I as an example. The symmetric-top CH_3I is in many ways equivalent to a linear triatomic molecule [36], since in both the ground and the first few excited states the I, the C, and the H_3 (C.M.) do not deviate significantly from the collinear configuration.

As mentioned in Section 6.1.C, CH_3I breaks apart to yield $\text{CH}_3(\nu) + \text{I}^*(^2P_{3/2})$ and $\text{CH}_3(\nu) + \text{I}(^2P_{3/2})$. The relevant quantum numbers for the bound states $|q\rangle$, $|q\rangle$ which make up the initial superposition state are E_f —the

energy and J_i and M_f —the total angular momentum and its z -projection, respectively; hence we denote the states as $|E_f, J_i, M_f\rangle$, etc. The products prime label m is composed of ν —the final CH_3 (umbrella) vibrational state, $\hat{\mathbf{k}} (= \varphi_k, \theta_k)$ —the CH_3 scattering angles relative to the polarization direction of the photolysis laser, and $q = 1, 2$ —the products prime electronic state index.

The molecule is a symmetric top rather than a simple rotator due to the presence of λ , the projection of the *total* angular momentum on the CH_3 -I axis. In general λ is a projection of both the electronic angular momentum and the rotation of the CH_3 group about the C-I axis. In the present discussion we ignore the nuclear component of λ and concentrate on the electronic component.

In the photoexcitation to the first (*A*) continuum of CH_3I , λ assumes the values 0 (the ground and the 3Q_0 states) and ± 1 (the 1Q_1 state). In the diabatic representation [28], $\lambda = 0$ correlates with $q = 1$ —the $\text{CH}_3 + \text{I}^*(^2P_{3/2})$ fragment-channel and $\lambda = \pm 1$ with $q = 2$ —the $\text{CH}_3 + \text{I}(^2P_{3/2})$ channel. We therefore use λ and q interchangeably in describing the products prime electronic states.

For a symmetric-top molecule the three dimensional photodissociation amplitude of Equation 6.27 can be written as [28], where \mathbf{d} is now along the electric field

$$\langle E, \hat{\mathbf{k}}, \nu, \lambda | \mathbf{d} | E_i, J_i, M_i \rangle = \frac{(2\mu k_\nu)^{1/2}}{\hbar} \sum_J \begin{pmatrix} J & 1 & J_i \\ -M_i & 0 & M_i \end{pmatrix} (2J+1)^{1/2} D_{\lambda, M_i}^J(\varphi_k, \theta_k, -\varphi_k) \epsilon(E, J, \lambda, \nu | E_i, J_i) \quad (6.41)$$

Here μ is the reduced-mass of the CH_3I pair, k_ν is the magnitude of the $\text{CH}_3(\nu)$ -I(λ) relative wave-vector, and $\epsilon(E, J, \lambda, \nu | E_i, J_i)$ are the (M_f -independent) reduced amplitudes, containing the essential dynamics of the photo-dissociation process [28].

With the use of Equation 6.11, the integral attributes which enter the general coherent control expression (Equation 6.13b), are,

$$\mathbf{d}^{(\lambda)}(E_f, J_f, M_f; E_i, J_i, M_i; E) = \sum_{\nu} \int d\hat{\mathbf{k}} \langle E_f, J_f, M_f | \mathbf{d}_e | E, \hat{\mathbf{k}}, \nu, \lambda \rangle \langle E, \hat{\mathbf{k}}, \nu, \lambda | \mathbf{d}_e | E_i, J_i, M_i \rangle$$

$$= \frac{8\pi\hbar}{\hbar^2} \delta_{M_i, M_j} \sum_{\nu, \lambda} k_{\nu\lambda} \begin{pmatrix} J & 1 & J_i \\ -M_i & 0 & M_i \end{pmatrix} \begin{pmatrix} J & 1 & J_j \\ -M_j & 0 & M_j \end{pmatrix} \times$$

$$(EJ\lambda_{\nu} \nu | E_i J_i J_i)^* (EJ\lambda_{\nu} \nu | E_j J_j J_j) \quad (6.42)$$

The δ_{M_i, M_j} factor arises from the angular integration and the orthogonality of the Wigner D functions [37]. We see immediately that even for the $i \neq j$ interference term, $M_i = M_j$. Since coherent control vanishes if the interference term vanishes, we conclude that for the superposition-state scenario, control with linearly polarized light is possible only when the states that make up the superposition state have *equal* magnetic quantum numbers.

This result is actually due to the fact that the two excitation pathways must be able to access continuum states with the same M quantum number. In the case of linear polarization the photoexcitation process cannot change M , hence the requirement that $M_i = M_j$ in the initial superposition state. For circular polarization M changes by ± 1 and the selection rule is that $M_i = M_j \pm 1$. These two different selection rules immediately preclude the use of a *single* bound state with two *different* polarizations, (linear + circular or two circular polarizations of opposite sense) for *integral* control. However there are no limitations on differential control [5] since two states of different M quantum numbers can interfere.

We now proceed to explore two cases of interest; the first, where the initial state is M -selected and the second where no such selection is assumed. Each of these cases is treated in turn.

M-Polarized Initial States

We consider exciting with linearly polarized light a superposition of two bound states: $|E_1 J_1 M_1\rangle$ and $|E_2 J_2 M_2 = M_1\rangle$. The choice $M_2 = M_1$ is a result of the earlier discussion and the use of linearly polarized light in the excitation step. The excitation by radiation with two colors raises the system to energy E as described above. Equation 6.13b, in conjunction with Equation 6.42, is now directly applicable.

The symmetry properties of the 3- j symbols [37] imply that,

$$\mathbf{d}^{(\lambda)}(E_i J_i M_i E_j J_j M_j E) = (-1)^{(J_i + J_j)} \mathbf{d}^{(\lambda)}(E_i J_i -M_i E_j J_j -M_j E) \quad (6.43)$$

Therefore, the relative product yield $R(1,2;E)$ is identical for the case of $|M_1\rangle$ and $-|M_1\rangle$ if $(J_1 + J_2)$ is even. In the case of odd $(J_1 + J_2)$, the interference term changes sign when going from $|M_1\rangle$ to $-|M_1\rangle$. The control map (i.e., yield versus S) and $(\theta_1 - \theta_2)$ of the M -polarized case is identical for the $|M_1\rangle$ and $-|M_1\rangle$ case, except for a shift in the relative phase $(\theta_1 - \theta_2)$ of π . For the *unpolarized* case, this result is shown below to lead to cancellation of the interference term for states of different parity.

Figures 6.11(a) and 6.12(a) display the yield of $I^*(2P_{1/2})$ for two different M -selected initial bound-state superpositions. Results are shown at $\omega_1 = 39638 \text{ cm}^{-1}$, which is near the absorption maximum. For the present discussion, the main feature worth noting is that the equal-parity case of Figure 6.12(a), where $J_1 = J_2 = 1$, is strikingly different from the unequal parity case of Figure 6.11(a), where $J_1 = 1$ and $J_2 = 2$. The equal-parity maps show a wider range of control as compared with the unequal parity results. In addition to these results, the actual value assumed by M of the initial beam is of importance. This is most noticeable in the unequal-parity case, where the $M = 1$ case of Figure 6.11(a), is drastically different than the $M = 0$ case of Figure 6.13 which shows *no phase control*. This loss of control follows from the properties of the 3- j symbols of Equation 6.42 which are zero whenever $M_1 = 0$ and $(J_1 + J_2)$ is odd [37].

M-Averaged Initial States

In this case the initial state is defined by the density matrix

$$\rho_0 = \frac{1}{J_1 + 1} \sum_{M_1} c_1 |E_1 J_1 M_1\rangle \langle E_1 J_1 M_1| + c_2 |E_2 J_2 M_1\rangle \langle E_2 J_2 M_1|$$

Each of the superposition states which make up our initial density matrix may be treated independently in the subsequent two-color irradiation which lifts the system to E . The resultant probability of observing product channel q at energy E , $P(q, E)$, is obtained as an average over the $(2J_1 + 1)$ superpositions,

$$P(q, E) = \frac{(\pi\hbar)^2}{2J_1 + 1} \sum_{i=1,2} \sum_{J_i} \sum_{M_i} F_{i,J_i} \mathbf{d}^{(\lambda)}(E_i J_i M_i E_j J_j M_j E) \quad (6.44)$$

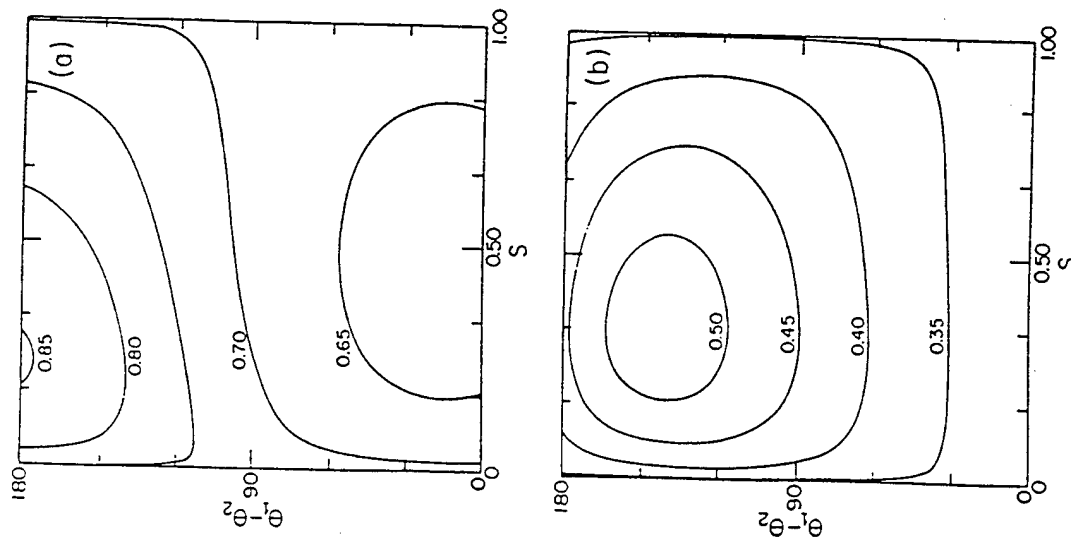


Figure 6.11 Contour plot of the yield of $I(^2P_{1/2})$ (i.e., percentage of I^* as product) in the photodissociation of CH_3I from a polarized superposition state composed of $v_1 = 0$, $J_1 = 1$, and $v_2 = 0$, $J_2 = 2$, where $M_1 = M_2 = 1$, at (a) $\omega_{E_1} = 39638 \text{ cm}^{-1}$ and (b) $\omega_{E_1} = 42367 \text{ cm}^{-1}$, $v = 0$ denotes the ground vibrational state of CH_3I . The abscissa is labelled by $S = x^2/(1+x^2)$, where x is the ratio of laser field intensities and the ordinate by the relative phase parameter $\theta = \theta_1 - \theta_2$. After Ref. [3].

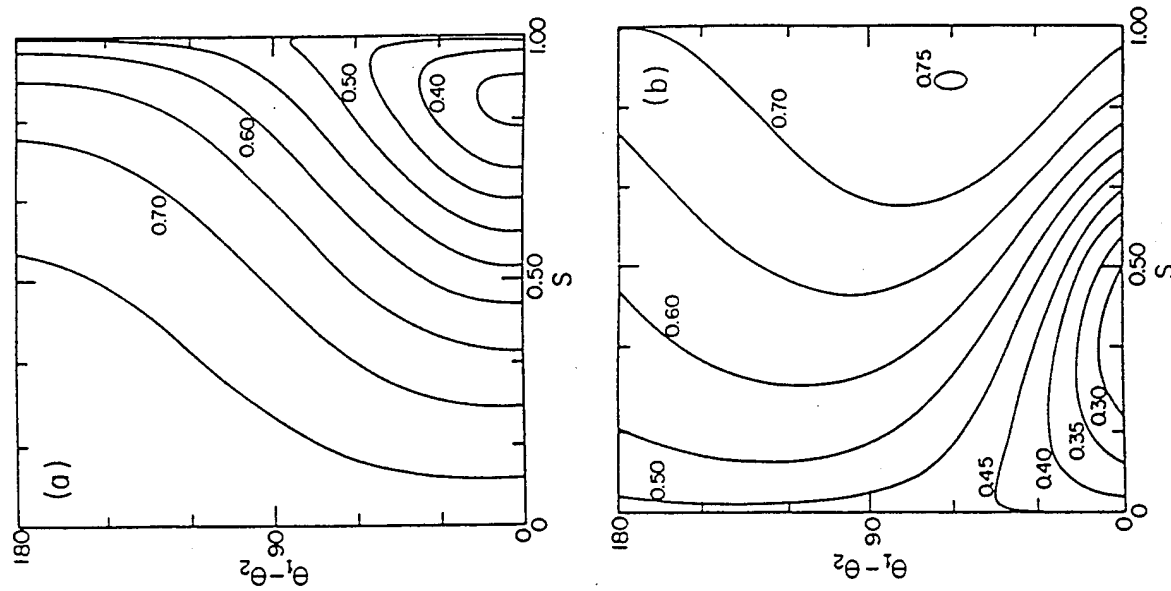


Figure 6.12 As in Figure 6.11 but $v_1 = 0$, $J_1 = 2$, $v_2 = 1$, $J_2 = 2$, $M_1 = M_2 = 0$, at (a) $\omega_{E_1} = 39638 \text{ cm}^{-1}$ and (b) $\omega_{E_1} = 42367 \text{ cm}^{-1}$, $v = 1$ denotes the first vibrationally excited state of CH_3I (essentially one quantum of the C-I stretch). After Ref. [3].

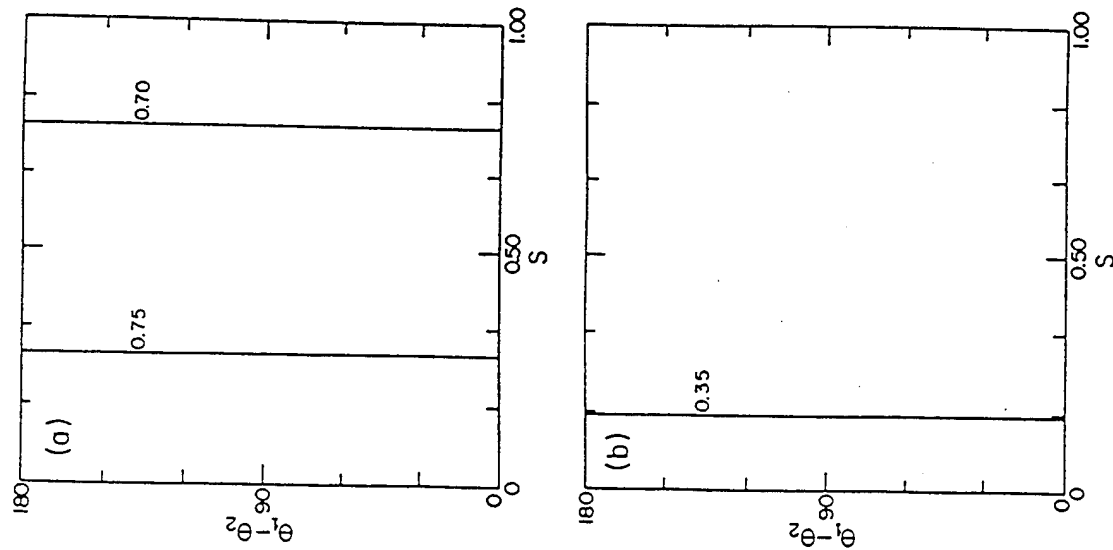


Figure 6.13 As in Figure 6.11 but $\nu_1 = 0$, $J_1 = 1$, $\nu_2 = 0$, $J_2 = 2$, $M_1 = M_2 = 0$. No phase control is seen since $J_1 + J_2$ is odd and $M_1 = 0$. (a) $\omega_{E_1} = 39638 \text{ cm}^{-1}$ and (b) $\omega_{E_1} = 42367 \text{ cm}^{-1}$. After Ref. [3].

where $F_{ij} \equiv c_i^* c_j \tilde{\epsilon}_i \tilde{\epsilon}_j$. From Equation 6.42 it follows that the M_1 -dependence of $\mathbf{d}^{(\lambda)}(E_i J_i M_i; E_j J_j M_j; E)$ is entirely contained in the 3- j product

$$\begin{pmatrix} J & 1 & J_i \\ -M_1 & 0 & M_1 \end{pmatrix} \begin{pmatrix} J & 1 & J_j \\ -M_1 & 0 & M_1 \end{pmatrix}$$

Hence, the M_1 summation can be performed separately. Defining,

$$C_{ij}(J) \equiv \frac{1}{2J_1 + 1} \sum_{M_1} \begin{pmatrix} J & 1 & J_i \\ -M_1 & 0 & M_1 \end{pmatrix} \begin{pmatrix} J & 1 & J_j \\ -M_1 & 0 & M_1 \end{pmatrix} F_{ij} \quad (6.45)$$

we have that

$$P(q, E) = \left(\frac{\pi}{\hbar} \right)^2 \sum_{i=1,2} \sum_{j=1,2} I^{(q)}(E_i J_i; E_j J_j; E) \quad (6.46)$$

where

$$I^{(q)}(E_i J_i; E_j J_j; E) \equiv \sum_{J, \nu} C_{ij}(J) (E J \lambda, \nu | E_i J_i)^* (E J \lambda, \nu | E_j J_j) \quad (6.47)$$

It follows immediately from the symmetry properties of the 3- j symbols [37] and Equation 6.45 that $I^{(q)}(E_i J_i; E_j J_j; E)$ is zero if $(J_1 + J_2)$ is odd; that is, yield control in M -averaged situations requires J_1 and J_2 of equal parity. Another way of reaching the same conclusion is to note that for odd $J_1 + J_2$, when we perform the M_1 summation, the positive M_1 terms cancel out the negative M_1 terms, and the $M_1 = 0$ term is identically zero. We conclude that for nonpolarized initial states, only two states of equal parity can be made to interfere allowing control of integral cross-sections.

The expression for the yield now follows directly as the ratio of $P(1, E)/\Sigma_q P(q, E)$ of Equation 6.46. Figure 6.14 shows the result for coherent radiative control of an initial M -averaged pair of states of *equal* parity at two different values of ω_1 . The range of control demonstrated is very wide: at the peak of the absorption, (Figure 6.14(a)), the $I^*(^2P_{1/2})$ quantum yield changes from 30%, for $S = 0.9$ and $\theta_1 - \theta_2 = 0^\circ$, to 75% for $S = 0.2$ and $\theta_1 - \theta_2 =$

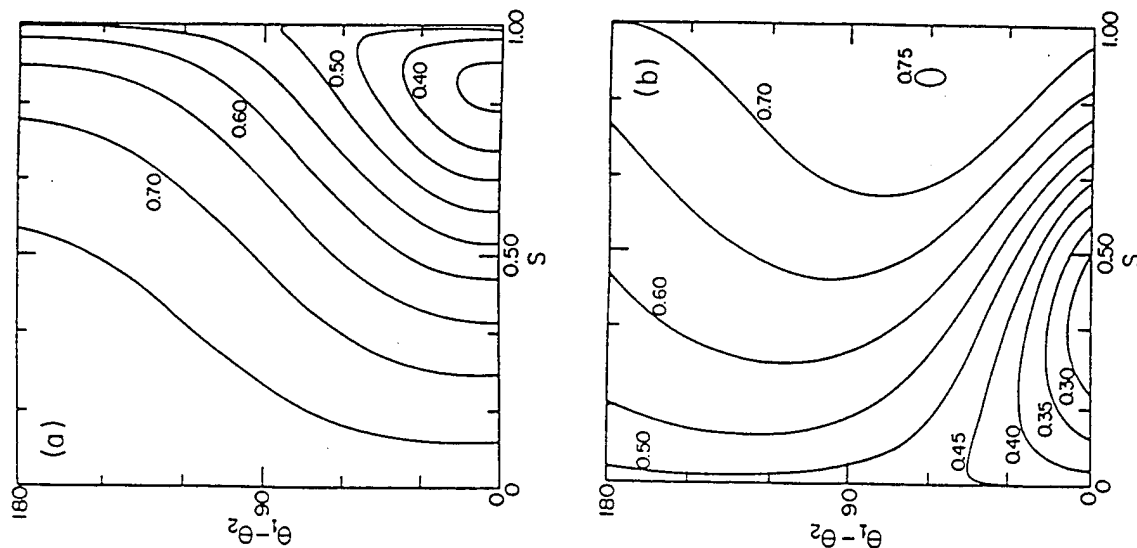


Figure 6.14 $I^{(2P_{1/2})}$ yield in the photodissociation of CH_3I starting from an M -averaged (unpolarized) ensemble of superposition states. The J and ν are as in Figure 6.12. (a) $\omega_{E_1} = 39639 \text{ cm}^{-1}$ and (b) $\omega_{E_1} = 42367 \text{ cm}^{-1}$. After Ref. [3].

140° . A comparison with the even $J_1 + J_2$ polarized case (Figure 6.12) shows that the range of control degrades only slightly with M -averaging. This is to be contrasted (Figure 6.11 versus Figure 6.13) with the odd $J_1 + J_2$ case.

B. Control in the Presence of Incoherence Effects

In practice there are a number of sources of incoherence which tend to diminish control. Prominent amongst these are effects due to an initial thermal distribution of states and effects due to partial coherence of the laser source. Hence, we describe one approach, based upon resonant two-photon photodissociation, which deals effectively with both problems and results in a viable scheme to control coherence in a thermal environment. An alternative method in which coherence is retained in the presence of collisions is discussed elsewhere [7].

Here we discuss a method [17] where it is possible to maintain control in a molecular system that is initially in thermal equilibrium by interfering two independent resonant two-photon routes to photodissociation. The resonant character of the excitations insure that only a selected state from the molecular thermal distribution participates. The proposed control scenario also provides a method for overcoming destructive interference loss due to phase jitter in the laser source and allows the reduction of contributions from uncontrolled ancillary photodissociation routes. Computational results support the feasibility and broad range of control afforded by this approach.

The specific scheme we advocate is depicted, for the particular case of Na_2 photodissociation, in Figure 6.15. Here the molecule is lifted from an initial bound state $|E_i, J_i, M_i\rangle$ to energy E via two independent two-photon routes. To introduce notation, first consider a single such two-photon route. Absorption of the first photon of frequency ω_1 lifts the system to a region close to an intermediate bound state $|E_m, J_m, M_m\rangle$, and a second photon of frequency ω_2 carries the system to the dissociating states $|E, \hat{k}, \hat{q}\rangle$, where the scattering angles are specified by $\hat{k} = (\theta_k, \phi_k)$. Here J is the angular momentum, M is the projection along the z -axis, and the values of energy, E_i and E_m , include specification of the vibrational quantum numbers. If we denote the phases of the coherent states by ϕ_1 and ϕ_2 , the wavevectors by \mathbf{k}_1 and \mathbf{k}_2 with overall phases $\theta_i = \mathbf{k}_i \cdot \mathbf{R} + \phi_i$ ($i = 1, 2$), and the electric field amplitudes by ϵ_1 and ϵ_2 , then the probability amplitude for resonant two-photon ($\omega_1 + \omega_2$) photodissociation is given [35] by

the square of the sum of the T -matrix elements from pathway a ($\omega_0 + \omega_0$) and pathway b ($\omega_+ + \omega_-$). That is, the probability into channel q

$$P(E, E, J, J, M_i; \omega_0, \omega_+, \omega_-) \equiv \int dk \left| T_{kq, i}(E, E, J, M_i, \omega_0, \omega_0) + T_{kq, i}(E, E, J, M_i, \omega_+, \omega_-) \right|^2 \quad (6.50)$$

Here $P^{(q)}(a)$ and $P^{(q)}(b)$ are the independent photodissociation probabilities associated with routes a and b respectively and $P^{(q)}(ab)$ is the interference term between them. Note that the two T -matrix elements in Equation 6.50 are associated with different lasers and as such contain different laser phases. Specifically, the overall phase of the three laser fields are

$$\theta_0 = k_0 \cdot R + \phi_0, \theta_+ = k_+ \cdot R + \phi_+, \text{ and } \theta_- = k_- \cdot R + \phi_-$$

where ϕ_0 , ϕ_+ , and ϕ_- are the photon phases, and k_0 , k_+ , and k_- are the wavevectors of the laser modes ω_0 , ω_+ , and ω_- whose electric field strengths are ϵ_0 , ϵ_+ , ϵ_- and intensities I_0 , I_+ , I_- .

The optical path-path interference term $P^{(q)}(ab)$ is given by

$$P^{(q)}(ab) = 2|F^{(q)}(ab)| \cos(\alpha_a^q - \alpha_b^q) \quad (6.51)$$

with relative phase

$$\alpha_a^q - \alpha_b^q = (\delta_a^q - \delta_b^q) + (2\theta_0 - \theta_+ - \theta_-) \quad (6.52)$$

where the amplitude $|F^{(q)}(ab)|$ and the molecular phase difference $(\delta_a^q - \delta_b^q)$ are defined by

$$|F^{(q)}(ab)| \exp[i(\delta_a^q - \delta_b^q)] \equiv \frac{8\pi\mu k_q}{\hbar^2} \sum_{J, P, \lambda \geq 0} \sum_{E_m, J_m} \sum_{M_i} \sum_{M_i'} \left(\begin{matrix} J & 1 & J_m \\ -M_i & 0 & M_i' \end{matrix} \right) \left(\begin{matrix} J & 1 & J_i \\ -M_i & 0 & M_i \end{matrix} \right) \times$$

$$\begin{pmatrix} J_m & 1 & J_i \\ -M_i & 0 & M_i \end{pmatrix} (E, E, J, i, \omega_0, \omega_0, q) (J, P, \lambda, E_m, J_m)^* (E, E, J, i, \omega_+, \omega_-, q) (J, P, \lambda, E_m, J_m) \quad (6.53)$$

Consider now the quantity of interest $R_{qq'}$, the branching ratio of the product in q -channel to that in q' -channel. Noting that in the weak field case $P^{(q)}(a)$ is proportional to ϵ_0^4 , $P^{(q)}(b)$ to $\epsilon_+^2 \epsilon_-^2$, and $P^{(q)}(ab)$ to $\epsilon_0^2 \epsilon_+ \epsilon_-$ we can write

$$R_{qq'} = \frac{\mu_{aa}^{(q)} + x^2 \mu_{bb}^{(q)} + 2x|\mu_{ab}^{(q)}| \cos(\alpha_a^q - \alpha_b^q) + (B^{(q)}/\epsilon_0^4)}{\mu_{aa}^{(q')} + x^2 \mu_{bb}^{(q')} + 2x|\mu_{ab}^{(q')}| \cos(\alpha_a^{q'} - \alpha_b^{q'}) + (B^{(q')}/\epsilon_0^4)} \quad (6.54)$$

where

$$\mu_{aa}^{(q)} = \frac{P^{(q)}(a)}{\epsilon_0^4}$$

$$\mu_{bb}^{(q)} = \frac{P^{(q)}(b)}{(\epsilon_+^2 \epsilon_-^2)}$$

$$|\mu_{ab}^{(q)}| = \frac{|F^{(q)}(ab)|}{(\epsilon_0^2 \epsilon_+ \epsilon_-)}$$

and

$$x = \frac{\epsilon_+ \epsilon_-}{\epsilon_0^2} = \frac{\sqrt{I_+ I_-}}{I_0}$$

The terms with $B^{(q)}$, $B^{(q')}$ correspond to resonant photodissociation routes to energies other than $E = E_i + 2\hbar\omega_0$ and hence [4] to terms which do not coherently interfere with the a and b pathways. Minimization of these terms, which result from absorption of $(\omega_0 + \omega_-)$, $(\omega_0 + \omega_+)$, $(\omega_+ + \omega_-)$, or $(\omega_+ + \omega_+)$, is discussed elsewhere [17]. Here we emphasize that the product ratio in Equation 6.54 depends upon both the laser intensities and relative laser phase. Hence manipulating these laboratory parameters allows for control over the relative cross-section between channels.

The proposed scenario embodied in Equation 6.54 also provides a means by which control can be improved by eliminating effects due to laser jitter. Specifically, the term $2\phi_0 - \phi_+ - \phi_-$ contained in the relative phase $\alpha_a^q - \alpha_b^q$ can be subject to the phase fluctuations arising from laser instabilities. If such fluctuations are sufficiently large then the interference term in Equation 6.54, and hence control, disappears [14]. The following experimentally desirable implementation of the two-photon plus two-photon scenario readily compensates for this problem. Specifically, consider generating $\omega_+ = \omega_0 + \delta$ and $\omega_- = \omega_0 - \delta$ in a parametric process by passing a beam of frequency $2\omega_0$ with phase $2\phi_0$ through a nonlinear crystal. This latter beam is assumed generated by second harmonic generation from the laser ω_0 with the phase ϕ_0 . Then the quantity $2\phi_0 - \phi_+ - \phi_-$ in the phase difference between the $(\omega_0 + \omega_0)$ and $(\omega_+ + \omega_-)$ routes is a constant. That is, in this particular scenario, fluctuations in ϕ_0 cancel and have no effect on the relative phase $\alpha_a^q - \alpha_b^q$. Thus the two-photon plus two-photon scenario is insensitive to the laser jitter of the incident laser fields.

To examine the range of control afforded by this scheme consider the photodissociation of Na_2 in the regime below the $\text{Na}(3d)$ threshold, where dissociation is to two product channels $\text{Na}(3s) + \text{Na}(3p)$ and $\text{Na}(3s) + \text{Na}(4s)$. Two-photon dissociation of Na_2 from a bound state of the $1\Sigma_g^+$ state occurs [35] in this region by initial excitation to an excited intermediate bound state $|E_m J_m M_m\rangle$. The latter is a superposition of states of the $A^1\Sigma_u^+$ and $b^3\Pi_u$ electronic curves, a consequence of spin-orbit coupling. That is, the two-photon photodissociation can be viewed [35] as occurring via intersystem crossing subsequent to absorption of the first photon. The continuum states reached in the excitation can be either of singlet or triplet character but, despite the multitude of electronic states involved in the computation, the predominant contributions to the products $\text{Na}(3p)$ and $\text{Na}(4s)$ are found to come from the $3\Pi_g$ and $3\Sigma_g^+$ states, respectively. Methods for computing the required photodissociation amplitude, which involves eleven electronic states, are discussed elsewhere [35]. Since the resonant character of the two-photon excitation allows us to select a single initial state from a thermal ensemble we consider here the specific case of $v_i = J_i = 0$ without loss of generality, where v_i, J_i denote the vibrational and rotational quantum numbers of the initial state.

The ratio R_{qq} depends on a number of laboratory control parameters including the ratio of laser intensities x , relative laser phase, and the ratio of ϵ_+ and ϵ_- via η . In addition, the relative cross-sections can be altered by

modifying the detuning. Typical control results are shown in Figure 6.16 which provides contour plots of the $\text{Na}(3p)$ yield (i.e., the ratio of the probability of observing $\text{Na}(3p)$ to the sum of the probabilities to form $\text{Na}(3p)$ plus $\text{Na}(4s)$). The figure axes are the ratio of the laser amplitudes x and the relative laser phase $\delta\theta = 2\theta_0 - \theta_+ - \theta_-$. Here $\omega_0 = 631.899$, $\omega_+ = 562.833$, and $\omega_- = 720.284$ nm and control is seen to be large, ranging from 30% $\text{Na}(3p)$ to 90% as $\delta\theta$ and x are varied.

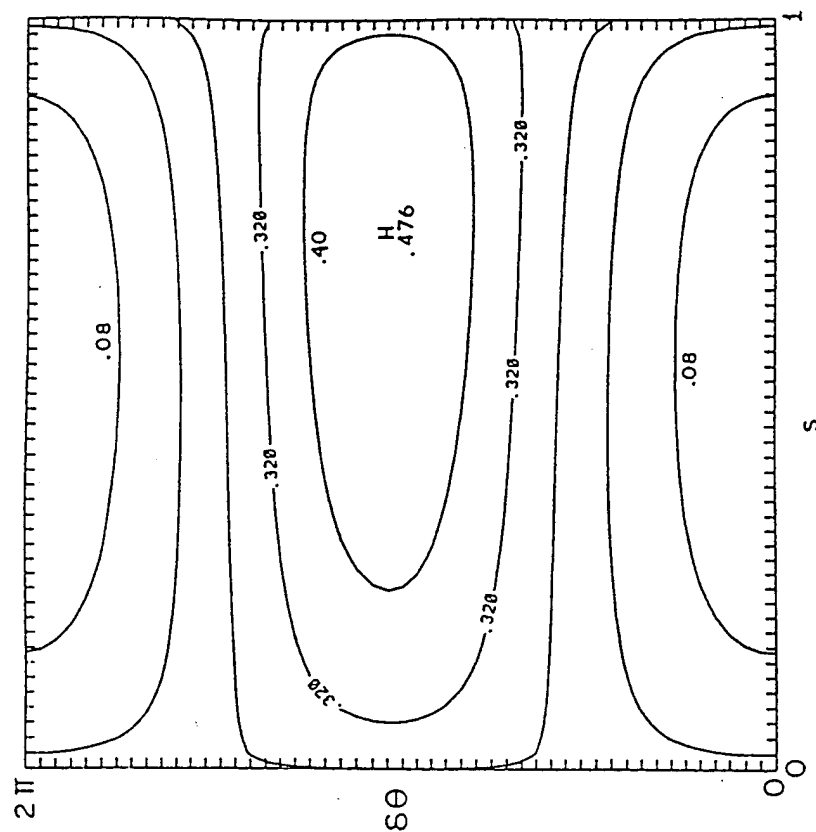


Figure 6.16 Contours of equal $\text{Na}(3p)$ yield. Ordinate is the relative laser phase and the abscissa is $S = x^2/(1 + x^2)$ where x is the field intensity ratio. Here $\omega_0 = 627.584$, $\omega_+ = 611.207$, $\omega_- = 644.863$ nm, and $\eta = 0.5$. See [17] for a discussion of η which can be used to minimize background contributions. Source: from [35].

Note that the proposed approach is not limited to the specific frequency scheme discussed previously. Essentially all that is required is that the two resonant photodissociation routes lead to interference and that the cumulative laser phases of the two routes be independent of laser jitter. As one sample extension, consider the case where paths *a* and *b* are composed of totally different photons, $\omega_+^{(a)}$ and $\omega_-^{(a)}$ and $\omega_+^{(b)}$ and $\omega_-^{(b)}$, with $\omega_+^{(a)} + \omega_-^{(a)} = \omega_+^{(b)} + \omega_-^{(b)}$. Both of these sets of frequencies can be generated, for example, by passing $2\omega_0$ light through nonlinear crystals, hence yielding two pathways whose relative phase is independent of laser jitter in the initial $2\omega_0$ source. Given these four frequencies we now have an additional degree of freedom in order to optimize control, although the experiment is considerably more complicated than in the three frequency case. Typical four-frequency results for Na_2 are provided elsewhere [17]. Note also that the control is not limited to two product channels. Computations [17] on higher energy Na_2 photodissociation, where more product arrangement channels are available, show equally large ranges of control for the three channel case.

6.4 NOVEL APPLICATIONS OF CONTROL

A. Control of Symmetry Breaking

The pump-dump scenario has been extended to include applications to symmetry breaking in chemical reactions [18]. We briefly review these developments in this section.

The possibility of controlling symmetry-breaking processes using coherent control techniques constitutes an exciting application of this field. In general, symmetry breaking occurs whenever a system executes a transition to a *nonsymmetric* eigenstate of the Hamiltonian. Strictly speaking, nonsymmetric eigenstates (i.e., states which do not belong to any of the symmetry-group representations) can occur if there exist several degenerate eigenstates, each belonging to a different irreducible representation. Any linear combination of such eigenstates is nonsymmetric.

In practice, symmetry breaking also occurs even if the degeneracy is only approximate, as in the problem of a symmetric double-well potential. If the barrier between the two wells is such that tunneling is miniscule, then the ground state of the system is composed, to all intents and purposes, of a doublet of *symmetric* and *antisymmetric* degenerate states. States localized

at either well can then result by taking the \pm linear combinations of this doublet. Because of the near degeneracy, these nonsymmetric localized states are essentially eigenstates of the Hamiltonian insofar as their time evolution can be immeasurably slow.

Nonsymmetric eigenstates of a symmetric Hamiltonian also occur in the continuous spectrum of a *BAB* type molecule. It is clear that the $|E, n, R\rangle$ state, which correlates asymptotically with the dissociation of the right *B* group, must be degenerate with the $|E, n, L\rangle$ state, which gives rise to the departure of the left *B* group. It is also possible to form a symmetric $|E, n, s\rangle$ and an antisymmetric $|E, n, a\rangle$ eigenstate of the same Hamiltonian by taking the \pm combination of these states. There is an important physical distinction between the nonsymmetric states and states which are symmetric/antisymmetric: Any experiment performed in the asymptotic *B-AB* or *BA-B* regions must, by necessity, measure the probability of populating a nonsymmetric state. This follows because when the *B-AB* distance or the *BA-B* distance is large, a given group *B* is either far away from or close to group *A*. Thus symmetric and antisymmetric states are not directly observable in the asymptotic regime.

We conclude that the very act of observation of the dissociated *BAB* molecule entails the collapse of the system to one of the nonsymmetric states. As long as the probability of collapse to the $|E, n, R\rangle$ state is equal to the probability of collapse to the $|E, n, L\rangle$ state, the collapse to a nonsymmetric state does not lead to a preference of *R* over *L* in an *ensemble* of molecules. This is the case when the above collapse (symmetry breaking) is *spontaneous* (i.e., occurring due to some (random) factors not in our control). Coherent control techniques allow us to influence these probabilities. In this case symmetry breaking is stimulated rather than spontaneous. This has far reaching physical and practical significance.

One of the most important cases of symmetry breaking arises when the two *B* groups (now denoted as *B* and *B'*) are not identical but are enantiomers of one another. (Two groups of atoms are said to be *enantiomers* of one another if one is the mirror image of the other). If these groups are also *chiral* (i.e., they lack a center of inversion symmetry) then the two enantiomers are distinguishable and can be detected through the distinctive direction of rotation of linearly polarized light.

The existence and role of enantiomers is recognized as one of the fundamental broken symmetries in nature [38]. It has motivated a long-

standing interest in asymmetric synthesis (i.e., a process which preferentially produces a specific chiral species). Contrary to the prevailing belief [39] that asymmetric synthesis must necessarily involve either chiral reactants, or chiral external system conditions such as chiral crystalline surfaces, we show below that preferential production of a chiral photofragment can occur even though the parent molecule is not chiral. In particular two results are demonstrated:

1. Ordinary photodissociation, using linearly polarized light, of a BAB' "prochiral" molecule may yield different cross-sections for the production of right-handed (B) and left-handed (B') products, when the projection of the angular momentum (m_j) of the products is selected; and
2. That this natural symmetry breaking may be enhanced and controlled using coherent lasers.

To treat this problem we return to the formulation of the pump-dump scenario with attention focused on control of the relative yield of two product arrangement channels but with angular momentum projection m_j fixed (Equation 6.40).

Explicitly considering the dissociation of BAB' into right- (R) and left-hand (L) products we have:

$$Y = \frac{P(L, m_j)}{P(L, m_j) + P(R, m_j)}$$

The yield Y is a function of the delay time $\tau = (t_d - t_x)$ and ratio $x = |c_1/c_2|$, the latter by detuning the initial excitation pulse. Active control over the products $B + AB'$ versus $B' + AB$ (i.e., a variation of Y with τ and x) and hence control over left- versus right-handed products, will result only if $P(R, m_j)$ and $P(L, m_j)$ have different functional dependences on x and τ .

We now show that $P(R, m_j)$ may be different from $P(L, m_j)$ for the $B'AB$ case. We first note that this molecule belongs to the C_s point group which is a group possessing only one symmetry plane. This plane, denoted as σ , is defined as the collection of the C_{2v} points (i.e., points satisfying the $B-A = A-B'$ condition), where $B-A$ designates the distance between the B and A groups. In order to do that we choose the intermediate state $|E_1\rangle$ to be symmetric and the state $|E_2\rangle$ to be antisymmetric with respect to reflection in the σ plane. Furthermore, we shall focus upon transitions between elec-

tronic states of the same representations (e.g., A' to A' or A'' to A''), where A' denotes the symmetric representation and A'' the antisymmetric representation of the C_s group). We further assume that the ground vibronic state belongs to the A' representation.

The first thing to demonstrate is that it is possible to excite simultaneously, by optical means, both the symmetric $|E_1\rangle$ and antisymmetric $|E_2\rangle$ states. Using Equation 6.35 we see that this requires the existence of both a symmetric \mathbf{d} component, denoted as \mathbf{d}_s , and an antisymmetric \mathbf{d} component, denoted \mathbf{d}_a , because, by the symmetry properties of $|E_1\rangle$ and $|E_2\rangle$,

$$\langle E_1 | \mathbf{d} | E_g \rangle = \langle E_1 | \mathbf{d}_s | E_g \rangle, \quad \langle E_2 | \mathbf{d} | E_g \rangle = \langle E_2 | \mathbf{d}_a | E_g \rangle \quad (6.55)$$

The existence of both dipole-moment components occurs in $A' \rightarrow A'$ electronic transitions whenever a bent $B'-A-B$ molecule deviates considerably from the equidistance C_{2v} geometries (where $\mathbf{d}_a = 0$). The effect is non-Franck-Condon in nature because we no longer assume that the dipole-moment does not vary with the nuclear configurations. (In the theory of vibronic-transitions terminology the existence of both \mathbf{d}_s and \mathbf{d}_a is due to a Herzberg-Teller intensity borrowing [42] mechanism).

We conclude that the excitation pulse can create a $|E_1\rangle$, $|E_2\rangle$ superposition consisting of two states of different reflection symmetry which is therefore nonsymmetric. We now wish to show that this nonsymmetry established by exciting *nongenerate bound* states translates to a nonsymmetry in the probability of populating the two *degenerate* $|E, n, R\rangle$, $|E, n, L\rangle$ *continuum* states. We proceed by examining the properties of the bound-free transition matrix elements of Equation 6.39 entering the probability expression of Equation 6.38.

Although the continuum states of interest $|E, n, q\rangle$ are nonsymmetric, they satisfy a closure relation since $\sigma |E, n, R\rangle = |E, n, L\rangle$ and vice-versa. Working with the symmetric and antisymmetric continuum eigenfunctions,

$$|E, n, R\rangle \equiv \frac{|E, n, s\rangle + |E, n, a\rangle}{\sqrt{2}}$$

$$|E, n, L\rangle \equiv \frac{|E, n, s\rangle - |E, n, a\rangle}{\sqrt{2}} \quad (6.56)$$

using the fact that $|E_1\rangle$ is symmetric and $|E_2\rangle$ antisymmetric, and adopting the notation $A_{s2} \equiv \langle E, n, s | \mathbf{d} | E_2 \rangle$, $S_{a1} \equiv \langle E, n, a | \mathbf{d} | E_1 \rangle$, etc., we have,

$$\begin{aligned} \mathbf{d}^{(q)} &= \sum' [|S_{s1}|^2 + |A_{a1}|^2 \pm 2\text{Re}(A_{a1}S_{s1}^*)] \\ \mathbf{d}_{22}^{(q)} &= \sum' [|A_{s2}|^2 + |S_{a2}|^2 \pm 2\text{Re}(A_{s2}S_{a2}^*)] \\ \mathbf{d}_2^{(q)} &= \sum' [S_{s1}A_{s2}^* + A_{a1}S_{a2}^* \pm S_{s1}S_{a2}^* \pm A_{a1}A_{s2}^*] \end{aligned} \quad (6.57)$$

where the plus sign applies for $q = R$ and the minus sign for $q = L$.

Equation 6.57 displays two noteworthy features:

1. $\mathbf{d}_{kk}^{(R)} \neq \mathbf{d}_{kk}^{(L)}$, $k = 1, 2$. That is, the system displays *natural symmetry breaking* in photodissociation from state $|E_1\rangle$ or state $|E_2\rangle$, with right- and left-handed product probabilities differing by $4\text{Re}(S_{s1}^*A_{a1})$ for excitation from $|E_1\rangle$ and $4\text{Re}(A_{s2}S_{a2}^*)$ for excitation from $|E_2\rangle$. Note that these symmetry-breaking terms may be relatively small since they rely upon non Franck-Condon contributions.
2. However, even in the Franck-Condon approximation: $\mathbf{d}_2^{(R)} \neq \mathbf{d}_2^{(L)}$. Thus laser controlled symmetry breaking, which depends upon $\mathbf{d}_2^{(q)}$ in accordance with Equation 6.38, is therefore possible, allowing enhancement of the enantiomer ratio for the m_j polarized product.

To demonstrate the extent of expected control, as well as the effect of m_j summation, we considered a model of the enantiomer selectivity (i.e., HOH photodissociation in three dimensions) where the two hydrogens are assumed distinguishable. The computation is done using the formulation and computational methodology of Segev et al. [43]. We briefly summarize the angular momentum algebra and some other details involved in performing three dimensional quantum calculations of triatomic photodissociation [44].

We first specify the relevant n and i quantum numbers which enter the bound-free matrix elements of Equation 6.39. For the continuum states, $n = \hat{\mathbf{k}}, v, j, m_j$ where $\hat{\mathbf{k}}$ is the scattering direction, v and j are the vibrational and rotational product quantum numbers, and m_j is the space-fixed z-projection of j . For the bound states $i = \{E_i, M_i, J_i, p_i\}$, where J_i , M_i , and p_i are, respectively, the bound state angular momentum, its space-fixed z-projection, and its parity. The full (6-dimensional) bound-free matrix element can be

written as a product of analytic functions involving $\hat{\mathbf{k}}$ and (three-dimensional) radial matrix elements,

$$\langle E, \hat{\mathbf{k}}, v, j, m_j, q | \mathbf{d} | E_i, M_i, J_i, p_i \rangle = \left(\frac{\mu k_{vj}}{2\pi^2 \hbar^2} \right)^{1/2} \sum_{\lambda} (2J_i + 1)^{1/2} (-1)^{M_i - J_i - m_j} D_{\lambda M_i}^J(\varphi_k, \theta_k, 0) D_{-\lambda - m_j}^J(\varphi_k, \theta_k, 0) \langle E, J, v, j, \lambda | E, J, p_i \rangle \quad (6.58)$$

where D are the rotation matrices, μ is the reduced mass, k_{vj} is the momentum of the products and $\langle E, J, v, j, \lambda | E, J, p_i \rangle$ is proportional to the radial partial wave matrix element [44] $\langle E, J, M, p, v, j, \lambda, q | \mathbf{d} | E_i, M_i, J_i, p_i \rangle$. Here λ is the projection of J along the body-fixed axis of the H-OH (c.m.) product separation.

The product of the bound-free matrix elements of Equation 6.58, which enter Equation 6.39, integrated over scattering angles and averaged over the initial [45] M_i ($= M_i$) quantum numbers, is [46]

$$\begin{aligned} (2J_i + 1)^{-1} \sum_{M_i} \int d\hat{\mathbf{k}} \langle E, M_i, J_i, p_i | \mathbf{d} | E, \hat{\mathbf{k}}, v, j, m_j, q \rangle \langle E, \hat{\mathbf{k}}, v, j, m_j, q | \mathbf{d} | E_i, M_i, J_i, p_i \rangle \\ = (-1)^{m_j} \frac{16\pi^2 \mu}{\hbar^2 (2J_i + 1)} \sum_{v, j} k_{vj} \sum_{\lambda, \lambda'} [(2J_i + 1)(2J_i + 1)]^{1/2} (-1)^{J_i - \lambda - \lambda' + J_i + j} \\ \sum_{\ell=0,2} (2\ell + 1) \begin{pmatrix} J_i & J_i & \ell \\ \lambda & -\lambda' & \lambda' - \lambda \end{pmatrix} \begin{pmatrix} j & j & \ell \\ \lambda & \lambda' & \lambda - \lambda' \end{pmatrix} \begin{pmatrix} 1 & 1 & \ell \\ 0 & 0 & 0 \end{pmatrix} \\ \begin{pmatrix} j & j & \ell \\ -m_j & m_j & 0 \end{pmatrix} \begin{pmatrix} 1 & 1 & \ell \\ J_i & J_i & J_i \end{pmatrix} \langle E, J, v, j, \lambda, p_i | \mathbf{d} | E_i, J_i, p_i \rangle \langle E, J, v, j, \lambda', p_i | \mathbf{d} | E_i, J_i, p_i \rangle \end{aligned} \quad (6.59)$$

Here $J_i = J_k$ has been assumed for simplicity.

These equations, in conjunction with the artificial channel method [44] for computing the T -matrix elements, were used to compute the yield Y of the HO + H (as distinct from the H + OH) product in a fixed m_j state. Specifically, Figure 6.17 shows the result of first exciting the superposition of symmetric plus asymmetric vibrational modes $[(1,0,0) + (0,0,1)]$ with $J_i = J_k = 0$ in the ground electronic state, followed by dissociation at 70,700 cm^{-1} to the B state using a pulse width of 200 cm^{-1} . Results show that

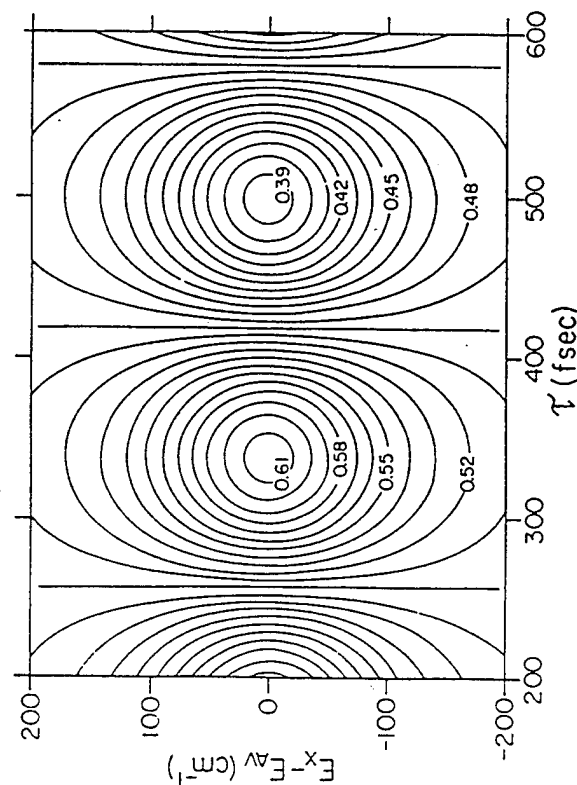


Figure 6.17 Contour plot of percent HO + H (as distinct from H + OH) in HOH. Ordinate is the detuning from $E_{av} = (E_2 - E_1)/2$, abscissa is time between pulses. Source: from [18].

varying the time delay between pulses allows for controlled variation of Y from 61–39%!

Finally we sketch the effect of a summation over product m_j states on symmetry breaking and chirality control. In this regard the three body model is particularly informative. Specifically, note that Equation 6.57 provides $d_{ij}^{(q)}$ in terms of products of matrix elements involving $|E, n, \alpha\rangle$ and $|E, n, \alpha'\rangle$. Focus attention on those products which involve both wavefunctions (e.g., $A_{a1} S_{a1}^*$). These matrix element products can be written in the form of Equation 6.59 where q and q' now refer to the antisymmetric or symmetric continuum states, rather than channels 1 and 2. Thus, for example, $A_{a1} S_{a1}^*$ results from using $|E, n, \alpha\rangle$ in Equation 6.58 to form A_{a1} and $|E, n, \alpha'\rangle$ to form S_{a1}^* . The resultant $A_{a1} S_{a1}^*$ has the form of Equation 6.59 with $f^{(q)}$ and $f^{(q')}$ associated with the symmetric and antisymmetric continuum wavefunctions, respectively. Consider now the effect of summing over m_j . Standard formulae [43, 44] imply that this summation introduces a $\delta_{\ell,0}$ which, in turn forces $\lambda = \lambda'$ via

the first and second $3j$ symbol in Equation 6.59. However, a rather involved argument [47] shows that t -matrix elements associated with symmetric continuum eigenfunctions and those associated with antisymmetric continuum eigenfunctions must have λ of different parities. Hence summing over m_j eliminates all contributions to Equation 6.57 which involve both $|E, n, \alpha\rangle$ and $|E, n, \alpha'\rangle$. Specifically, we find [47] after m_j summation:

$$d_{ij}^{(1)} = d_{ij}^{(2)} = \sum [S_{si} f_i^2 + |A_{ai}|^2] \quad (6.60)$$

$$d_{12}^{(1)} = d_{12}^{(2)} = \sum [S_{si} A_{sj}^* + A_{ai} S_{aj}^*] \quad (6.61)$$

That is, natural symmetry breaking is lost upon m_j summation, both channels $q = R$ and $q = L$ having equal photodissociation probabilities, and control over the enantiomer ratio is lost since the interference terms no longer distinguish the $q = R$ and $q = L$ channels [48].

Having thus demonstrated the principle of m_j -selected enantiomer control it remains to determine the extent to which realistic systems can be controlled. Such studies are in progress [47].

B. Control of Photocurrent Directionality

The possibility of controlling product channels applies not only to chemically or electronically distinct products but also to control over the distribution of internal states (e.g., rotation, vibration) of the product as well [2]. Thus, for example, one may use coherent pathways to produce inversion amongst product states. In this section we demonstrate that it is possible to control the product angular distribution using the scheme outlined in Section 6.1.C. Our specific application is to the case of photoionization so that the result is control over the direction of the photocurrent induced by the interference. An alternative method of controlling differential cross-sections by varying the degree of elliptic polarization of the light source is described elsewhere [5].

Properties of a photocurrent generated in a semiconductor are controlled by a bias voltage for a given concentration and spatial distribution of charge carriers [49]. The role of this voltage is to give *thermodynamic* preference to the flow of photoelectrons in one direction (the forward or backward direction in a p - n junction.) In a p -type or n -type semiconductor the probability of carrier photoemission (from a single impurity) without an

external voltage is anisotropic only inasmuch as the crystal possesses mass or dielectric constant anisotropies, but the probabilities of emission backward and forward along a given crystal axis are equal. Although photocurrents are commonly produced by laser illumination, the laser coherence does not affect the process.

Here we review our scheme [8] for generating and controlling photocurrents *without bias voltage*, relying instead on the coherence of the illuminating source. The method is an application of the scenario of Section 6.1.C to the photoionization of bound states of donors. Specifically, a superposition of two bound donor (or exciton) states is photoionized by two mutually phase-locked lasers at slightly different frequencies with the same polarization axis. The result is a current along the direction of polarization. The realization of the scheme is discussed for shallow-level donors in semiconductors.

Consider a semiconductor doped with shallow-level donors. The bound state wavefunction of such a donor is described by the hydrogenic effective-mass theory [50] with wavefunction:

$$\chi_n(r) = \langle n | \psi \rangle = V^{-1/2} \int_{-\infty}^{\infty} B_{n,k} u_k(r) e^{ik \cdot r} dk \quad (6.62)$$

Here $u_k(r)$ is the conduction band Bloch state correlated to the asymptotic free-electron momentum $\hbar k$, V is the normalization volume and $B_{n,k}$ is the corresponding Fourier component of the hydrogenic wavefunction envelope χ_n . For semiconductors with effective-mass anisotropy, the χ_n are evaluated variationally [51-54]. Although the theory described below holds for any superposition of bound donor states, a superposition of $|1s\rangle$ and $|2p\rangle$ states will be considered explicitly. For these cases a simple variational procedure [54], whose results agree reasonably well with those of more refined procedures [51-55], yields

$$\begin{aligned} \chi_{1s} &= \pi^{1/4} \exp \left\{ - \left[\frac{x^2 + y^2}{a^2 + z^2/b^2} \right]^{1/2} \right\} \\ \chi_{2p_o} &= \sqrt{2} \pi^{3/4} b^{-1} z \exp \left\{ - \left[\frac{(x^2 + y^2)}{a^2 + z^2/b^2} \right]^{1/2} \right\} \end{aligned} \quad (6.63)$$

Here the coordinates [normalized to the effective Bohr radius $a^* = \hbar^2/(m_{\perp} e^2)$] coincide with the main axes of the cubic crystal. Depending on the ratio $\gamma = m_{\perp}/m_{\parallel}$ (the parallel direction coinciding with z), the a and b parameters vary between $a = b = 1$ for nearly isotropic materials with $\gamma = 1$ (e.g., GaAs, GaSb, InAs) and $a \approx 4/3$, $b \approx (4/3)(4/\pi)^{1/2} \gamma^{1/2}$ for highly anisotropic materials (e.g., Si or Ge) with $\gamma < 1$.

Let a superposition of the $|1s\rangle$ and $|2p\rangle$ states be prepared by some coherent process. As pointed out previously, this can be achieved by a short coherent laser pulse or various other means. It is possible to discriminate against the excitation of the $|2p_{\pm 1}\rangle$ states either by frequency tuning, (e.g., the $2p_{\pm 1} - 2p_o$ splitting is ~ 5 meV in Si) or by linearly polarizing the laser along the z -axis. Consider now the simultaneous excitation of this superposition state to a kinetic energy level E_k in the conduction band continuum by two z -polarized infrared or visible lasers with frequencies $\omega_{1s}, \omega_{2p_o}$; the former lifts the $|1s\rangle$ state to E_k and the latter lifts the $|2p_o\rangle$ state to E_k . These excitations involve the energy conservation relation:

$$E_k = \frac{\hbar^2 k_{\perp}^2}{2m_{\perp}} + \frac{\hbar^2 k_z^2}{2m_{\parallel}} = \hbar\omega_n - |E_n| - \sum_p \hbar p \omega \quad (6.64)$$

Here the n -state energy is measured from the conduction-band edge and the last term accounts for the emission ($p > 0$) or absorption ($p < 0$) of p phonons of frequency ω . For the sake of simplicity, we shall use the zero phonon-frequency line [55, 56]; hence, $\hbar\omega_{1s} = E_k + |E_{1s}|$, $\hbar\omega_{2p_o} = E_k + |E_{2p_o}|$.

In what follows we consider only electric-dipole induced optical transitions with the electric field along the z axis. The electric dipole transition amplitudes from an impurity state $|n\rangle$ to the asymptotic (far from impurity) plane wave $\langle k | = V^{-1/2} e^{ik \cdot r} u_k(r)$ is

$$\langle k | \mu_z | n \rangle = \frac{-ie\hbar}{m_{\parallel}(E_k + |E_n|)} \left\langle k \left| \frac{-i\hbar \partial}{\partial z} \right| n \right\rangle \quad (6.65)$$

The last factor is, using Equation 6.62, simply given as

$$\langle k | \frac{-i\hbar \partial}{\partial z} | n \rangle = \hbar k_z \langle k | n \rangle = \hbar k_z B_{n,k} \quad (6.66)$$

We now consider the photoionization of the superposition state,

$$|\psi\rangle = c_1|1\rangle + c_2|2\rangle \quad (6.67)$$

where 1 denotes the 1s state and 2 the $2p_o$ state. We let a z-polarized two-color source, whose electric field is given as,

$$\mathbf{E}_z(t) = \mathbf{E}_1 \cos(\omega_1 t + \phi_1) + \mathbf{E}_2 \cos(\omega_2 t + \phi_2) \quad (6.68)$$

act on this superposition state. The rate (probability per unit time and unit solid angle) of photoemission to a conduction state with momentum $\hbar\mathbf{k}$ resulting from this action is,

$$P(\cos\theta) = \left(\frac{2\pi}{\hbar}\right) \rho(k) \left| \sum_{n=1,2} e^{-i\phi_n} \langle \mathbf{E}_n \cdot \mathbf{c}_n | \mu_z | n \rangle \right|^2 \quad (6.69)$$

Here,

$$\begin{aligned} \cos\theta &= \frac{k_z}{k}, \quad \sin\theta = \frac{k_\perp}{\gamma^{1/2}k} \\ k &= \frac{(2m_\parallel E_k)^{1/2}}{\hbar} \\ \rho(k) &= \left(\frac{m_\perp V}{8\pi^3 \hbar^2} \right) k \end{aligned} \quad (6.70)$$

and $\rho(k)$ is the density of final states. The Franck-Condon factor for the zero-phonon line has been set here to unity.

Denoting $c_n = |c_n| \exp(i\alpha_n)$ and using Equations 6.65 and 6.66 in Equation 6.69 gives the form:

$$\begin{aligned} P(\cos\theta) &= \\ [A_1 |B_{1s,k}|^2 + A_2 |B_{2p_o,k}|^2 + A_{12} \cos(\alpha_1 - \alpha_2 - \phi_1 + \phi_2 + \alpha_{12}) |B_{1s,k} B_{2p_o,k}| \cos^2\theta] \end{aligned} \quad (6.71)$$

where

$$\begin{aligned} A_n &= \frac{2\pi e^2 \hbar^3 k^2 \rho(k) |E_n c_n|^2}{m_\parallel^2 (E_k + E_n)^2} \quad (n=1,2) \\ A_{12} &= \frac{4\pi e^2 \hbar^3 k^2 \rho(k) |E_1 E_2 c_1 c_2|}{m_\parallel^2 (E_k + E_1)(E_k + E_2)} \end{aligned} \quad (6.72)$$

Here α_{12} is defined by $B_{1s,k} B_{2p_o,k}^* = |B_{1s,k} B_{2p_o,k}| \exp(i\alpha_{12})$ and $E_1 = |E_{1s}|$, $E_2 = |E_{2p_o}|$. The evaluation of $P(\cos\theta)$ requires the Fourier components $B_{n,k}$. For the present choice of impurity states and z axis these components are obtained from Equation 6.63 as,

$$\begin{aligned} B_{1s,k} &= \frac{8\pi^{1/2} a^2 \hbar V^{-1/2}}{G^2} \\ B_{2p_o,k} &= \frac{-i\sqrt{2}(32)a^2 b^2 \pi^{1/4} V^{-1/2} a^* k_z}{G^3} \end{aligned} \quad (6.73)$$

with

$$G = G(\cos^2\theta) = [1 + \gamma(a^* a k)^2 + (b^2 - a^2)\gamma(a^* k)^2 \cos^2\theta]$$

It is clear from Equation 6.73 that $\alpha_{12} = \pi/2$.

Given the above expression, the net current flowing in the z-direction is given as

$$\begin{aligned} I_z^+ &= \left(\frac{eNV\hbar}{m_\parallel} \right) \tau \times F \int_0^{2\pi} \int_0^\pi d\omega P(\cos\theta) k \cos\theta \\ &= 256 \left(\frac{eNV\hbar^4 k^3}{m_\parallel^3} \right) \tau \times F a^4 b^3 \pi^{2/2} \frac{|E_1 E_2 c_1 c_2|}{(E_k + E_1)(E_k + E_2)} \end{aligned}$$

$$\cos \left(\alpha_1 - \alpha_2 - \varphi_1 + \varphi_2 + \frac{\pi}{2} \right) \int_{-1}^{+1} dx \frac{x^4}{[G(x^2)]^5} \quad (6.74)$$

where τ is the free electron collisional relaxation time, N is the donor concentration in cm^{-3} , and F is the x - y cross-sectional area of the sample.

We note that contributions from the diagonal A_1 and A_2 terms are odd in $\cos \theta$ and that they have vanished, whereas the interference term induces a directional current flow! Thus coherent interference contributions result in a controlled directional current flow.

Several additional remarks are in order. First, the phases φ_1 and φ_2 of Equation 6.68 contain the spatial phase factors $\exp[i\mathbf{k} \cdot \mathbf{R}]$, where \mathbf{k} is the light wave vector. The difference in the spatial phases can be exactly offset by the phase difference $\alpha_1 - \alpha_2$ in the preparation step (e.g., in a Raman preparation of $|\psi\rangle$) or eliminated by phase matching. Second, there are substantial experimental simplifications associated with applying the photo-dissociating lasers at the same time as initiating the preparation of the superposition state. Third, two-color light also causes excitation (via ω_{2p_0}) of the $|1s\rangle$ level to the state at $[E_k + |E_{2p_0}| - |E_{1s}|]$ and of the $|2p_0\rangle$ level (via ω_{1s}) to the state at $[E_k + |E_{1s}| - |E_{2p_0}|]$ (i.e., the uncontrolled satellite contributions discussed previously). In this case, however, these terms contribute to the A_1 and A_2 terms in Equation 6.71 and hence do not contribute to degrade the controlled current I_z^+ .

The magnitude and sign of the current is controllable for a given host material and superposition state parameters via: a) the optical phase difference $\varphi_1 - \varphi_2$, b) the donor number N , and/or, c) the ionizing field strengths \mathcal{E}_1 and \mathcal{E}_2 and their frequencies ω_1 and ω_2 . To estimate a typical current, consider the I_z resulting from the following parameters: $\mathcal{E}_1 = \mathcal{E}_2 = 0.1$ Volts/cm, $k = 5 \times 10^7 \text{ cm}^{-1}$, $|c_1 c_2| = 0.25$, and $\tau = 10^{-14}$ to 10^{-13} sec. The latter corresponds to a mean free path ($\hbar k \tau / m$) of 100–1000 Å, a typical value for the ballistic electrons at the cited k value. Furthermore, $N(\text{Si})V = 10^{18} \text{ cm}^{-3}V$ where V is the effective interaction volume. For a sample of 0.1 micron \times 10 micron \times 10 micron, $V = 10^{-11} \text{ cm}^3$. Utilizing Equation 6.74 and these parameter values, we obtain a current $I_z = 10$ –100 mA. Thus, sizeable currents may be readily produced due to the high quantum efficiency of the silicon photoionization.

Equations 6.72–6.74 apply, evidently, to photoionization of other $\ln s \rightarrow -\ln' p_0$ superpositions, where $\ln - \ln' = 1$, upon substituting the appropriate

ate Fourier coefficients $B_{n\mathbf{k},\mathbf{k}}$ and $B_{n'p_0,\mathbf{k}}$. It may turn out to be more practical to use other states than those discussed earlier.

6.5 COHERENCE CHEMISTRY

Our discussion makes clear that the characteristic features which we invoke in order to control chemical reactions are purely quantum in nature. There is, for example, little classical about the time-dependent picture where the ultimate outcome of the de-excitation (i.e., product $\text{H} + \text{HD}$ or $\text{H}_2 + \text{D}$) depends entirely upon the phase and amplitude characteristics of the wavefunction. Indeed, as repeatedly emphasized, if, for example, collisional effects are sufficiently strong so as to randomize the phases then reaction control is lost. Hence reaction dynamics are intimately linked to the wavefunction phases which are controllable through coherent optical phase excitation.

These results must be viewed in light of the history of molecular reaction dynamics. Possibly the most useful result of the reaction dynamics research effort has been the recognition that the vast majority of qualitatively important phenomena in reaction dynamics are well described by classical mechanics. Quantum and semiclassical mechanics were viewed as necessary only insofar as they correct quantitative failures of classical mechanics for unusual circumstances and/or for the dynamics of very light particles. Therefore, it appeared to be correct to considering reaction dynamics in traditional chemistry to be essentially classical in character for the vast majority of naturally occurring molecular processes; coherence played no role. The approach which we have introduced above makes clear, however, that coherence phenomena have great potential for application. The quantum phase is always present and can be used to our advantage, even though it is irrelevant to traditional chemistry. By calling attention to the extreme importance of coherence phenomena to controlled chemistry we herald the introduction of a new focus in atomic and molecular science (i.e., introducing coherence in controlled environments to modify molecular processes) thus defining the area of coherence chemistry.

ACKNOWLEDGMENTS

We acknowledge support for this research by the U.S. Office of Naval Research.

REFERENCES

1. P. Brumer and M. Shapiro, *Chem. Phys. Lett.*, **126**, 541 (1986).
2. M. Shapiro and P. Brumer, *J. Chem. Phys.*, **84**, 4103 (1986).
3. P. Brumer and M. Shapiro, *Faraday Disc. Chem. Soc.*, **82**, 177 (1986).
4. M. Shapiro and P. Brumer, *J. Chem. Phys.*, **84**, 4103 (1986).
5. C. Asaro, P. Brumer and M. Shapiro, *Phys. Rev. Lett.*, **60**, 1634 (1988).
6. M. Shapiro, J. Hepburn and P. Brumer, *Chem. Phys. Lett.*, **149**, 451 (1988).
7. P. Brumer and M. Shapiro, *J. Chem. Phys.*, **90**, 6179 (1989).
8. G. Kurizki, M. Shapiro and P. Brumer, *Phys. Rev. B*, **39**, 3435 (1989).
9. T. Seideman, M. Shapiro and P. Brumer, *J. Chem. Phys.*, **90**, 7136 (1989).
10. J. Krause, M. Shapiro and P. Brumer, *J. Chem. Phys.*, **92**, 1126 (1990).
11. I. Levy, M. Shapiro and P. Brumer, *J. Chem. Phys.*, **93**, 2493 (1990).
12. P. Brumer and M. Shapiro, *Accounts Chem. Res.*, **22**, 407 (1989).
13. C. K. Chan, P. Brumer and M. Shapiro, *J. Chem. Phys.*, **94**, 2688 (1991).
14. X-P. Jiang, P. Brumer and M. Shapiro (to be published).
15. P. Brumer and M. Shapiro, *Chem. Phys.*, **139**, 221 (1989).
16. M. Shapiro and P. Brumer, *J. Chem. Phys.*, **97**, 6259 (1992).
17. X. Jiang, P. Brumer and M. Shapiro, (in preparation).
18. M. Shapiro and P. Brumer, *J. Chem. Phys.*, **95**, 8658 (1991).
19. J. Dods, M. Shapiro and P. Brumer, *Can. J. Chem.* (submitted); J. Dods, M.Sc. Dissertation, University of Toronto (1992).
20. For a discussion of the basic principles of coherence, quantum interference, time dependence, which are fundamental to coherent control; see, for example, J. D. Macomber, *The Dynamics of Spectroscopic Transitions*, J. Wiley, New York, 1976.
21. To see this requirement note that it should be possible to set up initial reactant conditions (i.e., relative velocities, internal rotation, and vibration states, etc.) so as to produce a wide variety of possible reaction outcomes (e.g., probabilities of observing products with different relative velocities, internal rotational and vibrational states, scattering angles, etc.). To properly describe these product states requires then a host of wavefunctions, all at energy E , which can be added arbitrarily together so as to yield this wide variety of allowed final states. This the Asymptotic Condition of Scattering Theory [see J. R. Taylor, *Scattering Theory*, J. Wiley, New York, 1972].
23. See, for example, R. D. Taylor and P. Brumer, *Disc. Faraday Society*, **75**, 17 (1983); P. Brumer and M. Shapiro (to be published).
24. Contrary to popular expectation, perturbation theory does not imply a small total photodissociation yield. Computational results (P. Brumer and M. Shapiro) indicate that perturbation theory is quantitatively correct for dissociation probabilities as large as 0.2.
25. R. Bersohn and M. Shapiro, *Ann. Rev. Phys. Chem.*, **33**, 409 (1982); M. Shapiro, *J. Chem. Phys.*, **56**, 2582 (1972).
26. M. S. Child, *Mol. Phys.*, **32**, 495 (1976).

27. M. Shapiro and P. Brumer, in *Methods of Laser Spectroscopy*, (A. Prior, A. Ben-Reuven and M. Rosenbluh, Eds.) Plenum, New York, 1986.
28. M. Shapiro, *J. Phys. Chem.*, **90**, 3644 (1986).
29. D. J. Tannor and S. A. Rice, *J. Chem. Phys.*, **83**, 5013 (1985); D. J. Tannor, R. Kosloff and S. A. Rice, *J. Chem. Phys.*, **85**, 5805 (1986).
30. See, for example, R. B. Bernstein and R. D. Levine, *Molecular Reaction Dynamics*, Oxford University Press, New York, 1987.
31. A. D. Bandrauk, J. M. Gauthier, J. F. McCann, *Chem. Phys. Lett.*, **200**, 399 (1992).
32. C. Chen, Y.-Y. Yin, and D. S. Elliott, *Phys. Rev. Lett.*, **64**, 507 (1990); C. Chen, Y.-Y. Yin, and D. S. Elliott, *Phys. Rev. Lett.*, **65**, 1737 (1990).
33. S. M. Park, S.-P. Lu, and R. J. Gordon, *J. Chem. Phys.*, **94**, 8622 (1991); S.-P. Lu, S. M. Park, Y. Xie, R. J. Gordon, *J. Chem. Phys.*, **96**, 6613 (1992).
34. B. A. Baranova, A. N. Chudinov, and B. Ya Zel prime dovitch, *Opt. Comm.*, **79**, 116 (1990).
35. Z. Chen, M. Shapiro and P. Brumer, *J. Chem. Phys.*, **98**, 6843 (1993).
36. M. Shapiro and R. Bersohn, *J. Chem. Phys.*, **73**, 3810 (1980).
37. A. R. Edmonds, *Angular Momentum in Quantum Mechanics*, 2nd edition, Princeton University Press, Princeton, 1960.
38. L. D. Barron, *Molecular Light Scattering and Optical Activity*, Cambridge University Press, Cambridge, 1982; R. G. Woolley, *Adv. Phys.*, **25**, 27 (1975); *Origins of Optical Activity in Nature*, (D. C. Walker, Ed.), Elsevier, Amsterdam, 1979.
39. For a discussion see L. D. Barron, *Chem. Soc. Rev.*, **15**, 189 (1986). For historical examples see J. A. Bel, *Bull. Soc. Chim. Fr.*, **22**, 337 (1874); J. H. Van't Hoff, *Die Lagerung der Atome und Raume*, 2nd. Ed., 1894, p. 30.
40. An example, although requiring a slight extension of the BAB prime notation, is the Norrish type II reaction: $D(CH_2)_3CO(CH_2)_3D$ prime dissociating to $DCHCH_2 + D$ prime $(CH_2)_3COCH_3$ and D prime $CHCH_2 + D(CH_2)_3COCH_3$ where D and D prime are enantiomers.
41. See T. Seideman, M. Shapiro and P. Brumer, *J. Chem. Phys.*, **90**, 7136 (1989); J. Krause, M. Shapiro and P. Brumer, *J. Chem. Phys.*, **92**, 1126 (1990); C. K. Chan, P. Brumer and M. Shapiro, *J. Chem. Phys.*, **94**, 2688 (1991) and references therein.
42. J. M. Hollas, *High Resolution Spectroscopy*, Butterworths, London, 1982.
43. E. Segev and M. Shapiro, *J. Chem. Phys.*, **77**, 5604 (1982).
44. G. G. Balint-Kurti and M. Shapiro, *Chem. Phys.*, **61**, 137 (1981).
45. $M_I = M_k$ since both $|E_I\rangle$ and $|E_k\rangle$ arise by excitation, with linearly polarized light, from a common eigenstate.
46. Equation 6.59 is a generalized version of Equation 6.48 [44].
47. M. Shapiro and P. Brumer, (to be published).
48. As an aside we note that control is not possible in collinear models since, in that case, d_1 and d_k can not both couple to the same electronically excited state.
49. K. Seeger, *Semiconductor Physics*, Springer Verlag, Berlin, 1973.

50. S. T. Pantelides, *Rev. Mod. Phys.*, **50**, 797 (1978).
51. R. A. Faulkner, *Phys. Rev.*, **184**, 713 (1969).
52. A. Kasami, *J. Phys. Soc. Japan*, **24**, 551 (1968).
53. A. Baldereschi and M. G. Diaz, *Nuov. Cim.*, **68B**, 217 (1970).
54. W. Kohn and J. M. Luttinger, *Phys. Rev.*, **98**, 915 (1955).
55. B. K. Ridley, *J. Phys.*, **C13**, 2015 (1980).
56. K. Huang and A. Rhy, *Proc. Roy. Soc. A*, **04**, 406 (1950).
57. D. Hsu and J. L. Skinner, *J. Chem. Phys.*, **81**, 1604 (1984); **81**, 5471 (1984).
58. M. J. M. Ziman, *The Principles of the Theory of Solids*, Cambridge University Press, 1965, Equation 7.16.

Two-color coherent control with SEP preparation: electronic branching in Na₂ photodissociation

JEFFREY DODS AND PAUL BRUMER¹

Chemical Physics Theory Group, Department of Chemistry, University of Toronto, Toronto, ON M5S 1A1, Canada

AND

MOSHE SHAPIRO

Department of Chemical Physics, The Weizmann Institute of Science, Rehovot, Israel 76100

Received August 24, 1993

This paper is dedicated to Professor John C. Polanyi on the occasion of his 65th birthday

JEFFREY DODS, PAUL BRUMER, and MOSHE SHAPIRO. *Can. J. Chem.* **72**, 958 (1994).

Extensive control over relative product yields is shown to result from weak laser photodissociation in a two-color coherent control scenario. Photodissociation takes place from a superposition state prepared by stimulated emission pumping. The method allows for control in the presence of laser phase jumps by using four-wave mixing to prepare the required laser frequencies. The near UV photodissociation of Na₂, resulting in the Na(3s) + Na(4s) and the Na(3s) + Na(3d) products, is used to illustrate the method.

JEFFREY DODS, PAUL BRUMER et MOSHE SHAPIRO. *Can. J. Chem.* **72**, 958 (1994).

On démontre que les rendements relatifs en produit peuvent être fortement contrôlés par une photodissociation faible au laser dans un scénario de contrôle cohérent en deux couleurs. La photodissociation se produit par un état de superposition préparé par un pompage stimulé d'émission. La méthode permet de réaliser un contrôle en présence de sauts de phase du laser en utilisant un mélange de quatre ondes pour préparer les fréquences laser requises. Pour illustrer la méthode, on utilise la photodissociation dans le proche UV du Na₂ qui conduit aux produits Na(3s) + Na(4s) et Na(3s) + Na(3d).

[Traduit par la rédaction]

1. Introduction

The past few decades have seen enormous progress in our understanding of the detailed dynamics of chemical reactions, and J.C. Polanyi's pioneering leadership in this area is widely acclaimed. This knowledge base has allowed recent progress (1, 2) towards an essential goal of practical chemistry, control over chemical reactions. Our technique of coherent radiative control (1) affords a method of controlling molecular dynamics by exploiting quantum interference phenomena. For example, in photodissociation of a molecule at energy E where a number of products are present, control over relative product yield can be achieved by introducing two or more simultaneous excitation routes. Varying the intensity and relative phases of the lasers used to excite the molecule allows one to directly alter the interference between these routes and hence to directly alter the reaction yield.

Thus far we have devised a number of scenarios that rely upon this interference principle and that utilize either CW or pulsed laser excitation sources. Here we introduce a specific scenario, which embellishes our first control scheme (3) and which allows us to bypass deleterious incoherence effects due to laser jitter.² Briefly, the scheme involves two steps: preparation of a molecular superposition state by stimulated emission pumping (SEP), followed by photodissociation after a suitable time delay. If the frequencies used are prepared by an appropriate nonlinear mixing scheme then we show that the method is insensitive to any laser jitter inherent in the light sources. In the next section we give a more detailed overview of the control scheme. Subsequent sections describe the details of the method and give applications to the photodissociation of Na₂.

2. One photon vs. one photon coherent control

2.1 Overview

The first coherent control scenario (3) considered the photo-

dissociation, at energy E , of a molecule in a superposition of two bound states $|E_1\rangle$ and $|E_2\rangle$. The ratio of dissociation products could be varied by altering the relative phase and intensity of two coherent sources, of frequencies $(E - E_i)/\hbar$ ($i = 1, 2$). In addition, we demonstrated, through a quantitative study of products in methyl iodide dissociation, that the range of product control can be extensive. A subsequent study of the utility of this scenario in the presence of collisions (5) showed that control survived over a reasonable temperature range.

In this paper we demonstrate that by preparing the initial state in a specific fashion we are able to construct an experimental scheme that is readily implemented and that minimizes deleterious effects due to laser jitter. In addition, the method allows for the preparation of superposition states where $(E_2 - E_1)$ can be large, aiding in the suppression of uncontrollable competitive photodissociation routes.

Briefly, we propose to use a frequency ω_0 to pump two dye lasers at frequencies ω_1 and ω_2 . The quantity $\hbar(\omega_1 - \omega_2)$ is chosen equal to $(E_j - E_i)$, the energy difference between $|E_j\rangle$ and $|E_i\rangle$, two vib-rotational levels on the ground electronic surface. The molecule (see Fig. 1) is then irradiated with ω_1 and ω_2 light for a fixed time period, resulting in preparation of the superposition state via stimulated emission pumping (6). After some selected time delay the molecule is photodissociated with two frequencies $(\omega_0 + \omega_1)$ and $(\omega_0 + \omega_2)$ prepared by mixing the ω_1 and ω_2 beams with ω_0 in a nonlinear crystal. Simultaneous excitation to energy E results, with interference effects controlled by the relative intensity, and phases of the two routes. Phase jitter effects are eliminated and uncontrollable satellite contributions can be minimized, as discussed below.

2.2 Superposition preparation

Consider the molecule, defined by Hamiltonian H_m with eigenstates $|E_j\rangle$ of energy E_j , which is subject to the time-dependent perturbation $V(t)$. The standard solution (7) is given by the wavefunction $|\psi(t)\rangle$:

¹ Author to whom correspondence may be addressed.

² For an alternate two-photon vs. two-photon control scheme for overcoming interference loss due to phase jumps and thermal effects see ref. 4.

$$[1] \quad |\psi(t)\rangle = \sum_j a_j(t) |E_j\rangle \exp(-iE_j t/\hbar)$$

where

$$[2] \quad a_j(t) \equiv \langle E_j | \psi^I(t) \rangle \\ = \langle E_j | T \exp \left(-\frac{i}{\hbar} \int_{t_0}^t V^I(t') dt' \right) | \psi(t_0) \rangle$$

Here T is the time-ordering operator and $V^I(t)$ and $|\psi^I(t)\rangle$ denote the perturbation and wavefunction in the interaction representation. That is

$$[3] \quad |\psi(t)\rangle = \exp(-iH_m t/\hbar) |\psi^I(t)\rangle$$

and

$$[5] \quad a_j(t) = \langle E_j | 1 - \frac{i}{\hbar} \int_{t_0}^t V^I(t') dt' - \frac{1}{2\hbar^2} \int_{t_0}^t V^I(t') dt' \int_{t_0}^{t'} V^I(t'') dt'' | E_i \rangle$$

Both the first and second matrix elements are zero, the first by orthogonality and the second (the first-order, one-photon transition) because the transition between $|E_i\rangle$ and $|E_j\rangle$, which belong to the same electronic surface, is assumed dipole forbidden.

To evaluate the third term we insert complete sets of states between the integrals. We can limit consideration to a particular vibration-rotation level of an intermediate electronic state (denoted $|E_N\rangle$) if ω_1 and ω_2 are tuned to resonance. Choosing ω_1 resonant with the $E_i \rightarrow E_N$ transition and ω_2 with the stimulated $E_N \rightarrow E_j$ emission, we can rewrite eq. [2] as

$$[6] \quad a_j(t) = -\frac{1}{2\hbar^2} \int_{t_0}^t dt' \exp(i(E_j - E_N)t'/\hbar) \langle E_j | V(t') | E_N \rangle \int_{t_0}^{t'} dt'' \exp(i(E_N - E_i)t''/\hbar) \langle E_N | V(t'') | E_i \rangle$$

Substituting the explicit form of $V(t)$ we obtain, in the rotating wave approximation (i.e., retaining absorption of $|E_i\rangle$ to $|E_N\rangle$ and emission from $|E_N\rangle$ to $|E_j\rangle$), that

$$[7] \quad a_j(t) = \frac{1}{4\hbar^2} \int_{t_0}^t dt' \exp(i(E_j - E_N + \hbar\omega_2)t'/\hbar + i\phi_2) \\ \times \epsilon_2(\omega_2) \langle E_j | d_{\epsilon_2} | E_N \rangle \int_{t_0}^{t'} dt'' \exp(i(E_N - E_i - \hbar\omega_1)t''/\hbar - i\phi_1) \epsilon_1(\omega_1) \langle E_N | d_{\epsilon_1} | E_i \rangle$$

Evaluating the integrals gives

$$[8] \quad a_j(t) = \frac{1}{8\hbar^2} (t - t_0)^2 \epsilon_1(\omega_1) \epsilon_2(\omega_2) \langle E_j | d_{\epsilon_2} | E_N \rangle \langle E_N | d_{\epsilon_1} | E_i \rangle \exp(i(\phi_2 - \phi_1))$$

$$[9] \quad \equiv a_j^p \exp(i(\phi_2 - \phi_1 + \beta_{ij}))$$

where a_j^p denotes the absolute magnitude of the post-preparation coefficient of state $|E_i\rangle$ and β_{ij} is the phase of $\langle E_j | d_{\epsilon_2} | E_N \rangle \langle E_N | d_{\epsilon_1} | E_i \rangle$. Equation [1] therefore acquires the explicit form

$$[10] \quad |\psi(t)\rangle = |E_i\rangle \exp(-iE_i t/\hbar) + a_j^p \exp(i(\phi_2 - \phi_1 + \beta_{ij} - E_j t/\hbar)) |E_j\rangle$$

Equation [10] neglects the term in $|E_N\rangle$, which is justified if, as below, subsequent photodissociation from $|E_N\rangle$ is negligible due to poor Franck-Condon factors.

It is convenient to begin the photodissociation at time zero. To allow this we shift the zero of time by starting the SEP preparation step at time $-(T + \tau_p)$ and terminating it at time $-T$. The molecular state at the time the SEP preparation is completed ($t = -T$) is then

$$[11] \quad |\psi(-T)\rangle = |E_i\rangle + a_j^p \exp(i(\phi_2 - \phi_1 + \beta_{ij})) |E_j\rangle$$

and the state at a time just before the turn on of the photodissociation laser is

$$[12] \quad |\psi(0)\rangle = |E_i\rangle \exp(-iE_i T/\hbar) + a_j^p \exp(i(\phi_2 - \phi_1 + \beta_{ij})) |E_j\rangle \exp(-iE_j T/\hbar)$$

$$V^I(t) = \exp(iH_m t/\hbar) V(t) \exp(-iH_m t/\hbar)$$

In the case of SEP preparation, $V(t)$ describes the influence of two laser fields with frequencies ω_1 and ω_2 , and amplitudes ϵ_1, ϵ_2 , i.e.,

$$[4] \quad V(t) = -d_{\epsilon_1} \epsilon_1(\omega_1) \cos(\omega_1 t + \phi_1) \\ - d_{\epsilon_2} \epsilon_2(\omega_2) \cos(\omega_2 t + \phi_2)$$

Here the d_{ϵ_i} is the component of the transition dipole moment operator along the direction of the i th linearly polarized electric field. Expanding the exponential function in eq. [2] in a power series, truncating after the third term, and assuming the initial state $|\psi(t_0)\rangle$ to be the i th vibration-rotation level of the ground electronic state with no population in states $|E_j\rangle \neq |E_i\rangle$, allows us to rewrite eq. [2] as

Thus the final outcome of the molecular preparation step leaves the molecule in a superposition of bound states with phases dictated by relative laser phase and time delay before the photodissociation pulse. Note also that the molecular state has acquired the relative laser phase $(\phi_2 - \phi_1)$, with positive phase contribution ϕ_2 from emission and negative, $-\phi_1$, from absorption. Below we will see that the form of these phases is crucial to the coherent control scheme.

2.3 Photodissociation of the superposition state

Consider now photodissociation of the prepared superposition state of eq. [12] by two CW lasers of frequency $\omega_{E_i} = (E - E_i)/\hbar$ and $\omega_{E_j} = (E - E_j)/\hbar$ (or by pulses containing these frequencies):

$$[13] \quad \epsilon(t) = \epsilon_4(\omega_{E_i}) \cos(\omega_{E_i}t + \phi_4) + \epsilon_3(\omega_{E_j}) \cos(\omega_{E_j}t + \phi_3)$$

To obtain the photodissociation amplitudes $b(Enq|t \rightarrow \infty)$ we expand the wavefunction as

$$[14] \quad |\psi(t)\rangle = \sum_i c_i(t)|E_i\rangle \exp\left(-\frac{i}{\hbar} E_i t\right) + \sum_{nq} \int dE' b(E'nq|t)|E'nq^-\rangle \exp\left(-\frac{i}{\hbar} E' t\right)$$

and solve for $b(Enq|t)$. Here $|Enq^-\rangle$ are incoming scattering wave functions which asymptotically go to products at energy E in arrangement channel q and internal quantum numbers n ; in diatomics, n is simply the scattering angle vector \hat{k} . Assuming the fields are sufficiently weak we have $c_i(t) = a_i^p$ at all times and, at long times, (3):

$$[15] \quad \left(\frac{\hbar}{i\pi}\right) b(Enq|t \rightarrow \infty) = \epsilon_4(\omega_{E_i}) \langle Enq^- | d_{\epsilon_4} | E_i \rangle \exp(-i(\phi_{\omega_{E_i}} + E_i T/\hbar)) \\ + a_j^p \epsilon_3(\omega_{E_j}) \langle Enq^- | d_{\epsilon_3} | E_j \rangle \exp(i(\phi_2 - \phi_1 + \beta_{ij} - \phi_{\omega_{E_j}} - E_j T/\hbar))$$

with $E = E_i + \hbar \omega_{E_i} = E_j + \hbar \omega_{E_j}$. The probability of forming product in product channel q at energy E is given by $P(q; E) = \lim_{t \rightarrow \infty} \sum_n |b(Enq|t)|^2$. This assumes a convenient form if we introduce the notation

$$[16] \quad d_{44}^q = \int d\hat{k} |\langle Enq^- | d_{\epsilon_4} | E_i \rangle|^2$$

$$[17] \quad d_{33}^q = \int d\hat{k} |\langle Enq^- | d_{\epsilon_3} | E_j \rangle|^2$$

$$[18] \quad d_{34}^q = |d_{34}^q| \exp(i\alpha_{34}^q) \\ = \int d\hat{k} \langle E_j | d_{\epsilon_3} | Enq^- \rangle \langle Enq^- | d_{\epsilon_4} | E_i \rangle$$

Expanding the square in $|b(Enq|t)|^2$ allows us to write the yield $R(q; E)$ to observe products in channel q , with energy E as

$$[19] \quad R(q; E) = \frac{P(q; E)}{P(q; E) + P(q'; E)}$$

with

$$[20] \quad P(q; E) \propto d_{44}^q + x^2 d_{33}^q + 2x |d_{34}^q| \cos(\Phi + \beta_{ij} + \alpha_{34}^q)$$

Here we have left out proportionality factors irrelevant to R and have introduced the notation:

$$[21] \quad \Phi = \phi_{\omega_{E_i}} - \phi_{\omega_{E_j}} + \phi_2 - \phi_1 + (E_i - E_j)T/\hbar$$

$$[22] \quad x = \frac{a_j^p \epsilon_3(\omega_{E_j})}{\epsilon_4(\omega_{E_i})}$$

Equation [20] comprises three terms, direct photodissociation of levels $|E_i\rangle$ and $|E_j\rangle$ plus an interference term between these routes. It is evident from eq. [20] that changing either x or Φ will result in a variation in the probability $P(q; E)$. Both variables comprise experimentally controllable parameters including the relative phases and intensities of the excitation sources in both steps, as well as the time delay T between preparation and dissociation. Varying these control parameters in the laboratory allows direct control over the interference term and hence over the product distribution.

Additional photodissociation at energies other than E , the so-called satellite contributions, also occur. These correspond to the photodissociation of $|E_i\rangle$ by absorption of ω_{E_j} to energy $E + E_i - E_j$ and the photodissociation of $|E_j\rangle$ by absorption of ω_{E_i} to energy $E + E_j - E_i$. Since there is only one pathway to each of these energies, they correspond to uncontrolled photodissociation pathways. However, this scenario allows large $(E_i - E_j)$ so that these absorptions may be placed outside of the continuum absorption range.

2.4 Countering phase incoherence

Relying on independent lasers for state creation and subsequent photodissociation has serious disadvantages. Specifically, if the four relative laser phases within Φ are unstable or uncorrelated then phase fluctuations during the interaction of the molecule with four independent lasers can lead to extensive phase averaging. Such phase averaging destroys the coherence vital to coherent control. However, a simple experimental scenario resolves this problem. In particular, consider using a single CW laser of frequency ω_0 to pump two dye lasers at frequencies ω_1 and ω_2 . The associated laser phases are denoted ϕ_0 , ϕ_1 , and ϕ_2 . The three frequencies are chosen such that $(\omega_0 + \omega_1) = \omega_{E_i}$, $(\omega_0 + \omega_2) = \omega_{E_j}$. If ω_1 and ω_0 , as

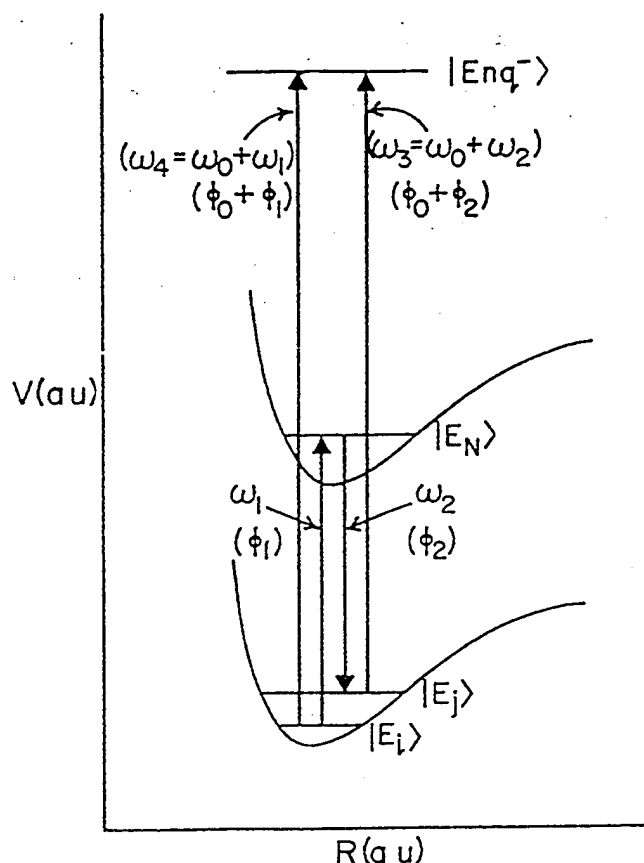


FIG. 1. Schematic of the coherent control scenario. The phase of route one (excitation by $\omega_0 + \omega_1$) imparts to the continuum state $\phi_0 + \phi_1$. Similarly, the phase imparted in route two (ω_1, ω_2) preparation followed by $\omega_0 + \omega_2$ dissociation equals $(\phi_1 - \phi_2 + \phi_0 + \phi_2) = (\phi_0 + \phi_1)$.

well as ω_2 and ω_0 , are mixed in a nonlinear crystal then the created frequencies $(\omega_0 + \omega_1) = \omega_{E_i}$ and $(\omega_0 + \omega_2) = \omega_{E_j}$ have phases $\phi_0 + \phi_1$ and $\phi_0 + \phi_2$, respectively.

With this mode of frequency preparation the phase Φ assumes the form:

$$[23] \quad \Phi = \phi_{\omega_{E_i}} - (\phi_1 - \phi_2 + \phi_{\omega_{E_j}}) + (E_i - E_j)T/\hbar$$

$$[24] \quad = (\phi_0 + \phi_1) - (\phi_1 - \phi_2 + \phi_0 + \phi_2) + (E_i - E_j)T/\hbar$$

$$[25] \quad = (E_i - E_j)T/\hbar$$

Thus the phase difference between the two routes is independent of the laser phases and, in particular, independent of the fluctuations in the laser sources.

An enlightening qualitative picture of the phases associated with the two excitation routes to dissociation is shown in Fig. 1. Route one to dissociation is excitation from level $|E_i\rangle$ via $\epsilon_4(\omega_{E_i})$; the created state acquires the phases $[-(\phi_0 + \phi_1)]$. Route two is a three-photon route, from $|E_i\rangle$ to $|E_N\rangle$ to $|E_j\rangle$ to the continuum. Phase accumulated along this route is $[-\phi_1 + \phi_2 - (\phi_0 + \phi_2)] = [-(\phi_0 + \phi_1)]$. Hence both excitation routes result in the same accumulated phase and the phase difference between them cancels.

Laboratory control over the phase then corresponds to varying T or, if preferred, deliberately introducing an additional phase delay between the two routes. We therefore extend the

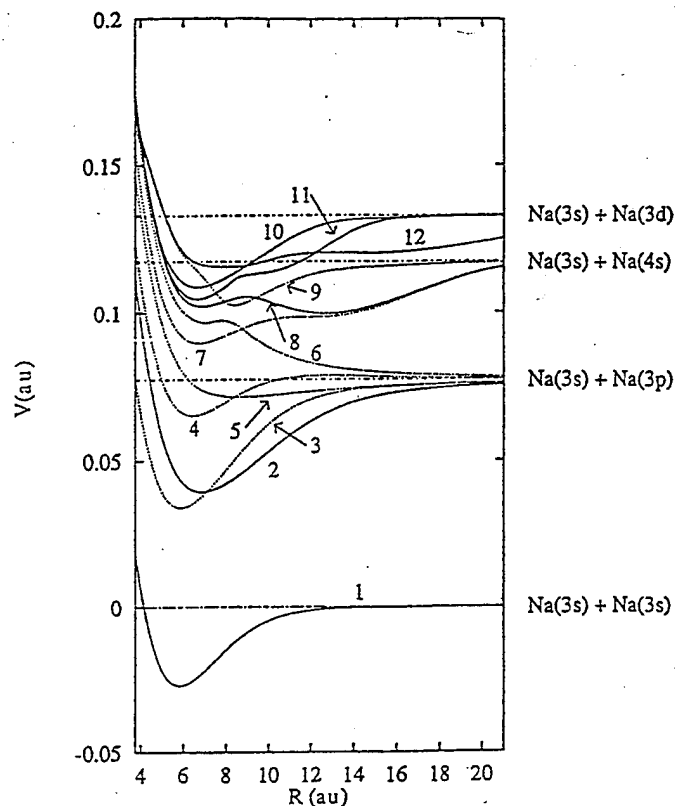


FIG. 2. The most relevant Na_2 potential curves are shown: (1) $^1\Sigma_g$, (2) $^1\Sigma_u$, (3) $^3\Pi_u$, (4) $^1\Pi_u$, (5) $^1\Pi_g$, (6) $^3\Sigma_u$, (7) $^1\Sigma_g$, (8) $^1\Sigma_u$, (9) $^3\Sigma_u$, (10) $^1\Pi_u$, (11) $^3\Pi_u$, (12) $^1\Sigma_u$. Additional states included in the computation but omitted here for clarity are as follows: one $^1\Sigma_g$, two $^3\Sigma_g$, and one $^3\Pi_g$, which are asymptotic to the $\text{Na}(3s) + \text{Na}(3p)$ product, and one $^3\Sigma_g$ state that is asymptotic to the $\text{Na}(3s) + \text{Na}(4s)$ product.

definition of Φ to include any experimentally introduced additional phase delay.

3. Results

Although this control scheme is applicable to a wide range of molecules, it is convenient to choose a particular system, e.g., Na_2 , to demonstrate the method. We first consider some photodissociation amplitudes characteristic of the energy range of interest. Appendix A provides additional details on the nature of these calculations; below we will discuss only the qualitative results of the photodissociation and the coherent control of products $\text{Na}(3s) + \text{Na}(4s)$ vs. $\text{Na}(3s) + \text{Na}(3d)$.

3.1 Na_2 photodissociation

A total of 17 Na_2 electronic states (8) were included in the computation. The 12 curves contributing most significantly are shown in Fig. 2, with the remainder omitted for clarity of presentation. Those which are dipole coupled to the ground state (9), and which are in the energy range of interest, are shown using solid lines. Since the ground state of Na_2 is a $^1\Sigma_g$, only singlets of ungerade symmetry are dipole coupled to this state. A small spin-orbit coupling does mix singlet states with triplets; only one triplet state need concern us in this study, the $^3\Pi_u$ curve numbered 11. Also shown are typical frequencies used to apply the coherent control scenario discussed above to this system. The low-lying potentials leading to the $\text{Na}(3s) + \text{Na}(3p)$ and $\text{Na}(3s) + \text{Na}(3s)$ have negligible Franck-Condon factors for the photodissociation energies of interest, but are necessary for the computation of the SEP preparation step.

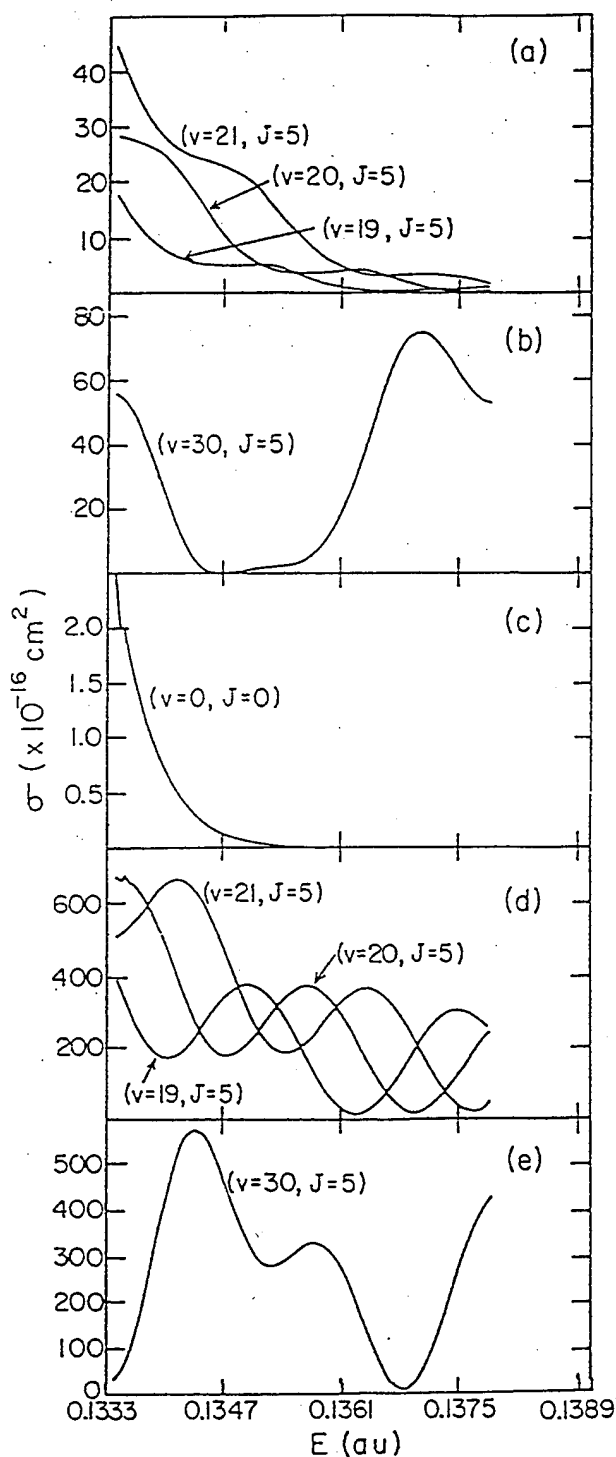


FIG. 3. Photodissociation cross sections into $\text{Na}(3s) + \text{Na}(4s)$ from $J = 5$, (a) $v = 19, 20, 21$; (b) $v = 30$. Photodissociation cross sections into $\text{Na}(3s) + \text{Na}(3d)$ vs. photon energy from Na_2 ; (c) into $v = 0, J = 0$; (d) $J = 5$, $v = 19, 20$, and 21 ; and (e) $v = 30$.

Our computations show that the Na_2 photodissociation cross section to the $\text{Na}(3s) + \text{Na}(4s)$ channel is extremely small for vibrational states $v = 0$ to $v = 15$. This is due to the large bond length of the ground $(1)^1\Sigma_g$ state of Na_2 , resulting in a small overlap between the $v = 0$ to $v = 15$ levels and the state $[(8)^1\Sigma_u]$ leading to the $\text{Na}(3s) + \text{Na}(4s)$ products. This low cross section is in contrast with the $\text{Na}(3s) + \text{Na}(3d)$ channel

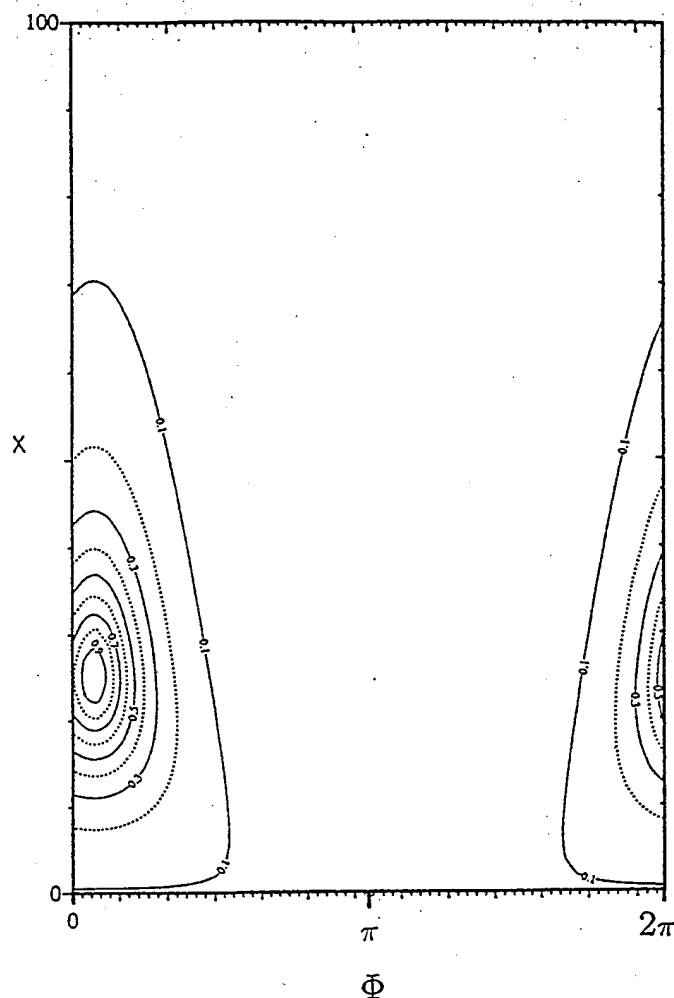
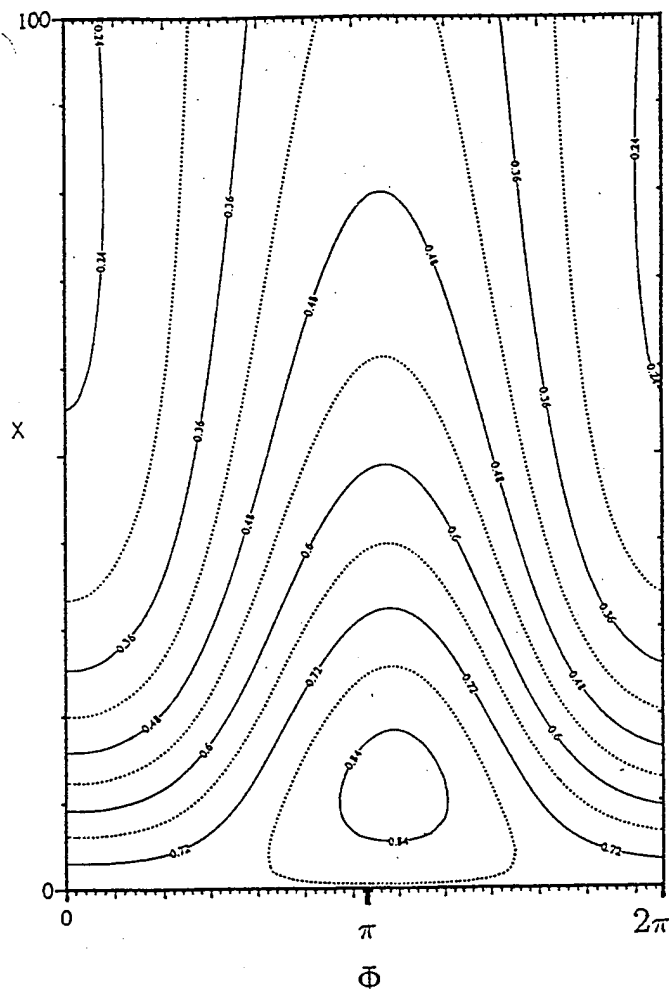


FIG. 4. Contours of constant $R(4s; E)$. The ordinate is the parameter x and the abscissa is the relative phase Φ . The control map is for the initial superposition of $v = 24, J = 0$ with $v' = 27, J = 0$.

cross section, which has a detectable magnitude starting with photodissociation of the Na_2 $v = 0$ state due to adequate overlap with the $(12)^1\Sigma_u$ state. The cross section for both channels increases as v increases. Figure 3 shows selected Na_2 photodissociation cross sections.

Figure 3a shows typical cross sections to the $\text{Na}(3s) + \text{Na}(4s)$ product channel. Adjacent bound states are seen to give similar cross sections. For $v = 19$ to $v = 21$, the decrease in cross section as photolysis energy increases is due to diminishing Franck-Condon factors on the repulsive wall of the excited surfaces. But $v = 30$ (Fig. 3b) has a different structure because the turning point of the bound state is outside the turning point of the excited state repulsive wall. A minimum is seen at about 0.1347 au of photon energy, followed by a peak at 0.1370 au.

Sample results for the $\text{Na}(3s) + \text{Na}(3d)$ channel are shown in Figs. 3c-e. The vibrationless level of the $(1)^1\Sigma_g$ state of Na_2 has a $\text{Na}(3s) + \text{Na}(3d)$ channel cross section that decays rapidly (Fig. 3c). By $v = 10$ the cross section develops clear oscillations, but by $v = 30$ (Fig. 3e) the oscillatory structure is no longer clear because there is significant interference from the Franck-Condon factors of the two strongly participating singlet states, the $(12)^1\Sigma_u$ and the $(10)^1\Pi_u$ states. This is in

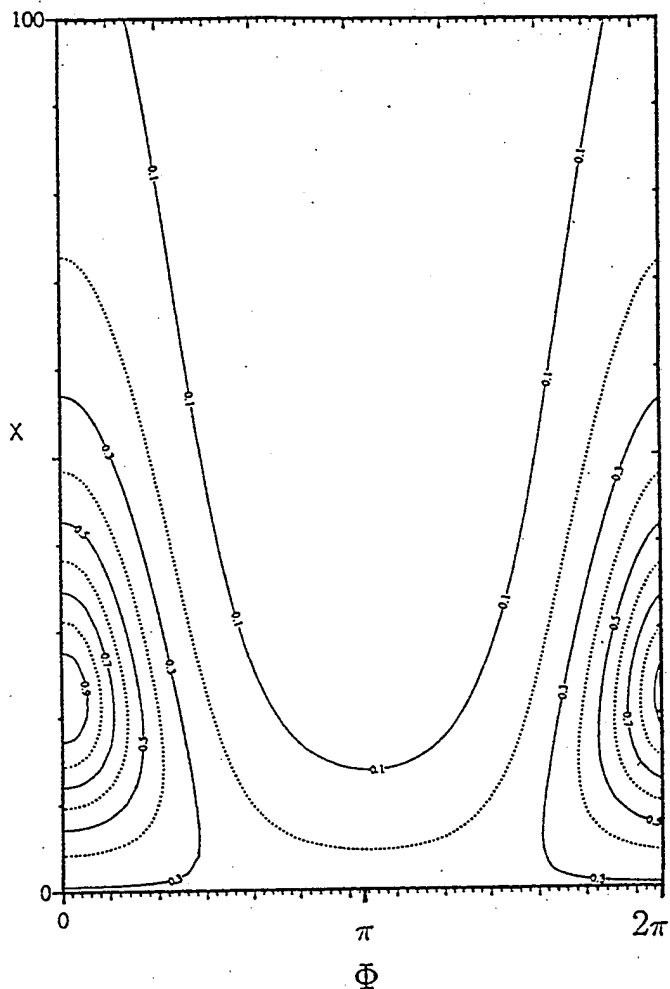
FIG. 5. As in Fig. 4 but with $J = 5$.

contrast with the results in Fig. 3d where the oscillatory structure is clear and where only one excited state, the $(12)^1\Sigma_u$, dominates the photodissociation. This state has a distinctly different location of its inner repulsive wall in the region of the $\text{Na}(3s) + \text{Na}(3d)$ channel threshold.

3.2 Coherent control of Na_2

Here we consider control over the fractional yield of the $q \equiv \text{Na}(3s) + \text{Na}(4s)$ vs. the $q' \equiv \text{Na}(3s) + \text{Na}(3d)$ channels. The vanishingly small cross section to produce $\text{Na}(3s) + \text{Na}(4s)$ for lower vibrational states prevents us from using low vibrational states for coherent control purposes. Below we describe control starting with the higher vibrational states ($v \geq 24$), which, if desired, can be experimentally created by the SEP pumping or by adiabatic passage techniques (10). We will use the availability of such techniques to our advantage by assuming that control can begin with the molecule in a high vibrational level of the ground electronic state.

Assume, for example, that we can begin the control experiment with the molecule in $v = 24$ and $J_i, M_i = 0$, where the latter denotes the angular momentum of the i th state and its z -projection. A survey (11) of Franck-Condon factors between this state and vib-rotational states of the $(2)^1\Sigma_u$ state shows that a superposition state comprising the $(v = 24, J = 0)$, and $(v = 27, J = 0)$ states could be conveniently formed via an $|E_N\rangle$ state with $v = 14, J = 1$. This corresponds to the

FIG. 6. As in Fig. 4 but with $J = 10$.

choice $\hbar\omega_1 = 12883 \text{ cm}^{-1}$ and $\hbar\omega_2 = 12538 \text{ cm}^{-1}$. Control results at $E = 29672 \text{ cm}^{-1}$ are shown in Fig. 4 where we plot $R(4s; E)$, the fractional yield of $4s$ as a function of the control parameters x and Φ . The figure shows contours of constant $R(4s; E)$ and indicates that the branching ratio can be varied between 10 and 90% by varying x and Φ . The maximum $\text{Na}(4s)$ yield is at $\Phi \sim 0.2\pi$ radians and the amplitude factor $x \sim 25$.

Figures 5 and 6 show results for initial states with higher rotational quantum numbers for which M averaging has been performed. Figure 5 shows results for the superpositions $(v = 24, J = 5)$, and $(v = 27, J = 5)$ at the slightly higher energy $E = 30046 \text{ cm}^{-1}$. Control of the $\text{Na}(4s)$ yield has been somewhat reduced (ranging from 0.24 to 0.84) relative to the case shown in Fig. 4. This is accompanied by a shift in the maximum in the $\text{Na}(4s)$ yield to $\Phi \sim 3.5\pi$ radians and $x \sim 10$. The $J_i = J_j = 10$ case (Fig. 6) shows very similar results to the $J_i = J_j = 0$ situation, with the range of control of 0.1–0.9 now restored.

As an example of the observed behavior of other combinations of bound state pairs, consider the case where the molecule is in the $v = 27, J = 0$ plus $v = 31, J = 0$ state, pumped via the intermediate $v = 21, |E_N\rangle$ state. This corresponds to using $\hbar\omega_1 = 13268 \text{ cm}^{-1}$ and $\hbar\omega_2 = 12837 \text{ cm}^{-1}$. The resultant $R(4s; E)$ control map at $E = 29607 \text{ cm}^{-1}$

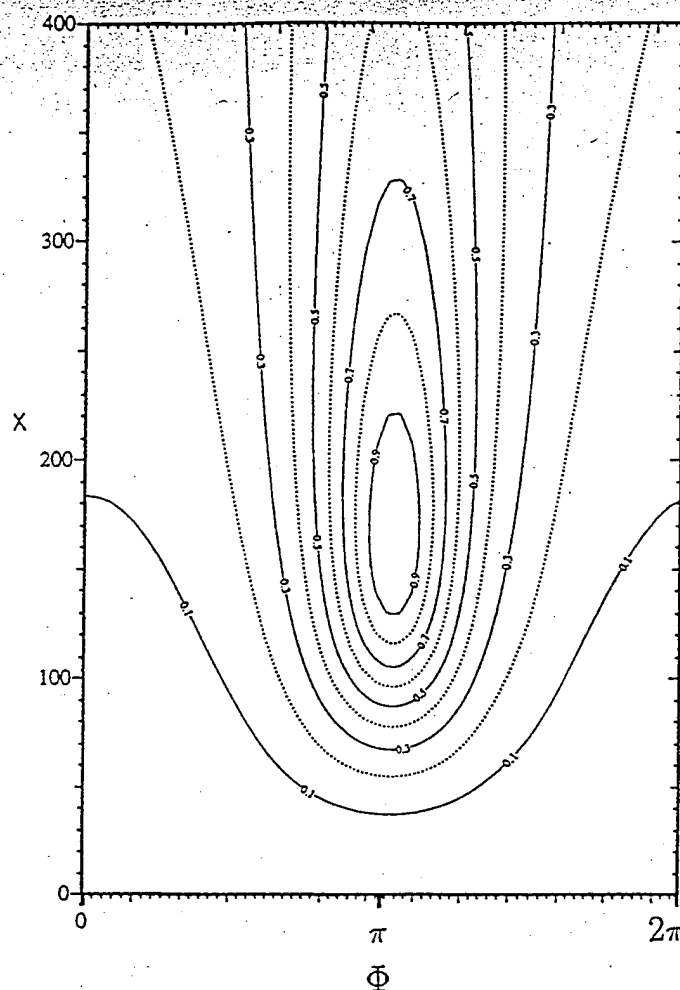


FIG. 7. As in Fig. 4 but with $\nu = 27$, and $\nu = 31$.

is shown in Fig. 7. The observed range of control is large, with the maximum in the Na(4s) yield appearing at very large x . This is a consequence of the relatively small Franck-Condon factor between the intermediate state and $\nu = 31$. That is, if

one of the excitation paths has a much weaker cross section, the electric field carrying that component to the continuum must be increased to compensate, resulting in large x .

4. Conclusion

We have proposed a SEP one photon vs. one photon coherent control scheme with a number of experimental advantages. Specifically, the scenario allows minimization of effects due to laser jitter and reduction of effects due to uncontrolled satellites. The scenario shows the possibility of a wide range of control, as demonstrated in computations on electronic branching in the photodissociation of Na₂.

Acknowledgements

This work was supported by the U.S. Office of Naval Research and by the Ontario Laser and Lightwave Research Centre.

1. P. Brumer and M. Shapiro. *Acc. Chem. Res.* **22**, 407 (1989); *Annu. Rev. Phys. Chem.* **42**, 257 (1992), and references therein.
2. S.A. Rice. *Science*, **258**, 412 (1992); W.S. Warren, H. Rabitz, and M. Dahleh. *Science*, **259**, 1581 (1993).
3. P. Brumer and M. Shapiro. *Chem. Phys. Lett.* **126**, 541 (1986).
4. Z. Chen, P. Brumer, and M. Shapiro. *J. Chem. Phys.* **98**, 6843 (1993).
5. M. Shapiro and P. Brumer. *J. Chem. Phys.* **90**, 6179 (1989).
6. C.E. Hamilton, J.L. Kinsey, and R.W. Field. *Annu. Rev. Phys. Chem.* **37**, 493 (1986).
7. P. Roman. *Advanced quantum theory*. Addison-Wesley, Reading, Mass. 1965.
8. G. Jeung. *J. Phys. B: At. Mol. Phys.* **16**, 4289 (1983); A. Schmidt. Ph.D. Dissertation, Univ. Kaiserslautern, Germany.
9. H. Lefebvre-Brion and R.W. Field. *Perturbations in the spectra of diatomic molecules*. Academic Press, Orlando, Fla. 1986.
10. U. Gaubatz, P. Rudecki, S. Shiemann, and K. Bergmann. *J. Chem. Phys.* **92**, 5363 (1990).
11. J. Dods. M.Sc. Dissertation, University of Toronto (1992).
12. I. Levy and M. Shapiro. *J. Chem. Phys.* **89**, 2900 (1988).
13. M. Shapiro and R. Bersohn. *Annu. Rev. Phys. Chem.* **33**, 409 (1982).
14. M. Shapiro and G.G. Balint-Kurti. *Chem. Phys.* **61**, 137 (1981), and references therein.

5. Appendix: Computational details

The bound-bound matrix elements, $\langle E_j | d | E_N \rangle \langle E_N | d | E_i \rangle$ that appear in $P(q; E)$ are calculated using uniform semiclassical wave functions.

To solve for the photodissociation amplitude, a considerable amount of manipulation is required. Here we only state the relevant results of the formulation (12, 13).

The amplitude $\langle Enq^- | d | E_i \rangle$ is obtained in accord with the method of Levy and Shapiro (12). Specifically we expand in partial waves

$$[A1] \quad \langle Enq^- | d | E_i \rangle \equiv \langle Enq^- | d | E_i, J_i, M_i \rangle \\ = \frac{\sqrt{2\mu k_\pi}}{h} \sum_{J, p, \lambda \geq 0} \begin{pmatrix} J & 1 & J_i \\ -M_i & 0 & M_i \end{pmatrix} \sqrt{2J+1} \mathcal{D}_{\lambda, M_i}^{J, p}(\phi_k, \theta_k, 0) t(E, p, \lambda, q | E_i, J_i)$$

where $\hat{k} = (\phi_k, \theta_k)$ is the direction of the recoiling fragments and λ is the magnitude of the electronic angular momentum about the internuclear axis. The $\mathcal{D}_{\lambda, M_i}^{J, p}$ are the parity-adapted rotation matrices defined, with parity $p = \pm 1$ as:

$$[A2] \quad \mathcal{D}_{\lambda, M_i}^{J, p} = \iota_\lambda [\mathcal{D}_{\lambda, M_i}^J + p \mathcal{D}_{-\lambda, M_i}^J]$$

where $t_\lambda = \sqrt{\frac{1}{2}}$ for $\lambda \neq 0$ and $t_\lambda = \frac{1}{2}$ for $\lambda = 0$. The quantity t is the reduced matrix element for photodissociation.

$$[A3] \quad t(EJp\lambda q|E_i J_i) = (-1)^\lambda t_\lambda \sqrt{(2J+1)(2J_i+1)} \begin{pmatrix} J & 1 & J_i \\ -\lambda & \lambda & 0 \end{pmatrix} (1+p(-1)^{J+1+J_i}) \\ \times \sum_{\xi} \int dR \Phi_{\xi}^{*(J,p-)}(R) (\xi|d|g) \Phi_{E_i}^{J_i}(R)$$

Here the sum over ξ is over all the electronic states that correlate with the same final channel. The $(\xi|d(R)|g)$ matrix element is the electronic transition dipole moment between the ground state and the ξ th state. The quantity $\Phi_{\xi}^{(J,p-)}(R)$ is the radial nuclear scattering wave function in electronic state's ξ and $\Phi_{E_i}^{J_i}(R)$ is the radial nuclear bound wavefunction with energy E_i .

The t matrix element is computed using the artificial channel method (14).

To calculate the probability $P(q; E)$ requires repeated use of this explicit form. For example, to calculate the first term d_{44}^q , we expand the $\mathcal{D}_{\lambda, M_i}^{J, p}$ and perform the integration over the scattering angle \hat{k} to arrive at:

$$[AA4] \quad d_{44}^q = \frac{8\pi\mu k_n}{\hbar^2} \sum_{J, p, \lambda \geq 0} \begin{pmatrix} J & 1 & J_i \\ -M_i & 0 & M_i \end{pmatrix}^2 |t(EJp\lambda nq|E_i J_i)|^2$$

Similarly, the other terms in $P(q; E)$ are given by:

$$[AA5] \quad d_{33}^q = \frac{8\pi\mu k_n}{\hbar^2} \sum_{J, p, \lambda \geq 0} \begin{pmatrix} J & 1 & J_j \\ -M_j & 0 & M_j \end{pmatrix}^2 |t(EJp\lambda q|E_j J_j)|^2$$

and

$$[AA6] \quad d_{34}^q = \frac{8\pi\mu k_n}{\hbar^2} \sum_{J, p, \lambda \geq 0} \begin{pmatrix} J & 1 & J_i \\ -M_i & 0 & M_i \end{pmatrix} \begin{pmatrix} J & 1 & J_j \\ -M_j & 0 & M_j \end{pmatrix} t(EJp\lambda q|E_i J_i) t^*(EJp\lambda q|E_j J_j)$$

In general, the sums over J extend over $J_i - 1, J_i, J_i + 1$ except for the $J_i = 0$ case for which there is only the $J = 1$ term.



ELSEVIER

7 October 1994

**CHEMICAL
PHYSICS
LETTERS**

Chemical Physics Letters 228 (1994) 289–294

Interference control of photodissociation branching ratios. Two-color frequency tuning of intense laser fields

Zhidang Chen, Moshe Shapiro¹, Paul Brumer

*Chemical Physics Theory Group and The Ontario Laser and Lightwave Research Center, University of Toronto,
Toronto, Canada M5S 1A1*

Received 11 July 1994

Abstract

Control over product probabilities and channel specific line shapes in molecular photodissociation is shown to result from quantum interference effects which can be manipulated by varying the frequencies of two intense laser fields. The laser fields, whose relative phase need not be well defined, have frequencies centered around two transitions: one between the continuum and an initially populated state and the second between the continuum and an initially unpopulated molecular bound state. Computations on Na₂ photodissociation show that control over product yields is extensive, with the branching ratio changing by a factor of ten as the frequencies are tuned over a convenient range.

Laser control of atomic and molecular processes is a rapidly developing field. Most recent innovations rely on using several lasers with well defined relative phase to excite a system [1–8]. The quantum interference between the laser induced multiple excitation routes depends upon both the laser intensities and their relative phases. Hence, by varying these laboratory parameters one varies the interference, leading to experimentally controllable molecular dynamics. Extensive control over processes such as branching in molecular photodissociation has been demonstrated computationally [1] and several experiments have supported the essential principle [6].

In this Letter, we demonstrate that high laser fields introduce nonlinear phenomena which allow novel and effective control scenarios. Specifically, we show that one can control channel specific line shapes and photodissociation branching ratios using two-color

irradiation with intense lasers whose relative phase need not be well defined. Control, which results from quantum interference between optically induced excitation routes, is achieved by changing the *frequencies* of the two intense lasers. The relative phase between lasers need not be well defined since the laser phases transferred to the molecule cancel in the multiphoton pathways induced by intense fields. In addition we show, in a computation on the photodissociation of Na₂, that the proposed approach allows for an extensive range of control over product probabilities.

These results constitute a significant advance in coherent control since they demonstrate the possibility of quantum-interference based control of photodissociation while avoiding the experimentally challenging problem of maintaining a well defined and stable relative laser phase. The results also contribute significantly to the theory of laser-induced continuum structure [9], extending the theory to molecules, with many bound states coupled to multiple

¹ Permanent address: Chemical Physics Department, The Weizmann Institute of Science, Rehovot, 76100 Israel.

continua. We show that the induced continuum structure in molecules can differ for continua coupled to different product channels, allowing for the selective enhancement of the cross section for a desired product arrangement channel.

The scenario is depicted in Fig. 1, here for the specific case of electronic branching in the photodissociation of an excited state of Na₂. A cw laser of frequency ω_1 excites a molecule from an initially populated bound state $|\epsilon_i\rangle$ to the dissociation continuum $|\epsilon, \mathbf{m}, q^-\rangle$ (where \mathbf{m} specifies the product quantum numbers and q labels the product arrangement channel) while a second laser, of frequency ω_2 , simultaneously couples the continuum to bound states $|\epsilon_j\rangle$ that are initially devoid of population. With both lasers on, dissociation to $|\epsilon, \mathbf{m}, q^-\rangle$ occurs via direct and indirect paths, $|\epsilon_i\rangle \rightarrow |\epsilon, \mathbf{m}, q^-\rangle$ and $|\epsilon_i\rangle \rightarrow |\epsilon', \mathbf{m}', q'^-\rangle \rightarrow |\epsilon_j\rangle \rightarrow |\epsilon, \mathbf{m}, q^-\rangle$. Contributions from these pathways to the product in a given channel q at energy ϵ interfere either constructively or destructively. As we show below, varying the frequencies and intensities of the two excitation lasers strongly affects this interference term, providing a means of controlling the photodissociation line shape and the branching ratio into different products.

To introduce notation and the computational method consider the photodissociation of a molecule

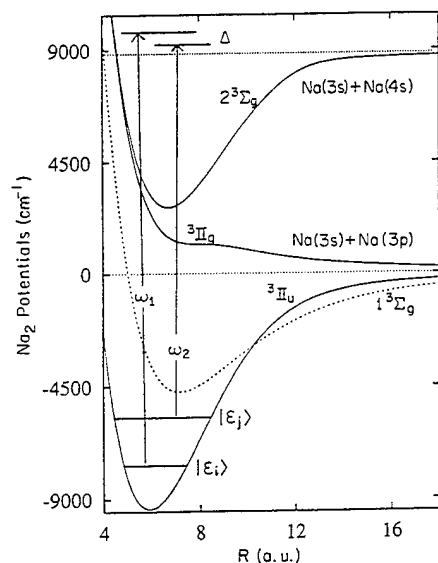


Fig. 1. Control scenario applied to the photodissociation of the $3^3\Pi_u$ state of Na₂. For the case considered in this paper $|\epsilon_i\rangle$ corresponds to $v=19$ with $\epsilon_{v=19} = -6512.8 \text{ cm}^{-1}$ and $|\epsilon_j\rangle$ is $v=31$ with $\epsilon_{v=31} = -4966.04 \text{ cm}^{-1}$.

with Hamiltonian H_M in the presence of a radiation field with Hamiltonian H_R . The total Hamiltonian $H = H_M + H_R + V$, where V is the molecule-field interaction. The radiation field is described by Fock states $|N_k\rangle \equiv |n_1^k, n_2^k, \dots\rangle$ with energy $\sum_l n_l^k \hbar \omega_l$. Eigenstates of H_M include bound states $|\epsilon_n\rangle$ and dissociative continuum states $|\epsilon, \mathbf{m}, q^-\rangle$. The latter correlate at large internuclear distances with states of the product in channel q with energy ϵ and quantum numbers \mathbf{m} . In general \mathbf{m} includes the scattering direction $\hat{\mathbf{k}}$.

Photodissociation dynamics is completely embodied [10] in the fully interacting eigenstates of the total Hamiltonian H , denoted $|(\epsilon, \mathbf{m}, q^-), N_k^-\rangle [H | (\epsilon, \mathbf{m}, q^-), N_k^-] = (\epsilon + \sum_l n_l^k \hbar \omega_l) |(\epsilon, \mathbf{m}, q^-), N_k^-\rangle$, where the minus superscript on N_k indicates that $|(\epsilon, \mathbf{m}, q^-), N_k^-\rangle$ becomes the non-interacting state $|(\epsilon, \mathbf{m}, q^-), N_k\rangle \equiv |\epsilon, \mathbf{m}, q^-\rangle |N_k\rangle$ when V is switched off. If the system is initially in the state $|\epsilon_i, N_i\rangle \equiv |\epsilon_i\rangle |N_i\rangle$ and the radiation field is switched on suddenly then the photodissociation amplitude to form the product state $|\epsilon, \mathbf{m}, q^-\rangle |N_k\rangle$ is given by [10] $\langle (\epsilon, \mathbf{m}, q^-), N_k^- | \epsilon_i, N_i \rangle$. Since $\langle (\epsilon, \mathbf{m}, q^-), N_k^- | \epsilon_i, N_i \rangle = 0$ then this overlap assumes the convenient form

$$\begin{aligned} &\langle (\epsilon, \mathbf{m}, q^-), N_k^- | \epsilon_i, N_i \rangle \\ &= \langle (\epsilon, \mathbf{m}, q^-), N_k^- | VG \left(\epsilon^+ + \sum_l n_l^k \hbar \omega_l \right) | \epsilon_i, N_i \rangle, \end{aligned} \quad (1)$$

by using the Lippmann-Schwinger equation $\langle (\epsilon, \mathbf{m}, q^-), N_k^- | = \langle (\epsilon, \mathbf{m}, q^-), N_k^- | + \langle (\epsilon, \mathbf{m}, q^-), N_k^- | VG (\epsilon^+ + \sum_l n_l^k \hbar \omega_l)$. Here $G(E) = 1/(E - H)$ and $\epsilon^+ = \epsilon + i\delta$ ($\delta \rightarrow 0^+$ at the end of the computation). Eq. (1) is exact and provides a connection between the dissociation amplitude and the VG matrix element. It is the latter which we compute exactly using a high field extension of the artificial channel method [11,12].

Two quantities are of interest: the channel specific line shape, that is

$$\begin{aligned} &A(\epsilon, q, N_k | \epsilon_i, N_i) \\ &= \int d\hat{\mathbf{k}} |\langle (\epsilon, \hat{\mathbf{k}}, q^-), N_k^- | \epsilon_i, N_i \rangle|^2, \end{aligned} \quad (2)$$

as a function of energy ϵ , and the total dissociation probability to channel q

$$P(q) = \sum_{N_k} \int d\epsilon A(\epsilon, q, N_k | \epsilon_i, N_i), \quad (3)$$

where the sum is over sets of photons that excite the molecule into the dissociation continuum. In writing Eq. (2) diatomic dissociation is assumed, so that $m = \hat{k}$.

To demonstrate the control scenario consider (see Fig. 1) photodissociation of Na_2 from the initial state $|\epsilon_i\rangle$ with vibrational quantum number $v_i = 19$ of the $^3\Pi_u$ electronic state [13], assumed prepared by excitation from the ground electronic state. Excitations from $|\epsilon_i\rangle$ by ω_1 and from initially empty $|\epsilon_j\rangle$ by ω_2 are to the dissociating continua where both $\text{Na}(3s) + \text{Na}(3p)$ and $\text{Na}(3s) + \text{Na}(4s)$ are produced. Computations were done with ω_1 chosen within the range $15430 \text{ cm}^{-1} < \omega_1 < 15700 \text{ cm}^{-1}$ with intensity $I_1 \sim 6 \times 10^9 \text{ W/cm}^2$, which is sufficiently energetic to dissociate levels of the $^3\Pi_u$ state with $v \geq 19$ to both products. The second laser has fixed frequency $\omega_2 = 13964 \text{ cm}^{-1}$ and fixed intensity $I_2 = 3.51 \times 10^{10} \text{ W/cm}^2$ and can dissociate levels with $v \geq 31$ to both products. Under these circumstances the dissociation from above threshold dissociation is found to be negligible. In the computations we also include contributions from the dissociation of $|\epsilon_i\rangle$ by ω_2 and of $|\epsilon_j\rangle$ by ω_1 , which can not be controlled by the interference effects discussed here, but are minimized under these circumstances. Results shown here are typical of those obtained in a broader class of computations which we have carried out. Studies which include rotations, which describe effects of laser intensities on control and which cover a wide range of laser powers and frequencies of the two lasers are to be included in a future publication [14].

Fig. 2 shows computed line shapes $A(\epsilon, q, N_k | \epsilon_i, N_i)$ (on a logarithmic scale) as a function of the product energy ϵ . Here $\omega_1 = 15456 \text{ cm}^{-1}$, $I_1 = 5.5 \times 10^9 \text{ W/cm}^2$, $N_i = (n_1, n_2)$ and $N_k = (n_1 - 1, n_2)$ where n_1 and n_2 are photon numbers of the lasers ω_1 and ω_2 , respectively. Results with both lasers on for the $\text{Na}(3p) + \text{Na}(3s)$ (curve (a)) and $\text{Na}(4s) + \text{Na}(3s)$ (curve (b)) product channels are shown. Fig. 3 contains similar results, but with $\omega_1 = 15511 \text{ cm}^{-1}$. In addition, the line shape for excitation with $\omega_1 = 15456 \text{ cm}^{-1}$ but with the ω_2 laser off is shown

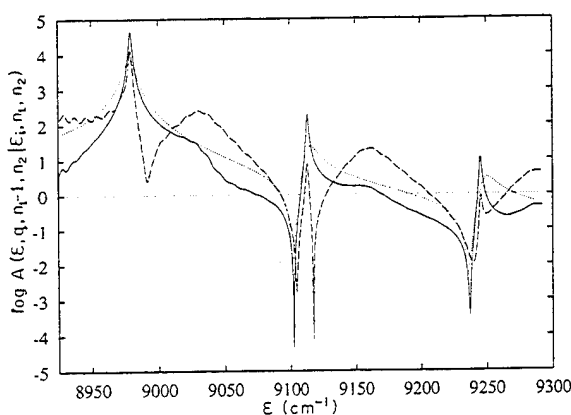


Fig. 2. $\log A(\epsilon, q, n_1 - 1, n_2 | \epsilon_i, n_1, n_2)$ as a function of ϵ (where the $\text{Na}(3s) + \text{Na}(3p)$ asymptote defines the zero energy). (—) $\text{Na}(3s) + \text{Na}(3p)$ product and (---) $\text{Na}(3s) + \text{Na}(4s)$ product, with both lasers on; (···) for the $\text{Na}(3s) + \text{Na}(4s)$ product with only one laser (ω_1) on. Here $\omega_1 = 15456 \text{ cm}^{-1}$, $\omega_2 = 13964 \text{ cm}^{-1}$, $I_1 = 5.5 \times 10^9 \text{ W/cm}^2$ and $I_2 = 3.51 \times 10^{10} \text{ W/cm}^2$.

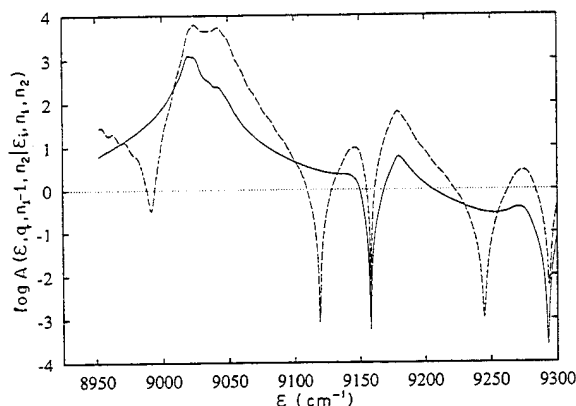


Fig. 3. (—, ---) As in Fig. 2 but with $\omega_1 = 15511 \text{ cm}^{-1}$.

in Fig. 2 (curve (c)) for the $\text{Na}(3s) + \text{Na}(4s)$ product; the $\text{Na}(3s) + \text{Na}(3p)$ result is similar.

Consider first $A(\epsilon, q, n_1 - 1, n_2 | \epsilon_i, n_1, n_2)$ associated with excitation by a single laser (Fig. 2, curve (c)). The line shape is comprised of a series of non-Lorentzian peaks and dips corresponding to resonance contributions from the dressed $v = 19, 20, 21$ vibrational states. The predominant contribution is the direct $v_i = 19$ excitation, with smaller $v = 20, 21$ contributions arising from stimulated emission and absorption from and to the continuum. Further, the overall shape between the peaks shows Fano-type interference [15] between the photodissociation pathways arising from the pairs of adjacent vibrational

states. Since significant dissociation is observed from states other than the initially populated $v_i=19$ it is clear that the power broadening is on the same order of magnitude as the vibrational level spacing.

With both ω_1 and ω_2 lasers on, each peak splits into two peaks in a manner which is dependent both upon asymptotic channel (compare curves (a) and (b) within each of Figs. 2 and 3) and frequency ω_1 (compare Fig. 2 with Fig. 3). An analysis of this structure is provided later below. Here we note the significant implication that by varying ω_1 we can control the channel specific line shapes $A(\epsilon, q, N_k | \epsilon_i, N_i)$. For example, comparing Figs. 2 and 3 shows that the increase in ω_1 results in a shift of the dominant peaks to higher ϵ . Products at $\epsilon \approx 9025 \text{ cm}^{-1}$ are strongly enhanced relative to the case in Fig. 2 and products at $\epsilon \approx 8980 \text{ cm}^{-1}$ are suppressed, etc. Tuning ω_2 or changing the laser intensities also changes the line shapes, as discussed elsewhere [14].

Integrating $A(\epsilon, q, N_k | \epsilon_i, N_i)$ over ϵ (Eq. (3)) for various ω_1 gives $P(q)$ as a function of ω_1 . The result of these computations are shown in Fig. 4 for both Na(3s) + Na(3p) (curve (a)) and Na(3s) + Na(4s) (curve (b)) channels, with $I_1 = 8.7 \times 10^9 \text{ W/cm}^2$, $I_2 = 3.51 \times 10^{10} \text{ W/cm}^2$ and $\omega_2 = 13964 \text{ cm}^{-1}$. The probability $P(q)$ is seen to oscillate strongly as a function of ω_1 . Only two periods are shown here, in which the distance between the peaks (or dips) is the

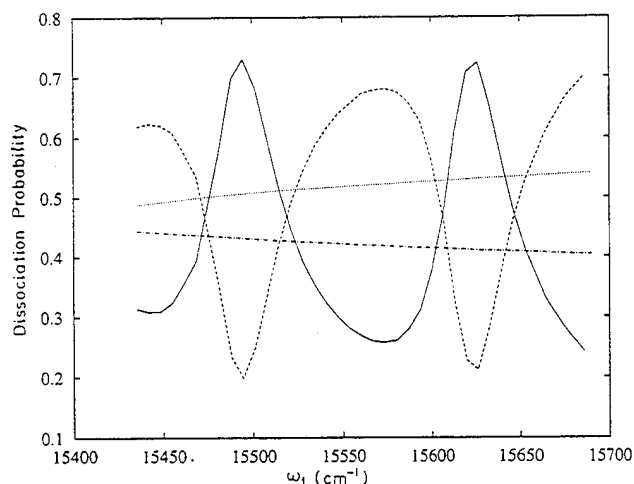


Fig. 4. Probability of forming (—) Na(3s) + Na(3p) and (---) Na(3s) + Na(4s) as a function of ω_1 , with $\omega_2 = 13964 \text{ cm}^{-1}$, $I_1 = 8.7 \times 10^9 \text{ W/cm}^2$ and $I_2 = 3.51 \times 10^{10} \text{ W/cm}^2$. Results for (— · —) Na(3s) + Na(3p) and (····) Na(3s) + Na(4s), respectively, with the ω_2 laser turned off.

vibrational spacing between $v=31$ and 32. The oscillations for the two product probabilities are out of phase with the sum being close to 0.93. Hence, for example, the probabilities of producing Na(3s) + Na(4s) and Na(3s) + Na(3p) at $\omega_1 = 15494 \text{ cm}^{-1}$ are 0.198 and 0.730, respectively. The reverse situation occurs at $\omega_1 = 15573 \text{ cm}^{-1}$ where 68% of product is Na(3s) + Na(4s). Thus varying ω_1 provides a straightforward method to control the branching ratio into final product channels. Tuning ω_2 results in a similar control [14]. These results are in sharp contrast with the essentially constant probabilities which obtain when only the ω_1 laser is on (Figs. 4c and 4d). Furthermore, and significantly, computations show that arbitrarily changing the relative phase between the ω_1 and ω_2 does not alter Figs. 2-4, indicating that the control process is independent of the relative laser phase. This is consistent with the model discussed below.

Reducing the laser power in these computations [14] shows the product probabilities oscillating with the same period as Fig. 4, but with narrower widths, indicating that this width, which measures the overlap of two resonance states, is partially determined by the power broadening.

The gross qualitative behavior seen in Figs. 2-4 can be readily understood in terms of a simple model which assumes excitation of the initial state $|1\rangle \equiv |\epsilon_i, n_1, n_2\rangle$ with laser ω_1 to the continuum $|\epsilon_q\rangle \equiv |(\epsilon, q^-), n_1-1, n_2\rangle$, which is coupled to state $|2\rangle \equiv |\epsilon_j, n_1-1, n_2+1\rangle$ by laser ω_2 ; finer details require inclusion of all bound states. If these two are the only contributing states then the photodissociation amplitude is given (Eq. (1)) by

$$\begin{aligned} \langle \epsilon_q | VG(E) | 1 \rangle &= \langle \epsilon_q | V | 1 \rangle \langle 1 | G(E) | 1 \rangle \\ &+ \langle \epsilon_q | V | 2 \rangle \langle 2 | G(E) | 1 \rangle. \end{aligned} \quad (4)$$

Substituting $E = \epsilon + (n_1-1)\hbar\omega_1 + n_2\hbar\omega_2$ into Eq. (4) and solving $(E - H_0 - V)G(E) = 1$ for the matrix elements of G , we obtain the dissociation probability

$$\begin{aligned} &|\langle \epsilon_q | VG | 1 \rangle|^2 \\ &= \left| \frac{(\epsilon - \epsilon_j - \hbar\omega_2 - \pi_{2,2}) \langle \epsilon_q | V | 1 \rangle + \langle \epsilon_q | V | 2 \rangle \pi_{2,1}}{(\epsilon - \chi_+)(\epsilon - \chi_-)} \right|^2 \end{aligned} \quad (5)$$

as a function of energy ϵ , where $\pi_{a,b}$ ($a, b=1, 2$) are optical potentials given by

$$\pi_{a,b} = \sum_q \int d\epsilon' \frac{\langle a|V|\epsilon'_q\rangle \langle \epsilon'_q|V|b\rangle}{\epsilon^+ - \epsilon'} \quad (6)$$

The energies χ_{\pm} , given by

$$2\chi_{\pm} = (\epsilon_i + \pi_{1,1} + \hbar\omega_1) + (\epsilon_j + \pi_{2,2} + \hbar\omega_2) \pm \sqrt{[(\epsilon_i + \pi_{1,1} + \hbar\omega_1) - (\epsilon_j + \pi_{2,2} + \hbar\omega_2)]^2 + 4\pi_{1,2}\pi_{2,1}} \quad (7)$$

are the eigenvalues associated with the diagonalization of the matrix coupling the two dressed states $|1\rangle$ and $|2\rangle$ via the continuum. The real and imaginary parts of $\pi_{a,a}$ give the shifts and broadenings of the two levels.

Eqs. (4)–(6) describe the photon fields by number states. Repeating the same argument using coherent states $|\alpha\rangle \equiv |\alpha_1\rangle \oplus |\alpha_2\rangle$, where $|\alpha_1\rangle$ and $|\alpha_2\rangle$ are coherent states describing the ω_1 and ω_2 fields, provides information on the role of relative laser phase. The coherent states $|\alpha_i\rangle$ ($i=1,2$) are defined in terms of the number states as $|\alpha_i\rangle = \sum_{n_i} P(\alpha_i, n_i) |n_i\rangle$, with $P(\alpha_i, n_i) = \alpha_i^{n_i} \exp(-\frac{1}{2}|\alpha_i|^2) / \sqrt{n_i!}$, where the quantities α_i can be parameterized by the average photon number \bar{n}_i and the phase ϕ_i of the ω_i laser: $\alpha_i = \sqrt{\bar{n}_i} \exp(i\phi_i)$. Replacing Eq. (4) by $\langle \epsilon, q^- | \langle \alpha | VG(E) | \epsilon_i \rangle | \alpha \rangle$, gives, within the rotating wave approximation,

$$\begin{aligned} \langle \epsilon, q^- | \langle \alpha | VG(E) | \epsilon_i \rangle | \alpha \rangle \\ = e^{i\phi_1} \langle \bar{\epsilon}_q | V | \bar{1} \rangle \langle \bar{1} | G(E) | \bar{1} \rangle \\ + e^{i\phi_2} e^{i(\phi_1 - \phi_2)} \langle \bar{\epsilon}_q | V | \bar{2} \rangle \langle \bar{2} | G(E) | \bar{1} \rangle. \end{aligned} \quad (8)$$

Here $|\bar{\epsilon}_q\rangle$, $|\bar{1}\rangle$ and $|\bar{2}\rangle$ are of the same form as $|\epsilon_q\rangle$, $|1\rangle$ and $|2\rangle$ with the argument now being the average photon numbers \bar{n}_1 and \bar{n}_2 , respectively. Because of the cancelation of the laser phase ϕ_2 in Eq. (8), the dissociation probability $|\langle \epsilon, q^- | \langle \alpha | VG(E) | \epsilon_i \rangle | \alpha \rangle|^2$ is then given by Eq. (5) with the photon numbers replace by the average photon number.

Eq. (5) shows photodissociation occurring via two pathways, $|1\rangle \rightarrow |\epsilon_q\rangle$ and $|1\rangle \rightarrow |\epsilon'_q\rangle \rightarrow |2\rangle \rightarrow |\epsilon_q\rangle$; interference between them can be constructive or destructive, depending on the relative sign of the two terms. This interference can be manipulated by varying the laser frequencies. The double peak structure seen in Figs. 2 and 3 is consistent with the form of

Eq. (5) wherein two peaks are predicted as the function of ϵ , at the two roots of the equations $\epsilon - \chi_{\pm} = 0$. For example, in the case of Fig. 2, the first double peak arises from the interaction between the dressed $v=19$ and $v=31$ levels of the $^3\Pi_u$ state whereas the decrease in photodissociation (compared to the curve (c)) in the middle of the double peak results from the destructive interference between them. A similar explanation applies to the second and third double peaks, which result mainly from the combined excitations of $v=20$ and 32 , and of $v=21$ and 33 , respectively. Note that the locations of the peaks are channel-independent but that the ratio of the heights of the peaks, given by the ratio of $|\langle \epsilon_q | V | 1 \rangle [\epsilon - \epsilon_j - \hbar\omega_2 - \pi_{2,2}] + \langle \epsilon_q | V | 2 \rangle \pi_{2,1}|^2$ evaluated at $\epsilon = \chi^+$ and χ^- , respectively, depends strongly on the laser frequencies, intensities and the channel index q . Thus Eq. (7) encompasses the channel dependence of the interference and hence the control over product probabilities.

Note also that Eq. (8) is consistent with a photodissociation amplitude wherein control of the line shape and product probabilities is independent of the relative phase of the two lasers. The absorption of an ω_2 photon contributes a phase factor $\exp(i\phi_2)$ that cancels the phase factor $\exp(-i\phi_2)$ arising by stimulated emission of the same frequency photon. This is clearly illustrated in Eq. (8) in which the second term carries an overall phase factor $\exp(i\phi_1)$, the same as the phase factor in the first term. The relative phase of the two dissociation routes, which enters the interference term, is therefore independent of both ϕ_1 and ϕ_2 .

This model fails, however, to include excitation and dissociation of neighboring vibrational states of $|\epsilon_i\rangle$ and $|\epsilon_j\rangle$. Nonetheless the computations in Figs. 2–4, which incorporate all vibrational states, clearly demonstrate the desired control. Further computations [14] which include rotations have also been performed. Inclusion of these rotational states leads to a series of multiple peak-and-dip structure in the line shape corresponding to the resonance contributions of multiple rotational states. Because of this, the dependence of the channel specific dissociation yield on ω_1 changes, but control over line shapes and product yields is still strong.

In summary, we have shown that extensive control of the line shape and the branching ratio in photodis-

sociation can be achieved by scanning the frequencies of two intense lasers and that this control is independent of the relative phase of the two laser routes.

This work was supported by the US Office of Naval Research under contract No. N00014-90-J-1014.

References

- [1] P. Brumer and M. Shapiro, *Ann. Rev. Phys. Chem.* 43 (1992) 257.
- [2] M.Yu. Ivanov, P.B. Corkum and P. Dietrich, *Laser Physics* 3 (1993) 375.
- [3] A.D. Bandrauk, J.-M. Gauthier and J.F. McCann, *Chem. Phys. Letters* 200 (1992) 399.
- [4] H.G. Muller, P.H. Bucksbaum, D.W. Schumacher and A. Zavriyev, *J. Phys. B* 23 (1990) 2761;
R.M. Potvliege and P.H.G. Smith, *J. Phys. B* 25 (1992) 2501.
- [5] K.J. Schafer and K.C. Kulander, *Phys. Rev. A* 45 (1992) 8026.
- [6] C. Chen, Y.-Y. Yin and D.S. Elliott, *Phys. Rev. Letters* 64 (1990) 507.
- [7] T. Nakajima and P. Lambropoulos, *Phys. Rev. Letters* 70 (1993) 1081.
- [8] E. Charron, A. Guisti-Suzor and F.H. Mies, *Phys. Rev. Letters* 71 (1993) 692.
- [9] P.L. Knight, M.A. Lauder and B.J. Dalton, *Phys. Rept.* 190 (1990) 1;
O. Faushder, D. Charalambidis, C. Fotakis, J. Zhang and P. Lambropoulos, *Phys. Rev. Letters* 70 (1993) 3004.
- [10] P. Brumer and M. Shapiro, *Advan. Chem. Phys.* 60 (1986) 371.
- [11] M. Shapiro, *J. Chem. Phys.* 56 (1972) 2582;
G.G. Balint-Kurti and M. Shapiro, *Advan. Chem. Phys.* 60 (1986) 403.
- [12] M. Shapiro and H. Bony, *J. Chem. Phys.* 83 (1985) 1588;
A.D. Bandrauk and O. Atabek, *Advan. Chem. Phys.* 73 (1989) 823.
- [13] I. Schmidt, Ph.D. Thesis, Kaiserslautern University (1987).
- [14] Z. Chen, M. Shapiro and P. Brumer, to be submitted.
- [15] U. Fano, *Phys. Rev.* 124 (1961) 1866.

Relative Laser Phase in the Coherent Control and Interference Control of Photodissociation Branching Ratios

PAUL BRUMER,^a ZHIDANG CHEN,^a AND MOSHE SHAPIRO^{b,*}

^aChemical Physics Theory Group, Department of Chemistry, University of Toronto, Toronto, M5S 1A1 Canada

^bDepartment of Chemical Physics, The Weizmann Institute of Science, Rehovot 76100, Israel

(Received 25 January 1994)

Abstract. Product properties in molecular photodissociation can be controlled by simultaneous excitation through a number of coherent excitation routes. Examples of simplified methods for maintaining laser phase coherence of the multiple routes, required for control, are described. Of particular interest is a new high field approach where multiple paths are generated in such a manner as to make relatively coherent lasers unnecessary.

1. INTRODUCTION

Control over the yield of chemical reactions is the essence of practical chemistry, and the ability to use lasers to achieve this goal is one primary thrust within modern Chemical Physics. The theory of coherent radiative control of chemical reactions¹ affords a direct method for controlling isolated molecule reaction dynamics using phase properties of lasers, with a large range of yield control expected in laboratory scenarios. In addition, the theory of coherent control provides deep insights into the essential features of reaction dynamics and quantum interference, which are necessary to achieve control over elementary chemical processes.

Coherent radiative control relies upon the fundamental quantum mechanical principle that multiple coherent (i.e., phase-preserving) pathways to the same final state interfere with one another. In our case, the final state is a continuum system at energy E with a number of open arrangement channels (e.g., a molecule in the dissociative continuum), and the independent pathways correspond to excitation via distinct coherent optical excitation routes. By judicious choice of these pathways we are able to control the interference from within the laboratory and hence control the outcome of the molecular processes.

Reliance upon quantum interference effects necessitates that the *relative* phase of the multiple excitation routes be well defined. This can be difficult to achieve

when the two routes require independent light sources. In this paper we focus on two methods to simplify the problem of maintaining the laser-induced component of the relative phase. In doing so we emphasize some of the essential characteristics of coherent control, display results on photodissociation of Na_2 , and introduce a new frequency-based control scenario.

This paper is structured as follows: the role of the relative phase in coherent control is introduced, in section 2, via a resonant 2-photon vs. 2-photon absorption scenario. In addition to providing a means of controlling reactions in a thermal environment, this approach advocates the use of nonlinear optics techniques to prepare light sources whose relative phase is easily maintained. Section 3 introduces a new high field scheme where the second route is a self-cancelling phase route in the molecule. Under these circumstances, we are able to show that the two external laser fields need not be relatively coherent and that the relative *frequency* is a useful control variable. We term this behavior "interference control", rather than coherent control, to emphasize these aspects of the control scenario.

In this paper we focus on the dissociation of diatomic molecules, although the theory is essentially identical for polyatomic systems. Computational results on control in Na_2 photodissociation are used throughout.

*Author to whom correspondence should be addressed.

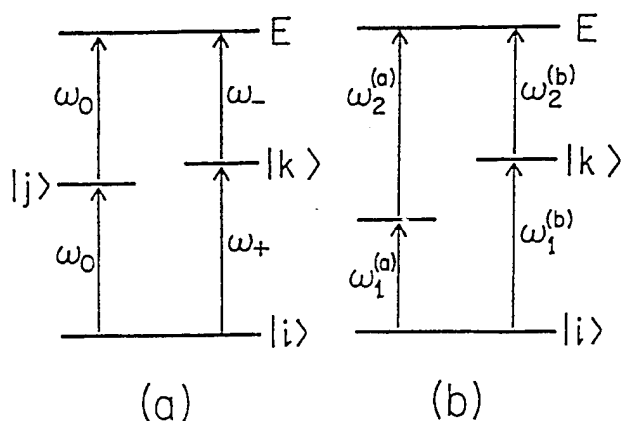


Fig. 1. Schematic of resonant 2-photon vs. 2-photon control scenarios using: (a) three frequencies; (b) four frequencies. Here $|i\rangle$ denotes the initial system bound state and $|j\rangle$ and $|k\rangle$ are molecular bound states which are optically accessible from $|i\rangle$. Energy E is in the continuum from which several product states are accessible.

2. COHERENT CONTROL: RESONANT 2-PHOTON VS. 2-PHOTON EXCITATION

Consider irradiating a molecule which is in a bound eigenstate i with three interrelated excitation frequencies ω_0 , ω_+ , and ω_- . Here $2\hbar\omega_0 = \hbar(\omega_+ + \omega_-)$ is sufficiently energetic to excite the molecule to energy E in the dissociative continuum. If $\hbar\omega_+$ and $\hbar\omega_0$ are each chosen resonant with a bound-bound molecular transition emanating from $|i\rangle$, then the two simultaneous resonant two-photon processes shown in Fig. 1a occur (as do several other transitions). The two optical excitation paths shown in Fig. 1a interfere and allow for control of the photodissociation yield, as described below.

Resonant 2-Photon Dissociation

Consider first² photodissociation via one 2-photon pathway with generic frequencies ω_1 , ω_2 . The molecule assumed initially in an eigenstate, $|i\rangle = |E_i, J_i, M_i\rangle$ of the molecular Hamiltonian H_M , total angular momentum J and its z -projection with eigenvalues E_i, J_i, M_i photodissociates, under excitation, to a number of different product channels labeled by q . Absorption of the first photon of frequency ω_1 lifts the system to a region close to an intermediate bound state $|m\rangle = |E_m, J_m, M_m\rangle$, and a second photon of frequency ω_2 carries the system to the dissociating states $|E, \mathbf{k}, q\rangle$. These continuum states are of energy E , and correlate with the product in arrangement channel q which scatter into angles $\mathbf{k} = (\theta_k, \phi_k)$. Here the J 's are the angular momentum, M 's are their projection along the z -axis, and the values of bound state energy, E_i and E_m , include specification of the vibrational quantum numbers. Photon states of the incident lasers are described by the coherent states which contain phase infor-

mation about the laser modes. Specifically, if we denote the phases of the coherent states of the laser modes by ϕ_1 and ϕ_2 , the wave vectors by \mathbf{k}_1 and \mathbf{k}_2 with overall phases

$$\theta_1 = \mathbf{k}_1 \cdot \mathbf{r} + \phi_1, \quad \theta_2 = \mathbf{k}_2 \cdot \mathbf{r} + \phi_2 \quad (1)$$

and the electric field amplitudes by ϵ_1 and ϵ_2 , then the probability amplitude for resonant 2-photon photodissociation by $(\omega_1 + \omega_2)$ is given² by

$$\begin{aligned} T_{kq,i}(E, E_i, J_i, M_i, \omega_2, \omega_1) \\ = \sum_{E_m, J_m} \frac{\langle E, \mathbf{k}, q | d_2 \epsilon_2 | E_m, J_m, M_m \rangle \langle E_m, J_m, M_m | d_1 \epsilon_1 | E_i, J_i, M_i \rangle}{\hbar\omega_1 - (E_m + \Delta_m - E_i) + i\Gamma_m/\hbar} \\ \times \exp[i(\theta_1 + \theta_2)] \\ = \sqrt{\frac{2\mu k_q}{\hbar}} \sum_{\lambda, 0 \leq J} \sum_J \begin{pmatrix} J & 1 & J_m \\ -M & 0 & M \end{pmatrix} \begin{pmatrix} J_m & 1 & J_i \\ -M & 0 & M \end{pmatrix} \\ \times \sqrt{2J+1} D_{\lambda, M_i}^{J, p}(\phi_k, \theta_k, 0) t(E, E_i, J_i, \omega_2, \omega_1, q | J, p, \lambda, E_m, J_m) \\ \times \exp[i(\theta_1 + \theta_2)] \end{aligned} \quad (2)$$

Here d_i is the component of the dipole moment along the electric-field vector of the i^{th} laser mode, $E = E_i + (\omega_1 + \omega_2)$, Δ_m and Γ_m are respectively the radiative shift and width of the intermediate state, μ is the reduced mass, and k_q is the relative momentum of the dissociated product in q -channel. The $D_{\lambda, M_i}^{J, p}$ is the parity adapted rotation matrix,³ with λ being the magnitude of the projection on the internuclear axis of the electronic angular momentum and $(-1)^p$ the parity of the rotation matrix. We have assumed for simplicity that the lasers are linearly-polarized and that their electric-field vectors are parallel. The second step in eq 2 comes from the usual procedure of expanding the molecular wave functions in partial waves followed by the integration over rotational wave functions. Given eq 2, the probability of photodissociation is given by:

$$\begin{aligned} P^{q,i}(E, E_i, J_i; \omega_2, \omega_1) \\ = \frac{1}{2J_i+1} \sum_{M_i} P^{q,i}(E, E_i, J_i, M_i; \omega_2, \omega_1) \\ = \frac{1}{2J_i+1} \sum_{M_i} \int d\mathbf{k} |T_{kq,i}(E, E_i, J_i, M_i, \omega_2, \omega_1)|^2 \\ = \frac{8\pi\mu k_q}{(2J_i+1)\hbar^2} \sum_{M_i, J, p, \lambda \geq 0} \left| \sum_{E_m, J_m} \begin{pmatrix} J & 1 & J_m \\ -M_i & 0 & M_i \end{pmatrix} \begin{pmatrix} J_m & 1 & J_i \\ -M_i & 0 & M_i \end{pmatrix} \right. \\ \left. \times t(E, E_i, J_i, \omega_2, \omega_1, q | J, p, \lambda, E_m, J_m) \right|^2 \end{aligned} \quad (3)$$

where we have averaged over M_i since no initial M_i selection is assumed.

The essence of the photodissociation lies in the molecular 2-photon t -matrix element whose structure has

been analyzed in detail elsewhere.² Note that the T -matrix element in eq 2 is a complex quantity, whose phase is the sum of the laser phase $\theta_1 + \theta_2$ and the molecular phase, i.e., the phase of t . Methods for computing these matrix elements for Na_2 involving the fourteen electronic states shown in Fig. 2, are discussed elsewhere.²

Finally, note that only the levels closest to the resonance $\hbar\omega_1 = (E_m + \Delta_m - E_i)$ contribute significantly to the dissociation probability. This feature is enormously useful in the case of excitation from a thermal bath. That is, *it allows us to selectively photodissociate molecules from a thermal bath, reestablishing coherence necessary for quantum interference based control.*

Below, we utilize these methods to compute the required amplitudes for coherent control in Na_2 .

Coherent Control via Resonant 2-Photon vs. 2-Photon Interference

Consider now irradiating a molecule in state $|i\rangle = |E_i, J_i, M_i\rangle$ with several frequencies which induce independent simultaneous two-photon resonant transitions.⁴ A typical general case (see Fig. 1b) involves excitation with four different photon frequencies, $\omega_1^{(a)}$, $\omega_2^{(a)}$, $\omega_1^{(b)}$, and $\omega_2^{(b)}$, where $\omega_1^{(a)}$ and $\omega_1^{(b)}$ are resonant with intermediate bound states $|j\rangle$ and $|k\rangle$, where $\hbar(\omega_1^{(a)} + \omega_2^{(a)}) =$

$\hbar(\omega_1^{(b)} + \omega_2^{(b)})$, and where the excitation is sufficiently energetic to lead to dissociation. Under these conditions there are at least two independent paths to the same final state, which we denote "a" and "b". Path a consists of $(\omega_1^{(a)} + \omega_2^{(a)})$ excitation, and path b of excitation with $(\omega_1^{(b)} + \omega_2^{(b)})$. The photodissociation probability is then

$$P^{(q)}(E, E_i, J_i | \omega_2^{(a)}, \omega_1^{(a)}; \omega_2^{(b)}, \omega_1^{(b)}) \\ \equiv \frac{1}{2J_i+1} \sum_{M_i} \int d\mathbf{k} |T_{kq,i}(E, E_i, J_i, M_i, \omega_2^{(a)}, \omega_1^{(a)}) \\ + T_{kq,i}(E, E_i, J_i, M_i, \omega_2^{(b)}, \omega_1^{(b)})|^2 \quad (4)$$

where $E = E_i + \hbar(\omega_2^{(a)} + \omega_1^{(a)})$. Since no M -selection prior to laser excitation is assumed, we have averaged over the quantum number M_i . The right-hand side is the sum of three terms: two independent photodissociation probabilities from each of the two paths, and interference between them.

For the sake of simplicity, consider the simpler three color case (Fig. 1a) where $\omega_1^{(a)} + \omega_2^{(a)} = \omega_0$ and denote $\omega_1^{(b)} = \omega_+$ and $\omega_2^{(b)} = \omega_-$.

The overall phase of the three laser fields are

$$\theta_0 = \mathbf{k}_0 \cdot \mathbf{r} + \phi_0, \theta_+ = \mathbf{k}_+ \cdot \mathbf{r} + \phi_+, \text{ and } \theta_- = \mathbf{k}_- \cdot \mathbf{r} + \phi_- \quad (5)$$

where ϕ_0 , ϕ_+ , and ϕ_- are the photon phases. Here \mathbf{k}_0 , \mathbf{k}_+ , and \mathbf{k}_- are the wave vectors of the laser modes ω_0 , ω_+ , and ω_- , whose electric field strengths are ϵ_0 , ϵ_+ , ϵ_- and intensities are I_0 , I_+ , I_- . Photodissociation occurs at $E = E_i + 2\hbar\omega_0 = E_i + \hbar(\omega_+ + \omega_-)$, where ω_0 and ω_+ are chosen resonant with intermediate bound state levels. Applying eq 4, we write the probability of photodissociation from pathway "a" ($\omega_0 + \omega_0$) and pathway "b" ($\omega_+ + \omega_-$) as

$$P^{(q)}(E, E_i, J_i; a, b) \equiv P^{(q)}(E, E_i, J_i | \omega_0, \omega_0; \omega_+, \omega_-) \\ = P^{(q)}(a) + P^{(q)}(b) + P^{(q)}(ab) \quad (6)$$

Here, $P^{(q)}(a)$ and $P^{(q)}(b)$ are the independent photodissociation probabilities associated with routes a and b ,

$$P^{(q)}(a) \equiv P^{(q)}(E, E_i, J_i; \omega_0, \omega_0) \quad (7)$$

$$P^{(q)}(b) \equiv P^{(q)}(E, E_i, J_i; \omega_+, \omega_-) \quad (8)$$

with the right-hand sides defined as in eq 3, and $P^{(q)}(ab)$ is the interference term between them, discussed below. Note that the paths a and b in eq 6 are associated with different lasers and as such contain different laser phases.

The optical path-path interference term $P^{(q)}(ab)$ is expressed by

$$P^{(q)}(ab) = 2|F^{(q)}(ab)| \cos(\alpha_a^q - \alpha_b^q) \quad (9)$$

where the relative phase $(\alpha_a^q - \alpha_b^q)$ between the two paths has two contributions:

$$\alpha_a^q - \alpha_b^q = (\delta_a^q - \delta_b^q) + \delta\theta, \delta\theta = 2\theta_0 - \theta_+ - \theta_- \quad (10)$$

Here $\delta\theta$ is the relative laser phases between the two

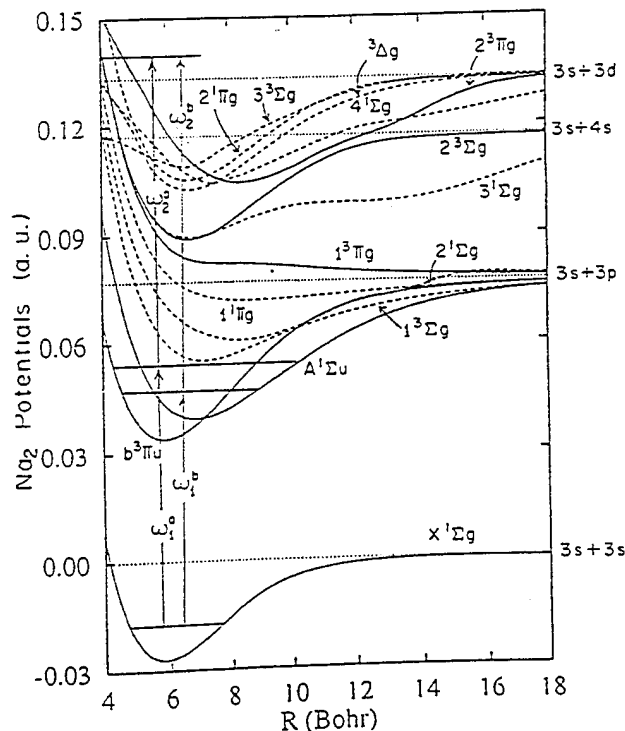


Fig. 2. Fourteen Na_2 potential energy curves involved in the photodissociation computation. Arrows indicate typical conditions for the resonant 2-photon vs. 2-photon coherent control scenario.

paths and $(\delta_a^q - \delta_b^q)$ is the "molecular phase". The latter term, along with the amplitude $|F^{(q)}(ab)|$, is defined through the identity

$$\begin{aligned} & |F^{(q)}(ab)| \exp[i(\delta_a^q - \delta_b^q)] \\ &= \frac{8\pi\mu k_q}{(2J_i+1)\hbar^2} \sum_{M_i, J_i, p, \lambda} \sum_{E_m} \sum_{J_m} \begin{pmatrix} J & 1 & J_m \\ -M_i & 0 & M_i \end{pmatrix} \\ & \times \begin{pmatrix} J_m & 1 & J_i \\ -M_i & 0 & M_i \end{pmatrix} \begin{pmatrix} J & 1 & J'_m \\ -M_i & 0 & M'_i \end{pmatrix} \begin{pmatrix} J'_m & 1 & J_i \\ -M'_i & 0 & M_i \end{pmatrix} \\ & \times t(E, E_i, J_i, \omega_0, \omega_+, q | Jp\lambda, E_m, J_m) \\ & \times t^*(E, E_i, J_i, \omega_-, \omega_+, q | Jp\lambda, E'_m, J'_m) \quad (11) \end{aligned}$$

Equation 6 embodies the essential principles of coherent control. That is, the reaction probability into channel q is given by contributions from the two direct routes, plus an interference term between them. It is worthwhile emphasizing that the interference term can be of either positive or negative sign, enhancing or reducing the probability of product formation in the product channel q . Both the direct and interference terms depend on the laboratory parameters; in this particular case on the laser intensities and relative laser phase $\delta\theta$. Hence by varying these laser characteristics in the laboratory we gain direct control over the quantum interference term and hence over the probability and yield of the reaction.

The probability of product in the q -channel is actually the sum of $P^{(q)}(E, E_i, J_i; a, b)$ at energy $E = E_i + 2\hbar\omega_0$ (eq 6) and background terms $B^{(q)}$ which correspond to contributions of resonant photodissociation routes to energies other than E , and hence⁵ to terms which do not coherently interfere with the a and b pathways. In particular, $B^{(q)}$ corresponds to absorption of $(\omega_0 + \omega_-)$, $(\omega_0 + \omega_+)$, $(\omega_+ + \omega_0)$, or $(\omega_+ + \omega_-)$, leading to photodissociation at energies $E_- = E_i + \hbar(\omega_0 + \omega_-)$, $E_+ = E_i + \hbar(\omega_0 + \omega_+)$, and $E_{++} = E_i + \hbar(\omega_0 + \omega_-)$, respectively.

The actual quantity of interest for reactivity control is the branching ratio of the product in q -channel to that in q' -channel, denoted by $R_{qq'}$ (there is little interest in enhancing probabilities in both channels since this can be achieved by other simpler techniques, e.g., by raising laser power, and this does not necessarily enhance reaction selectivity). In the weak field case $P^{(q)}(a)$ is proportional to ϵ_0^4 , $P^{(q)}(b)$ to $\epsilon_+^2 \epsilon_-^2$, and $P^{(q)}(ab)$ to $\epsilon_0^2 \epsilon_+ \epsilon_-$, so that we can write the branching ratio

$$\begin{aligned} R_{qq'} &= \frac{P^{(q)}(E, E_i, J_i; a, b) + B^{(q)}}{P^{(q')}(E, E_i, J_i; a, b) + B^{(q')}} \\ &= \frac{\epsilon_0^4 \mu_{aa}^{(q)} + \epsilon_+^2 \epsilon_-^2 \mu_{bb}^{(q)} + 2\epsilon_0^2 \epsilon_+ \epsilon_- |\mu_{ab}^{(q)}| \cos(\alpha_a^q - \alpha_b^q) + B^{(q)}}{\epsilon_0^4 \mu_{aa}^{(q')} + \epsilon_+^2 \epsilon_-^2 \mu_{bb}^{(q')} + 2\epsilon_0^2 \epsilon_+ \epsilon_- |\mu_{ab}^{(q')}| \cos(\alpha_a^{q'} - \alpha_b^{q'}) + B^{(q')}} \quad (12) \end{aligned}$$

where $\mu_{aa}^{(q)} = P^{(q)}(a)/\epsilon_0^4$, $\mu_{bb}^{(q)} = P^{(q)}(b)/\epsilon_+^2 \epsilon_-^2$, and $|\mu_{ab}^{(q)}| = |F^{(q)}(ab)|/(\epsilon_0^2 \epsilon_+ \epsilon_-)$. The terms $B^{(q)}$ and $B^{(q')}$ are independent of the relative laser phase $\delta\theta$, and can be minimized by appropriate choice of laser parameters, as discussed elsewhere.⁴ Here we just emphasize that the product ratio in eq 12 depends upon both the laser intensities and the relative laser phase. Hence manipulating these laboratory parameters allows for control over the relative cross section between channels.

Typical control results for the three-frequency arrangement (Fig. 1a) have been previously published⁴ in both the energy regime where photodissociation yields two products [Na(3p) + Na(3s), and Na(3s) + Na(4s)] as well as three products [Na(3p) + Na(3s), Na(3s) + Na(4s), and Na(3s) + Na(3d)]. Typical control results show that the range of yield control is extensive, with yields varying, for example, over a range of 50% with changes in laser parameters. Fewer control results with the four-frequency arrangement (Fig. 1b) have been published, but the control range is similar.

The typical structure of the control plot is shown in Fig. 3 for the four-field case where we display contours of constant product fraction in a given channel vs. $\delta\theta$ and x . Here $x = \epsilon_+^{(b)} \epsilon_-^{(b)} / \epsilon_+^{(a)} \epsilon_-^{(a)}$, i.e., x is the ratio of the product of laser amplitudes in the two pathways. The frequencies chosen correspond to $\omega_1^{(a)} = 17,737 \text{ cm}^{-1}$, $\omega_2^{(a)} = 16,774 \text{ cm}^{-1}$, $\omega_1^{(b)} = 18,004 \text{ cm}^{-1}$, $\omega_2^{(b)} = 16,507 \text{ cm}^{-1}$. Na₂ is initially in the sixth vibrational level ($v_i = 5$) of the ground electronic state. These frequencies induce resonant excitation from $v_i = 5$ (via $\omega_1^{(a)}$) to $v_m = 38$ of the $A^1 \Sigma_u^+$ electronic state, and (via $\omega_1^{(b)}$) to $v_m = 41$ of the same electronic state.

Figure 3 makes clear that there is substantial variation of the product yield as a function of the relative laser phase $\delta\theta$. At constant x , this is due solely to quantum interference which alters the cross term between the two optical excitation pathways.

The range of control shown in Fig. 3 is substantial, but larger variations [e.g., a range of 15% yield to 95% yield of Na(3s) + Na(3d)] have been seen with other parameter choices.⁴ Comparisons of this kind are important to gain an appreciation of the dependence of control on laser parameters.

3. LABORATORY STABILIZATION OF THE RELATIVE PHASE

Figure 1 and the associated eqs 6–10 provide an example of one coherent control scenario. Reliance upon the laboratory-controllable relative phase $\delta\theta$ is paramount. Under ideal circumstances, $\delta\theta$ is entirely within the control of the experimentalist. However, in actuality the laser phase can drift and jitter, reducing the range of control. Small uncontrolled relative phase fluctuations,

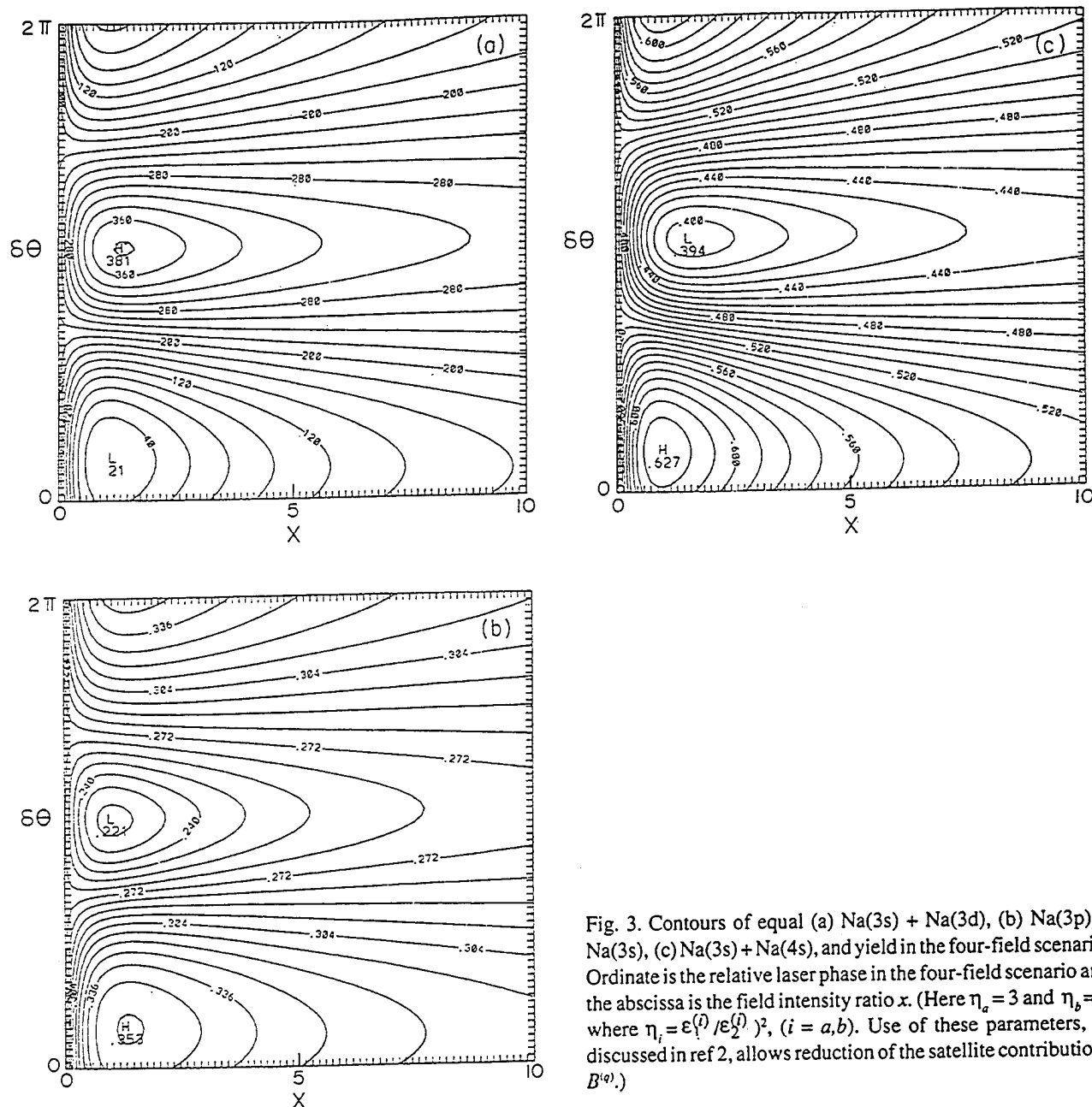


Fig. 3. Contours of equal (a) Na(3s) + Na(3d), (b) Na(3p) + Na(3s), (c) Na(3s) + Na(4s), and yield in the four-field scenario. Ordinate is the relative laser phase in the four-field scenario and the abscissa is the field intensity ratio x . (Here $\eta_a = 3$ and $\eta_b = 1$ where $\eta_i = \epsilon_i^{(i)} / \epsilon_2^{(i)2}$, ($i = a, b$). Use of these parameters, as discussed in ref 2, allows reduction of the satellite contributions $B^{(q)}$.)

say, due to difficulties in sustaining a stable laser phase in one of the sources, act to reduce the range of possible control. Indeed if the relative phase varies extensively, then $\cos(\alpha_a^q - \alpha_b^q)$, and hence $P^{(q)}(ab)$, approaches zero. Control is then lost. Laboratory methods for attaining relatively stable relative phases are therefore necessary; several examples are discussed in this section.

Consider first the nature of the relative laser phase $\delta\theta = 2\theta_0 - \theta_+ - \theta_-$ (eq 10) which embodies a generally useful rule. That is, consider any laser excitation pathway consisting of a number of steps involving energy absorption from fields with phase $\theta_i^{(abs)}$ and stimulated emission induced by fields with phase $\theta_j^{(em)}$. Then, in accord with perturbation theory, the overall laser phase associated

with that route⁶ is $\Theta = -\sum_i \theta_i^{(abs)} + \sum_j \theta_j^{(em)}$. For example, in the case of Fig. 1a, one route acquires phase $-2\theta_0$ through 2-photon absorption of $\hbar\omega_0$ and the second acquires the phase $(-\theta_+ - \theta_-)$ from absorption of $\hbar\omega_+$ and $\hbar\omega_-$. The difference in the phase of these two routes is then $\delta\theta$, the quantity appearing in eq 10.

Nonlinear optical techniques can be used to minimize uncontrolled variations in the relative phase due to laser jitter. Specifically, consider generating $\omega_+ = \omega_0 + \epsilon$ and $\omega_- = \omega_0 - \epsilon$ in a parametric process by passing a beam of frequency $2\omega_0$ through a nonlinear crystal. This latter beam is assumed generated by second harmonic generation from the laser ω_0 with the phase θ_0 . Then⁷ the quantity $\delta\theta = 2\theta_0 - \theta_+ - \theta_-$ is a constant. That is, in this particular

approach all frequencies emanate from a single original frequency ω_0 , and fluctuations arising from θ_0 cancel between the two sources. *In this fashion the 2-photon plus 2-photon scenario is made insensitive to the laser jitter of the incident laser fields.*

Such considerations of laser phase are quite general and allow development of specific nonlinear optics schemes appropriate to a given scenario. Consider, as a second example, an early coherent control scenario.⁸ There we considered a molecule in an initial superposition of two bound states, $|E_i\rangle$, $|E_j\rangle$ of energies E_i and E_j . The superposition state was then irradiated with two laser frequencies $\omega_3 = (E - E_i)/\hbar$ and $\omega_4 = (E - E_j)/\hbar$ which lift $|E_j\rangle$ and $|E_i\rangle$, respectively, to the dissociative continuum at energy E . Interference between the photodissociation of $|E_i\rangle$ and $|E_j\rangle$ by the two laser fields allows for coherent control over the final products at energy E .

Once again the relative laser phase $\theta_4 - \theta_3$ is a control parameter, where θ_k is the phase of the field of frequency ω_k . Consider then the following approach (see Fig. 4) which allows for preparation of the initial superposition state and subsequent dissociation so that the relative laser phase is insensitive to drift and jitter of the excitation sources.

Let a portion of a CW laser source at energy $\hbar\omega_0$ pump two dye lasers which in turn generate frequencies ω_1 and ω_2 . ω_1 and ω_2 are then each mixed with ω_0 in two nonlinear crystals, to produce two new frequencies, $\omega_4 = \omega_0 + \omega_1$ and $\omega_3 = \omega_0 + \omega_2$. The net result of this procedure is four working frequencies: ω_k , $k = 1, \dots, 4$ with phases θ_k , $k = 1, \dots, 4$. Further, the phases θ_3 and θ_4 are $\theta_3 = \theta_0 + \theta_2$ and $\theta_4 = \theta_0 + \theta_1$, respectively, due to the nature of their

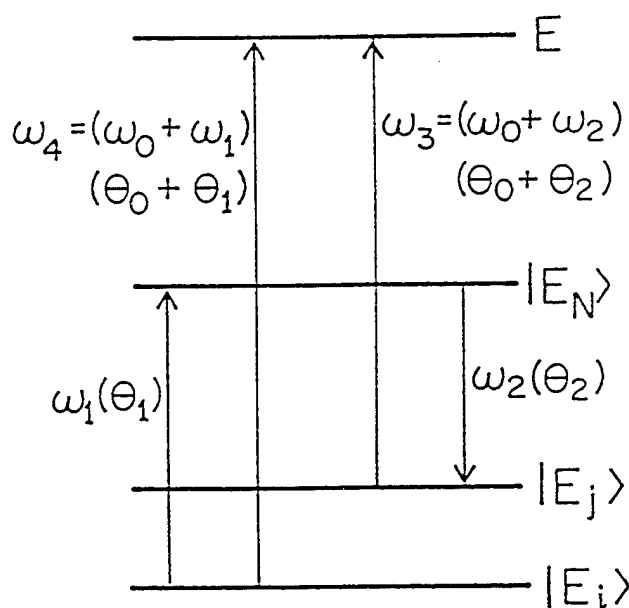


Fig. 4. Schematic of preparation and dissociation of a coherent superposition of bound states $|E_j\rangle$ and $|E_i\rangle$, which results in cancellation of the relative phase of the two dissociation routes.

preparation.

Consider now irradiating the molecule, initially in state $|E_i\rangle$, with the four fields (Fig. 4). The sequence of absorption and stimulated emission ω_1 followed by ω_2 produces a superposition of $|E_i\rangle$ and $|E_j\rangle$ which is subsequently dissociated by ω_3 and ω_4 . If the initial phase of $|E_i\rangle$ is χ , then the resultant phase of $|E_j\rangle$, prior to excitation to dissociation, is $\chi - \theta_1 + \theta_2$, in accord with the rules discussed above. Path *a* to dissociation, excitation of $|E_j\rangle$ by ω_4 , acquires the overall phase $\chi - \theta_4 = \chi - \theta_0 - \theta_1$. Similarly, path *b*, excitation of $|E_i\rangle$ by ω_3 , gives a phase $(\chi - \theta_1 + \theta_2) - \theta_3 = (\chi - \theta_1 + \theta_2) - (\theta_0 + \theta_2) = \chi - \theta_0 - \theta_1$. Hence, both pathways acquire the same laser phase so that the difference in phase between paths *a* and *b*, upon which the control depends, is now zero! A phase difference between the two routes is then easily added by, e.g., delaying one frequency relative to the others. Thus, this overall arrangement leads to a relative phase which is insensitive to the phase jitter and drift of the sources. Computations on this scenario¹⁰ for Na_2 photodissociation show extensive yield control.

Both these examples utilize rather detailed nonlinear optical schemes to successfully eliminate experimental problems associated with phase fluctuations in the light sources. The result is a relatively sophisticated preparation of the optical frequencies. However, the relatively straightforward "phase rule" discussed above does, however, suggest a new and simple approach to quantum-based control which does not use the phase as a control parameter at all. This is discussed in the next section.

4. INTERFERENCE CONTROL: TWO-FREQUENCY CONTROL OF PHOTODISSOCIATION YIELDS

The proposed scenario¹¹ is depicted in Fig. 5a. A CW laser of frequency ω_1 excites a molecule from an initially

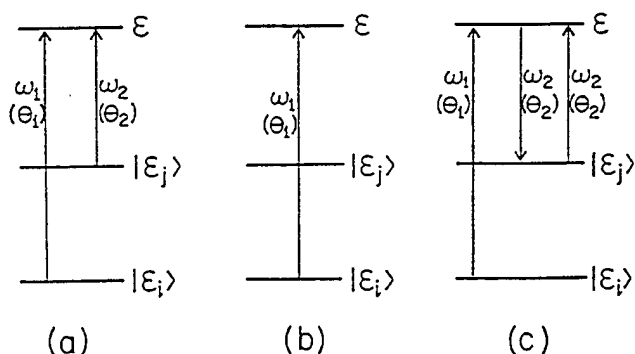


Fig. 5. (a) Schematic of incoherent frequency control scenario. Here $|E_i\rangle$ is an initially populated bound state and $|E_j\rangle$ is an initially unpopulated bound state which is coupled to the continuum at energy ϵ by a laser of frequency ω_2 . (b) 1-photon pathway inherent in panel a. (c) 3-photon pathway inherent in panel a.

populated bound state $|e_i\rangle$ to the dissociation continuum $|\epsilon, \mathbf{m}, q^-\rangle$ at energy ϵ (where \mathbf{m} specifies the product quantum numbers and q labels the product arrangement channel), while a second intense laser, of frequency ω_2 , simultaneously couples the continuum to bound states $|e_j\rangle$ that are initially devoid of population. In the simplest picture, with both lasers on, dissociation to $|\epsilon, \mathbf{m}, q^-\rangle$ occurs via direct and indirect dissociation paths, $|e_i\rangle \rightarrow |\epsilon, \mathbf{m}, q^-\rangle$ and $|e_i\rangle \rightarrow |\epsilon, \mathbf{m}', q^-\rangle \rightarrow |e_j\rangle \rightarrow |\epsilon, \mathbf{m}, q^-\rangle$, as shown in Fig. 5b,c. Contributions from these pathways to the probability of dissociation into a given channel q at product energy ϵ interfere either constructively or destructively.

Consider now the expected behavior of the relative phase of the two pathways. Here we make an argument based upon perturbation theory, which is substantiated by a full field model¹¹ below and by exact computation. In accord with the perturbation theory argument of Section 2, if θ_i denotes the phase of the field of frequency ω_i , then the pathway in Fig. 5b imparts the laser phase $-\theta_i$ to path a . Similarly, the phase imparted in the Fig. 5c pathway is $-\theta_1 + \theta_2 - \theta_2 = -\theta_1$. Thus the relative phase of the two paths is zero, a consequence of the internal cancellation of the θ_2 phase in the absorption and stimulated emission step. The resultant scenario is therefore totally insensitive to the phase jitter or drift of either laser. Further, unlike the scenarios above, one can not add an additional phase to one pathway which does not appear in the other pathway. Hence variation of phase is no longer a useful control parameter. Further note that if the fields are weak then the three-photon pathway will only be significant when $\omega_2 = (\epsilon - \epsilon_j)/\hbar$, i.e., on resonance. Thus in the weak field limit varying frequency does not afford a means of control. Below we show, however, that using stronger fields allows highly efficient yield control with variation of the frequencies ω_1 and ω_2 .

To introduce notation and the computational method, consider the photodissociation of a molecule with Hamiltonian H_M in the presence of a radiation field with Hamiltonian H_R . The total Hamiltonian $H = H_M + H_R + V$, where V is the molecule-field interaction. The radiation field is described by Fock states $|n_k\rangle$ with energy $n_k \hbar \omega_k$. (In the case of several frequencies, the repeated index in $n_k \omega_k$ implies the sum over the modes.) Eigenstates of H_M include bound states $|e_n\rangle$ and dissociative continuum states $|\epsilon, \mathbf{m}, q^-\rangle$. The latter correlate at large internuclear distances with states of the product in channel q with energy ϵ and quantum numbers \mathbf{m} . In general, \mathbf{m} includes the scattering direction $\hat{\mathbf{k}}$.

Photodissociation dynamics is completely embodied¹² in the fully interacting eigenstates of the total Hamiltonian H , denoted $|\langle \epsilon, \mathbf{m}, q^-, n_k^- \rangle| [H |\langle \epsilon, \mathbf{m}, q^-, n_k^- \rangle| = (\epsilon + n_k \hbar \omega_k) |\langle \epsilon, \mathbf{m}, q^-, n_k^- \rangle|]$, where the minus superscript on n_k

indicates that $|\langle \epsilon, \mathbf{m}, q^-, n_k^- \rangle|$ becomes the noninteracting state $|\langle \epsilon, \mathbf{m}, q^-, n_k \rangle| \equiv |\langle \epsilon, \mathbf{m}, q^- \rangle| |n_k\rangle$ when V is switched off. If the system is initially in the state $|\epsilon_i, n_i\rangle \equiv |e_i\rangle |n_i\rangle$ and the radiation field is switched on suddenly, then the photodissociation amplitude to form the product state $|\epsilon, \mathbf{m}, q^-\rangle |n_k\rangle$ is given by¹² $\langle \langle \epsilon, \mathbf{m}, q^-, n_k^- | \epsilon_i, n_i \rangle \rangle$. Since $\langle \langle \epsilon, \mathbf{m}, q^-, n_k^- | \epsilon_i, n_i \rangle \rangle = 0$, this overlap assumes the convenient form

$$\langle \langle \epsilon, \mathbf{m}, q^-, n_k^- | \epsilon_i, n_i \rangle \rangle = \langle \langle \epsilon, \mathbf{m}, q^-, n_k^- | VG(\epsilon^* + n_k \hbar \omega_k) | \epsilon_i, n_i \rangle \rangle \quad (13)$$

by using the Lippmann-Schwinger equation $\langle \langle \epsilon, \mathbf{m}, q^-, n_k^- | = \langle \langle \epsilon, \mathbf{m}, q^-, n_k^- | + \langle \langle \epsilon, \mathbf{m}, q^-, n_k^- | VG(\epsilon^* + n_k \hbar \omega_k)$. Here $G(E) = 1/(E - H)$ and $\epsilon^* = \epsilon + i\delta$, with $\delta \rightarrow 0^+$ at the end of the computation. Equation 13 is exact and provides a connection between the photodissociation amplitude and the VG matrix element. It is the latter which we compute exactly using a high field extension of the artificial channel method.¹³

Two quantities are of interest: the channel specific line shape, that is

$$A(\epsilon, q, n_k | \epsilon_i, n_i) = \int d\hat{\mathbf{k}} |\langle \langle \epsilon, \hat{\mathbf{k}}, q^-, n_k^- | \epsilon_i, n_i \rangle \rangle|^2 \quad (14)$$

as a function of energy ϵ , and the total dissociation probability to channel q

$$P(q) = \sum_{n_k} \int d\epsilon A(\epsilon, q, n_k | \epsilon_i, n_i) \quad (15)$$

where the sum is over photons that excite the molecule above the dissociation threshold. In writing eq 14 diatomic dissociation is assumed, so that $\mathbf{m} = \hat{\mathbf{k}}$.

To demonstrate the control scenario, consider photodissociation of Na_2 from the initial state $|e_i\rangle$ with vibrational quantum number $v_i=18$ of the ${}^3\Pi_u$ electronic state, assumed prepared by excitation from the ground electronic state. Excitations from $|e_i\rangle$ by ω_1 and from initially empty $|e_j\rangle$ by ω_2 arrive at the dissociating continua, producing $\text{Na}(3s) + \text{Na}(3p)$ and $\text{Na}(3s) + \text{Na}(4s)$. Computations were done with a range of ω_1 with intensity I_1 which is sufficiently energetic to dissociate levels of the ${}^3\Pi_u$ state with $v \geq 18$ to both $\text{Na}(3s) + \text{Na}(3p)$ and $\text{Na}(3s) + \text{Na}(4s)$. The second laser has fixed frequency $\omega_2 = 13,964 \text{ cm}^{-1}$ and intensity $I_2 = 3.51 \times 10^{10} \text{ W/cm}^2$, and can dissociate levels with $v \geq 31$ to both products. Under these circumstances the dissociation from above threshold dissociation is found to be negligible. In the computations we also include contributions from the dissociation of $|e_i\rangle$ by ω_2 and of $|e_j\rangle$ by ω_1 , which cannot be controlled by the interference effects discussed here, but are minimized under these circumstances. Results shown here are typical of those obtained in a broader class of computations which we have carried out. Studies which include rotations describing effects of laser intensities on control and covering a wide range of laser powers and

frequencies of the two lasers are to be included in a future publication.¹⁴

Figure 6 shows computed line shapes $A(\epsilon, q, n_k | \epsilon_r, n_r)$ (on a logarithmic scale) as a function of the product translational energy ϵ , with $\omega_2 = 13,964 \text{ cm}^{-1}$, $\omega_1 = 15,617 \text{ cm}^{-1}$, $I_1 = 8.7 \times 10^9 \text{ W/cm}^2$, and $I_2 = 3.51 \times 10^{10} \text{ W/cm}^2$. Results for both the Na(3p) + Na(3s) and Na(4s) + Na(3s) product channels are shown. These frequencies correspond to a state $|e_r\rangle$ with $v_i = 18$, and that of $|e_r\rangle$ with $v_i = 31$. The line shape $A(\epsilon, q, n_k | \epsilon_r, n_r)$ is comprised of a series of sharp non-Lorentzian peaks and dips, each followed by a broader peak. The predominant contribution corresponds to direct $v_i = 18$ excitation, whereas the subsequent smaller sets of features correspond to $v = 19, 20$ contributions arising from stimulated emission and absorption from and to the continuum. In this figure the structure "sharp peak followed by a dip followed by a broad peak" arises due to quantum interference between the two pathways shown in Fig. 5b,c, and higher-order absorption-emission sequences. Single photon absorption by ω_1 , by comparison,¹¹ shows only a series of sharp non-Lorentzian peaks and dips and not the double-peak structure of Fig. 6. Note that it is significant that dissociation is observed from states other than the initially populated $v_i = 18$, clearly indicating that the power broadening is on the same order of magnitude as the vibrational level spacing.

Computations of $A(\epsilon, q, n_k | \epsilon_r, n_r)$ at different frequencies ω_1 or ω_2 show the same structure as Fig. 6 but differ quantitatively. This has the significant implication that by varying ω_1 we can control the channel specific line shapes $A(\epsilon, q, n_k | \epsilon_r, n_r)$ as we have indeed demonstrated elsewhere.¹¹ Further, integrating $A(\epsilon, q, n_k | \epsilon_r, n_r)$ over ϵ (eq 15) for various ω_1 (or ω_2) values gives $P(q)$ as a function of ω_1 . Thus by varying ω_1 or ω_2 we can alter the probability of forming product in channel q . A typical result of these computations,

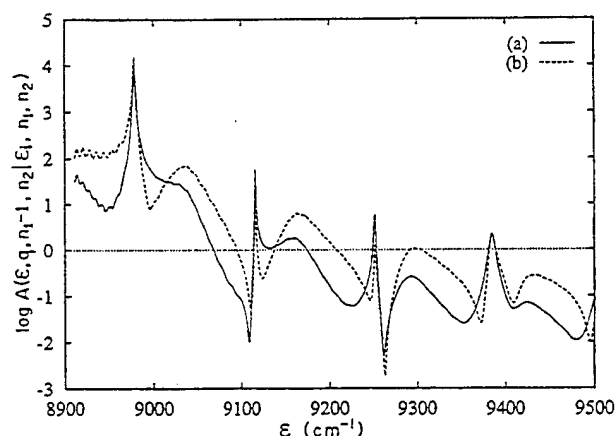


Fig. 6. $\log A(\epsilon, q, n_k | \epsilon_r, n_r)$ as a function of ϵ (where the Na(3p) + Na(3s) asymptote defines the zero energy). (a) Na(3s) + Na(3p) product and (b) Na(3s) + Na(4s) product.

where ω_1 is varied, is shown in Fig. 7 for both Na(3s) + Na(3p) [curve (a)] and Na(3s) + Na(4s) [curve (b)] channels. All fixed parameters are as used to obtain Fig. 6.

The probability $P(q)$ is seen to oscillate strongly as a function of ω_1 , with the distance between the peaks (or dips) being the vibrational spacing between $v = 31$ and 32. The oscillations for the two product channels are out of phase. Hence, for example, the probabilities of producing Na(3s) + Na(4s) and Na(3s) + Na(3p) at $\omega_1 = 15,680 \text{ cm}^{-1}$ are 0.18 and 0.68, respectively. The reverse situation occurs at $\omega_1 = 15,780 \text{ cm}^{-1}$, where 68% of product is Na(3s) + Na(4s). Thus varying ω_1 provides a straightforward method to control the branching ratio into final product channels. Furthermore, and significantly, computations show that arbitrarily changing the relative phase between the ω_1 and ω_2 does not alter the line shape or control results. This computationally confirms the argument given above showing that this approach is insensitive to the relative laser phase.

Two further comments are significant. First, Fig. 7 displays a repetitive periodic-type structure, where several values of ω_1 give essentially the same value of $P(q)$. This interesting feature arises since as ω_1 varies it couples different bound states $|j\rangle$ with the continuum at energy ϵ . Any of these initially-empty bound states is equally successful in introducing the three-photon pathway (Fig. 5c) which competes with the one-photon absorption of ω_1 . This is a convenient feature which allows the experimentalist a wide range of possible choices of ω_2 with no loss of success in control. Second, although the "period" of the oscillation is fixed by the vibrational level spacing, the width of the features depends upon the laser power. Specifically, as the sources become weaker, the range over which control varies reduces. Thus, the range over which control varies is a function of the laser power through power broadening.

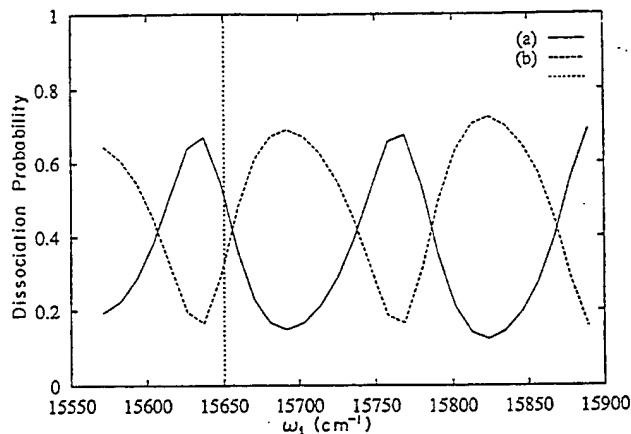


Fig. 7. Probability of forming (a) Na(3s) + Na(3p) and (b) Na(3s) + Na(4s) as a function of ω_1 , with $\omega_2 = 13,964 \text{ cm}^{-1}$, $I_1 = 8.7 \times 10^9 \text{ W/cm}^2$, and $I_2 = 3.51 \times 10^{10} \text{ W/cm}^2$.

5. SUMMARY

We have provided a discussion of two types of methods of maintaining relative laser phase stability in coherent control scenarios for altering the yield in photodissociation. The first approach relies on the judicious use of nonlinear optics techniques to produce a relative phase which is insensitive to the drift or jitter of the laser sources. The second type of method introduces specific multiphoton pathways in which laser phase contributions between the two interfering paths cancel. In this method it is the variation of relative laser frequencies which is the operant control variable. Computations on the photodissociation of Na_2 show large ranges of control in each of these scenarios.

Acknowledgment. This work was supported by the U.S. Office of Naval Research under contract number N00014-90-J-1014.

REFERENCES AND NOTES

- (1) Brumer, P.; Shapiro, M. *Acc. Chem. Res.* 1989, **22**: 407; *Annu. Rev. Phys. Chem.* 1992, **43**: 257.
- (2) Chen, Z.; Brumer, P.; Shapiro, M. *J. Chem. Phys.* 1993, **98**: 8647.
- (3) Levy, I.; Shapiro, M. 1988, **89**: 2900.
- (4) Chen, Z.; Brumer, P.; Shapiro, M. *J. Chem. Phys.* 1993, **98**: 6843.
- (5) Shapiro, M.; Brumer, P. *J. Chem. Phys.* 1986, **84**: 540.
- (6) The phase convention assumed here is such that the electric field term is of the form $\cos(\omega t + \theta)$. Opposite signs for the absorption and emission contributions arise if one uses $\cos(\omega t - \theta)$.
- (7) Schubert, M.; Wilhelmi, B. *Nonlinear Optics and Quantum Electronics*. Wiley: New York, 1986.
- (8) Brumer, P.; Shapiro, M. *Chem. Phys. Lett.* 1986, **126**: 541.
- (9) Yariv, A. *Quantum Electronics*. 2d ed. Wiley: New York, 1975. See chapter 16.
- (10) Dods, J.; Brumer, P.; Shapiro, M. *Can. J. Chem.*, in press.
- (11) Chen, Z.; Shapiro, M.; Brumer, P. *Phys. Rev. Lett.* Submitted for publication.
- (12) Brumer, P.; Shapiro, M. *Adv. Chem. Phys.* 1986, **60**: 371, Lawley, K.P., Ed.; Wiley-Interscience: New York, 1986.
- (13) Balint-Kurti, G.G.; Shapiro, M. *Adv. Chem. Phys.* 1986, **60**: 403; Shapiro, M.; Bony, H. *J. Chem. Phys.* 1985, **83**: 1588; Bandrauk, A.D.; Atabek, O. *Adv. Chem. Phys.* 1989, **73**: 823.
- (14) Chen, Z.; Brumer, P.; Shapiro, M. In preparation.

Coherent and incoherent laser control of photochemical reactions

by MOSHE SHAPIRO

Chemical Physics Department, Weizmann Institute of Science,
Rehovot, Israel 76100

and PAUL BRUMER

Chemistry Physics Theory Group, Department of Chemistry,
University of Toronto, Toronto, Canada M5S 1A1

Coherent radiative control provides a quantum-interference-based method for controlling molecular dynamics. This theory is reviewed and applications to a variety of processes including photodissociation, asymmetric synthesis and the control of currents in semiconductors are discussed. State-of-the-art computations on the photodissociation of CH_3I , IBr , Na_2 and H_2O are presented to show that a wide range of yield control is possible under suitable laboratory conditions. The role of coherent relative laser phase is emphasized and, in a most recent development, shown to be insignificant in appropriately designed high-field control experiments.

1. Introduction

Selectivity is at the heart of chemistry and the control of reactions using lasers has been a goal for decades. Recently, we [1-20] and other groups [21-30] have demonstrated theoretically that one can achieve this goal by using quantum interference phenomena. We showed that phases acquired by a quantum systems while excited by lasers enable one to control quantum interferences, and hence the outcome of many dynamical processes. Initial experimental tests [31-36] of our approach, termed coherent control, confirm many of the theoretical predictions and prove the viability of the method.

The purpose of this review is to provide an introduction to the concepts (for a discussion of the basic principles of coherence, quantum interference and time dependence, which are fundamental to coherent control see, for example, [37]) underlying coherent control and to discuss its current status in both chemistry and physics. Section 1 provides an introduction to the basics of coherent control, followed by a detailed discussion of two control scenarios in § 2. In § 3 we discuss selection rules to control and in § 4 the issue of control of a thermal ensemble. Section 5 describes the control of symmetry breaking, and § 6 describes the production of photocurrents in semiconductors. Finally, in § 7 we discuss extensions of coherent control to the strong-laser-field domain.

1.2. *Aspects of scattering theory and reaction dynamics*

The processes that we wish to control include branching 'half'-collisions,



and 'full' collisions,



In the above, A, B and C are atoms, groups of atoms, electrons or photons, m and m' denote the internal (vibrational, rotational and photon occupation) quantum numbers of the reactants or products.

Given $\Psi(t=0)$, the system wavefunction at an initial time, the evolution of the system is determined by the time-dependent material Schrödinger equation

$$H_M \Psi(t) = i\hbar \frac{\partial \Psi(t)}{\partial t}. \quad (5)$$

where H_M is the system Hamiltonian. The wavefunction at long times, that is when the products are well separated, provides the probabilities of forming the products. The approach to be followed here consists of expressing the time evolution in terms of $|E_i\rangle$, the solutions of the time-independent Schrödinger equation

$$H_M |E_i\rangle = E_i |E_i\rangle. \quad (6)$$

The long-time behaviour of $\Psi(t)$ is intimately connected with the nature of the time-independent continuum energy eigenstates. For every continuum energy value E , each of the possible outcomes observed in the product region is represented by an independent wavefunction. The fact that such a set of degenerate wavefunctions of the separated products exists implies the existence of a set of degenerate eigenfunctions of the total Hamiltonian (which is the asymptotic condition of scattering theory [38]), and a one-to-one correlation between the two sets. This 'boundary' condition is expressed more precisely by denoting the different possible chemical products of the break-up of ABC in equation (2) by an index q (e.g. $q=1$ denotes the A + BC products), and all additional identifying state labels by m . The set of continuum eigenfunctions of the material Hamiltonian

$$H_M |E, m, q^-\rangle = E |E, m, q^-\rangle \quad (7)$$

is now defined via the requirement that asymptotically every $|E, m, q^-\rangle$ state goes over to a state of the separated products, denoted $|E, m, q^0\rangle$, which is of energy E , chemical identity q and remaining quantum numbers m . The 'minus' superscript serves to indicate this choice of boundary condition.

The description of the system in terms of $|E, m, q^-\rangle$ has an important advantage. Expressing the state of the system in the present in terms of these states, that is writing and initial continuum state as

$$\Psi(t=0) = \sum_{q,m} \int dE c_{q,m}(E) |E, m, q^-\rangle, \quad (8)$$

means that we know the fate of the system in the future. Since each of the $|E, m, q^-\rangle$ states correlates with a *single* product state, the probability of observing each $|E, m, q^0\rangle$ product state is simply given by $|c_{q,m}(E)|^2$, the *preparation* probabilities. The probability of producing a chemical product q in the future is therefore given as

$$P_q = \sum_m \int dE |c_{q,m}(E)|^2. \quad (9)$$

The fact that the state of the system in the distant future is pre-determined by the initially created state is, admittedly, intuitively obvious. However, the consequences of this simple fact are often ignored. For example, arguments such as 'intramolecular energy scrambling makes reaction control difficult', are misleading: a general wave

packet may show wondrously complicated temporal behaviour, and yet equation (9) tells us that the probability of producing product q in the long-time limit is merely the energy average of the preparation probabilities. Since the preparation coefficients are also determined by the energy eigenstates, we see that the long-time limit is an average property of the states which make up a given wave packet.

Another consequence of equation (9) is that pulse shaping which merely changes the phases of the preparation coefficients will have absolutely no effect on the q products yields [13]. Likewise, shortening of a pulse, which results in broadening of the power spectrum of that pulse, will modify the $c_{q,m}(E)$ coefficients to *all* the q channels and will not necessarily 'help beat out IVR'.

Below we demonstrate that the key to laser control is to change one $c_{q,m}(E)$ coefficient relative to another $c_{q',m}(E)$ coefficient *at the same energy*. In order to understand how this can be done we discuss now the process of preparation.

1.2. Perturbation theory, system preparation and coherence

Consider the effect of an electric field on an initially bound molecule. The molecule is assumed to be in an eigenstate $|E_g\rangle$ of the radiation-free Hamiltonian H_M before being subjected to a perturbing incident radiation field $\varepsilon(t)$. The overall Hamiltonian is then given by

$$H = H_M - \mathbf{d}[\bar{\varepsilon}(t) + \bar{\varepsilon}^*(t)], \quad (10)$$

where \mathbf{d} is the component of the dipole moment along the electric field.

Consider now the case in which the impinging photon is energetic enough to dissociate the molecule. It is then necessary to expand $|\Psi(t)\rangle$ in the bound and scattering eigenstates of the radiation-free Hamiltonian:

$$|\Psi(t)\rangle = \sum_i c_i(t) |E_i\rangle \exp\left(-\frac{iE_i t}{\hbar}\right) + \sum_{m,q} \int dE c_{E,m,q}(t) |E, m, q^-\rangle \exp\left(-\frac{iEt}{\hbar}\right). \quad (11)$$

Insertion of equation (11) into the time-dependent Schrödinger equation results in a set of first-order differential equations for the $c_v(t)$ coefficients, where v represents either the bound (i) or scattering (E, m, q) indices.

For weak fields the use of first-order perturbation theory gives, for the post-pulse preparation coefficient,

$$c_{E,m,q}(t \gg \Gamma) = \frac{(2\pi)^{1/2}}{i\hbar} \varepsilon(\omega_{E,E_g}) \langle E, m, q^- | \mathbf{d} | E_g \rangle, \quad (12)$$

where Γ is the pulse duration and

$$\varepsilon(\omega) = \frac{1}{(2\pi)^{1/2}} \int_{-\infty}^{\infty} \exp(i\omega t) \bar{\varepsilon}(t) dt. \quad (13)$$

where $\omega_{E,E_g} = (E - E_g)/\hbar$.

The process described above amounts to the creation of a pure state (i.e. a state for which a phase may be defined) in the continuum by a well defined electric field. As long as there are no random collisions, this state will remain pure (i.e. will retain its phase), a feature of some importance to the discussion below.

It follows from equations (9) and (12) that the probability $P(E, q)$ of forming asymptotic product in arrangement q is

$$P(E, q) = \sum_m |c_{E,m,q}(t \gg \Gamma)|^2 = \frac{2\pi}{\hbar^2} \sum_m |\varepsilon(\omega_{E,E_g}) \langle E_g | \mathbf{d} | E, m, q^- \rangle|^2 \quad (14)$$

and that the branching ratio $R(1, 2; E)$ between the $q=1$ products and the $q=2$ products at energy E is given as

$$R(1, 2; E) = \frac{\sum_m |\langle E_g | \mathbf{d} | E, m, 1^- \rangle|^2}{\sum_m |\langle E_g | \mathbf{d} | E, m, 2^- \rangle|^2}. \quad (15)$$

1.3. Coherent radiative control of chemical reactions

We now address the issue of how to alter the above yield ratio $R(1, 2; E)$ in a systematic fashion. Equation (15) makes clear that (at least in the weak-field regimen) this cannot be achieved by altering the laser intensity, since the field strength cancels out in the expression for R . Any other quantity which appears in a similar form in both the numerator and the denominator cannot serve as a handle on yield control.

Quantum interference phenomena can, however, alter the numerator or denominator of R in an independent and controlled way. This can be achieved by accessing the final continuum state via two or more interfering pathways. One of the first examples which we studied [1] involves preparing a molecule in a superposition $c_1|\phi_1\rangle + c_2|\phi_2\rangle$ state and exciting the two components to the same final continuum energy E by using two continuous-wave (CW) sources (figure 1). The field employed is of the form

$$\tilde{\epsilon}(t) = \epsilon_1 \exp(-i\omega_1 t + i\chi_1) + \epsilon_2 \exp(-i\omega_2 t + i\chi_2), \quad (16)$$

where $\hbar\omega_i = E - E_i$. A straightforward computation [1] yields

$$R(1, 2; E) = \frac{\sum_m |\langle \tilde{\epsilon}_1 c_1 \phi_1 + \tilde{\epsilon}_2 c_2 \phi_2 | \mathbf{d} | E, m, 1^- \rangle|^2}{\sum_m |\langle \tilde{\epsilon}_1 c_1 \phi_1 + \tilde{\epsilon}_2 c_2 \phi_2 | \mathbf{d} | E, m, 2^- \rangle|^2}, \quad (17)$$

where $\tilde{\epsilon} = \epsilon_i \exp(i\chi_i)$. Expanding the square gives

$$R(1, 2; E) = \frac{\sum_m [|\tilde{\epsilon}_1 c_1 \langle \phi_1 | \mathbf{d} | E, m, 1^- \rangle|^2 + |\tilde{\epsilon}_2 c_2 \langle \phi_2 | \mathbf{d} | E, m, 1^- \rangle|^2 + 2 \operatorname{Re} [c_1 c_2^* \tilde{\epsilon}_1 \tilde{\epsilon}_2^* \langle \phi_1 | \mathbf{d} | E, m, 1^- \rangle]]}{\sum_m [|\tilde{\epsilon}_1 c_1 \langle \phi_1 | \mathbf{d} | E, m, 2^- \rangle|^2 + |\tilde{\epsilon}_2 c_2 \langle \phi_2 | \mathbf{d} | E, m, 2^- \rangle|^2 + 2 \operatorname{Re} [c_1 c_2^* \tilde{\epsilon}_1 \tilde{\epsilon}_2^* \langle \phi_1 | \mathbf{d} | E, m, 2^- \rangle]]}. \quad (18)$$

The structure of the numerator and denominator of equation (18) is of the type desired, that is each has a term associated with the excitation of the $|\phi_1\rangle$ state, a term associated with the excitation of the $|\phi_2\rangle$ state, and a term corresponding to the interference between the two excitation routes. The interference term, which can be either constructive or destructive, is in general different for the two product channels.

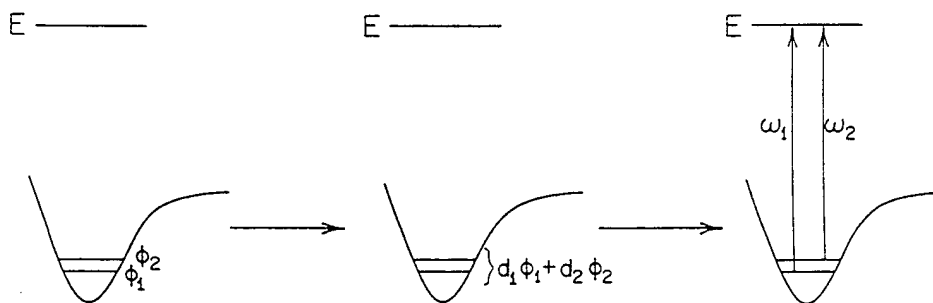


Figure 1. A general two-step scheme for inducing controllable quantum interference effects into the continuum state at energy E . The two bound states ϕ_1 and ϕ_2 belong to a lower electronic state whereas the level at energy E is that of an excited electronic state. Coherence introduced in the first step is carried into the continuum (from [12]).

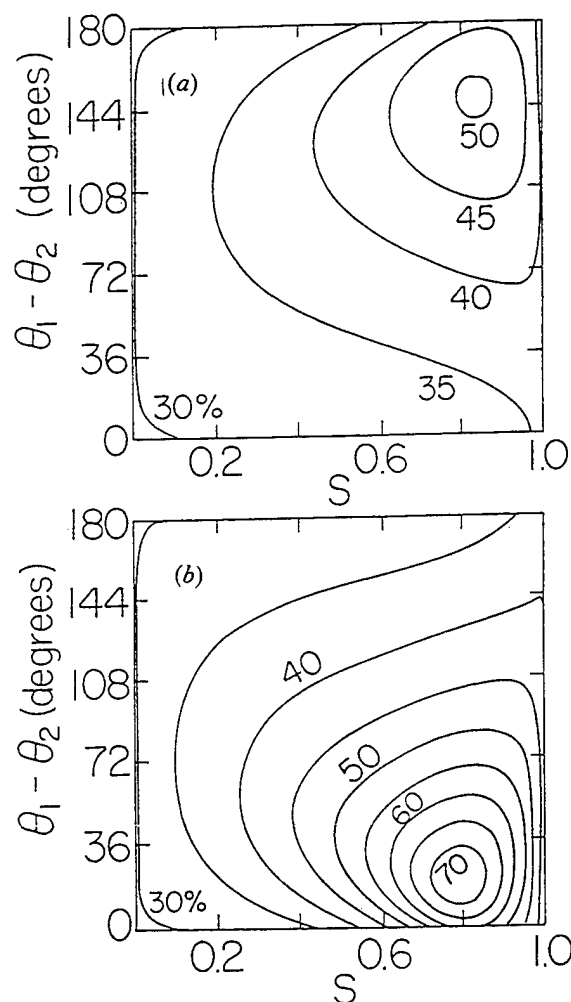


Figure 2. Contour plot of the yield of I^* (i.e. fraction of I^* as product) in the photodissociation of CH_3I from a superposition state comprised of (a) $(v_1, J_1, M_1) = (0, 0, 0) + (v_2, J_2, M_2) = (0, 1, 0)$ and (b) $(0, 0, 0) + (0, 2, 0)$. Here v_i , J_i and M_i are the vibrational, rotational and rotational projection quantum numbers respectively of the i th bound state (from [1]).

What makes equation (18) so important *in practice* is that the interference term has coefficients whose magnitude and sign depend upon *experimentally controllable* parameters. Thus the experimentalist can manipulate laboratory parameters and, in doing so, directly alter the reaction product yield by varying the magnitude of the interference term. In the case of equation (18) the experimental parameters which alter the yield [1] are contained in the complex quantity $A = \tilde{\epsilon}_2 c_2 / \tilde{\epsilon}_1 c_1$. Both $x \equiv |A|$ and $\theta_1 - \theta_2 \equiv \arg(A)$ can be controlled separately in the experiment.

Results of a specific computational example based upon equation (18) are shown in figure 2. Here we consider control over the relative probability of forming $I(^2P_{3/2})$ as against $I(^2P_{1/2})$, denoted I and I^* respectively, in the dissociation of methyl iodide:



The computations were carried out with realistic potential surfaces [39, 40] within the framework of a fully quantum photodissociation theory [40, 41]. Figure 2 shows a

typical plot of the yield of I^* as a function of $\theta_1 - \theta_2$ and $S \equiv x^2/(1+x^2)$. ($S=0$ corresponds to $\tilde{\epsilon}_1=0$, and $S=1$ corresponds to $\tilde{\epsilon}_2=0$.) We see that our ability to control the process ('range of control') is almost complete: as we change S and $\theta_1 - \theta_2$, the yield varies from 30 to 70% I. Higher and lower ratios can also be achieved [42] with different choices of the initial pair of states $|\phi_1\rangle$ and $|\phi_2\rangle$.

These ideas can be naturally extended to the control of N products, using an initial superposition of N states [17]. Experimentally, the creation of an initial superposition of two (or more) states may be achieved by acting on a single ground state with a light pulse whose frequency width spans the levels of interest [9–11]. Alternatively, one can employ stimulated emission pumping through an intermediate electronic state [20]. The 'real-time' analogue of the above scenario with two CW frequencies, in which the superposition state preparation is affected by a single broad-band pulse and the dissociation by a second pulse, is discussed in detail in § 2.2.

2. Representative control scenarios

As mentioned above, the two-step approach of figures 1 and 2 is simply one particular implementation of coherent control; numerous other scenarios may be designed. They all rely upon the same 'coherent-control principle' that, *in order to achieve control, one must drive a state through multiple independent optical excitation routes to the same final state*.

It is helpful to think of coherent control as analogous to a double-slit (or multiple-slit) experiment; the tuning in of a desired product ratio R , accomplished by varying the external laser parameters (e.g. A), is analogous to probing different regions of a screen on which the double-slit interference patterns are imaged. Control arises because these interference patterns are different for different final channels (because of the different molecular phases).

It would seem that laser incoherence would lead to loss of control since incoherence implies that the phases of $\tilde{\epsilon}_1$ and $\tilde{\epsilon}_2$ in equation (18) are random. An ensemble average of these phases is expected to lead to the disappearance of the interference term. This is only true, however, in the fully incoherent limit. Control can persist in the presence of some laser incoherence [19] or when the initial state is described by a *mixed*, as distinct from *pure*, state [7]. Most surprising is the fact, described below, that, by utilizing strong laser fields, one can attain quantum interference control with completely *incoherent* sources [43].

We now describe in more detail two additional control scenarios.

2.1. Interference between n -photon and m -photon routes (' $n+m$ ' control)

So far, we exploited quantum interference phenomena by dissociating a superposition of several energy eigenstates with a single-type (one-photon absorption) process. It is possible instead to start with a *single* energy eigenstate and to employ interference between optical routes of *different* types. Such is the interference between two multiphoton processes of different multiplicities. In order to satisfy the coherent-control principle, which requires that we reach the same final energy E , we must use photons of commensurate frequencies, that is frequencies which satisfy an $m\omega_1 = n\omega_2$ relation, with integer m and n . Selection rules dictate the acceptable n, m pairs.

As the simplest example, we examine a one-photon process interfering with a three-photon process ('3+1' control). Let H_g and H_e be the nuclear Hamiltonians for the ground state and the excited electronic state respectively. H_g is assumed to have a

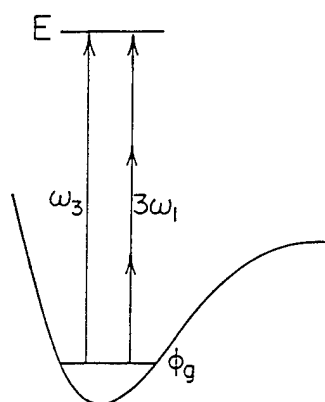


Figure 3. A multiple-optical-route scheme to induce controllable quantum interference effects into the continuum state at energy E . Here the level ϕ_g is a bound state of a lower electronic state and that at E is a continuum state of the excited electronic state. Simultaneous application of frequencies ω_1 and $\omega_3 = 3\omega_1$ leads to interference in the continuum state (from [12]).

discrete spectrum and H_e to possess a continuous spectrum. The molecule, initially in an eigenstate $|E_i\rangle$ of H_g , is subjected to two electric fields (figure 3) given by

$$\varepsilon(t) = \varepsilon_1 \cos(\omega_1 t + \mathbf{k}_1 \cdot \mathbf{R} + \theta_1) + \varepsilon_3 \cos(\omega_3 t + \mathbf{k}_3 \cdot \mathbf{R} + \theta_3). \quad (21)$$

Here $\omega_3 = 3\omega_1$, $\varepsilon_l = \varepsilon_l \hat{\varepsilon}_l$, $l = 1, 3$; ε_l is the magnitude and $\hat{\varepsilon}_l$ is the polarization of the electric fields. The two fields are chosen parallel, with $\mathbf{k}_3 = 3\mathbf{k}_1$.

The probability $P(E, q; E_i)$ of producing a product with energy E in arrangement q from a state $|E_i\rangle$ is given by

$$P(E, q; E_i) = P_3(E, q; E_i) + P_{13}(E, q; E_i) + P_1(E, q; E_i), \quad (22)$$

where $P_1(E, q; E_i)$ and $P_3(E, q; E_i)$ are the probabilities of dissociation due to the ω_1 and ω_3 excitation, and $P_{13}(E, q; E_i)$ is the term due to interference between the two excitation routes.

In the weak-field limit, $P_3(E, q; E_i)$ is given by

$$P_3(E, q; E_i) = \left(\frac{\pi}{\hbar}\right)^2 \varepsilon_3^2 F_3^{(q)}, \quad (23)$$

where

$$F_3^{(q)} = \sum_n |\langle E, n, q^- | (\hat{\varepsilon}_3 \cdot \mathbf{d})_{e,g} | E_i \rangle|^2, \quad (24)$$

\mathbf{d} is the electric dipolar operator and

$$(\hat{\varepsilon}_3 \cdot \mathbf{d})_{e,g} = \langle e | \hat{\varepsilon}_3 \cdot \mathbf{d} | g \rangle, \quad (25)$$

with $|g\rangle$ and $|e\rangle$ denoting the ground state and excited electronic state respectively. $P_1(E, q; E_i)$ is given in third-order perturbation theory by [6]

$$P_1(E, q; E_i) = \left(\frac{\pi}{\hbar}\right)^2 \varepsilon_1^6 F_1^{(q)}, \quad (26)$$

where

$$F_1^{(q)} = \sum_n |\langle E, n, q^- | T | E_i \rangle|^2, \quad (27)$$

with

$$T = (\hat{\mathbf{e}}_1 \cdot \mathbf{d})_{e,g} (E_i - H_g + 2\hbar\omega_1)^{-1} (\hat{\mathbf{e}}_1 \cdot \mathbf{d})_{g,e} (E_i - H_e + \hbar\omega_1)^{-1} (\hat{\mathbf{e}}_1 \cdot \mathbf{d})_{e,g}. \quad (28)$$

We assumed that $E_i + 2\hbar\omega_1$ is below the dissociation threshold and that dissociation occurs from the excited electronic state only.

A similar derivation [6] gives the cross-term in equation (22) as

$$P_{13}(E, q; E_i) = -2 \left(\frac{\pi}{\hbar} \right)^2 \varepsilon_3 \varepsilon_1^3 \cos(\theta_3 - 3\theta_1 + \delta_{13}^{(q)}) |F_{13}^{(q)}| \quad (29)$$

with the amplitude $|F_{13}^{(q)}|$ and phase $\delta_{13}^{(q)}$ defined by

$$|F_{13}^{(q)}| \exp(i\delta_{13}^{(q)}) = \sum_n \langle E_i | T | E, n, q^- \rangle \langle E, n, q^- | (\hat{\mathbf{e}}_3 \cdot \mathbf{d})_{e,g} | E_i \rangle. \quad (30)$$

The branching ratio $R_{qq'}$ between the q and q' products can then be written as

$$R_{qq'} = \frac{P(E, q; E_i)}{P(E, q'; E_i)} = \frac{\varepsilon_3^2 F_3^{(q)} - 2\varepsilon_3 \varepsilon_1^3 \cos(\theta_3 - 3\theta_1 + \delta_{13}^{(q)}) |F_{13}^{(q)}| + \varepsilon_1^6 F_1^{(q)}}{\varepsilon_3^2 F_3^{(q')} - 2\varepsilon_3 \varepsilon_1^3 \cos(\theta_3 - 3\theta_1 + \delta_{13}^{(q')}) |F_{13}^{(q')}| + \varepsilon_1^6 F_1^{(q')}} \quad (31)$$

Next we rewrite equation (31) in a more convenient form. We define a dimensionless parameter $\bar{\varepsilon}_l$ and a parameter x as follows:

$$\varepsilon_l = \bar{\varepsilon}_l \varepsilon_0 \text{ for } l = 1, 3, \quad x = \frac{\bar{\varepsilon}_1^3}{\bar{\varepsilon}_3}. \quad (32)$$

The quantity ε_0 essentially carries the unit for the electric fields; variations in the magnitude of ε_0 can also be used to account for unknown transition dipole moments. Utilizing these parameters, equation (31) becomes

$$R_{qq'} = \frac{F_3^{(q)} - 2x \cos(\theta_3 - 3\theta_1 + \delta_{13}^{(q)}) \varepsilon_0^2 |F_{13}^{(q)}| + x^2 \varepsilon_0^4 F_1^{(q)}}{F_3^{(q')} - 2x \cos(\theta_3 - 3\theta_1 + \delta_{13}^{(q')}) \varepsilon_0^2 |F_{13}^{(q')}| + x^2 \varepsilon_0^4 F_1^{(q')}} \quad (33)$$

The numerator and denominator of equation (33) contain contributions from two independent routes and an interference term. Since the interference term is controllable through variation in laboratory parameters, so too is the product ratio $R_{qq'}$. Thus the principle upon which this control scenario is based is the same as in the first example above, although the interference is introduced in an entirely different way.

Experimental control over $R_{qq'}$ is obtained by varying the difference $\theta_3 - 3\theta_1$ and the parameter x . The former is the phase difference between the ω_3 and the ω_1 laser fields and the latter, via equation (32), incorporates the ratio of the two laser amplitudes. Experimentally one envisages using 'tripling' to produce ω_3 from ω_1 ; the subsequent variation in the phase of one of these beams provides a straightforward method of altering $\theta_3 - 3\theta_1$. Indeed, generating ω_3 from ω_1 allows for compensation of any phase jumps in the two laser sources. Thus the relative phase $\omega_3 - 3\omega_1$ is well defined.

With the qualitative principle of interfering pathways established, it remains to determine the quantitative extent to which coherent control alters the yield ratio in a realistic system. To this end we consider an application to one-photon as against three-photon ('3+1') photodissociation of IBr. In particular, we focus on the energy regime where IBr dissociates to both I ($^2P_{3/2} + \text{Br } ^2P_{3/2}$) and I ($^2P_{3/2} + \text{Br}^* ^2P_{1/2}$). The IBr potential curves and coupling strengths used in the calculation, taken from the work of Child [44], are shown in figure 4.

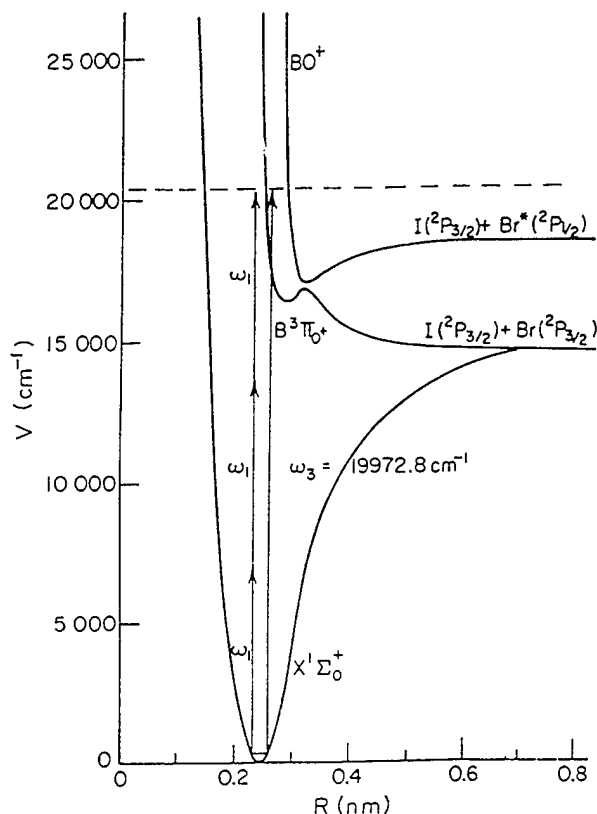


Figure 4. IBr potential curves relevant in the one-plus-three-photon-induced dissociation (from [14]).

A complete computation requires inclusion of angular momentum. A detailed discussion of the role of angular momentum is given in § 3. Here we simply display the results of the quantum calculation which fully incorporates all the rotational states involved in the '3 + 1' coherent control of IBr. Two different cases were examined: those corresponding to fixed initial magnetic quantum numbers M_i and those corresponding to averaging over a random distribution of M_i for fixed J_i . Results typical of those obtained are shown in figures 5 and 6, where we provide a contour plot of the yield of $\text{Br}^* 2\text{P}_{1/2}$ for the case of excitation from $J_i = 1$, $M_i = 0$, and $J_f = 42$ with an average over M_f , as a function of laser control parameters (relative intensity and phase). The range of control in each case is vast with, remarkably, no loss of control with averaging over M_f .

As pointed out above, '3 + 1' is not necessarily the only viable control scenario in the ' $n + m$ ' family. It has the advantage that one may generate one of the frequencies (the tripled photon) from the other. This is indeed the reason why the '3 + 1' route was the first control scenario to be implemented experimentally (see discussion below).

As discussed in § 3, control of *integral* (in contrast with *differential*) cross-sections requires that the $|E, n, q^-\rangle$ continuum states be made up of equal parity $|J, M\rangle$ angular momentum states. This means that, in the ' $m + n$ ' control scheme, the integer n must have the same parity as the integer m . Thus, studies of a '2 + 2' scheme for the control of Na_2 photodissociation [18, 45] (discussed in detail in § 4) and of a '2 + 4' scenario for the control of the Cl_2 photodissociation [46], have been published. In addition, studies of '3 + 1' control with strong fields have also appeared [47, 48]. These studies and others [47] have verified that ' $n + m$ ' control is viable even when strong fields are used,

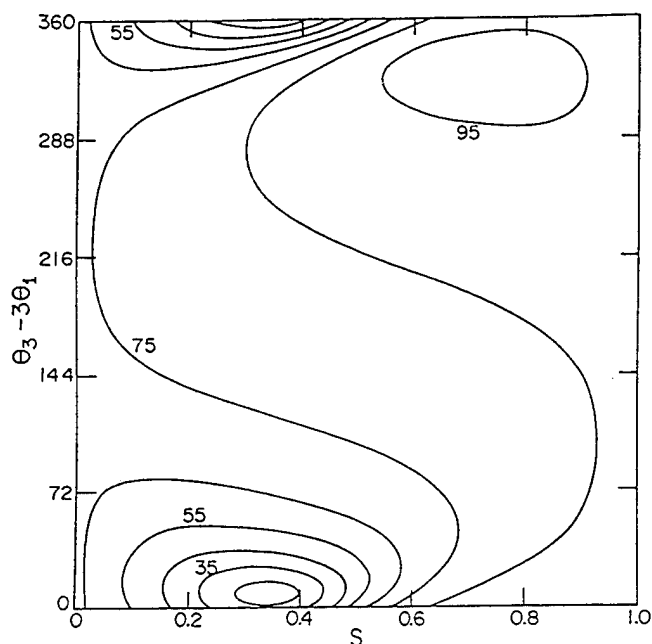


Figure 5. Contour plot of the yield of $\text{Br}^*(^2\text{P}_{1/2})$ (percentage of Br^* as product) in photodissociation of IBr from an initial bound state in $\text{X } ^1\Sigma_0^+$ with $v=0$, $J_i=1$ and $M_i=0$. Results arise from simultaneous (ω_1, ω_3) excitation ($\omega_3=3\omega_1$), with $\omega_1=6657.5 \text{ cm}^{-1}$ (from [14]).

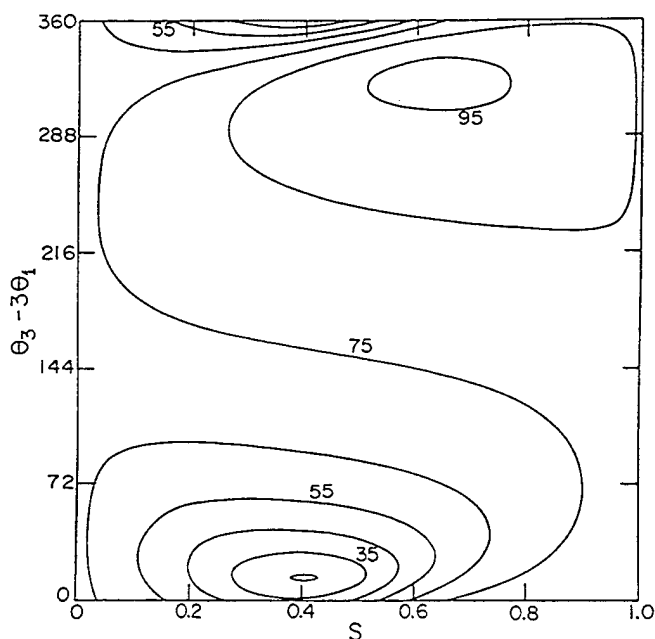


Figure 6. As in figure 5 but for $v=0$, $J_i=42$, $\omega_1=6635.0 \text{ cm}^{-1}$ and M averaged ($\varepsilon_0=\frac{1}{8}$) (from [14]).

although the dependence on the x amplitude and the $\theta_n - 3\theta_m$ phase factors are no longer as transparent as in the weak-field case discussed above.

The weak-field '3 + 1' scenario has now been experimentally implemented in part in REMPI-type experiments. The experiments demonstrated control of the total ionization rate, first in Hg [31], and then in HCl and CO [32]. In the case of HCl [32], the molecule was excited to an intermediate $^3\Sigma^-(\Omega^+)$ vibrational resonance, using a combination of three ω_1 ($\lambda_1 = 336$ nm) photons and one ω_3 ($\lambda_3 = 112$ nm) photon. The ω_3 beam was generated from an ω_1 beam by tripling in a Kr gas cell. Ionization of the intermediate state takes place by absorption of one additional ω_1 photon.

The relative phase of the light fields was varied by passing the ω_1 and ω_2 beams through a second Ar or H₂ ('tuning') gas cell of variable pressure. The HCl REMPI experiments verified the prediction of a sinusoidal dependence of the ionization rates on the relative phase of the two exciting lasers of equation (33). The HCl experiment also verified the prediction of equation (33) of the dependence of the strength of the sinusoidal modulation of the ionization current on the x amplitude factor.

As discussed in § 3, if one is content with controlling angular distributions, one can lift the equal-parity restriction. The absorption of two photons of perpendicular polarizations [5, 8], or of two photons interfering with their second-harmonic photon ('2 + 1' scenario) [8, 35, 36], results in states of different parities. Although such processes do not lead to control of integral quantities, they do allow for control of differential cross-sections. The '1 + 2' scenario (discussed in § 4) has been implemented experimentally for the control of photocurrent directionality in semiconductors, using no bias voltage [35].

2.2. The pump-dump scheme

A useful extension of the scenario outlined in § 1.3 is a 'pump-dump' scheme, in which an initial superposition of bound states is prepared with one laser pulse and subsequently dissociated with another. The scenario is shown qualitatively in figure 7. The pump and dump steps are assumed to be temporally separated by a time delay τ .

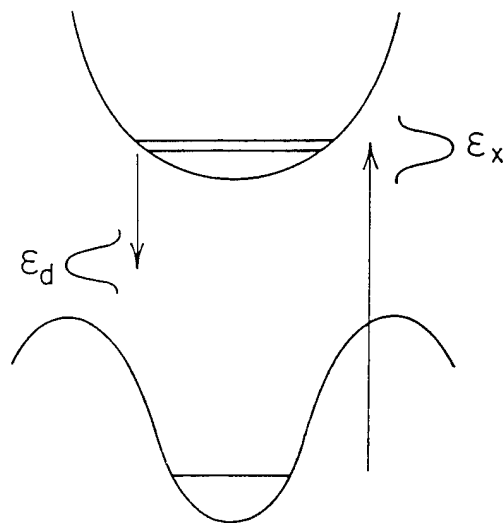


Figure 7. Coherent radiative control via a picosecond pulse scheme. In this case a single level is excited with a laser pulse to produce a superposition of two bound states in an excited electronic state. Subsequent de-excitation of this state to the continuum of the ground state allows control over the reaction on the ground state surface (from [12]).

The analysis below shows that under these circumstances the control parameters are the central frequency of the pump pulse and the time delay between the two pulses.

Consider a molecule, initially ($t=0$) in eigenstate $|E_g\rangle$ of Hamiltonian H_M , subjected to two transform limited light pulses. The field $\bar{e}(t)$ consists of two temporally separated pulses, that is $\bar{e}(t) = \bar{e}_x(t) + \bar{e}_d(t)$, with the Fourier transform of $\bar{e}_x(t)$ denoted $\varepsilon_x(\omega)$, etc. For convenience, we have chosen Gaussian pulses peaking at $t=t_x$ and t_d , respectively. As discussed in § 1.2, the $\bar{e}_x(t)$ pulse induces a transition to a linear combination of two excited bound electronic states with nuclear eigenfunctions $|E_1\rangle$ and $|E_2\rangle$, and the $\bar{e}_d(t)$ pulse dissociates the molecule by further exciting it to the continuous part of the spectrum. Both fields are chosen to be sufficiently weak for perturbation theory to be valid. Contrary to popular expectation, perturbation theory does not imply a small total photodissociation yield. Computational results [50] indicate that perturbation theory is quantitatively correct for dissociation probabilities as large as 0.2.

The superposition state prepared by the $\bar{e}_x(t)$ pulse, whose width is chosen to encompass just the two E_1 and E_2 levels, is given in first-order perturbation theory as

$$|\phi(t)\rangle = |E_g\rangle \exp\left(-\frac{iE_g t}{\hbar}\right) + c_1 |E_1\rangle \exp\left(-\frac{iE_1 t}{\hbar}\right) + c_2 |E_2\rangle \exp\left(-\frac{iE_2 t}{\hbar}\right), \quad (34)$$

where

$$c_k = \frac{(2\pi)^{1/2}}{i\hbar} \langle E_k | \mathbf{d} | E_g \rangle \varepsilon_x(\omega_{kg}), \quad k=1,2, \quad (35)$$

with $\omega_{kg} \equiv (E_k - E_g)/\hbar$.

After a delay time of $\tau \equiv t_d - t_x$ the system is subjected to the $\bar{e}_d(t)$ pulse. It follows from equation (34) that after this delay time each preparation coefficient has picked up an extra factor of $\exp(-iE_k \tau/\hbar)$, $k=1,2$. Hence, the phase of c_1 relative to c_2 at that time increases by $-(E_1 - E_2)\tau/\hbar = \omega_{2,1}\tau$. Thus the natural two-state time evolution replaces the relative laser phase of the two-frequency control scenario of § 1.3.

After the decay of the $\bar{e}_d(t)$ pulse the system wavefunction is given as

$$|\psi(t)\rangle = |\phi(t)\rangle + \sum_{n,q} \int dE B(E, n, q|t) |E, n, q^-\rangle \exp\left(-\frac{iEt}{\hbar}\right). \quad (36)$$

The probability of observing the q fragments at total energy E in the remote future is therefore given as

$$\begin{aligned} P(E, q) &= \sum_n |B(E, n, q|t=\infty)|^2 \\ &= \frac{2\pi}{\hbar^2} \sum_n \left| \sum_{k=1,2} c_k \langle E, n, q^- | \mathbf{d} | E_k \rangle \varepsilon_d(\omega_{EE_k}) \right|^2, \end{aligned} \quad (37)$$

where $\omega_{EE_k} = (E - E_k)/\hbar$, and c_k is given by equation (35).

Expanding the square and using the Gaussian pulse shape give

$$P(E, q) = \frac{2\pi}{\hbar^2} [|c_1|^2 \mathbf{d}_{1,1}^{(q)} \varepsilon_1^2 + |c_2|^2 \mathbf{d}_{2,2}^{(q)} \varepsilon_2^2 + 2 |c_1 c_2^* \varepsilon_1 \varepsilon_2 \mathbf{d}_{1,2}^{(q)}| \cos(\omega_{2,1}(t_d - t_x) + \alpha_{1,2}^{(q)}(E) + \phi)], \quad (38)$$

where $\varepsilon_i = |\varepsilon_d(\omega_{EE_i})|$, $\omega_{2,1} = (E_2 - E_1)/\hbar$ and the phases ϕ , $\alpha_{1,2}^{(q)}(E)$ are defined by

$$\langle E_1 | \mathbf{d} | E_g \rangle \langle E_g | \mathbf{d} | E_2 \rangle \equiv |\langle E_1 | \mathbf{d} | E_g \rangle \langle E_g | \mathbf{d} | E_2 \rangle| \exp(i\phi)$$

$$\mathbf{d}_{i,k}^{(q)}(E) \equiv |\mathbf{d}_{i,k}^{(q)}(E)| \exp[i\alpha_{i,k}^{(q)}(E)] = \sum_n \langle E, n, q^- | \mathbf{d} | E_i \rangle \langle E_k | \mathbf{d} | E, n, q^- \rangle. \quad (39)$$

Integrating over E to encompass the full width of the second pulse and forming the ratio $Y = P(q)/\Sigma_q P(q)$ give the ratio of products in each of the two arrangement channels, that is the quantity that we wish to control. Once again it is the sum of two direct photodissociation contributions, plus an interference term.

Examination of equation (38) makes clear that the product ratio Y can be varied by changing the delay time $\tau = t_d - t_x$ or ratio $x = |c_1/c_2|$; the latter is not conveniently done by detuning the initial excitation pulse.

It is enlightening to consider this scenario as applied [9] to a model branching photodissociation reaction with masses of D and H, that is



in which one uses the first pulse to excite a pair of states in a binding (Rydberg) electronic state and the second pulse to dissociate the system by de-exciting it back to the ground state. Typical results (see also [9]) for control are shown in figure 8 where the yield is seen to vary from 16 to 72% as the time delay and tuning of the initial excitation pulse are varied. This is an extreme range of control, especially in light of the fact that the two product channels differ only in mass factors.

It is highly instructive to examine the nature of the superposition state prepared in the initial excitation (equation 34) and its time evolution during the delay between pulses. An example of such a state is shown in figure 9 where we plot the wavefunction for a collinear model of the reaction of equation (40). Specifically, the coordinates are the reaction coordinate S and its orthogonal conjugate x . The wavefunction is shown evolving over half of its total possible period. Examination of figure 9 shows that de-exciting this superposition state (figure 9b) would yield a substantially different

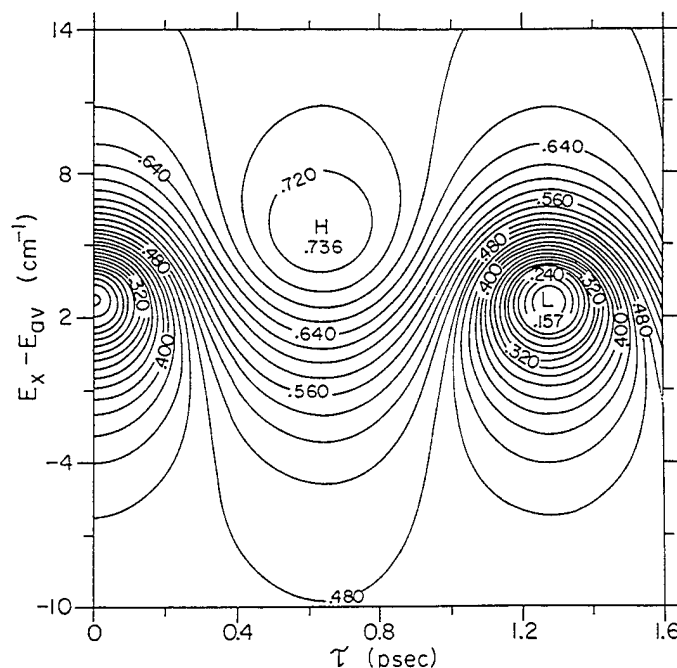


Figure 8. Contour plot of the DH yield in the reaction $\text{D} + \text{H}_2 \rightarrow \text{DH} + \text{H}$. The control parameters are the difference in energy between the excitation pulse centre energy E_x and the average energy E_{av} of the two excited levels and the time τ between the pulses. Although the abscissa begins at zero and spans approximately one period, the results are periodic in the delay time (from [9]).

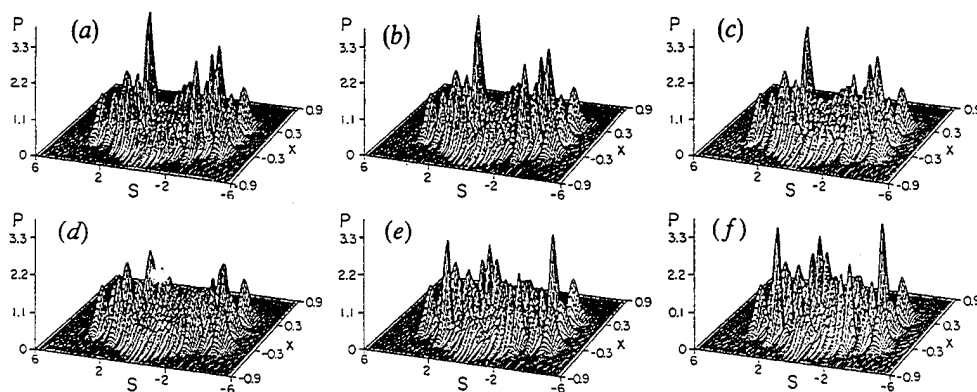
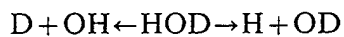


Figure 9. Time evolution of the square of the wavefunction for a superposition state comprised of levels 56 and 57 of the G1 surface of H_3 . The probability is shown as a function of the reaction coordinate S and orthogonal distance x at times of (a) 0, (b) 0.0825 ps, (c) 0.165 ps, (d) 0.33 ps, (e) 0.495 ps and (f) 0.66 ps, which correspond to equal fractions of one half of the period $2\pi/\omega_{2,1}$ (from [9]).

product yield from de-exciting at the time in figure 9 (e). However, there is clearly no particular preference of the wavefunction for large positive or large negative S at these particular times, which would be the case if the reaction control were a result of some spatial characteristics of the wavefunction. Rather, the essential control characteristics of the wavefunction are carried in the quantum amplitude and phase of the created superposition state.

A second example of pump-dump control [11] is provided by the example of IBr photodissociation. Specifically, we showed that it is possible to control the Br^* against Br yield in this process, using two conveniently chosen picosecond pulses. The first pulse was chosen to prepare a linear superposition of two bound states which arise from mixing of the X and A states. A subsequent pulse pumps this superposition to dissociation where the relative yields of Br and Br^* are examined. Results typical of those obtained are shown in figure 10 where the relative yield is shown as a function of the delay between pulses and the detuning of the pump pulse from the energetic centre of the two bound states in the initial superposition. The results show the vast range of control which is possible with this relatively simple experimental set-up. Once again it is worth noting that both the potential energy surfaces and the quantum photodissociation computations are 'state of the art', so that the results should be representative of results expected in the laboratory.

Theoretical work on similar pump-dump scenarios for the control of the



dissociation via the B state [51] of HOD and the A state [52] of HOD have recently been published. Experimental work on the control of this system is now in progress [53].

3. Selection rules

We now discuss in greater detail issues of *selection rules* in coherent control. We show that there are some strict limitations on the types of scenario which can be used to control integral properties. The term 'integral' (as distinct from 'differential') is used here to describe any quantity in which averaging over angles and/or final polarizations takes place in the detection process. The most obvious of such integral quantities is the total yield of a reaction.

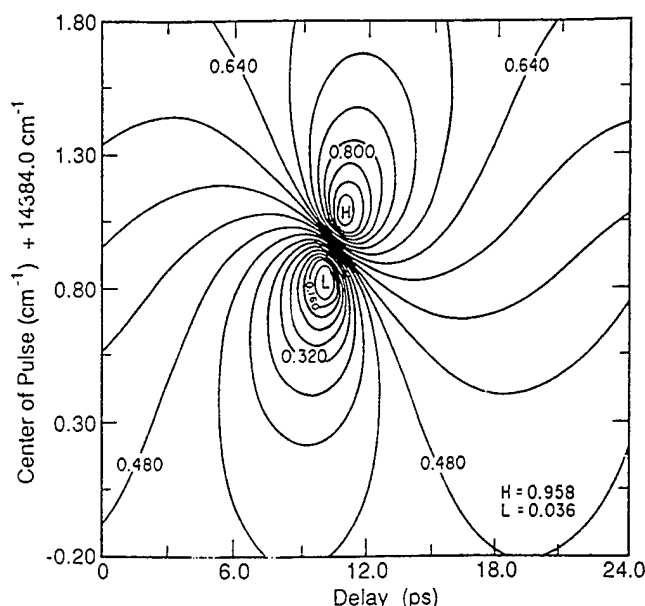


Figure 10. Computed control over the Br yield as a function of E_x (the excitation pulse detuning) and τ (the time delay between the pulses) (from [11]). Br yield $\Delta_d = 20 \text{ cm}^{-1}$, $\Delta_x = 2 \text{ cm}^{-1}$, $E_d = 15\,230 \text{ cm}^{-1}$.

Most of the limitations imposed on the control of integral quantities do not apply to the control of differential attributes. Examples of differential quantities of interest include the control of current directionality [8] (see §6), and of the angular distributions of photofragments [5].

The discussion below can be summarized in terms of two general selection rules for integral control.

- (a) *The (two) interfering pathways must be able to access continuum states with the same magnetic quantum numbers.* This rule holds even when the initial states are *M* polarized.
- (b) *If the initial state is not *M* polarized, integral control can only be achieved via interference between continuum states of equal parity.* Two pathways which generate states of opposite parity, such as one-photon and two-photon absorption, cannot lead to integral control of unpolarized initial states. However, these pathways can [5, 8] and do [35, 36] lead to differential control of unpolarized states or integral control of polarized beams (subject to selection rule (a)).

In order to see how these selection rules come about we use a symmetric-top molecule as a working example and the superposition-state control scenario outlined in §1.3. To be more specific, we consider CH_3I . This symmetric-top molecule is in many ways equivalent to a linear triatomic molecule [39], since in both the ground and the first few excited states the I, and C and the H_3 (CM) do not deviate significantly from the collinear configuration.

CH_3I dissociates to yield $\text{CH}_3(\text{v}) + \text{I}^* {}^2\text{P}_{1/2}$ and $\text{CH}_3(\text{v}) + \text{I}^2\text{P}_{3/2}$. The relevant quantum numbers for the bound states $|\phi_i\rangle$, $|\phi_j\rangle$ which make up the initial superposition state are the energy E_i and the total angular momentum and its *z* projection, J_i and M_i respectively; hence we denote the states as $|E_i, J_i, M_i\rangle$, etc. The products' label *m* is composed of the final CH_3 (umbrella) vibrational state *v*, the CH_3

scattering angles relative to the polarization direction of the photolysis laser $\hat{\mathbf{k}} (= \phi_k, \theta_k)$, and the products' electronic state index $q = 1$ or $q = 2$.

The molecule is a symmetric top rather than a simple rotator owing to the presence of λ , the projection of the *total* angular momentum on the $\text{CH}_3\text{-I}$ axis. In general, λ is a projection of both the electronic angular momentum and the rotation of the CH_3 group about the C-I axis. In the present discussion we ignore the nuclear component of λ and concentrate on the electronic component.

In the photoexcitation to the first (A) continuum of CH_3I , λ assumes the values 0 (the ground and the $^3\text{Q}_0$ states) and ± 1 (the $^1\text{Q}_1$ state). In the diabatic representation [40], $\lambda = 0$ correlates with $q = 1$, the $\text{CH}_3 + \text{I}^* \ ^2\text{P}_{1/2}$ fragment channels and $\lambda = \pm 1$ with $q = 2$, the $\text{CH}_3 + \text{I}^* \ ^2\text{P}_{3/2}$ channel. We therefore use λ and q interchangeably in describing the products' electronic states.

For a symmetric-top molecule the three-dimensional photodissociation amplitude can be written as [40]

$$\langle E, \hat{\mathbf{k}}, v, \lambda^- | d_e | E_i, J_i, M_i \rangle = \frac{(2\mu k_{v\lambda})^{1/2}}{h} \sum_J \begin{pmatrix} J & 1 & J_i \\ -M_i & 0 & M_i \end{pmatrix} (2J+1)^{1/2} D_{\lambda, M_i}^J(\phi_k, \theta_k, -\phi_k) t(E, J, \lambda, v | E_i, J_i). \quad (41)$$

Here μ is the reduced-mass of the $\text{CH}_3\text{-I}$ pair, $k_{v\lambda}$ is the magnitude of the $\text{CH}_3(v)$ to $\text{I}(\lambda)$ relative wave-vector, and $t(E, J, \lambda, v | E_i, J_i)$ are the (M_i -independent) reduced amplitudes, containing the essential dynamics of the photodissociation process [40].

With the use of equation (41), the integral attributes which enter the general coherent control expression (equation (18)) are

$$\begin{aligned} d^{(\lambda)}(E_i, J_i, M_i; E_j, J_j, M_j; E) &= \sum_v \int d\hat{\mathbf{k}} \langle E_i, J_i, M_i | d_e | E, \hat{\mathbf{k}}, v, \lambda^- \rangle \langle E, \hat{\mathbf{k}}, v, \lambda^- | d_e | E_j, J_j, M_j \rangle \\ &= \frac{8\pi\mu}{\hbar^2} \delta_{M_i, M_j} \sum_{v, J} k_{v\lambda} \begin{pmatrix} J & 1 & J_i \\ -M_i & 0 & M_i \end{pmatrix} \begin{pmatrix} J & 1 & J_j \\ -M_j & 0 & M_j \end{pmatrix} \\ &\quad \times t(E, J, \lambda, v | E_i, J_i) t^*(E, J, \lambda, v | E_j, J_j). \end{aligned} \quad (42)$$

The δ_{M_i, M_j} factor arises from the angular integration and the orthogonality of the Wigner D functions [54]. We see immediately that, even for the $i \neq j$ interference term, $M_i = M_j$ is required for non-zero $d^{(\lambda)}$. Since coherent control vanishes if the interference term vanishes, we conclude that, for the superposition-state scenario, control with linearly polarized light is possible only when the states which make up the superposition state have *equal* magnetic quantum numbers.

This requirement is actually because the two excitation pathways must be able to access continuum states with the same M quantum number. In the case of linear polarization the photoexcitation process cannot change M ; hence we have the requirement that $M_i = M_j$ in the initial superposition state. For circular polarization, M changes by ± 1 and the appropriate selection rule is that $M_i = M_j \pm 1$. These two opposed selection rules immediately preclude the use of a *single* bound state with two *different* polarizations (linear + circular or two circular polarizations of opposite sense) for *integral* control. However, there are no limitations on differential control [5] since two states of different quantum numbers M can interfere under these circumstances.

We now proceed to explore two cases of interest; the first, where the initial state is M selected, and the second where no such selection is assumed. These cases are treated below.

3.1. *M-polarized initial states*

We consider exciting a superposition of two bound states: $|E_1, J_1, M_1\rangle$ and $|E_2, J_2, M_2 = M_1\rangle$ with linearly polarized light. The choice $M_2 = M_1$ is consistent with the above discussion for linearly polarized light. The excitation by radiation with two colours raises the system to energy E as described above in §1.3. Equation (18), in conjunction with equation (42), is not directly applicable.

The symmetry properties of the 3- j symbols [54] imply that

$$d^{(\lambda)}(E_i, J_i, M_i; E_j, J_j, M_j; E) = (-1)^{(J_i + J_j)} d^{(\lambda)}(E_i, J_i, -M_i; E_j, J_j, -M_j; E). \quad (43)$$

Therefore the relative product yields $R(1, 2; E)$ are identical for the case of $|M_1|$ and $-|M_1|$ if $J_1 + J_2$ is even. In the case of odd $J_1 + J_2$, the interference term changes sign when going from $|M_1|$ to $-|M_1|$. The control maps (i.e. yield against S and $\theta_1 - \theta_2$) of the M -polarized case are identical for the $|M_1|$ and $-|M_1|$ case, except for a shift in the relative phase $\theta_1 - \theta_2$ of π . For the *unpolarized* case, this result is shown below to lead to cancellation of the interference term for states of different parities.

Figures 11(a) and 12(a) display the yield of $I^* {}^2P_{1/2}$ for two different M -selected initial bound-state superpositions. Results are shown at $\omega_1 = 39\,638\text{ cm}^{-1}$, which is near the absorption maximum. For our present discussion, the main feature worth noting is that the equal-parity case in figure 12(a), where $J_1 = J_2 = 2$, is strikingly different from the unequal-parity case in figure 11(a), where $J_1 = 1$ and $J_2 = 2$. The equal-parity maps show a wider range of control compared with the unequal-parity results.

In addition to the above, the actual value assumed by M of the initial beam is of importance. This is most noticeable in the unequal-parity case, where the $M = 1$ case in figure 11(a) is drastically different from the $M = 0$ case in figure 13 which shows *no phase control*. This loss of control follows from the properties of the 3- j symbols of equation (42) which are zero whenever $M_1 = 0$ and $J_1 + J_2$ is odd [54].

3.2. *M-averaged initial states*

In this case the initial state is defined by the density matrix

$$\rho_0 = \frac{1}{J_1 + 1} \sum_{M_1} c_1 |E_1, J_1, M_1\rangle \langle E_1, J_1, M_1| + c_2 |E_2, J_2, M_1\rangle \langle E_2, J_2, M_1|. \quad (44)$$

Each of the superposition states which make up our initial density matrix may be treated independently in the subsequent two-colour irradiation which lifts the system to E . The resultant probability $P(q, E)$ of observing product channel q at energy E is obtained as an average over the $2J_1 + 1$ superpositions:

$$P(q, E) = \frac{(\pi/\hbar)^2}{2J_1 + 1} \sum_{i=1,2} \sum_{j=1,2} \sum_{M_1} F_{i,j} d^{(\lambda)}(E_i, J_i, M_i; E_j, J_j, M_j; E), \quad (45)$$

where $F_{i,j} \equiv c_i c_j^* \tilde{\epsilon}_i \tilde{\epsilon}_j^*$. From equation (42) it follows that the M_1 dependence of $d^{(\lambda)}(E_i, J_i, M_i; E_j, J_j, M_j; E)$ is entirely contained in the 3- j product

$$\begin{pmatrix} J & 1 & J_i \\ -M_1 & 0 & M_1 \end{pmatrix} \begin{pmatrix} J & 1 & J_j \\ -M_1 & 0 & M_1 \end{pmatrix}. \quad (46)$$

Hence, the M_1 summation can be performed separately. Defining

$$C_{i,j}(J) \equiv \frac{1}{2J_1 + 1} \sum_{M_1} \begin{pmatrix} J & 1 & J_i \\ -M_1 & 0 & M_1 \end{pmatrix} \begin{pmatrix} J & 1 & J_j \\ -M_1 & 0 & M_1 \end{pmatrix} F_{i,j}, \quad (47)$$

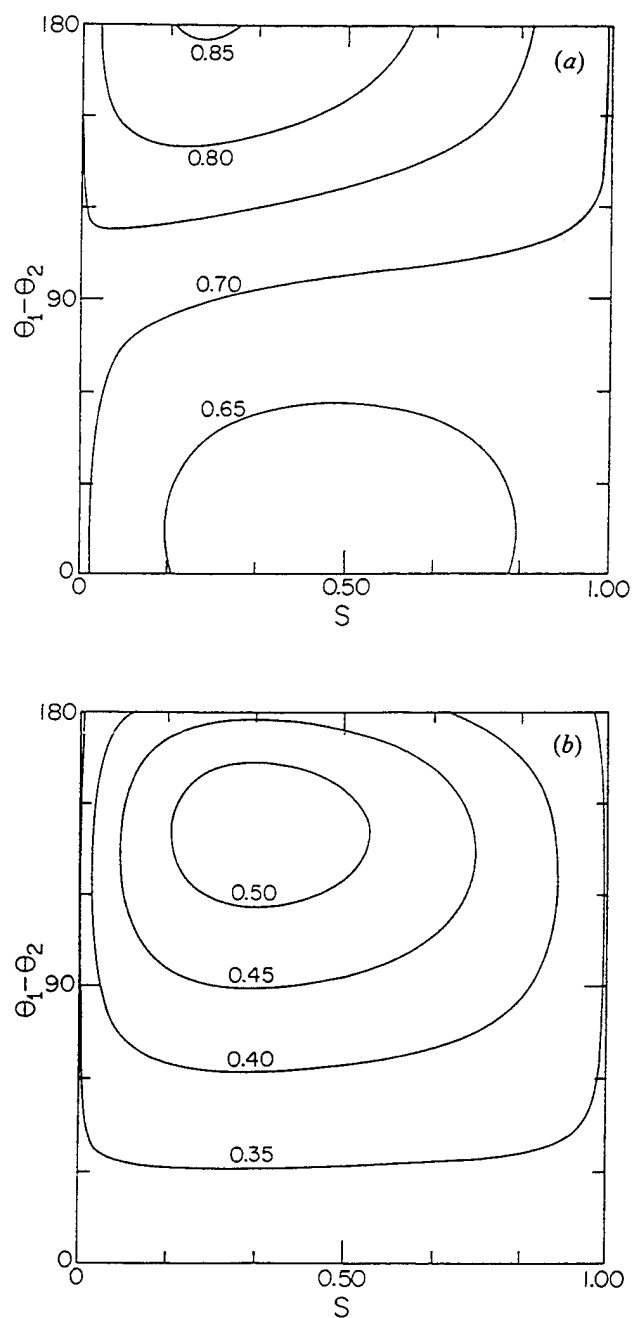


Figure 11. Contour plot of the yield of $I^*(^2P_{1/2})$ (i.e. percentage of I^* as product) in the photodissociation of CH_3I from a polarized superposition state composed of $v_1=0, J_1=1$ and $v_2=0, J_2=2$, where $M_1=M_2=1$, at (a) $\omega_{E_1}=39\,638\text{ cm}^{-1}$ and (b) $\omega_{E_1}=42\,367\text{ cm}^{-1}$. $v=0$ denotes the ground vibrational state of CH_3I . The abscissa is labelled by $S=x^2/(1+x^2)$, where x is the ratio of laser field intensities and the ordinate by the relative phase parameter $\theta=\theta_1-\theta_2$ (after [3]).

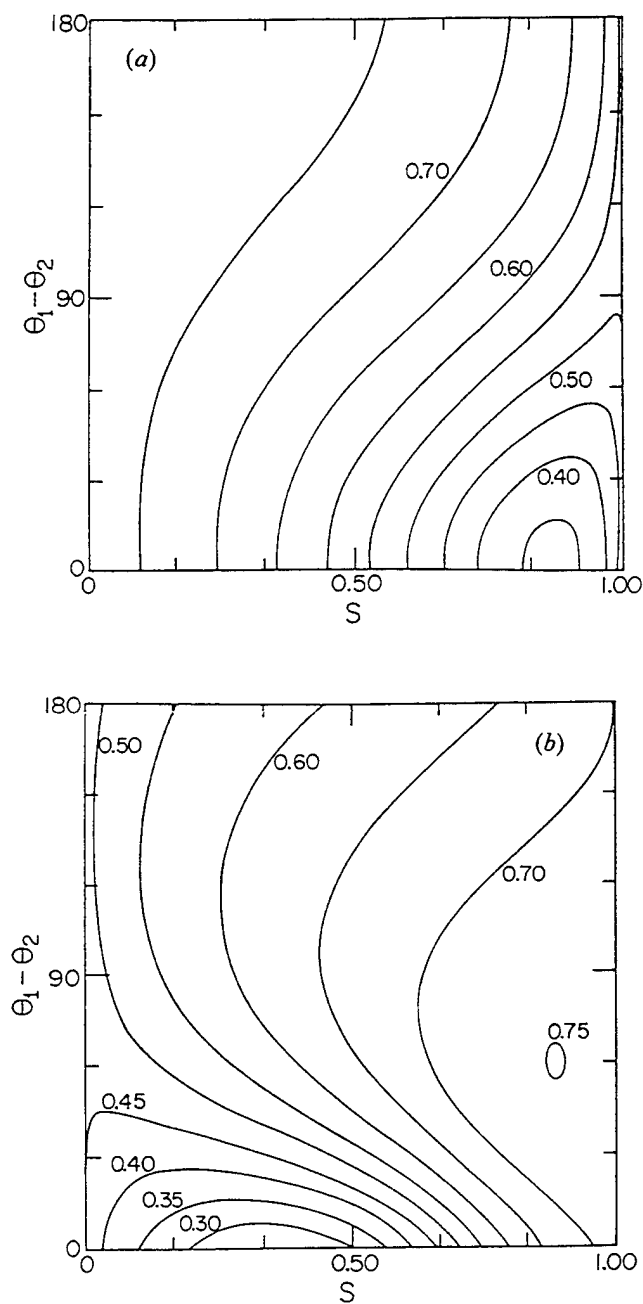


Figure 12. As in figure 11 but $v_1=0, J_1=2, v_2=1, J_2=2, M_1=M_2=0$, at (a) $\omega_{E_1}=39\,638\text{ cm}^{-1}$ and (b) $\omega_{E_1}=42\,367\text{ cm}^{-1}$. $v=1$ denotes the first vibrationally excited state of CH_3I (essentially the first excitation of the C-I stretch (after [3])).

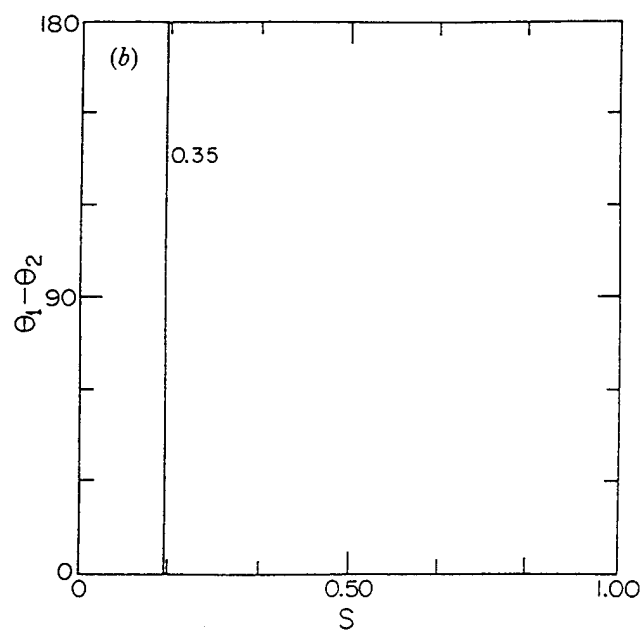
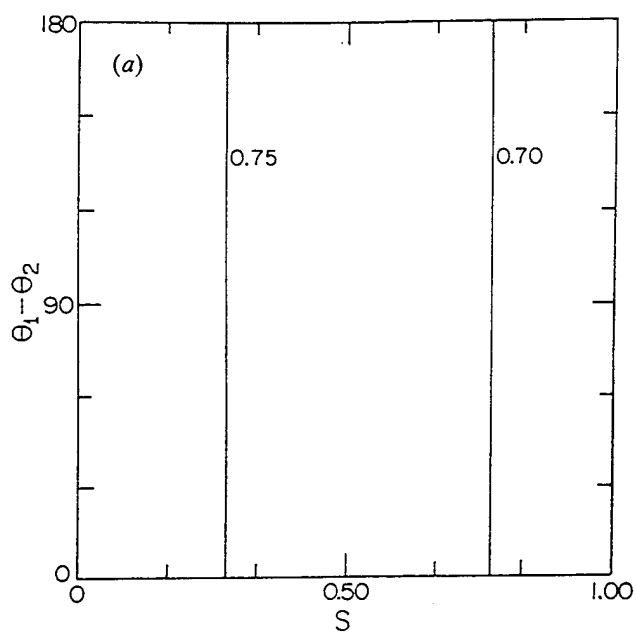


Figure 13. As in figure 11 but $v_1=0, J_1=1, v_2=0, J_2=2, M_1=M_2=0$ (no phase control is seen since J_1+J_2 is odd and $M_1=0$): (a) $\omega_{E_1}=39\,638\text{ cm}^{-1}$; (b) $\omega_{E_1}=42\,367\text{ cm}^{-1}$ (after [3]).

we have that

$$P(q, E) = \left(\frac{\pi}{h}\right)^2 \sum_{i=1,2} \sum_{j=1,2} t^{(q)}(E_i, J_i; E_j, J_j; E), \quad (48)$$

where

$$t^{(q)}(E_i, J_i; E_j, J_j; E) \equiv \sum_{J, v} C_{i,j}(J) t(E, J, \lambda, v | E_i, J_i) t^*(E, J, \lambda, v | E_j, J_j). \quad (49)$$

It follows immediately from the symmetry properties of the 3- j symbols [54] and equations (47) that $t^{(q)}(E_1, J_1; E_2, J_2; E)$ is zero if $J_1 + J_2$ is odd, that is yield control in

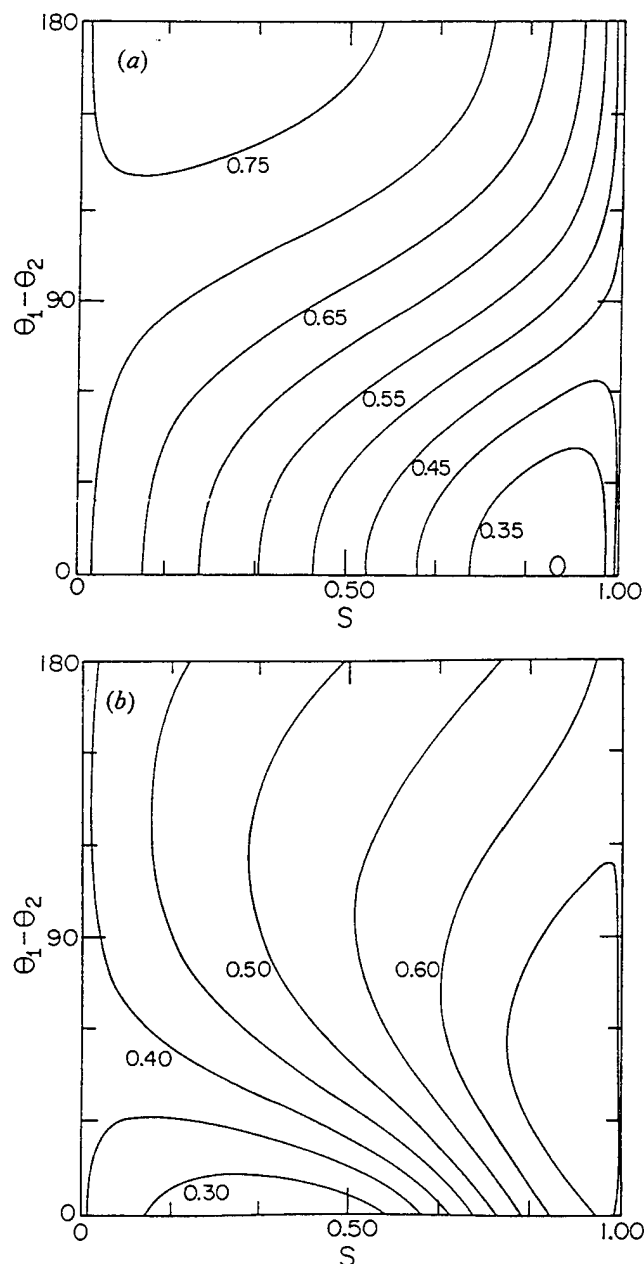


Figure 14. $I^*(^2P_{1/2})$ yield in the photodissociation of CH_3I starting from an M -averaged (unpolarized) ensemble of superposition states, where the J and v are as in figure 12: (a) $\omega_{E_1} = 39\,639\text{ cm}^{-1}$; and (b) $\omega_{E_1} = 42\,367\text{ cm}^{-1}$ (after [3]).

M -averaged situations requires J_1 and J_2 of equal parity. Another way of reaching the same conclusion is to note, as discussed above, that for odd $J_1 + J_2$, when we perform the M_1 summation, the positive M_1 terms cancel out the negative M_1 terms and the $M_1 = 0$ term is identically zero. We conclude that, for unpolarized initial states, only two states of equal parity can be made to interfere such that control of integral quantities arises.

The expression for the yield $R(1,2;E)$ now follows directly as the ratio of $P(1,E)/P(2,E)$ in equation (48). Figure 14 shows the result for coherent radiative control of an initial M -averaged pair of states of equal parity at two different values of ω_1 . The range of control demonstrated is very wide; at the peak of the absorption (figure 14(a), the $I^*(^2P_{1/2})$ quantum yield changes from 30%, for $S=0.9$ and $\theta_1 - \theta_2 = 0^\circ$, to 75% for $S=0.2$ and $\theta_1 - \theta_2 = 140^\circ$. A comparison with the even $J_1 + J_2$ polarized case (figure 12) shows that the range of control degrades only slightly with M averaging. This is to be contrasted (figure 11 compared with 13) with the odd $J_1 + J_2$ case.

4. '2+2' control of a thermal ensemble

In practice there are a number of sources of incoherence which tend to diminish control. Prominent amongst these are effects due to an initial thermal distribution of states and effects due to partial coherence of the laser source. Below we describe one approach, based upon a resonant '2+2' scenario, which deals effectively with both problems. An alternative method in which coherence is retained in the presence of collisions has been discussed elsewhere [7].

The specific scheme that we advocate is depicted, for the particular case of Na_2 photodissociation, in figure 15. Here the molecule is lifted from an initial bound state $|E_i, J_i, M_i\rangle$ to energy E via two independent two-photon routes. To introduce notation, first consider a single such two-photon route. Absorption of the first photon of frequency ω_1 lifts the system to a region close to an intermediate bound state $|E_m, J_m, M_m\rangle$, and a second photon of frequency ω_2 carries the system to the dissociating states $|E, \mathbf{k}, q^-\rangle$, where the scattering angles are specified by $\mathbf{k} = (\theta_k, \phi_k)$. Here the J values are the angular momentum, the M values are their projection along the z axis, and the values of energy E_i and E_m include specification of the vibrational quantum numbers. Specifically, if we denote the phases of the coherent states by ϕ_1 and ϕ_2 , the wave-vectors by \mathbf{k}_1 and \mathbf{k}_2 with overall phases $\theta_i = \mathbf{k}_i \cdot \mathbf{R} + \phi_i$ ($i=1,2$) and the electric field amplitudes by ε_1 and ε_2 , then the probability amplitude for resonant two-photon ($\omega_1 + \omega_2$) photodissociation is given [18, 45] by

$$\begin{aligned}
 & T_{\mathbf{k}q,i}(E, E_i, J_i, M_i, \omega_2, \omega_1) \\
 &= \sum_{E_m, J_m} \frac{\langle E, \mathbf{k}, q^- | \mathbf{d}_2 \varepsilon_2 | E_m, J_m, M_m \rangle \langle E_m, J_m, M_m | \mathbf{d}_1 \varepsilon_1 | E_i, J_i, M_i \rangle}{\omega_1 - (E_m + \delta_m - E_i) + i\Gamma_m} \exp[i(\theta_1 + \theta_2)] \\
 &= \frac{(2\mu k_q)^{1/2}}{h} \sum_{J, p, \lambda \geq 0} \sum_{E_m, J_m} \begin{pmatrix} J & 1 & J_m \\ -M_i & 0 & M_i \end{pmatrix} \begin{pmatrix} J_m & 1 & J_i \\ -M_i & 0 & M_i \end{pmatrix} \\
 & \times (2J+1)^{1/2} D_{\lambda, M_i}^{Jp}(\theta_k, \phi_k, 0) t(E, E_i, J_i, \omega_2, \omega_1, q | Jp\lambda, E_m, J_m) \exp[i(\theta_1 + \theta_2)]. \quad (50)
 \end{aligned}$$

Here \mathbf{d}_i is the component of the dipole moment along the electric field vector of the i th laser mode, $E = E_i + (\omega_1 + \omega_2)$, δ_m and Γ_m are the radiative shift and width respectively of the intermediate state, μ is the reduced mass, and k_q is the relative momentum of the dissociated product in the q channel. The D_{λ, M_i}^{Jp} is the parity-adopted rotation matrix

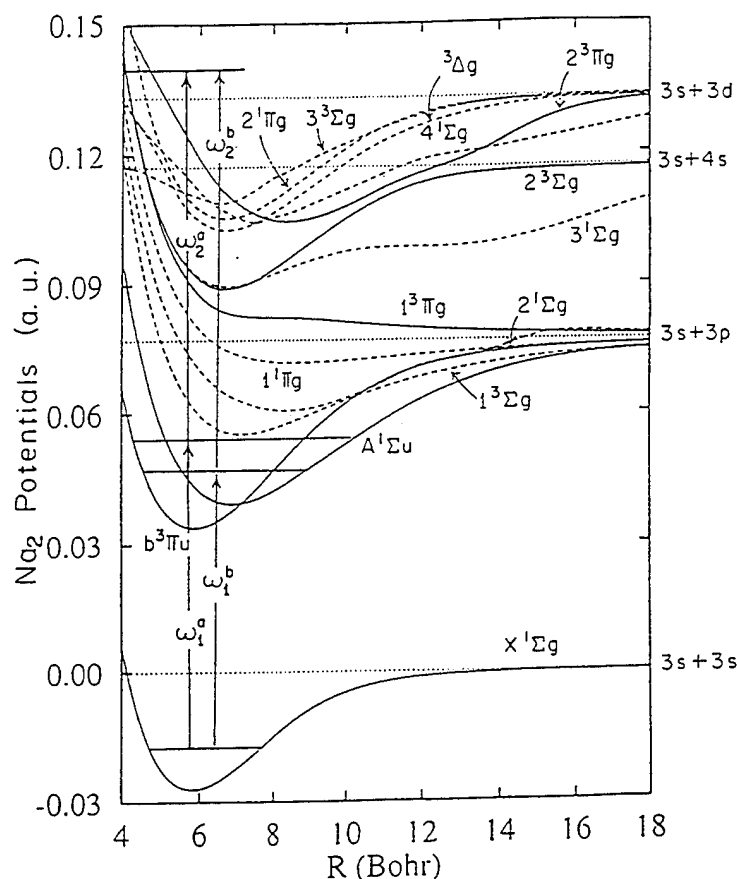


Figure 15. Two resonant two-photon paths in the photodissociation of Na₂ (from [18]).

[55] with λ the magnitude of the projection on the internuclear axis of the electronic angular momentum and $(-1)^J p$ the parity of the rotation matrix. We have set $\hbar \equiv 1$, and assumed for simplicity lasers which are linearly polarized, with parallel electric field vectors. Note that the T-matrix element in equation (50) is a complex quantity, whose phase is the sum of the laser phase $\theta_1 + \theta_2$ and the molecular phase, that is the phase of t .

The probability of producing the fragments in the q channel is obtained by integrating the square of equation (50) over the scattering angles $\hat{\mathbf{k}}$, with the result

$$\begin{aligned}
 P^{(q)}(E, E_i J_i M_i, \omega_2, \omega_1) &= \int d\hat{\mathbf{k}} |T_{\hat{\mathbf{k}}q,i}(E, E_i J_i M_i, \omega_2, \omega_1)|^2 \\
 &= \frac{8\pi\mu k_q}{h^2} \sum_{J,p,\lambda \geq 0} \left| \sum_{E_m, J_m} \begin{pmatrix} J & 1 & J_m \\ -M_i & 0 & M_i \end{pmatrix} \begin{pmatrix} J_m & 1 & J_i \\ -M_i & 0 & M_i \end{pmatrix} \right. \\
 &\quad \times t(E, E_i J_i, \omega_2, \omega_1, q | J p \lambda, E_m J_m) \Big|^2. \quad (51)
 \end{aligned}$$

Because the t-matrix element contains a factor of $[\omega_1 - (E_m + \delta_m - E_i) + i\Gamma_m]^{-1}$ the probability is greatly enhanced by the approximate inverse square of the detuning $\Delta = \omega_1 - (E_m + \delta_m - E_i)$ as long as the line width $\Gamma_m < \Delta$. Hence only the levels closest to the resonance $\Delta = 0$ contribute significantly to the dissociation probability. This allows us to photodissociate molecules selectively from a thermal bath, reestablishing coherence necessary for quantum interference based control and overcoming dephasing effects due to collisions.

Consider then the following coherent control scenario. A molecule is irradiated with three interrelated frequencies ω_0 , ω_+ and ω_- where photodissociation occurs at $E = E_i + 2\omega_0 = E_i + (\omega_+ + \omega_-)$ and where ω_0 and ω_+ are chosen to be resonant with intermediate bound-state levels. The probability of photodissociation at energy E into arrangement channel q is then given by the square of the sum of the T-matrix elements from pathway a ($\omega_0 + \omega_0$) and pathway b ($\omega_+ + \omega_-$). That is, the probability into channel q

$$P_q(E, E_i J_i M_i; \omega_0, \omega_+, \omega_-) \equiv \int d\mathbf{k} |T_{\mathbf{k}q, i}(E, E_i J_i M_i; \omega_0, \omega_0) + T_{\mathbf{k}q, i}(E, E_i J_i M_i; \omega_+, \omega_-)|^2 \\ \equiv P^{(q)}(a) + P^{(q)}(b) + P^{(q)}(ab). \quad (52)$$

Here $P^{(q)}(a)$ and $P^{(q)}(b)$ are the independent photodissociation probabilities associated with routes a and b , respectively, and $P^{(q)}(ab)$ is the interference term between them, discussed below. Note that the two T-matrix elements in equation (52) are associated with different lasers and as such contain different laser phases. Specifically, the overall phase of the three laser fields are $\theta_0 = \mathbf{k}_0 \cdot \mathbf{R} + \phi_0$, $\theta_+ = \mathbf{k}_+ \cdot \mathbf{R} + \phi_+$ and $\theta_- = \mathbf{k}_- \cdot \mathbf{R} + \phi_-$, where ϕ_0 , ϕ_+ and ϕ_- are the photon phases, and \mathbf{k}_0 , \mathbf{k}_+ and \mathbf{k}_- are the wave-vectors of the laser modes ω_0 , ω_+ and ω_- , whose electric field strengths are ε_0 , ε_+ and ε_- and intensities I_0 , I_+ and I_- .

The optical path-path interference term $P^{(q)}(ab)$ is given by

$$P^{(q)}(ab) = 2[F^{(q)}(ab)] \cos(\alpha_a^q - \alpha_b^q), \quad (53)$$

with the relative phase

$$\alpha_a^q - \alpha_b^q = (\delta_a^q - \delta_b^q) + (2\theta_0 - \theta_+ - \theta_-), \quad (54)$$

where the amplitude $|F^{(q)}(ab)|$ and the molecular phase difference $\delta_a^q - \delta_b^q$ are defined by

$$|F^{(q)}(ab)| \exp[i(\delta_a^q - \delta_b^q)] \\ = \frac{8\pi k_q}{h^2} \sum_{J, p, \lambda \geq 0} \sum_{E_m, J_m} \sum_{E'_m, J'_m} \begin{pmatrix} J & 1 & J_m \\ -M_i & 0 & M_i \end{pmatrix} \begin{pmatrix} J_m & 1 & J_i \\ -M_i & 0 & M_i \end{pmatrix} \begin{pmatrix} J & 1 & J'_m \\ -M_i & 0 & M_i \end{pmatrix} \\ \times \begin{pmatrix} J'_m & 1 & J_i \\ -M_i & 0 & M_i \end{pmatrix} t(E, E_i J_i, \omega_0, \omega_0, q|Jp\lambda, E_m J_m) t^*(E, E_i J_i, \omega_-, \omega_+, q|Jp\lambda, E'_m J'_m). \quad (55)$$

Consider now the quantity $R_{qq'}$ of interest, which is the branching ratio of the product in the q channel to that in the q' channel. Noting that in the weak-field case $P^{(q)}(a)$ is proportional to ε_0^4 , $P^{(q)}(b)$ to $\varepsilon_+^2 \varepsilon_-^2$, and $P^{(q)}(ab)$ to $\varepsilon_0^2 \varepsilon_+ \varepsilon_-$, we can write

$$R_{qq'} = \frac{\mu_{aa}^{(q)} + x^2 \mu_{bb}^{(q)} + 2x |\mu_{ab}^{(q)}| \cos(\alpha_a^q - \alpha_b^q) + B^{(q)}/\varepsilon_0^4}{\mu_{aa}^{(q')} + x^2 \mu_{bb}^{(q')} + 2x |\mu_{ab}^{(q')}| \cos(\alpha_a^{q'} - \alpha_b^{q'}) + B^{(q')}/\varepsilon_0^4}, \quad (56)$$

where $\mu_{aa}^{(q)} = P^{(q)}(a)/\varepsilon_0^4$, $\mu_{bb}^{(q)} = P^{(q)}(b)/\varepsilon_+^2 \varepsilon_-^2$ and $|\mu_{ab}^{(q)}| = |F^{(q)}(ab)|/\varepsilon_0^2 \varepsilon_+ \varepsilon_-$ and $x = \varepsilon_+ \varepsilon_- / \varepsilon_0^2 = (I_+ I_-)^{1/2} / I_0$. The terms with $B^{(q)}$ and $B^{(q')}$, described below correspond to resonant photodissociation routes to energies other than $E = E_i + 2\hbar\omega_0$ and hence [4] to terms which do not coherently interfere with the pathways a and b . Minimization of these terms, due to absorption of $\omega_0 + \omega_-$, $\omega_0 + \omega_+$, $\omega_+ + \omega_0$ or $\omega_+ + \omega_+$, has been discussed elsewhere [18, 45]. Here we just emphasize that the product ratio in equation (56) depends upon both the laser intensities and the relative laser phase. Hence manipulating these laboratory parameters allows for control over the relative cross-section between channels.

The proposed scenario, embodied in equation (56), also provides a means by which control can be improved by eliminating effects due to laser jitter. Specifically, the term $2\phi_0 - \phi_+ - \phi_-$ contained in the relative phase $\alpha_a^q - \alpha_b^q$ can be subject to the phase fluctuations arising from laser instabilities. If such fluctuations are sufficiently large, then the interference term in equation (56), and hence control, disappears [19]. The following experimentally desirable implementation of the above two-photon-plus-two-photon scenario readily compensates for this problem. Specifically, consider generating $\omega_+ = \omega_0 + \delta$ and $\omega_- = \omega_0 - \delta$ in a parametric process by passing a beam of frequency $2\omega_0$ through a nonlinear crystal. This latter beam is assumed to be generated by second-harmonic generation from the laser ω_0 with the phase ϕ_0 . Then the quantity $2\phi_0 - \phi_+ - \phi_-$ in the phase difference between the $\omega_0 + \omega_0$ and $\omega_+ + \omega_-$ routes is a constant. That is, in this particular scenario, fluctuations in ϕ_0 cancel and have no effect on the relative phase $\alpha_a^q - \alpha_b^q$. Thus the two-photon-plus-two-photon scenario is insensitive to the laser jitter of the incident laser fields.

To examine the range of control afforded by this scheme consider the photodissociation of Na_2 in the regimen below the Na (3d) threshold where dissociation is to two product channels $\text{Na} (3s) + \text{Na} (3p)$ and $\text{Na} (3s) + \text{Na} (4s)$. Two-photon dissociation of Na_2 from a bound state of the $^1\Sigma_g^+$ state occurs [18,45] in this region by initial excitation to an excited intermediate bound state $|E_m J_m M_m\rangle$. The latter is a superposition of states of the $A^1\Sigma_u^+$ and $b^3\Pi_u$ electronic curves, a consequence of spin-orbit coupling. That is, the two-photon photodissociation can be viewed [45] as occurring via intersystem crossing subsequent to absorption of the first photon. The continuum states reached in the excitation can be either of singlet or triplet character but, despite the multitude of electronic states involved in the computation, the predominant contributions to the products $\text{Na} (3p)$ and $\text{Na} (4s)$ are found to come from the $^3\Pi_g$ and $^3\Sigma_g^+$ states, respectively. Methods for computing the required photodissociation amplitude, which involves eleven electronic states have been discussed elsewhere [45]. Since the resonant character of the two-photon excitation allows us to select a single initial state from a thermal ensemble, we consider here the specific case of $v_i = J_i = 0$ without loss of generality, where v_i and J_i denote the vibrational and the rotational quantum numbers respectively of the initial state.

The ratio $R_{qq'}$ depends on a number of laboratory control parameters including the relative laser intensities x , the relative laser phase and the ratio of ε_+ to ε_- via η . In addition, the relative cross-sections can be altered by modifying the detuning. Typical control results are shown in figure 16 which provides contour plots of the Na (3p) yield (i.e. the ratio of the probability of observing Na (3p) to the sum of the probabilities to form Na (3p) plus Na (4s)). The figure axes are the ratio x of the laser amplitudes and the relative laser phase $\delta\theta = 2\theta_0 - \theta_+ - \theta_-$. Here $\omega_0 = 631.899$ nm, $\omega_+ = 562.833$ nm and $\omega_- = 720.284$ nm and control is seen to be large, ranging from 30 to 90% Na (3p) as $\delta\theta$ and x are varied.

Note that the proposed approach is not limited to the specific frequency scheme discussed above. Essentially all that is required is that the two resonant photodissociation routes lead to interference and that the cumulative laser phases of the two routes be independent of laser jitter. As one sample extension, consider the case where paths a and b are composed of totally different photons, $\omega_+^{(a)}$ and $\omega_-^{(a)}$ and $\omega_+^{(b)}$ and $\omega_-^{(b)}$, with $\omega_+^{(a)} + \omega_-^{(a)} = \omega_+^{(b)} + \omega_-^{(b)}$. Both these sets of frequencies can be generated, for example, by passing $2\omega_0$ light through nonlinear crystals, hence yielding two pathways whose relative phase is independent of laser jitter in the initial $2\omega_0$ source. Given these four frequencies, we now have an additional degree of freedom in order to optimize control,

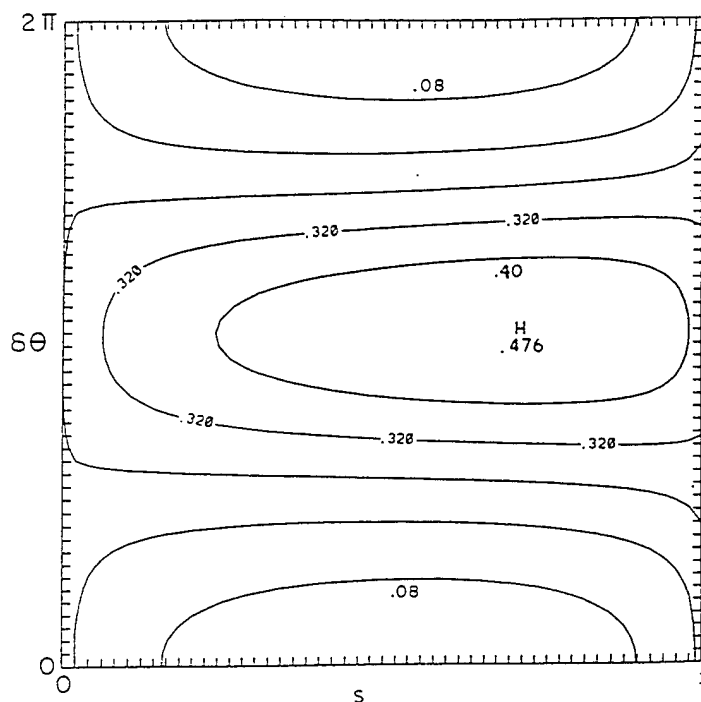


Figure 16. Contours of equal Na(3p) yield. The ordinate is the relative laser phase and the abscissa is $S=x^2/(1+x^2)$ where x is the field intensity ratio. Here $\omega_0=627.584$ nm, $\omega_+=611.207$ nm, $\omega_-=644.863$ nm and $\eta=0.5$. See [18] for a discussion of η which can be used to minimize background contributions (from [45]).

although the experiment is considerably more complicated than in the three-frequency case. Typical results for Na₂ have been provided elsewhere [18, 45]. Note also that the control is not limited to two-product channels, such as those discussed above. Recent computations [45] on higher-energy Na₂ photodissociation, where more product arrangement channels are available, show equally large ranges of control for the three-channel case.

5. Control of symmetry breaking

Weak-field phase interference has one remarkable property; it can lead to controlled *symmetry breaking* [15]. Below we show that the pump-dump scheme described above §2.2) can lead to symmetry breaking in systems with three-dimensional spherical symmetry and to the generation of chirality, provided that magnetic quantum state selection is performed. Other mechanisms for collinear symmetry breaking in *strong* fields have recently been proposed [56, 57]. There, it was shown that one can generate *even* high harmonics by exciting a symmetric double quantum well. However, in contrast with the symmetry-breaking scenario described below, the generation of even harmonics is not expected to exist in systems with three-dimensional spherical symmetry.

In general, symmetry breaking occurs whenever a system executes a transition to a *asymmetric* eigenstate of the Hamiltonian. Strictly speaking, asymmetric eigenstates (i.e. states which do not belong to any of the symmetry group representations) can occur if several degenerate eigenstates exist, each belonging to a different irreducible representation. Any linear combination of such eigenstates is asymmetric.

In practice, symmetry breaking also occurs even if the degeneracy is only approximate, as in the problem of a symmetric double-well potential. If the barrier between the two wells is such that tunnelling is very small, then the ground state of the system is composed, to all intents and purposes, of a doublet of (symmetric and antisymmetric) degenerate states. States localized at either well can then result by taking the \pm linear combinations of this doublet. Because of the near degeneracy, these asymmetric localized states are essentially eigenstates of the Hamiltonian insofar as their time evolution can be immeasurably slow.

Asymmetric eigenstates of a symmetric Hamiltonian also occur in the continuous spectrum of a BAB-type molecule. It is clear that the $|E, n, R^- \rangle$ state, which correlates asymptotically with the dissociation of the right B group, must be degenerate with the $|E, n, L^- \rangle$ state, giving rise to the departure of the left B group. It is also possible to form symmetric $|E, n, s^- \rangle$ and antisymmetric $|E, n, a^- \rangle$ eigenstates of the same Hamiltonian by taking the \pm combination of these states. There is an important physical distinction between the asymmetric states and states which are symmetric-antisymmetric: Any experiment performed in the asymptotic B — AB or BA — B regions must, by necessity, measure the probability of populating an asymmetric state. This follows because, when the B — AB distance or the BA — B distance is large, a given group B is either far away from or close to group A. Thus symmetric and antisymmetric states are not directly observable in the asymptotic regime.

We conclude that the very act of observation of the dissociated molecule entails the collapse of the system to one of the asymmetric states. As long as the probability of collapse to the $|E, n, R^- \rangle$ state is equal to the probability of collapse to the $|E, n, L^- \rangle$ state, the collapse to an asymmetric state does not lead to a preference of R over L in an ensemble of molecules. This is the case when the above collapse ('symmetry breaking') is spontaneous, that is occurring owing to some (random) factors not in our control. CC techniques allow us to influence these probabilities. In this case, symmetry breaking is stimulated rather than spontaneous. This has a far-reaching physical and practical significance.

One of the most important cases of symmetry breaking arises when the two B groups (now denoted as B and B') are not identical, but are enantiomers of one another. (Two groups of atoms are said to be enantiomers of one another if one is the mirror image of the other. If these groups are also 'chiral', i.e. they lack a centre of inversion symmetry, then the two enantiomers are distinguishable and can be detected through the distinctive direction of rotation of linearly polarized light.)

The existence and role of enantiomers is recognized as one of the fundamental broken symmetries in nature [58]. It has motivated a long-standing interest in asymmetric synthesis, that is a process which preferentially produces a specific chiral species. Contrary to the prevailing belief (for a discussion see [59]; for historical examples see [60]) that asymmetric synthesis must necessarily involve either chiral reactants, or chiral external system conditions such as chiral crystalline surfaces, we show below that preferential production of a chiral photofragment can occur even though the parent molecule is not chiral. In particular two results are demonstrated.

- (1) Ordinary photodissociation, using linearly polarized light, of a BAB' 'pro-chiral' molecule may yield different cross-sections for the production of right-handed (B) and left-handed (B') products, when the direction of the angular momentum m_j of the products is selected.
- (2) This natural symmetry breaking may be enhanced and controlled using coherent lasers.

To treat this problem we return to the formulation of the pump-dump scenario described above, with attention focused on control of the relative yield of two product arrangement channels, but with angular momentum projection m_j fixed. That is

$$Y = P(q, m_j) / \sum_q P(q, m_j), \quad (57)$$

Explicitly considering the dissociation of BAB' into right-handed products R and left-handed products L we have

$$Y = \frac{P(L, m_j)}{[P(L, m_j) + P(R, m_j)]}. \quad (58)$$

As above, the product ratio Y is a function of the delay time $\tau = t_d - t_x$ and the ratio $x = |c_1/c_2|$, the latter by detuning the initial excitation pulse. Active control over the products $B + AB'$ against $B' + AB$, that is a variation in Y with τ and x , and hence control over left-handed against right-handed products, will result only if $P(R, m_j)$ and $P(L, m_j)$ have different functional dependences on x and τ .

We now show that $P(R, m_j)$ may be different from $P(L, m_j)$ for the $B'AB$ case. We first note that this molecule belongs to the C_s point group which is a group possessing only one symmetry plane. This plane, denoted as σ , is defined as the collection of the C_{2v} points, that is points satisfying the $B - - A = A - - B'$ condition, where $B - - A$ designates the distance between the B and A groups. We choose the intermediate state $|E_1\rangle$ to be *symmetric* and the state $|E_2\rangle$ to be *antisymmetric* with respect to reflection in the σ plane. Furthermore, we shall focus upon transitions between electronic states of the same representations, for example A' to A' or A'' to A'' (where A' denotes the symmetric representation and A'' the antisymmetric representation the C_s group). We further assume that the ground vibronic state belongs to the A' representation.

The first thing to demonstrate is that it is possible to excite simultaneously, by optical means, both the symmetric $|E_1\rangle$ and antisymmetric $|E_2\rangle$ states. Using equation (35) we see that this requires the existence of both a symmetric \mathbf{d} component, denoted as \mathbf{d}_s , and an antisymmetric \mathbf{d} component, denoted \mathbf{d}_a , because, by symmetry properties of $|E_1\rangle$ and $|E_2\rangle$,

$$\langle E_1 | \mathbf{d} | E_g \rangle = \langle E_1 | \mathbf{d}_s | E_g \rangle, \quad \langle E_2 | \mathbf{d} | E_g \rangle = \langle E_2 | \mathbf{d}_a | E_g \rangle. \quad (59)$$

The existence of both dipole moment components occurs in $A' \rightarrow A'$ electronic transitions whenever a bent $B' - - A - - B$ molecule deviates considerably from the equidistant C_{2v} geometries (where $\mathbf{d}_a = 0$). The effect is non-Franck-Condon in nature, because we no longer assume that the dipole moment does not vary with the nuclear configurations. (In the theory of vibronic transitions terminology this existence of both \mathbf{d}_s and \mathbf{d}_a , is due to a Herzberg-Teller intensity borrowing [61] mechanism.)

We conclude that the excitation pulse *can* create a $|E_1\rangle$, $|E_2\rangle$ superposition consisting of two states of different reflection symmetry, which is therefore asymmetric. We now wish to show that this asymmetry established by exciting *non-degenerate bound* states translates to an asymmetry in the probability of populating the two *degenerate* $|E, n, R^-\rangle$, $|E, n, L^-\rangle$ continuum states. We proceed by examining the properties of the bound-free transition matrix elements of equation (39) entering the probability expression of equation (38).

Although the continuum states $|E, n, q^-\rangle$ of interest are asymmetric, they satisfy a closure relation, since $\sigma|E, n, R^-\rangle = |E, n, L^-\rangle$ and vice versa. Working with the symmetric and antisymmetric continuum eigenfunctions

$$|E, n, R^-\rangle \equiv \frac{(|E, n, s^-\rangle + |E, n, a^-\rangle)}{2^{1/2}}, \quad (60)$$

$$|E, n, L^-\rangle \equiv \frac{(|E, n, s^-\rangle - |E, n, a^-\rangle)}{2^{1/2}}, \quad (61)$$

using the fact that $|E_1\rangle$ is symmetric and $|E_2\rangle$ antisymmetric, and adopting the notation $A_{s2} \equiv \langle E, n, s^- | \mathbf{d}_a | E_2 \rangle$, $S_{a1} \equiv \langle E, n, a^- | \mathbf{d}_s | E_1 \rangle$, etc., we have

$$\mathbf{d}_{11}^{(q)} = \Sigma' [|S_{s1}|^2 + |A_{a1}|^2 \pm 2 \operatorname{Re}(A_{a1} S_{s1}^*)], \quad (62)$$

$$\mathbf{d}_{22}^{(q)} = \Sigma' [|A_{s2}|^2 + |S_{a2}|^2 \pm 2 \operatorname{Re}(A_{s2} S_{a2}^*)], \quad (63)$$

$$\mathbf{d}_{12}^{(q)} = \Sigma' (S_{s1} A_{s2}^* + A_{a1} S_{s2}^* \pm S_{s1} S_{a2}^* \pm A_{a1} A_{s2}^*), \quad (64)$$

where the plus sign applies for $q = R$ and the minus sign for $q = L$. Here the sum is over all quantum numbers other than m_j .

Equation (64) displays two noteworthy features.

- (1) $\mathbf{d}_{kk}^{(R)} \neq \mathbf{d}_{kk}^{(L)}$, $k = 1, 2$. That is, the system displays *natural symmetry breaking* in photodissociation from state $|E_1\rangle$ or state $|E_2\rangle$, with right- and left-handed product probabilities differing by $4\Sigma' \operatorname{Re}(S_{s1}^* A_{a1})$ for excitation from $|E_1\rangle$ and $4\Sigma' \operatorname{Re}(A_{s2} S_{a2}^*)$ for excitation from $|E_2\rangle$. Note that these symmetry-breaking terms may be relatively small since they rely upon non-Franck-Condon contributions.
- (2) However, even in the Franck-Condon approximation, $\mathbf{d}_{12}^{(R)} \neq \mathbf{d}_{12}^{(L)}$. Thus laser-controlled symmetry breaking, which depends upon $\mathbf{d}_{12}^{(q)}$ in accordance with equation (38), is therefore possible, allowing enhancement of the enantiomer ratio for the m_j polarized product.

To demonstrate the extent of expected control, as well as the effect of m_j summation, we considered a model of the enantiomer selectivity, that is HOH photodissociation in three dimensions, where the two hydrogen atoms are assumed distinguishable. The computation is done using the formulation and computational methodology of Segev and Shapiro [62]. Below we briefly summarize the angular momentum algebra and some other details involved in performing three-dimensional quantum calculations of triatomic photodissociation [63].

We first specify the relevant quantum numbers n and i which enter the bound-free matrix elements in equation (39). For the continuum states, $n = \{\mathbf{k}, v, j, m_j\}$ where \mathbf{k} is the scattering direction, v and j are the vibrational and rotational product quantum numbers and m_j is the space-fixed z projection of j . For the bound states $i = \{E_i, M_i, J_i, p_i\}$, where J_i , M_i and p_i are the bound state angular momentum, its space-fixed z projection and its parity respectively. The full (six-dimensional) bound-free matrix element can be written as a product of analytical functions involving \hat{k} and (three-dimensional) radial matrix elements:

$$\begin{aligned} & \langle E, \mathbf{k}, v, j, m_j, q^- | \mathbf{d} | E_i, M_i, J_i, p_i \rangle \\ &= \left(\frac{\mu k_{vj}}{2\pi^2 \hbar^2} \right)^{1/2} \sum_{J\lambda} (2J+1)^{1/2} (-1)^{M_i - j - m_j} D_{\lambda M_i}^J \\ & \quad \times (\phi_k, \theta_k, 0) D_{-\lambda - m_j}^i (\phi_k, \theta_k, 0) t^{(q)}(E, J, v, j, \lambda | E_i, J_i, p_i), \end{aligned} \quad (65)$$

where \mathbf{D} are the rotation matrices, μ is the reduced mass, k_{vj} is the momentum of the products and $t^{(a)}(E, J, v, j, \lambda | E_i J_i p_i)$ is proportional to the radial partial wave matrix element [63] $\langle E, J, M, p, v, j, \lambda, q^- | \mathbf{d} | E_i, M_i, J_i, p_i \rangle$. Here λ is the projection of J along the body fixed axis of the H-OH (CM) product separation.

The product of the bound-free matrix elements in equation (65), which enter equation (39), integrated over scattering angles and average over the initial $M_k (= M_i)$ quantum numbers ($M_i = M_k$ since both $|E_i\rangle$ and $|E_k\rangle$ arise by excitation, with linearly polarized light, from a common eigenstate)

$$\begin{aligned}
 & (2J_i + 1)^{-1} \sum_{M_i} \int d\mathbf{k} \langle E_k, M_k, J_k, p_k | \mathbf{d} | E, \mathbf{k}, v, j, m_j, q'^- \rangle \langle E, \mathbf{k}, v, j, m_j, q^- | \mathbf{d} | E_i, M_i, J_i, p_i \rangle \\
 &= (-1)^{m_j} \frac{16\pi^2 v \mu}{\hbar^2 (2J_i + 1)} \sum_{vj} k_{vj} \sum_{J\lambda J'\lambda'} [(2J+1)(2J'+1)]^{1/2} (-1)^{(\lambda-\lambda'+J+J'+J_i)} \\
 & \sum_{l=0,2} (2l+1) \begin{pmatrix} J & J' & l \\ \lambda & -\lambda' & \lambda'-\lambda \end{pmatrix} \begin{pmatrix} j & j & l \\ -\lambda & \lambda' & \lambda-\lambda' \end{pmatrix} \begin{pmatrix} 1 & 1 & l \\ 0 & 0 & 0 \end{pmatrix} \\
 & \times \begin{pmatrix} j & j & l \\ -m_j & m_j & 0 \end{pmatrix} \begin{pmatrix} 1 & 1 & l \\ J & J' & J_i \end{pmatrix} t^{(a)}(E J v j \lambda p | E_i J_i p_i) t^{(a')*}(E J' v j \lambda' p | E_k J_k p_k). \quad (66)
 \end{aligned}$$

Here $J_i = J_k$ has been assumed for simplicity. Equation (66) is a generalized version of equation (48) [63].

These equations, in conjunction with the artificial channel method [63] for computing the t -matrix elements, were used to compute the ratio Y of the HO + H (as distinct from the H + OH) product in a fixed m_j state. Specifically, figure 17 shows the result of first exciting the superposition of symmetric plus asymmetric vibrational modes $[(1, 0, 0) + (0, 0, 1)]$ with $J_i = J_k = 0$ in the ground electronic state, followed by dissociation at $70\,700\text{ cm}^{-1}$ to the B state using a pulse width of 200 cm^{-1} . Results show that varying the time delay between pulses allows for controlled variation of Y from 61 to 39%!

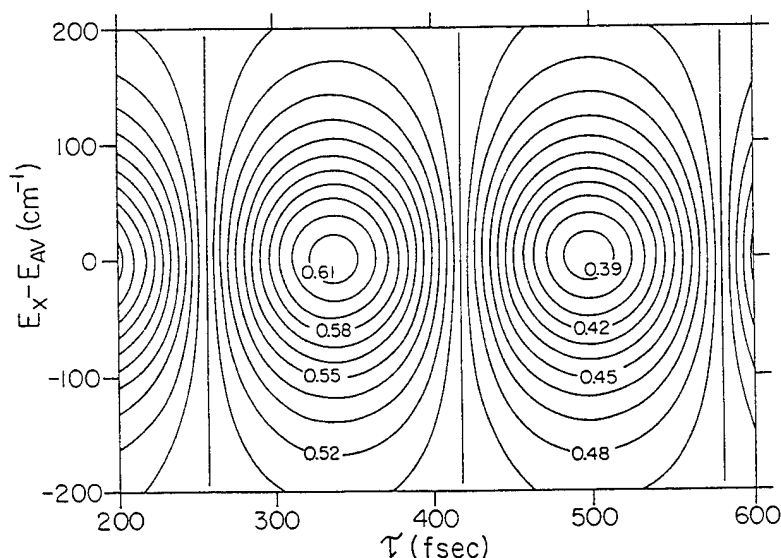


Figure 17. Contour plot of percentage HO + H (as distinct from H + OH) in HOH. The ordinate is the detuning from $E_{av} = \frac{1}{2}(E_2 - E_1)$; the abscissa is the time between pulses (from [15]).

Finally we sketch the effect of a summation over product m_j states on symmetry breaking and chirality control. In this regard the three-body model is particularly informative. Specifically, note that equation (64) provides $d_{i,k}^{(q)}$ in terms of products of matrix elements involving $|E, n, a^- \rangle$ and $|E, n, s^- \rangle$. Focus attention on those products which involve both wavefunctions, for example $A_{a1} S_{s1}^*$. These matrix element products can be written in the form of equation (66) where q and q' now refer to the antisymmetric or symmetric continuum states, rather than channels 1 and 2. Thus, for example, $A_{a1} S_{s1}^*$ results from using $|E, n, a^- \rangle$ in equation (65) to form A_{a1} and $|E, n, s^- \rangle$ to form S_{s1}^* . The resultant $A_{a1} S_{s1}^*$ has the form of equation (66) with $t^{(q)}$ and $t^{(q')}$ associated with the symmetric and antisymmetric continuum wavefunctions, respectively. Consider now the effect of summing over m_j . Standard formulae [62, 63] imply that this summation introduces a $\delta_{l,0}$ which, in turn forces $\lambda = \lambda'$ via the first and second $3j$ symbol in equation (66). However, a rather involved argument [64] shows that t -matrix elements associated with symmetric continuum eigenfunctions and those associated with antisymmetric continuum eigenfunctions must have λ of different parities. Hence summing over m_j eliminates all contributions to equation (64) which involve both $|E, n, a^- \rangle$ and $|E, n, s^- \rangle$. Specifically, we find [64] that after m_j summation

$$d_{ii}^{(1)} = d_{ii}^{(2)} = \sum (|S_{si}|^2 + |A_{ai}|^2), \quad (67)$$

$$d_{12}^{(1)} = d_{12}^{(2)} = \sum (S_{si} A_{sj}^* + A_{ai} S_{aj}^*). \quad (68)$$

That is, natural symmetry breaking is lost upon m_j summation, both channels $q = R$ and $q = L$ having equal photodissociation probabilities, and control over the enantiomer ratio is lost since the interference terms no longer distinguish the $q = R$ and $q = L$ channels. (As an aside we note that control is not possible in collinear models since, in that case, d_a and d_s cannot both couple to the same electronically excited state.)

Having thus demonstrated the principle of m_j selected enantiomer control it remains to determine the extent to which realistic systems can be controlled. Such studies are in progress.

6. Control of photocurrent directionality

In this section we demonstrate that it is possible to control the product angular distribution using the scheme outlines in § 1.3. Our specific application is to the case of photoionization so that the result is control over the direction of the photocurrent induced by the interference. An alternative method of controlling differential cross-sections by varying the degree of elliptic polarization of the light source has been described elsewhere [5].

Properties of a photocurrent generated in a semiconductor are usually controlled by a bias voltage [65]. The role of this voltage is to give *thermodynamic* preference to the flow of photoelectrons in one direction (the forward or backward direction in a p-n junction.) In a p- or n-type semiconductor the probability of carrier photoemission (from a single impurity) without an external voltage is anisotropic only inasmuch as the crystal possesses mass or dielectric constant anisotropies, but the probabilities of emission backward and forward along a given crystal axis are equal. Although photocurrents are commonly produced by laser illumination, the laser coherence does not affect the process.

Here we describe a scheme [8] for generating and controlling photocurrents *without bias voltage*, relying instead on the coherence of the illuminating source. The method is an application of the scenario of § 1.3 to the photoionization of bound states

of donors. Specifically, a superposition of two bound donor (or exciton) states is photoionized by two mutually phase-locked lasers at slightly different frequencies with the same polarization axis. The result is a current along the direction of polarization. The realization of the scheme is discussed for shallow-level donors in semiconductors.

Consider a semiconductor doped with shallow-level donors. The bound-state wavefunction of such a donor is successfully described by the hydrogenic effective-mass theory [66] with wavefunction

$$\chi_n(\mathbf{r}) = \langle \mathbf{r} | \mathbf{n} \rangle = V^{-1/2} \int_{-\infty}^{\infty} B_{n,\mathbf{k}} u_{\mathbf{k}}(\mathbf{r}) \exp(i\mathbf{k} \cdot \mathbf{r}) d\mathbf{k}. \quad (69)$$

Here $u_{\mathbf{k}}(\mathbf{r})$ is the conduction-band Bloch state correlated to the asymptotic free-electron momentum $\hbar\mathbf{k}$, V is the normalization volume and $B_{n,\mathbf{k}}$ is the corresponding Fourier component of the hydrogenic wavefunction envelope χ_n . For semiconductors with effective-mass anisotropy, the χ_n are evaluated variationally [67–70]. Although the theory described below holds for any superposition of bound donor states, a superposition of $|1s\rangle$ and $|2p_0\rangle$ states will be considered explicitly. For these cases a simple variational procedure [70], whose results agree reasonably well with those of more refined procedures [67–71], yields

$$\begin{aligned} \chi_{1s} &= \pi^{1/3} \exp \left[- \left(\frac{x^2 + y^2}{a^2} + \frac{z^2}{b^2} \right)^{1/2} \right], \\ \chi_{2p_0} &= 2^{1/2} \pi^{3/4} b^{-1} z \exp \left[- \left(\frac{x^2 + y^2}{a^2} + \frac{z^2}{b^2} \right)^{1/2} \right]. \end{aligned} \quad (70)$$

Here the coordinates (normalized to the effective Bohr radius $a^* = \hbar^2/m_{\perp}e^2$) coincide with the main axes of the cubic crystal. Depending on the ratio $\gamma = m_{\perp}/m_{\parallel}$ (the parallel direction coinciding with z), the parameters a and b vary between $a = b = 1$ for nearly isotropic materials with $\gamma = 1$ (e.g. GaAs, GaSb or InAs) and $a \approx \frac{4}{3}\pi$ and $b \approx \frac{1}{3}(4/\pi)^{2/3}\gamma^{1/3}$ for highly anisotropic materials (e.g. Si or Ge) with $\gamma \ll 1$.

Let a superposition of the $|1s\rangle$ and $|2p_0\rangle$ states be prepared by some coherent process. As pointed out before, this can be achieved by a short coherent laser pulse or various other means. It is possible to discriminate against the excitation of the $|2p_{\pm 1}\rangle$ states either by frequency tuning (e.g. the $2p_{\pm 1} - 2p_0$ splitting is about 5 meV in Si), or by linearly polarizing the laser along the z axis. Consider now the simultaneous excitation of this superposition state to a kinetic energy level E_k in the conduction-band continuum by two z -polarized infrared or visible lasers with frequencies ω_{1s} and ω_{2p_0} ; the former lifts the $|1s\rangle$ state to E_k and the latter lifts the $|2p_0\rangle$ state to E_k . These excitations involve the energy conservation relation

$$E_k = \frac{\hbar^2 k_{\perp}^2}{2m_{\perp}} + \frac{\hbar^2 k_z^2}{2m_{\parallel}} = \hbar\omega_n - |E_n| - \sum_p p\hbar\omega. \quad (71)$$

Here the n -state energy is measured from the conduction-band edge and the last term accounts for the emission ($p > 0$) or absorption ($p < 0$) of p phonons of frequency ω . For simplicity, we shall use the zero-phonon-frequency line [71, 72]; hence, $\hbar\omega_{1s} = E_k + |E_{1s}|$, $\hbar\omega_{2p_0} = E_k + |E_{2p_0}|$.

In what follows we consider only electric-dipole-induced optical transitions with the electric field along the z -axis. The electric dipole transition

amplitudes from an impurity state $|n\rangle$ to the asymptotic (far from impurity) plane wave $\langle \mathbf{r}|\mathbf{k}\rangle = V^{-1/2} \exp(i\mathbf{k} \cdot \mathbf{r}) u_{\mathbf{k}}(\mathbf{r})$ is

$$\langle \mathbf{k}|\mu_z|n\rangle = \frac{-ie\hbar}{m_{\parallel}(E_{\mathbf{k}} + |E_n|)} \langle \mathbf{k}|\left(-i\hbar \frac{\partial}{\partial z}\right)|n\rangle. \quad (72)$$

The last factor is, using equation (69), simply given as

$$\langle \mathbf{k}|-i\hbar \frac{\partial}{\partial z}|n\rangle = \hbar \mathbf{k}_z \langle \mathbf{k}|n\rangle = \hbar \mathbf{k}_z B_{n,\mathbf{k}}. \quad (73)$$

We now consider the photoionization of the superposition state

$$|\psi\rangle = c_1|1\rangle + c_2|2\rangle, \quad (74)$$

where 1 denotes the 1s state and 2 the 2p₀ state. We let a z-polarized two-colour source, whose electric field is given as

$$\varepsilon_z(t) = \varepsilon_1 \cos(\omega_1 t + \phi_1) + \varepsilon_2 \cos(\omega_2 t + \phi_2) \quad (75)$$

act on this superposition state. The rate (probability per unit time and unit solid angle) of photoemission to a conduction state with momentum $\hbar \mathbf{k}$ resulting from this action is

$$P(\cos \theta) = \frac{2\pi}{\hbar} \rho(k) \left| \sum_{n=1,2} \exp(-i\phi_n) \varepsilon_n c_n \langle \mathbf{k}|\mu_z|n\rangle \right|^2. \quad (76)$$

Here,

$$\begin{aligned} \cos \theta &= \frac{kz}{k}, \quad \sin \theta = \frac{k_{\perp}}{\gamma^{1/2} k}, \\ k &= \frac{(2m_{\parallel} E_k)^{1/2}}{\hbar}, \\ \rho(k) &= \frac{m_{\perp} V}{8\pi^3 \hbar^2 k} \end{aligned} \quad (77)$$

and $\rho(k)$ is the density of final states. The Franck-Condon factor for the zero-phonon-frequency line has been set here to unity.

Denoting $c_n = |c_n| \exp(i\alpha_n)$ and using equations (72) and (73) in equation (76) gives the form

$$\begin{aligned} P(\cos \theta) &= \\ [A_1 |B_{1s,\mathbf{k}}|^2 + A_2 |B_{2p_0,\mathbf{k}}|^2 + A_{12} \cos(\alpha_1 - \alpha_2 - \phi_1 + \phi_2 + \alpha_{12}) |B_{1s,\mathbf{k}} B_{2p_0,\mathbf{k}}|] \cos^2 \theta, \end{aligned} \quad (78)$$

where

$$\begin{aligned} A_n &= \frac{2\pi e^2 \hbar^3 k^2 \rho(k) |\varepsilon_n c_n|^2}{m_{\parallel}^2 (E_k + E_n)^2} \quad (n=1,2), \\ A_{12} &= \frac{4\pi e^2 \hbar^3 k^2 \rho(k) |\varepsilon_1 \varepsilon_2 c_1 c_2|}{m_{\parallel}^2 (E_k + E_1)(E_k + E_2)}. \end{aligned} \quad (79)$$

Here α_{12} is defined by $B_{1s,\mathbf{k}} B_{2p_0,\mathbf{k}}^* = |B_{1s,\mathbf{k}} B_{2p_0,\mathbf{k}}| \exp(i\alpha_{12})$ and $E_1 = |E_{1s}|$, $E_2 = |E_{2p_0}|$.

The evaluation of $P(\cos \theta)$ requires the Fourier components $B_{n,k}$. For the present choice of impurity states and z -axis these components are obtained from equation (70) as

$$B_{1s,k} = \frac{8\pi^{4/3}a^2bV^{-1/2}}{G^2},$$

$$B_{2p_0,k} = \frac{-i2^{1/2}(32)a^2b^2\pi^{7/4}V^{-1/2}a^*k_z}{G^3}, \quad (80)$$

with

$$G = G(\cos^2 \theta) = [1 + \gamma(a^*ak)^2 + (b^2 - a^2\gamma)(a^*k)^2 \cos^2 \theta]. \quad (81)$$

It is clear from equation (80) that $\alpha_{12} = \frac{1}{2}\pi$.

Given the above expression, the net current flowing in the z direction is given as

$$I_z^+ = \frac{eNV\hbar}{m_{||}} \tau F \int_0^{2\pi} \int_0^\pi d\Omega P(\cos \theta) k \cos \theta$$

$$= 256 \frac{eNV\hbar^4 k^5}{m_{||}^3} \tau F a^4 b^3 \pi^{25/12} \frac{|\varepsilon_1 \varepsilon_2 c_1 c_2|}{(E_k + E_1)(E_k + E_2)}$$

$$\times \cos(\alpha_1 - \alpha_2 - \phi_1 + \phi_2 + \frac{1}{2}\pi) \int_{-1}^{+1} dx \frac{x^4}{[G(x^2)]^5}, \quad (82)$$

where τ is the free-electron collisional relaxation time, N is the donor concentration in reciprocal cubic centimetres and F is the x - y cross-sectional area of the sample.

We note that contributions from the diagonal A_1 and A_2 terms are odd in $\cos \theta$ and have vanished, whereas the interference term induces a directional current flow! Thus coherent interference contributions result in a controlled directional current flow.

Several additional remarks are in order. First, the phases ϕ_1 and ϕ_2 of equation (75) contain the spatial phase factors $\exp(i\mathbf{k} \cdot \mathbf{R})$, where \mathbf{k} is the light wave-vector. The difference in the spatial phases can be exactly offset by the phase difference $\alpha_1 - \alpha_2$ in the preparation step (e.g. in a Raman preparation of $|\psi\rangle$), or eliminated by phase matching. Second, there are substantial experimental simplifications associated with applying the photodissociating lasers at the same time as initiating the preparation of the superposition state. Third, two-colour light also causes excitation (via ω_{2p_0}) of the $|1s\rangle$ level to the state at $E_k + |E_{2p_0}| - |E_{1s}|$ and of the $|2p_0\rangle$ level (via ω_{1s}) to the state at $E_k + |E_{1s}| - |E_{p_0}|$, that is the uncontrolled satellite contributions discussed above. In this case, however, these terms contribute to the A_1 and A_2 terms in equation (78) and hence do not contribute to degrade the controlled current I_z^+ .

The magnitude and sign of the current are controllable for a given host material and superposition state parameters via first, the optical phase difference $\phi_1 - \phi_2$, second, the donor number N and/or third, the ionizing field strengths ε_1 and ε_2 and their frequencies ω_1 and ω_2 . To estimate a typical current, consider the I_z resulting from the following parameters: $\varepsilon_1 = \varepsilon_2 = 0.1 \text{ V cm}^{-1}$, $k = 5 \times 10^7 \text{ cm}^{-1}$, $|c_1 c_2| = 0.25$ and $\tau = 10^{-14} - 10^{-13} \text{ s}$. The latter corresponds to a mean free path $\hbar k \tau / m$ of 100–1000 Å, a typical value for the ballistic electrons at the cited k value. Further $N(\text{Si})V = 10^{18} \text{ cm}^{-3} V$ where V is the effective interaction volume. For a sample of $0.1 \times 10 \times 10 \mu\text{m}$, $V = 10^{-11} \text{ cm}^3$. Utilizing equation (82), and these parameter values, we obtain a current $I_z = 10\text{--}100 \text{ mA}$. Thus sizeable currents may be readily produced, owing to the high quantum efficiency of the silicon photoionization.

Equations (79)–(82) apply, evidently, to photoionization of other $|ns\rangle - |n'p_0\rangle$ superpositions, where $|n - n'| = 1$, upon substituting the appropriate Fourier coefficients $B_{ns, \mathbf{k}}$ and $B_{n'p_0, \mathbf{k}}$. It may turn out to be more practical to use other states than those discussed above.

7. Control with intense laser fields

We now discuss some extensions of coherent control to strong laser fields. Parallel work involving other strong-field scenarios has been done by Bandrauk and co-workers [46], Bardsley and co-workers [47], Guisti-Suzor and co-workers [48], Corkum and co-workers [49] and Nakajima and Lambropoulos [73]. Here we concentrate on a strong-field control scenario in which the dependence on the relative phase between the two laser beams, and hence on laser coherence, disappears. As a result, coherence plays no role in this scenario (except for being intimately linked with the existence of the narrow-band laser sources needed for its execution). Although the unimportance of coherence means that we lose phase control, the effect still depends on quantum interference phenomena. The scenario is therefore called interference control.

To illustrate interference control we look at the control of the electronic states of Na_2 atoms generated by the photodissociation of Na_2 , a process treated in the context of weak-field coherent control in §4. We envisage a scenario, depicted in figure 18, in which we employ two laser sources. One laser (not necessarily intense) with centre frequency ω_1 is used to excite a molecule from an initially populated bound state $|E_i\rangle$ to a dissociative state $|E, m, q^-\rangle$. A second laser, with frequency ω_2 , is used to couple

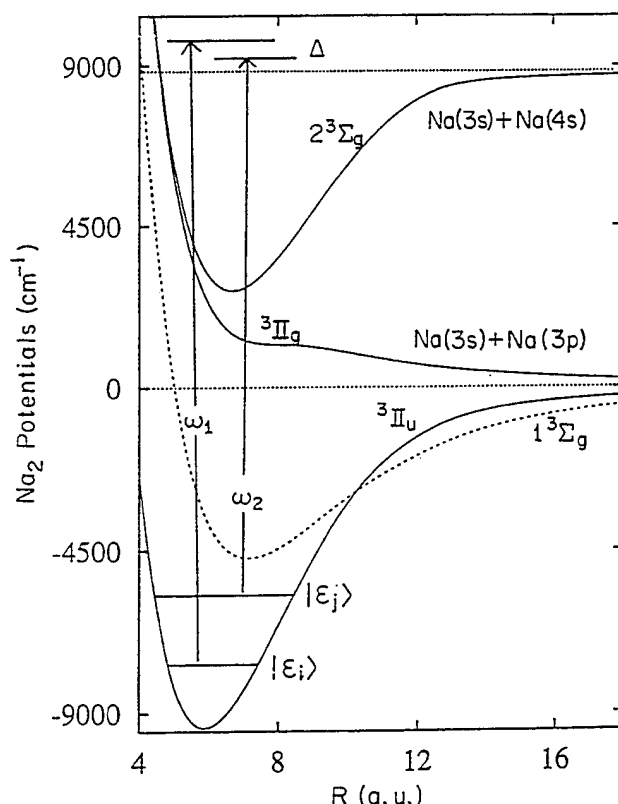


Figure 18. Control scenario applied to the photodissociation of the ${}^3\Pi_u$ state of Na_2 . For the case considered in this paper, $|E_i\rangle$ corresponds to $v=19$ with $E_{v=19} = -6512.8 \text{ cm}^{-1}$ and $|E_j\rangle$ is $v=31$ with $E_{v=31} = -4966.04 \text{ cm}^{-1}$.

('dress') the continuum with some (initially unpopulated) bound states $|E_j\rangle$. With both lasers on, dissociation to $|E, m, q^-\rangle$ occurs via one direct, that is $|E_i\rangle \rightarrow |E, m, q^-\rangle$, pathway and a multitude of indirect, for example $|E_i\rangle \rightarrow |E, m, q^-\rangle \rightarrow |E_j\rangle \rightarrow |E, m, q^-\rangle$, pathways. The interference between these pathways to form a given channel q at product energy E can be either constructive or destructive. As we show below, varying the frequencies and intensities of the two excitation lasers strongly affects this interference term, providing a means of controlling the photodissociation line shape and the branching ratio into different products.

With this scenario in mind we now briefly discuss the methodology of dealing with strong laser fields and the extension of coherent control ideas to this domain. We consider the photodissociation of a molecule with Hamiltonian H_M in the presence of a radiation field with Hamiltonian H_R , whose eigenstates are the Fock states $|n_k\rangle$ with energy $n_k\hbar\omega_k$. (In the case of several frequencies the repeated index in $n_k\omega_k$ implies the sum over the modes.)

Strong-field dynamics are completely embodied [74] in the fully interacting eigenstates of the total Hamiltonian H , that is $H_M + H_R + V$, where V is the light-matter interaction, denoted $|(E, m, q^-), n_k^-\rangle$:

$$H|(E, m, q^-), n_k^-\rangle = (E + n_k\hbar\omega_k)|(E, m, q^-), n_k^-\rangle. \quad (83)$$

The minus superscript on n_k is used in exactly the same way as in the weak-field domain; it is a reminder that each $|(E, m, q^-), n_k^-\rangle$ state correlates to a non-interacting $|(E, m, q^-), n_k\rangle \equiv |E, m, q^-\rangle |n_k\rangle$ state when the light-matter interaction V is switched off.

If the system is initially in the $|E_i, n_i\rangle \equiv |E_i\rangle |n_i\rangle$ state and we suddenly switch on V , the photodissociation amplitude to form in the future the product state $|E, m, q^-\rangle |n_k\rangle$ is simply given [74] as the overlap between the initial and fully interacting state $\langle (E, m, q^-), n_k^- | E_i, n_i \rangle$. This overlap assumes the convenient form

$$\langle (E, m, q^-), n_k^- | E_i, n_i \rangle = \langle (E, m, q^-), n_k | V G(E^+ + n_k\hbar\omega_k) | E_i, n_i \rangle, \quad (84)$$

by using the Lippmann-Schwinger equation

$$\langle (E, m, q^-), n_k^- | = \langle (E, m, q^-), n_k | + \langle (E, m, q^-), n_k | V G(E^+ + n_k\hbar\omega_k). \quad (85)$$

Here $G(\mathcal{E}) = 1/(\mathcal{E} - H)$ and $E^+ = E + i\delta$, with $\delta \rightarrow 0^+$ at the end of the computation. Equation (84) is exact and provides a connection between the photodissociation amplitude and the VG matrix element. It is the latter which we compute exactly using a high-field extension of the artificial channel method [75, 76].

Two quantities are of interest: the channel specific line shape given by

$$A(E, q, n_k | E_i, n_i) = \int d\mathbf{k} |\langle (E, \mathbf{k}, q^-), n_k^- | E_i, n_i \rangle|^2, \quad (86)$$

and the total dissociation probability to channel q given by

$$P(q) = \sum_{n_k} \int dE A(E, q, n_k | E_i, n_i). \quad (87)$$

In equation (87) the sum is over photons that excite the molecule above the dissociation threshold. In writing equation (86), diatomic dissociation is assumed, so that $m = \mathbf{k}$.

Consider for example the photodissociation of Na_2 from the $|E_i\rangle = |v=19, {}^3\Pi_u\rangle$ initial state, where v denotes the vibrational quantum number in the ${}^3\Pi_u$ electronic potential (the potential curves and the relevant electronic dipole moments are taken

from [79]) (figure 18). $|E_i\rangle$ is assumed to have been prepared by previous excitation from the ground electronic state. Excitations from $|E_i\rangle$ by ω_1 and mixing of the initially unpopulated $|E_j\rangle$ by ω_2 to the dissociating continua produce Na (3s) + Na (3p) and Na (3s) + Na (4s). Computations were done with ω_1 chosen within the range $15\,430 < \omega_1 < 15\,700\text{ cm}^{-1}$ with intensity $I_1 \approx 10^{10}\text{ W cm}^{-2}$, which is sufficiently energetic to dissociate levels of the $^3\Pi_u$ state with $v \geq 19$ to both Na (3s) + Na (3p) and Na (3s) + Na (4s). The second laser has fixed frequency $\omega_2 = 13\,964\text{ cm}^{-1}$ and intensity $I_2 = 3.2 \times 10^{11}\text{ W cm}^{-2}$ and can dissociate levels with $v \geq 26$ to both products. Under these circumstances the contribution of above threshold dissociation is found to be negligible. However, cognizance must be taken of the possibility of dissociation of $|E_i\rangle$ by ω_2 and of $|E_j\rangle$ by ω_1 . These processes do not interfere and cannot be controlled. Hence we must find the range of parameters that minimizes them.

Figure 19 shows computed line shapes $A(E, q, n_k | E_i, n_i)$ (on a logarithmic scale) as a function of the product translational energy E , with $\omega_2 = 13\,964\text{ cm}^{-1}$, $\omega_1 = 15\,546\text{ cm}^{-1}$, $I_1 = 5.5 \times 10^9\text{ W cm}^{-2}$ and $I_2 = 3.51 \times 10^{10}\text{ W cm}^{-2}$. Results for both the Na (3p) + Na (3s) and Na (4s) + Na (3s) product channels are shown. Figure 20 contains similar results, but with $\omega_1 = 15\,511\text{ cm}^{-1}$. In addition, the line shape for excitation with the laser of frequency $\omega_1 = 15\,456\text{ cm}^{-1}$ only (ω_2 laser off) is shown in figure 19 for the Na (3s) + Na (4s) product; the Na (3p) + Na (4s) result is similar.

Consider first $A(E, q, n_k | E_i, n_i)$ associated with excitation by a single laser (figure 19, dotted curve). The line shape is comprised of a series of non-Lorentzian peaks and dips corresponding to resonance contributions from the dressed $v = 19, 20, 21$ vibrational states. The predominant contribution is the direct $v_i = 19$ excitation, with smaller $v = 20, 21$ contributions arising from stimulated emission and absorption from and to

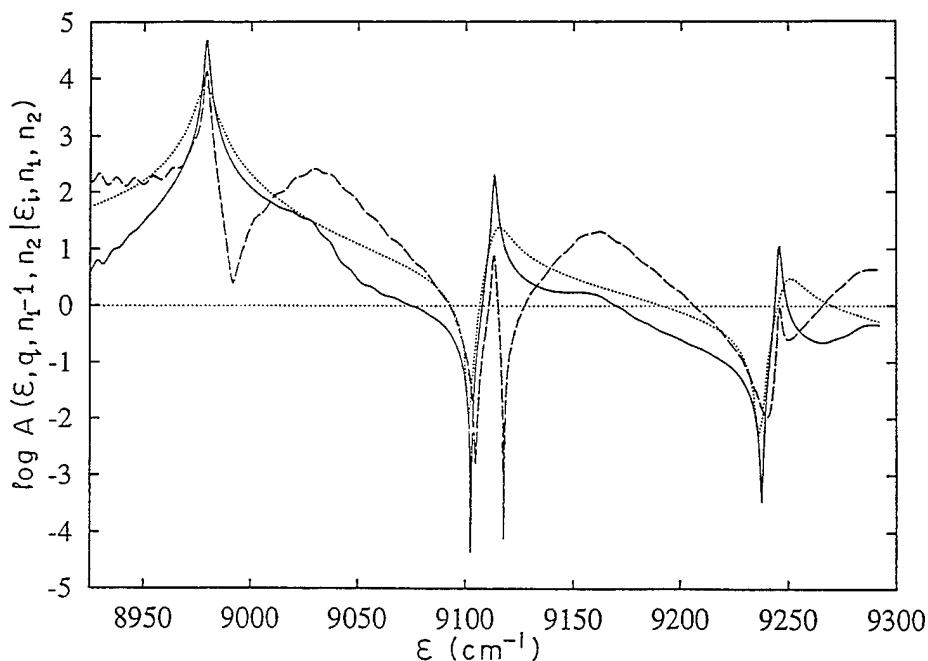


Figure 19. $\log [A(E, q, n_k | E_i, n_i)]$ as a function of E (where the Na (3p) + Na (3s) asymptote defines the zero energy): (—), Na (3s) + Na (3p) product with both lasers on; (---) Na (3s) + Na (4s) product, with both lasers on; (.....) Na (3s) + Na (4s) product with only one laser (ω_1) on. Here $\omega_1 = 15\,456\text{ cm}^{-1}$, $\omega_2 = 13\,964\text{ cm}^{-1}$, $I_1 = 5.5 \times 10^9\text{ W cm}^{-2}$ and $I_2 = 3.51 \times 10^{10}\text{ W cm}^{-2}$.

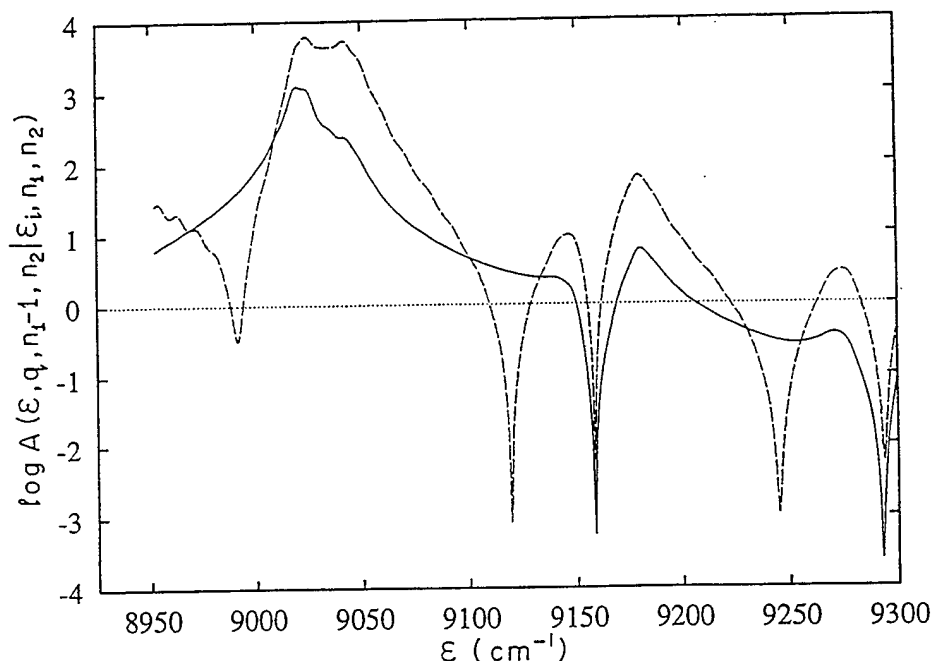


Figure 20. As in figure 19 but with $\omega_1 = 15\,511\text{ cm}^{-1}$: (—), Na(3s) + Na(3p) product with both lasers on; (---), Na(3s) + Na(4s) product with both lasers on.

the continuum. Further, the overall shape between the peaks shows Fano-type interference between the photodissociation pathways arising from the pairs of adjacent vibrational states. Since significant dissociation is observed from states other than the initially populated $v_i = 19$, it is clear that the power broadening is of the same order of magnitude as the vibrational level spacing.

With both ω_1 and ω_2 lasers on, each peak splits into two peaks in a manner which is dependent both upon asymptotic channel (compare solid and broken curves in figures 19 and 20) and frequency ω_1 (compare figure 19 with 20). An analysis of this structure is provided below. Here we note the significant implication that by varying ω_1 we can control the channel specific line shapes $A(E, n_k | E_i, n_i)$. For example, comparing figures 19 and 20 shows that the increase in ω_1 results in a shift of the dominant peaks to higher E . Products at $E \approx 9025\text{ cm}^{-1}$ are strongly enhanced relative to the case in figure 19 products at $E \approx 8980\text{ cm}^{-1}$ are suppressed, etc. Tuning ω_2 or changing the laser intensities also changes the line shapes, as discussed elsewhere [43].

Integrating $A(E, q, n_k | E_i, n_i)$ over E (equation 87) for various ω_1 values give $P(q)$ as a function of ω_1 . The result of these computations are shown in figure 21 for both Na(3s) + Na(3p) (solid curve) and Na(3s) + Na(4s) (broken curve) channels, with $I_1 = 8.7 \times 10^9\text{ W cm}^{-2}$, $I_2 = 3.51 \times 10\text{ W cm}^{-2}$ and $\omega_2 = 13\,964\text{ cm}^{-1}$. The probability $P(q)$ is seen to oscillate strongly as a function of ω_1 , with the distance between the peaks (or dips) being the vibrational spacing between $v = 31$ and 32. The oscillations for the two product channels are out of phase. Hence, for example, the probabilities of producing Na(3s) + Na(4s) and Na(3s) + Na(3p) at $\omega_1 = 15\,494\text{ cm}^{-1}$ are 0.198 and 0.730, respectively. The reverse situation occurs at $\omega_1 = 15\,573\text{ cm}^{-1}$ where the total dissociation probability remains 0.93 but where 68% of product is Na(3s) + Na(4s). Thus varying ω_1 provides a straightforward method of controlling the branching ratio into final product channels. Furthermore, and significantly, computations show that

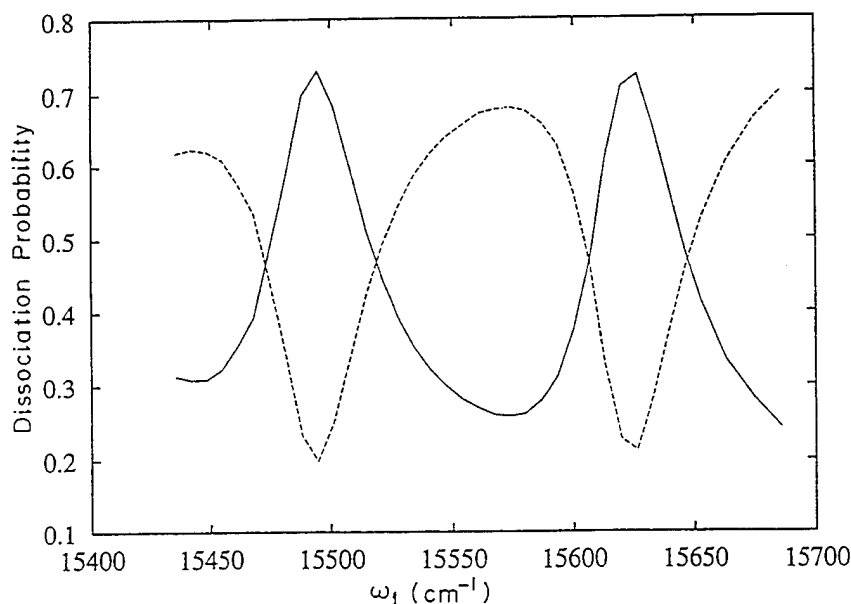


Figure 21. Probability of forming Na(3s) + Na(3p) (—) and Na(3s) + Na(4s) (---) as a function of ω_1 , with $\omega_2 = 13\,964\text{ cm}^{-1}$, $I_1 = 8.7 \times 10^9\text{ W cm}^{-2}$ and $I_2 = 3.51 \times 10^{10}\text{ W cm}^{-2}$.

arbitrarily changing the relative phase between the ω_1 and ω_2 does not alter figures 19–21, indicating that the control process is independent of the relative laser phase. This is consistent with the model discussed below.

Reducing the laser power in these computations [43] narrows the frequency range over which the product probability oscillates, clearly indicating that this range is at least partially determined by the power broadening.

The qualitative behaviour seen in figures 19–21 can be readily understood in terms of a simple model which assumes excitation of the initial state $|1\rangle \equiv |E_i, n_1, n_2\rangle$ with laser ω_1 to the continuum $|E_q\rangle \equiv |(E, q^-), n_1 - 1, n_2\rangle$, which is coupled to state $|2\rangle \equiv |E_j, n_1, n_2 + 1\rangle$ with laser ω_2 . If these are the only contributing states, then the photodissociation amplitude is given by

$$\langle E_q | \mathbf{V} \mathbf{G}(\mathcal{E}) | 1 \rangle = \langle E_q | \mathbf{V} | 1 \rangle \langle 1 | \mathbf{G}(\mathcal{E}) | 1 \rangle + \langle E_q | \mathbf{V} | 2 \rangle \langle 2 | \mathbf{G}(\mathcal{E}) | 1 \rangle, \quad (88)$$

where $\mathcal{E} = E^+ + (n_1 - 1)\hbar\omega_1 + n_2\hbar\omega_2$. Using $(\mathcal{E} - H_0 - \mathbf{V})\mathbf{G}(\mathcal{E}) = 1$, we obtain coupled equations for the matrix elements of \mathbf{G} which can be solved. Substituting the results into equation (88), gives

$$\langle E_q | \mathbf{V} \mathbf{G}(\mathcal{E}) | 1 \rangle = \frac{(\mathcal{E} - E_2 - \pi_{2,2}(E))\langle E_q | \mathbf{V} | 1 \rangle + \langle E_q | \mathbf{V} | 2 \rangle \pi_{2,1}(E)}{[E - E_1 - \pi_{1,1}(E)][E - E_2 - \pi_{2,2}(E)] - \pi_{1,2}(E)\pi_{2,1}(E)}, \quad (89)$$

where $E_1 = E_i + n_1\hbar\omega_1 + n_2\hbar\omega_2$, $E_2 = E_j + (n_1 - 1)\hbar\omega_1 + (n_2 + 1)\hbar\omega_2$ and $\pi_{a,b}(a, b = 1, 2)$ is given by

$$\pi_{a,b}(E) = \sum_q \int dE' \frac{\langle a | \mathbf{V} | E'_q \rangle \langle E'_q | \mathbf{V} | b \rangle}{E - E' - (n_1 - 1)\hbar\omega_1 - n_2\hbar\omega_2}. \quad (90)$$

The E dependence of equation (89) can be exposed by substituting

$$\mathcal{E} = E^+ + (n_1 - 1)\hbar\omega_1 + n_2\hbar\omega_2$$

into equation (89). Denoting $\pi_{a,b}(E)$ at this energy by $\pi_{a,b}$, we have

$$|\langle E_q | \mathbf{V} \mathbf{G}(\mathcal{E}) | 1 \rangle|^2 = \left| \frac{(\mathcal{E} - E_j - \hbar\omega_2 - \pi_{2,2}) \langle E_q | \mathbf{V} | 1 \rangle + \langle E_q | \mathbf{V} | 2 \rangle \pi_{2,1}}{(\mathcal{E} - \chi_+)(\mathcal{E} - \chi_-)} \right|, \quad (91)$$

where

$$2\chi_{\pm} = (E_i + \pi_{1,1} + \hbar\omega_1) + (E_j + \pi_{2,2} + \hbar\omega_2) \pm \{[(E_i + \pi_{1,1} + \hbar\omega_1) - (E_j + \pi_{2,2} + \hbar\omega_2)]^2 + 4\pi_{1,2}\pi_{2,1}\}^{1/2}. \quad (92)$$

χ_{\pm} are the eigenvalues associated with the diagonalization of the matrix coupling the two dressed states, of energy $E_i + \pi_{1,1} + \hbar\omega_1$ and $E_j + \pi_{2,2} + \hbar\omega_2$ via the continuum. The real and imaginary parts of $\pi_{a,a}(a=1,2)$ give the shifts and broadenings of the two levels.

Equation (91) shows photodissociation occurring via two pathways, $|E_i, n_1, n_2\rangle \rightarrow |(E, q^-), n_1 - 1, n_2\rangle$ and $|E_i, n_1, n_2\rangle \rightarrow |E_j, n_1 - 1, n_2 + 1\rangle \rightarrow |(E, q^-), n_1 - 1, n_2\rangle$; interference between them can be constructive or destructive, depending on the relative sign of the two terms. This interference can be manipulated by varying the laser frequencies. The double-peak structure seen in figures 19 and 20 is consistent with the form of equation (91) wherein two peaks are predicted as the function of \mathcal{E} , at the two roots of the equations $\mathcal{E} - \chi_{\pm} = 0$. For example, in the case of figure 19, the first double peak arises from the interaction between the dressed $v=19$ and $v=31$ levels of the $^3\Pi_u$ state whereas the decrease in photodissociation (compared with the dotted curve) in the middle of the double-peak results from the destructive interference between them. A similar explanation applies to the second and third double peaks, which result mainly from the combined excitations of $v=20$ and 32 and of $v=21$ and 33 , respectively. Note that the locations of the peaks are channel independent but that the ratio of the heights of the peaks, given by the ratio of $|\langle E_q | \mathbf{V} | 1 \rangle (\mathcal{E} - E_j - \hbar\omega_2 - \pi_{2,2}) + \langle E_q | \mathbf{V} | 2 \rangle \pi_{2,1}|^2$ evaluated at $\mathcal{E} = \chi^+$ and χ^- respectively, depends strongly on the laser frequencies, intensities and the channel index q . Thus equation (92) encompasses the channel dependence of the interference and hence the control over product possibilities.

Note also that equation (91) is consistent with a photodissociation amplitude wherein control of the line shape and product probabilities is independent of the relative phase of the two routes. That is, if ϕ_1 and ϕ_2 are the phases of the two lasers (including the spatial phases $\mathbf{K}_1 \cdot \mathbf{r}$, $\mathbf{K}_2 \cdot \mathbf{r}$), then absorption of an ω_1 or ω_2 photon contributes a phase factor $\exp(i\phi_1)$ or $\exp(i\phi_2)$ to the matrix elements of \mathbf{V} . Similarly, stimulated emission of one photon of ω_1 or ω_2 contributes a phase factor $\exp(-i\phi_1)$ or $\exp(-i\phi_2)$ to the matrix elements of \mathbf{V} . Therefore the second term in denominator of equation (91) carries an overall phase factor $\exp(i\phi_2) \exp(i\phi_1 - i\phi_2) = \exp(i\phi_1)$, which is the same as the phase factor in the first term. The *relative* phase of the two routes, which enters the interference term, is therefore independent of both ϕ_1 and ϕ_2 .

This model fails, however, to include excitation and dissociation of neighbouring vibrational states of $|E_i\rangle$ and $|E_j\rangle$. Nonetheless the computations in figures 19–21, which incorporate all vibrational states, clearly demonstrate the desired control. Further computations [45], which include rotations have also been performed. Inclusion of these rotational states leads to a series of multiple peak-and-dip structure in the line shape corresponding to the resonance contributions of multiple rotational states. Because of this, the dependence of the channel specific dissociation yield on ω_1 changes, but control over line shapes and product yields is still strong.

8. Conclusions

Our discussion makes clear that the characteristic features which we invoke in order to control chemical reactions are purely quantum in nature. There is, for example, little classical about the time-dependent picture where the ultimate outcome of the de-excitation, that is product $H + HD$ or $H_2 + D$ depends entirely upon the phase and amplitude characteristics of the wavefunction. Indeed, as repeatedly emphasized above, if for example collisional effects are sufficiently strong as to randomize the phases, then reaction control is lost. Hence reaction dynamics are intimately linked to the wavefunction phases which are controllable through coherent optical phase excitation.

These results must be viewed in the light of the history of molecular reaction dynamics over the past two decades. Possibly the most useful result of the reaction dynamics research effort has been the recognition that the vast majority of qualitatively important phenomena in reaction dynamics are well described by classical mechanics. Quantum and semiclassical mechanics were viewed as necessary only insofar as they correct quantitative failures of classical mechanics for unusual circumstances and/or for the dynamics of very light particles. Considering reaction dynamics in traditional chemistry to be essentially classical in character therefore appeared to be essentially correct for the vast majority of naturally occurring molecular processes. Coherence played no role. The approach which we have introduced above makes clear, however, that coherence phenomena have great potential for application. The quantum phase is always present and can be used to our advantage, even though it is irrelevant to traditional chemistry. By calling attention to the extreme importance of coherence phenomena to controlled chemistry we herald the introduction of a new focus in atomic and molecular science, that is introducing coherence in controlled environments to modify molecular processes, thus defining the area of coherence chemistry.

Acknowledgments

We acknowledge support for this research by the US Office of Naval Research and the Ontario Laser and Lightwave Research Centre.

References

- [1] BRUMER, P., and SHAPIRO, M., 1986, *Chem. Phys. Lett.*, **126**, 541.
- [2] SHAPIRO, M., and BRUMER, P., 1986, *J. chem. Phys.*, **84**, 4103.
- [3] BRUMER, P., and SHAPIRO, M., 1986, *Discuss. Faraday Soc.*, **82**, 177.
- [4] SHAPIRO, M., and BRUMER, P., 1986, *J. chem. Phys.*, **84**, 4103.
- [5] ASARO, C., BRUMER, P., and SHAPIRO, M., 1988, *Phys. Rev. Lett.*, **60**, 1634.
- [6] SHAPIRO, M., HEPBURN, J., and BRUMER, P., 1988, *Chem. Phys. Lett.*, **149**, 451.
- [7] BRUMER, P., and SHAPIRO, M., 1989, *J. chem. Phys.*, **90**, 6179.
- [8] KURIZKI, G., SHAPIRO, M., and BRUMER, P., 1989, *Phys. Rev. B*, **39**, 3435.
- [9] SEIDEMAN, T., SHAPIRO, M., and BRUMER, P., 1989, *J. chem. Phys.*, **90**, 7136.
- [10] KRAUSE, J., SHAPIRO, M., and BRUMER, P., 1990, *J. chem. Phys.*, **92**, 1126.
- [11] LEVY, I., SHAPIRO, M., and BRUMER, P., 1990, *J. chem. Phys.*, **93**, 2493.
- [12] BRUMER, P., and SHAPIRO, M., 1989, *Accts Chem. Res.*, **22**, 407.
- [13] BRUMER, P., and SHAPIRO, M., 1984, *Chem. Phys.*, **139**, 221.
- [14] CHAN, C. K., BRUMER, P., and SHAPIRO, M., 1991, *J. chem. Phys.*, **94**, 2688.
- [15] SHAPIRO, M., and BRUMER, P., 1991, *J. chem. Phys.*, **95**, 8658.
- [16] BRUMER, P., and SHAPIRO, M., 1992, *A. Rev. phys. Chem.*, **43**, 257.
- [17] SHAPIRO, M., and BRUMER, P., 1992, *J. chem. Phys.*, **97**, 6259.
- [18] CHEN, Z., BRUMER, P., and SHAPIRO, M., 1992, *Chem. Phys. Lett.*, **198**, 498.
- [19] JIANG, X.-P., BRUMER, P., and SHAPIRO, M., 1994, *J. chem. Phys.* (submitted).
- [20] DODS, J., BRUMER, P., and SHAPIRO, M., 1994, *Can. J. Chem.* (in press).

- [21] TANNOR, D. J., and RICE, S. A., 1985, *J. chem. Phys.*, **83**, 5013; TANNOR, D. J., KOSLOFF, R., and RICE, S. A., 1986, *J. chem. Phys.*, **85**, 5805.
- [22] RICE, S. A., TANNOR, D. J., and KOSLOFF, R., 1986, *J. chem. Soc., Faraday Trans. II*, **82**, 2423.
- [23] TANNOR, D. J., and RICE, S. A., 1988, *Adv. chem. Phys.*, **70**, 441.
- [24] KOSLOFF, R., RICE, S. A., GASPARD, P., TERSIGNI, S., and TANNOR, D. J., 1989, *Chem. Phys.*, **139**, 201.
- [25] TERSIGNI, S., GASPARD, P., and RICE, S. A., 1990, *J. chem. Phys.*, **93**, 1670.
- [26] SHI, S., WOODY, A., and RABITZ, H., 1988, *J. chem. Phys.*, **88**, 6870; SHI, S., and RABITZ, H., 1989, *Chem. Phys.*, **139**, 185.
- [27] PEIRCE, A. P., DAHLEH, M., and RABITZ, H., 1988, *Phys. Rev. A*, **37**, 4950.
- [28] SHI, S., and RABITZ, H., 1990, *J. chem. Phys.*, **92**, 364.
- [29] KRAUSE, J. L., WHITNELL, R. M., WILSON, K. R., YAN, Y., and MUKAMEL, S., 1993, *J. chem. Phys.*, **99**, 6562.
- [30] JAKUBETZ, W., JUST, B., MANZ, J., and SCHREIER, H.-J., 1990, *J. phys. Chem.*, **94**, 2294.
- [31] CHEN, C., YIN, Y.-Y., and ELLIOTT, D. S., 1990, *Phys. Rev. Lett.*, **64**, 507; 1990, *Ibid.*, **65**, 1737.
- [32] PARK, S. M., LU, S.-P., and GORDON, R. J., 1991, *J. chem. Phys.*, **94**, 8622; LU, S.-P., PARK, S. M., XIE, Y., and GORDON, R. J., 1992, *J. chem. Phys.*, **96**, 6613.
- [33] SCHERER, N. F., RUGGIERO, A. J., DU, M., and FLEMING, G. R., 1990, *J. chem. Phys.*, **93**, 856.
- [34] BOLLER, K. J., IMAMOGLU, A., and HARRIS, S. E., 1991, *Phys. Rev. Lett.*, **66**, 2593.
- [35] BARANOVA, B. A., CHUDINOV, A. N., and ZEL'DOVITCH, B. YA., 1990, *Optics Commun.*, **79**, 116.
- [36] YIN, Y.-Y., CHEN, C., ELLIOTT, D. S., and SMITH, A. V., 1992, *Phys. Rev. Lett.*, **69**, 2353.
- [37] MACOMBER, J. D., 1976, *The Dynamics of Spectroscopic Transitions* (New York: Wiley).
- [38] TAYLOR, J. R., 1972, *Scattering Theory* (New York: Wiley).
- [39] SHAPIRO, M., and BERSOHN, R., 1980, *J. chem. Phys.*, **73**, 3810.
- [40] SHAPIRO, M., 1986, *J. phys. Chem.*, **90**, 3644.
- [41] SHAPIRO, M., 1972, *J. chem. Phys.*, **56**, 2582.
- [42] SHAPIRO, M., and BRUMER, P., 1986, *Methods of Laser Spectroscopy*, edited by A. Prior, A. Ben-Reuven and M. Rosenbluh (New York: Plenum).
- [43] CHEN, Z., SHAPIRO, M., and BRUMER, P., 1994, *Phys. Rev. Lett.* (submitted).
- [44] CHILD, M. S., 1976, *Molec. Phys.*, **32**, 495.
- [45] CHEN, Z., BRUMER, P., and SHAPIRO, M., 1993, *J. chem. Phys.*, **98**, 6843.
- [46] CHELKOWSKI, S., and BANDRAUK, A. D., 1991, *Chem. Phys. Lett.*, **186**, 284; BANDRAUK, A. D., GAUTHIER, J. M., and MCCANN, J. F., 1992, *Chem. Phys. Lett.*, **200**, 399.
- [47] SZÖKE, A., KULANDER, K. C., and BARDSLEY, J. N., 1991, *J. Phys. B*, **24**, 3165; POTVLIEGE, R. M., and SMITH, P. H. G., 1992, *J. Phys. B*, **25**, 2501.
- [48] CHARRON, E., GUISTI-SUZOR, A., and MIES, F. H., 1993, *Phys. Rev. Lett.*, **71**, 692.
- [49] CHELKOWSKI, S., BANDRAUK, A. D., and CORKUM, P. D., 1990, *Phys. Rev. Lett.*, **65**, 2355.
- [50] BRUMER, P., and SHAPIRO, M., 1994 (to be published).
- [51] SHAPIRO, M., and BRUMER, P., 1993, *J. chem. Phys.*, **98**, 201.
- [52] HENRIKSEN, N. E., and AMSTRUP, B., 1993, *Chem. Phys. Lett.*, **213**, 65; 1993, *J. chem. Phys.*, **97**, 8285.
- [53] WILSON, K. R., 1993, private communication.
- [54] EDMONDS, A. R., 1960, *Angular Momentum in Quantum Mechanics*, 2nd Edn (Princeton University Press).
- [55] LEVY, I., and SHAPIRO, M., 1988, *J. chem. Phys.*, **89**, 2900.
- [56] BAVLI, R., and METIU, 1992, *Phys. Rev. Lett.*, **69**, 1986.
- [57] IVANOV, M. YU., CORKUM, P. B., and DIETRICH, P., 1993, *Laser Phys.*, **3**, 375.
- [58] WOOLLEY, R. G., 1975, *Adv. Phys.*, **25**, 27; 1979, *Origins of Optical Activity in Nature*, edited by D. C. Walker (Amsterdam: Elsevier); BARRON, L. D., 1982, *Molecular Light Scattering and Optical Activity* (Cambridge University Press).
- [59] BARRON, L. D., 1986, *Chem. Soc. Rev.*, **15**, 189.
- [60] BEL, J. A., 1874, *Bull. Soc. chim. Fr.*, **22**, 337; VAN'T HOFF, J. H., 1894, *Die Lagerung der Atome und Raume*, 2nd Edn, p. 30.
- [61] HOLLAS, J. M., 1982, *High Resolution Spectroscopy* (London: Butterworths).
- [62] SEGEV, E., and SHAPIRO, M., 1982, *J. chem. Phys.*, **77**, 5604.
- [63] BALINT-KURTI, G. G., and SHAPIRO, M., 1981, *Chem. Phys.*, **61**, 137.

- [64] SHAPIRO, M., and BRUMER, P., 1994 (to be published).
- [65] SEEGER, K., 1973, *Semiconductor Physics* (Berlin: Springer Verlag).
- [86] PANTELIDES, S. T., 1978, *Rev. mod. Phys.*, **50**, 797.
- [67] FAULKNER, R. A., 1969, *Phys. Rev.*, **184**, 713.
- [68] KASAMI, A., 1968, *J. phys. Soc. Japan*, **24**, 551.
- [69] BALDERESCHI, A., and DIAZ, M. G., 1970, *Nuovo Cim. B*, **68**, 217.
- [70] KOHN, W., and LUTTINGER, J. M., 1955, *Phys. Rev.*, **98**, 915.
- [71] RIDLEY, B. K., 1980, *J. Phys. C*, **13**, 2015.
- [72] HUANG, K., and RHYS, A., 1950, *Proc. R. Soc. A*, **204**, 406.
- [73] NAKAJIMA, T., and LAMBROPOULOS, P., 1993, *Phys. Rev. Lett.*, **70**, 1081.
- [74] BRUMER, P., and SHAPIRO, M., 1986, *Adv. chem. Phys.*, **60**, 371.
- [75] SHAPIRO, M., and BONY, H., 1985, *J. chem. Phys.*, **83**, 1588; BALINT-KURTI, G. G., and SHAPIRO, M., 1986, *Adv. chem. Phys.*, **60**, 403.
- [76] BANDRAUK, A. D., and ATABEK, O., 1989, *Adv. chem. Phys.*, **73**, 823.
- [79] SCHMIDT, I., 1987, PhD thesis, Kaiserslautern University.

Uniform Semiclassical Wave-Packet Propagation and Eigenstate Extraction in a Smooth Chaotic System

Daniel Provost and Paul Brumer

Chemical Physics Theory Group, Department of Chemistry, University of Toronto, Toronto, Canada M5S 1A1

(Received 2 June 1994)

A uniform semiclassical propagator is used to time evolve a wave packet in a smooth Hamiltonian system at energies for which the underlying classical motion is chaotic. The propagated wave packet is Fourier transformed to yield a scarred eigenstate.

PACS numbers: 05.45.+b, 03.65.Sq

Semiclassical mechanics attempts to elucidate and utilize the relationship between classical dynamics and its quantum counterpart in the small \hbar regime [1]. For bound conservative Hamiltonian systems, two goals may be identified: to develop useful methods for the semiclassical propagation of wave packets and to obtain estimates for the quantum eigenvalues and eigenfunctions using classical trajectories. Both have been achieved for classically integrable systems [2]. For classically chaotic systems, however, the situation is still unresolved.

For the case of eigenfunction or eigenvalue determination, most semiclassical studies of bound Hamiltonian systems have been done in the energy domain. After all, the eigenvalues and eigenfunctions are time independent quantities and should therefore be related to classical manifolds that are time invariant. When the corresponding classical system is integrable, the classical motion is restricted to tori, and their quantization produces good semiclassical estimates for the eigenvalues and the eigenfunctions [2]. This is in contrast to the case where the classical system is chaotic: The only time invariant structures other than the energy shell are then the periodic orbits. Consequently, periodic orbits are at the center of the semiclassical efforts in the energy domain for chaotic systems [3]. For example, Gutzwiller's trace formula [4] uses the periodic orbits to explain oscillations in the density of states, and a similar expression due to Bogomolny [5] explains the accentuations and attenuations in the average coordinate probability density about the classical periodic orbits, the so-called scars.

At present, however, we cannot obtain individual eigenvalues or eigenfunctions for generic chaotic Hamiltonians using periodic orbit theory. There are two main reasons for this. The first is numerical: to obtain an energy resolution of ϵ requires all periodic orbits with period $\tau < \tau_{\max} \sim 2\pi\hbar/\epsilon$, a quantity which grows exponentially in the chaotic regime [6]. Because of this exponential proliferation of contributing orbits, single eigenvalues can be obtained only for very special systems. The second reason is theoretical and deals with the possible divergence of the semiclassical expressions as we try to resolve an eigenvalue or eigenstate. This divergence can be traced back to the noncommutativity of the limits $\hbar \rightarrow 0$ and $\tau_{\max} \rightarrow \infty$.

Similarly, considerable difficulties abound in attempting semiclassical propagation in chaotic systems over reasonable time periods. For example, Van Vleck-Gutzwiller type propagators [2,7] require trajectories satisfying two-point boundary value conditions. Chaotic dynamics makes finding such trajectories extremely difficult. Hence, generally useful long time propagators are sorely needed to study chaotic dynamics. The availability of such methods would also aid in finding desired eigenvalues and eigenfunctions. In particular, if the propagation time is comparable to the Heisenberg time, $\tau_H = 2\pi\hbar/D$, where D is the mean level spacing, then Fourier transforming the propagated wave packet exposes the semiclassical eigenvalues and eigenfunctions.

Despite the inherent difficulties, some progress has recently been made toward developing useful propagation methods in the chaotic regime. For example, Tomsovic and Heller propagated wave packets [8], using the Van Vleck-Gutzwiller propagator, and extracted a scarred eigenstate of the stadium billiard [9]. In doing so they propagated past the so-called log time [10], $t_{\log} \sim \frac{1}{\lambda} \log N_{TF}(E)$, where λ is the largest Lyapunov exponent of the chaotic flow [11] and $N_{TF}(E)$ is the number of Planck cells in the phase space volume enclosed by a shell of energy E . This time was expected to limit the utility of nonuniform propagators of the Van Vleck-Gutzwiller type [7] since it was thought to be accompanied by the exponential proliferation of caustics. However, Schulman [12] has recently shown that their success in "breaking the log time barrier" arises from pathologies of the particular system chosen, the stadium billiard, where most caustics are found near the walls. For more realistic systems it is unclear whether nonuniform semiclassical expressions can be used for sufficiently long times.

In this Letter we use a uniform semiclassical propagator to get the time evolution of a wave packet in a smooth Hamiltonian system at energies for which the underlying classical motion is chaotic. By uniform we mean that there are no caustics (singularities) in our expressions. We then Fourier transform this propagation to obtain a scarred eigenstate. The method is straightforward and has no caustics-based time limitations. Furthermore,

trajectories satisfying two-point boundary values conditions are not required.

To obtain the time evolution of a wave packet $|\Psi\rangle$ we consider the following expression:

$$\langle\Psi|e^{-i\hat{H}t/\hbar}|\mathbf{q}_i\rangle = \int d\mathbf{p}_f \langle\Psi|\mathbf{p}_f\rangle \langle\mathbf{p}_f|e^{-i\hat{H}t/\hbar}|\mathbf{q}_i\rangle. \quad (1)$$

Then $\Psi(\mathbf{q}_i, t) = \langle\Psi|e^{-i\hat{H}(-t)/\hbar}|\mathbf{q}_i\rangle^*$. A semiclassical approximation for Eq. (1) is obtained by replacing $\langle\mathbf{p}_f|e^{-i\hat{H}t/\hbar}|\mathbf{q}_i\rangle$ with a Van Vleck-Gutzwiller type of expression [13]:

$$\langle\mathbf{p}_f|e^{-i\hat{H}t/\hbar}|\mathbf{q}_i\rangle_{sc} = \frac{1}{(2\pi\hbar)^{n/2}} \sum \frac{1}{|\sqrt{\det(D)}|} \times \exp\{i\phi/\hbar - i\nu\pi/2\}. \quad (2)$$

The sum is over all classical trajectories that connect \mathbf{q}_i with \mathbf{p}_f in a time t ; the sum is indexed by the initial momenta \mathbf{p}_i such that

$$\mathbf{q}(0) = \mathbf{q}_i, \quad \mathbf{p}(0) = \mathbf{p}_i, \quad \text{and} \quad \mathbf{p}(t) = \mathbf{p}_f. \quad (3)$$

The matrix D is one of the four stability matrices which describe how trajectories in the immediate vicinity of a given classical trajectory behave:

$$\begin{pmatrix} \delta\mathbf{q}(t) \\ \delta\mathbf{p}(t) \end{pmatrix} = \begin{pmatrix} A & B \\ C & D \end{pmatrix} \begin{pmatrix} \delta\mathbf{q}(0) \\ \delta\mathbf{p}(0) \end{pmatrix}. \quad (4)$$

The function $\phi(\mathbf{q}_i, \mathbf{p}_i, t)$ is a generator of the classical motion and is given by

$$\phi(\mathbf{q}_i, \mathbf{p}_i, t) = -\mathbf{p}(t)\mathbf{q}(t) + \int_0^t [\mathbf{p}(\tau)\dot{\mathbf{q}}(\tau) - H]d\tau. \quad (5)$$

Finally the index $\nu[\mathbf{q}_i, \mathbf{p}_i, t]$ is given by [13,14]:

$$\nu[\mathbf{q}_i, \mathbf{p}_i, t] = \frac{1}{\pi} \lim_{\epsilon \rightarrow 0^+} \arg\{\det(D + i\epsilon B)\}, \quad (6)$$

with $\nu[\mathbf{q}_i, \mathbf{p}_i, t=0] = 0$. The matrices D and B are defined by Eq. (4). It can be shown that Eq. (6) is equivalent to directly derived Maslov indices [15].

Inserting the semiclassical expression given in Eq. (2) into Eq. (1), we obtain

$$\langle\Psi|e^{-i\hat{H}t/\hbar}|\mathbf{q}_i\rangle_{sc} = \frac{1}{(2\pi\hbar)^{n/2}} \int d\mathbf{p}_i \langle\Psi|\mathbf{p}(t)\rangle |\det(D)|^{1/2} \times \exp\{i\phi/\hbar - i\nu\pi/2\}, \quad (7)$$

where $\mathbf{p}(t)$ is the momentum resulting from propagation beginning at $(\mathbf{q}_i, \mathbf{p}_i)$. To obtain Eq. (7) we made the change of integration variables from $\mathbf{p}_f [= \mathbf{p}(t)]$ to \mathbf{p}_i . Note that this expression has no singularities. In fact, although expression (2) develops caustics (i.e., singularities caused by the focusing of classical trajectories) as time progresses, Eq. (7) is uniform [13]. This expression is in the form of an initial value representation [14-16], i.e., it allows propagation of trajectories starting at $(\mathbf{q}_i, \mathbf{p}_i)$ and

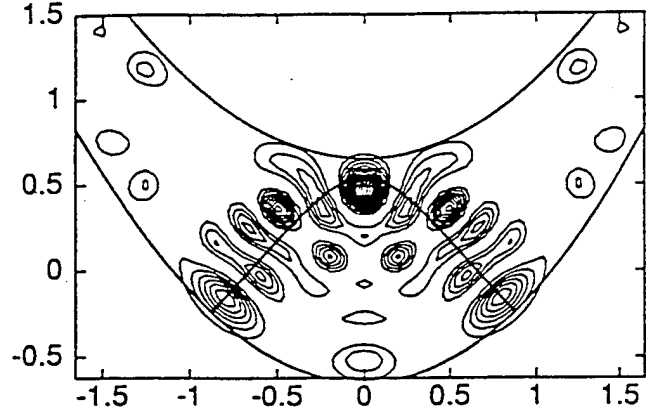


FIG. 1. Contours of the coordinate space probability density of the 42nd even (in x) eigenstate, showing striking scarring by a symmetric libration. The equipotential contour at $E = 0.4249$, the energy of this eigenstate, is also shown.

does not require [as does, e.g., Eq. (2)] trajectories that satisfy two-point boundary conditions.

We use Eq. (7) to propagate a coherent state (Gaussian wave packet) in the following smooth Hamiltonian system:

$$H = \frac{1}{2}(p_x^2 + p_y^2) + 0.05x^2 + (y - \frac{1}{2}x^2)^2. \quad (8)$$

In contrast to billiard systems, this Hamiltonian has a smooth potential and is generic in the sense that the energy cannot be scaled away. Its classical dynamics have been studied extensively [17], and it has been used, in the energy domain, to semiclassically study the scarring of wave functions [18]. The exact quantal wave functions and energies were obtained as in [18], with $\hbar = 0.05$. In Fig. 1 we show the coordinate probability density of the 42nd even (in x) eigenstate; it has energy $E = 0.4249$. We also show the simple symmetric libration that scars it extensively.

Here we consider propagation of a wave packet in this classically chaotic regime, extracting this eigenstate semiclassically. To do so we center a coherent state on

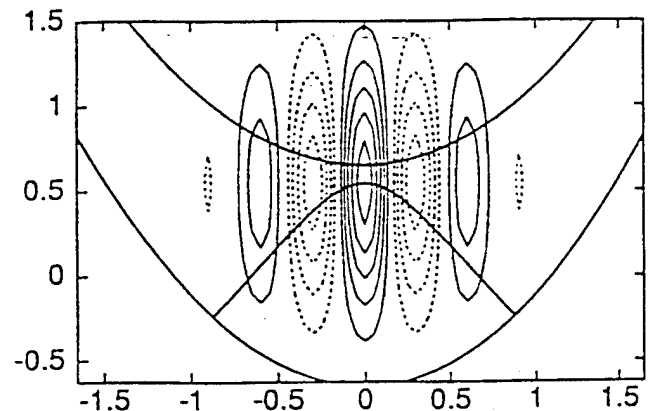


FIG. 2. The coordinate representation of the real part of the coherent state to be propagated. Solid contours are positive, dashed are negative. The contour spacing is 0.2 in Figs. 2-5.

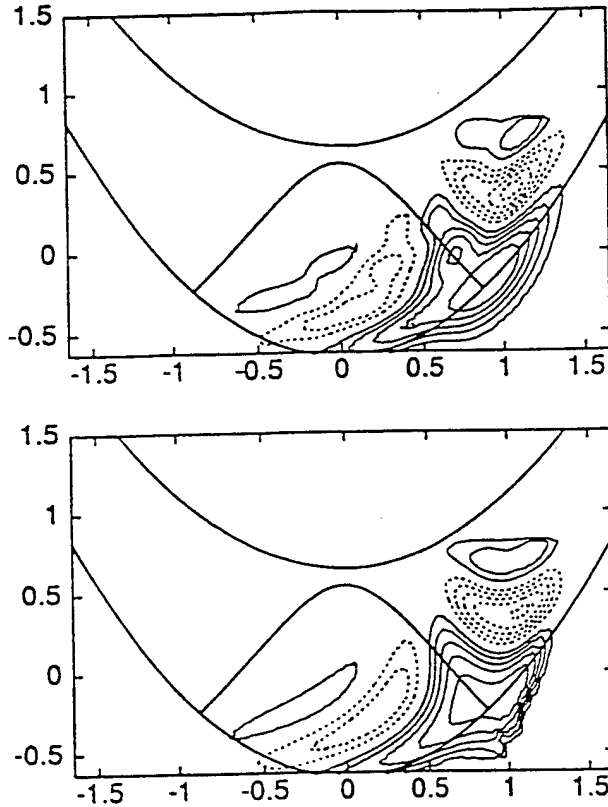


FIG. 3. The real part of the wave packet propagated for a time $t = \tau/4$, where τ is the period of the symmetric libration. Top: exact quantal propagation. Bottom: semiclassical propagation.

this periodic orbit; the coherent state we chose has the following coordinate representation:

$$\langle q|\Psi\rangle = \left(\frac{1}{\pi b^2}\right)^{1/2} \exp\left\{-\frac{(q - \bar{q})^2}{2b^2} + \frac{i\bar{p}}{\hbar}\left(q - \frac{\bar{q}}{2}\right)\right\}. \quad (9)$$

with $b = 0.5$, and (\bar{q}, \bar{p}) is the point where the symmetric libration intersects the y axis. In Fig. 2 we show the real part of the coordinate representation of this coherent state, chosen large in coordinate space so that it is well localized in momentum space. This feature allows us to search out the relevant regions in momentum space where Eq. (7) must be evaluated and to carry out the integration with low order quadrature methods. Note that we do not evaluate Eq. (7) by stationary phase and hence avoid the root search problem and caustics associated with coalescing trajectories.

Our calculations of the semiclassical wave-packet propagation is illustrated in Figs. 3–5 and are compared with the exact propagation. The agreement between the exact quantal and semiclassical pictures is excellent, even past the log time which we estimate to be $t_{\log} \sim 1.5\tau$, where τ is the period of the symmetric libration. In Fig. 6 we show the Fourier transform of our exact and semiclassical wave-packet propagations, with $\tau_{\max} = 2.5\tau$. Since we also have the wave-packet propagations backwards

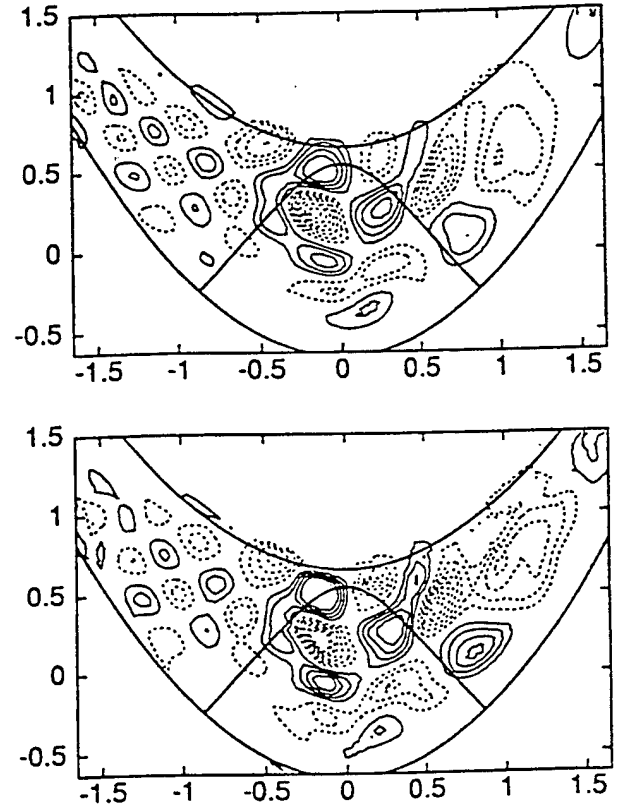


FIG. 4. Same as Fig. 3 but for $t = \tau$.

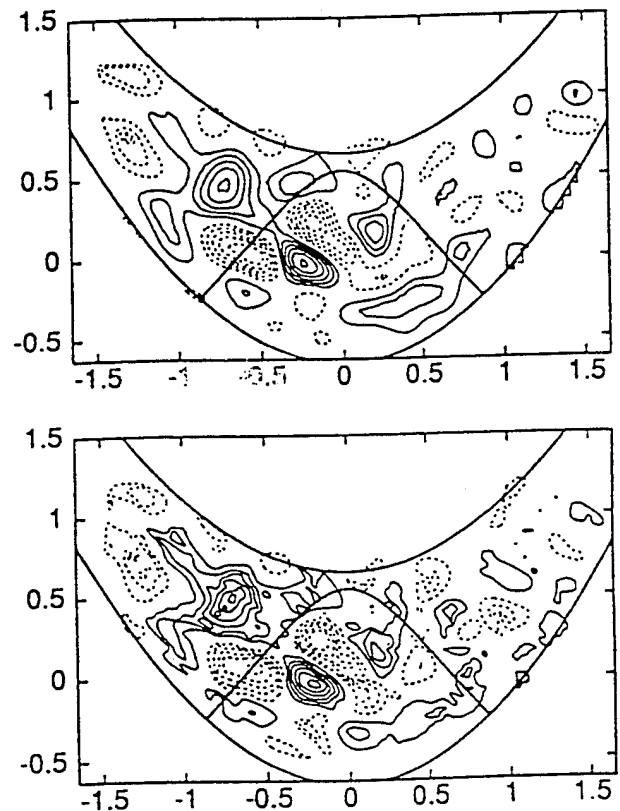


FIG. 5. Same as Fig. 3 but for $t = 2\tau$.

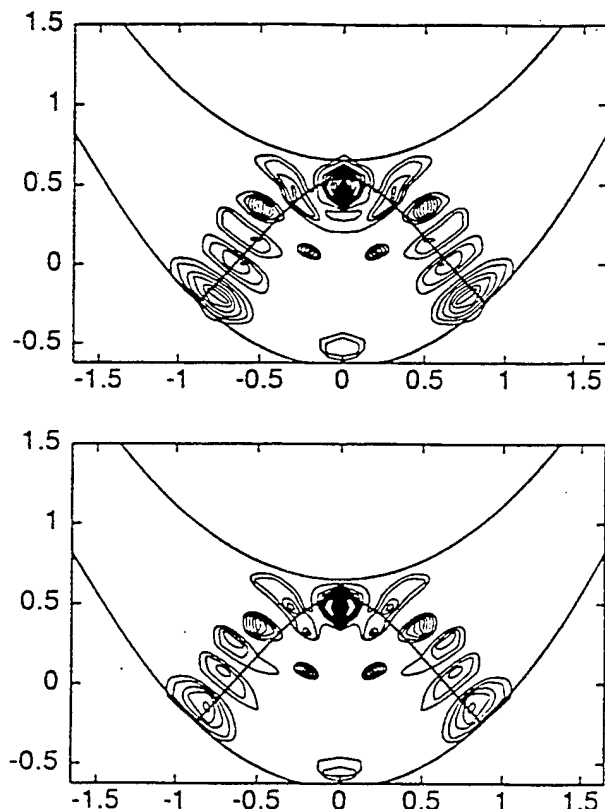


FIG. 6. The Fourier transform of the wave-packet propagation with $E = 0.4249$ and $t_{\max} = 2.5\tau$. Top: from exact quantal propagation. Bottom: from semiclassical propagation.

in time, we expect to get an energy resolution equivalent to a propagation time of 5.0τ . This is smaller than the Heisenberg time, which is $\tau_H \sim 8.0\tau$ at $E = 0.4249$. However, due to the special wave packet we chose, we are able to resolve most of the eigenstate, and agreement between the semiclassical and quantum results is excellent. It is important to realize that a similar calculation in the energy domain using Bogomolny's formula [18] would not produce the nodal structure which is seen to exist along the libration, even if all the periodic orbits with periods up to τ_H were included.

The resultant figures clearly demonstrate that this uniform propagation method is capable of accurate propagation in chaotic systems over sufficiently long times to extract accurate eigenstates. Further studies over longer time periods and for larger systems are well warranted and are in progress.

This work was supported in part by funds provided by the Ontario Laser and Lightwave Research Center

and the U.S. Office of Naval Research under Contract No. N00014-90-J-1014.

- [1] By small \hbar regime we mean where the dimensionless quantity formed from a combination of physical parameters with \hbar in the numerator can be made small.
- [2] See, for example, A.M. Ozorio de Almeida, *Hamiltonian Systems: Chaos and Quantization* (Cambridge University Press, Cambridge, 1988); M.C. Gutzwiller, *Chaos in Classical and Quantum Mechanics* (Springer-Verlag, Berlin, 1991); M.S. Child, *Semiclassical Mechanics with Molecular Applications* (Oxford University Press, Oxford, 1991).
- [3] See, for example, the following special issue on periodic orbit theories: *Chaos* 2 (1992).
- [4] M.C. Gutzwiller, *J. Math. Phys.* **12**, 343 (1971); R. Balian and C. Bloch, *Ann. Phys. (N.Y.)* **69**, 76 (1972).
- [5] E.B. Bogomolny, *Physica (Amsterdam)* **31D**, 169 (1988); M.V. Berry, *Proc. R. Soc. London A* **423**, 219 (1989).
- [6] R. Bowen, *Lecture Notes in Mathematics*, **470** (1975).
- [7] J.H. Van Vleck, *Proc. Natl. Acad. Sci. U.S.A.* **14**, 178 (1928).
- [8] S. Tomsovic and E.J. Heller, *Phys. Rev. Lett.* **67**, 664 (1991); M.A. Sepulveda, S. Tomsovic, and E.J. Heller, *Phys. Rev. Lett.* **69**, 402 (1992).
- [9] S. Tomsovic and E.J. Heller, *Phys. Rev. Lett.* **70**, 1405 (1993).
- [10] M.V. Berry and N.L. Balasz, *J. Phys. A* **12**, 625 (1979); M.V. Berry, N.L. Balasz, M. Tabor, and A. Voros, *Ann. Phys. (N.Y.)* **122**, 26 (1979).
- [11] S. Tomsovic (private communication).
- [12] L.S. Schulman, *J. Phys. A* **27**, 1703 (1994).
- [13] J.R. Klauder, *Phys. Rev. Lett.* **56**, 897 (1986); J.R. Klauder, *Ann. Phys. (N.Y.)* **180**, 108 (1987); J.R. Klauder, *Phys. Rev. Lett.* **59**, 748 (1987).
- [14] K.G. Kay, *J. Chem. Phys.* **100**, 4432 (1994); K.G. Kay, *J. Chem. Phys.* **101**, 2250 (1994).
- [15] G. Campolieti and P. Brumer, *Phys. Rev. A* **50**, 997 (1994).
- [16] W.H. Miller, *J. Chem. Phys.* **53**, 3578 (1970); W.H. Miller, *J. Chem. Phys.* **95**, 9428 (1991); G. Campolieti and P. Brumer, *J. Chem. Phys.* **96**, 5969 (1992).
- [17] M. Baranger and K.T.R. Davies, *Ann. Phys. (N.Y.)* **177**, 330 (1987).
- [18] D. Provost and M. Baranger, *Phys. Rev. Lett.* **71**, 662 (1993); D. Provost, in "Coherent States: Past, Present and Future," edited by D.H. Feng, J.R. Klauder, and M.R. Strayer (World Scientific, Singapore, to be published).

an Article from | **SCIENTIFIC
AMERICAN**

MARCH, 1995 VOL. 272 NO. 3

Laser Control of Chemical Reactions

For years, chemists have sought to control reactions with lasers—and have mostly failed. Success may come from exploiting subtle quantum effects resulting from the interaction of light and matter

by Paul Brumer and Moshe Shapiro

Although the science of chemistry has made considerable progress in the past century, the main principles behind the industrial practice of chemistry have remained basically unchanged. Methods for breaking and re-forming chemical bonds still often rely heavily on altering the temperature and pressure of the reaction or adding a catalyst. This approach is often ineffective because it takes no account of our understanding of the motions of molecules. As a result, bulk reactions are often inefficient, generating large quantities of useless by-products in addition to the desired materials.

Recently investigators have devised new techniques, based on illuminating chemical compounds with lasers, that can potentially control the paths taken by reactions. These methods promise to alter the yields in selected ways by exploiting an essential feature of quantum mechanics—namely, the wavelike properties of both light and matter. The latest calculations show that lasers

can be enormously effective in steering a reaction down a preferred pathway.

The idea of using lasers to drive reactions is not revolutionary—in fact, attempts to do so began shortly after the first laser was invented about 35 years ago. These devices emit radiation of a precise frequency, or color, and thus can impart a well-defined parcel of energy to a given target. Chemical bonds were seen as individual springs of different strengths, each of which vibrated when given a certain amount of energy. The hope was that lasers could be tuned to attack a particular bond, weakening or breaking it and thereby encouraging one product to form in lieu of another.

But this approach, called mode-selective chemistry, has seen only limited success. In fact, it is doomed to fail for the vast majority of molecules because it assumes that chemical bonds are largely independent of one another. Only a few compounds have bonds that meet this requirement. Rather most bonds are strongly interdependent: energy readily flows between them. As a consequence, the energy imparted by the laser is distributed throughout the molecule in a fashion similar to that resulting from traditional, and far cheaper, sources.

The latest approach, called coherent control, has grown out of research begun in the mid-1980s, when investigators began to take a look at properties of laser light that had been ignored in earlier considerations of chemical control. One such property is the coherence of laser light. "Coherence" relates to the way that atoms emit light. In conventional light sources, such as household bulbs, electricity heats up the filament, exciting tungsten atoms. The atoms spontaneously lose this energy by giving off a bit of light. Each atom, however, emits light independently of the other atoms. The total light from the

filament therefore consists of a jumble of waves from individual atoms. In a way, light from ordinary sources resembles a column of soldiers marching out of step with one another. Physicists say that such light is incoherent, or out of phase. In contrast, atoms in lasers act together. Consequently, all the waves that make up the entire laser beam match perfectly, behaving like soldiers marching in step.

Coherent light readily displays an important property—constructive and destructive interference. The term "interference" does not necessarily mean that the waves disturb one another's trajectories; it refers to the way all waves (including those on water) combine. In constructive interference, the crests or troughs of two (or more) waves meet so that the wave heights or dips add together. The wave therefore becomes bigger and deeper (in other words, the amplitude of the wave increases). In destructive interference, crest meets trough, and the wave is extinguished.

Interfering Light Waves

The phenomena of constructive and destructive interference become apparent if we shine a laser beam on an opaque plate that has two narrow slits cut into it. Each slit acts as a new source of light waves. The waves emanating from each slit, which fan out, can then interfere with each other. The interference can be rendered visible if we place a viewing screen just beyond the slits. The screen will show a pattern of dark and light stripes, or fringes. The light areas correspond to constructive interference; the dark areas, destructive interference.

The latest technique to control molecules takes advantage of the fact that light is not the only entity that displays interference. In accordance with a basic

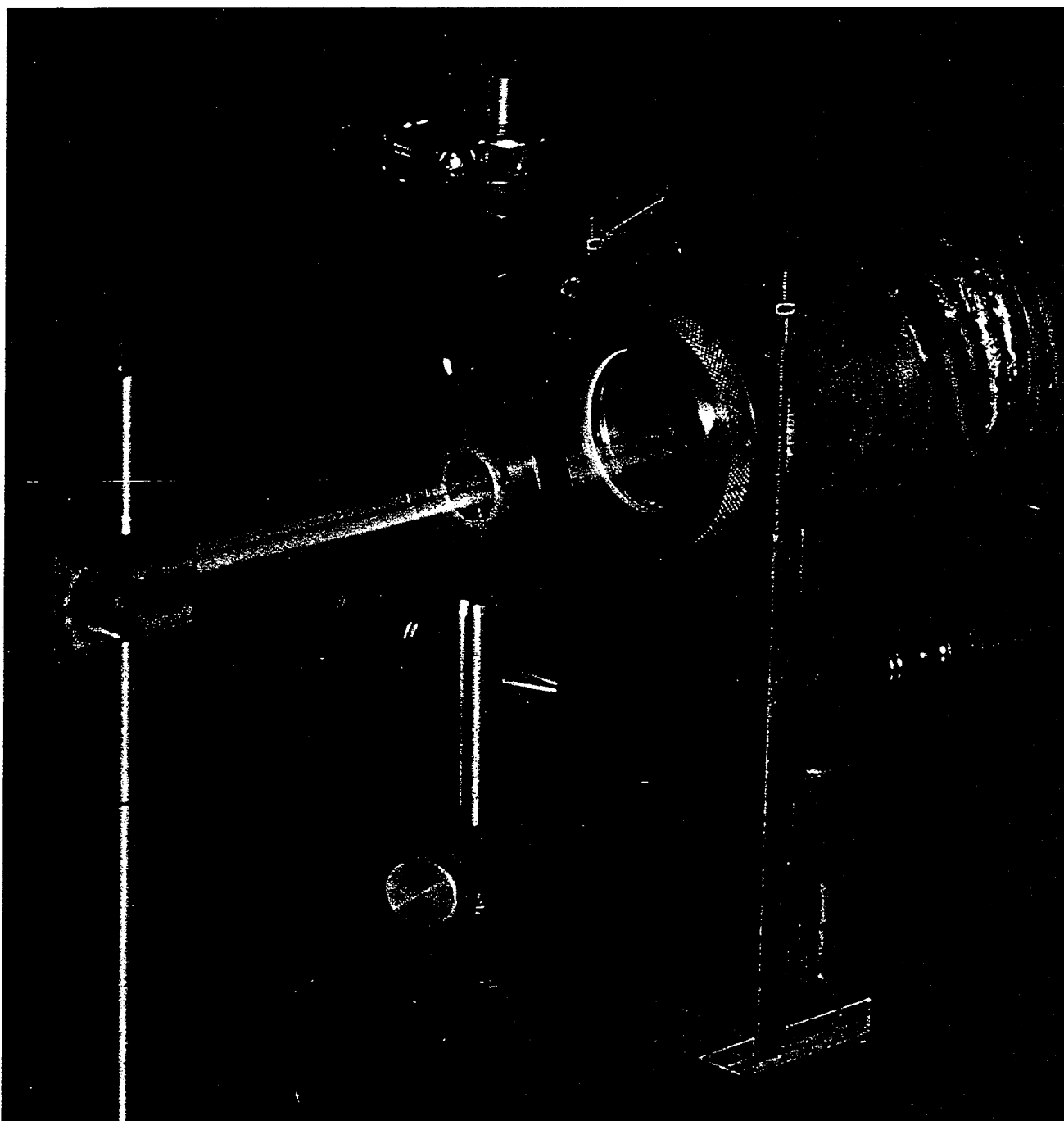
PAUL BRUMER and MOSHE SHAPIRO have been research collaborators since they met at Harvard University more than 20 years ago. Brumer is a professor in the chemical physics theory group at the University of Toronto and is currently a Killam Research Fellow. He recently received the Chemical Institute of Canada's Palladium Medal, one of the organization's highest awards. He earned his Ph.D. from Harvard. Shapiro obtained his Ph.D. from the Hebrew University of Jerusalem. The Jacques Mimran Professor of Theoretical Chemical Physics at the Weizmann Institute of Science in Rehovot, Israel, he has also held several visiting appointments throughout the U.S., Europe and Canada. The authors gratefully acknowledge funding and support from the U.S. Office of Naval Research.

principle of quantum mechanics, particles such as electrons, atoms and molecules can also behave as waves that can interfere with one another [see "The Duality in Matter and Light," by Berthold-Georg Englert, Marlan O. Scully and Herbert Walther; *SCIENTIFIC AMERICAN*, December 1994]. Experiments have fully confirmed the existence of such matter waves and of the associated interference of particles.

How can chemists exploit interference phenomena to control reactions? Numerous techniques have been developed, but the simplest one trains two different lasers beams on molecules. Each beam excites the wavelike aspect of the molecules in a particular way. These two matter waves can then interfere with each other. Constructive interference, in turn, may result in the formation of a particular product. Destruc-

tive interference would result in the absence of that product or the enhanced formation of another. It turns out that we can control the interference pattern—that is, the yield of the reaction products—by adjusting the coherence and intensity properties of the two laser beams.

A more specific explanation incorporates an abstraction known as a wave function, which physicists use to de-



RICK ROSEN SABA

LASER BEAMS fired into a vessel filled with paired sodium atoms, or dimers, can control the breakup of the molecules. The beams, each of a different frequency (appearing as yellow and red), place the molecules into quantum states that

interfere with one another. Each molecule subsequently breaks up into one sodium atom in its normal state and another sodium atom in any of several excited states. The particular state formed is governed by the degree of interference.

scribe atomic and molecular systems. Consider a molecule made of three components connected in a line—call them A, B and C. Because particles behave as waves, physicists can describe the initial state of the molecule with a mathematical entity—a wave function. It embodies all available information about the state of a particle and its motions, or dynamics. For example, the square of the wave function gives the probability of finding the molecule in a particular geometry. Wave functions serve as the basic descriptive tool of quantum mechanics.

Now imagine that we can break the ABC molecule apart in two ways. Either the bond between A and B can break, or the one between B and C. Thus, two pairs of compounds are possible: A and BC or AB and C. To produce either possibility, we must add energy to the molecule. We can irradiate it with a photon of a particular frequency (and thus impart a known amount of energy to it), which the molecule absorbs. If the photon is sufficiently energetic, it brings the ABC molecule to the final state—that is, to the energy level at which ABC dissociates into two products. The wave function describing the ABC molecule in this state incorporates two kinds of information. One is the wave nature of the laser light impinging on the molecule; the second is the quantum-mechanical wave nature of the molecule itself.

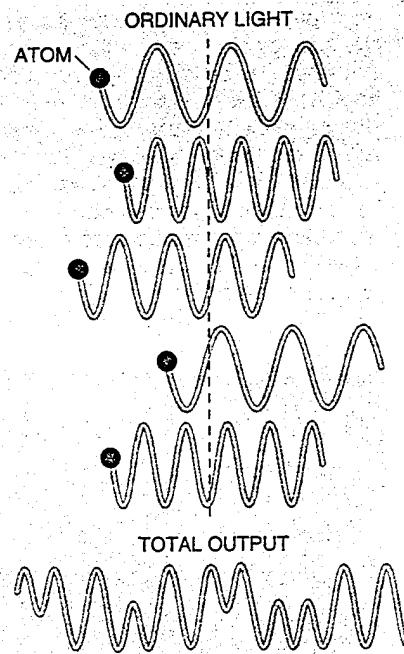
But what if we irradiate the molecule at one third the frequency (that is, with light carrying one third the energy)? In this case, the molecule would have to

PHASE COHERENCE refers to the way atoms emit radiant energy. In ordinary sources such as lightbulbs, excited atoms spontaneously give off light independently of one another. Hence, the light waves from each do not “line up,” and the total output over time consists of random emissions (left). In laser light (right), all the atoms emit in phase, so the output is coherent.

absorb three photons instead of one in order to dissociate. The molecular wave function at the point of dissociation would then be different, reflecting the fact that the molecule absorbed three photons rather than just one.

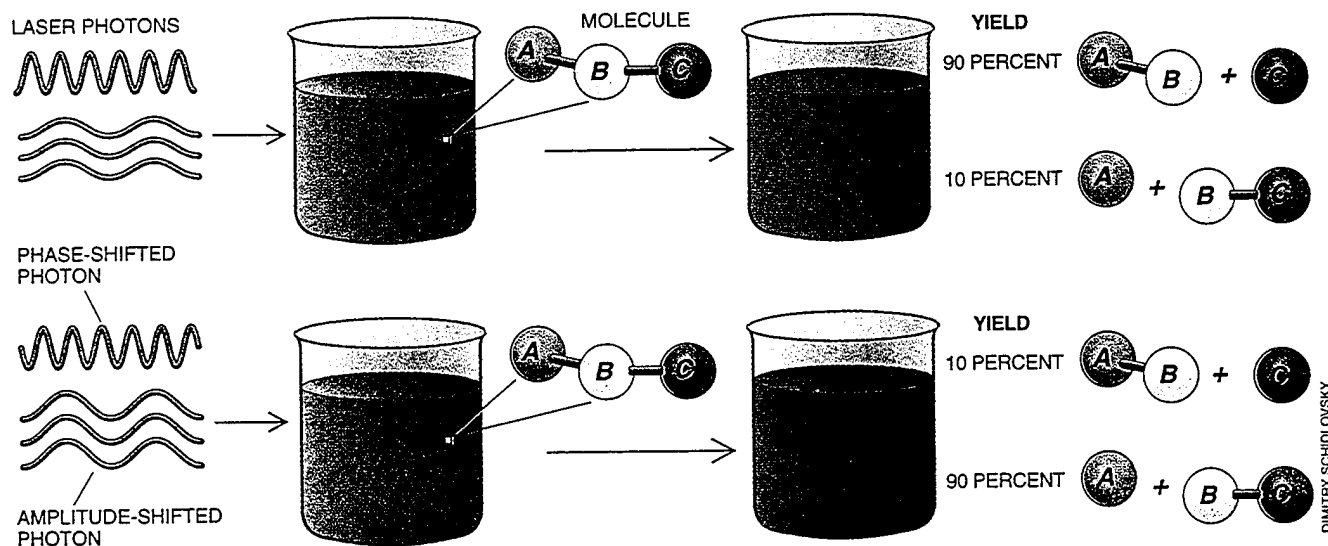
We can control molecular motion if we simultaneously irradiate ABC with both light fields. Doing so produces two distinct wave functions at the energy of dissociation. The two modes of excitation interfere, just as coherent light does when it passes through two slits [see box on page 38]. It may seem strange that two reaction pathways can interfere, but such interference is the essence of quantum mechanics.

Fortunately for chemists seeking to control molecules, the mathematical term describing the interference differs for the two possible outcomes of the reaction. We can create predominantly A and BC or mostly AB and C by adjusting the interference term. The interference, and hence the amount of each product, depends on the relative amplitude and phase of the two original laser beams, and so it can be altered by adjusting these characteristics. Note



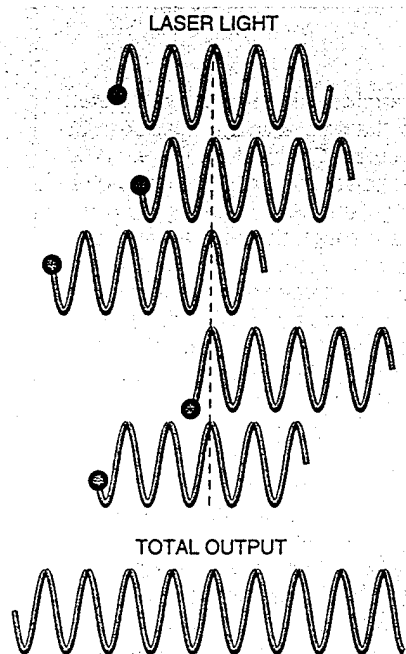
that because control relies on interference, the method does not require the use of intense lasers. In other words, weak light can have a substantial effect on the dynamics of molecules.

Working with Chi K. Chan, then at the University of Toronto, we studied the dissociation of the diatomic molecule iodine monobromine (IBr). This molecule can separate into I + Br or I + Br*, where the asterisk indicates that the bromine atom has excess energy. Our calculations predict that varying the intensities and relative phase of two la-



CONTROLLED CHEMICAL DISSOCIATION can be accomplished if a compound is irradiated simultaneously by two types of laser photons, one of which is more energetic than the other. For instance, the molecule ABC can dissociate if it absorbs a photon of a certain energy, or three photons, each with one

third the energy. The wave functions associated with the excitation by each type of photon quantum-mechanically interfere with one another. The extent of the interference—and hence, the yield—is controlled by adjusting the relative amplitude (the height of the wave) and the phase of the laser light.



DIMITRY SCHIDLOVSKY

ser beams would provide an enormous range of control over the reaction. We would be able to vary the amount of energetic bromine produced to ensure that it accounted for between 25 and 95 percent of the total product formed. This degree of control far exceeds the hopes of conventional industrial chemistry, which seeks to improve reaction selectivity by about 10 percent. Experiments by Daniel S. Elliott of Purdue University have demonstrated the success of this approach for controlling the ionization of atoms. Robert J. Gordon

of the University of Illinois at Chicago has also obtained beautiful results in the control of diatomic and polyatomic molecules.

This form of coherent control is not restricted to the use of one photon and three photons at one third the energy. Rather quantum mechanics permits control over the probability that a particular reaction will occur if each of the two paths corresponds to the absorption of either an even number or an odd number of photons. For example, Andre Bandrauk of the University of Sherbrooke in Quebec has computationally displayed extensive control over the photodissociation of a chlorine molecule into energetic and nonenergetic atoms when the molecule absorbs two photons from one laser beam and four photons, each of half the energy, from the second laser beam. Similarly, we have shown that using one photon in conjunction with two photons, each of half the energy, can be used to control the direction that molecules take when they leave the reaction region. Such an ability may render the separation of products easier and thereby boost the efficiency of the reaction.

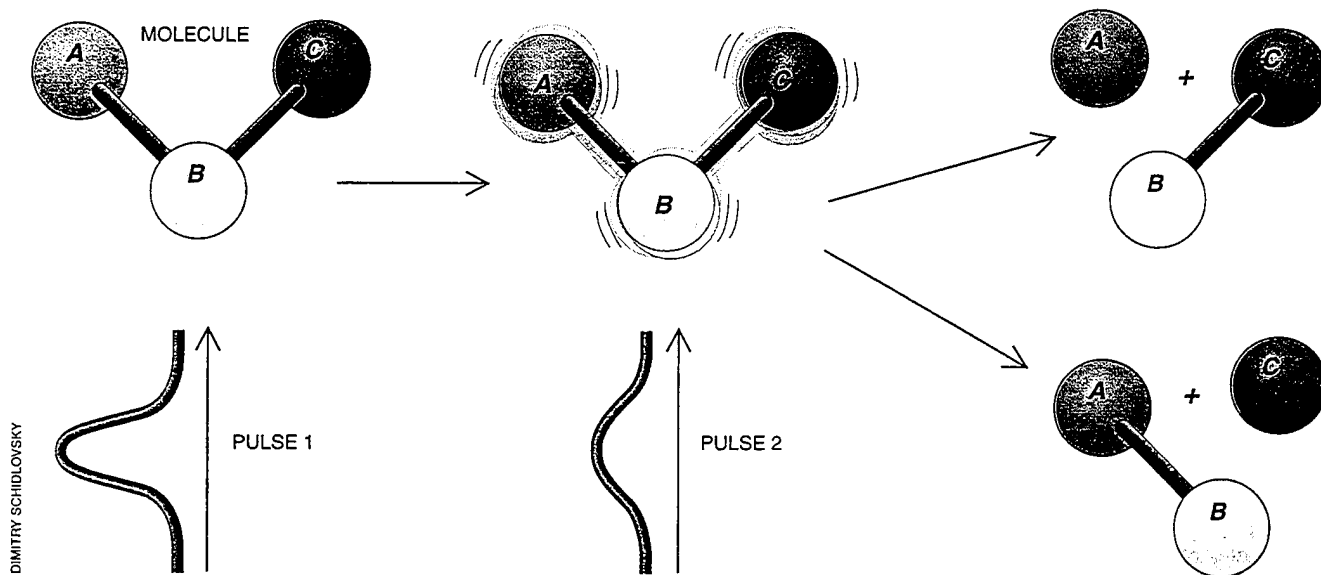
Current Limitations

Although the concepts behind controlling reactions with coherent light apply to a wide range of isolated molecules, there are at least two obstacles to their immediate broad application. One is that the efficiency of laser control drops substantially when the

light waves or the molecular wave functions have ill-defined phases. Loss of phase definition occurs mainly because of collisions between molecules, which increase with higher temperature and pressure and which commonly occur in industrial environments. Further work is necessary to be able to introduce coherent control into modern commercial settings. Consequently, at present, the schemes must be applied in cleverly designed environments or must be restricted to a limited class of reactions. For instance, current technology works well on dilute gases, where the molecules are far apart and so collide less frequently.

The second major obstacle, now beginning to seem surmountable, involves the phase of the laser light. Given two arbitrary laser sources, we generally do not know the extent to which the light from one will be in phase with the other. In addition, the phase difference is affected by any instabilities in the equipment. An unstable phase difference between the two lasers reduces the degree of interference and control.

Sophisticated optical techniques have the potential to eliminate such phase problems. For example, photons may be generated by passing light at one frequency through a particular material that is thereby induced to emit light at another frequency. This process yields two light fields whose phase relations are well defined. We can further control the phase differences between the two light sources by temporarily slowing one light beam relative to the other.



TWO-PULSE LASER STRATEGY can also govern the yield of a chemical reaction. The first pulse places the molecule in a superposition state—in other words, it sets the molecule vibrating and rotating in a particular way. The motion depends on

the characteristics of the molecule and the laser. The second pulse causes the molecule to break up. The differences in yield are controlled by varying the time between pulses and by changing the frequencies that make up the pulses.

Interference and Coherent Control

Perhaps the most unusual aspect of quantum mechanics is that, under certain circumstances, matter behaves just as waves do. In particular, it displays interference. Because this property is essential to the ability of lasers to control chemical reactions, some of the mathematics and more technical quantum-mechanical concepts underlying the phenomenon may be of interest.

Interference arises from the way waves add together. The rule for combining many different waves is first to sum their amplitudes (the height of the wave) and then square the result. Consider the interference of two waves whose amplitudes at a given position and time are a and b . The intensity of each wave is a^2 and b^2 . The combined amplitude, c , is the sum $c = a + b$, and the combined intensity is $c^2 = (a + b)^2 = a^2 + b^2 + 2ab$.

Note that the combined intensity is not merely the sum of the intensities of each wave (which would be $a^2 + b^2$), but that an additional interference term, $2ab$, contributes. If a and b are both positive or both negative, this interference term is positive. The resulting intensity, c^2 , is thus greater than the simple sum of intensities of each wave. The interference in this case is said to be constructive. If a is positive and b is negative (or vice versa), the interference term is negative, and the resulting intensity is smaller than the simple sum of the individual intensities. Interference in this case is said to be destructive.

The variation in intensity produced by interfering light waves can be seen in the famous double-slit experiment, in which a beam of coherent light passes through two slits and onto a screen (diagram). The bright regions on the screen arise from the constructive interference between the two beams of light passing through the two slits; dark regions result from the destructive interference. Intensities in between these two extremes arise from the combi-

nations of maxima and minima meeting at the screen.

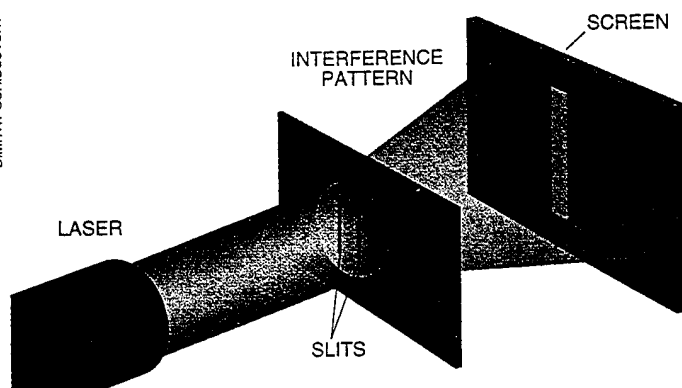
Now consider replacing the light with particles such as electrons, atoms or molecules. Classical intuition would suggest that the emergent pattern on the screen would resemble two nearly rectangular blobs, resulting from the direct passage of particles through the slits. In fact—and this is the essential feature of quantum mechanics—the observed pattern can clearly display an interference pattern. That is, the particles can show behavior characteristic of waves (as long as the particles are themselves “coherent”—that is, prepared so that they have well-defined wave functions). There is simply no way to explain these

observations on the basis of a classical theory of particles.

For this reason, the proper description of particle dynamics in quantum mechanics entails a wave function that, as in the case for waves, is described by both an amplitude and a phase. In the double-slit experiment applied to particles, quantum wave functions arriving at the screen via the slits interfere with one another. Most significant is another unusual

feature of the quantum world: interference arises because we do not know through which of the slits the particles passed. If we do record such information, the interference pattern disappears.

The two-slit experiment embodies the fundamental quantum principle that two (or more) phase-preserving routes that a molecule can take to some final state can be made to interfere. In the case of the one-photon plus three-photon experiment mentioned in the main body of the article, we do not know which of the two possible excitation routes leads to the observed final state. Hence, the two routes interfere. This optically induced interference forms the foundation for coherent radiative control of molecular processes.



INTERFERENCE FRINGES are made if coherent light passes through two slits. Particles such as molecules also interfere in this way.

Another way to control phase problems relies on intense laser beams, the focus of many recent investigations. With Zhidang Chen of the University of Toronto, we have shown that such lasers make it possible to bypass the need for radiation having well-defined and carefully controlled phases. In addition, such strong-field methods have the potential to increase substantially the absolute yield of the reaction and to overcome unwanted collisional effects. A particular scheme has just been used experimentally at the Weizmann Institute of Science in Israel by Irit Sofer, Alexander Shnitman, Ilya Golub, Amnon Yogev and us to demonstrate con-

trol over the various products formed in the dissociation of paired sodium molecules.

Using Pulses

Because interference of molecular pathways is the key to governing reactions, any laser scenario that induces such interference may serve as a means of controlling reactions. Instead of shining two steady beams on a target, one might use ultrashort pulses of laser light. Modern lasers can generate bursts as short as 10^{-14} second. Unlike continuous-wave radiation, a light pulse is made up of a collection of distinct fre-

quencies and, hence, of a collection of photons with different energies. Such light also has a perhaps counterintuitive property. The briefer the pulse, the broader the range of energies within it.

This property plays a major role in pulsed-laser methods for controlling the outcomes of chemical reactions. By delivering a range of energies, a pulse can induce motion (such as vibration or rotation) in a molecule, which in turn affects the way it interacts with other light pulses. Ordinarily a molecule such as ABC exists at a specific (that is, quantized) energy value. A system at one of these fixed energies resides in a so-called stationary state and does not move over

time. For a molecule to undergo the dynamics, it must live in several energy levels at once. Such an assemblage of energy levels is called a superposition state. The wave function describing the superposition state is the sum of wave functions representing stationary states of different energies. To construct it, researchers shine a pulse of coherent laser light on the molecule. The way the molecule then moves depends on the nature of the light pulse and its interaction with the molecule. Thus, we can effect dynamic changes in the molecule by shifting the relative contribution of the frequencies that compose the pulse—that is, by shaping the pulse.

Several researchers have developed these ideas. They include Stuart A. Rice of the University of Chicago, David J. Tannor of Notre Dame University, Herschel Rabitz of Princeton University, Ronnie Kosloff of the Hebrew University of Jerusalem and Kent R. Wilson of the University of California at San Diego. Their results show that pulses built out of a complicated mixture of frequencies are required to control molecular dynamics optimally, but simple approximations often suffice to break apart molecules in a controlled way.

Although a single light pulse can alter the dynamics of a molecule, it does not by itself afford an active means of controlling the yield of a chemical reaction. Rather an idea originally introduced by Rice and Tannor and subsequently extended by us in collaboration with Tamar Seideman, now at the National Research Council of Canada, does allow for control with pulses. Specifically, one needs to employ a two-pulse sequence. The first pulse places the molecule in a superposition state that dictates how that molecule will later respond to the follow-up pulse. The second pulse breaks up the molecule into different products.

Although not apparent, this scenario is similar to that using continuous-wave lasers in that quantum interference between wave functions is responsible for the control. Interference between molecular wave functions, however, is now created by the various frequencies within the two light pulses incident on the molecule. The interference, and hence the yield of the products formed, can be altered easily by varying the interval between the two pulses and the frequencies that make up the first laser pulse. Hence, unlike the continuous-wave laser experiments in which a steady stream of products is formed, pulsed lasers let us take advantage of time as an experimental variable.

Indeed, computational studies by Izhak Levy, formerly at the Weizmann In-

stitute, and us show that the range of control is potentially quite extensive. In an analysis of the dissociation of diatomic molecules, we showed that the yield can be varied so that the desired product accounts for between 3 percent of the total yield and 95 percent, depending on the laser settings selected. One can basically turn a process completely on or off. For polyatomic molecules, control is not as extensive but is considerable nonetheless. We have, for instance, successfully applied this approach to the dissociation of monodeuterated water (HOD), made of hydrogen, oxygen and deuterium, to produce controllable amounts of $H + OD$ or $D + OH$.

Help for Pharmaceuticals

One of the first real-world applications of laser control may well be enjoyed by the pharmaceutical industry. Currently chemists must take care to ensure that reaction products adopt a specific conformation. Often the same molecule can exist in two forms, known as enantiomers. Like our right and left hands, enantiomers are mirror images of each other. Indeed, such molecules are often referred to as right- or left-handed. Drug companies expend considerable effort to form compounds with the correct handedness because often one enantiomer is biologically active, and the other is either inactive or harmful.

Laser control could be a solution for achieving the correct outcome. We examined the dissociation of a compound that can break up into either right- or left-handed forms—call the substance ABA' , where A and A' are enantiomers. The reaction can produce A and BA' or A' and BA . Because ABA' is highly symmetrical, traditional dissociation of ABA' by absorption of light does not push the reaction in any particular direction; the result is an equal yield of A and A' . But our studies show that under certain conditions (in particular, in the presence of a weak magnetic field) the two-pulse scheme can be used to control enantiomeric yield so that we can produce A rather than A' .

Procedures based on quantum interference can do more than control chemical reactions. They can be used to produce entirely novel kinds of technology. The methods can allow workers to select the particular energy state of the products of a chemical reaction. These products could in turn generate laser light at frequencies not obtainable with current equipment. Even more interesting, Paul B. Corkum of the National Research Council of Canada has proposed using interference effects to build lasers

that emit supershort bursts of light, on the timescale of 10^{-16} second. This interval is about one tenth the length of pulses from the best lasers in use today.

With Gershon Kurizki of the Weizmann Institute, we have proposed using quantum interference to regulate the flow of electrons in semiconductors. One can design two pathways by which a donor atom loses an electron on absorption of light. These paths can be made to interfere. Controlling this interference means that the direction of the ejected electrons—and hence the direction of the electric current—can be regulated. The result would be a fast optical switch, perhaps on the order of 10^{-12} second, many times faster than present-day switches. Experimental evidence for such directional control has now been obtained by Boris Zeldovich, now at the University of Central Florida, in photoelectric detectors, by Corkum in semiconductor devices and by Elliott in atoms that are ionized by light.

The advent of quantum mechanics introduced new concepts in the understanding of nature. But we are now moving past the role of passive observer. As we approach the 21st century, it is clear that we can extend quantum-mechanical ideas to open up unprecedented possibilities for gaining further control over atomic, molecular and electronic processes.

FURTHER READING

- COHERENT PULSE SEQUENCE CONTROL OF PRODUCT FORMATION IN CHEMICAL REACTIONS. D. J. Tannor and S. A. Rice in *Advances in Chemical Physics*, Vol. 70, Part 1, pages 441-523; 1988.
- INTERFERENCE BETWEEN OPTICAL TRANSITIONS. C. Chen, Y.-Y. Yin and D. S. Elliott in *Physical Review Letters*, Vol. 64, No. 5, pages 507-510; January 29, 1990.
- CONTROLLED PHOTON INDUCED SYMMETRY BREAKING CHIRAL MOLECULAR PRODUCTS FROM ACHIRAL PRECURSORS. M. Shapiro and P. Brumer in *Journal of Chemical Physics*, Vol. 95, No. 11, pages 8658-8661; December 1, 1991.
- COHERENT LASER CONTROL OF BOUND-TO-BOUND TRANSITIONS OF HCL AND CO. S.-P. Lu, S. M. Park, Y. Xie and R. J. Gordon in *Journal of Chemical Physics*, Vol. 96, No. 9, pages 6613-6620; May 1, 1992.
- COHERENT AND INCOHERENT LASER CONTROL OF PHOTO CHEMICAL REACTIONS. M. Shapiro and P. Brumer in *International Reviews in Physical Chemistry*, Vol. 13, No. 2, pages 187-229; September 1994.
- COHERENCE CHEMISTRY: CONTROLLING CHEMICAL REACTIONS WITH LASERS. P. Brumer and M. Shapiro in *Accounts of Chemical Research*, Vol. 22, No. 12, pages 407-413; December 1994.

Interference control without laser coherence: Molecular photodissociation

Zhidang Chen, Moshe Shapiro,^{a)} and Paul Brumer
Chemical Physics Theory Group, Department of Chemistry, University of Toronto, Toronto M5S 1A1, Canada

(Received 21 October 1994; accepted 6 January 1995)

Control over channel-specific line shapes and branching ratios in photodissociation is shown to be achievable by irradiating a molecule with two intense cw lasers whose relative phase need not be well defined. Control results from quantum interference between nonlinear pathways induced by the intense fields, within which the relative laser phase cancels. The interference, and hence the product yields, can be manipulated by changing the relative frequencies and intensities of the two lasers. In this paper this theory of high field control is developed, and computations on the photodissociation of Na₂ are presented. Control over product yields is shown to be extensive, even with inclusion of rotational states. For example, the branching ratio between the Na(3s)+Na(3p) and Na(3s)+Na(4s) products can change by as much as a factor of 10 as the frequencies are tuned. © 1995 American Institute of Physics.

I. INTRODUCTION

Controlling atomic and molecular processes via external variation of laser parameters is a rapidly developing field. Most recent innovations rely on using several lasers with well-defined relative phase to excite a system.¹⁻⁸ This simultaneous excitation induces quantum interference effects between laser-induced multiple excitation routes. These interferences, and hence the molecular dynamics, may be altered by varying the laser intensities and their relative phase. Further, computations on molecular photodissociation show that control over product yields is extensive^{1,3} and several experiments have demonstrated the validity of the essential coherent control principle.⁴

The vast majority of proposed control scenarios have relied upon the use of lasers whose relative phase is controllable and well defined. In this paper we show that simultaneous irradiation of a molecule with two intense laser fields allows for a control scenario in which relative laser phase need not be maintained. Rather, the essential control parameter influencing the quantum interference effect is the relative frequency of the two lasers. This scenario, which bears some relationship to studies of laser-induced continuum structure^{9,10} and laser-induced transparency,¹¹ is shown to allow for extensive control over the probability of dissociation as a function of translational energy (channel-specific line shape) as well as the total yield of a given product.

The proposed control scenario is straightforward: an intense laser of frequency ω_1 excites a molecule from an initially populated bound state $|\epsilon_i\rangle$ to a continuum $|\epsilon, m, q^-\rangle$ (where m specifies the product quantum numbers and q labels the product arrangement channel) while a second laser ω_2 simultaneously couples initially unpopulated bound states $|\epsilon_j\rangle$ to the same continuum. With both lasers on, dissociation to $|\epsilon, m, q^-\rangle$ occurs via direct and indirect dissociation pathways, the two lowest orders of which are $|\epsilon_i\rangle \rightarrow |\epsilon, m, q^-\rangle$ and $|\epsilon_i\rangle \rightarrow |\epsilon', m', q'^-\rangle \rightarrow |\epsilon_j\rangle \rightarrow |\epsilon, m, q^-\rangle$. Contributions

from these pathways to the product in a given channel q at energy ϵ interfere (either constructively or destructively) with one another. Varying the frequencies and intensities of the lasers alters the interference and hence the dissociation line shape and the yield of product into a given channel.

This paper is organized as follows. We develop, in Sec. II, a molecular photodissociation theory for molecules in intense laser fields. The proposed control scenario emerges by applying this theory to excitation with two laser fields, characterized as described in Sec. II B. Results of computations examining the extent of possible control are provided in Sec. III, where we demonstrate extensive control over the branching ratio into Na(3s)+Na(3p) vs Na(3s)+Na(4s). Indeed the absolute controlled yield is extensive as well, since the cw fields induce virtually 100% dissociation. Section IV contains a brief summary. Preliminary results on this scenario have been reported elsewhere.¹²

II. MOLECULE-INTENSE LASER INTERACTION

A. Photodissociation

Consider first a molecular photodissociation theory for intense radiation fields. The total system Hamiltonian H is the sum of the molecular part H_M , radiation part H_R , and the interaction between them V

$$H = H_M + H_R + V \equiv H_0 + V. \quad (1)$$

The Hamiltonian H_M of an isolated molecule AB can be conveniently written as the sum of the nuclear kinetic terms, $K(R)$ and $k(r)$, and the electronic term $H_{el}(q|R, r)$,

$$H_M = K(R) + k(r) + H_{el}(q|R, r), \quad (2)$$

where R is the displacement vector between A and B , r are the remaining nuclear coordinates, and q denotes the collection of all electronic coordinates. As the molecule dissociates ($R \equiv |R| \rightarrow \infty$), H_M approaches its asymptotic form H_M^∞ while $H_{el}(q|R, r)$ approaches $h_{el}(q, r)$,

$$\lim_{R \rightarrow \infty} H_M = H_M^\infty, \quad (3)$$

^{a)}Permanent address: Chemical Physics Department, Weizmann Institute of Science, Rehovot, Israel.

$$H_M^\infty = K(\mathbf{R}) + [k(\mathbf{r}) + h_{\text{el}}(\mathbf{q}, \mathbf{r})], \quad (4)$$

where the term in the brackets in the right-hand side of Eq. (4) is the Hamiltonian of the separated fragments *A* and *B*.

Photodissociation occurs as a transition from a molecular bound state $|\epsilon_b\rangle$ to dissociating eigenstates $|\epsilon, \mathbf{m}, q^-\rangle$ in the presence of radiation fields. Here $|\epsilon_b\rangle$ and $|\epsilon, \mathbf{m}, q^-\rangle$ are eigenstates of H_M with discrete energy ϵ_b and continuous energy ϵ , respectively. That is,

$$H_M|\epsilon_b\rangle = \epsilon_b|\epsilon_b\rangle, \quad (5)$$

$$H_M|\epsilon, \mathbf{m}, q^-\rangle = \epsilon|\epsilon, \mathbf{m}, q^-\rangle. \quad (6)$$

The properties of the eigenstates imply that

$$\langle \epsilon_b | \epsilon, \mathbf{m}, q^- \rangle = 0, \quad (7)$$

$$\langle \epsilon', \mathbf{m}', q'^- | \epsilon, \mathbf{m}, q^- \rangle = \delta(\epsilon' - \epsilon) \delta_{\mathbf{m}', \mathbf{m}} \delta_{q', q}. \quad (8)$$

The minus sign on *q* denotes the incoming boundary condition that at large *t* the states $\exp(-i\epsilon t/\hbar)|\epsilon, \mathbf{m}, q^-\rangle$ approach well-defined states $\exp(-i\epsilon t/\hbar)|\epsilon, \mathbf{m}, q\rangle$, where $|\epsilon, \mathbf{m}, q\rangle$ are eigenstates of the asymptotic Hamiltonian H_M^∞

$$H_M^\infty|\epsilon, \mathbf{m}, q\rangle = \epsilon|\epsilon, \mathbf{m}, q\rangle. \quad (9)$$

The quantity *m*, being good quantum numbers of H_M^∞ , specify, in conjunction with the energy ϵ and the arrangement channel label *q*, the states $|\epsilon, \mathbf{m}, q\rangle$ of the fragment products. In the case of diatomic photodissociation the quantum number *m* refers to scattering angles $\hat{\mathbf{k}}$.

The presence of radiation is conveniently described by the eigenstates of H_R : $H_R|N_k\rangle \equiv H_R|n_1^{(k)}, n_2^{(k)}, \dots\rangle = E_{N_k}|N_k\rangle$ with energy $E_{N_k} = \sum n_l^{(k)} \hbar \omega_l$. The letters *k* = *i* and *f* will be used to label the initial and final states, respectively. The eigenstates of $H_0 \equiv H_M + H_R$ are the direct product of the molecular and photon states; e.g., $|\epsilon, \mathbf{m}, q^-, N_f\rangle \equiv |\epsilon, \mathbf{m}, q^-\rangle |N_f\rangle$. The molecule-radiation interaction *V* can be expressed in the dipole approximation as

$$V = -\boldsymbol{\mu} \cdot \boldsymbol{\mathcal{E}}, \quad \boldsymbol{\mathcal{E}} = i \sum_l \epsilon_l (\mathbf{e}_l a_l - \mathbf{e}_l^* a_l^\dagger), \quad (10)$$

where $\boldsymbol{\mu}$ is the electric dipole operator, $\epsilon_l = (2\pi\hbar\omega_l/L^3)^{1/2}$, \mathbf{e}_l and ω_l are the polarization vector and angular frequency of mode *l*, respectively, and a_l , a_l^\dagger are annihilation and creation operators.

The dynamics of photodissociation is completely embodied¹⁵ in the fully interacting state $|\epsilon, \mathbf{m}, q^-, N_k^-\rangle$ of the total Hamiltonian *H*,

$$H|\epsilon, \mathbf{m}, q^-, N_k^-\rangle = (\epsilon + E_{N_k})|\epsilon, \mathbf{m}, q^-, N_k^-\rangle, \quad (11)$$

where the minus superscript on N_k indicates that when the radiative interaction *V* is switched off, the state $|\epsilon, \mathbf{m}, q^-, N_k^-\rangle$ becomes the noninteracting state $|\epsilon, \mathbf{m}, q^-, N_k\rangle$. The fully interacting state $|\epsilon, \mathbf{m}, q^-, N_k^-\rangle$ satisfies the Lippmann-Schwinger equation¹⁴

$$\begin{aligned} \langle \epsilon, \mathbf{m}, q^-, N_k^- | &= \langle \epsilon, \mathbf{m}, q^-, N_k | \\ &+ \langle \epsilon, \mathbf{m}, q^-, N_k | VG(\epsilon^+ + E_{N_k}), \end{aligned} \quad (12)$$

where $G(E) = 1/(E - H)$ is the resolvent operator, and ϵ^+ denotes $\epsilon + i\delta$ with $\delta \rightarrow 0^+$ at the end of the calculations. If the system is initially in $|\epsilon_i, N_i\rangle \equiv |\epsilon_i\rangle |N_i\rangle$ and the radiation field is switched on suddenly then the photodissociation amplitude to form the product state $|\epsilon, \mathbf{m}, q^-, N_f\rangle$ is given by¹³ $\langle \epsilon, \mathbf{m}, q^-, N_f | \epsilon_i, N_i \rangle$. Since $\langle \epsilon, \mathbf{m}, q^-, N_f | \epsilon_i, N_i \rangle = 0$ then this overlap assumes the convenient form

$$\begin{aligned} \langle \epsilon, \mathbf{m}, q^-, N_f | \epsilon_i, N_i \rangle \\ = \langle \epsilon, \mathbf{m}, q^-, N_f | VG(\epsilon^+ + E_{N_f}) | \epsilon_i, N_i \rangle, \end{aligned} \quad (13)$$

through use of Eq. (12).

Two quantities are of interest: the channel-specific line shape $A(\epsilon, q, N_f | \epsilon_i, N_i)$, i.e., the probability of dissociation into channel *q* with energy ϵ ,

$$A(\epsilon, q, N_f | \epsilon_i, N_i) = \int d\hat{\mathbf{k}} |\langle \epsilon, \hat{\mathbf{k}}, q^-, N_f | \epsilon_i, N_i \rangle|^2, \quad (14)$$

and the total dissociation probability to channel *q*

$$P(q) = \sum_{N_f} \int d\epsilon A(\epsilon, q, N_f | \epsilon_i, N_i), \quad (15)$$

where the sum is over sets of photons that lift the molecule above the dissociation continua. [In writing Eq. (14) diatomic dissociation is assumed, so that $\mathbf{m} = \hat{\mathbf{k}}$.] Equation (13) is an exact expression which provides a connection between the dissociation amplitude and the *VG* matrix element. It is the latter which we compute exactly using a high field extension of the artificial channel method,^{15,16} as described later below.

We first examine the general structure of the photodissociation amplitude $\langle \epsilon, \mathbf{m}, q^-, N_f | VG(E^+) | \epsilon_i, N_i \rangle$ ($E^+ = \epsilon^+ + E_{N_f}$). To this end, we introduce the projection operators *P* and *Q*

$$P = \sum_{\mathbf{m}, q} \sum_{N_k} d\epsilon |\epsilon, \mathbf{m}, q^-, N_k\rangle \langle \epsilon, \mathbf{m}, q^-, N_k|, \quad (16)$$

$$Q = \sum_j |\epsilon_j, N_j\rangle \langle \epsilon_j, N_j|, \quad (17)$$

which project out continuous and bound parts of eigenstates of H_0 [Eq. (1)], respectively. Note that with *P*, *Q* thus defined, the photodissociation amplitude is also given by

$$\begin{aligned} \langle \epsilon, \mathbf{m}, q^-, N_f | VG(E^+) | \epsilon_i, N_i \rangle \\ = \langle \epsilon, \mathbf{m}, q^-, N_f | P VG(E^+) Q | \epsilon_i, N_i \rangle. \end{aligned} \quad (18)$$

Consider then the operator *PVGQ*:

$$PVGQ = PV(Q + P)GQ = PVQGQ + PVPQGQ. \quad (19)$$

The operators *QGQ* and *PGQ* can be expressed¹⁷ as

$$QG(E^+)Q = \frac{Q}{E^+ - QH_0Q - QR(E^+)Q}, \quad (20)$$

$$PG(E^+)Q = \frac{P}{E^+ - PH_0P - PVP} VQG(E^+)Q, \quad (21)$$

where $R(E^+)$, the level-shift operator, is given by¹⁷

$$R(E^+) = V + V \frac{P}{E^+ - PH_0P - PVP} V. \quad (22)$$

Substituting Eqs. (20) and (21) into Eq. (19) yields

$$\begin{aligned} PVG(E^+)Q &= PR(E^+)QGQ \\ &= PR(E^+)Q \frac{1}{E^+ - QH_0Q - QR(E^+)Q} Q. \end{aligned} \quad (23)$$

It is convenient to separate the operator QRQ in the denominator of Eq. (23) into diagonal and off-diagonal parts

$$QRQ = \sum_j Q_j R Q_j + \sum_{j,j'} ' Q_j R Q_{j'}, \quad (24)$$

where $Q_j = |\epsilon_j, N_j\rangle \langle \epsilon_j, N_j|$ and where the prime on the double summation indicates $j \neq j'$. Using Eq. (24) and the operator identity

$$\frac{1}{A-B} = \frac{1}{A} + \frac{1}{A} B \frac{1}{A-B}, \quad (25)$$

we rewrite

$$\begin{aligned} \frac{1}{E^+ - QH_0Q - QR(E^+)Q} &= \frac{1}{E^+ - QH_0Q - \sum_j Q_j R(E^+) Q_j} \\ &+ \frac{1}{E^+ - QH_0Q - \sum_j Q_j R(E^+) Q_j} \left(\sum_{j,j'} ' Q_j R(E^+) Q_{j'} \right) \frac{1}{E^+ - QH_0Q - QR(E^+)Q}. \end{aligned} \quad (26)$$

By iteration, Eq. (26) can be expanded as

$$\begin{aligned} \frac{1}{E^+ - QH_0Q - QR(E^+)Q} &= \frac{1}{E^+ - QH_0Q - \sum_j Q_j R(E^+) Q_j} + \frac{1}{E^+ - QH_0Q - \sum_j Q_j R(E^+) Q_j} \left[\left(\sum_{j,j'} ' Q_j R(E^+) Q_{j'} \right) \right. \\ &+ \left. \left(\sum_{j,j'} ' Q_j R(E^+) Q_{j'} \right) \frac{1}{E^+ - QH_0Q - \sum_j Q_j R(E^+) Q_j} \left(\sum_{j,j'} ' Q_j R(E^+) Q_{j'} \right) + \dots \right] \\ &\times \frac{1}{E^+ - QH_0Q - \sum_j Q_j R(E^+) Q_j}. \end{aligned} \quad (27)$$

We can evaluate the matrix element of Eq. (23), using Eq. (27), since the operator $1/[E^+ - QH_0Q - \sum_j Q_j R(E^+) Q_j]$ is diagonal in Q subspace. The resulting photodissociation amplitude can be written as the sum of the terms

$$\begin{aligned} \langle (\epsilon, m, q^-), N_f | VG(E^+) | \epsilon_i, N_i \rangle &= \frac{1}{E^+ - \epsilon_i - E_{N_i} - R_{i,i}(E^+)} \times \left(\langle (\epsilon, m, q^-), N_f | R(E^+) | \epsilon_i, N_i \rangle \right. \\ &+ \sum_{j(\neq i)} \frac{\langle (\epsilon, m, q^-), N_f | R(E^+) | \epsilon_j, N_j \rangle \langle \epsilon_j, N_j | R(E^+) | \epsilon_i, N_i \rangle}{[E^+ - \epsilon_j - E_{N_j} - R_{j,j}(E^+)]} \\ &+ \sum_{j,j'(\neq i)} \frac{\langle (\epsilon, m, q^-), N_f | R(E^+) | \epsilon_{j'}, N_{j'} \rangle \langle \epsilon_{j'}, N_{j'} | R(E^+) | \epsilon_j, N_j \rangle \langle \epsilon_j, N_j | R(E^+) | \epsilon_i, N_i \rangle}{[E^+ - \epsilon_{j'} - E_{N_{j'}} - R_{j',j'}(E^+)] [E^+ - \epsilon_j - E_{N_j} - R_{j,j}(E^+)]} \\ &+ \dots \Bigg), \end{aligned} \quad (28)$$

where $E^+ = \epsilon^+ + E_{N_f}$. We have written out three groups of terms explicitly, which give insight into the photodissociation process, but we emphasize that the numerical method utilized below allows us to compute $\langle (\epsilon, m, q^-), N_f | VG(E^+) | \epsilon_i, N_i \rangle$ directly.

Equation (28) is completely general. It may be simplified, under the conditions of this paper, by noting that the incident radiation is such that it only effectively couples

states in the Q space to those in the P space. Under these circumstances $QVQ = PVP = 0$ and

$$\langle (\epsilon, m, q^-), N_f | R(E^+) | \epsilon_i, N_i \rangle = \langle (\epsilon, m, q^-), N_f | V | \epsilon_i, N_i \rangle. \quad (29)$$

The other matrix elements of R in Eq. (28) assume the following forms: the diagonal elements $R_{j,j}$ of $R(E^+)$ in the Q subspace given by

$$R_{j,j}(E^+) = \langle \epsilon_j, N_j | R(E^+) | \epsilon_j, N_j \rangle \quad (30)$$

$$= \Delta_j(E) - \frac{i}{2} \Gamma_j(E), \quad (31)$$

where, by taking $\delta \rightarrow 0$, we have

$$\Delta_j(E) = \langle \epsilon_j, N_j | V \frac{P_v}{E - PHP} V | \epsilon_j, N_j \rangle, \quad (32)$$

$$\Gamma_j(E) = 2\pi \langle \epsilon_j, N_j | VP \delta(E - PHP) PV | \epsilon_j, N_j \rangle, \quad (33)$$

which are the field-induced shift and broadening, respectively. In Eq. (32), P_v denotes the principle part of the integration. Equation (28) also involves the off-diagonal elements $R_{j,i}(E^+)$ ($j \neq i$)

$$\langle \epsilon_j, N_j | R(E^+) | \epsilon_i, N_i \rangle = \langle \epsilon_j, N_j | V \frac{P}{E^+ - PHP} V | \epsilon_i, N_i \rangle \quad (34)$$

which describes Raman-type coupling between two bound states, via the continuum.

The photodissociation amplitude in Eq. (28) is therefore seen to be comprised of transitions from the initial state $|\epsilon_i, N_i\rangle$ to the dissociation continuum $|\epsilon, m, q^-, N_f\rangle$ via various dissociation pathways: $|\epsilon, m, q^-, N_f\rangle \leftarrow |\epsilon_i, N_i\rangle$, $|\epsilon, m, q^-, N_f\rangle \leftarrow |\epsilon_j, N_j\rangle \leftarrow |\epsilon', m', q'^-, N'\rangle \leftarrow |\epsilon_i, N_i\rangle$, etc. The interference between these pathways, which can be constructive or destructive, leads to the possibility of controlling molecular photodissociation by varying the laser parameters, as discussed below.

To gain further insight into Eq. (28) we consider some specific applications. The simplest case is weak field single photon dissociation in which only the first term on the right-hand side of Eq. (28) need be considered. If n_1 and ω_1 are

the photon number and frequency of the excitation laser, respectively, then $|N_i\rangle = |n_1\rangle$, $|N_f\rangle = |n_1 - 1\rangle$, and $E^+ = \epsilon^+ + (n_1 - 1)\hbar\omega_1$. The photodissociation amplitude becomes

$$\begin{aligned} & \langle (\epsilon, m, q^-), n_1 - 1 | VG(E^+) | \epsilon_i, n_1 \rangle \\ &= \frac{\langle (\epsilon, m, q^-), n_1 - 1 | V | \epsilon_i, n_1 \rangle}{\epsilon^+ - \epsilon_i - \hbar\omega_1 - \Delta_i + i\Gamma_i/2}, \end{aligned} \quad (35)$$

where the shift and broadening of the initial state are given by

$$\Delta_i = P_v \sum_{m,q} \int d\epsilon \frac{|\langle (\epsilon, m, q^-), n_1 - 1 | V | \epsilon_i, n_1 \rangle|^2}{\epsilon_i + \hbar\omega_1 - \epsilon}, \quad (36)$$

$$\begin{aligned} \Gamma_i &= 2\pi \sum_{m,q} \int d\epsilon |\langle (\epsilon, m, q^-), n_1 - 1 | V | \epsilon_i, n_1 \rangle|^2 \\ &\times \delta(\epsilon_i + \hbar\omega_1 - \epsilon), \end{aligned} \quad (37)$$

as in the weak field perturbation theory. The resultant expression, Eq. (35) is the same as that obtained by applying Fano's configuration interaction theory (Ref. 18) in conjunction with the isolated resonance approximation (i.e., the assumption that only one bound state is dissociated) and the neglect of free-free transitions.

For intense fields the power broadening of the initial bound state can become comparable to, or larger than, the spacing between the bound states, and the isolated resonance approximation is no longer valid. Under these circumstances, the contribution from the neighboring states, which are initially devoid of population, should be included via the second group terms in Eq. (28). The photodissociation amplitude becomes

$$\begin{aligned} & \langle (\epsilon, m, q^-), n_1 - 1 | VG(E^+) | \epsilon_i, n_1 \rangle \\ &= \left[\langle (\epsilon, m, q^-), n_1 - 1 | V | \epsilon_i, n_1 \rangle + \sum_{l \neq i} \frac{\langle (\epsilon, m, q^-), n_1 - 1 | V | \epsilon_l, n_1 \rangle \langle \epsilon_l, n_1 | R(E^+) | \epsilon_i, n_1 \rangle}{\epsilon^+ - \epsilon_l - \hbar\omega_1 - \Delta_l + i\Gamma_l/2} + \dots \right] \\ &\times \frac{1}{\epsilon^+ - \epsilon_i - \hbar\omega_1 - \Delta_i + i\Gamma_i/2}, \end{aligned} \quad (38)$$

where we have used $E = \epsilon + (n_1 - 1)\hbar\omega_1$. Here $\langle \epsilon_l, n_1 | R(E^+) | \epsilon_i, n_1 \rangle$ is given by Eq. (34) with $E^+ = \epsilon^+ + (n_1 - 1)\hbar\omega_1$, and the leading term is

$$\langle \epsilon_l, n_1 | R(E^+) | \epsilon_i, n_1 \rangle \approx \sum_{m,q} \int d\epsilon' \frac{\langle \epsilon_l, n_1 | V | (\epsilon', m, q^-), n_1 - 1 \rangle \langle (\epsilon', m, q^-), n_1 - 1 | V | \epsilon_i, n_1 \rangle}{\epsilon^+ - \epsilon'}, \quad (39)$$

describing the coupling between $|\epsilon_i\rangle$ and $|\epsilon_l\rangle$ via absorption and emission. Practically, only those $|\epsilon_l\rangle$ such that $|\epsilon_l - \epsilon_i| < \Gamma_i$ contribute in Eq. (38). The two dissociation pathways in Eq. (38), $|\epsilon, m, q^-, n_1 - 1\rangle \leftarrow |\epsilon_i, n_1\rangle$ and $|\epsilon, m, q^-, n_1 - 1\rangle \leftarrow |\epsilon_l, n_1\rangle \leftarrow |(\epsilon', m', q'^-), n_1 - 1\rangle \leftarrow |\epsilon_i, n_1\rangle$, terminate in the same dissociation continuum and interfere. The resultant line shape [Eq. (14)] should demonstrate a se-

ries of peaks at $\epsilon = \epsilon_b (b = i, l, \dots) + \hbar\omega_1$ and a series of dips where the two paths destructively interfere with one another. This structure is the molecular analog of Fano-interference,²⁰ and, as shown below, is observed in our numerical study.

B. Control of photodissociation cross sections

Consider now the effect of applying two cw laser fields, of frequency ω_1 and ω_2 and photon numbers n_1 and

n_2 ($|N_i\rangle = |n_1, n_2\rangle$). The molecule-radiation interaction V is given by the sum of the perturbations due to each of the laser fields

$$V = V_1 + V_2 = -\boldsymbol{\mu} \cdot \mathcal{E}_1 - \boldsymbol{\mu} \cdot \mathcal{E}_2, \quad (40)$$

where \mathcal{E}_1 and \mathcal{E}_2 are the electric field vectors associated with ω_1 and ω_2 . The laser of frequency ω_1 excites the molecule from the $|\epsilon_i\rangle$ to the dissociative continuum $|\epsilon, m, q^-\rangle$ while the second laser ω_2 simultaneously couples the continuum to bound states $|\epsilon_j\rangle$ that are initially devoid of population. Laser frequencies are chosen such that $\epsilon_i + \hbar\omega_1 \approx \epsilon_j + \hbar\omega_2$. Under these circumstances $|\epsilon_j\rangle$ can be populated by stimu-

lated emission from the continuum. As shown below, with these frequencies there are three predominant routes to dissociation leading to three different energy regimes; (i) dissociation of the initial $|\epsilon_i\rangle$ state by ω_2 to energy $\epsilon \approx \epsilon_i + \hbar\omega_2$; (ii) dissociation of $|\epsilon_j\rangle$ by ω_1 to energy $\epsilon \approx \epsilon_j + \hbar\omega_1$, and (iii) the dissociation of $|\epsilon_i\rangle$ by ω_1 and of $|\epsilon_j\rangle$ by ω_2 , both to energy $\epsilon \approx \epsilon_i + \hbar\omega_1 \approx \epsilon_j + \hbar\omega_2$. The third route involves two interfering pathways while the other two, termed satellite contributions, do not. This interference is the key to the control scenario discussed below. For the third route, the leading terms in the dissociation amplitude at $\epsilon \approx \epsilon_i + \hbar\omega_1$ are

$$\begin{aligned} \langle (\epsilon, m, q^-, n_1 - 1, n_2) | VG(E^+) | \epsilon_i, n_1, n_2 \rangle &= a + b, \\ a &= \left(\langle (\epsilon, m, q^-, n_1 - 1) | V_1 | \epsilon_i, n_1 \rangle + \sum_{l(i \neq i)} \frac{\langle (\epsilon, m, q^-, n_1 - 1) | V_1 | \epsilon_l, n_1 \rangle \langle \epsilon_l, n_1 | R_1(E^+) | \epsilon_i, n_1 \rangle}{\epsilon^+ - \epsilon_l - \hbar\omega_1 - R_{l,i}} \right) \frac{1}{\epsilon^+ - \epsilon_i - \hbar\omega_1 - R_{i,i}}, \quad (41) \\ b &= \sum_{j(i \neq i)} \frac{\langle (\epsilon, m, q^-, n_2) | V_2 | \epsilon_j, n_2 + 1 \rangle \langle \epsilon_j, n_1 - 1, n_2 + 1 | R(E^+) | \epsilon_i, n_1, n_2 \rangle}{(\epsilon^+ - \epsilon_j - \hbar\omega_2 - R_{j,j})(\epsilon^+ - \epsilon_i - \hbar\omega_1 - R_{i,i})}, \end{aligned}$$

where $\langle \epsilon_l, n_1 | R_1(E^+) | \epsilon_i, n_1 \rangle$ is given by Eq. (39) with V replaced by V_1 , and

$$\langle \epsilon_j, n_1 - 1, n_2 + 1 | R(E^+) | \epsilon_i, n_1, n_2 \rangle \approx \sum_{m,q} \int d\epsilon' \frac{\langle \epsilon_j, n_2 + 1 | V_2 | (\epsilon', m, q^-, n_2) \rangle \langle (\epsilon', m, q^-, n_1 - 1) | V_1 | \epsilon_i, n_1 \rangle}{\epsilon^+ - \epsilon'}. \quad (42)$$

Note that we have used $E = \epsilon + (n_1 - 1)\hbar\omega_1 + n_2\hbar\omega_2$ in Eq. (28) to obtain Eq. (41).

The term a in Eq. (41) results from the direct dissociation path $|\epsilon_i\rangle \rightarrow |\epsilon, m, q^-\rangle$ induced by ω_1 [path (a)], including the contribution for neighboring state $|\epsilon_l\rangle$. Term b describes the indirect dissociation path $|\epsilon_i\rangle \rightarrow |\epsilon', m', q'^-\rangle \rightarrow |\epsilon_j\rangle \rightarrow |\epsilon, m, q^-\rangle$ induced by ω_1 plus ω_2 [path (b)]. The coupling between $|\epsilon_i\rangle$ and $|\epsilon_j\rangle$ in Eq. (42) results from absorption of one ω_1 photon and stimulated emission of an ω_2 photon. This results in additional peaks in the line shape at $\epsilon \approx \epsilon_j + \omega_2$ and additional minima at points where term a cancels term b . It is important to note that the relative sign of the two groups of terms depends on laser frequency, resulting in a sensitivity of the line shape to frequency.

The above results are readily understood from an alternate perspective, the dressed-molecule representation. From this viewpoint, the multiple bound states of the bound electronic manifold are embedded in the continuum by the lasers ω_1 and ω_2 , and dissociate. Only those bound states which effectively overlap with the $|\epsilon_i\rangle|n_1\rangle|n_2\rangle$ dressed states contribute significantly. The resulting dissociation line shape therefore displays a series of peaks and dips, reflecting the interference pattern from the multiple dissociation pathways.

The interference term arising from squaring Eq. (41), and hence control, is in principle a function of the relative phase of the two contributing terms. Consider then the contribution of the relative phase of pathway (a) and (b) to control. We rely, for this argument, on Eq. (41) but a proper model based on coherent states¹² gives the same result. If θ_i

denotes the phase of the field of frequency ω_i (including the spatial phases $\mathbf{k}_1 \cdot \mathbf{r}$ and $\mathbf{k}_2 \cdot \mathbf{r}$) then pathway (a) imparts the laser phase²¹ θ_1 to the molecule. Similarly the phase imparted in the pathway (b) is $\theta_1 - \theta_2 + \theta_2 = \theta_1$. As a result the relative phase of the two paths is independent of the laser phases, a consequence of the internal cancellation of the θ_2 phase when ω_2 photons are emitted and absorbed. The resultant control scenario is therefore expected to be insensitive to the phase jitter or drift of either laser. Hence, although there are multiple interfering pathways to dissociation in this scenario, variation of the laser phases can no longer be used as a parameter to control dissociation yields. However, as shown below, highly efficient yield control results through variation of the frequencies ω_1 and ω_2 .

C. Computational method

From the computational viewpoint, it is greatly advantageous to compute $\langle (\epsilon, m, q^-, N_f) | VG(E^+) | \epsilon_i, N_i \rangle$ [Eq. (28)] directly, rather than many terms in the expansion on the right-hand side of Eq. (28). The direct computations are done with the artificial channel method, as described below. This method¹⁵ rewrites the photodissociation process as a full collision problem by introducing an artificial open channel which couples to the initial physical bound manifold. As a result the artificial channel serves as an incoming channel of an artificial full collision problem, and the physical continua serve as outgoing channels. The resultant problem is then amenable to treatment by full collision problem techniques, from which photodissociation probability can be obtained.

This method has been applied, for example, to single and multiphoton dissociation problems using single artificial channel configurations,¹⁵ and high field photodissociation problems using two artificial channel configurations.¹⁶ Here we show that using a two artificial channel arrangement allows us to compute the photodissociation amplitude $\langle(\epsilon, m, q^-), N_f|VG|\epsilon_i, N_i\rangle$ directly.

To this end, we multiply both sides of the equation $G = G_0 + GVG_0$ (Ref. 17) by V , yielding

$$VG = VG_0 + VGVG_0, \quad (43)$$

where $G_0 = 1/(E - H_0)$. Using Eq. (43), we rewrite the transition operator $T = V + VGV$ as

$$T(E) = V + VG_0(E)V + VG(E)VG_0(E)V. \quad (44)$$

We now introduce two artificial states, an open channel $|\tilde{A}, N_i\rangle$ and a closed channel $|\tilde{\epsilon}_b\rangle$ where the tilde denotes the artificial character of the states. The physical system plus the two artificial channels now comprise a full collision problem, in which the incoming flux flows from the artificial open channel to the physical continua. The dressed state $|\tilde{A}, N_i\rangle$ is as-

sumed to weakly couple to the $|\tilde{\epsilon}_b, N_i\rangle$ by an artificial interaction $\langle\tilde{\epsilon}_b, N_i|W_a|\tilde{A}, N_i\rangle$ and the $|\tilde{\epsilon}_b, N_i\rangle$ to the physical bound manifold $|\epsilon_b, N_i\rangle$ by another artificial coupling $\langle\epsilon_b, N_i|W_b|\tilde{\epsilon}_b, N_i\rangle$. The W_a and W_b can be regarded as components of the interaction V that connect $|\tilde{A}, N_i\rangle$ to $|\tilde{\epsilon}_b, N_i\rangle$ and $|\tilde{\epsilon}_b, N_i\rangle$ to $|\epsilon_b, N_i\rangle$ but which do not affect the couplings between the physical states. Further, to avoid any disturbance to $|\tilde{\epsilon}_b\rangle$ and $|\epsilon_b\rangle$ due to the introduction of the artificial interactions, the reverse coupling elements $\langle\tilde{A}, N_i|W_a|\tilde{\epsilon}_b, N_i\rangle$ and $\langle\tilde{\epsilon}_b, N_i|W_b|\epsilon_b, N_i\rangle$ are set to zero in the computation. All couplings between the physical states are included in the computations, including absorption and stimulated emission processes induced by the intense lasers between bound-free and free-free manifolds.

We now show that the computation of T -matrix element between $\langle(\epsilon, m, q^-), N_f|$ and $|\tilde{A}, N_i\rangle$ allows us to extract the photodissociation amplitude of interest. Consider the matrix element $\langle(\epsilon, m, q^-), N_f|T|\tilde{A}, N_i\rangle$, from Eq. (44). The first two terms in the right-hand side are zero because $|\langle(\epsilon, m, q^-), N_f\rangle$ does not directly couple to the artificial states $|\tilde{A}, N_i\rangle$ and $|\tilde{\epsilon}_b, N_i\rangle$. The third term in Eq. (44) can be rewritten, given that V couples the $|\tilde{A}, N_i\rangle$ to $|\tilde{\epsilon}_b, N_i\rangle$ and $|\tilde{\epsilon}_b, N_i\rangle$ to $|\epsilon_b, N_i\rangle$ only, as

$$\langle(\epsilon, m, q^-), N_f|T(E)|\tilde{A}, N_i\rangle = \sum_{\tilde{\epsilon}_b} \sum_{\epsilon_b} \frac{\langle(\epsilon, m, q^-), N_f|VG(E)|\epsilon_b, N_i\rangle \langle\epsilon_b, N_i|W_b|\tilde{\epsilon}_b, N_i\rangle \langle\tilde{\epsilon}_b, N_i|W_a|\tilde{A}, N_i\rangle}{E - \tilde{\epsilon}_b - E_{N_i}}. \quad (45)$$

To simplify, we set W_b to be unity, and $|\tilde{\epsilon}_b\rangle$ to be a copy of the initial bound manifold $|\epsilon_b\rangle$, but shifted in energy by an amount α . The advantage of this choice¹⁶ is that the summation over $\tilde{\epsilon}_b$ in Eq. (45) can be done now, due to orthogonality of rovibrational states of the same electronic state. Substituting $E = \epsilon^+ + E_{N_f}$, we write the final result as

$$\langle(\epsilon, m, q^-), N_f|T(\epsilon^+ + E_{N_f})|\tilde{A}, N_i\rangle = \sum_b \frac{\langle(\epsilon, m, q^-), N_f|VG(\epsilon^+ + E_{N_f})|\epsilon_b, N_i\rangle \langle\tilde{\epsilon}_b, N_i|W_a|\tilde{A}, N_i\rangle}{\epsilon^+ + E_{N_f} - \epsilon_b - E_{N_i} - \alpha}. \quad (46)$$

Equation (46) has the same structure as that in which one uses one artificial channel,¹⁵ so that the previous computational techniques are applicable with minor modifications. Specifically, by computing the residues of the T -matrix element at $\epsilon = \epsilon_i + E_{N_i} + \alpha - E_{N_f}$, we obtain $\langle(\epsilon, m, q^-), N_f|VG(\epsilon^+ + E_{N_f})|\epsilon_i, N_i\rangle$ at that energy, which is the desired photodissociation amplitude. Varying α gives the photodissociation amplitude and the line shape at various energy ϵ for given photon energies and coupling strength. The total dissociation yield is obtained from Eq. (15).

III. CONTROL OF PHOTODISSOCIATION LINE SHAPES

As an example of this approach we consider high field dissociation of Na_2 which produces $\text{Na}(3s) + \text{Na}(4s)$ and $\text{Na}(3s) + \text{Na}(3p)$, where excitation is out of a previously populated level of the $^3\Pi_u$ state (Fig. 1). The relevant electronic potentials and dipole transition functions are taken from Ref. 19.

Consider first dissociation with a single cw laser of frequency ω_1 . A typical dissociation line shape is shown in Fig. 2. Here the initial state $|\epsilon_i\rangle$ is chosen with vibrational quantum number $v_i = 18$ and rotational quantum number $J = 0$ ($\epsilon_{v_i=18} = -6662.9 \text{ cm}^{-1}$) in the $^3\Pi_u$ excited electronic state. The laser, with $\omega_1 = 15617 \text{ cm}^{-1}$ and intensity $I_1 = 8.7 \times 10^9 \text{ W/cm}^2$, is sufficiently energetic to dissociate levels of the $^3\Pi_u$ state with $v \geq 18$ to both $\text{Na}(3s) + \text{Na}(3p)$ and $\text{Na}(3s) + \text{Na}(4s)$ products. Under these circumstances above threshold dissociation is negligible, as is the dissociation through the $1^3\Sigma_g$ electronic state (the dashed line in Fig. 1). Figure 2 shows computed line shapes $A(\epsilon, q, n_1 - 1|\epsilon_i, n_1)$ (on a logarithmic scale) as a function of the product translational energy ϵ . Results for the $\text{Na}(3p) + \text{Na}(3s)$ [curve (a)] and $\text{Na}(4s) + \text{Na}(3s)$ [curve (b)] product channels are shown, where the computation only includes the rotational states $J = 1$ of the $2^3\Sigma_g$ and $^3\Pi_g$ electronic states. (The inclusion of additional rotational states is discussed below.) Line shapes for both products are seen to be similar in structure, showing a series of non-Lorentzian

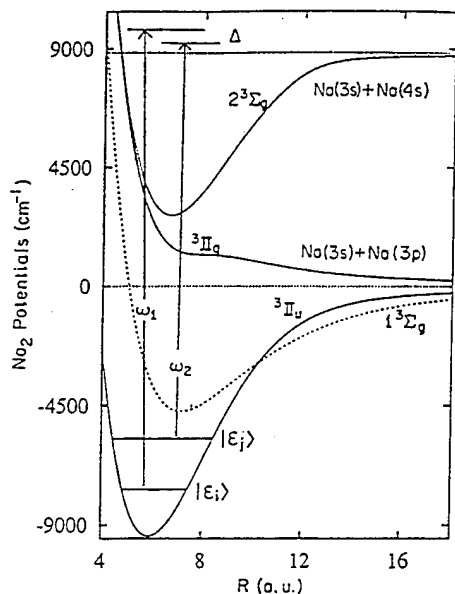


FIG. 1. Relevant potential energy curves of Na_2 included in the computation. Two lasers, of frequencies ω_1 and ω_2 , couple the dissociation continua to the bound states $|\epsilon_i\rangle$ and $|\epsilon_j\rangle$ in the ${}^3\Pi_u$ state, where the $|\epsilon_i\rangle$ is initially populated and the $|\epsilon_j\rangle$ initially unpopulated. Here $\Delta = \hbar(\omega_1 - \omega_2) + \epsilon_i - \epsilon_j$.

peaks and dips corresponding to resonance contributions from various v states. The predominant contribution is the direct $v_i=18$ dissociation (at $\epsilon=8975 \text{ cm}^{-1}$), with smaller contributions from the initially empty $v=19, 20, 21$ states, which are populated by stimulated emission from the continua and are subsequently dissociated. The overall shape between the peaks shows Fano-type interferences²⁰ between the photodissociation pathways arising from the pairs of adjacent vibrational states. All of the features observed in Fig. 2 are consistent with an analysis based on Eq. (38).

Including rotations complicates the structure of the line shape. Figure 3, for example, shows $A(\epsilon, q, n_1 - 1 | \epsilon_i, n_i)$ for the $\text{Na}(3s) + \text{Na}(3p)$ product, where we include rotational couplings among $J=0, 2, 4$ of the ${}^3\Pi_u$ state, and $J=1, 3, 5$

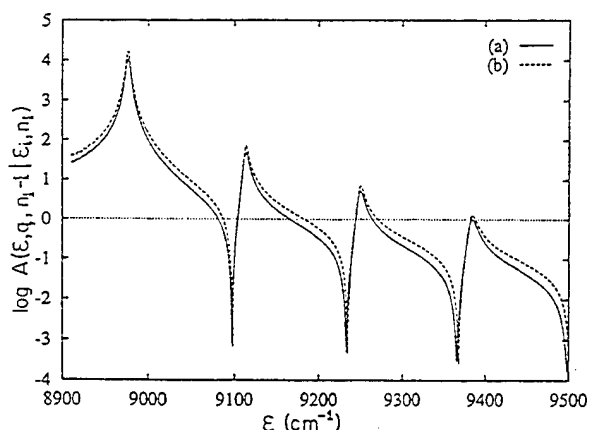


FIG. 2. $\log A(\epsilon, q, n_1 - 1 | \epsilon_i, n_i)$ vs ϵ for photodissociation with a single excitation laser of frequency ω_1 . (a) $\text{Na}(3s) + \text{Na}(3p)$ product and (b) $\text{Na}(3s) + \text{Na}(4s)$ product. Here $\omega_1 = 15\,617 \text{ cm}^{-1}$, $I_1 = 8.7 \times 10^9 \text{ W/cm}^2$. The initial molecular state is $v_i=18$, $J=0$ of the ${}^3\Pi_u$ state and the $\text{Na}(3s) + \text{Na}(3p)$ asymptote defines the zero of energy ϵ throughout this paper.

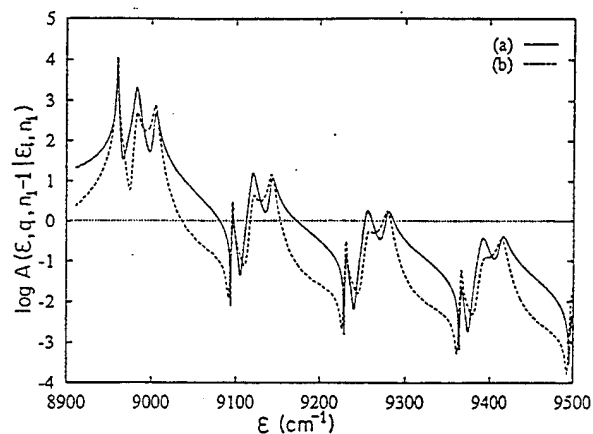


FIG. 3. $\log A(\epsilon, q, n_1 - 1 | \epsilon_i, n_i)$ vs ϵ for the $\text{Na}(3s) + \text{Na}(3p)$ product, including rotational coupling. For products dissociating with (a) $J=1$ and (b) $J=3$ in the ${}^3\Pi_g$ electronic state ($\omega_1 = 15\,617 \text{ cm}^{-1}$ and $I_1 = 8.7 \times 10^9 \text{ W/cm}^2$).

of the $2\,{}^3\Sigma_g^-$ and ${}^3\Pi_g$ states, with laser frequencies and intensities as in Fig. 2. Specifically, the initially populated $J=0$ and empty $J=2, 4$, $v=18$ states of the ${}^3\Pi_u$ couple to the $J=1, 3, 5$ states of the $2\,{}^3\Sigma_g^-$ and ${}^3\Pi_g$, producing three peaks in the line shapes. Curves (a) and (b) show line shapes for the products dissociated from the $J=1$ and $J=3$ states of the ${}^3\Pi_g$ state, respectively. The $J=5$ probability has a similar structure but is small and is not shown here. Similar results are shown in Fig. 4, but for the other product, $\text{Na}(4s) + \text{Na}(3s)$, dissociating from the $J=1$ and $J=3$ components of the $2\,{}^3\Sigma_g^-$ state. The single peaks in Fig. 2 are seen to be replaced by a triple-peak structure, corresponding to the contributions from the rotational states. Of note is that the spacing between pairs of rotational peaks in Figs. 3 and 4 is about ten times larger than the corresponding zero-field rotational spacings. This increased rotational spacing is due to the shifting and broadening of the bound rotational states that are coupled to one another via the continuum. In Fig. 5 we show the same line shapes as in Fig. 3, but with the intensity I_1 reduced to $3.16 \times 10^9 \text{ W/cm}^2$. Spacings between the rota-

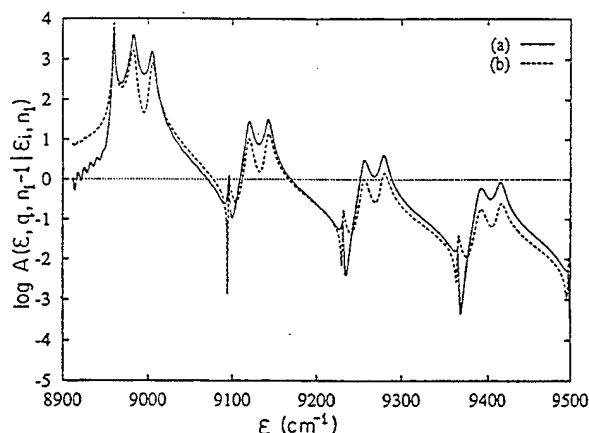


FIG. 4. As in Fig. 3, but for the $\text{Na}(3s) + \text{Na}(4s)$ product dissociated out of the $2\,{}^3\Sigma_g^-$ state. For product dissociating with (a) $J=1$ and (b) $J=3$.

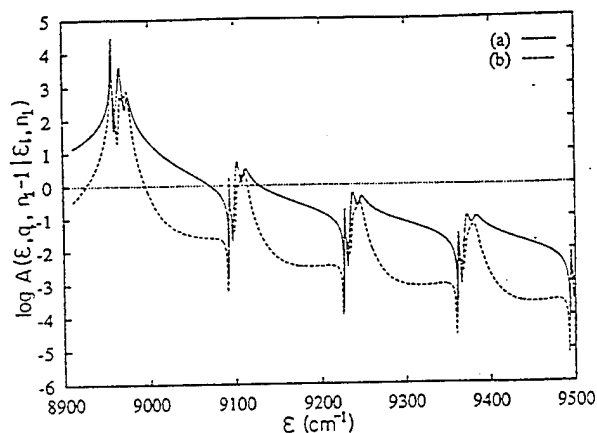


FIG. 5. As in Fig. 3, but with the laser intensity reduced to $I_1 = 3.16 \times 10^9$ W/cm².

tional peaks are reduced, consistent with this power broadening perspective.

We now consider the effect of a second laser ω_2 , which embeds initially empty states $|\epsilon_j\rangle$ into the continuum (see Fig. 1).²⁰ Only those $|\epsilon_j\rangle$ that are located around $\epsilon_i + \hbar(\omega_1 - \omega_2)$ are effectively excited and dissociated. Figures 6 and 7 show $\log A(\epsilon, q, N_f | \epsilon_i, N_i)$ as a function of ϵ for products Na(3p) + Na(3s) and Na(4s) + Na(3s), for various ω_1 and with the same ω_2 . In Fig. 6, $N_i = (n_1, n_2)$, $N_f = (n_1 - 1, n_2)$, $\omega_1 = 15\,617$ cm⁻¹; in Fig. 7 $\omega_1 = 15\,683$ cm⁻¹. The ω_1 laser is sufficiently energetic to dissociate $v \geq 18$ states of the $^3\Pi_u$, and the ω_2 laser ($\omega_2 = 14\,591$ cm⁻¹, $I_2 = 3.51 \times 10^{10}$ W/cm²) can dissociate levels $v \geq 26$ of the $^3\Pi_u$ to both products. At this I_2 intensity, and with the known dipole moment between the $^3\Pi_u$ and the $2\,^3\Sigma_g$, the Rabi frequency¹⁶ is 499 cm⁻¹, much larger than the vibrational spacing of 135 cm⁻¹ in the neighborhood of $v_i = 18$. To expose the essential physics only $J=0$ of the bound manifold and $J=1$ of the continua are included in the com-

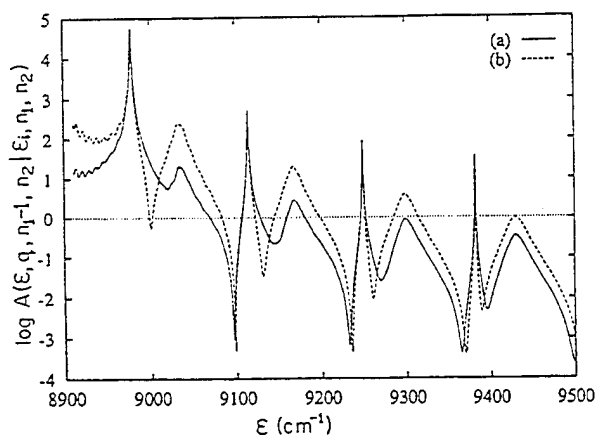


FIG. 6. $\log A(\epsilon, q, n_i - 1, n_2 | \epsilon_i, n_i, n_2)$ vs ϵ , with two lasers on. (a) Na(3s) + Na(3p) product and (b) Na(3s) + Na(4s) product. Here $\omega_1 = 15\,617$ cm⁻¹, $\omega_2 = 14\,591$ cm⁻¹, $I_1 = 8.7 \times 10^9$ W/cm², and $I_2 = 3.5 \times 10^{10}$ W/cm², and the detuning $\Delta = \hbar(\omega_1 - \omega_2) + \epsilon_{v=18} - \epsilon_{v=26} < 0$. Initially the molecule is in $v_i = 18$, $J=0$ of the $^3\Pi_u$ state. Rotational and satellite couplings are set to zero.

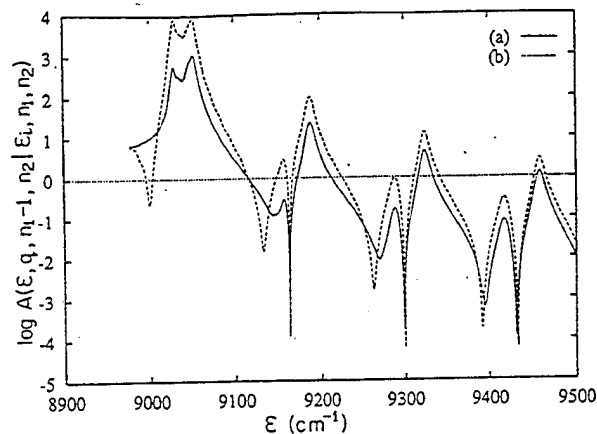


FIG. 7. As in Fig. 6, but with $\omega_1 = 15\,683$ so that $\Delta = \hbar(\omega_1 - \omega_2) + \epsilon_{v=18} - \epsilon_{v=26} > 0$.

putation and the satellite terms are not included. Comparing Figs. 2 and 6 we see that with both ω_1 and ω_2 lasers on, each peak in Fig. 2 is split into two in a way which depends on the asymptotic channel [compare curves (a) and (b) within each of Figs. 6 and 7]. There is also a dependence on the frequency ω_1 (compare Fig. 6 with Fig. 7). This behavior is in direct contrast to that in the single excitation laser case (Fig. 2) where the line shapes are not sensitive to either the product channel index q or to the frequency ω_1 . The channel dependence in Figs. 6 and 7, in accord with Eq. (41), results from the interference characteristics of the two dissociation pathways induced by ω_1 and ω_2 .

Figures 6 and 7 show a series of double-peak structures, associated with the dressed states $v=18$ and $v=26$ pair (the first double peak), the $v=19$ and $v=27$ pair (the second double peak), etc., of the $^3\Pi_u$ state. The ω_1 in Fig. 6 is such that the detuning $\Delta = \hbar(\omega_1 - \omega_2) + \epsilon_{v=18} - \epsilon_{v=26}$ is less than 0, while in Fig. 7, Δ is greater than zero. As a consequence the dominant peak (arising from the $v=18$ state) is located on the left-hand side in Fig. 6, and on the right-hand side in Fig. 7, of the $v=26$ peak. The dip in the middle of the two peaks results from destructive interference between the two pathways. A similar situation applies for the second and third sets of peaks. Note that while the locations of the peaks are independent of the channel index, the ratio of the heights of the peaks and the locations of the dips strongly depend on the laser frequencies and on the channel index q . This being the case, we can control the channel specific line shapes $A(\epsilon, q, N_f | \epsilon_i, N_i)$ by varying ω_1 . For example, a comparison of Figs. 6 and 7 shows that increasing ω_1 shifts the dominant peaks to higher ϵ , with products at $\epsilon \approx 9030$ cm⁻¹ strongly enhanced and products at $\epsilon \approx 8980$ cm⁻¹ suppressed.

The line shapes can also be changed by varying laser intensities; Fig. 8 shows one example. In this case all molecule and laser parameters are as in Fig. 6, except that the intensity I_1 of the ω_1 laser is increased to 2.24×10^{10} W/cm². Figures 8 and 6 differ in peak strengths and peak separations as a result of the change in coupling between the bound and the continuum states.

In Figs. 6–8, rotational and satellite contributions were set to zero to expose the basic interference effect. Including

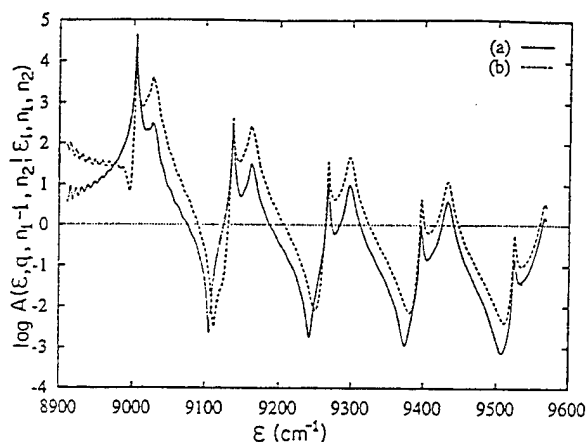


FIG. 8. As in Fig. 6, but with higher ω_1 intensity, $I_1 = 2.24 \times 10^{10}$ W/cm 2 .

rotations leads to additional peaks in the line shapes. We discuss the effect of rotational contributions to the control of the total dissociation yields below. Here we focus on the effect of satellite contributions.

The satellite contributions are defined as those which cannot be controlled. They can, however, be minimized by proper choice of the laser intensities and frequencies. Figure 9 shows an example of the satellite contributions to the line shape for the same laser parameters as in Fig. 6, save for ω_2 which is set at 13 964 cm $^{-1}$. The results in Fig. 9 show the product emerging in three distinct ϵ regions. The line shapes on the far right (10 500 < ϵ < 10 900 cm $^{-1}$) correspond to $A(\epsilon, q, n_1 - 2, n_2 + 1 | \epsilon_i, n_1, n_2)$, resulting from the dissociation of the $v \geq 31$ states by ω_1 , which produces Na(3p) + Na(3s) [curve (a)] and Na(4s) + Na(3s) [curve (b)]. The line shape on the far left (7300 < ϵ < 7700 cm $^{-1}$) shows $A(\epsilon, q, n_1, n_2 - 1 | \epsilon_i, n_1, n_2)$, resulting from the dissociation of $v \geq v_i = 18$ by ω_2 , which is only sufficiently energetic to produce Na(3p) + Na(3s) atoms. The line shape in the middle, $A(\epsilon, q, n_1 - 1, n_2 | \epsilon_i, n_1, n_2)$, which resembles that in Fig. 6, comes from interference contributions, i.e., the disso-

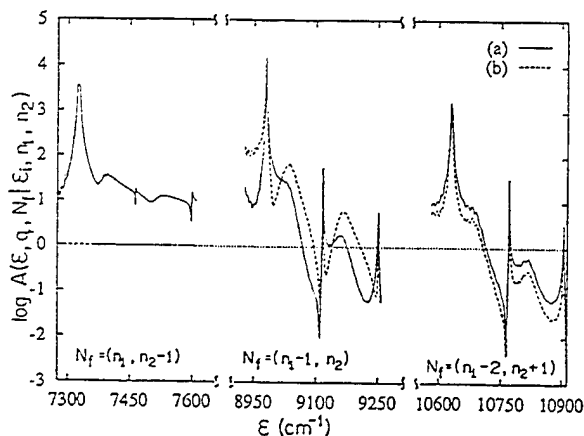


FIG. 9. As in Fig. 6, but with $\omega_2 = 13\,964$ cm $^{-1}$ and with the inclusion of satellite contributions. The far left displays $A(\epsilon, q, n_1, n_2 - 1 | \epsilon_i, n_1, n_2)$, the middle $A(\epsilon, q, n_1 - 1, n_2 | \epsilon_i, n_1, n_2)$, and the far right $A(\epsilon, q, n_1 - 2, n_2 + 1 | \epsilon_i, n_1, n_2)$.

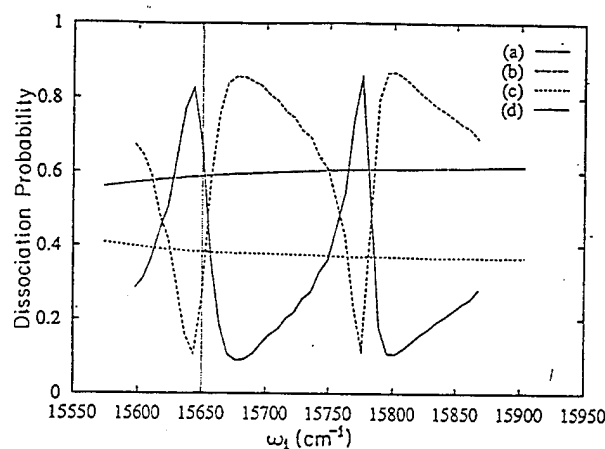


FIG. 10. $P(q)$ as a function of ω_1 . In (a) and (b) both lasers are on, while in (c) and (d) the ω_2 laser is off. (a) and (c) show the Na(3s) + Na(3p) product whereas (b) and (d) show that Na(3s) + Na(4s) product. The molecule is initially in $v_i = 18$, $J = 0$ of the $^3\Pi_u$ state; rotational and satellite terms are neglected.

ciation of $|\epsilon_i\rangle$ by ω_1 plus that of $|\epsilon_j\rangle$ by ω_2 . Note that while the satellite contributions display the characteristic double-peak structure, due to the resonant coupling of the $|\epsilon_i\rangle$ and $|\epsilon_j\rangle$ via the continuum, they are not channel-dependent (compare the curves at the far right to those in the middle of Fig. 9). However, as long as the interference contributions substantially exceed the satellite contributions we can expect channel-sensitive control over the line shape by tuning the laser frequencies.

IV. CONTROL OF PHOTODISSOCIATION BRANCHING RATIOS

Results in the last section show that two high field lasers with appropriate frequencies allow for novel and effective q dependent control over $A(\epsilon, q, N_f | \epsilon_i, n_1, n_2)$. Hence, in accord with Eq. (15), control over the yield into different products q is expected. A sample of our extensive computations displaying yield control for various laser frequencies and intensities is provided below.

To demonstrate the essence of yield control we first ignore rotational effects and satellite contributions. Figure 10 shows the total dissociation probability $P(q)$ as a function of ω_1 for both the Na(3s) + Na(3p) [curve (a)] and Na(3s) + Na(4s) [curve (b)] products for the same parameters as in Fig. 6. The vertical line indicates the value of ω_1 at which $\hbar(\omega_1 - \omega_2) = \epsilon_v = 26 - \epsilon_v = 18$ with $J = 0$. For comparison we also plot, as curves (c) and (d), $P(q)$ for Na(3s) + Na(3p) and for Na(3s) + Na(4s) for the case where the ω_2 laser is shut off. In the one laser case $P(q)$ is seen to be flat as ω_1 is varied, in contrast to the two laser case where it oscillates strongly. The oscillations for the two product probabilities in Fig. 10 are seen to be out of phase, with the sum of dissociation probabilities being close to 0.94. Thus, essentially total dissociation is obtained, with the ratio of the products varying widely between the two channels as ω_1 is tuned. For example, the probabilities of producing Na(3s) + Na(3p) and Na(3s) + Na(4s) at $\omega_1 = 15\,670$ cm $^{-1}$ is 10% and 84%, respectively, but the reverse situation occurs at $\omega_1 = 15\,775$

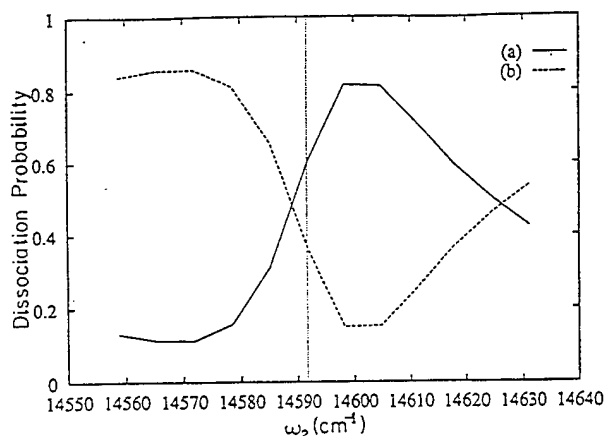


FIG. 11. As in (a) and (b) of Fig. 10, but here ω_2 is tuned with $\omega_1 = 15\,650\text{ cm}^{-1}$ fixed.

cm^{-1} , where 86% of product is $\text{Na}(3s) + \text{Na}(3p)$. Thus, varying ω_1 provides a straightforward method of extensive control over the branching ratio into final product channels.

Figure 10 shows two periods of $P(q)$, with the distance between the peaks (or dips) corresponding to the vibrational spacing between $v = 26$ and 27. The origin of this oscillatory behavior is readily evident: as ω_1 increases by an amount equal to the vibrational spacing with ω_2 fixed, $|\epsilon_i\rangle$ couples to the next bound state $|\epsilon_{j+1}\rangle$. In essence, then, any of initially empty bound states $|\epsilon_j\rangle$ can be used as an intermediary in a path which interferes with the direct dissociation from $|\epsilon_i\rangle$. This is a convenient feature which gives the experimentalist a wide range of possible choices of ω_1 and ω_2 , with no loss of control.

Tuning ω_2 and fixing ω_1 results in equally successful control. In Fig. 11, we show $P(q)$ as a function of ω_2 , where $\omega_1 = 15\,650.4\text{ cm}^{-1}$, $I_1 = 8.7 \times 10^9\text{ W/cm}^2$, and $I_2 = 3.51 \times 10^{10}\text{ W/cm}^2$. The molecule is initially in the $v_i = 18$, $J = 0$ state, and the value of the ω_1 and ω_2 effectively couple the $|\epsilon_{v=18}\rangle$ ($J = 0$) and $|\epsilon_{v=26}\rangle$ ($J = 0$) states. Once again control is extensive. Only one period of the oscillation in $P(q)$ is shown; the pattern repeats for ω_2 larger than $14\,630\text{ cm}^{-1}$.

Changing the laser power alters the linewidths of the power broadened bound states, affecting the control. By reducing the laser power the line widths narrow and $|\epsilon_i\rangle$ decouples from $|\epsilon_j\rangle$ when the sum of their line widths becomes smaller than the detuning Δ . Sample effects due to intensity variation are shown in Figs. 12 and 13. Here ω_2 is fixed at $14\,591\text{ cm}^{-1}$, so as to couple the $v = 26$, $J = 0$ state to the initial $v_i = 15$, $J = 0$ in the $^3\Pi_u$ state when $\omega_1 = 16\,064\text{ cm}^{-1}$ (Resonant coupling occurs at the vertical line in the figure). The laser intensities in Fig. 12 are $I_1 = 8.7 \times 10^9$, $I_2 = 3.5 \times 10^{10}$, and $I_1 = 1.4 \times 10^7$, $I_2 = 1.4 \times 10^9$ in Fig. 13. In both cases the product probabilities oscillate with the same period. However, the region over which $P(q)$ changes significantly at the weaker laser intensity is substantially smaller than at the larger intensity, indicating that the width of the region, which measures the overlap of the two resonance states, is at least partially determined by the power broadening. In the limit of even weaker laser intensities (not

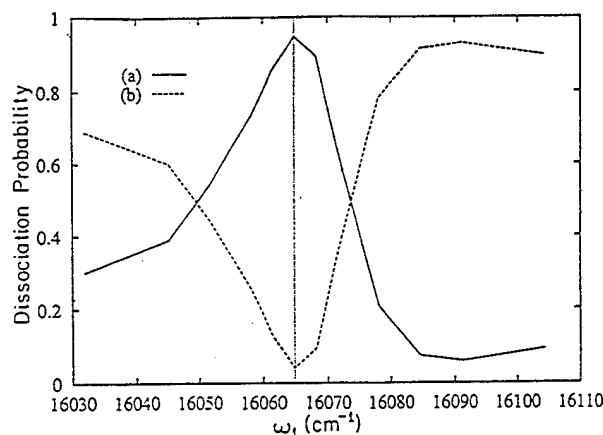


FIG. 12. As in (a) and (b) of Fig. 10, but with the molecule initially in $v_i = 15$, $J = 0$. ($I_1 = 8.7 \times 10^9\text{ W/cm}^2$, $I_2 = 3.5 \times 10^{10}\text{ W/cm}^2$, and $\omega_2 = 14\,591\text{ cm}^{-1}$.) The vertical line indicates the point of resonant coupling of the two bound states.

shown here), e.g., $I_1 = 10^5$ and $I_2 = 10^6\text{ W/cm}^2$, $P(q)$ is essentially flat except in the immediate vicinity of frequencies which satisfy $\hbar(\omega_1 - \omega_2) = \epsilon_j - \epsilon_i$.

Significantly, additional computations show that the results in Figs. 2–13 are insensitive to the relative phase of the ω_1 and ω_2 fields, a result which is consistent with the theory discussed above. As a consequence, *the two lasers need not be phase coherent in order to achieve control*. Any drift or jitter in the laser phase in a practical environment will not alter the outcome of the control experiment, simplifying experimental conditions considerably.

Consider now the effect of including rotational states. One expects two compensatory effects. First, rotational contributions ought to broaden the line shapes, increasing the overlap between $|\epsilon_i\rangle$ and $|\epsilon_j\rangle$ (cf. Figs. 3 and 4), enhancing control. Second, rotational excitation introduces additional noninterfering pathways which tend to diminish the range of control, especially when the laser intensities are high and rotational excitation is significant. Figures 14 and 15 do indeed demonstrate this field-dependent effect. Figure 14 shows $P(q)$ vs ω_1 without [Fig. 14(a)] and with [Fig. 14(b)]

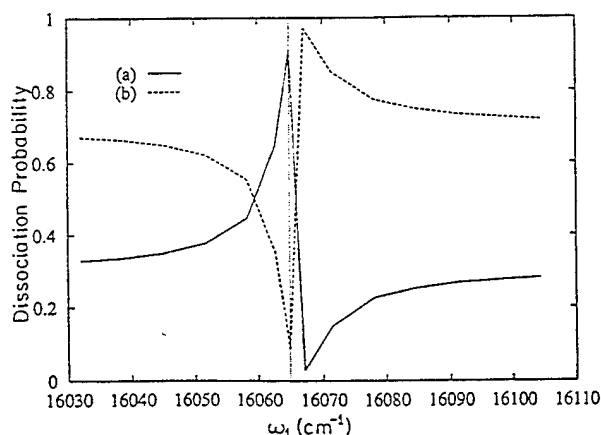


FIG. 13. As in Fig. 12, but with the laser intensities reduced to $I_1 = 1.4 \times 10^7\text{ W/cm}^2$, $I_2 = 1.4 \times 10^9\text{ W/cm}^2$.

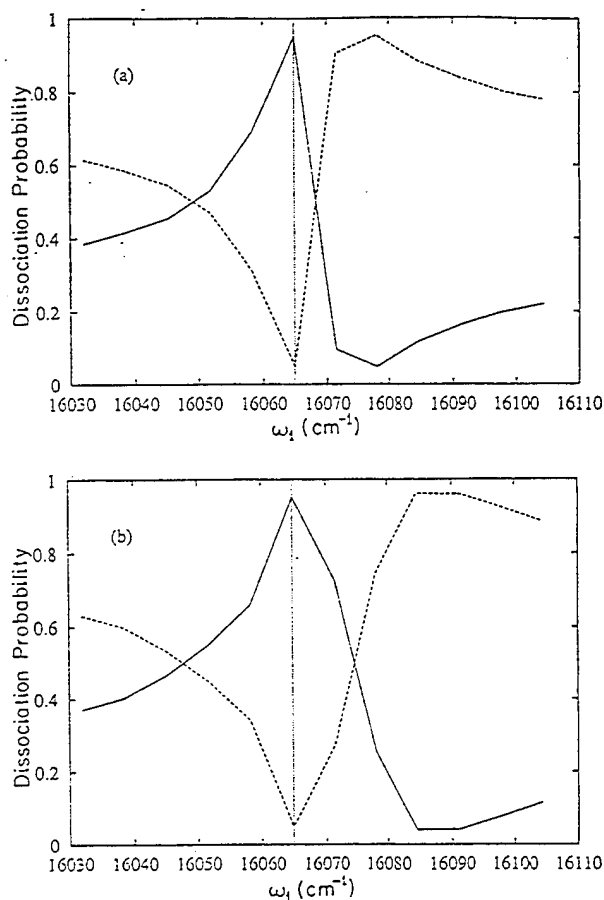


FIG. 14. $P(q)$ vs ω_1 for $\text{Na}(3s)+\text{Na}(3p)$ (solid lines) and for $\text{Na}(3s)+\text{Na}(4s)$ (dashed lines). Rotational couplings are excluded in (a), and included in (b). Here, $I_1=8.7 \times 10^7$, $I_2=5.6 \times 10^9$ W/cm², and the frequency $\omega_2=14\,491$ cm⁻¹ is fixed. The initial molecular state is $v_i=15$, $J=0$ of the $^3\Pi_u$. Satellite terms are neglected.

rotational states (i.e., $J=0,2,4$ states of the $^3\Pi_u$ and the $J=1,3,5$ states of the $^3\Pi_g$ and $2\ ^3\Sigma_g$). Here the laser fields are relatively weak ($I_1=8.7 \times 10^7$, $I_2=5.6 \times 10^9$ W/cm²) and rotation leads to a wider range of ω_1 over which control is achieved. A higher intensity result is shown in Fig. 15 and is to be compared to results without rotation in Fig. 10. Here

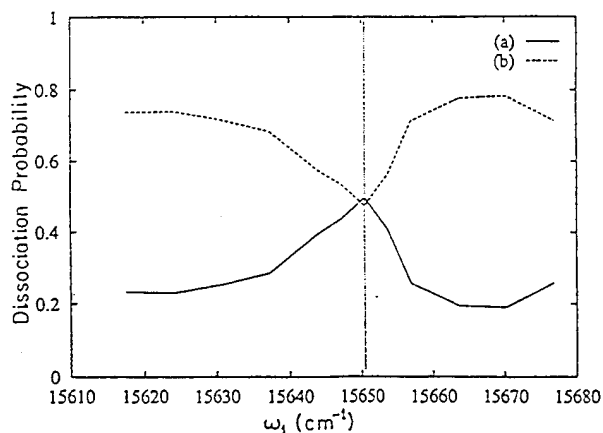


FIG. 15. As in Fig. 14(b), but with the initial state in $v_i=18$, $J=0$ and with higher laser intensities, $I_1=8.7 \times 10^9$, $I_2=3.51 \times 10^{10}$ W/cm².

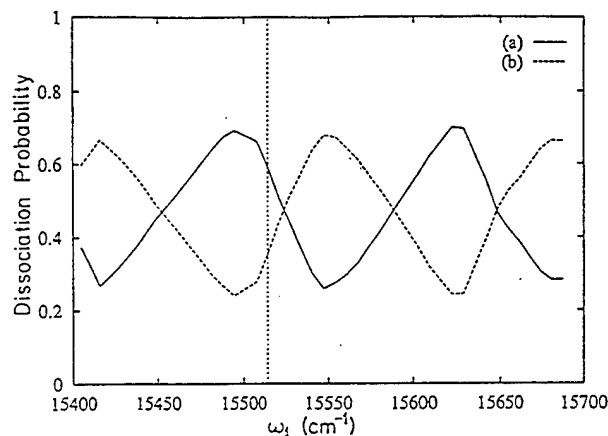


FIG. 16. Probability of forming (a) $\text{Na}(3s)+\text{Na}(3p)$ and (b) $\text{Na}(3s)+\text{Na}(4s)$ as a function of ω_1 , with $\omega_2=13\,964$ cm⁻¹, $I_1=8.7 \times 10^9$ W/cm², and $I_2=3.51 \times 10^{10}$ W/cm². The molecule is initially in $v_i=19$, $J=0$ of the $^3\Pi_u$ electronic state and $\hbar(\omega_1-\omega_2)+(\epsilon_{v=19}-\epsilon_{v=31})=0$ at $\omega_1=15\,514$ cm⁻¹. Both satellite terms and rotational couplings are included.

the presence of rotational states is seen to reduce the ω_1 range over which $P(q)$ varies and to substantially reduce the range of control. Nonetheless, we still observe a change of as much as a factor of 3 in the branching ratio as the frequency ω_1 is varied.

Finally, we consider results which include all effects, i.e., both rotational terms and satellite contributions. Figure 16 shows such a result where $v_i=19$, $J=0$ of the $^3\Pi_u$ state. Rotational couplings among the $J=0,2$ of the $^3\Pi_u$ and the $J=1,3$ of the $^3\Pi_g$ and $2\ ^3\Sigma_g$ are included in the computation. Control over the product probability remains extensive, with the ratio $P(q=3s+3p)/P(q=3s+4s)$ ranging from 0.3 to 3 as ω_1 is tuned.

V. SUMMARY

We have shown that extensive control of the line shape and the branching ratio in photodissociation can be achieved by scanning the relative frequencies of two intense lasers. The control is independent of the phase of the two laser routes. Computations on Na_2 photodissociation show that control over product yields is extensive, with the branching ratio changing by as much as a factor of 10 as the frequencies are tuned.

ACKNOWLEDGMENT

This work was supported by the U.S. Office of Naval Research under Contract No. N00014-90-J-1014.

¹ P. Brumer and M. Shapiro, *Acc. Chem. Res.* **22**, 407 (1989); *Annu. Rev. Phys. Chem.* **43**, 257 (1992); M. Shapiro and P. Brumer, *Int. Reviews Phys. Chem.* **13**, 187 (1994).

² M. Yu. Ivanov, P. B. Corkum, and P. Dietrich, *Laser Phys.* **3**, 375 (1993).

³ A. D. Bandrauk, J.-M. Gauthier, and J. F. McCann, *Chem. Phys. Lett.* **200**, 399 (1992).

⁴ C. Chen, Y.-Y. Yin, and D. S. Elliott, *Phys. Rev. Lett.*, **64**, 507 (1990); S.-P. Lu, S. M. Park, Y. Xie, and R. J. Gordon, *J. Chem. Phys.* **96**, 6613 (1992); E. Dupont, P. B. Corkum, H. C. Liu, M. Buchanan, and Z. R. Wasilewski, *Phys. Rev. Lett.* (submitted); I. Sofer, A. Shnitman, I. Gollub, A. Yogev, M. Shapiro, Z. Chen, and P. Brumer (unpublished).

⁵ T. Nakajima and P. Lambropoulos, *Phys. Rev. Lett.* **70**, 1081 (1993).

- ⁶H. G. Muller, P. H. Bucksbaum, D. W. Schumacher, and A. Zavriyev, *J. Phys. B* **23**, 2761 (1990); R. M. Potvliege and P. H. G. Smith, *ibid.* **25**, 2501 (1992).
- ⁷K. J. Schafer and K. C. Kulander, *Phys. Rev. A* **45**, 8026 (1992).
- ⁸E. Charron, A. Guisti-Suzor, and F. H. Mies, *Phys. Rev. Lett.* **71**, 692 (1993).
- ⁹See, for example, P. L. Knight, M. A. Lauder, and B. J. Dalton, *Phys. Rep.* **190**, 1 (1990), and references therein.
- ¹⁰O. Faucher, D. Charalambidis, C. Fotakis, J. Zhang, and P. Lambropoulos, *Phys. Rev. Lett.* **70**, 3004 (1993).
- ¹¹K. J. Boller, A. Imamoglu, and S. E. Harris, *Phys. Rev. Lett.* **66**, 2593 (1991).
- ¹²Z. Chen, M. Shapiro, and P. Brumer, *Chem. Phys. Lett.* **228**, 289 (1994).
- ¹³P. Brumer and M. Shapiro, *Adv. Chem. Phys.* **60**, 371 (1986).
- ¹⁴R. D. Levine, *Quantum Mechanics of Molecular Rate Processes* (Clarendon, Oxford, England, 1969).
- ¹⁵M. Shapiro, *J. Chem. Phys.* **56**, 2582 (1972); G. G. Balint-Kurti and M. Shapiro, *Adv. Chem. Phys.* **60**, 403, (1986); M. Shapiro and H. Bony, *J. Chem. Phys.* **83**, 1588 (1985); Z. Chen, M. Shapiro, and P. Brumer, *ibid.* **98**, 8647 (1993).
- ¹⁶A. D. Bandrauk and O. Atabek, *Adv. Chem. Phys.* **73**, 823 (1989); S. Miret-Artes, O. Atabek, and A. D. Bandrauk, *Phys. Rev. A* **45**, 8056 (1992).
- ¹⁷C. Cohen-Tannoudji, J. Dupont-Roc, and G. Grynberg, *Atom-Photon Interactions* (Wiley, New York, 1992).
- ¹⁸U. Fano, *Phys. Rev.* **124**, 1866 (1961).
- ¹⁹The potential curves and the relevant electronic dipole moments are from I. Schmidt, Ph.D. thesis, Kaiserslautern University, 1987; W. Meyer (private communication).
- ²⁰A similar laser arrangement was used to study CARS involving a resonant absorption to the continuum. See A. D. Bandrauk, M. Giroux, and G. Turcotte, *J. Phys. Chem.* **89**, 4473 (1985).

Abstract

Quantum mechanics is shown to impose a rigid limitation on the extent to which dynamics can be controlled. Specifically, consider a system in an initial subspace \mathcal{H}_0 of dimensionality M_0 , which evolves to populate subspaces $\mathcal{H}_1, \mathcal{H}_2$ of dimensionality M_1, M_2 . Then, if $M_2 \geq M_0$, it is possible to prevent transitions from \mathcal{H}_0 into \mathcal{H}_2 only under extremely stringent conditions. Classical mechanics is shown to impose no such limitation.

Using coherent external fields to induce quantum interference effects in atomic and molecular systems provides a powerful means of controlling system dynamics at its most fundamental level.¹⁻⁴ For example, recent theoretical considerations, and experimental verification⁵, show that realistically achievable laser configurations can be used to substantially alter product yields in molecular photodissociation processes⁶. As interest in the possibilities afforded by such directed dynamics grows, so does the need for general principles which delimit the range of possible control.

In this letter we demonstrate that quantum mechanics imposes a stringent general limitation on the extent of possible control. Uncontrolled free system evolution is also seen to be similarly limited.

We focus attention on a system whose Hamiltonian eigenstates are partitioned into bases for three subspaces $\mathcal{H}_0, \mathcal{H}_1, \mathcal{H}_2$ of dimensionality M_0, M_1 and M_2 , respectively. States in \mathcal{H}_i ($i = 0, 1, 2$) are denoted $|i, n_k\rangle$, where $n_k = 1, \dots, M_i$ labels the state and i labels the subspace. Dynamics initiated in \mathcal{H}_0 can flow into $\mathcal{H}_0, \mathcal{H}_1$ and \mathcal{H}_2 under the influence of a unitary operator⁷ S . The object of control here is to direct dynamics from \mathcal{H}_0 into $\mathcal{H}_0 \oplus \mathcal{H}_1$, while excluding transitions to \mathcal{H}_2 . Clearly this is a trivial problem if there are states in \mathcal{H}_0 with nonzero S-matrix elements solely to states in one \mathcal{H}_i . Hence we restrict attention to the more general case where each state in \mathcal{H}_0 has a nonzero probability of undergoing a transition to at least one state in either \mathcal{H}_0 or \mathcal{H}_1 and to \mathcal{H}_2 . We then show that only under extremely stringent conditions is it possible to construct an initial superposition state in \mathcal{H}_0 which directs the system entirely from \mathcal{H}_0 into $\mathcal{H}_0 \oplus \mathcal{H}_1$ if $M_2 \geq M_0$. No such restrictions arise in classical mechanics.

Since any initial state in \mathcal{H}_0 is comprised of an incoherent weighted sum over pure

states, it suffices to consider a single pure initial state. Consider then the dynamics of an initial wavefunction $|i_0\rangle$ which is comprised of a linear superposition of states in \mathcal{H}_0 :

$$|i_0\rangle = \sum_{n_i=1}^{M_0} c_{n_i} |0, n_i\rangle \quad (1)$$

and note that the operator S operates as:

$$S|0, n_i\rangle = \sum_{j=1}^2 \sum_{n_k=1}^{M_j} S_{n_i, n_k}^{(0,j)} |j, n_k\rangle \quad (2)$$

By construction, \mathcal{H}_1 and \mathcal{H}_2 are comprised of states accessible from \mathcal{H}_0 via S ; i.e., the matrix elements $S_{n_i, n_k}^{(0,j)}$ are nonzero.

The final state, resulting from the operation of S on $|i_0\rangle$, is given by:

$$S|i_0\rangle = \sum_{n_i=1}^{M_0} c_{n_i} \sum_{j=1}^2 \sum_{n_k=1}^{M_j} S_{n_i, n_k}^{(0,j)} |j, n_k\rangle \quad (3)$$

Projecting this state onto $\langle 2, n_f |$, squaring and summing over n_f gives the probability of finding the system in \mathcal{H}_2 :

$$P(\mathcal{H}_2) = \sum_{n_f} \left| \sum_{n_i=1}^{M_0} c_{n_i} S_{n_i, n_f}^{(0,2)} \right|^2 \quad (4)$$

Under what conditions can we prevent dynamics into \mathcal{H}_2 ? To do so requires $P(\mathcal{H}_2) = 0$, i.e.

$$\sum_{n_i=1}^{M_0} c_{n_i} S_{n_i, n_f}^{(0,2)} = 0, \quad (5)$$

for $n_f = 1, \dots, M_2$, or

$$S_{M_0, M_2} C_{M_0} = 0 \quad (6)$$

where S_{M_0, M_2} is an $M_0 \times M_2$ dimensional matrix and C_{M_0} is an M_0 dimensional vector.

Equation (6) has nontrivial solutions if and only if⁸ the rank of S_{M_0, M_2} is less than M_0 . This is certainly the case⁹ for $M_2 < M_0$. However, for $M_2 \geq M_0$ the rank of S_{M_0, M_2} is greater than or equal to M_0 unless all $M_0 \times M_0$ dimensional submatrices of S_{M_0, M_2} are

singular. That is, denoting the k^{th} such submatrix by $S_{M_0, M_0}^{(k)}$ ($k = 1, \dots, [M_2!/(M_2 - M_0)!M_0!]$), nontrivial solutions are only possible if

$$\det S_{M_0, M_0}^{(k)} = 0 \quad (7)$$

for all k . Clearly this imposes very stringent conditions on the possibility of the desired control, making it virtually impossible under generic conditions.

The inability to direct dynamics from \mathcal{H}_0 away from \mathcal{H}_2 under typical conditions, if $M_2 \geq M_0$, is entirely a quantum limitation. To see this consider the analogous situation classically. Here one examines a phase space region A_0 of volume M_0 containing trajectories which flow into final phase space regions A_0 , A_1 and A_2 , of volume M_0 , M_1 and M_2 . To design, for example, an initial state in A_0 which goes solely into A_1 simply (1) allow all trajectories to evolve from A_0 and settle into A_0 , A_1 or A_2 ; (2) time reverse just those trajectories which went from A_0 into A_1 , to give a distribution in A_0 . The resultant distribution, when propagated forward in time, will evolve solely from A_0 to A_1 .

The simplest way to understand the difference between the classical and quantum results is to note that in classical mechanics each classical state (i.e. each trajectory) goes from A_0 into a specific A_i . This is not the case quantum mechanically where each \mathcal{H}_0 state has nonzero S matrix elements with states in both $\mathcal{H}_0 \oplus \mathcal{H}_1$ and \mathcal{H}_2 .

The quantum restriction we have obtained is completely general, applying to both systems which are controlled, in which case S defines a process which we design for control purposes, as well as to uncontrolled system evolution in which S is dictated by nature. The result establishes an important inequality between the dimension of the subspace (\mathcal{H}_2) which we desire not to populate and the initial subspace (\mathcal{H}_0). Further, unlike quantum entropy arguments for example, the result imposes a fundamental restriction on

the dynamical evolution of the wavefunction itself. No observer or measurement need be invoked.

Acknowledgments:

This work was supported by the U.S. Office of Naval Research under contract number N00014-90-J-1014, and by the Ontario Laser and Lightwave Research Centre.

References

- [1] For recent reviews, see, P. Brumer and M. Shapiro, *Ann. Rev. Phys. Chem.* **43**, 257 (1992); M. Shapiro and P. Brumer, *Int. Reviews Phys. Chem.* **13**, 187 (1994); For the initial paper see P. Brumer and M. Shapiro, *Chem. Phys. Letters* **126**, 541 (1986).
- [2] D. J. Tannor and S.A. Rice, *Adv. Chem. Phys.* **70**, 441 (1988); D.J. Tannor, in "Molecules in Laser Fields", pg. 287, ed. A. Bandrauk, (Marcel Dekker, 1994);
- [3] W. Warren, H. Rabitz and M. Dahleh, *Science* **259**, 1581 (1993); H. Rabitz, in "Laser Techniques for State-Selected and State-to-State Chemistry II", ed. J.W. Hepburn, SPIE-Int. Soc. Opt. Eng. **2124**, 84 (1994).
- [4] Y. Yan, R.E. Gillilan, R.M. Whitnell and K.R. Wilson, *J. Phys. Chem.* **97**, 2320 (1993)
- [5] I. Sofer, A. Shnitman, I. Gollub, A. Yogev, M. Shapiro, Z. Chen and P. Brumer (manuscript in preparation).
- [6] See, e.g., control of Na_2 photodissociation in Z. Chen, P. Brumer and M. Shapiro, *J. Chem. Phys.* **98**, 6843 (1993); J. Dods, P. Brumer and M. Shapiro, *Can. J. Chem.* **72**, 958 (1994); Z. Chen, M. Shapiro, and P. Brumer, *Chem. Phys. Letters* (in press)
- [7] S , the extension of the scattering S matrix to arbitrary systems and processes carries the system from the initial to the final state of the unperturbed system. It contains all parameters, including time dependences, which are external to the unperturbed system.
- [8] F.E. Hohn, *Elementary Matrix Algebra*, (MacMillan Co., N.Y., 1964)

[9] In the case of $M_2 < M_0$ dynamics directed solely into $\mathcal{H}_0 \oplus \mathcal{H}_1$ *may* be possible if the set of solutions c_{n_i} obtained is normalizeable, i.e. $\sum_{n_i=1}^{M_0} |c_{n_i}|^2 = 1$. Otherwise the solutions which exist are nonphysical.

Incoherent Interference Control of Photodissociation in the Strong Field Domain

Zhidang Chen, Moshe Shapiro* and Paul Brumer

Chemical Physics Theory Group, Department of Chemistry

and The Ontario Laser and Lightwave Research Center

University of Toronto, Toronto, M5S 1A1 Canada

(January 17, 1995)

Abstract

Control over channel specific line shapes and branching ratios in photodissociation is achievable by irradiating a molecule with two intense CW lasers whose relative phase need not be well defined. Control results from quantum interference between nonlinear pathways induced by the intense fields, within which the relative laser phase cancels. The interference, and hence the product yields, can be manipulated by changing the relative frequencies and intensities of the two lasers. In this paper this theory of high field control is described, and computations on the photodissociation of Na_2 are discussed. Control over product yields is shown to be extensive, even with inclusion of rotational states. For example, the branching ratio between the $\text{Na}(3s)+\text{Na}(3p)$ and $\text{Na}(3s)+\text{Na}(4s)$ products can change by as much as a factor of ten as the frequencies are tuned.

I. INTRODUCTION

Attempts to control atomic and molecular processes with lasers is an important problem of longstanding interest. Initial efforts to reach this goal proposed using intense laser fields

whose interaction energy with the atomic or molecular system was sufficiently large so as to compete with ionization and binding energies. These early efforts were generally unsuccessful since increasing the cross section of the desired process was often accompanied by undesirable side effects. Similarly, frequency based approaches, e.g. tuning the laser frequency to match that of a particular bond which we desire to break (the so called mode-selective approach) have been limited to molecules with light atoms where vibrational motion of the target bond is effectively decoupled from the remainder of the molecule.

Since the late 1980's we, and other researchers, demonstrated that the coherence properties of *weak* lasers could be used effectively to control molecular reactions [1]- [13]. Consider for example control over the relative cross section of the three products formed in the photodissociation of a molecule ABC , e.g.



As one example of a control scenario, say one photoexcites ABC to a particular energy and total angular momentum using two different lasers (e.g., absorption of one photon of frequency ω and three photons of frequency $\omega/3$). Under these circumstances there are two independent pathways to the final products. These two routes can interfere destructively or constructively, depending on the relative phase and intensity of the two lasers. The resultant interference depends upon the particular product channel. Thus, by varying laser parameters one can selectively alter the interference term to favor production of one product over another [5].

The essential principle of coherent control, the name given to this approach, is that *control over molecular processes may be achieved by exciting a system to the same final state through several independent optical excitation routes*. Using this essential principle one may design a host of scenarios for controlling a wide variety of processes, including total photodissociation cross sections, differential photodissociation cross sections [1], current directions in semiconductors [7], bimolecular collision processes [8], etc. Detailed state-of-

the-art computational studies of these control scenarios show that extensive control over product channel cross sections is possible [1,3]. In addition, a number of experimental studies have verified the essential principles of coherent control [6].

The vast majority of proposed control scenarios have relied upon the use of lasers whose relative phase is controllable and well defined. This places a strong requirement on the required laser arrangement. In this paper we review work showing that simultaneous irradiation of a molecule with two intense laser fields allows for a control scenario in which relative laser phase need not be maintained. Rather, the essential control parameter influencing the quantum interference effect is the relative frequency of the two lasers. This scenario, which bears some relationship to studies of laser induced continuum structure [14,15] and laser induced transparency [16], is shown to allow for extensive control over the probability of dissociation as a function of translational energy (channel specific line shape) as well as the total yield of a given product.

The proposed control scenario is straightforward: an intense laser of frequency ω_1 excites a molecule from an initially populated bound state $|\varepsilon_i\rangle$ to a continuum state $|\varepsilon, \mathbf{m}, q^-\rangle$ at energy ε (where \mathbf{m} specifies the product quantum numbers and q labels the product arrangement channel) while a second laser ω_2 simultaneously couples initially unpopulated bound states $|\varepsilon_j\rangle$ to the same continuum. With both lasers on, dissociation to $|\varepsilon, \mathbf{m}, q^-\rangle$ occurs via direct and indirect dissociation pathways, the two lowest orders of which are $|\varepsilon_i\rangle \rightarrow |\varepsilon, \mathbf{m}, q^-\rangle$ and $|\varepsilon_i\rangle \rightarrow |\varepsilon', \mathbf{m}', q'^-\rangle \rightarrow |\varepsilon_j\rangle \rightarrow |\varepsilon, \mathbf{m}, q^-\rangle$. Contributions from these pathways to the product in a given channel q at energy ε interfere (either constructively or destructively) with one another. Varying the frequencies and intensities of the lasers alters the interference and hence the dissociation line shape and the yield of product into a given channel. Since the resultant scenario, as shown below, is independent of the laser phase, we call this “incoherent interference control”, as distinct from coherent control.

In this paper we review our recent work [17–19] in this area. We develop, in Section II, a molecular photodissociation theory for molecules in intense laser fields. The proposed control scenario emerges by applying this theory to excitation with two specifically chosen laser

fields, as described in Sect. IIB. Two types of control scenarios are described, one photon plus one photon and two photon plus one photon control. Results of computations examining the extent of possible control are provided in Section III and IV, where we demonstrate extensive control over the branching ratio into $\text{Na}(3s)+\text{Na}(3p)$ vs. $\text{Na}(3s) + \text{Na}(3d)$ vs. $\text{Na}(3s)+\text{Na}(4s)$. Indeed the absolute controlled yield is extensive as well, since the CW fields induce virtually 100% dissociation. Section IV contains a brief summary.

II. QUANTUM DYNAMICS OF PHOTODISSOCIATION IN INTENSE FIELDS

In this section we sketch the quantum theory of photodissociation in intense CW laser fields. This theory is then used to develop incoherent interference control. Section IID discusses the numerical method which enables us to exactly compute photodissociation probabilities in intense fields.

A. Photodissociation

The Hamiltonian H of a molecule in the presence of a radiation field is the sum of the molecular part H_M , the radiation part H_R and the interaction V between them:

$$H = H_M + H_R + V \equiv H_0 + V. \quad (2)$$

The Hamiltonian H_M of an isolated molecule AB (where A and B are molecular moieties) can be conveniently written as the sum of the nuclear kinetic terms, $K(\mathbf{R})$ and $k(\mathbf{r})$, and the electronic term $H_{el}(\mathbf{q}|\mathbf{R}, \mathbf{r})$,

$$H_M = K(\mathbf{R}) + k(\mathbf{r}) + H_{el}(\mathbf{q}|\mathbf{R}, \mathbf{r}), \quad (3)$$

where \mathbf{R} is the displacement vector between A and B , \mathbf{r} are the remaining nuclear coordinates, and \mathbf{q} denotes the collection of all electronic coordinates. As the molecule dissociates, ($R \equiv |\mathbf{R}| \rightarrow \infty$), H_M approaches its asymptotic form H_M^∞ while $H_{el}(\mathbf{q}|\mathbf{R}, \mathbf{r})$ approaches $h_{el}(\mathbf{q}, \mathbf{r})$,

$$\lim_{R \rightarrow \infty} H_M = H_M^\infty, \quad (4)$$

$$H_M^\infty = K(\mathbf{R}) + [k(\mathbf{r}) + h_{el}(\mathbf{q}, \mathbf{r})]. \quad (5)$$

The term in the brackets on the right hand side of Eq.(5) is the Hamiltonian of the separated fragments A and B .

Photodissociation occurs as a result of a transition from a molecular bound state $|\varepsilon_b\rangle$ to dissociating eigenstates $|\varepsilon, \mathbf{m}, q^-\rangle$ in the presence of radiation fields. Here \mathbf{m} specifies the product quantum numbers, ε is the state energy, q labels the product arrangement channel, and $|\varepsilon_b\rangle$ and $|\varepsilon, \mathbf{m}, q^-\rangle$ are eigenstates of H_M with discrete energy ε_b and continuous energy ε , respectively. That is,

$$H_M|\varepsilon_b\rangle = \varepsilon_b|\varepsilon_b\rangle, \quad (6)$$

$$H_M|\varepsilon, \mathbf{m}, q^-\rangle = \varepsilon|\varepsilon, \mathbf{m}, q^-\rangle. \quad (7)$$

The eigenstates are normalized so that

$$\langle \varepsilon_b | \varepsilon, \mathbf{m}, q^- \rangle = 0, \quad (8)$$

$$\langle \varepsilon', \mathbf{m}', q'^- | \varepsilon, \mathbf{m}, q^- \rangle = \delta(\varepsilon' - \varepsilon) \delta_{\mathbf{m}', \mathbf{m}} \delta_{q', q}. \quad (9)$$

The minus sign on q denotes the incoming boundary condition i.e. that at large time t the states $\exp(-i\varepsilon t/\hbar)|\varepsilon, \mathbf{m}, q^-\rangle$ approach well-defined states $\exp(-i\varepsilon t/\hbar)|\varepsilon, \mathbf{m}, q\rangle$, where $|\varepsilon, \mathbf{m}, q\rangle$ are eigenstates of the asymptotic product Hamiltonian H_M^∞ ,

$$H_M^\infty|\varepsilon, \mathbf{m}, q\rangle = \varepsilon|\varepsilon, \mathbf{m}, q\rangle. \quad (10)$$

The quantity \mathbf{m} , being good quantum numbers of H_M^∞ , specify, in conjunction with the energy ε and the arrangement channel label q , the states $|\varepsilon, \mathbf{m}, q\rangle$ of the fragment products. In the case of diatomic photodissociation the quantum number \mathbf{m} refers to scattering angles $\hat{\mathbf{k}}$.

The presence of radiation is conveniently described by the number eigenstates of H_R ,

$$H_R|N_k\rangle \equiv H_R|n_1^{(k)}, n_2^{(k)}, \dots\rangle = E_{N_k}|N_k\rangle \quad (11)$$

with energy $E_{N_k} = \sum_l n_l^{(k)} \hbar \omega_l$, which is the sum of photon energies in all possible modes. The letters $k = i$ and f will be used to label the initial and final states, respectively. The eigenstates of $H_0 \equiv H_M + H_R$ are the direct product of the molecular and photon states; e.g., $|(\varepsilon, \mathbf{m}, q^-), N_f\rangle \equiv |\varepsilon, \mathbf{m}, q^-|N_f\rangle$. The molecule-radiation interaction V can be expressed in the dipole approximation as

$$V = -\boldsymbol{\mu} \cdot \boldsymbol{\mathcal{E}}, \quad \boldsymbol{\mathcal{E}} = i \sum_l \epsilon_l (\mathbf{e}_l a_l - \mathbf{e}_l^* a_l^\dagger), \quad (12)$$

where $\boldsymbol{\mu}$ is the electric dipole operator, $\boldsymbol{\mathcal{E}}$ the amplitude of the radiation electric field, $\epsilon_l = (2\pi \hbar \omega_l / L^3)^{1/2}$, \mathbf{e}_l and ω_l are the polarization vector and angular frequency of mode l , respectively, and a_l, a_l^\dagger are annihilation and creation operators of photons in mode l .

The dynamics of photodissociation is completely described by the fully interacting state $|(\varepsilon, \mathbf{m}, q^-), N_k^-\rangle$ of the total Hamiltonian H ,

$$H|(\varepsilon, \mathbf{m}, q^-), N_k^-\rangle = (\varepsilon + E_{N_k})|(\varepsilon, \mathbf{m}, q^-), N_k^-\rangle, \quad (13)$$

where the minus superscript on N_k indicates the boundary condition that when the radiative interaction V is switched off, the state $|(\varepsilon, \mathbf{m}, q^-), N_k^-\rangle$ becomes the non-interacting state $|(\varepsilon, \mathbf{m}, q^-), N_k\rangle$. The states $|(\varepsilon, \mathbf{m}, q^-), N_k^-\rangle$ satisfy the Lippmann-Schwinger equation [20],

$$\langle(\varepsilon, \mathbf{m}, q^-), N_k^-| = \langle(\varepsilon, \mathbf{m}, q^-), N_k| + \langle(\varepsilon, \mathbf{m}, q^-), N_k|VG(\varepsilon^+ + E_{N_k}) \quad (14)$$

Here $G(E) = 1/(E - H)$ is the resolvent operator, and ε^+ denotes $\varepsilon + i\delta$ with $\delta \rightarrow 0^+$ at the end of the calculations. If the system is initially in $|\varepsilon_i, N_i\rangle \equiv |\varepsilon_i\rangle|N_i\rangle$ and the radiation field is switched on suddenly then the photodissociation amplitude to form the product state $|\varepsilon, \mathbf{m}, q^-|N_f\rangle$ is given by the overlap integral $\langle(\varepsilon, \mathbf{m}, q^-), N_f^-|\varepsilon_i, N_i\rangle$. Since $\langle(\varepsilon, \mathbf{m}, q^-), N_f|\varepsilon_i, N_i\rangle = 0$ this overlap assumes the form

$$\langle(\varepsilon, \mathbf{m}, q^-), N_f^-|\varepsilon_i, N_i\rangle = \langle(\varepsilon, \mathbf{m}, q^-), N_f|VG(\varepsilon^+ + E_{N_f})|\varepsilon_i, N_i\rangle, \quad (15)$$

through use of Eq.(14). Thus, the operator VG gives a complete description of the photodissociation process, up to all orders of the laser-molecule interaction.

Equation (15) is an exact expression which provides a connection between the dissociation amplitude and the VG matrix element. The required matrix elements of VG can be computed directly using the artificial method [18] originally introduced by Shapiro for weak radiation fields [21] and extended to high fields [22,23]. The numerical approach is discussed in Section IID.

Two quantities are of interest: the channel specific line shape $A(\varepsilon, q, N_f|\varepsilon_i, N_i)$, i.e. the probability of dissociation into channel q with energy ε ,

$$A(\varepsilon, q, N_f|\varepsilon_i, N_i) = \int d\hat{\mathbf{k}} | \langle (\varepsilon, \hat{\mathbf{k}}, q^-), N_f^- | \varepsilon_i, N_i \rangle |^2, \quad (16)$$

and the total dissociation probability to channel q

$$P(q) = \sum_{N_f} \int d\varepsilon A(\varepsilon, q, N_f|\varepsilon_i, N_i), \quad (17)$$

where the sum is over sets of photons that lift the molecule above the dissociation threshold. [In writing Eq. (16) diatomic dissociation is assumed, so that $\mathbf{m} = \hat{\mathbf{k}}$].

Our computations [17–19] are based upon a direct calculation of the full photodissociation amplitude $\langle (\varepsilon, \mathbf{m}, q^-), N_f | VG(E^+) | \varepsilon_i, N_i \rangle$ ($E^+ = \varepsilon^+ + E_{N_f}$), but to gain insight into the physics it is of interest to examine the general structure of this quantity. It is highly complex since the molecular response to intense laser fields is generally highly nonlinear with multiple absorption and emission processes occurring. For example, stimulated emission from bound as well as from continuous states can be as strong as absorption processes. As a result, Raman-type couplings via absorption and emission lead to the overlap between two bound vib-rotational states in the same or different electronic manifolds, which is otherwise negligible in weak field regime. Multiple absorption and emission induce multiple reaction pathways in molecules, resulting in profound effects in molecular dynamics [18]. As a result it is generally impossible to obtain a closed form for the VG matrix element in high field regime. It is possible, however, to obtain an expansion of the VG matrix element in terms of the level-shift operator $R(E^+)$, as we show below. This expression provides insight into photodissociation dynamics in intense radiation fields.

To this end we introduce the projection operators P and Q

$$P = \sum_{\mathbf{m}, q} \sum_{N_k} \int d\epsilon |(\epsilon, \mathbf{m}, q^-), N_k\rangle \langle (\epsilon, \mathbf{m}, q^-), N_k| \quad (18)$$

$$Q = \sum_j |\epsilon_j, N_j\rangle \langle \epsilon_j, N_j|, \quad (19)$$

which project out continuous and bound parts of eigenstates of H_0 [Eq. (2)], respectively.

Note that with P, Q thus defined, the photodissociation amplitude is also given by:

$$\langle (\epsilon, \mathbf{m}, q^-), N_f | VG(E^+) | \epsilon_i, N_i \rangle = \langle (\epsilon, \mathbf{m}, q^-), N_f | PVG(E^+) Q | \epsilon_i, N_i \rangle. \quad (20)$$

Consider then the operator $PVGQ$:

$$PVGQ = PV(Q + P)GQ = PVQGQ + PVPGQ. \quad (21)$$

The operators QGQ and PGQ can be expressed [24] as

$$QG(E^+)Q = \frac{Q}{E^+ - QH_0Q - QR(E^+)Q}, \quad (22)$$

$$PG(E^+)Q = \frac{P}{E^+ - PH_0P - PVP} VQG(E^+)Q, \quad (23)$$

where $R(E^+)$, the level-shift operator, is given by [24]

$$R(E^+) = V + V \frac{P}{E^+ - PH_0P - PVP} V. \quad (24)$$

Substituting Eqs.(22) and (23) into Eq.(21) yields

$$PVG(E^+)Q = PR(E^+)QGQ = PR(E^+)Q \frac{1}{E^+ - QH_0Q - QR(E^+)Q} Q. \quad (25)$$

It is convenient to separate the operator QRQ in the denominator of Eq.(25) into diagonal and off-diagonal parts

$$QRQ = \sum_j Q_j R Q_j + \sum_{j \neq j'} Q_j R Q_{j'} \quad (26)$$

where $Q_j = |\epsilon_j, N_j\rangle \langle \epsilon_j, N_j|$. Using Eq.(26) and the operator identity

$$\frac{1}{A - B} = \frac{1}{A} + \frac{1}{A} B \frac{1}{A - B}, \quad (27)$$

we rewrite

$$\frac{1}{E^+ - QH_0Q - QR(E^+)Q} = \frac{1}{E^+ - QH_0Q - \sum_j Q_j R(E^+) Q_j} + \frac{1}{E^+ - QH_0Q - \sum_j Q_j R(E^+) Q_j} \left(\sum_{j \neq j'} Q_j R(E^+) Q_{j'} \right) \frac{1}{E^+ - QH_0Q - QR(E^+)Q}. \quad (28)$$

By iteration, Eq.(28) can be expanded as

$$\begin{aligned} \frac{1}{E^+ - QH_0Q - QR(E^+)Q} &= \frac{1}{E^+ - QH_0Q - \sum_j Q_j R(E^+) Q_j} \\ &+ \frac{1}{E^+ - QH_0Q - \sum_j Q_j R(E^+) Q_j} \left[\left(\sum_{j \neq j'} Q_j R(E^+) Q_{j'} \right) \right. \\ &+ \left. \left(\sum_{j \neq j'} Q_j R(E^+) Q_{j'} \right) \frac{1}{E^+ - QH_0Q - \sum_j Q_j R(E^+) Q_j} \left(\sum_{j \neq j'} Q_j R(E^+) Q_{j'} \right) + \dots \right] \\ &\times \frac{1}{E^+ - QH_0Q - \sum_j Q_j R(E^+) Q_j}. \end{aligned} \quad (29)$$

We can evaluate the matrix element of Eq.(25), using Eq.(29), since the operator $1/(E^+ - QH_0Q - \sum_j Q_j R(E^+) Q_j)$ is diagonal in Q -subspace. The resulting photodissociation amplitude can be written as the sum of the terms:

$$\begin{aligned} &\langle (\varepsilon, \mathbf{m}, q^-), N_f | VG(E^+) | \varepsilon_i, N_i \rangle \\ &= \frac{1}{E^+ - \varepsilon_i - E_{N_i} - R_{i,i}(E^+)} \times \left[\langle (\varepsilon, \mathbf{m}, q^-), N_f | R(E^+) | \varepsilon_i, N_i \rangle \right. \\ &+ \sum_{j \neq i} \frac{\langle (\varepsilon, \mathbf{m}, q^-), N_f | R(E^+) | \varepsilon_j, N_j \rangle \langle \varepsilon_j, N_j | R(E^+) | \varepsilon_i, N_i \rangle}{[E^+ - \varepsilon_j - E_{N_j} - R_{j,j}(E^+)]} \\ &+ \sum_{j \neq j' \neq i} \frac{\langle (\varepsilon, \mathbf{m}, q^-), N_f | R(E^+) | \varepsilon_{j'}, N_{j'} \rangle \langle \varepsilon_{j'}, N_{j'} | R(E^+) | \varepsilon_j, N_j \rangle \langle \varepsilon_j, N_j | R(E^+) | \varepsilon_i, N_i \rangle}{[E^+ - \varepsilon_{j'} - E_{N_{j'}} - R_{j',j'}(E^+)] [E^+ - \varepsilon_j - E_{N_j} - R_{j,j}(E^+)]} \\ &+ \dots \Big], \end{aligned} \quad (30)$$

where $E^+ = \varepsilon^+ + E_{N_f}$. We have written out three groups of terms explicitly, but we emphasize that the numerical method utilized below allows us to compute $\langle (\varepsilon, \mathbf{m}, q^-), N_f | VG(E^+) | \varepsilon_i, N_i \rangle$ directly.

Equation (30) shows that numerous terms contribute to the photodissociation amplitude. Each of the terms is associated with a transition pathway. Multiple pathways induced by intense fields interfere with one another, either constructively or destructively, depending on

the relative phases among them. By manipulating the frequencies we can effectively control the transition probability, as we discuss below.

Equation (30) provides a completely general expression for terms in the laser-molecule interaction. The expression may be simplified, however, under the conditions of this paper, by noting that the incident radiation is such that it only effectively couples states in the Q space to those in the P space. Under these circumstances $PVP = 0$, which is tantamount to neglecting above-threshold dissociation, and

$$\langle (\varepsilon, \mathbf{m}, q^-), N_f | R(E^+) | \varepsilon_j, N_j \rangle = \langle (\varepsilon, \mathbf{m}, q^-), N_f | V | \varepsilon_j, N_j \rangle \quad (31)$$

The other matrix elements of R in Eq.(30) assume the following forms: the diagonal elements $R_{j,j}$ of $R(E^+)$ in the Q -subspace given by

$$R_{j,j}(E^+) = \langle \varepsilon_j, N_j | R(E^+) | \varepsilon_j, N_j \rangle \quad (32)$$

$$= \Delta_j(E) - \frac{i}{2}\Gamma_j(E), \quad (33)$$

where, by taking $\delta \rightarrow 0$, we have

$$\Delta_j(E) = \langle \varepsilon_j, N_j | V \frac{P_v}{E - PHP} V | \varepsilon_j, N_j \rangle, \quad (34)$$

$$\Gamma_j(E) = 2\pi \langle \varepsilon_j, N_j | VP\delta(E - PHP)PV | \varepsilon_j, N_j \rangle, \quad (35)$$

which are the field-induced shift and broadening, respectively. In Eq.(34), P_v denotes the principle part of the integration. Equation (30) also involves the off-diagonal elements $R_{j,i}(E^+)$ ($j \neq i$)

$$\langle \varepsilon_j, N_j | R(E^+) | \varepsilon_i, N_i \rangle = \langle \varepsilon_j, N_j | V | \varepsilon_i, N_i \rangle + \langle \varepsilon_j, N_j | V \frac{P}{E^+ - PHP} V | \varepsilon_i, N_i \rangle. \quad (36)$$

the second term of which describes second order coupling between two bound states, mediated by the continuum. If the $|\varepsilon_j\rangle$ and $|\varepsilon_i\rangle$ belong to the same electronic manifold the first term is zero in the dipole approximation.

The photodissociation amplitude in Eq.(30) is therefore seen to be comprised of transitions from the initial state $|\varepsilon_i, N_i\rangle$ to the dissociation continuum $|(\varepsilon, \mathbf{m}, q^-), N_f\rangle$ via

various dissociation pathways: $|(\varepsilon, \mathbf{m}, q^-), N_f\rangle \leftarrow |\varepsilon_i, N_i\rangle$, $|(\varepsilon, \mathbf{m}, q^-), N_f\rangle \leftarrow |\varepsilon_j, N_j\rangle \leftarrow |(\varepsilon', \mathbf{m}', q'^-), N'\rangle \leftarrow |\varepsilon_i, N_i\rangle$, etc.

Equation (30) can be truncated at various levels to examine a particular process. The simplest case is weak field single photon dissociation, where the isolated resonance approximation (i.e. the assumption that only one bound state is dissociated) applies. In this case only the first term on the right hand side of Eq.(30) need be considered. The resultant expression [18] turns out to be the same as that obtained by applying Fano's configuration interaction theory [25] in conjunction with the isolated resonance approximation and the neglect of free-free transitions.

For higher fields where the power broadening of the initial bound state is comparable to, or larger than, the spacing between the bound states, the isolated resonance approximation is no longer valid. Under these circumstances, the contribution from the neighboring states, which are initially unpopulated, should be included via the second group terms in Eq.(30). If n_1 and ω_1 are the photon number and frequency of the excitation laser, respectively then $|N_i\rangle = |n_1\rangle$, $|N_f\rangle = |n_1 - 1\rangle$ and $E^+ = \varepsilon^+ + (n_1 - 1)\hbar\omega_1$. The photodissociation amplitude becomes

$$\begin{aligned} \langle (\varepsilon, \mathbf{m}, q^-), n_1 - 1 | V G(E^+) | \varepsilon_i, n_1 \rangle &= \left[\langle (\varepsilon, \mathbf{m}, q^-), n_1 - 1 | V | \varepsilon_i, n_1 \rangle \right. \\ &+ \sum_{l \neq i} \frac{\langle (\varepsilon, \mathbf{m}, q^-), n_1 - 1 | V | \varepsilon_l, n_1 \rangle \langle \varepsilon_l, n_1 | R(\varepsilon^+) | \varepsilon_i, n_1 \rangle}{\varepsilon^+ - \varepsilon_l - \hbar\omega_1 - \Delta_l + i\Gamma_l/2} \Big] \\ &\times \frac{1}{\varepsilon^+ - \varepsilon_i - \hbar\omega_1 - \Delta_i + i\Gamma_i/2}, \end{aligned} \quad (37)$$

where Δ_i and Γ_i are the shift and broadening of the initial state, respectively. Here $\langle \varepsilon_l, n_1 | R(\varepsilon^+) | \varepsilon_i, n_1 \rangle$ is given by Eq.(36) with $E^+ = \varepsilon^+ + (n_1 - 1)\hbar\omega_1$, and the leading term is

$$\langle \varepsilon_l, n_1 | R(\varepsilon^+) | \varepsilon_i, n_1 \rangle \simeq \sum_{\mathbf{m}, q} \int d\varepsilon' \frac{\langle \varepsilon_l, n_1 | V | (\varepsilon', \mathbf{m}, q^-), n_1 - 1 \rangle \langle (\varepsilon', \mathbf{m}, q^-), n_1 - 1 | V | \varepsilon_i, n_1 \rangle}{\varepsilon^+ - \varepsilon'}, \quad (38)$$

describing the coupling between $|\varepsilon_i\rangle$ and $|\varepsilon_l\rangle$ via absorption and emission mediated by the continuum. Practically, only those $|\varepsilon_l\rangle$ such that $|\varepsilon_l - \varepsilon_i| < \Gamma_i$ contribute in Eq.(37). The two

dissociation pathways in Eq.(37), $|(\varepsilon, \mathbf{m}, q^-), n_1 - 1\rangle \leftarrow |\varepsilon_i, n_1\rangle$ and $|(\varepsilon, \mathbf{m}, q^-), n_1 - 1\rangle \leftarrow |\varepsilon_l, n_1\rangle \leftarrow |(\varepsilon', \mathbf{m}', q'^-), n_1 - 1\rangle \leftarrow |\varepsilon_i, n_1\rangle$, terminate in the same dissociation continuum and interfere. The resultant line shape [Eq.(16)] should demonstrate a series of peaks at $\varepsilon \simeq \varepsilon_b (b = i, l, \dots) + \hbar\omega_1$ and a series of dips where the two paths destructively interfere with one another. This structure is the molecular analogue of Fano-interference [25], and is observed in our numerical study.

B. Control of One-Photon Dissociation: One Plus One Arrangement

Consider now the effect of simultaneously applying two CW laser fields, of frequency ω_1 and ω_2 and photon numbers n_1 and n_2 ($|N_i\rangle = |n_1, n_2\rangle$). The molecule-radiation interaction V is given by the sum of the potentials due to each of the laser fields:

$$V = V_1 + V_2 = -\boldsymbol{\mu} \cdot \boldsymbol{\mathcal{E}}_1 - \boldsymbol{\mu} \cdot \boldsymbol{\mathcal{E}}_2, \quad (39)$$

where $\boldsymbol{\mathcal{E}}_1$ and $\boldsymbol{\mathcal{E}}_2$ are the electric field vectors associated with ω_1 and ω_2 . One photon absorption of frequency ω_1 excites the molecule from the initial state $|\varepsilon_i\rangle$ to the dissociative continuum $|\varepsilon, \mathbf{m}, q^-\rangle$ while the second laser ω_2 simultaneously couples the continuum to bound states $|\varepsilon_j\rangle$ that are initially devoid of population. Multiple absorptions and emissions of ω_1 and ω_2 couple numerous bound states to the continuum. We call this scenario the “one plus one arrangement”. An example of this scenario applied to Na_2 molecule is shown in Fig. 1 where laser frequencies are chosen such that $\varepsilon_i + \hbar\omega_1 \approx \varepsilon_j + \hbar\omega_2$. Under these circumstances $|\varepsilon_j\rangle$ can be populated by stimulated emission from the continuum. Given these frequencies there are three routes to dissociation in lowest order leading to three different energy regimes; (i) dissociation of the initial $|\varepsilon_i\rangle$ state by ω_2 to energy $\varepsilon \approx \varepsilon_i + \hbar\omega_2$; (ii) dissociation of $|\varepsilon_j\rangle$ by ω_1 to energy $\varepsilon \approx \varepsilon_j + \hbar\omega_1$, and (iii) the dissociation of $|\varepsilon_i\rangle$ by ω_1 and of $|\varepsilon_j\rangle$ by ω_2 , both to energy $\varepsilon \approx \varepsilon_i + \hbar\omega_1 \approx \varepsilon_j + \hbar\omega_2$. The third route involves two interfering pathways while the other two, termed satellite contributions, do not. This interference, and similar higher order interference contributions, is the key to control in this scenario. For the third route, the leading terms in the photodissociation amplitude at $\varepsilon \approx \varepsilon_i + \hbar\omega_1$ are

$$\langle (\varepsilon, \mathbf{m}, q^-), n_1 - 1, n_2 | VG(E^+) | \varepsilon_i, n_1, n_2 \rangle = A + B, \quad (40)$$

$$A = \left[\langle (\varepsilon, \mathbf{m}, q^-), n_1 - 1 | V_1 | \varepsilon_i, n_1 \rangle + \sum_{l \neq i} \frac{\langle (\varepsilon, \mathbf{m}, q^-), n_1 - 1 | V_1 | \varepsilon_l, n_1 \rangle \langle \varepsilon_l, n_1 | R_1(\varepsilon^+) | \varepsilon_i, n_1 \rangle}{\varepsilon^+ - \varepsilon_l - \hbar\omega_1 - R_{l,l}} \right] \\ \times \frac{1}{\varepsilon^+ - \varepsilon_i - \hbar\omega_1 - R_{i,i}}, \\ B = \sum_{j \neq i} \frac{\langle (\varepsilon, \mathbf{m}, q^-), n_2 | V_2 | \varepsilon_j, n_2 + 1 \rangle \langle \varepsilon_j, n_1 - 1, n_2 + 1 | R(\varepsilon^+) | \varepsilon_i, n_1, n_2 \rangle}{(\varepsilon^+ - \varepsilon_j - \hbar\omega_2 - R_{j,j})(\varepsilon^+ - \varepsilon_i - \hbar\omega_1 - R_{i,i})}, \quad (41)$$

where $\langle \varepsilon_l, n_1 | R_1(\varepsilon^+) | \varepsilon_i, n_1 \rangle$ is given by Eq.(38) with V replaced by V_1 , and

$$\langle \varepsilon_j, n_1 - 1, n_2 + 1 | R(\varepsilon^+) | \varepsilon_i, n_1, n_2 \rangle \\ \approx \sum_{\mathbf{m}, q} \int d\varepsilon' \frac{\langle \varepsilon_j, n_2 + 1 | V_2 | (\varepsilon', \mathbf{m}, q^-), n_2 \rangle \langle (\varepsilon', \mathbf{m}, q^-), n_1 - 1 | V_1 | \varepsilon_i, n_1 \rangle}{\varepsilon^+ - \varepsilon'}. \quad (42)$$

Note that we have used $E = \varepsilon + (n_1 - 1)\hbar\omega_1 + n_2\hbar\omega_2$ in Eq.(30) to obtain Eq.(41).

The A term in Eq.(41) results from a direct one-photon dissociation path $|\varepsilon_i\rangle \rightarrow |\varepsilon, \mathbf{m}, q^-\rangle$ induced by ω_1 , including the contribution for neighboring state $|\varepsilon_l\rangle$. Term B describes the indirect dissociation path $|\varepsilon_i\rangle \rightarrow |\varepsilon', \mathbf{m}', q'^-\rangle \rightarrow |\varepsilon_j\rangle \rightarrow |\varepsilon, \mathbf{m}, q^-\rangle$ induced by ω_1 plus ω_2 . The coupling between $|\varepsilon_i\rangle$ and $|\varepsilon_j\rangle$ in Eq.(42) results from absorption of one ω_1 photon and stimulated emission of an ω_2 photon. This results in additional peaks in the line shape at $\varepsilon \simeq \varepsilon_j + \omega_2$ and additional minima at points where term A cancels term B . Higher order terms in the expansion of Eq. (40) correspond to additional sequences of absorption and emission of photons of frequencies ω_1 and ω_2 . It is important to note that the relative signs of all of these terms depend on laser frequencies, resulting in a sensitivity of the line shape to frequency.

These results are readily understood from an alternate perspective, the dressed-molecule picture. From this viewpoint the bound states of the bound electronic manifold are embedded in the continuum by the lasers ω_1 and ω_2 , and dissociate. Those bound states which effectively overlap one another strongly interfere. The resulting dissociation line shape therefore displays a series of peaks and dips, reflecting the interference pattern from the multiple dissociation pathways. The characteristic of the interference depends on the frequencies and intensities of the lasers, leading to the control of dissociation product distribution via variation of laser parameters.

Equation (41) are written in terms of the number representation for photon states. However, a complete analysis of the interference between the A and B and higher order paths necessitates an understanding of the role of the photon phase. For this reason we sketch the same argument using coherent states. Here $|\alpha_1\rangle$ and $|\alpha_2\rangle$ are coherent states describing the ω_1 and ω_2 fields and are defined as ($i = 1, 2$)

$$|\alpha_i\rangle = \sum_{n_i} P(\alpha_i, n_i) |n_i\rangle, \quad (43)$$

with

$$P(\alpha_i, n_i) = \alpha_i^{n_i} \exp(-|\alpha_i|^2/2) / \sqrt{n_i!}, \quad (44)$$

The quantity α_i can be parameterized by the average photon number \bar{n}_i and the phase ϕ_i (including the spatial phase $\mathbf{k}_i \cdot \mathbf{r}$) of the ω_i laser as: $\alpha_i = \sqrt{\bar{n}_i} \exp(i\phi_i)$. Note that at high intensities (large \bar{n}_i) the Poisson distribution in Eq.(44) is sharply peaked at $n_i = \bar{n}_i$. Replacing Eq.(41) by $\langle \alpha | \langle \varepsilon, q^- | VG(E^+) | \varepsilon_i \rangle | \alpha \rangle$ with $|\alpha\rangle \equiv |\alpha_1\rangle \oplus |\alpha_2\rangle$, gives, within the rotating wave approximation,

$$\langle \alpha | \langle \varepsilon, \mathbf{m}, q^- | VG(E^+) | \varepsilon_i \rangle | \alpha \rangle = e^{i\phi_1} \bar{A} + e^{i\phi_2} e^{i(\phi_1 - \phi_2)} \bar{B}, \quad (45)$$

where \bar{A} and \bar{B} are of the same form as A and B in Eq.(41) but with the photon numbers n_1 and n_2 replaced by the average photon numbers \bar{n}_1 and \bar{n}_2 . Because of the cancelation of the laser phase ϕ_2 in Eq.(45), the dissociation probability $|\langle \alpha | \langle \varepsilon, \mathbf{m}, q^- | VG(E^+) | \varepsilon_i \rangle | \alpha \rangle|^2$ is given by Eq.(41) with n_i replaced by \bar{n}_i . The same argument applies to higher order terms, within the rotating wave approximation.

Equation (45) shows that the laser phase imparted to the molecule in the path A is ϕ_1 , and the phase imparted in the path B is $\phi_1 - \phi_2 + \phi_2 = \phi_1$. As a result the relative phase of the two paths is independent of the laser phases, a consequence of the internal cancellation of the ϕ_2 phase when ω_2 photons are emitted and absorbed. A similar cancellation occurs (within the rotating wave approximation) in the higher order terms to energy $E \approx \varepsilon_i + \hbar\omega_1$, which are composed of repeated iterations of emission and absorption of ω_2 or ω_1 . The resultant

control scenario is therefore expected to be insensitive to the phase jitter or phase drift of either laser. Hence, although there are multiple interfering pathways to dissociation in this scenario, variation of laser phases no longer serves as a means of controlling dissociation yields, as it does in coherent control [1]. However, as shown in Section III, highly efficient yield control results from varying the frequencies ω_1 and ω_2 .

C. Control of Two-Photon Dissociation: Two plus One Arrangement

In this section we discuss a related scenario that controls resonant two-photon, rather than one-photon, dissociation. The resonant character of the two photon process not only greatly enhances the dissociation probability, but also provides a means of selectively exciting molecules out of a thermal distribution, a feature of considerable importance for controlling reactions in a thermal environment.

Consider a molecule in an initial bound state $|\varepsilon_i\rangle$ that, by absorbing two photons of frequency ω_1 , is excited to a continuum $|\varepsilon, \mathbf{m}, q^-\rangle$ via a resonant intermediate state $|\varepsilon_{j_1}\rangle$. For the purpose of control, a second ("control") laser ω_2 simultaneously couples the continuum to initially unpopulated bound states $|\varepsilon_{j_2}\rangle$ to generate new pathways for photodissociation (see Fig. 2). For example, the state $|\varepsilon_{j_2}\rangle$ can be populated by stimulated emission from the continuum and subsequently dissociated by absorption. The laser frequencies are chosen such that $\hbar\omega_1 \approx \varepsilon_{j_1} - \varepsilon_i$, that is, the ω_1 is in resonance with ε_{j_1} , and $\varepsilon_i + 2\hbar\omega_1 \approx \varepsilon_{j_2} + \hbar\omega_2$. The initial state of the total system is $|\varepsilon_i, N_i\rangle = |\varepsilon_i, n_1, n_2\rangle$, and the final state is $|\varepsilon, \mathbf{m}, q^-, n_1 - 2, n_2\rangle$. We term the scenario the "two plus one arrangement".

In this case, as above, the exact photodissociation amplitude is given by Eq. (15). Physical insight emerges by considering the leading terms in the expansion of the photodissociation amplitude [Eq.(30)] given by

$$\langle (\varepsilon, \mathbf{m}, q^-), n_1 - 2, n_2 | VG(E^+) | \varepsilon_i, n_1, n_2 \rangle = C + D + \dots \quad (46)$$

$$C = \sum_{j_1 \neq i} \frac{\langle (\varepsilon, \mathbf{m}, q^-), n_1 - 2 | V_1 | \varepsilon_{j_1}, n_1 - 1 \rangle \langle \varepsilon_{j_1}, n_1 - 1 | V_1 | \varepsilon_i, n_1 \rangle}{(\varepsilon^+ - \varepsilon_{j_1} - \hbar\omega_1 - R_{j_1, j_1})(\varepsilon^+ - \varepsilon_i - 2\hbar\omega_1 - R_{i, i})} \quad (47)$$

$$D = \sum_{j_1 \neq i, j_2 \neq i, j_1 \neq j_2} \frac{\langle (\varepsilon, \mathbf{m}, q^-), n_2 | V_2 | \varepsilon_{j_2}, n_2 + 1 \rangle R_{j_2, j_1} \langle \varepsilon_{j_1}, n_1 - 1 | V_1 | \varepsilon_i, n_1 \rangle}{(\varepsilon^+ - \varepsilon_{j_2} - \hbar\omega_2 - R_{j_2, j_2})(\varepsilon^+ - \varepsilon_{j_1} - \hbar\omega_1 - R_{j_1, j_1})(\varepsilon^+ - \varepsilon_i - 2\hbar\omega_1 - R_{i, i})} \quad (48)$$

where we have used $E = \varepsilon + (n_1 - 2)\hbar\omega_1 + n_2\hbar\omega_2$ in Eq.(30) to obtain Eq.(46). The R_{j_2, j_1} term in Eq.(48) is given by

$$R_{j_2, j_1} \equiv \langle \varepsilon_{j_2}, n_1 - 2, n_2 + 1 | R(\varepsilon^+) | \varepsilon_{j_1}, n_1 - 1, n_2 \rangle \\ = \sum_{\mathbf{m}', q'} \int d\varepsilon' \frac{\langle \varepsilon_{j_2}, n_2 + 1 | V_2 | (\varepsilon', \mathbf{m}', q'^-), n_2 \rangle \langle (\varepsilon', \mathbf{m}', q'^-), n_1 - 2 | V_1 | \varepsilon_{j_1}, n_1 - 1 \rangle}{\varepsilon^+ - \varepsilon'}. \quad (49)$$

and describes the coupling between $|\varepsilon_{j_1}\rangle$ and $|\varepsilon_{j_2}\rangle$ resulting from the absorption of one ω_1 photon and the stimulated emission of an ω_2 photon.

For the fields described by coherent states $|\alpha\rangle \equiv |\alpha_1\rangle \oplus |\alpha_2\rangle$, the leading terms in the photodissociation amplitude are given by

$$\langle \varepsilon, \mathbf{m}, q^- | \langle \alpha | VG(E) | \varepsilon_i \rangle | \alpha \rangle = e^{2i\phi_1} \bar{C} + e^{i\phi_2} e^{i(2\phi_1 - \phi_2)} \bar{D} + \dots, \quad (50)$$

where \bar{C} and \bar{D} are of the same form as C and D in Eq.(46) but with the photon numbers n_1 and n_2 replaced by the average photon numbers \bar{n}_1 and \bar{n}_2 . Once again, because of the cancellation of the laser phase ϕ_2 in Eq.(50), the leading terms in the dissociation probability $|\langle \alpha | \langle \varepsilon, \mathbf{m}, q^- | VG(E) | \varepsilon_i \rangle | \alpha \rangle|^2$ are given by Eq.(46) with n_i replaced by \bar{n}_i . The resultant control over the two-photon process is independent of the phase jitter or phase drift of either laser. Similarly, all higher order terms in the expansion [Eq.(46)], within the rotating wave approximation, lead to laser phase free contributions to the probability of dissociation.

D. Computational Method

From the computational viewpoint, it is greatly advantageous to compute $\langle (\varepsilon, \mathbf{m}, q^-), N_f | VG(E^+) | \varepsilon_i, N_i \rangle$ [Eq.(15)] directly, rather than to evaluate the many terms in the expansion on the right hand side of Eq.(30). These computations can be done by using the artificial channel method, as described below. This method [21–23] rewrites the

photodissociation process as a full collision problem by introducing an artificial open channel which couples to the initial physical bound manifold. As a result the artificial channel serves as an incoming channel of an artificial full collision problem, and the physical continua serve as outgoing channels. The resultant full collision problem is then amenable to treatment by well developed full collision problem techniques, from which photodissociation probabilities can be extracted. This artificial channel method has been applied to single and multiphoton dissociation problems using a single artificial channel configuration [21], and to high field photodissociation problems using a one [22] and two artificial channel configuration [23]. We emphasize that while the single artificial channel method leads to the direct computation of the T -matrix element $\langle (\epsilon, \mathbf{m}, q^-), N_f | T | \epsilon_i, N_i \rangle$, using the two-artificial channel arrangement allows us to exactly compute, as we show here, the desired photodissociation amplitude $\langle (\epsilon, \mathbf{m}, q^-), N_f | VG | \epsilon_i, N_i \rangle$.

The essence of the artificial channel approach is readily explained. First, multiply both sides of the equation $G = G_0 + GVG_0$ [24] by V , yielding

$$VG = VG_0 + VGVG_0, \quad (51)$$

where $G_0 = 1/(E - H_0)$. Using Eq.(51), we rewrite the transition operator $T = V + VGV$ as

$$T(E) = V + VG_0(E)V + VG(E)VG_0(E)V. \quad (52)$$

Now introduce two artificial states, an open channel $|\tilde{A}\rangle$ and a closed channel $|\tilde{\epsilon}_b\rangle$ where the tilde denotes the artificial character of these states. The physical system plus the two artificial channels now comprise a full collision problem, in which the incoming flux flows from the artificial open channel to the physical continua. The dressed state $|\tilde{A}, N_i\rangle$ is (weakly) coupled to the $|\tilde{\epsilon}_b, N_i\rangle$ by an artificial interaction $\langle \tilde{\epsilon}_b, N_i | W_a | \tilde{A}, N_i \rangle$ and the $|\tilde{\epsilon}_b, N_i\rangle$ to the physical bound manifold $|\epsilon_b, N_i\rangle$ by another artificial coupling $\langle \epsilon_b, N_i | W_b | \tilde{\epsilon}_b, N_i \rangle$. The potentials W_a and W_b can be regarded as components of the interaction V that connect $|\tilde{A}, N_i\rangle$ to $|\tilde{\epsilon}_b, N_i\rangle$ and $|\tilde{\epsilon}_b, N_i\rangle$ to $|\epsilon_b, N_i\rangle$ but which do not affect the couplings between the physical states. Further, to avoid any disturbance to $|\tilde{\epsilon}_b\rangle$ and $|\epsilon_b\rangle$ due to the introduction of the

artificial interactions, the reverse coupling elements $\langle \tilde{A}, N_i | W_a | \tilde{\epsilon}_b, N_i \rangle$ and $\langle \tilde{\epsilon}_b, N_i | W_b | \epsilon_b, N_i \rangle$ are set to zero in the computation. All couplings between the physical states are included in the computations, including absorption and stimulated emission processes induced by the intense lasers between bound-free and free-free manifolds.

We now show that the computation of T-matrix element between $\langle (\epsilon, \mathbf{m}, q^-), N_f |$ and $| \tilde{A}, N_i \rangle$ allows us to extract the photodissociation amplitude of interest. Consider the matrix element $\langle (\epsilon, \mathbf{m}, q^-), N_f | T | \tilde{A}, N_i \rangle$, from Eq.(52). The first two terms in the right hand side are zero because $| (\epsilon, \mathbf{m}, q^-), N_f \rangle$ does not directly couple to the artificial states $| \tilde{A}, N_i \rangle$ and $| \tilde{\epsilon}_b, N_i \rangle$. The third term in Eq.(52) can be rewritten, given that V couples the $| \tilde{A}, N_i \rangle$ to $| \tilde{\epsilon}_b, N_i \rangle$ and $| \tilde{\epsilon}_b, N_i \rangle$ to $| \epsilon_b, N_i \rangle$ only, as

$$\begin{aligned} & \langle (\epsilon, \mathbf{m}, q^-), N_f | T(E) | \tilde{A}, N_i \rangle \\ &= \sum_{\tilde{\epsilon}_b} \sum_{\epsilon_b} \frac{\langle (\epsilon, \mathbf{m}, q^-), N_f | VG(E) | \epsilon_b, N_i \rangle \langle \epsilon_b, N_i | W_b | \tilde{\epsilon}_b, N_i \rangle \langle \tilde{\epsilon}_b, N_i | W_a | \tilde{A}, N_i \rangle}{E - \tilde{\epsilon}_b - E_{N_i}}, \end{aligned} \quad (53)$$

To simplify, we set W_b to equal unity, and $| \tilde{\epsilon}_b \rangle$ to be a copy of the initial bound manifold $| \epsilon_b \rangle$, but shifted in energy by an amount E_α . The advantage of this choice [23] is that the summation over $\tilde{\epsilon}_b$ in Eq.(53) can now be done due to orthogonality of rovibrational states in the same electronic state. Substituting $E = \epsilon^+ + E_{N_f}$, we write the final result as

$$\langle (\epsilon, \mathbf{m}, q^-), N_f | T(\epsilon^+ + E_{N_f}) | \tilde{A}, N_i \rangle = \sum_b \frac{\langle (\epsilon, \mathbf{m}, q^-), N_f | VG(\epsilon^+ + E_{N_f}) | \epsilon_b, N_i \rangle \langle \epsilon_b, N_i | W_a | \tilde{A}, N_i \rangle}{\epsilon^+ + E_{N_f} - \epsilon_b - E_{N_i} - E_\alpha}. \quad (54)$$

Equation (54) has the same structure as that in which one uses one artificial channel [22], so that the previous computational techniques are applicable with minor modifications. Specifically, by computing the residues of the T -matrix element at $\epsilon = \epsilon_i + E_{N_i} + E_\alpha - E_{N_f}$, we obtain $\langle (\epsilon, \mathbf{m}, q^-), N_f | VG(\epsilon^+ + E_{N_f}) | \epsilon_i, N_i \rangle$ at that energy, which is the desired photodissociation amplitude. Varying E_α gives the photodissociation amplitude and the line shape at various energy ϵ for given photon energies and coupling strength. The total dissociation yield is obtained from Eq.(17). Note the advantage of the original artificial channel idea, that the desired matrix element giving the photodissociation amplitude is

obtained without doing the integral over the continuum wavefunctions, thus avoiding the difficult problem of computing oscillatory integrands.

The theory above allows us to study photodissociation dynamics for realistic molecules. In the next two sections, we demonstrate that by manipulating the intense-laser induced interference in molecules, one can significantly alter the outcome of the photodissociation process. Results shown here are typical of those obtained in a wide range of computations which we have carried out.

III. CONTROL OF PHOTODISSOCIATION: ONE PLUS ONE ARRANGEMENT

A. Control of The Line Shape in Na_2

As an example of the one-plus-one arrangement we first consider the intense field dissociation of Na_2 , where excitation is out of a previously populated level $|\epsilon_i\rangle$ of the $^3\Pi_u$ state. In this case the one-photon absorption (Fig. 1) generates products $\text{Na}(3s)+\text{Na}(4s)$ and $\text{Na}(3s)+\text{Na}(3p)$. The relevant electronic potentials and dipole transition functions throughout this paper are taken from Ref. [26].

Note first the characteristics of dissociation with a single CW laser of frequency ω_1 . Numerous numerical computations [18] show that the computed line shape $A(\epsilon, q, n_1 - 1|\epsilon_i, n_1)$ for both the $\text{Na}(3s) + \text{Na}(3p)$ and $\text{Na}(3s) + \text{Na}(4s)$ products are similar in structure, displaying a series of non-Lorentzian peaks and dips corresponding to stimulated emission to, and absorption from, various v, J states. The line shapes are found to be relatively insensitive to the frequency ω_1 . The situation is quite different when we consider dissociation in the presence of two lasers, one of frequency ω_1 and one of frequency ω_2 , arranged as shown in Fig 1. The first laser couples the initially populated $|\epsilon_i\rangle$ state to the continuum and the second embeds initially empty states $|\epsilon_j\rangle$ into the continuum (see Fig. 1). Only those $|\epsilon_j\rangle$ that are located around $\epsilon_i + \hbar(\omega_1 - \omega_2)$ are found to be effectively excited and dissociated. Typical lineshapes are shown in Figs. 3 and 4 which display $\log A(\epsilon, q, N_f|\epsilon_i, N_i)$ vs. ϵ for

products $\text{Na}(3p)+\text{Na}(3s)$ and $\text{Na}(4s)+\text{Na}(3s)$, for two values of ω_1 with the same ω_2 . In Fig. 3, $\omega_1 = 15,617 \text{ cm}^{-1}$; in Fig. 4 $\omega_1 = 15,683 \text{ cm}^{-1}$. The ω_1 laser is sufficiently energetic to dissociate $v \geq v_i = 18$ states of the $^3\Pi_u$ electronic state, and the ω_2 laser ($\omega_2 = 14,591 \text{ cm}^{-1}$, $I_2 = 3.51 \times 10^{10} \text{ W/cm}^2$) can dissociate levels $v \geq 26$ of the $^3\Pi_u$ to both products. To expose the essential physics only $J = 0$ of the bound manifold and $J = 1$ of the continua are included in the computation and the satellite terms are not included. It is clear that with both ω_1 and ω_2 lasers on the line shape is dependent on the asymptotic channel [compare curves (a) and (b) within each of Figs. 3 and 4]. This channel dependence, in accord with Eq.(40), results from the interference characteristics of the multiple dissociation pathways induced by ω_1 and ω_2 . Also evident is a dependence on the frequency ω_1 [compare Fig. 3 with Fig. 4]. This behavior is in direct contrast to the case where only the ω_1 laser is operating, where the line shapes are not sensitive to either the product channel index q or to the frequency ω_1 .

The detailed nature of Figs. 3 and 4 are of interest. They show a series of double peak structures, associated with the dressed states $v = 18$ and $v = 26$ pair (the first double peak), the $v = 19$ and $v = 27$ pair (the second double peak), etc. of the $^3\Pi_u$ state. The ω_1 in Fig. 3 is such that the detuning $\Delta = \hbar(\omega_1 - \omega_2) + \varepsilon_{v=18} - \varepsilon_{v=26}$ is less than 0, while in Fig. 4, Δ is greater than zero. As a consequence the dominant peak (arising from the $v=18$ state) is located on the left in Fig. 3, and on the right in Fig. 4, of the $v = 26$ peak. The dip in the middle of the two peaks results from destructive interference between the two pathways. A similar explanation applies to the second and third sets of peaks. Note that while the locations of the peaks are independent of the channel index, the ratio of the heights of the peaks and the locations of the dips strongly depend on the laser frequencies and on the channel index q . This being the case, we can control the channel specific line shape $A(\varepsilon, q, N_f | \varepsilon_i, N_i)$ by varying ω_1 . For example, a comparison of Figs. 3 and 4 shows that increasing ω_1 shifts the dominant peaks to higher ε , with products at $\varepsilon \approx 9030 \text{ cm}^{-1}$ strongly enhanced and products at $\varepsilon \approx 8980 \text{ cm}^{-1}$ suppressed. The line shape can also be changed by varying laser intensities as discussed elsewhere [18].

In Figs. 3-4, rotational and satellite contributions were set to zero to expose the basic interference effect. Including rotations leads to additional peaks in the line shape. We discuss the effect of rotational contributions to the control of the total dissociation yields below. Here we focus on the effect of satellite contributions.

The satellite contributions are defined as those contributions which cannot be controlled. They can, however, be minimized by proper choice of the laser intensities and frequencies. Figure 5 shows an example of the satellite contributions to the line shape for the same laser parameters as in Fig. 3, except for ω_2 which is set at $13,964 \text{ cm}^{-1}$. The results in Fig. 5 show the product emerging in three distinct ε regions. The line shapes on the far right ($10500 < \varepsilon < 10900 \text{ cm}^{-1}$) correspond to $A(\varepsilon, q, n_1 - 2, n_2 + 1 | \varepsilon_i, n_1, n_2)$, resulting from the dissociation of the $v \geq 31$ states by ω_1 , which produces both Na(3p)+Na(3s) [curve (a)] and Na(4s)+Na(3s) [curve (b)]. The line shape on the far left ($7300 < \varepsilon < 7700 \text{ cm}^{-1}$) shows $A(\varepsilon, q, n_1, n_2 - 1 | \varepsilon_i, n_1, n_2)$, resulting from the dissociation of $v \geq v_i = 18$ by ω_2 , which is only sufficiently energetic to produce Na(3p)+Na(3s) atoms. The line shape in the middle, $A(\varepsilon, q, n_1 - 1, n_2 | \varepsilon_i, n_1, n_2)$, which resembles that in Fig. 3, comes from interference contributions, i.e. the dissociation of $|\varepsilon_i\rangle$ by ω_1 plus that of $|\varepsilon_j\rangle$ by ω_2 . Note that while the satellite contributions display the characteristic double-peak structure, due to the resonant coupling of the $|\varepsilon_i\rangle$ and $|\varepsilon_j\rangle$ via the continuum, they are not channel-dependent [compare the curves at the far right to those in the middle of Fig. 5]. However, as long as the interference contributions substantially exceed the satellite contributions we can expect channel-sensitive control over the line shape by tuning the laser frequencies.

B. Control of the Branching Ratios in Na₂

Results in the last section show that two high field lasers with appropriate frequencies allow for novel and effective q dependent control over $A(\varepsilon, q, N_f | \varepsilon_i, n_1, n_2)$. Hence, in accord with Eq.(17), control over the yield $P(q)$ into different products q is expected. A sample of our extensive computations [17,18] displaying yield control for various laser frequencies and

intensities is provided below.

To demonstrate the essence of yield control we again first ignore rotational effects and satellite contributions. Figure 6 shows the total dissociation probability $P(q)$ as a function of ω_1 for both the Na(3s)+Na(3p) [curve (a)] and Na(3s)+Na(4s) [curve (b)] products for the same parameters as in Fig. 3. The vertical dotted line indicates the value of ω_1 at which $\hbar(\omega_1 - \omega_2) = \varepsilon_{v=26} - \varepsilon_{v=18}$ with $J = 0$. For comparison we also plot, as curves (c) and (d), $P(q)$ for Na(3s)+Na(3p) and for Na(3s)+Na(4s) for the case where the ω_2 laser is shut off. In the one laser case (ω_2 intensity set equal to zero) $P(q)$ is seen to be flat as ω_1 is varied, in contrast to the two laser case where it oscillates strongly. The oscillations for the two product probabilities in Fig. 6 are seen to be out of phase, with the sum of dissociation probabilities being close to 0.94. Thus, essentially total dissociation is obtained, with the ratio of the products varying widely between the two channels as ω_1 is tuned. For example, the probabilities of producing Na(3s)+Na(3p) and Na(3s)+Na(4s) at $\omega_1 = 15,670 \text{ cm}^{-1}$ is 10% and 84%, respectively, but the reverse situation occurs at $\omega_1 = 15,775 \text{ cm}^{-1}$, where 86% of product is Na(3s)+Na(3p). Thus, varying ω_1 provides a straightforward method of extensive control over the branching ratio into final product channels.

Figure 6 shows two periods of $P(q)$; the distance between the peaks (or dips) corresponds to the vibrational spacing between $v = 26$ and 27. The origin of this oscillatory behavior is readily evident: as ω_1 increases by an amount equal to the vibrational spacing with ω_2 fixed, $|\varepsilon_i\rangle$ couples to the next bound state $|\varepsilon_{j+1}\rangle$. In essence, then, any of initially empty bound states $|\varepsilon_j\rangle$ can be used as an intermediary in a path which interferes with the direct dissociation from $|\varepsilon_i\rangle$. This convenient feature gives the experimentalist a wide range of possible choices of ω_1 and ω_2 , with no loss of control.

Changing the laser power alters the linewidths of the power broadened bound states, affecting the control. By reducing the laser power the linewidths narrow and $|\varepsilon_i\rangle$ decouples from $|\varepsilon_j\rangle$ when the sum of their linewidths becomes smaller than the detuning Δ . Sample effects due to intensity variation are discussed in Reference [18], as is the demonstration that tuning ω_2 with fixed ω_1 results in equally successful control.

Significantly, additional computations show that the results all of our control computations are insensitive to the relative phase of the ω_1 and ω_2 fields, a result which is consistent with the theory discussed above. As a consequence, *the two lasers need not be phase coherent in order to achieve control*. Any drift or jitter in the laser phase in a practical environment will not alter the outcome of the control experiment, simplifying experimental conditions considerably.

Consider now the effect of including rotational states and satellite terms. Figure 7 shows results which include both rotational terms and satellite contributions. Here $v_i = 19, J = 0$ of the $^3\Pi_u$ state. Rotational couplings among the $J = 0, 2$ of the $^3\Pi_u$ and the $J = 1, 3$ of the $1^3\Pi_g$ and $2^3\Sigma_g$ are included in the computation. Control over the product probability remains extensive, with the ratio of the probability of forming $\text{Na}(3s) + \text{Na}(3p)$ to $\text{Na}(3s) + \text{Na}(4s)$ ranging from 0.3 to 3 as ω_1 is tuned.

IV. CONTROL OF PHOTODISSOCIATION: TWO PLUS ONE ARRANGEMENT

A. Control of the Line Shape in Na_2

In the above scenario one photon excitation is sufficient to excite the system to the continuum. In many molecules, and particularly in a thermal environment, it is advantageous to do two photon excitation through an intermediate resonance. This allows selective excitation of molecules with initial thermally distributed populations. In this section we display control of such a two photon dissociation process. Computations are presented for Na_2 , where the initial state is the ground electronic state, unlike the previous section where we assume that the Na_2 molecule was previously prepared in a bound level of the electronically excited $^3\Pi_u$ state.

In the two photon scenario the molecule, initially in a bound vib-rotational level $|\varepsilon_i\rangle$ of the ground electronic state absorbs two ω_1 photons and in doing so undergoes a transition to the continuum $|\varepsilon, m, q^-\rangle$ via resonant intermediate states $|\varepsilon_{j_1}\rangle$. The latter are themselves

comprised of a superposition of ro-vibrational states associated with the $A^1\Sigma_u$ and $b^3\Pi_u$ electronic curves, a consequence of spin-orbit coupling [27]. Control over the dissociation is achieved by applying another laser of frequency ω_2 (Fig. 2) which couple the continuum to a previously unpopulated level. The continuum states reached in the two photon excitation can be either of singlet or triplet character but the predominant contributions to the products $\text{Na}(3p)+\text{Na}(3s)$, $\text{Na}(4s)+\text{Na}(3s)$ and $\text{Na}(3d)+\text{Na}(3s)$ are found, in the energy regime of interest, to come from the $1^3\Pi_g$, $2^3\Sigma_g$ and $2^3\Pi_g$ states [27] shown in Fig. 2. Our computations, however, also include the electronic states $1^1\Sigma_g$, $1^1\Pi_g$, and $3^1\Sigma_g$, which correlates asymptotically with the $\text{Na}(3s)+\text{Na}(3p)$ atoms, and the $2^1\Sigma_g$, which asymptotically correlates with the $\text{Na}(3s)+\text{Na}(4s)$ product [27].

Consider first the line shape $A(\varepsilon, q, n_1 - 2|\varepsilon_i, n_1)$ of ‘pure’ two photon dissociation resulting from illumination with a single CW laser of frequency ω_1 , i.e. with the intensity of the laser ω_2 set to zero. Under these circumstances line shapes for all the products are found to be similar in structure [19]. The situation is quite different in the presence of both lasers. Figures 8 and 9 show the line shape as $\log A(\varepsilon, q, n_1 - 2, n_2|\varepsilon_i, n_1, n_2)$ vs. ε for two different values of ω_2 . The solid line corresponds to the $\text{Na}(3p)+\text{Na}(3s)$ dissociation product and the dashed line depicts the $\text{Na}(4s)+\text{Na}(3s)$ products. Here the intensity of the control laser is $I_2 = 3.5 \times 10^{10} \text{ W/cm}^2$, at the frequency $\omega_2 = 14939.6 \text{ cm}^{-1}$ in Fig. 8 and 14961.5 cm^{-1} in Fig. 9. As in the above scenario of greatest importance is the fact that the ω_2 dependence of the line shape differs for the two product channels (compare dashed and solid curves within the same figure), and that the lineshapes are ω_2 dependent (compare Fig. 8 with Fig. 9).

The introduction of the ω_2 laser results in a four-peak line shape structure which are combined contributions from the dressed states $|\varepsilon_i\rangle$, $|\varepsilon_{j_2}\rangle$ and $|\varepsilon_{j_1}\rangle$. The structure is easily understood. The first, third and fourth peaks in the region $26350 < \varepsilon < 26500 \text{ cm}^{-1}$ are associated, from the left to the right, with the resonant contributions of the dressed $|\varepsilon_i\rangle$ and $|\varepsilon_{j_1}\rangle$, respectively, the latter being a doublet due to spin-orbit coupling [27]. With the given laser frequency, the $|v = 0, J = 0, 1^1\Sigma_g\rangle$ ($|\varepsilon_i\rangle$) is in quasi-resonance with $|v = 14, J = 1, 1^1\Sigma_u\rangle$, which forms a doublet by spin-orbit coupling with $|v = 19, J = 1, 3^1\Pi_u\rangle$. The dissociation

of these states contribute to the three peaks. These peaks occur in the absence of the ω_2 laser. The additional fourth peak, which appears as the second in the set of four peaks, arises from the dissociation of the $|\varepsilon_{j_2}\rangle$ level. For example, the dissociation of $|v = 28, J = 1, {}^3\Pi_u\rangle$ contributes the peak at $\varepsilon = 26433 \text{ cm}^{-1}$ in Fig. 9 and at $\varepsilon = 26453 \text{ cm}^{-1}$ in Fig. 10. A comparison of these figures show that increasing ω_2 causes a blue-shift in the position of the second peak of the four-peak structure, as well as a change in the peak intensities. The profound effect of the ω_2 laser on the line shape is due to the interference of the pathway induced by ω_2 with the original 2-photon dissociation path.

Computations in Figs. 8 and 9 only include $J = 0$ of ${}^1\Sigma_g$, $J = 1$ of ${}^1\Sigma_u$ and ${}^3\Pi_u$, and $J = 0$ of the continua. In cases where more rotational states contribute, as with initial higher J , the multiple rotational states lead to additional peaks in the line shape [19].

In this instance, unlike the one-plu-one arrangement, varying ω_1 is not an effective way to control the photodissociation since maintaining resonant excitation with the intermediate bound state is useful to enhance the photodissociation probability.

B. Control of the Branching Ratios

Integrating $A(\varepsilon, q, n_1 - 2, n_2 | \varepsilon_i, n_1, n_2)$ over ε [Eq. (17)] for various ω_2 gives $P(q)$ as a function of ω_2 . Having demonstrated that control over the line shape is indeed possible, we now show that extensive control over the relative cross section for production of the different products q can be achieved as well.

Figure 10 shows the channel specific dissociation probability $P(q)$ as a function of ω_2 for the Na(3s)+Na(3p) [curve (a)], Na(3s)+Na(4s) [curve (b)] and Na(3s)+Na(3d) [curve (c)] products, where the initial state is $v_i = 0, J_i = 0$ of the ${}^1\Sigma_g$ state. The laser parameters are: $\omega_1 = 17880.2 \text{ cm}^{-1}$, $I_1 = 3.16 \times 10^8 \text{ W/cm}^2$, and $I_2 = 2.75 \times 10^9 \text{ W/cm}^2$. To demonstrate the essential physics we only include the rotation states $J = 0$ of ${}^1\Sigma_g$, $J = 1$ of ${}^1\Sigma_u$ and ${}^3\Pi_u$, and $J = 0$ of the continua in the computation (the inclusion of rotational states are discussed below). For most values of ω_2 , the Na(3s)+Na(3d) product dominates. For example, in Fig.

10 with $\omega_2=13340 \text{ cm}^{-1}$, the probabilities of generating the Na(3s)+Na(3d), Na(3s)+Na(4s) and Na(3s)+Na(3p) products are 11.8 %, 0.24 % and 0.06 %, respectively. These are close to the corresponding values of $P(q)$ for 'pure' 2-photon dissociation with the ω_2 laser off, which are 11 %, 0.3 % and 0.10 %. However, the situation is quite the opposite when ω_2 is tuned to, for example, 13328 cm^{-1} , where the Na(3s)+Na(3p) product cross section is 5.6 times larger than the Na(3s)+Na(3d) (see Fig. 10).

Figure 10 shows that $P(q)$ is an almost periodic function of ω_2 , with the period being the vibrational spacings at energy ε_{j_2} . The change in $P(q)$ as a function of ω_2 results from the change in product distribution induced by ω_2 laser. The strong redistribution among the dissociation products occurs when ω_2 satisfies the equation

$$\varepsilon_{j_2} + \hbar\omega_2 \approx \varepsilon_{j_1} + \hbar\omega_1. \quad (55)$$

That is, the effective overlap between $|\varepsilon_{j_2}\rangle$ and $|\varepsilon_{j_1}\rangle$ strongly enhances the interference between the dissociation pathways, and thus the control at these ω_2 values is profound. With ω_1 fixed, the increase (decrease) in ω_2 by an amount equal to $\varepsilon_{j_2} - \varepsilon_{j_2-1}$ ($\varepsilon_{j_2+1} - \varepsilon_{j_2}$) brings the level $|\varepsilon_{j_2-1}\rangle$ ($|\varepsilon_{j_2+1}\rangle$) close to equality in Eq.(55). Therefore $P(q)$ as a function of ω_2 shows an almost periodic structure, with the period equal to the vibrational spacing. This is indeed evident in Figure 10. Here the distance in ω_2 values between the two Na(3s)+Na(3d) dips corresponds to the vibrational spacing between $v = 89, J=1$ and $v = 90, J=1$ of the $^3\Pi_u$. In essence, then, as in the one plus one arrangement, any of the unpopulated bound states $|\varepsilon_{j_2}\rangle$ can be used to provide the second pathway which interferes with the direct two photon dissociation pathway from $|\varepsilon_i\rangle$. This is a convenient feature which gives the experimentalist a wide range of possible choices of ω_2 , with no loss of control.

Initiating excitation from states with higher initial J leads to more complex control patterns. Figure 11 demonstrates such an example, which shows $P(q)$ as a function of ω_2 for each of the three products Na(3s)+Na(3p) [denoted $P(3p)$], Na(3s)+Na(4s) [denoted $P(4s)$] and Na(3s)+Na(3d) [denoted $P(4s)$] products. The initial state $|\varepsilon_i\rangle$ is chosen to be $v_i = 0$ and $J_i = 32$ (Fig. 12). The computations include the $J = 31, 33$ of the $^1\Sigma_u$ and

$^3\Pi_u$ and the $J = 32$, $J = 34$ of the continua, with $\omega_1 = 17720.8 \text{ cm}^{-1}$, and the intensities $I_1 = 1.72 \times 10^8 \text{ W/cm}^2$ and $I_2 = 2.84 \times 10^8 \text{ W/cm}^2$.

In Figs. 11(a) and 11(b) there are four peaks in $P(3p)$ and $P(4s)$, and in Fig. 11(c) there are four dips in $P(3d)$, as ω_2 is tuned. Similar to the structure in Figs. 10, it is due to the contributions from numerous rotational states. Given the relatively weak laser intensities here, the power-broadening in each of the rotational states is found smaller than the spacing between the high rotational states $J = 31$ and $J = 33$. Thus, as ω_2 is varied, the two rotational components, $J_2=31$ and 33 , of the $|v_{j_2}\rangle$ level, successively overlap with the two rotational components, $J_1 = 31, 33$, of the $|v_{j_1}\rangle$, generating the four-peak structure in the controlled dissociation probabilities. The first peak in Figs. 11(a) and 11(b) (and the first dip in Fig. 11(c)) is due to the overlap of the dressed $J_1 = 31$ and $J_2 = 33$ states, the second due to $J_1 = 31$ and $J_2 = 31$, and the third due to $J_1 = 33$ and $J_2 = 33$. This behavior is typical of that observed in the numerous computations which we have performed.

Further computations show that excitations out of different initial states produce curves similar to those in Fig. 11, but with extrema at different frequencies. Thus, excitations out of a thermally weighted distribution of initial states is expected to show control, but with numerous peaks and valleys, as a function of ω_2 . This is indeed in accord with recent experiments [9].

V. SUMMARY

We have described a general approach to controlling molecular photodissociation using intense laser fields. The approach relies upon the generation of numerous interfering excitation pathways to the continuum by two lasers whose frequencies are resonant with one and two photon absorption to the continuum. The resultant technique allows for control over molecular photodissociation without concern for experimental difficulties associated with maintaining relative laser coherence and cooling the molecules to reduce thermal population effects. In applications to Na_2 the resultant control is seen to be extensive, allowing for

significant redistribution amongst products by varying the frequencies of the incident lasers.

ACKNOWLEDGMENTS

This work was supported by the U.S. Office of Naval Research under contract number N00014-90-J-1014.

REFERENCES

* Permanent Address: Chemical Physics Department, Weizmann Institute of Science, Rehovot, Israel

- [1] P. Brumer and M. Shapiro, *Accounts of Chem. Res.* **22**, 407 (1989); P. Brumer and M. Shapiro, *Ann. Rev. Phys. Chem.* **43**, 257 (1992); M. Shapiro and P. Brumer, *Int. Reviews Phys. Chem.* **13**, 187 (1994).
- [2] M. Yu. Ivanov, P.B. Corkum and P. Dietrich, *Laser Physics* **3**, 375 (1993).
- [3] A.D. Bandrauk, J-M. Gauthier and J.F. McCann, *Chem. Phys. Lett.* **200**, 399 (1992).
- [4] D.J. Tannor, and S.A. Rice, *Adv. Chem. Phys.* **70**, 441 (1988); S. Tersigni, P. Gaspard and S.A. Rice, *J. Chem. Phys.* **93**, 1670, (1990); S. Shi, and H. Rabitz, *J. Chem. Phys.* **92**, 364 (1990); J.L. Krause, R.M. Whitnell, K.R. Wilson, Y. Yan and S. Mukamel, *J. Chem. Phys.* **99**, 6562 (1993)
- [5] M. Shapiro, J. Hepburn and P. Brumer *Chem. Phys. Lett.* **149**, 451 (1988); C.K. Chan, P. Brumer and M. Shapiro, *J. Chem. Phys.* **94**, 2688 (1991).
- [6] C. Chen, Y-Y. Yin, and D.S. Elliott, *Phys. Rev. Lett.*, **64**, 507 (1990); S-P. Lu, S.M. Park, Y. Xie, and R.J. Gordon, *J. Chem. Phys.*, **96**, 6613 (1992); E. Dupont, P.B. Corkum, H.C. Liu, M. Buchanan and Z.R. Wasilewski, *Phys. Rev. Letters* (submitted);
- [7] G. Kurizki, M. Shapiro and P. Brumer, *Phys. Rev. B* **39**, 3435 (1989).
- [8] J. Krause, M. Shapiro and P. Brumer, *J. Chem. Phys.* **92**, 1126 (1990).
- [9] I. Sofer, A. Shnitman, I. Golub, A. Yogeve, M. Shapiro, Z. Chen and P. Brumer, (manuscript in preparation)
- [10] T. Nakajima and P. Lambropoulos, *Phys. Rev. Lett.*, **70**, 1081 (1993).
- [11] H.G. Muller, P.H. Bucksbaum, D.W. Schumacher and A. Zavriyev, *J. Phys. B* **23** 2761 (1990); R.M. Potvliege and P.H.G. Smith, *J. Phys. B* **25** 2501 (1992).

- [12] K.J. Schafer and K.C. Kulander, *Phys. Rev. A* **45**, 8026 (1992).
- [13] E. Charron, A. Guisti-Suzor and F.H. Mies, *Phys. Rev. Lett.* **71**, 692 (1993).
- [14] See, for example, P.L. Knight, M.A. Lauder and B.J. Dalton, *Phys. Rep.* **190**, 1 (1990), and references therein.
- [15] O. Faucher, D. Charalambidis, C. Fotakis, J. Zhang and P. Lambropoulos, *Phys. Rev. Lett.*, **70**, 3004 (1993).
- [16] K.J. Boller, A. Imamoglu and S.E. Harris, *Phys. Rev. Lett.*, **66**, 2593 (1991).
- [17] Z. Chen, M. Shapiro and P. Brumer, *Chem. Phys. Letters* **228**, 289 (1994).
- [18] Z. Chen, M. Shapiro and P. Brumer, *J. Chem. Phys.*, (in press).
- [19] Z. Chen, M. Shapiro and P. Brumer, *Phys. Rev. A* (submitted).
- [20] P. Brumer and M. Shapiro, *Adv. Chem. Phys.* **60**, 371 (1986).
- [21] M. Shapiro, *J. Chem. Phys.* **56** 2582 (1972).
- [22] M. Shapiro and H. Bony, *J. Chem. Phys.* **83**, 1588 (1985); G. G. Balint-Kurti and M. Shapiro, *Adv. Chem. Phys.* **60** 403, (1986), Z. Chen, M. Shapiro, and P. Brumer, *J. Chem. Phys.*, **98**, 8647 (1993).
- [23] A. D. Bandrauk and O. Atabek, *Adv. Chem. Phys.* **73** 823, J. O. Hirschfelder, Ed, (Wiley, New York, 1989); S. Miret-Artes, O. Atabek and A. D. Bandrauk, *Phys. Rev. A* **45**, 8056 (1992).
- [24] C. Cohen-Tannoudji, J. Dupont-Roc and G. Grynberg, *Atom-Photon Interactions* (John Wiley & Sons, 1992).
- [25] U. Fano, *Phys. Rev.* **124**, 1866 (1961).
- [26] The potential curves and the relevant electronic dipole moments are from I. Schmidt, Ph.D. Thesis, Kaiserslautern University, 1987; W. Meyer, private communication.

[27] Z. Chen, M. Shapiro and P. Brumer, J. Chem. Phys. **98**, 8647 (1993).

FIGURES

FIG. 1. Na_2 potential energy curves. Only the major contributors to the one plus one controlled dissociation are included in the figure. For additional curves included in the computation, see Ref. 17. Two lasers, of frequencies ω_1 and ω_2 , couple the dissociation continua to the bound states $|\varepsilon_i\rangle$ and $|\varepsilon_j\rangle$ in the $^3\Pi_u$ state, where the $|\varepsilon_i\rangle$ is initially populated and the $|\varepsilon_j\rangle$ are initially unpopulated. Here $\Delta = \hbar(\omega_1 - \omega_2) + \varepsilon_i - \varepsilon_j$.

FIG. 2. Relevant potential energy curves of Na_2 included in the computations for two plus one arrangement. The resonant two photon dissociation occurs by coupling the bound states $|\varepsilon_i\rangle$ with the ω_1 laser to the dissociation continua via intermediate states $|\varepsilon_{j_1}\rangle$. The control laser ω_2 couples the continua to the bound states $|\varepsilon_{j_2}\rangle$ which is initially unpopulated.

FIG. 3. $\log A(\varepsilon, q, n_1 - 1, n_2 | \varepsilon_i, n_1, n_2)$ vs. ε , with two lasers on. (a) $\text{Na}(3s) + \text{Na}(3p)$ product and (b) $\text{Na}(3s) + \text{Na}(4s)$ product. Here $\omega_1 = 15,617 \text{ cm}^{-1}$, $\omega_2 = 14,591 \text{ cm}^{-1}$, $I_1 = 8.7 \times 10^9 \text{ W/cm}^2$ and $I_2 = 3.5 \times 10^{10} \text{ W/cm}^2$, and the detuning $\Delta = \hbar(\omega_1 - \omega_2) + \varepsilon_{v=18} - \varepsilon_{v=26} < 0$. Initially the molecule is in $v_i = 18, J = 0$ of the $^3\Pi_u$ state. Rotational and satellite couplings are set to zero.

FIG. 4. As in Figure 3, but with $\omega_1 = 15,683 \text{ cm}^{-1}$ so that $\Delta = \hbar(\omega_1 - \omega_2) + \varepsilon_{v=18} - \varepsilon_{v=26} > 0$.

FIG. 5. As in Figure 3, but with $\omega_2 = 13,964 \text{ cm}^{-1}$ and with the inclusion of satellite contributions. The far left displays $A(\varepsilon, q, n_1, n_2 - 1 | \varepsilon_i, n_1, n_2)$, the middle $A(\varepsilon, q, n_1 - 1, n_2 | \varepsilon_i, n_1, n_2)$, and the far right $A(\varepsilon, q, n_1 - 2, n_2 + 1 | \varepsilon_i, n_1, n_2)$.

FIG. 6. $P(q)$ as a function of ω_1 . In (a) and (b) both lasers are on, while in (c) and (d) the ω_2 laser is off. (a) and (c) show the $\text{Na}(3s) + \text{Na}(3p)$ product whereas (b) and (d) show that $\text{Na}(3s) + \text{Na}(4s)$ product. The molecule is initially in $v_i = 18, J = 0$ of the $^3\Pi_u$ state; rotational and satellite terms are neglected.

FIG. 7. Probability of forming (a) Na(3s)+Na(3p) and (b) Na(3s)+Na(4s) as a function of ω_1 , with $\omega_2 = 13,964 \text{ cm}^{-1}$, $I_1 = 8.7 \times 10^9 \text{ W/cm}^2$ and $I_2 = 3.51 \times 10^{10} \text{ W/cm}^2$. The molecule is initially in $v_i = 19, J = 0$ of the $^3\Pi_u$ electronic state and $\hbar(\omega_1 - \omega_2) + (\varepsilon_{v=19} - \varepsilon_{v=31}) = 0$ at $\omega_1 = 15,514 \text{ cm}^{-1}$. Both satellite terms and rotational couplings are included.

FIG. 8. $\log A(\varepsilon, q, n_1 - 2, n_2 | \varepsilon_i, n_1, n_2)$ vs. ε , with two lasers on. (a) Na(3s)+Na(3p) product and (b) Na(3s)+Na(4s) product. Here $\omega_2 = 14939.6 \text{ cm}^{-1}$, and the intensity $I_2 = 3.5 \times 10^{10} \text{ W/cm}^2$, $\omega_1 = 16154.7 \text{ cm}^{-1}$ and $I_1 = 8.7 \times 10^9 \text{ W/cm}^2$.

FIG. 9. As in Fig. 8, but with $\omega_2 = 14961.5 \text{ cm}^{-1}$.

FIG. 10. $P(q)$ as a function of ω_2 . (a) for the Na(3s)+Na(3p) product, (b) for the Na(3s)+Na(4s) product, and (c) for the Na(3s)+Na(3d) product. The molecule is initially in $v_i = 0, J_i = 0$ of the $^1\Sigma_g$ state. $\omega_1 = 17880.2 \text{ cm}^{-1}$, $I_1 = 3.16 \times 10^8 \text{ W/cm}^2$, and $I_2 = 2.75 \times 10^9 \text{ W/cm}^2$.

FIG. 11. $P(q)$ as a function of ω_2 , with rotational couplings included. (a) for the Na(3s)+Na(3p) product, (b) for the Na(3s)+Na(4s) product, and (c) for the Na(3s)+Na(3d) product. The molecule is initially in $v_i = 0, J_i = 32$ of the $^1\Sigma_g$ state. $\omega_1 = 17720.8 \text{ cm}^{-1}$, $I_1 = 1.72 \times 10^8 \text{ W/cm}^2$, and $I_2 = 2.84 \times 10^8 \text{ W/cm}^2$.

Fig 1

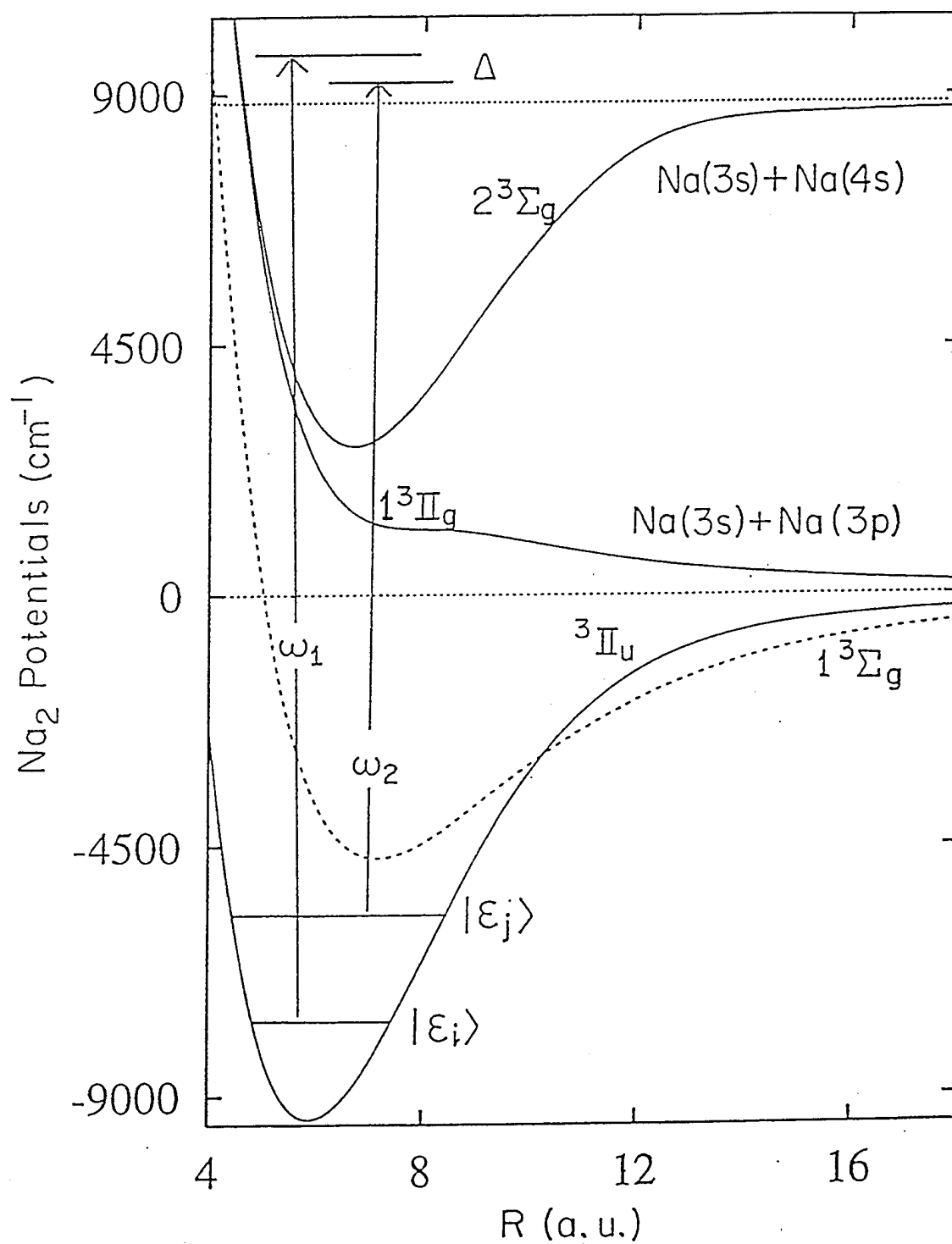


Fig 2

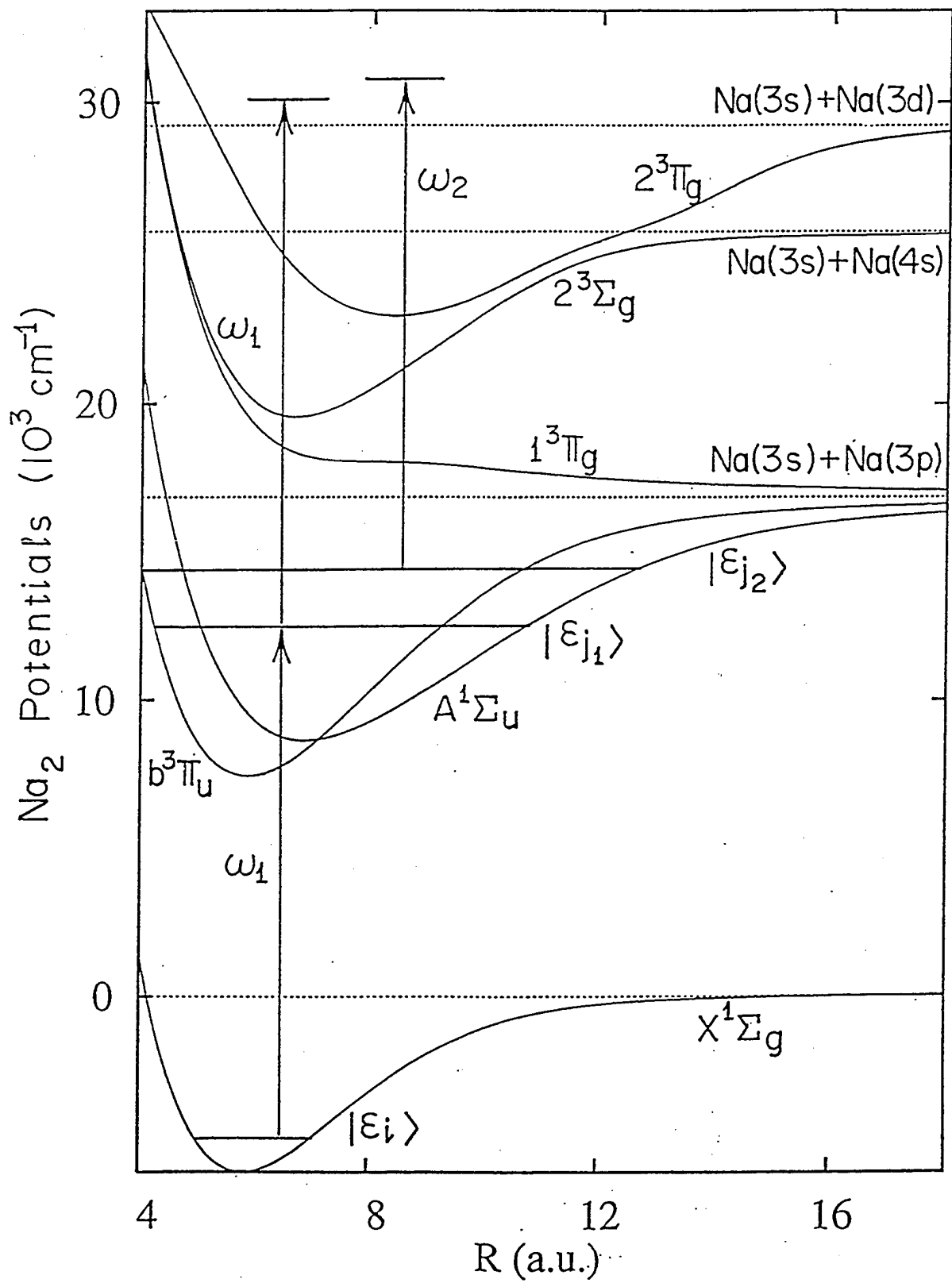
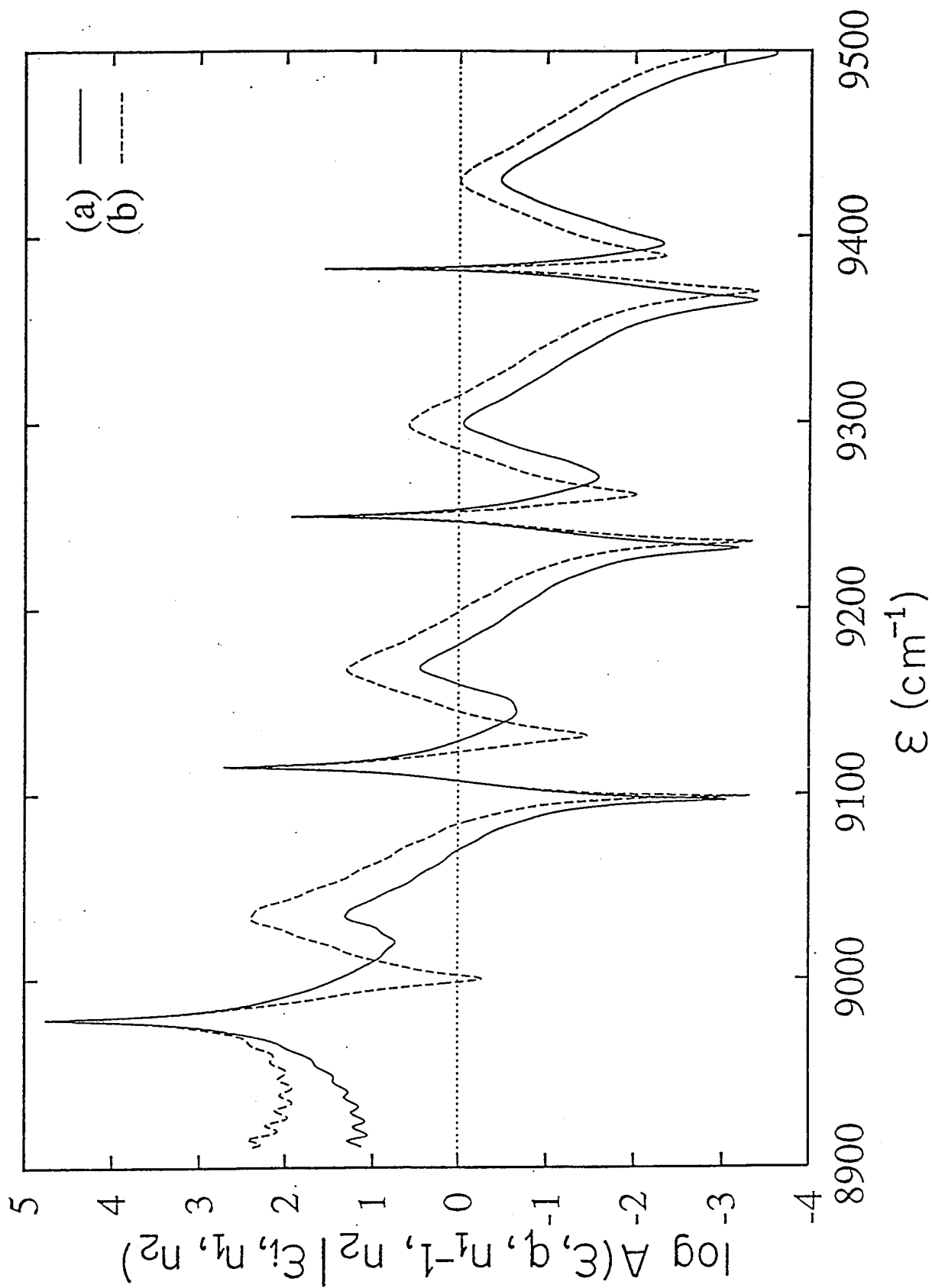
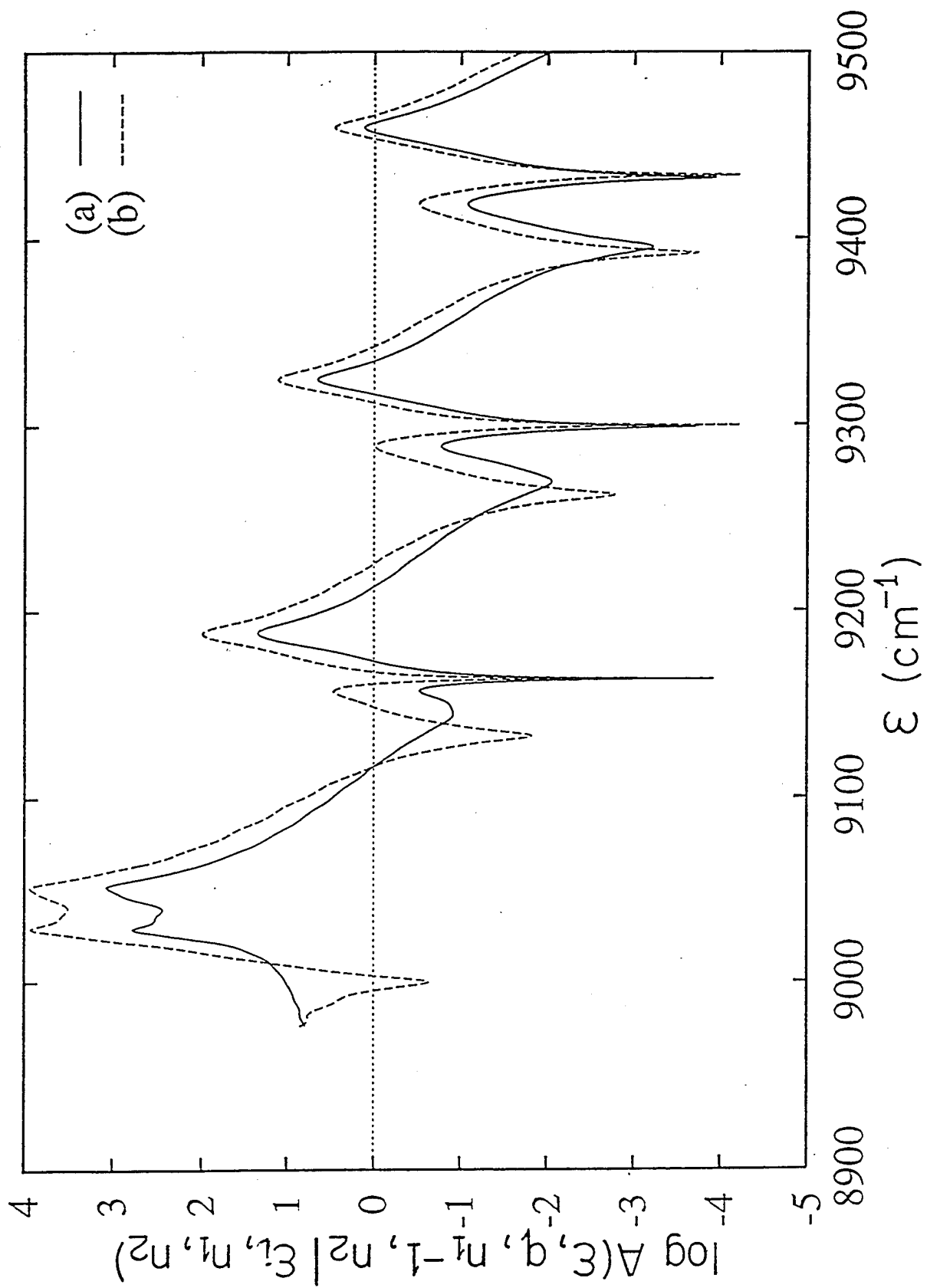
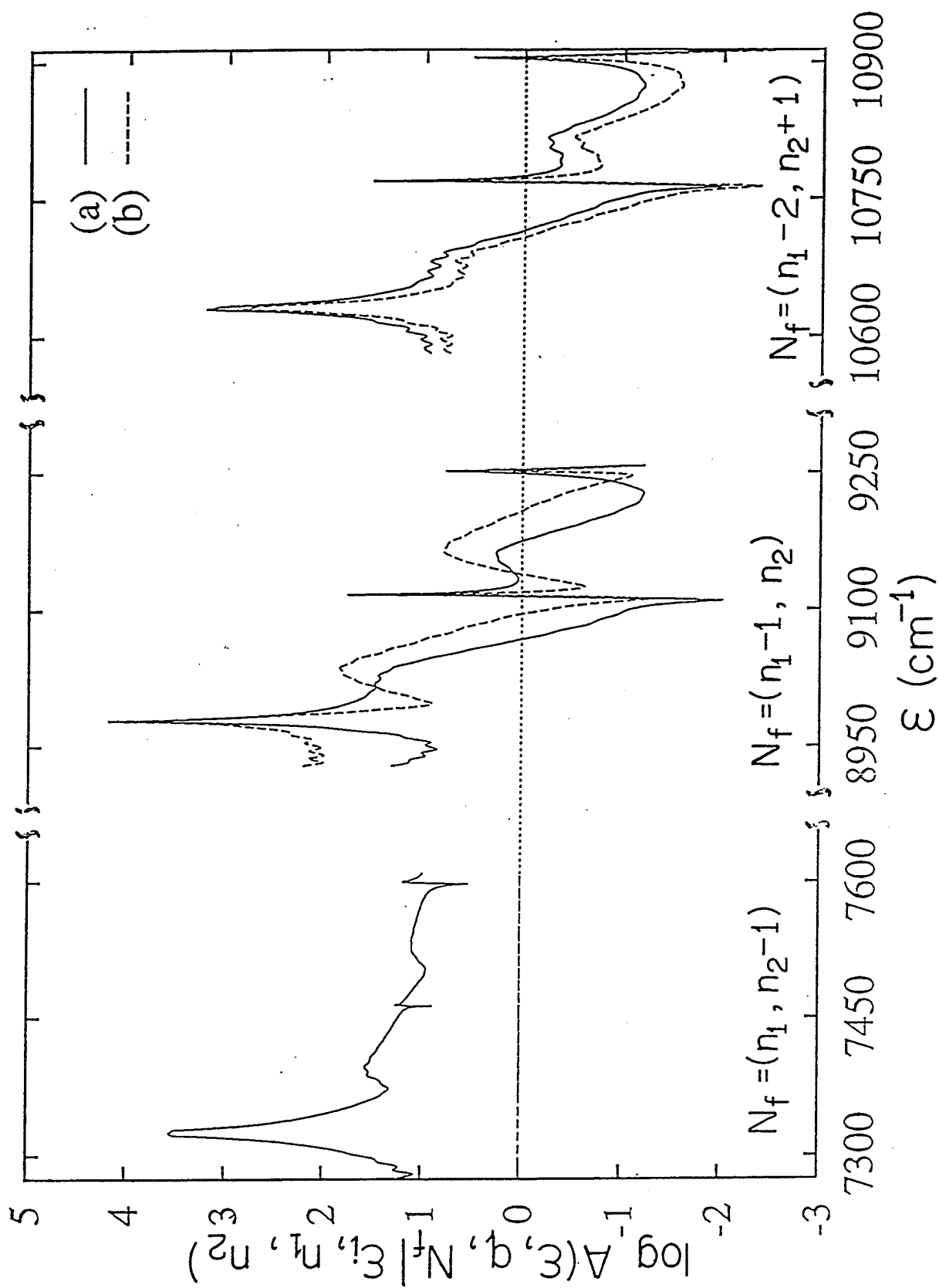


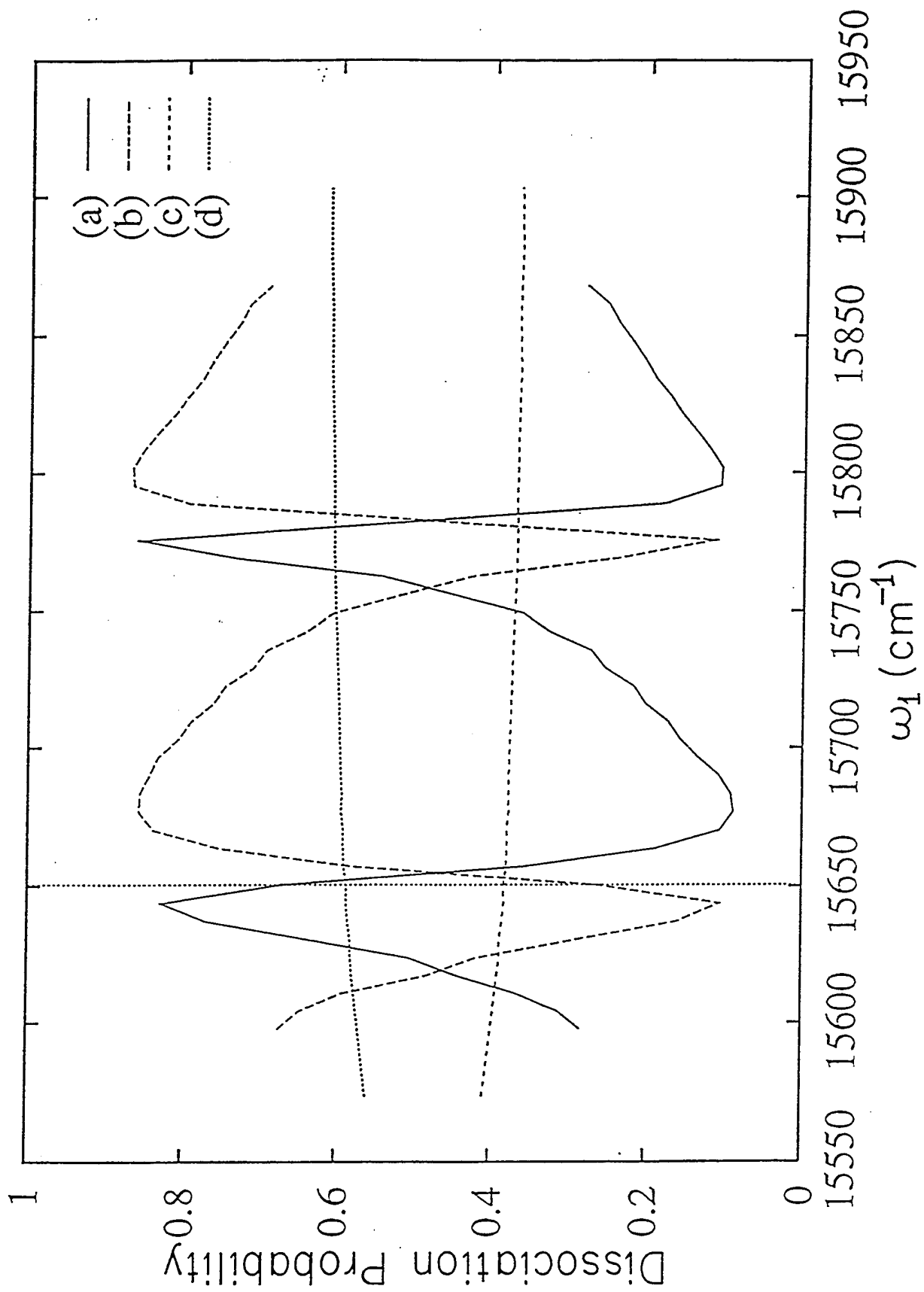
Fig 3

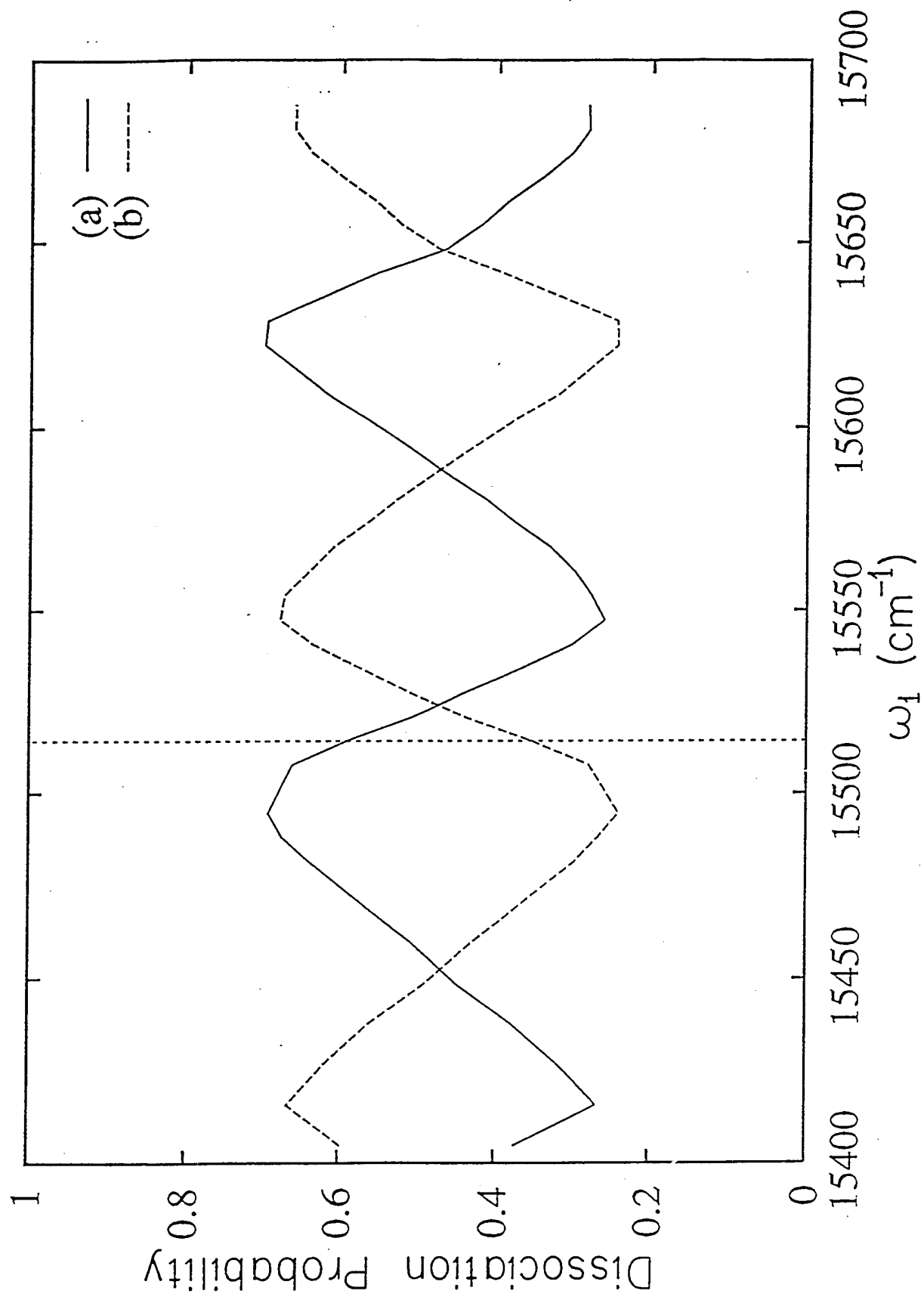




1-6
 4







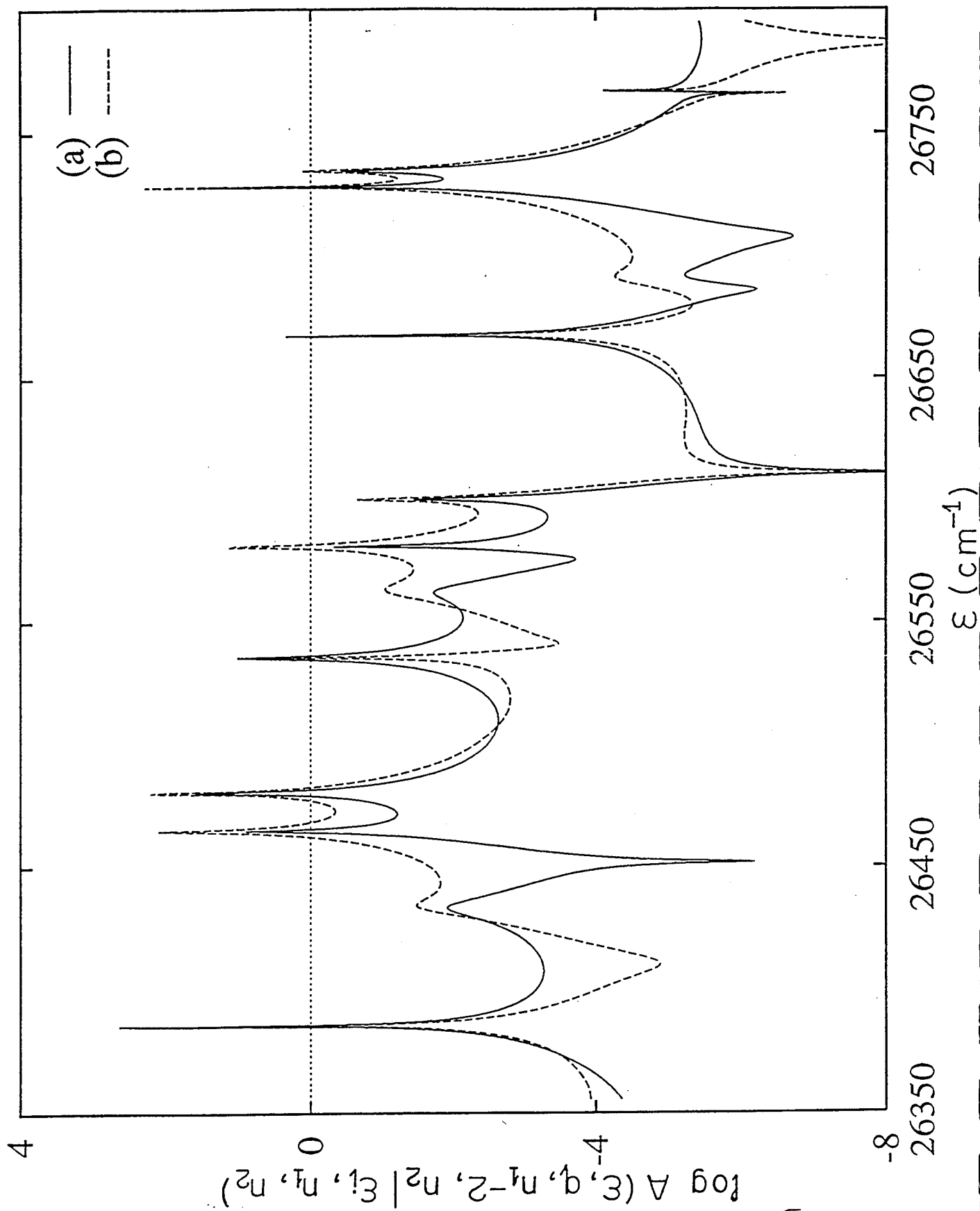
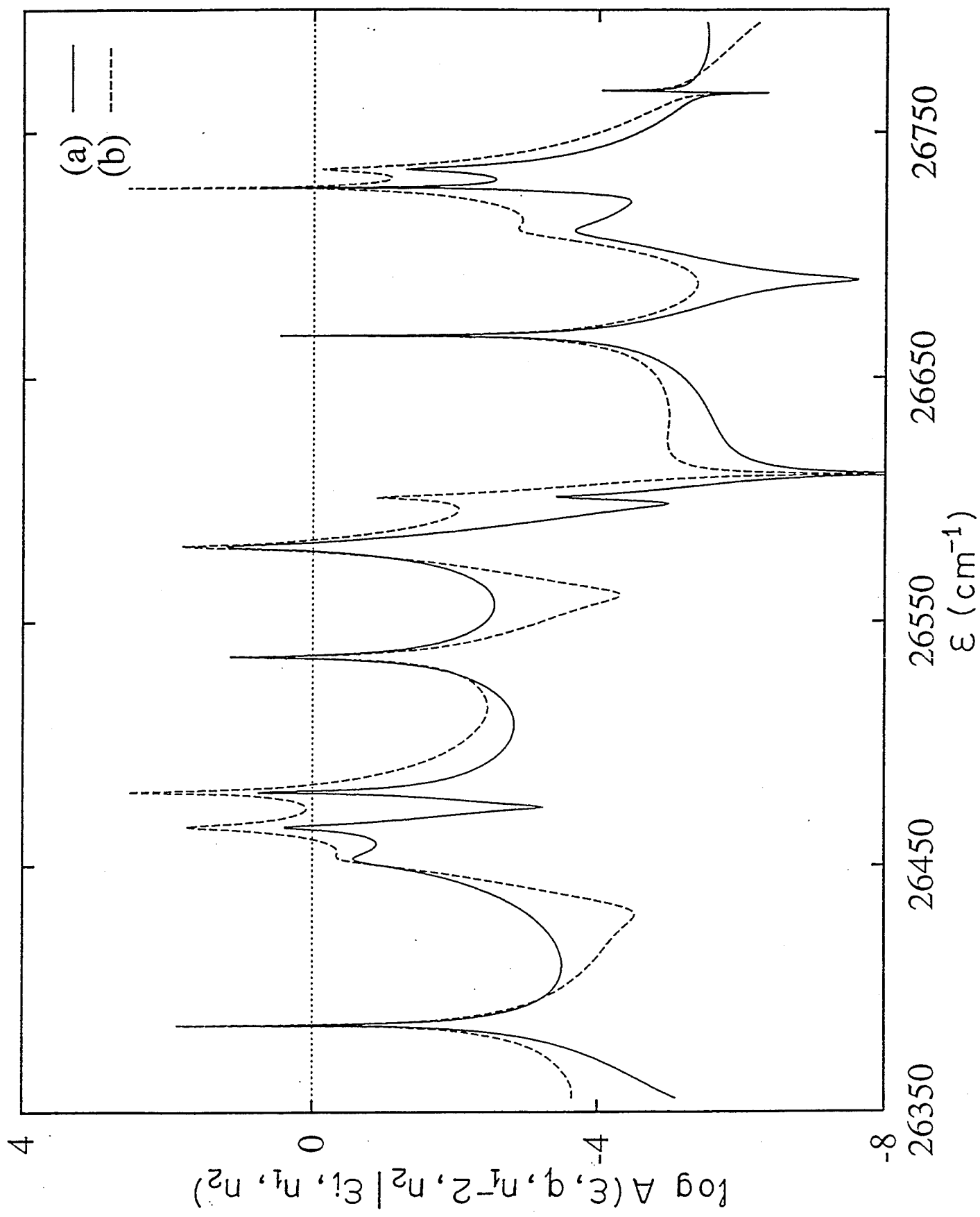
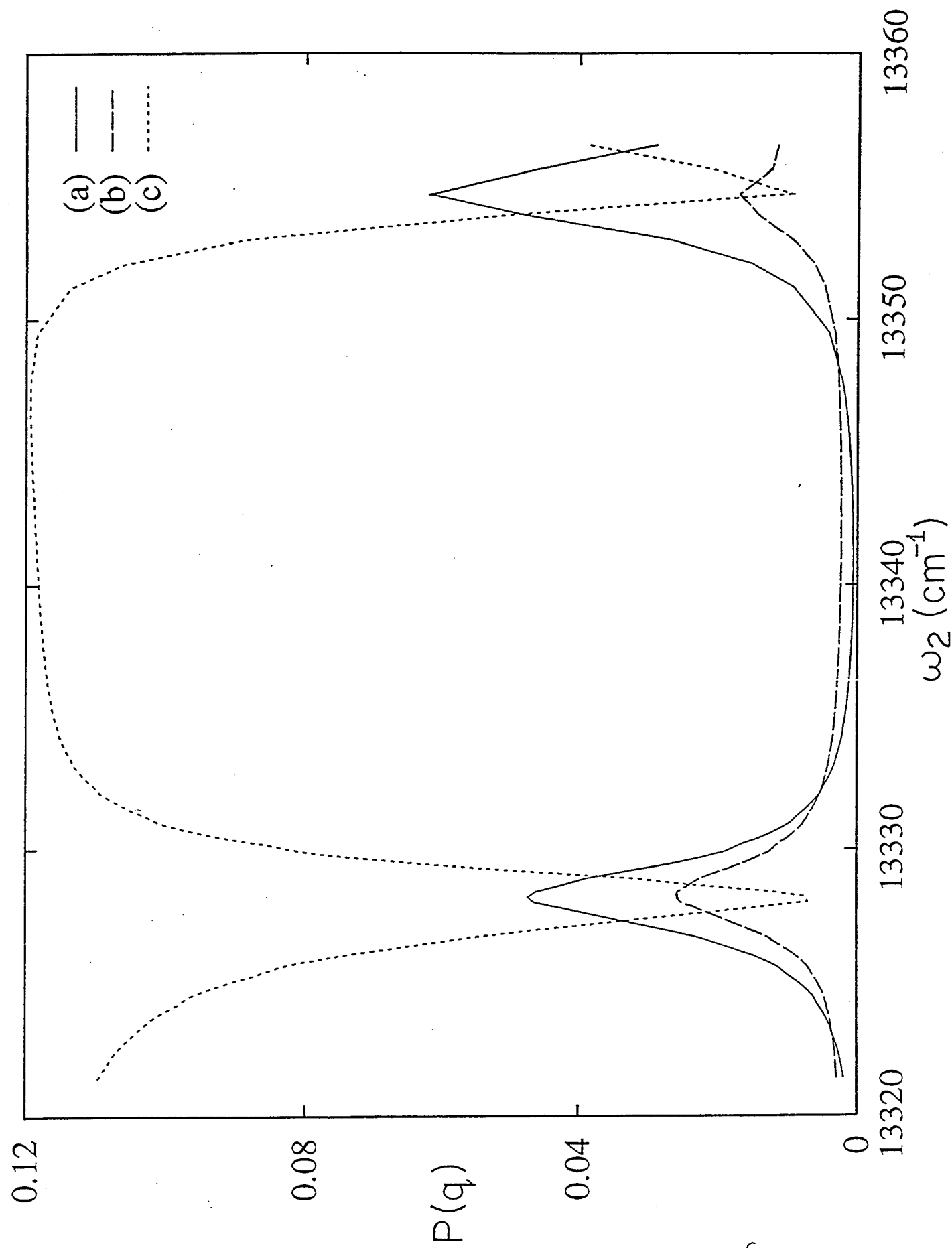
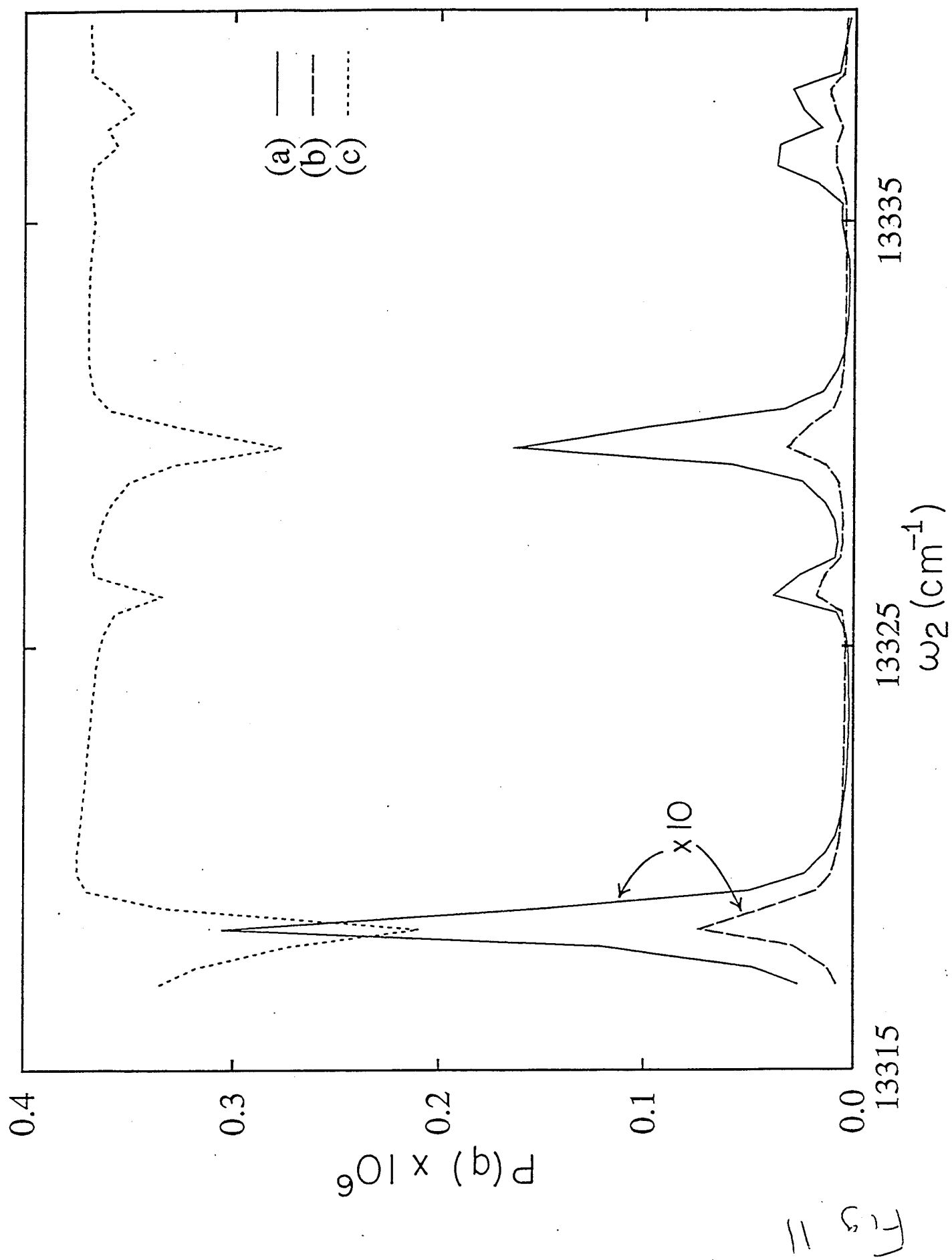


Fig 9







Phase and Intensity Control of Integral and Differential Above Threshold Ionization Rates

Ricardo A. Blank and Moshe Shapiro

Department of Chemical Physics,

Weizmann Institute of Science,

Rehovot 76100, Israel

(May 15, 1995)

Abstract

Theory of Coherent Control of Above Threshold Ionization (ATI) of Hydrogen using light fields composed of a fundamental frequency and its third harmonic, is developed. *Phase* control and *intensity* control over *integral* and *differential* quantities is demonstrated. Modulation of the first ATI kinetic energy peak height by more than 70 %, variation in the first two peaks ratio of up to a factor of 4, and separation in the alignment of the first two ATI peaks by as much as $\sim 50^\circ$, as a function of the relative phase between the two fields, are demonstrated. Intensity control, in which both partial and total integral ATI rates attain a local maximum at a specific combination of light intensities, is predicted to occur.

PACS numbers: 32.80.Rm; 32.80.Bx; 42.50.Hz

Typeset using REVTeX

The possibility of Coherent Control (CC) [1] of Above Threshold Ionization (ATI) by interfering two frequencies has attracted both experimental [2–6] and theoretical [7–14] interest in the last few years. Early on, two-color schemes were used to modify the ponderomotive shifts of ionization thresholds [2,3,7]. In such studies a combination of a strong (typically *ir*) laser, used to shift the ionization potential, and a weaker *uv* laser, used to ionize the atom, was often considered. Subsequent works dealt with the use of a fundamental frequency and its second harmonics [4–6,8,10,11,13] (the “1+2” scenario) [15,16], or the use of a fundamental frequency and its third harmonics [8–10,12,14] (the “1+3” scenario) [17–19]. Control was achieved with respect to: the modulations of both the total ionization rate and the relative magnitude of the different ATI kinetic energy peaks [4,9–12,18]; the backward/forward ratio [15,16] of photo-electrons [5,6,8,11]; the transition from the multiphoton regime to the tunneling-ionization regime [6,11,13], and stabilization induced by very intense fields [14].

The above studies have mainly concentrated on varying the relative phase of the two beams at fixed intensities. This type of control may be termed *phase control*. Following the general guidelines of CC theory [1,17], we know that the two-color interference effects ought also to be a sensitive function of the intensity ratio. This type of control may be termed *intensity control*. In this paper we explore the combination of phase *and* intensity control on ATI processes. We show that through this combination we achieve a dramatic improvement in the control and altogether new effects. In particular we demonstrate “1+3” control over *integral* rates (e.g. partial and total ionization rates), as well as *differential* quantities such as the the angular alignment of each ATI kinetic energy peak. The demonstration is achieved by performing numerically-exact computations of 3D Hydrogen in a strong electromagnetic field, using the Artificial Channel Method [21–23].

The essence of CC [1] is the coherent interference between different pathways leading to the same final state. CC interference effects can generally be classified according to whether the same angular momentum (l) states or different l states contribute to a given asymptotic channel [20]. In general, paths involving the same l states allow for integral control while paths involving different l states result in differential control.

As shown in Fig. 1, in the present work both types of interferences are considered. Depicted are possible pathways, such as the two-photon pathways associated with the $S=0$ peak, which involve the same l states ($l = 0$ and the $l = 2$), leading to integral control, and possible pathways, such as those contributing to the $S=1$ peak, which involve different l states, leading mainly to differential control.

We first present results of integral (Fig. 2) and differential (Fig. 3) *phase control*, in which control is achieved by varying the relative phase of the two beams. Though in this part we keep the intensities constant, the magnitude of the effect depends strongly on the actual intensity values chosen. Therefore, two sets of intensities are considered: One intensity set, “set A”, defined as, $I(\omega) = 6.216 \times 10^{-3}$ a.u., $I(3\omega) = 3.108 \times 10^{-3}$ a.u., results in good integral control. In contrast, the other intensity set, “set B”, for which $I(\omega) = 6.216 \times 10^{-3}$ a.u., $I(3\omega) = 1.554 \times 10^{-4}$ a.u., gives rise to good differential control.

Figure 2 shows the variation of the rates for the first three ATI kinetic energy peaks as a function of the phase between the two lasers. For set A intensities (Fig.2a), a large modulation (of more than 70%) in the $S=0$ ionization rate is obtained. [The percentage-modulation is defined as $(I_{max} - I_{min})/I_{max}$]. In addition, the ratio between the first two kinetic energy peaks can be made to vary by as much as 4. (See the right-hand scale of Fig.2a.) In contrast, for set B intensities shown in Fig.2b, the relative phase seems to have only a minor effect on the partial ionization-rates.

Figure 3b demonstrates differential control in which *directional separation* of two ATI kinetic energy peaks is achieved. This is accomplished by diverting one of the ATI peaks (the $S=1$ peak) away from the polarization direction. We see that contrary to the “1+2” scenario [4-6,8,10,11,13] which leads to change in backward/forward ratio (i.e. *orientation*) [15,16], the “1+3” scenario used here leads to change in *alignment*.

The degree of control over the alignment is calculated using the expression for the differential rate to a specific final kinetic energy. Assuming that we start from $l = 0$ bound states, the differential rate, $dR/d\Omega$, is,

$$\frac{dR}{d\Omega} \propto \left| \frac{1}{k} \sum_{l=0}^{\infty} i^l \exp[i\eta_l] Y_{l,0}(\theta) T_{l,0}(k) \right|^2. \quad (1)$$

In the above, θ is the angle between the polarization direction and that of the ejected electron, k is the magnitude of the momentum of the ejected electron, η_l is the Coulombic phase shift ($\eta_l = \arg\Gamma(l+1+i/k)$), and $T_{l,0}(k)$ are the T matrix element between the bound and each of the scattering states correlating asymptotically with an l partial wave and a k momentum value.

Figure 3 shows the differential rates as a function of the spatial angle and the relative phase between the lasers, for the $S=0$ and $S=1$ peaks, at set A intensities (left hand side), and set B intensities (right hand side). For set A we see that although the $S=0$ peak does depend on the relative phase, both the $S=0$ and $S=1$ peaks remain centered about $\theta = 0$ for all phases. In contrast, for set B the two peaks behave differently, the $S=1$ peak varies strongly with α , while the $S=0$ angular distribution is almost invariant to α . Thus, at $\alpha = 2$ radians the $S=1$ peak is maximal at $\theta = 50^\circ$ and minimal in the polarization direction ($\theta = 0^\circ$). For $\alpha = 5$ radians the $S=1$ angular dependence is reversed. Because the $S=0$ peak is essentially zero for $\theta \sim 50^\circ$, tuning the α phase to 2 radians results in dramatic directional control.

The effect we have just described illustrates the power of the present scenario in controlling ATI processes. Past one- and two-color ATI schemes [5,6,11,22] result in the photoelectrons being aligned about the field polarization direction [24]. (See however [27]). By using “1+3” interferences we are able to completely divert the alignment of a *specific* ATI kinetic energy peak ($S=1$ in this case) away from the polarization direction.

In Fig. 4 we demonstrate a different effect, that of *intensity* control over *integral* partial (and total) ionization rate. In Fig.4a we plot the rates of the first three ATI kinetic energy peaks as a function of $I(\omega)$ in the presence and absence of the second laser (of frequency 3ω). In Fig.4b we scan the 3ω laser intensity while keeping $I(\omega)$ constant. We note that when the intensity of one of the lasers is very high with respect to the other, the 2-color rates converge, as they should, to the 1-color rates, which rises monotonically with intensity.

In contrast, the 2-color rates attain a maximum at a *particular* combination of intensities, irrespective of the value of the relative phase (which is kept constant at $\alpha = 0$).

The resonant-type behavior of the ionization rate is a result of constructive interference between the $|S = 1, l = 1, n_\omega - 3, n_{3\omega} \rangle$ and $|S = 1, l = 1, n_\omega, n_{3\omega} - 1 \rangle$ dressed continuum states. In the above, n_ω and $n_{3\omega}$ represent the initial number of the ω and 3ω photons. As illustrated in Fig. 1, the $S=1$ peak serves as “doorway” state to all other ATI peaks. Hence the resonance between the above two states affects all other ATI peaks.

We speculate that the ionization rates attain a local maximum because at the specific values of intensities of Fig. 4 the AC Stark shifts associated with the above two states are identical. In support of this hypothesis we note that the ionization rates attain a local maximum whenever $U_p(\omega) - U_p(3\omega)$ - the 1-photon minus the 3-photon classical ponderomotive potentials - given as $2\pi e^2/(m_e c)[I(\omega)/\omega^2 - I(3\omega)/9\omega^2]$ equals the same ($\sim 4.2 \times 10^{-4}$ a.u.) value. It appears that whenever the ponderomotive potentials differ by this amount the actual AC stark shifts of the two levels are identical, giving rise to resonance between the two dressed states. This point must however be clarified further.

In conclusion, we have shown that *extensive* integral and differential CC of ATI processes is attainable, provided a judicious choice of relative intensities is made. Most striking is the demonstration of directional separation, by as much as $\sim 50^\circ$, of one ATI kinetic energy peak from another, and the diversion of the alignment away from the light polarization direction. Of great importance too is the demonstration of intensity control in which both partial and total integral ATI rates attain a maximum at a specific combination of light intensities.

Acknowledgments

This work was supported by the U.S.-Israel Binational Foundation and by the U.S. Office of Naval Research under contract number N00014-90-J-1014.

REFERENCES

- [1] For a recent review, see, e.g., M. Shapiro and P. Brumer, in *International Reviews in Physical Chemistry* **13** 187 (Taylor & Francis, London, 1994).
- [2] R. Trainham, G. H. Fletcher, N. B. Mansour, and D. J. Larson, *Phys. Rev. Lett.* **59**, 2291 (1987).
- [3] D. Normand, L.A. Lompre, A. L'Huilier, J. Morellec, M. Ferray, J. Lanvancier, G. Mainfray, and C Manus, *J. Opt. Am. B* **6**, 1513 (1989).
- [4] H. G. Muller, P. H. Bucksbaum, D. W. Schumacher, and A. Zavriyev, *J. Phys. B* **23**, 2761 (1990).
- [5] Y. Y. Yin, C. Chen, and D. S. Elliot, *Phys. Rev. Lett.* **69** 2353 (1992).
- [6] D. W. Schumacher, F. Weihe, H. G. Muller, and P. H. Bucksbaum, *Phys. Rev. Lett.* **73** 1344 (1994).
- [7] M. Dorr and R. Shakeshaft, *Phys. Rev. A* **40**, 459 (1989).
- [8] A. Szoke, K.C. Kulander, and J.N. Bardsley, *J. Phys. B*, **24**, 3165 (1991).
- [9] R.M. Potvliege and P.H.G. Smith, *J. Phys. B*, **24**, L641 (1991).
- [10] R.M. Potvliege and P.H.G. Smith, *J. Phys. B*, **25**, 2501 (1992).
- [11] K. J. Schafer and K. C. Kulander, *Phys. Rev. A*, **45**, 8026 (1992).
- [12] T. Nakajima, P. Lambropoulos, S. Cavalieri, and M. Matera, *Phys. Rev. A*, **46**, 7315 (1992).
- [13] N. B. Baranova, H. R. Reiss, and B. Y. Zel'dovich, *Phys. Rev. A*, **48**, 1497 (1993).
- [14] M. Protopapas, P. L. Knight, and K. Burnett, *Phys. Rev. A* **49**, 1945 (1994).
- [15] G. Kurizki, M. Shapiro and P. Brumer, *Phys. Rev. B*, **39** 3435 (1989).

- [16] B.A. Baranova, A.N. Chudinov, and B. Ya. Zel'dovitch, *Opt. Comm.*, **79**, 116 (1990).
- [17] M. Shapiro, J. W. Hepburn, and P. Brumer, *Chem. Phys. Lett.* **149**, 451 (1988).
- [18] C. Chen, Y. Y. Yin, and S. S. Elliot, *Phys. Rev. Lett.* **64**, 507 (1990).
- [19] S.M. Park, S-P. Lu, and R.J. Gordon, *J. Chem. Phys.* **94**, 8622 (1991); S-P. Lu, S.M. Park, Y. Xie, and R.J. Gordon, *J. Chem. Phys.* **96**, 6613 (1992).
- [20] C. K. Chan, P. Brumer and M. Shapiro, *J. Chem. Phys.* **94**, 2688 (1991)
- [21] M. Shapiro, *J. Chem. Phys.* **56** 2582 (1972).
- [22] R.A. Blank and M. Shapiro, *Phys. Rev. A* **50**, 3234 (1994).
- [23] R.A. Blank and M. Shapiro, "Resonances and Interferences in Above Threshold Ionization", (submitted to *Phys. Rev. A Rapid Communications*).
- [24] This is indeed the main justification for the use of 1-D models in ATI, see Ref. [25], or strong field photodissociation see Ref. [26].
- [25] Q. Su and J.H. Eberly, *Laser Physics* **2**, 598 (1992).
- [26] E. Charron, A. Giusti-Suzor, and F.H. Mies, *Phys. Rev. Lett.* **71**, 692 (1993); *Phys. Rev. A* **49**, R641 (1994).
- [27] A recent 1-color work [28] reports the observation of side-lobes in the angular distribution of some of the higher ATI peaks in Xenon, though the majority of the electrons are still ejected in the polarization direction.
- [28] B. Yang, K.J. Schafer, B. Walker, K.C. Kulander, P. Agostini, and L.F. DiMauro, *Phys. Rev. Lett.* **71**, 3770 (1993).

FIGURES

FIG. 1. Present scheme for CC of Hydrogenic ATI electrons. Drawn are the ground state ($1s$) dressed with $n_{3\omega}$ big-photons and n_{ω} small-photons, the threshold limit (broken line), and the positions of the first three ATI peaks. Also shown are the number of ω and 3ω photons connecting the ground state with each of the ATI continuum states and the l -values involved.

FIG. 2. Integral control of the ATI peaks as a function of the phase between the two lasers for intensity sets A and B.

FIG. 3. Differential rates for the $S=0$ and $S=1$ peaks as a function of the relative phase between the lasers, for intensity sets A and B.

FIG. 4. Ionization rates of the first three ATI peaks for a fixed phase ($\alpha = 0$) as a function of,

a) $I(\omega)$, at a fixed value of $I(3\omega)$ ($= 3.108 \times 10^{-3}$ a.u.);

b) $I(3\omega)$, at a fixed value of $I(\omega)$ ($= 1.10 \times 10^{-3}$ a.u.).

Also plotted are the 1-color results. (The number in parenthesis distinguishes between the 1 and 2 color cases).

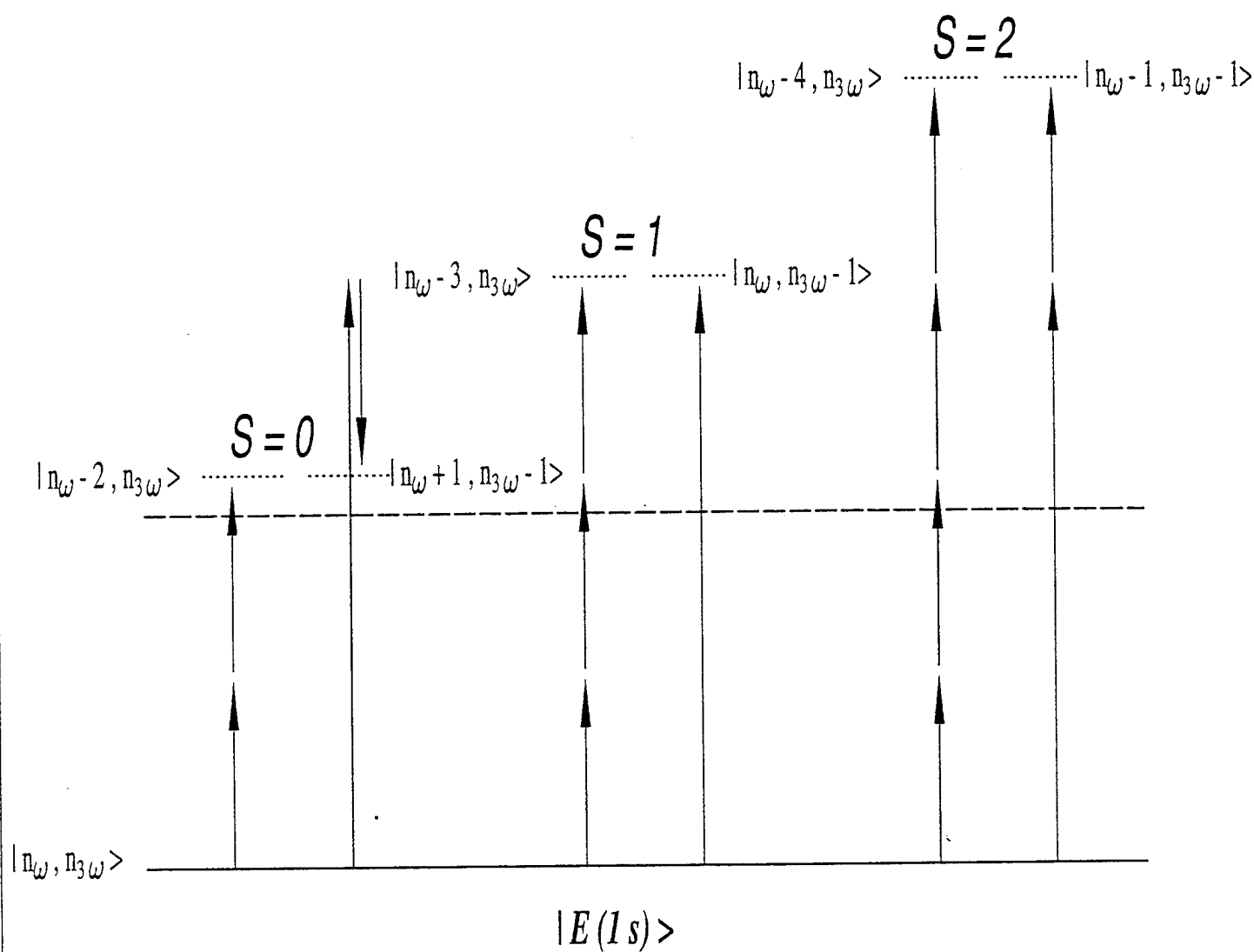
“1 + 3” ATI Level Scheme

($\omega = .2567$ au.)

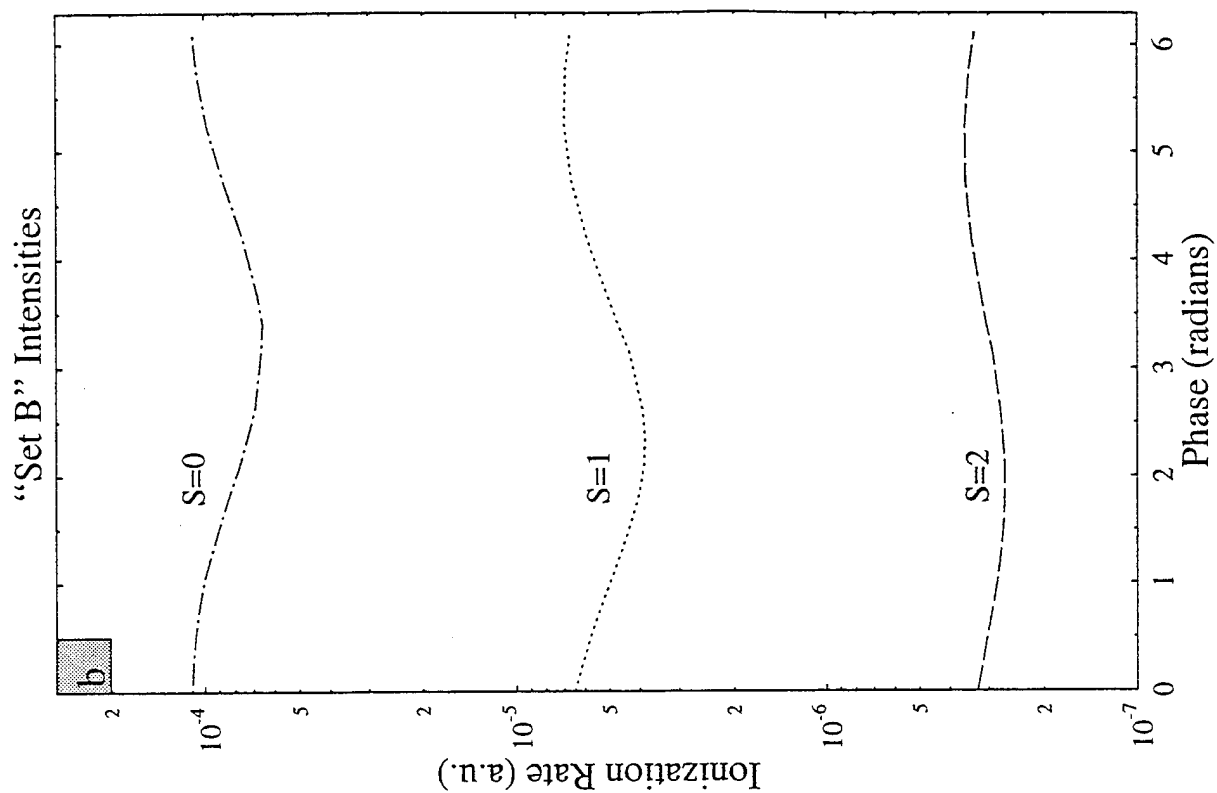
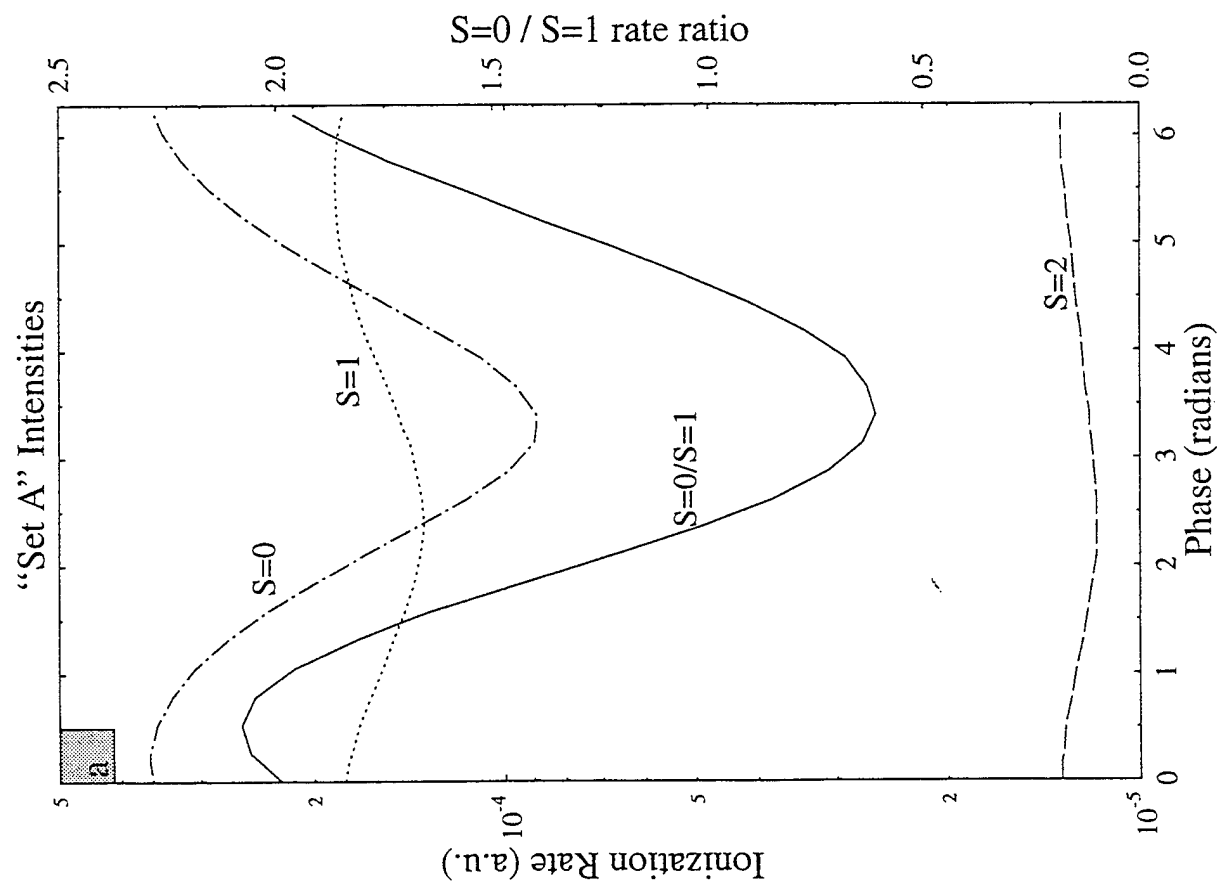
$l=0,2$ $l=0,2$

$l=1,3$ $l=1$

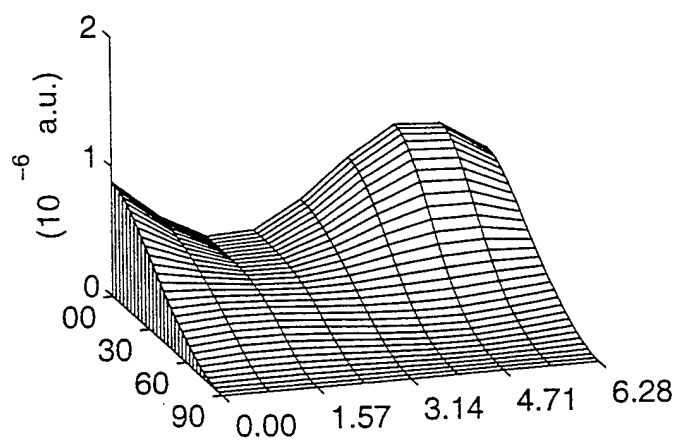
$l=0,2,4$ $l=0,2$



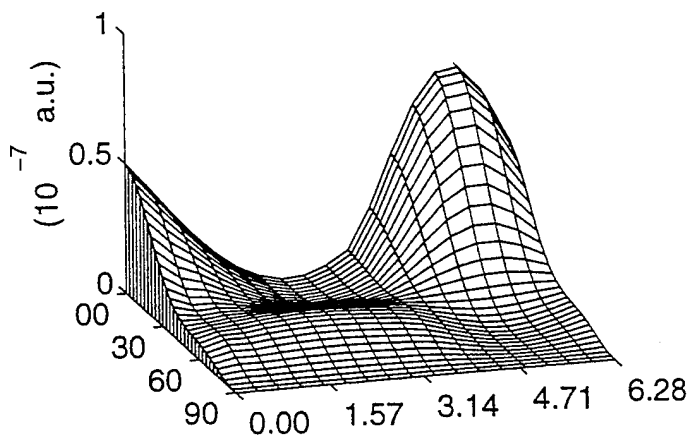
Phase control of the Ionization Rates



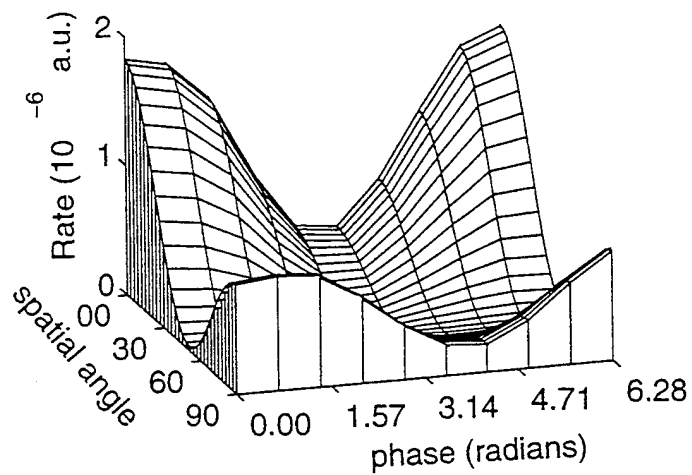
S=1 (set A)



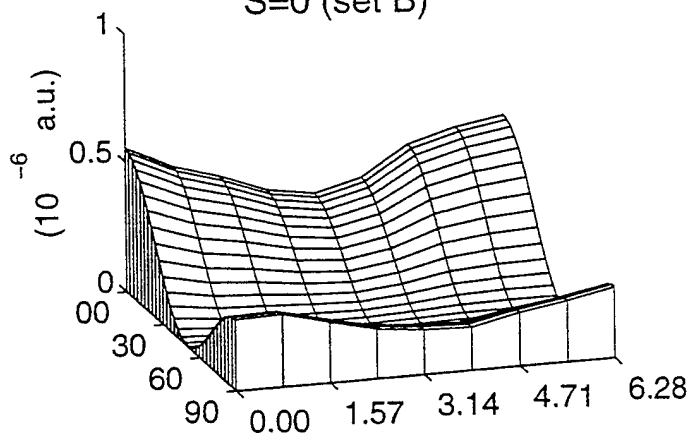
S=1 (set B)



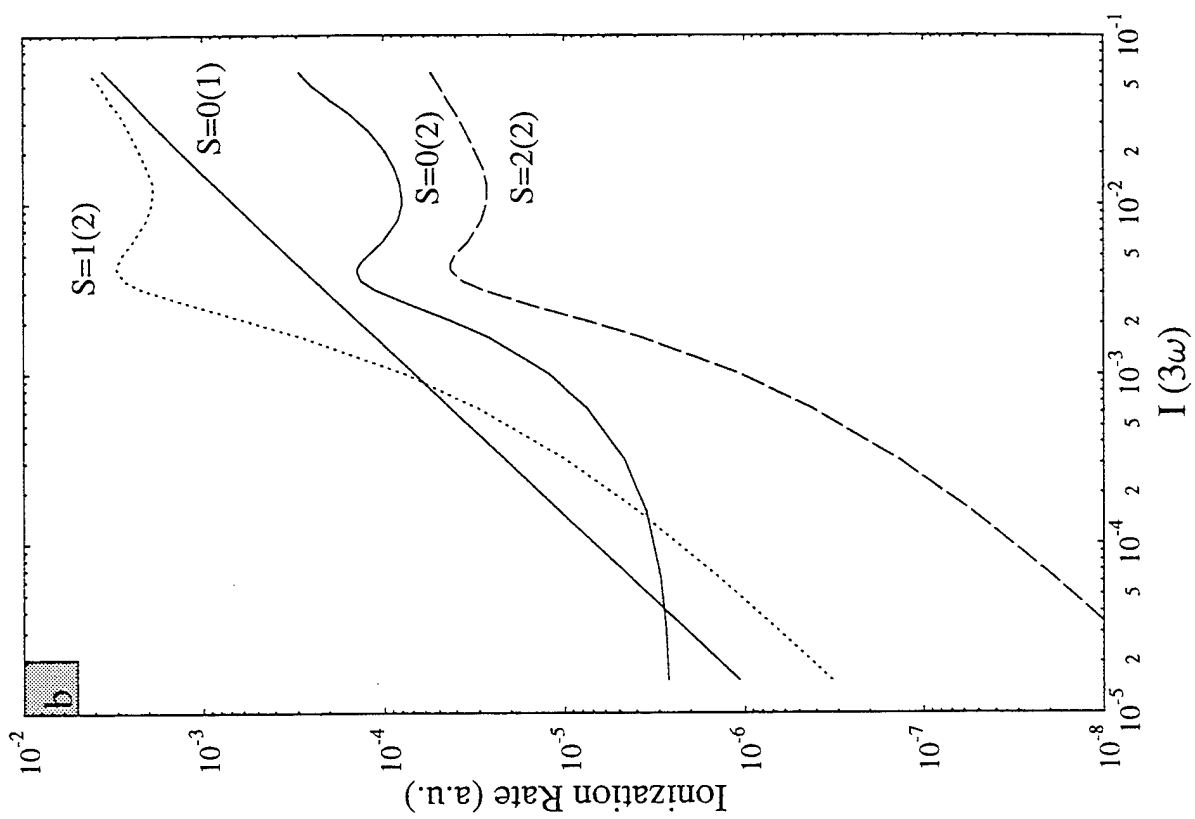
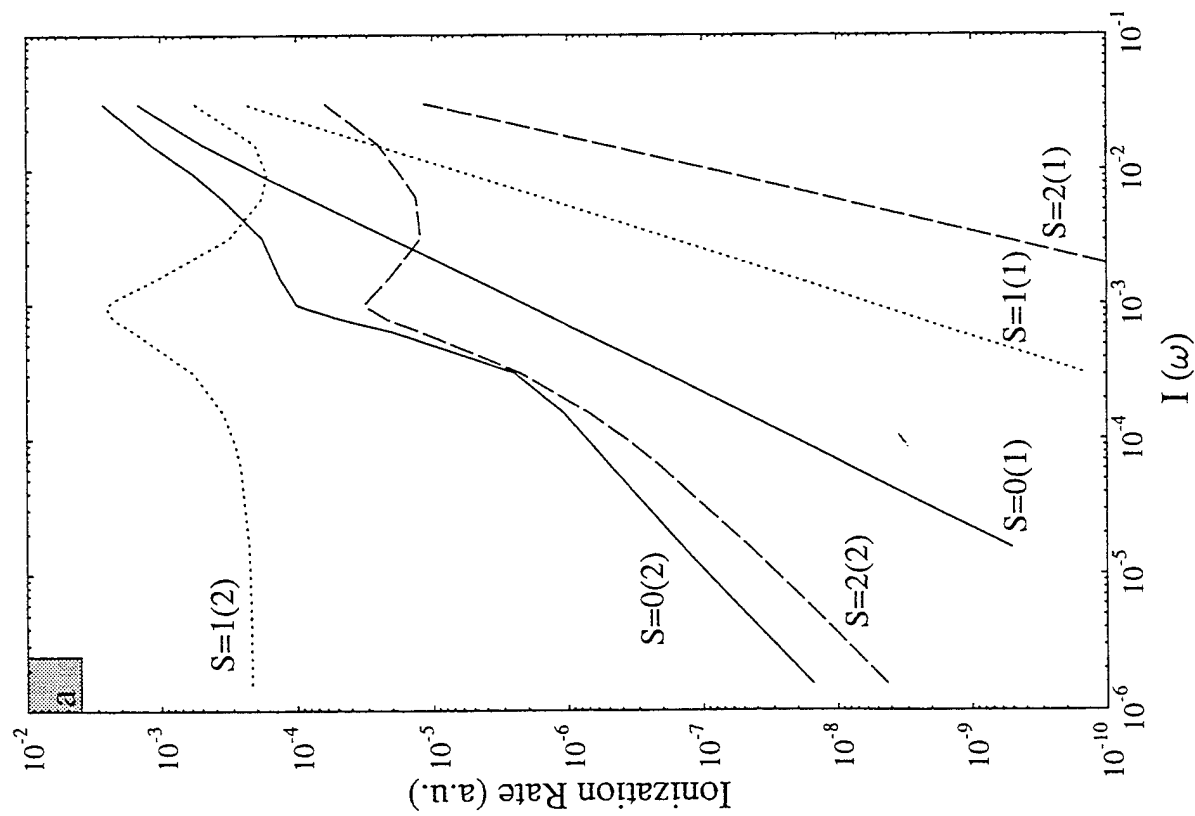
S=0 (set A)



S=0 (set B)



Intensity Control of Ionization Rates



Incoherent Interference Control of Two-Photon Dissociation

Zhidang Chen, Moshe Shapiro* and Paul Brumer

Chemical Physics Theory Group, Department of Chemistry

and The Ontario Laser and Lightwave Research Center

University of Toronto, Toronto, M5S 1A1 Canada

(April 20, 1995)

Abstract

Control over product probabilities and channel specific line shapes in resonant two photon dissociation is shown to result from quantum interference effects induced by illumination with a second laser. Control over product yield and selectivity is achieved by varying the frequency of this control laser, which need not to be coherent with the excitation laser. Computations on Na_2 photodissociation show that control over product selectivity is extensive.

I. INTRODUCTION

Developing methods to control atomic and molecular systems using lasers has been the subject of great interest [1]- [12]. Coherent control provides a fundamental principle by which this goal can be reached. Specifically, by exciting a system with several lasers we induce a number of pathways to the same final state. These pathways interfere, the interference term being a function of the final product channel and the laser parameters. By varying these laser parameters one alters the interference terms and hence the cross section to produce a particular product (or to achieve a particular goal). Experimental results [7] support the validity of this approach and computational results have indicated a wide range of achievable control.

Most recently we have shown [11,12] that intense laser fields can be used to introduce nonlinear phenomena which allow novel and effective control scenarios. Specifically, we showed that one can control channel specific line shapes and photodissociation branching ratios using two color irradiation with intense lasers. Control, which results from quantum interference between optically induced excitation routes, is achieved by changing the *frequencies* of the two intense lasers. Significantly, unlike coherent control scenarios, the relative phase of the two lasers need not be well defined since the laser phases transferred to the molecule cancel in the multiphoton pathways induced by intense fields. We term this control principle “incoherent interference control”.

Previously [11,12] we showed that laser induced interference control can be effectively used to control molecular one photon dissociation. Here we study control of resonant two photon dissociation. The resonant character of the two photon process not only greatly enhances the dissociation probability, but also provides selective excitation of molecules out of the thermal distribution, a feature which is of great use in the control of reactions in a thermal environment. Indeed, the scenario described herein is being successfully applied in an experimental study of photodissociation of Na_2 in a heat pipe [13].

The control scenario operates as follows. Consider a molecule in an initial bound state $|\varepsilon_i\rangle$ which absorbs two photons of frequency ω_1 and, in doing so, is excited to a continuum $|\varepsilon, \mathbf{m}, q^-\rangle$ via a resonant intermediate state $|\varepsilon_{j_1}\rangle$. Here $|\varepsilon, \mathbf{m}, q^-\rangle$ are exact molecular eigenstates describing the continuum which yields product in arrangement channel q , energy ε and quantum numbers \mathbf{m} . The outcome of this photodissociation process can be controlled by applying a “control laser” ω_2 which couples initially unpopulated bound states $|\varepsilon_{j_2}\rangle$ to the same continuum. With both lasers on, dissociation to $|\varepsilon, \mathbf{m}, q^-\rangle$ occurs via numerous dissociation pathways. To lowest order these are the routes $|\varepsilon_i\rangle \rightarrow |\varepsilon_{j_1}\rangle \rightarrow |\varepsilon, \mathbf{m}, q^-\rangle$ as well as $|\varepsilon_i\rangle \rightarrow |\varepsilon_{j_1}\rangle \rightarrow |\varepsilon', \mathbf{m}', q'^-\rangle \rightarrow |\varepsilon_{j_2}\rangle \rightarrow |\varepsilon, \mathbf{m}, q^-\rangle$. Contributions from these multiple pathways to the product in a given channel q at energy ε interfere (either constructively or destructively) with one another. Varying the frequency and intensity of the control laser alters the interference and hence the dissociation line shape and the yield of product into a

given channel.

The theory of this two photon plus one photon control scenario is described in Section II. Numerical examples on the control of Na₂ two photon dissociation are presented in Section III.

II. CONTROLLED TWO-PHOTON DISSOCIATION: THEORY

Recently, we described a general theory [12] of molecular photodissociation using intense CW radiation fields. The theory enables us to exactly compute the photodissociation probability, and can be applied to single and multiphoton dissociation processes. Here we focus on control of two-photon dissociation.

Consider a molecule with Hamiltonian H_M interacting with a radiation field with Hamiltonian H_R through potential V . The total Hamiltonian H is then given by:

$$H = H_M + H_R + V \equiv H_0 + V. \quad (1)$$

Absorption of a sufficient number of photons, corresponding to a transition from the molecular bound state $|\varepsilon_b\rangle$ to the continuum $|\varepsilon, \mathbf{m}, q^-\rangle$, leads to dissociation. Here $|\varepsilon_b\rangle$ and $|\varepsilon, \mathbf{m}, q^-\rangle$ are eigenstates of H_M with discrete energy ε_b and continuous energy ε , respectively. The minus superscript denotes incoming boundary conditions, i.e. that at large t the states $\exp(-i\varepsilon t/\hbar)|\varepsilon, \mathbf{m}, q^-\rangle$ approach $\exp(-i\varepsilon t/\hbar)|\varepsilon, \mathbf{m}, q\rangle$ where $|\varepsilon, \mathbf{m}, q\rangle$ describes the product fragments. Specifically, $|\varepsilon, \mathbf{m}, q\rangle$ is an eigenstate of H_M with the dissociation products separated by large distance from one another.

The presence of CW radiation is conveniently described by the number eigenstates of H_R :

$$H_R|N_k\rangle \equiv H_R|n_1^{(k)}, n_2^{(k)}, \dots\rangle = E_{N_k}|N_k\rangle \quad (2)$$

with energy $E_{N_k} = \sum_l n_l^{(k)} \hbar \omega_l$. The letters $k = i$ and f are used to label the initial and final states, respectively. The eigenstates of $H_0 \equiv H_M + H_R$ are a direct product of the molecular and photon states; e.g., $|\varepsilon, \mathbf{m}, q^-, N_f\rangle \equiv |\varepsilon, \mathbf{m}, q^-\rangle |N_f\rangle$.

The molecule-radiation interaction V can be expressed in the dipole approximation as

$$V = -\boldsymbol{\mu} \cdot \boldsymbol{\mathcal{E}}, \quad \boldsymbol{\mathcal{E}} = i \sum_l \epsilon_l (\mathbf{e}_l a_l - \mathbf{e}_l^* a_l^\dagger), \quad (3)$$

where $\boldsymbol{\mu}$ is the electric dipole operator, $\boldsymbol{\mathcal{E}}$ is the amplitude of the radiation electric field, $\epsilon_l = (2\pi\hbar\omega_l/L^3)^{1/2}$, \mathbf{e}_l , ω_l are the polarization vector and angular frequency of mode l , respectively, and a_l , a_l^\dagger are photon annihilation and creation operators.

The dynamics of photodissociation is completely described by the fully interacting state $|(\epsilon, \mathbf{m}, q^-), N_k^-\rangle$, which is an eigenstate of the total Hamiltonian H ,

$$H|(\epsilon, \mathbf{m}, q^-), N_k^-\rangle = (\epsilon + E_{N_k})|(\epsilon, \mathbf{m}, q^-), N_k^-\rangle. \quad (4)$$

The minus superscript on N_k indicates that when the radiative interaction V is switched off the state $|(\epsilon, \mathbf{m}, q^-), N_k^-\rangle$ becomes the non-interacting state $|(\epsilon, \mathbf{m}, q^-), N_k\rangle$. These $|(\epsilon, \mathbf{m}, q^-), N_k^-\rangle$ states satisfy the Lippmann-Schwinger equation [14],

$$\langle(\epsilon, \mathbf{m}, q^-), N_k^-| = \langle(\epsilon, \mathbf{m}, q^-), N_k| + \langle(\epsilon, \mathbf{m}, q^-), N_k|VG(\epsilon^+ + E_{N_k}) \quad (5)$$

where $G(E) = 1/(E - H)$ is the resolvent operator, and ϵ^+ denotes $\epsilon + i\delta$ with $\delta \rightarrow 0^+$ at the end of the calculation. If the system is initially in $|\epsilon_i, N_i\rangle \equiv |\epsilon_i\rangle|N_i\rangle$ and the radiation field is switched on suddenly then the photodissociation amplitude to form the product state $|\epsilon, \mathbf{m}, q^-|N_f\rangle$ is given by $\langle(\epsilon, \mathbf{m}, q^-), N_f^-|\epsilon_i, N_i\rangle$. Since $\langle(\epsilon, \mathbf{m}, q^-), N_f|\epsilon_i, N_i\rangle = 0$ then this overlap assumes the convenient form

$$\langle(\epsilon, \mathbf{m}, q^-), N_f^-|\epsilon_i, N_i\rangle = \langle(\epsilon, \mathbf{m}, q^-), N_f|VG(\epsilon^+ + E_{N_f})|\epsilon_i, N_i\rangle, \quad (6)$$

through use of Eq.(5). Equation (6) is an exact expression which provides a connection between the dissociation amplitude and the VG matrix element. The latter can be computed exactly by using a high field extension of the artificial channel method [12,15]. Note that the operator VG gives a full description of the dissociation process, up to all orders of the laser-molecule interaction.

Two quantities are of interest: the channel specific line shape $A(\epsilon, q, N_f|\epsilon_i, N_i)$, i.e. the probability of dissociation into channel q with energy ϵ ,

$$A(\varepsilon, q, N_f | \varepsilon_i, N_i) = \int d\hat{\mathbf{k}} | \langle (\varepsilon, \hat{\mathbf{k}}, q^-), N_f^- | VG(\varepsilon^+ + E_{N_f}) | \varepsilon_i, N_i \rangle |^2, \quad (7)$$

and the total dissociation probability to channel q

$$P(q) = \sum_{N_f} \int d\varepsilon A(\varepsilon, q, N_f | \varepsilon_i, N_i), \quad (8)$$

where the sum is over sets of photons that lift the molecule above the threshold for dissociation. [In writing Eq. (7) diatomic dissociation is assumed, so that $\mathbf{m} = \hat{\mathbf{k}}$].

Molecular response to the presence of intense laser fields is generally highly nonlinear, allowing multiple absorption and emission processes. For example, stimulated emission from bound as well as from continuous states can be as strong as absorption processes. As a result, Raman-type couplings via absorption and emission lead to the overlap between two bound vib-rotational states in the same or different electronic manifolds, which is otherwise negligible in weak field regime. Multiple absorption and emission induce multiple reaction pathways in molecules, resulting in profound effects in molecular dynamics [12]. As a result it is generally impossible to obtain a closed form for the VG matrix element in high field regime. However, it is possible to gain physical insight into the photodissociation process by examining the leading terms in an expansion [12] of the VG matrix element in terms of the level-shift operator $R(E^+)$. Here $R(E^+)$ is given [16] by

$$R(E^+) = V + V \frac{P}{E^+ - PH_0P - PVP} V. \quad (9)$$

where the projection operator P and its complementary operator Q are given by

$$P = \sum_{\mathbf{m}, q} \sum_{N_k} \int d\varepsilon | (\varepsilon, \mathbf{m}, q^-), N_k \rangle \langle (\varepsilon, \mathbf{m}, q^-), N_k | \quad (10)$$

$$Q = \sum_{\varepsilon_j} \sum_{N_j} | \varepsilon_j, N_j \rangle \langle \varepsilon_j, N_j |, \quad (11)$$

which project out continuous and bound parts of eigenstates of H_0 [Eq. (1)], respectively. With P , Q and $R(E^+)$ thus defined, the photodissociation amplitude can be expanded [12] as

$$\begin{aligned}
& \langle (\varepsilon, \mathbf{m}, q^-), N_f | V G(E^+) | \varepsilon_i, N_i \rangle \\
&= \frac{1}{E^+ - \varepsilon_i - E_{N_i} - R_{i,i}(E^+)} \times \left[\langle (\varepsilon, \mathbf{m}, q^-), N_f | R(E^+) | \varepsilon_i, N_i \rangle \right. \\
&+ \sum_{j \neq i} \frac{\langle (\varepsilon, \mathbf{m}, q^-), N_f | R(E^+) | \varepsilon_j, N_j \rangle \langle \varepsilon_j, N_j | R(E^+) | \varepsilon_i, N_i \rangle}{[E^+ - \varepsilon_j - E_{N_j} - R_{j,j}(E^+)]} \\
&+ \sum_{j,j' (j \neq j' \neq i)} \frac{\langle (\varepsilon, \mathbf{m}, q^-), N_f | R(E^+) | \varepsilon_{j'}, N_{j'} \rangle \langle \varepsilon_{j'}, N_{j'} | R(E^+) | \varepsilon_j, N_j \rangle \langle \varepsilon_j, N_j | R(E^+) | \varepsilon_i, N_i \rangle}{[E^+ - \varepsilon_{j'} - E_{N_{j'}} - R_{j',j'}(E^+)] [E^+ - \varepsilon_j - E_{N_j} - R_{j,j}(E^+)]} \\
&+ \dots], \tag{12}
\end{aligned}$$

with $E^+ = \varepsilon^+ + E_{N_f}$. Equation (12) shows that with intense fields there are multiple reaction pathways which contribute to the bound-free transition. Each term on the right hand side is associated with a pathway. Multiple pathways interfere one another, either constructively or destructively, depending on the relative phases of the various terms. By manipulating the phases we can effectively control the transition probability, as we discuss below.

The R -matrix elements in Eq.(12) assume the following forms. The element between bound and continuum states, for example, $\langle (\varepsilon, \mathbf{m}, q^-), N_f | R(E^+) | \varepsilon_j, N_j \rangle$, is composed of two terms, the direct transition term [via the first term in Eq.(9)] and the indirect term [via the second term of Eq.(9)]. The latter may be simplified, under the conditions of this paper, by noting that the incident radiation is such that it only effectively couples states in the Q -space to those in the P -space. (The simplification is then amount to neglecting above-threshold dissociation which is not essential in the numerical examples discussed below.) Under these circumstances $PVP = 0$ and

$$\langle (\varepsilon, \mathbf{m}, q^-), N_f | R(E^+) | \varepsilon_j, N_j \rangle = \langle (\varepsilon, \mathbf{m}, q^-), N_f | V | \varepsilon_j, N_j \rangle. \tag{13}$$

In Eq.(12) the diagonal element $R_{j,j}$ of $R(E^+)$ in the Q -space, for example, is given by

$$R_{j,j}(E^+) = \langle \varepsilon_j, N_j | R(E^+) | \varepsilon_j, N_j \rangle \tag{14}$$

$$= \Delta_j(E) - \frac{i}{2} \Gamma_j(E), \tag{15}$$

where, by taking $\delta \rightarrow 0$, we have

$$\Delta_j(E) = \langle \varepsilon_j, N_j | V \frac{P_v}{E - PHP} V | \varepsilon_j, N_j \rangle, \tag{16}$$

$$\Gamma_j(E) = 2\pi \langle \varepsilon_j, N_j | VP \delta(E - PHP) PV | \varepsilon_j, N_j \rangle, \tag{17}$$

which are the field-induced shift and broadening, respectively. Here P_v denotes the principle part of the integration. The third type of the the R -matrix element in Eq.(12) is the off-diagonal element between two bound states:

$$\langle \varepsilon_j, N_j | R(E^+) | \varepsilon_i, N_i \rangle = \langle \varepsilon_j, N_j | V \frac{P}{E^+ - PHP} V | \varepsilon_i, N_i \rangle \quad (i \neq j) \quad (18)$$

which describes second order coupling between two bound states mediated by the continuum.

In Eq.(12), partial summations have been performed to account for level-shifts and level broadening so that the expression is devoid of singularities. The resultant expression provides insight into photodissociation processes in intense fields, as becomes evident later below.

Consider now the case of a molecule in the presence of two laser fields, of frequency ω_1 and ω_2 . The initial state of the total system is $|\varepsilon_i, N_i\rangle = |\varepsilon_i, n_1, n_2\rangle$, where n_1 and n_2 are the initial occupation numbers of the field modes ω_1 and ω_2 , respectively. The molecule-radiation interaction V is given by the sum of the potentials due the two laser fields:

$$V = V_1 + V_2 = -\boldsymbol{\mu} \cdot \boldsymbol{\mathcal{E}}_1 - \boldsymbol{\mu} \cdot \boldsymbol{\mathcal{E}}_2, \quad (19)$$

where $\boldsymbol{\mathcal{E}}_1$ and $\boldsymbol{\mathcal{E}}_2$ are the electric field vectors associated with ω_1 and ω_2 . Laser frequencies are chosen such that $\hbar\omega_1 \approx \varepsilon_{j_1} - \varepsilon_i$, i.e., the ω_1 is in resonance with $|\varepsilon_{j_1}\rangle$, and $\varepsilon_i + 2\hbar\omega_1 \approx \varepsilon_{j_2} + \hbar\omega_2$, that is, $2\hbar\omega_1 - \hbar\omega_2$ is in resonance with $|\varepsilon_{j_2}\rangle$ (see Fig. 1 for the application to Na_2). Inserting Eq. (19) into Eq (6) gives the photodissociation matrix element which we compute. To gain insight into the terms contained within this expression we examine the leading terms in an expansion of Eq.(12) in V , which are

$$\langle (\varepsilon, \mathbf{m}, q^-), n_1 - 2, n_2 | VG(E^+) | \varepsilon_i, n_1, n_2 \rangle = A + B + \dots \quad (20)$$

$$A = \sum_{j_1 \neq i} \frac{\langle (\varepsilon, \mathbf{m}, q^-), n_1 - 2 | V_1 | \varepsilon_{j_1}, n_1 - 1 \rangle \langle \varepsilon_{j_1}, n_1 - 1 | V_1 | \varepsilon_i, n_1 \rangle}{(\varepsilon^+ - \varepsilon_{j_1} - \hbar\omega_1 - R_{j_1, j_1})(\varepsilon^+ - \varepsilon_i - 2\hbar\omega_1 - R_{i, i})} \quad (21)$$

$$B = \sum_{j_1, j_2 (j_1 \neq j_2 \neq i)} \frac{\langle (\varepsilon, \mathbf{m}, q^-), n_2 | V_2 | \varepsilon_{j_2}, n_2 + 1 \rangle R_{j_2, j_1} \langle \varepsilon_{j_1}, n_1 - 1 | V_1 | \varepsilon_i, n_1 \rangle}{(\varepsilon^+ - \varepsilon_{j_2} - \hbar\omega_2 - R_{j_2, j_2})(\varepsilon^+ - \varepsilon_{j_1} - \hbar\omega_1 - R_{j_1, j_1})(\varepsilon^+ - \varepsilon_i - 2\hbar\omega_1 - R_{i, i})} \quad (22)$$

where we have used $E = \varepsilon + (n_1 - 2)\hbar\omega_1 + n_2\hbar\omega_2$ in Eq.(12) to obtain Eq.(20). The R_{j_2,j_1} in Eq.(20) is given by

$$R_{j_2,j_1} \equiv \langle \varepsilon_{j_2}, n_1 - 2, n_2 + 1 | R(\varepsilon^+) | \varepsilon_{j_1}, n_1 - 1, n_2 \rangle$$

$$= \sum_{\mathbf{m}', q'} \int d\varepsilon' \frac{\langle \varepsilon_{j_2}, n_2 + 1 | V_2 | (\varepsilon', \mathbf{m}', q'^-), n_2 \rangle \langle (\varepsilon', \mathbf{m}', q'^-), n_1 - 2 | V_1 | \varepsilon_{j_1}, n_1 - 1 \rangle}{\varepsilon^+ - \varepsilon'}. \quad (23)$$

and describes the coupling between $|\varepsilon_{j_1}\rangle$ and $|\varepsilon_{j_2}\rangle$, resulted from absorption of one ω_1 photon and stimulated emission of an ω_2 photon. Similar sequential absorption and emission terms result from the higher order contributions to Eq.(12).

The term A in Eq.(21) describes the direct resonant two photon dissociation path $|\varepsilon_i\rangle \rightarrow |\varepsilon, \mathbf{m}, q^-\rangle$ via the intermediate states $|\varepsilon_{j_1}\rangle$ [path (A)]. The term B describes the dissociation path $|\varepsilon_i\rangle \rightarrow |\varepsilon', \mathbf{m}', q'^-\rangle \rightarrow |\varepsilon_{j_2}\rangle \rightarrow |\varepsilon, \mathbf{m}, q^-\rangle$ induced by ω_1 plus ω_2 [path (B)]. It is important to note that the relative sign of the A and B terms depend on the frequency ω_2 , resulting in a sensitivity of the line shape to the frequency of the control laser. That is, by tuning ω_2 , we alter the interference character between the paths A and B , and thus the line shape. Higher order terms in the expansion of Eq. (20) correspond to paths with multiple absorption and emission of ω_1 and ω_2 photons.

Equation (20) describes the photon fields by number states. However, a complete analysis of interference between the A and B paths necessitates an understanding of the role of the photon phase. Hence we sketch the same argument using coherent states $|\alpha\rangle \equiv |\alpha_1\rangle \oplus |\alpha_2\rangle$. Here $|\alpha_1\rangle$ and $|\alpha_2\rangle$ are coherent states describing the ω_1 and ω_2 fields and are defined as ($i = 1, 2$)

$$|\alpha_i\rangle = \sum_{n_i} P(\alpha_i, n_i) |n_i\rangle, \quad (24)$$

with

$$P(\alpha_i, n_i) = \alpha_i^{n_i} \exp(-|\alpha_i|^2/2) / \sqrt{n_i!}. \quad (25)$$

The quantity α_i can be parameterized by the average photon number \bar{n}_i and the phase ϕ_i (including the spatial phase $\mathbf{k}_i \cdot \mathbf{r}$) of the ω_i laser as: $\alpha_i = \sqrt{\bar{n}_i} \exp(i\phi_i)$. Note that at high intensities (large \bar{n}_i) the Poisson distribution in Eq.(25) is sharply peaked at $n_i = \bar{n}_i$.

Replacing Eq.(20) by $\langle \alpha | \langle \varepsilon, \mathbf{m}, q^- | VG(E^+) | \varepsilon_i \rangle | \alpha \rangle$, gives, within the rotating wave approximation,

$$\langle \alpha | \langle \varepsilon, \mathbf{m}, q^- | VG(E^+) | \varepsilon_i \rangle | \alpha \rangle = e^{2i\phi_1} \bar{A} + e^{i\phi_2} e^{i(2\phi_1 - \phi_2)} \bar{B} + \dots, \quad (26)$$

where \bar{A} and \bar{B} are of the same form as A and B in Eq.(20) but with the photon numbers n_1 and n_2 replaced by the average photon numbers \bar{n}_1 and \bar{n}_2 . Hence, the leading terms in the dissociation probability $|\langle \alpha | \langle \varepsilon, \mathbf{m}, q^- | VG(E) | \varepsilon_i \rangle | \alpha \rangle|^2$ can be obtained from Eq.(20) by replacing the photon numbers n_i by the average photon number \bar{n}_i and, most significantly, the photodissociation probability will be independent of the laser phase. Examination of the higher order terms in the expansion of Eq. (12) (within the rotating wave approximation) shows a similar cancellation of the laser phase. Thus, although the laser phase does not serve as a useful control parameter, varying ω_2 should alter the interference term between routes and hence affect the product distribution. Extensive control of the line shape and the product selectivity using this approach is demonstrated in Section 3 where computations on the photodissociation of Na_2 are presented.

From the computational viewpoint, it is greatly advantageous to compute $\langle (\varepsilon, \mathbf{m}, q^-), n_1 - 2, n_2 | VG(E^+) | \varepsilon_i, n_1, n_2 \rangle$ [Eq.(12)] directly. Such a direct computation is possible using a high field extension of the artificial channel method, as described in Ref. [12] and as utilized below.

III. CONTROL OF TWO-PHOTON DISSOCIATION IN Na_2

Consider now the control of Na_2 two photon dissociation, which occurs by resonant absorption of two ω_1 photons to the continuum $|\varepsilon, \mathbf{m}, q^- \rangle$, from a bound state $|\varepsilon_i \rangle$ of the Na_2 ground electronic state (see Fig. 1). The frequency ω_1 is in resonance with an intermediate bound state $|\varepsilon_{j_1} \rangle$, which is itself a superposition of states of the $A^1\Sigma_u$ and $b^3\Pi_u$ electronic curves, a consequence of spin-orbit coupling [17]. The control laser ω_2 simultaneously couples the continua to the bound states $|\varepsilon_{j_2} \rangle$, creating additional dissociation pathways which

interfere with the direct path for two-photon dissociation. The continuum states reached in the two photon excitation can either be of singlet or triplet character but the predominant contributions to the products $\text{Na}(3p)+\text{Na}(3s)$, $\text{Na}(4s)+\text{Na}(3s)$ and $\text{Na}(3d)+\text{Na}(3s)$ in the energy range of interest are found to arise from the $1^3\Pi_g$, $^3\Sigma_g$ and $2^3\Pi_g$ states which are shown in Fig. 1. (The relevant electronic potentials and dipole transition functions are taken from Ref. [18]). Also included in the computations are the electronic states $1^1\Sigma_g$, $1^1\Pi_g$, and $^3\Sigma_g$, which correlate asymptotically with $\text{Na}(3s)+\text{Na}(3p)$ atoms, and the $2^1\Sigma_g$, which correlates asymptotically with the $\text{Na}(3s)+\text{Na}(4s)$ product [17]. The contributions from these states are much smaller than those from the states shown in Fig. 1. The basic features of the control scenario are most readily seen by first studying a case which includes a minimum of rotational states. Thus in Figs. 2 to 4 we only include $J = 0$ of $1^1\Sigma_g$, $J = 1$ of $1^1\Sigma_u$ and $^3\Pi_u$, and $J = 0$ of the continua. Later figures show cases involving additional rotational levels.

Results shown below neglect the contribution from the two photon dissociation of Na_2 by $\omega_1 + \omega_2$. These contributions are negligible in the region of ω_2 where $P(q)$ varies significantly, i.e. in the regions where the product yield is controlled.

Consider first the line shape associated with of a 'pure' two photon dissociation using a single CW laser of frequency ω_1 . The intensity of the control laser ω_2 is set to zero. The dissociation line shape $A(\epsilon, q, n_1 - 2|\epsilon_i, n_1)$ is obtained by integrating the square of Eq.(21) over $\hat{\mathbf{k}}$ ($\mathbf{m} = \hat{\mathbf{k}}$ for Na_2). A typical resultant dissociation line shape is shown in Fig. 2, with $A(\epsilon, q, n_1 - 2|\epsilon_i, n_1)$ (on a logarithmic scale) shown as a function of the product translational energy ϵ . In this case the laser frequency is $\omega_1 = 16154.7 \text{ cm}^{-1}$ with an intensity $I_1 = 8.7 \times 10^9 \text{ W/cm}^2$ so that the energy of the two photon excitation is below the $\text{Na}(3d)+\text{Na}(3s)$ threshold, but above the $\text{Na}(4s)+\text{Na}(3s)$ thresholds. Two products, $\text{Na}(3p) + \text{Na}(3s)$ and $\text{Na}(4s) + \text{Na}(3s)$, are therefore energetically accessible. The solid line denotes the $\text{Na}(3p)+\text{Na}(3s)$ product and the dashed line denotes the $\text{Na}(4s)+\text{Na}(3s)$ atoms. The initial state $|\epsilon_i\rangle$ is chosen with vibrational quantum number $v_i = 0$ and rotational quantum number $J = 0$ in the ground electronic state.

Line shapes for both products are seen to be similar in structure, showing three sets of structure with three peaks. The first set of three peaks in the region $26350 < \varepsilon < 26500$ cm^{-1} are associated, from the left to the right, with the resonant contributions of the dressed $|\varepsilon_i\rangle$ and $|\varepsilon_{j_1}\rangle$ states, respectively, the latter being a doublet due to spin-orbit coupling [17]. Specifically, with the given laser frequency, the dressed $|v=0, J=0, {}^1\Sigma_g\rangle$ state, is in quasi-resonance with $|v=14, J=1, {}^1\Sigma_u\rangle$, which is spin-orbit coupled to $|v=19, J=1, {}^3\Pi_u\rangle$. The dissociation of these three states contribute to the first set of three peaks. Note that the spacings between the peaks are much larger than the corresponding zero-field spacings because of the laser-induced shifting and broadening. A similar explanation applies to the remaining sets of the three peaks, which arise from the dissociation of the higher dressed states $|\varepsilon_{i+1}\rangle$ and $|\varepsilon_{j_1+1}\rangle$, which are populated by stimulated emission.

Consider now the effect of introducing the second laser. Figures 3 and 4 show the logarithm of the line shape $A(\varepsilon, q, n_1 - 2, n_2 | \varepsilon_i, n_1, n_2)$ as a function of ε for two different values of ω_2 (ω_2 is 14939.6 cm^{-1} in Fig. 3 and 14961.5 cm^{-1} in Fig. 4, with $I_2 = 3.5 \times 10^{10} \text{ W/cm}^2$). Other than the introduction of the ω_2 laser, the system parameters are the same as in Fig. 2. The solid line denotes the Na(3p)+Na(3s) product and the dashed line corresponds to the Na(4s)+Na(3s) pair. Consideration of Figs. 3 and 4 reveals two significant features. First, the line shape shows considerable channel dependence [compare dashed and solid lines within the same figure], and the line shapes are ω_2 -dependent (compare Fig. 3 with Fig. 4). This is in direct contrast to the results in Fig. 2, which are not sensitive to the channel index q . The profound effect of the ω_2 laser on the line shape is due to the interference of the pathways induced by ω_2 with the 2-photon dissociation path.

Both Figs. 3 and 4 show that adding the frequency ω_2 introduces a new peak, resulting in a repetitive four-peak structure in the line shape arising from the combined contributions of the dressed states $|\varepsilon_i\rangle$, $|\varepsilon_{j_2}\rangle$ and $|\varepsilon_{j_1}\rangle$. Thus, the additional fourth peak comes from the dissociation of the level $|\varepsilon_{j_2}\rangle$. For example, the dissociation of $|v=28, J=1, {}^3\Pi_u\rangle$ contributes a peak at $\varepsilon = 26433 \text{ cm}^{-1}$ in Fig. 3 and at $\varepsilon = 26453 \text{ cm}^{-1}$ in Fig. 4. Increasing ω_2 causes a blue-shift in the position of the second peak of the four-peak structure, as well

as a change in the peak strengths.

As previously noted, computations resulting in Figs. 2 to 4 only include $J = 0$ of the ground electronic state, $J = 1$ of $^1\Sigma_u$ and $^3\Pi_u$, and $J = 0$ of the continua. Including multiple rotational states lead to additional peaks in the line shape. Figure 5 shows one example. Here the initial state $|\varepsilon_i\rangle$ is chosen to be $(v_i = 0, J_i = 32)$ of the $^1\Sigma_g$ state. The computation includes also the $J = 31, J = 33$ of $^1\Sigma_u$ and $^3\Pi_u$, and the $J = 30, J = 32, J = 34$ of the continua and the rotational selection rule $\Delta J = \pm 1$ applies. Here $\omega_1 = 17720.8 \text{ cm}^{-1}$, $\omega_2 = 13332.8 \text{ cm}^{-1}$, the intensities $I_1 = 1.72 \times 10^8 \text{ W/cm}^2$ and $I_2 = 2.84 \times 10^8 \text{ W/cm}^2$. In this instance the higher energy $\text{Na}(3d) + \text{Na}(3s)$ channel is open as well, a consequence of the larger ω_1 value. The $\text{Na}(3d) + \text{Na}(3s)$ line shape is shown in Fig. 5c, while the line shape for the $\text{Na}(3p) + \text{Na}(3s)$ and $\text{Na}(4s) + \text{Na}(3s)$ channels are shown in Fig. 5a and 5b. The line shapes are far more complicated than those shown earlier, showing multiple peaks and dips due to the couplings of the numerous vib-rotational bound states. However, comparing Figs. 5a, 5b and 5c clearly shows a strongly channel dependent line shape. Once again this is due to the difference in interference characteristics for different channels when both ω_1 and ω_2 lasers are on.

With control over the line shape now established we now show that varying ω_2 also results in control over the dissociation yield into different product channels q . Integrating $A(\varepsilon, q, n_1 - 2, n_2 | \varepsilon_i, n_1, n_2)$ over ε [Eq. (8)] for various ω_2 gives the total dissociation probability $P(q)$ as a function of ω_2 . Sample results are shown in Figs. 6 and 7 which display $P(q)$ as a function of ω_2 for the products $\text{Na}(3s) + \text{Na}(3p)$ [solid curve], $\text{Na}(3s) + \text{Na}(4s)$ [dashed curve] and $\text{Na}(3s) + \text{Na}(3d)$ [dotted curve]. In Fig. 6 Na_2 is initially in $v_i = J_i = 0$ of the ground electronic state whereas in Fig. 7 it is in $v_i = 1, J_i = 0$. The laser parameters are the same in both figures: $\omega_1 = 17880.2 \text{ cm}^{-1}$, $I_1 = 3.16 \times 10^8 \text{ W/cm}^2$, and $I_2 = 2.75 \times 10^9 \text{ W/cm}^2$. Once again, to expose the basic physics, we only include the rotational states $J = 0$ of $^1\Sigma_g$, $J = 1$ of $^1\Sigma_u$ and $^3\Pi_u$, and $J = 0$ of the continua; the inclusion of additional rotational states is discussed later below. The results in Figs. 6 and 7 show extensive variation of the relative yield of the different products as a function of ω_2 . For example, in

Fig. 6 the Na(3s)+Na(3d) product dominates entirely at most values of ω_2 , but the yield of Na(3s)+Na(3p) exceeds that of Na(3s)+Na(3d) by a factor of five at $\omega_2 \approx 13327$ and 13355 cm^{-1} . More specifically, in Fig. 6 the probabilities of generating the Na(3s)+Na(3d), Na(3s)+Na(4s) and Na(3s)+Na(3p) products at $\omega_2=13340 \text{ cm}^{-1}$, are 11.8 %, 0.24 % and 0.06 %, respectively. These are close to the corresponding values of $P(q)$ for the 'pure' 2-photon dissociation with the ω_2 laser off, which are 11 %, 0.3 % and 0.10 % for $q=3d$, $4s$, and $3p$. However, with ω_2 tuned to 13328 cm^{-1} , for example, the probability of forming Na(3s)+Na(3p) is 5.6 times larger than that of Na(3s)+Na(3d) (see Fig. 6). Similar behavior is seen in Fig. 7. Thus, extensive control over the product selectivity in the 2-photon dissociation process is clearly demonstrated.

Figures 6 and 7 show that $P(q)$ is almost a periodic function of ω_2 . The ω_2 values at which there is a strong variation in $P(q)$ satisfy the equation

$$\varepsilon_{j_2} + \hbar\omega_2 \approx \varepsilon_{j_1} + \hbar\omega_1. \quad (27)$$

At these frequencies, the dressed $|\varepsilon_{j_2}\rangle$ and $|\varepsilon_{j_1}\rangle$ states effectively overlap, strongly enhancing the interference between the dissociation pathways. Thus, with ω_1 fixed, increasing (decreasing) ω_2 by an amount equal to $\varepsilon_{j_2} - \varepsilon_{j_2-1}$ ($\varepsilon_{j_2+1} - \varepsilon_{j_2}$) brings the next lower level $|\varepsilon_{j_2-1}\rangle$ (higher level $|\varepsilon_{j_2+1}\rangle$) into the overlap region. As a consequence $P(q)$ displays, as a function of ω_2 , an almost periodic structure with period equal to the level spacing in the neighborhood of ε_{j_2} . For example, in Fig. 6 the distance between the two values of ω_2 in which there is a minimum in the Na(3s)+Na(3d) probability corresponds to the spacing between the levels $v = 89, J=1$ and $v = 90, J=1$ of the $^3\Pi_u$ electronic state. Similarly, in Fig. 7 the three dips are separated by the vibrational spacings between $(v = 100, J=1)$ and $(v = 99, J=1)$, and between $(v = 99, J=1)$ and $(v = 98, J=1)$ of the $^3\Pi_u$ electronic state, respectively.

As a consequence of this behavior, any of a host of bound states $|\varepsilon_{j_2}\rangle$ can be used to mediate the second pathway which interferes with the direct two photon dissociation pathway from $|\varepsilon_i\rangle$. This is a convenient feature which gives the experimentalist a wide

range of possible choices of ω_2 , with no loss of control.

In order to determine the magnitude of the satellite contribution associated with the two photon dissociation by $\omega_1 + \omega_2$ we carried out an extensive study of this contribution for the case shown in Fig. 6. The overall probability associated with this contribution was found to be insignificant (5×10^{-4}) in the important ω_2 regions in Fig. 6.

Cases involving more rotational states lead to more complex control patterns. Figures 8 and 9 show two examples, which show $P(q)$ as a function of ω_2 for each of the three products Na(3s)+Na(3p) [denoted $P(3p)$], Na(3s)+Na(4s) [denoted $P(4s)$] and Na(3s)+Na(3d) [denoted $P(3d)$]. Results for excitation from two initial states $|\varepsilon_i\rangle$ are shown: $v_i = 0$, $J_i = 32$ (Fig. 8) and $v_i = 0$, $J_i = 33$ (Fig. 9), both in the ground electronic state. Computations leading to Fig. 8 include the $J = 31, 33$ states of the $^1\Sigma_u$ and $^3\Pi_u$ electronic states and the $J = 32, J = 34$ of the continua; in Fig. 9 the $J = 32, J = 34$ of the $^1\Sigma_u$ and $^3\Pi_u$ and the $J = 33, J = 35$ of the continua are included. [In Fig. 8 the $J = 30$ continuum term, whose contribution to the line shapes was found to be an order of magnitude smaller than the other J contributions, was neglected. Similarly, the $J = 31$ contribution to Fig. 9 was neglected.] In both cases, $\omega_1 = 17720.8 \text{ cm}^{-1}$, the intensities $I_1 = 1.72 \times 10^8 \text{ W/cm}^2$ and $I_2 = 2.84 \times 10^8 \text{ W/cm}^2$. The line shape for the $J_i = 32$ case is that shown in Fig. 5.

Figures 8 shows four peaks in $P(3p)$ and $P(4s)$, and four corresponding dips in $P(3d)$, as ω_2 is tuned. The structure is more complex than that in Figs. 6 and 7, and is due to the couplings between rotational states. In addition the magnitude of $P(q)$ is substantially reduced due to excitation out of higher J states. Given the relatively weak laser intensities used here, the power-broadening in each of the rotational states is smaller than the rotational level spacing, allowing one to see the individual peaks. As ω_2 is varied the two dressed rotational $|v_{j_2}\rangle$ levels, with quantum numbers $J_2=31$ and 33, successively overlap with the two dressed $|v_{j_1}\rangle$ rotational states, $J_1 = 31, 33$, generating the four-peak structure in $P(q)$. In particular, the first $P(3p)$ and $P(4s)$ peak [and the first $P(3d)$ dip] is due to the coupling between the $J_1 = 31$ and $J_2 = 33$ states, the second due to the coupling between the $J_1 = 31$ and $J_2 = 31$, and the third due to the coupling between the $J_1 = 33$ and $J_2 = 33$. A similar

situation occurs in Fig. 9, where the first $P(3p)$ and $P(4s)$ peak [and first $P(3d)$ dip] is due to the coupling between the $J_1 = 32$ and $J_2 = 34$ states, the second (at $\omega_2 = 13324 \text{ cm}^{-1}$, but much suppressed) due to the coupling between the $J_1 = 32$ and $J_2 = 34$, and the third due to the coupling between the $J_1 = 34$ and $J_2 = 34$.

Some minimal appreciation of the expected $P(q)$ in the case of control in a thermal environment [13] results by computing a weighted sum of Figs. 8 and 9. Since the positions of the peaks and valleys in these two figures are dissimilar, one expects to produce a spiky control pattern. Figure 10 shows a plot of the ratio $P(4s)/P(3d)$ [Fig. 10(a)] and the ratio $P(3p)/P(3d)$ [Fig. 10(b)] as a function of ω_2 , assuming that the initial populations in $(v_i = 0, J_i = 32)$ and $(v_i = 0, J_i = 33)$ are equal. Due to the selectivity of the resonant 2-photon process, which in this case favors dissociation from $(v_i = 0, J_i = 32)$ (Fig. 8), the contribution to the control is largely weighted by the results in Fig. 8. Nonetheless, an increasing number of peaks are evident in Fig. 10 due to the contributions of more initial states. Although this is a simplified model, it suggests that the control should survive in a thermal environment, although a complicated $P(q)$ is anticipated. This is in accord with currently ongoing experiments [13].

IV. SUMMARY

We have shown that the resonant 2-photon dissociation of molecules can be controlled by illuminating the system with an independent intense laser, which need not be coherent relative to the excitation laser. The control results from laser induced interference, which depends upon the frequency of the control laser. Computations on photodissociation in Na_2 show that control over three different product yields is extensive.

ACKNOWLEDGMENTS

This work was supported by the U.S. Office of Naval Research under contract number N00014-90-J-1014.

REFERENCES

* Permanent Address: Chemical Physics Department, The Weizmann Institute of Science, Rehovot, 76100 Israel

- [1] P. Brumer and M. Shapiro, *Accounts of Chem. Res.* **22**, 407 (1989); P. Brumer and M. Shapiro, *Ann. Rev. Phys. Chem.* **43**, 257 (1992); M. Shapiro and P. Brumer, *Int. Reviews Phys. Chem.* **13**, 187 (1994).
- [2] M. Yu. Ivanov, P.B. Corkum and P. Dietrich, *Laser Physics* **3**, 375 (1993).
- [3] A.D. Bandrauk, J-M. Gauthier and J.F. McCann, *Chem. Phys. Lett.* **200**, 399 (1992).
- [4] D.J. Tannor, and S.A. Rice, *Adv. Chem. Phys.* **70**, 441 (1988); S. Tersigni, P. Gaspard and S.A. Rice, *J. Chem. Phys.* **93**, 1670, (1990); S. Shi, and H. Rabitz, *J. Chem. Phys.* **92**, 364 (1990); J.L. Krause, R.M. Whitnell, K.R. Wilson, Y. Yan and S. Mukamel, *J. Chem. Phys.* **99**, 6562 (1993)
- [5] H.G. Muller, P.H. Bucksbaum, D.W. Schumacher and A. Zavriyev, *J. Phys. B* **23**, 2761 (1990); R.M. Potvliege and P.H.G. Smith, *J. Phys. B* **25**, 2501 (1992).
- [6] K.J. Schafer and K.C. Kulander, *Phys. Rev. A* **45**, 8026 (1992).
- [7] C. Chen, Y-Y. Yin, and D.S. Elliott, *Phys. Rev. Lett.*, **64**, 507 (1990). S-P. Lu, S.M. Park, Y. Xie, and R.J. Gordon, *J. Chem. Phys.*, **96**, 6613 (1992).
- [8] T. Nakajima and P. Lambropoulos, *Phys. Rev. Lett.*, **70**, 1081 (1993).
- [9] E. Charron, A. Guisti-Suzor and F.H. Mies, *Phys. Rev. Lett.* **71**, 692 (1993).
- [10] P.L. Knight, M.A. Lauder and B.J. Dalton, *Phys. Reports* **190**, 1 (1990); O. Faushder, D. Charalambidis, C. Fotakis, J. Zhang and P. Lambropoulos, *Phys. Rev. Lett.* **70**, 3004 (1993)
- [11] Z. Chen, M. Shapiro and P. Brumer, *Chem. Phys. Lett.* **228**, 289 (1994).

- [12] Z. Chen, M. Shapiro and P. Brumer, *J. Chem. Phys.* (in press)
- [13] I. Sofer, A. Shnitman, I. Golub, A. Yogeve, M. Shapiro, Z. Chen and P. Brumer, (work in progress)
- [14] R. D. Levine, *Quantum Mechanics of Molecular Rate Processes*, (Clarendon, Oxford, England, 1969); P. Brumer and M. Shapiro, *Adv. Chem. Phys.* **60**, 371 (1986).
- [15] M. Shapiro and H. Bony, *J. Chem. Phys.* **83**, 1588 (1985); G. G. Balint-Kurti and M. Shapiro, *Adv. Chem. Phys.* **60** 403, (1986); A. D. Bandrauk and O. Atabek, *Adv. Chem. Phys.* **73** 823, J. O. Hirschfelder, Ed, (Wiley, New York, 1989).
- [16] C. Cohen-Tannoudji, J. Dupont-Roc and G. Grynberg, *Atom-Photon Interactions* (John Wiley & Sons, 1992).
- [17] Z. Chen, M. Shapiro and P. Brumer, *J. Chem. Phys.* **98**, 8647 (1993).
- [18] I. Schmidt, Ph.D. Thesis, Kaiserslautern University, 1987.

FIGURES

FIG. 1. Na_2 potential energy curves. Only the major contributors to dissociation are included in the figure. For additional curves included in the computation, see text. Resonant two photon dissociation occurs by coupling the bound states $|\epsilon_i\rangle$, with the ω_1 laser, to the dissociation continua via intermediate states $|\epsilon_{j_1}\rangle$. The control laser ω_2 couples the continua to the initially unpopulated bound states $|\epsilon_{j_2}\rangle$.

FIG. 2. The line shape for pure 2-photon dissociation: $\log A(\epsilon, q, n_1 - 2|\epsilon_i, n_1)$ vs. ϵ for (a) the $\text{Na}(3s)+\text{Na}(3p)$ product (solid curve), and (b) the $\text{Na}(3s)+\text{Na}(4s)$ product (dashed curve). Here $\omega_1 = 16154.7 \text{ cm}^{-1}$ and $I_1 = 8.7 \times 10^9 \text{ W/cm}^2$.

FIG. 3. The line shape for photodissociation with two lasers on. $\log A(\epsilon, q, n_1 - 2, n_2|\epsilon_i, n_1, n_2)$ vs. ϵ for (a) $\text{Na}(3s)+\text{Na}(3p)$ product (solid curve), (b) $\text{Na}(3s)+\text{Na}(4s)$ product (dashed curve). The control laser parameters are $\omega_2 = 14939.6 \text{ cm}^{-1}$, and the intensity $I_2 = 3.5 \times 10^{10} \text{ W/cm}^2$. Other parameters are as in Fig. 2.

FIG. 4. As in Fig. 3, but with $\omega_2 = 14961.5 \text{ cm}^{-1}$.

FIG. 5. $\log A(\epsilon, q, n_1 - 2, n_2|\epsilon_i, n_1, n_2)$ vs. ϵ , with rotations included. (a) $\text{Na}(3s)+\text{Na}(3p)$ product, (b) $\text{Na}(3s)+\text{Na}(4s)$ product, and (c) $\text{Na}(3s)+\text{Na}(3d)$ product. Here $\omega_1 = 17720.8 \text{ cm}^{-1}$, $\omega_2 = 13332.8 \text{ cm}^{-1}$, and the intensities $I_1 = 1.72 \times 10^8 \text{ W/cm}^2$ and $I_2 = 2.84 \times 10^8 \text{ W/cm}^2$.

FIG. 6. Probability of dissociation into channel q , $P(q)$, as a function of ω_2 : for the (a) $\text{Na}(3s)+\text{Na}(3p)$ product (solid curve), (b) for the $\text{Na}(3s)+\text{Na}(4s)$ product (dashed curve), and (c) for the $\text{Na}(3s)+\text{Na}(3d)$ product (dotted curve). The molecule is initially in $v_i = 0, J_i = 0$ of the ground electronic state. Here $\omega_1 = 17880.2 \text{ cm}^{-1}$, $I_1 = 3.16 \times 10^8 \text{ W/cm}^2$, and $I_2 = 2.75 \times 10^9 \text{ W/cm}^2$.

FIG. 7. As in Fig. 6, but the molecule is initially in $v_i = 1, J_i = 0$ of the ground electronic state.

FIG. 8. $P(q)$ as a function of ω_2 , for higher initial rotational state. (a) for the Na(3s)+Na(3p) product (solid curve), (b) for the Na(3s)+Na(4s) product (dashed curve), and (c) for the Na(3s)+Na(3d) product (dotted curve). Both curves (a) and (b) have been multiplied by a factor of ten to better display the results. The molecule is initially in $v_i = 0, J_i = 32$ of the ground electronic state. $\omega_1 = 17720.8 \text{ cm}^{-1}$, $I_1 = 1.72 \times 10^8 \text{ W/cm}^2$, and $I_2 = 2.84 \times 10^8 \text{ W/cm}^2$.

FIG. 9. As in Fig. 8, but with the molecule initially in $v_i = 0, J_i = 33$ of the ground electronic state.

FIG. 10. The ratios of photodissociation products vs. ω_2 , assuming the molecule is initially populated with equal probability in $(v_i = 0, J_i = 32)$ and $(v_i = 0, J_i = 33)$ of ground electronic. (a) For $P(4s)/P(3d)$ and (b) for $P(3p)/P(3d)$. Here $\omega_1 = 17720.8 \text{ cm}^{-1}$, $I_1 = 1.72 \times 10^8 \text{ W/cm}^2$ and $I_2 = 2.84 \times 10^8 \text{ W/cm}^2$.

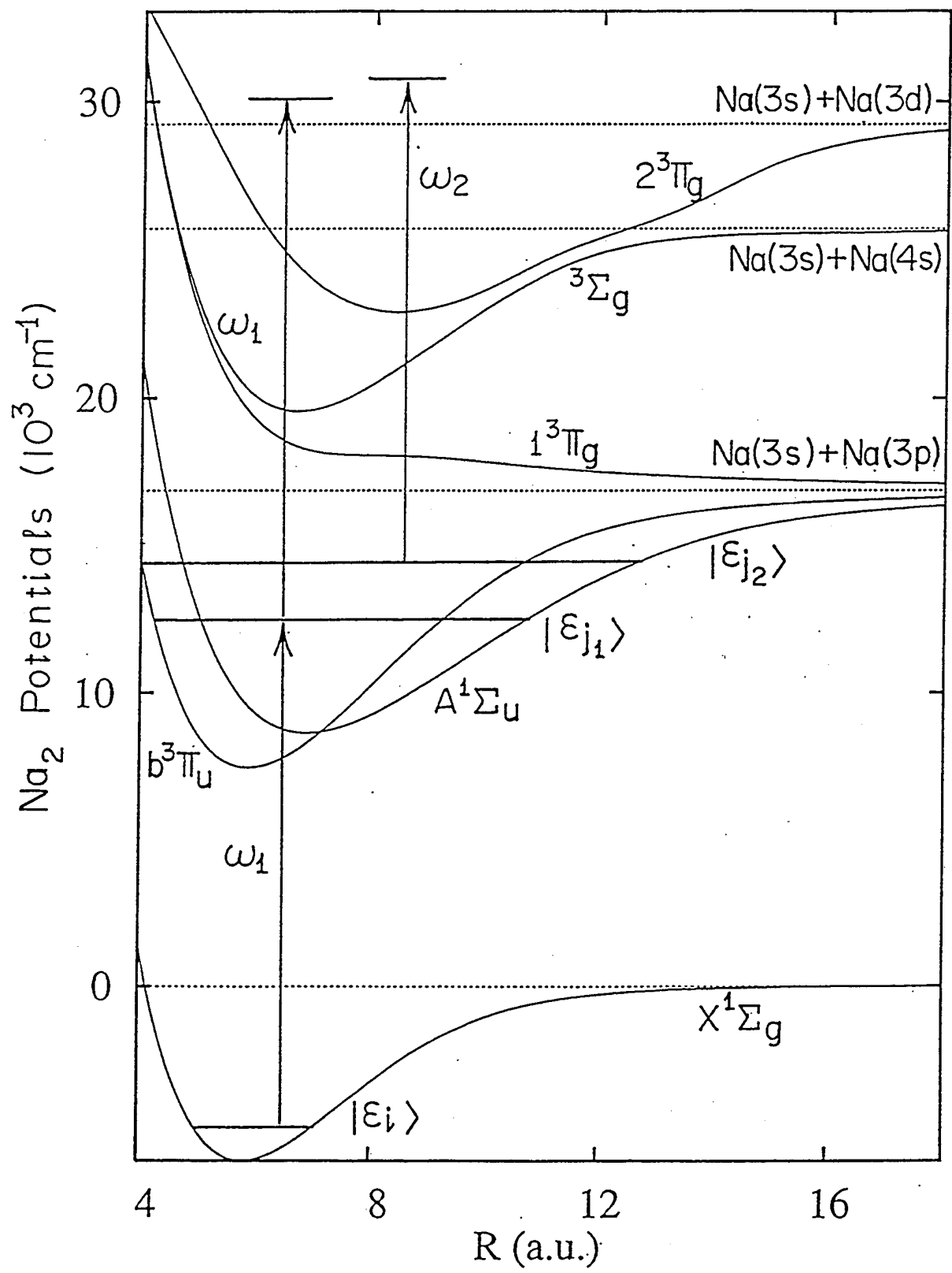


Fig 1

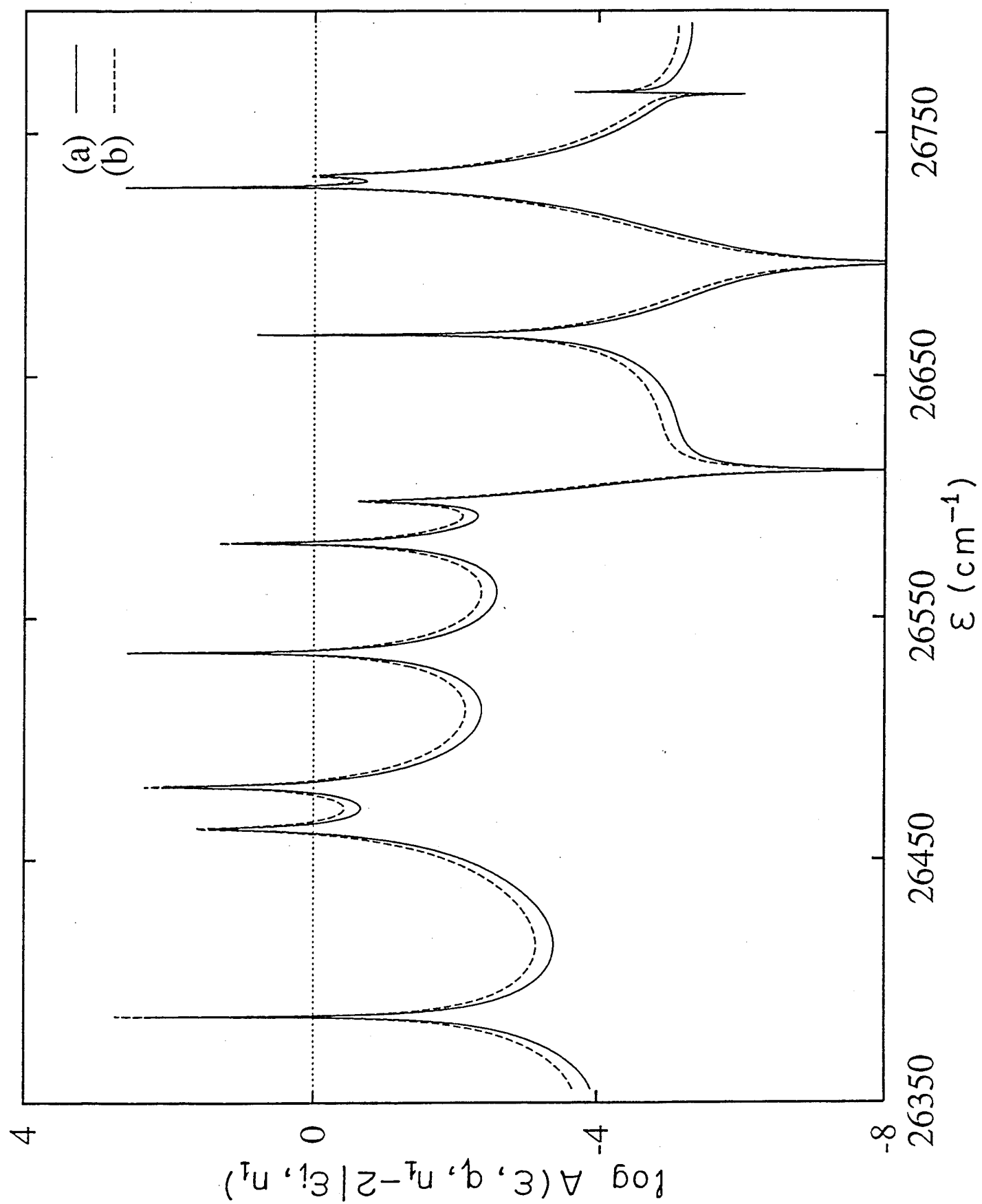


Fig 2

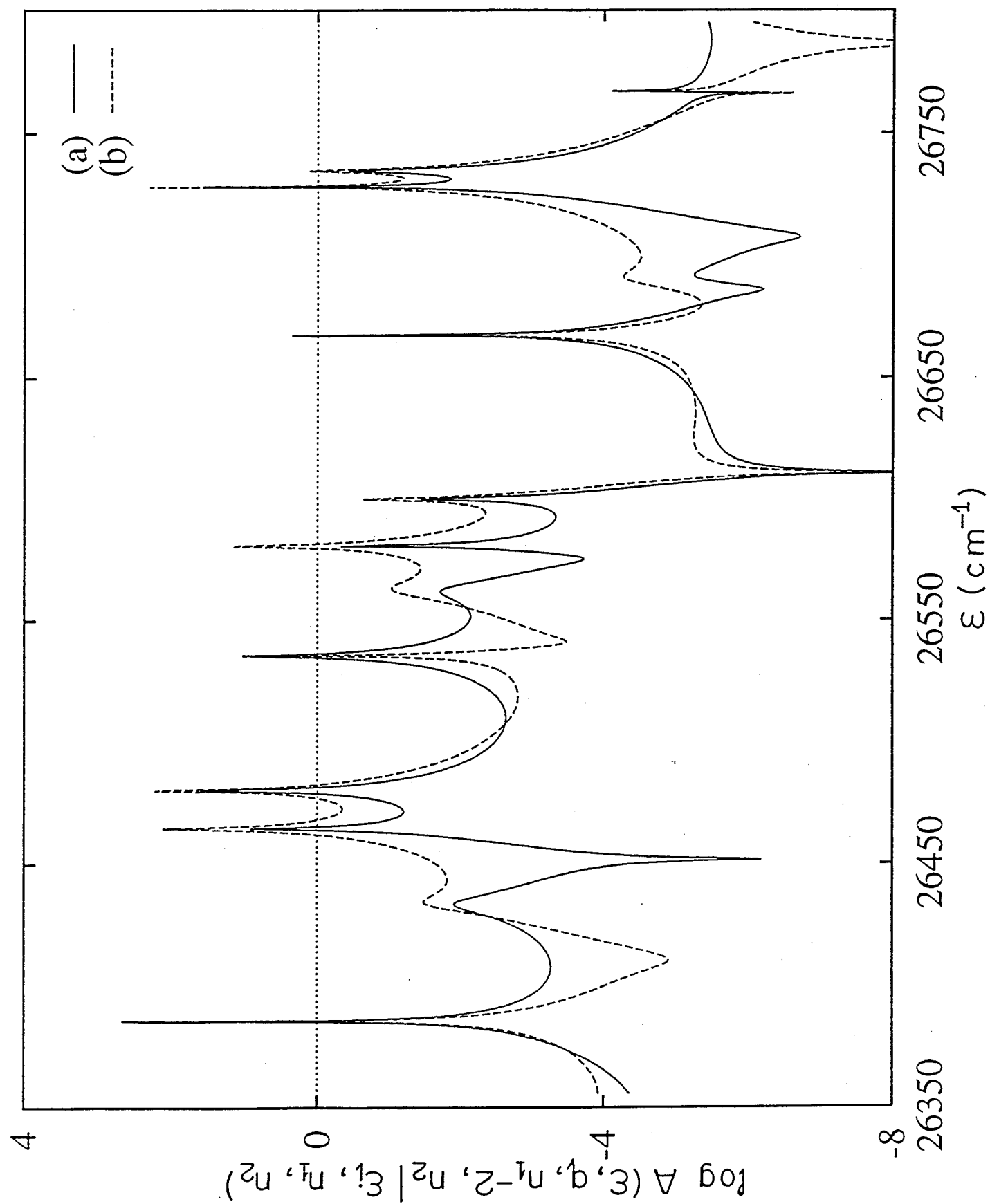


Fig 3

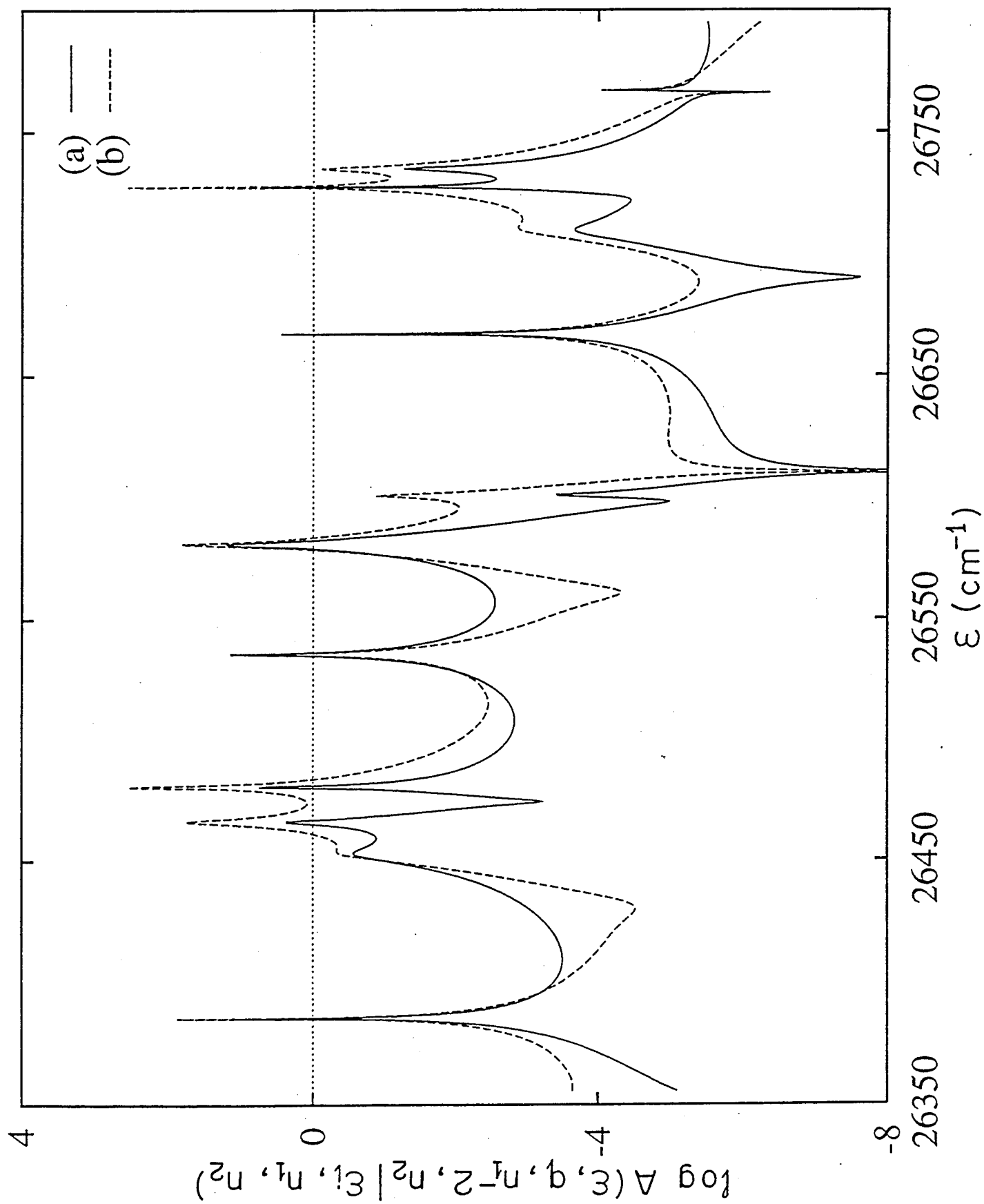
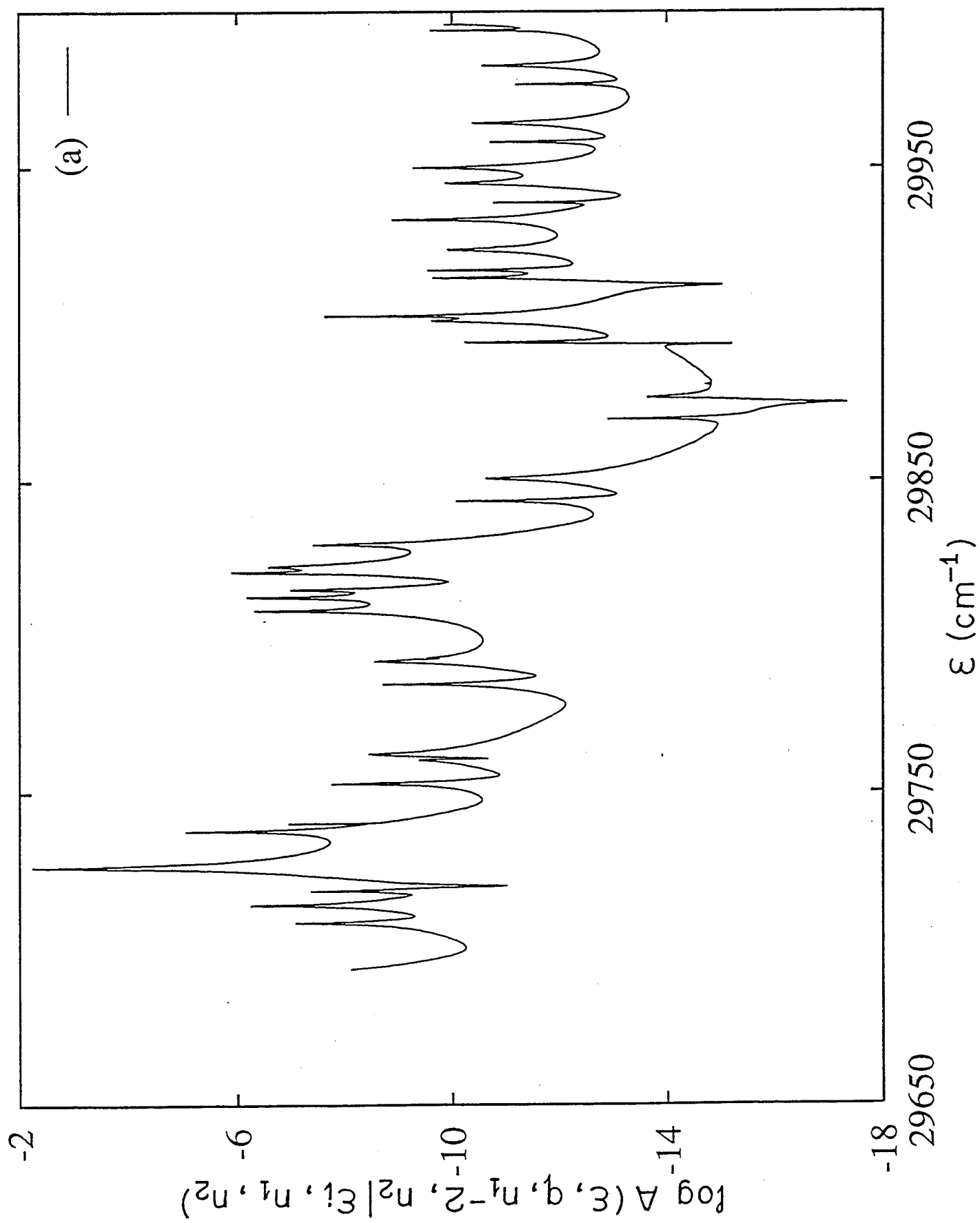


Fig 4

Fig 5a



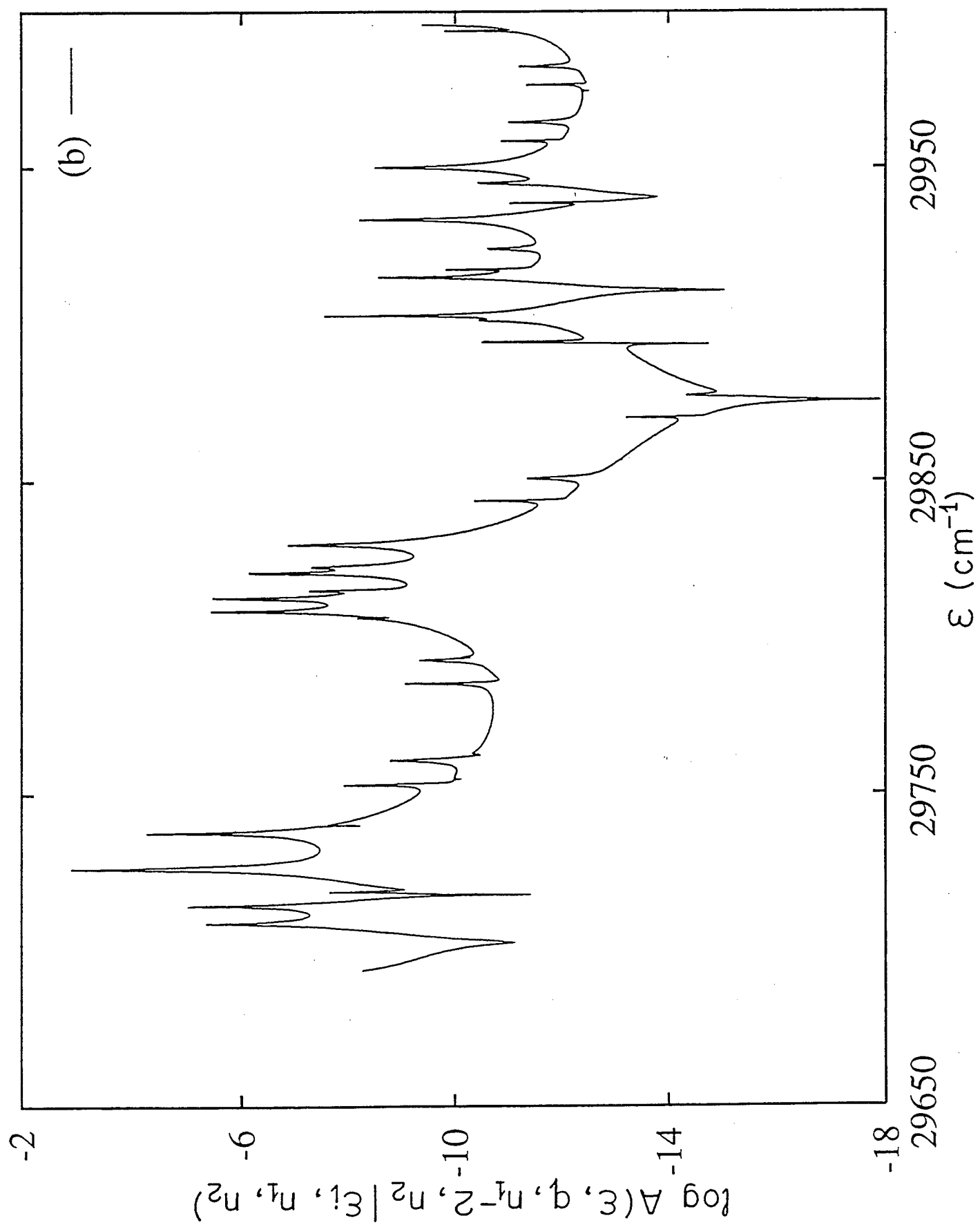


Fig 56

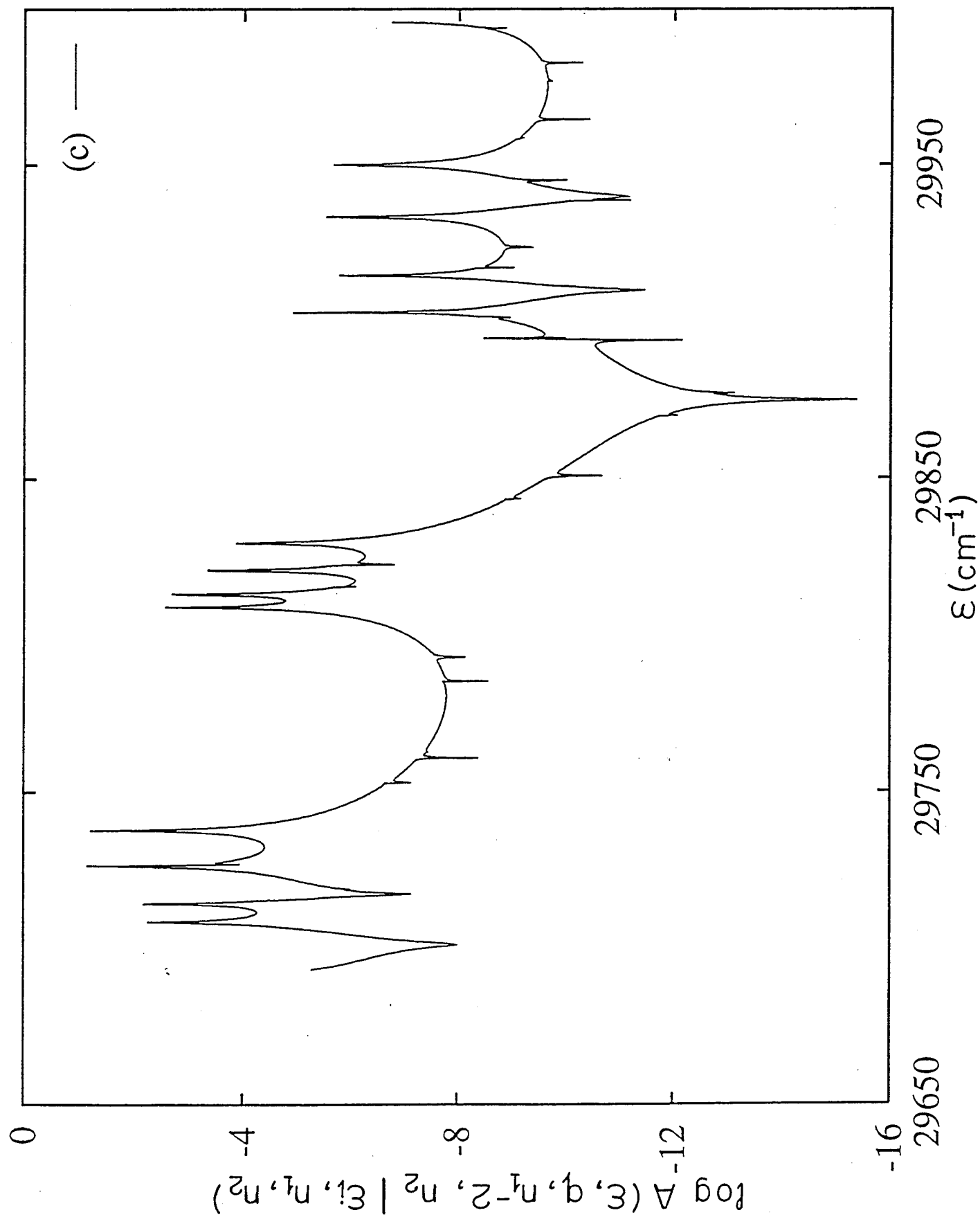
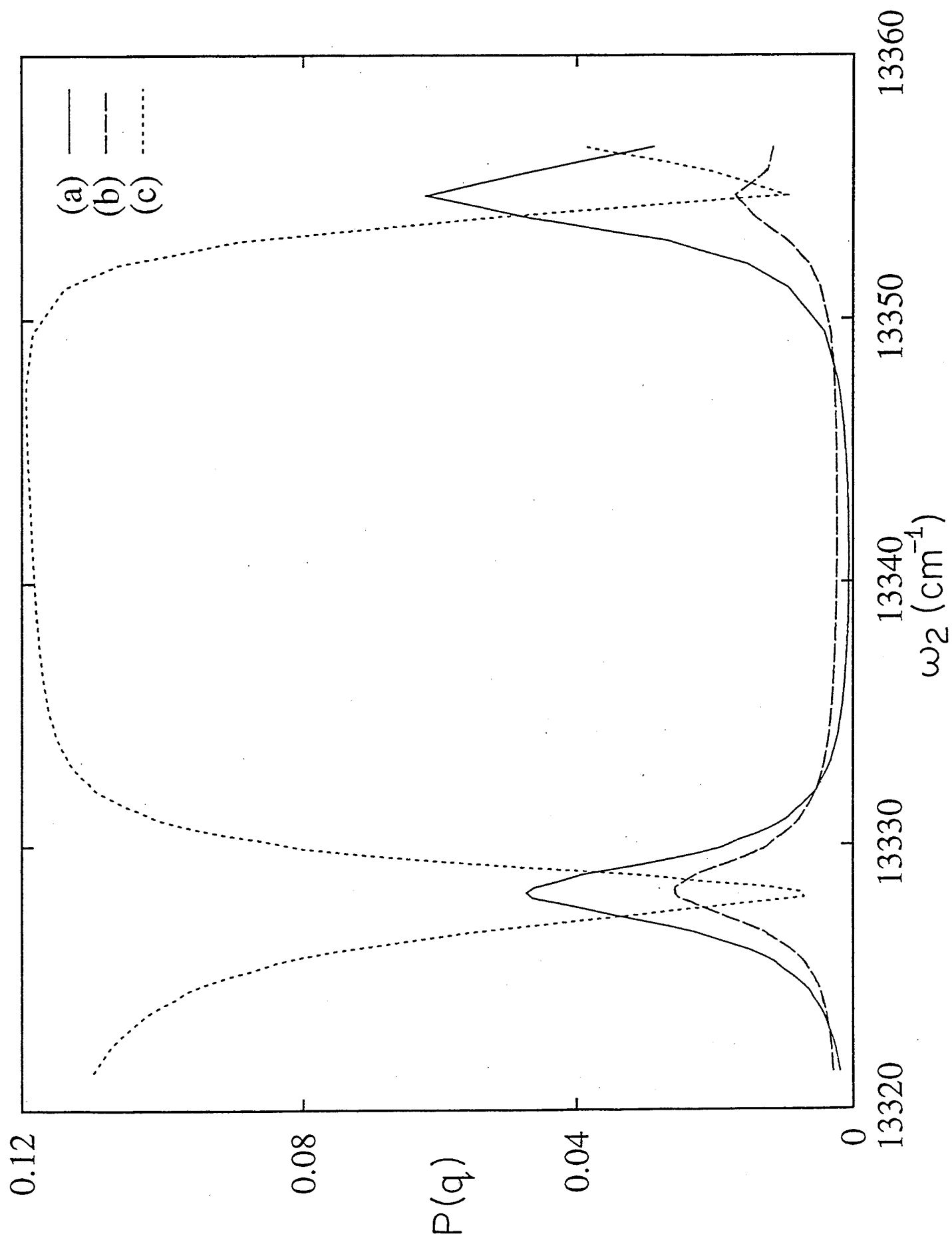
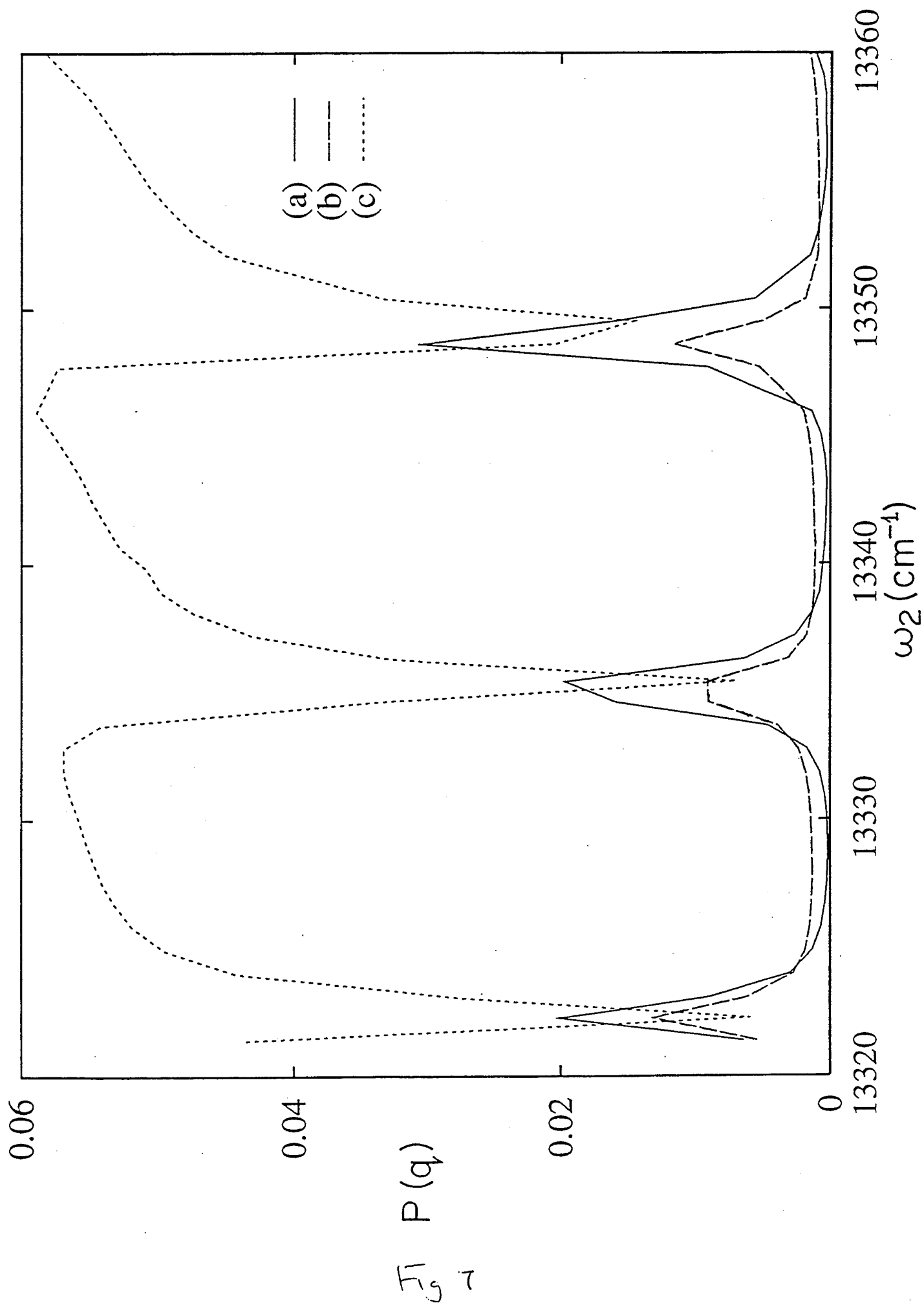
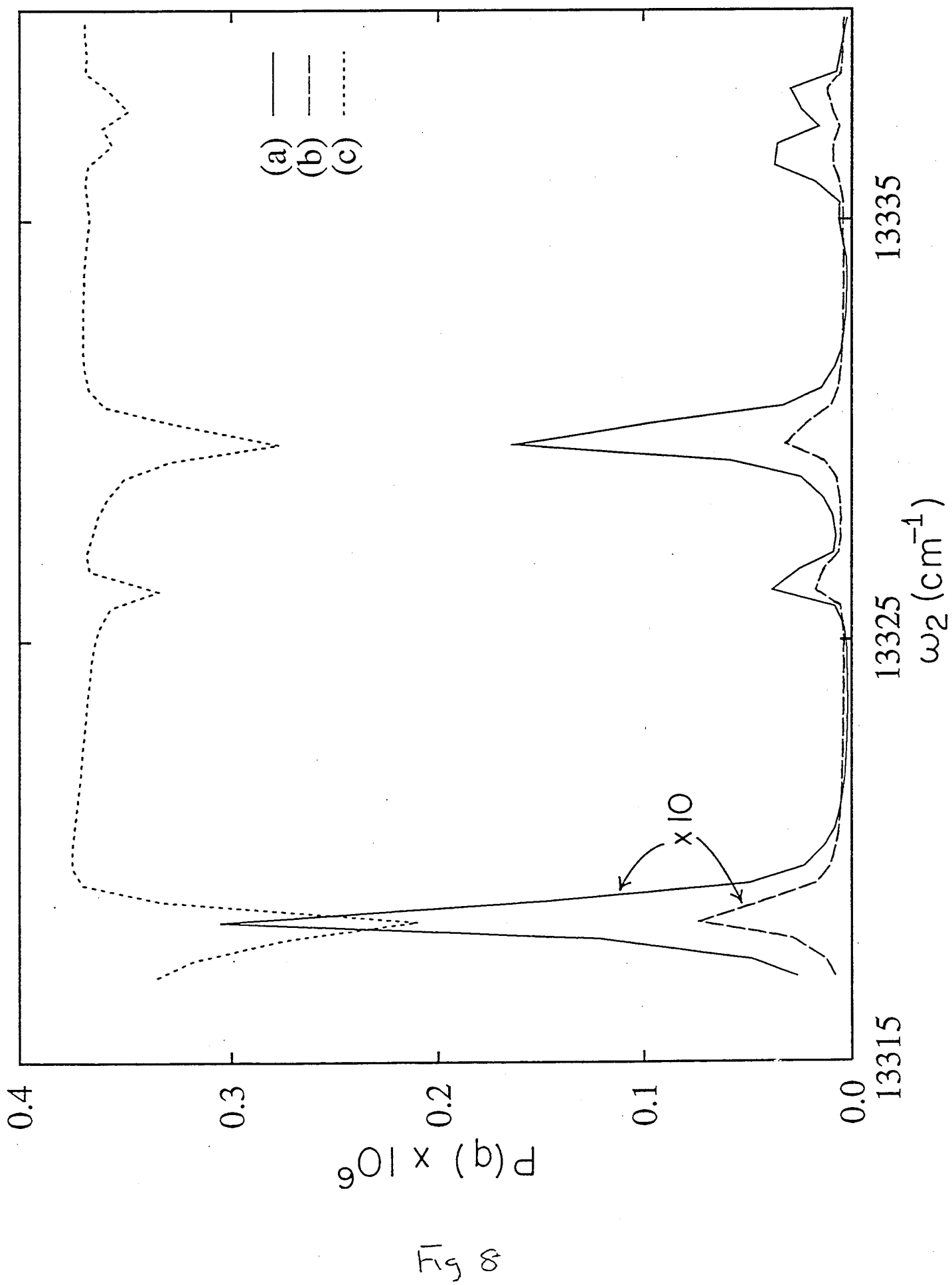


Fig 6







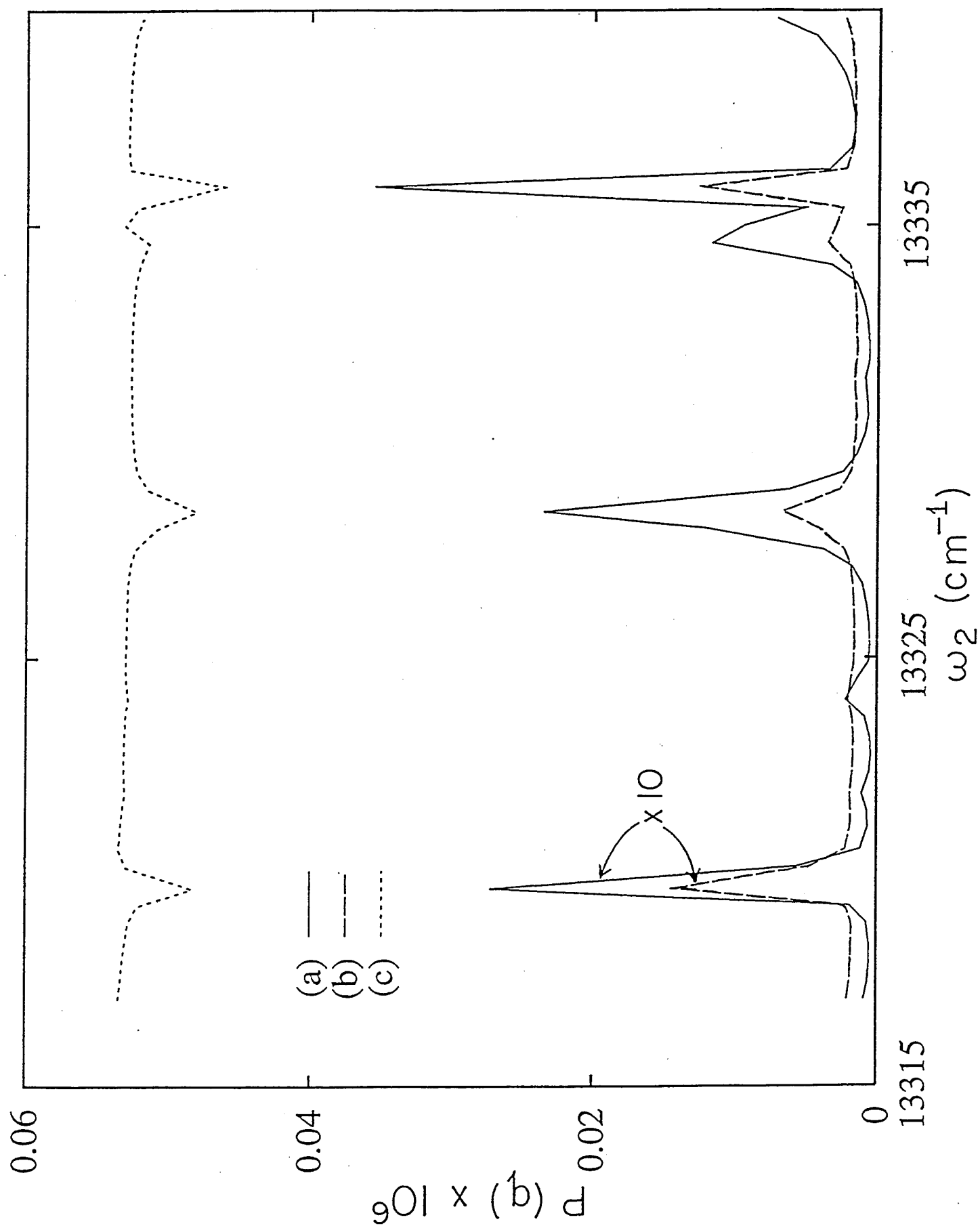
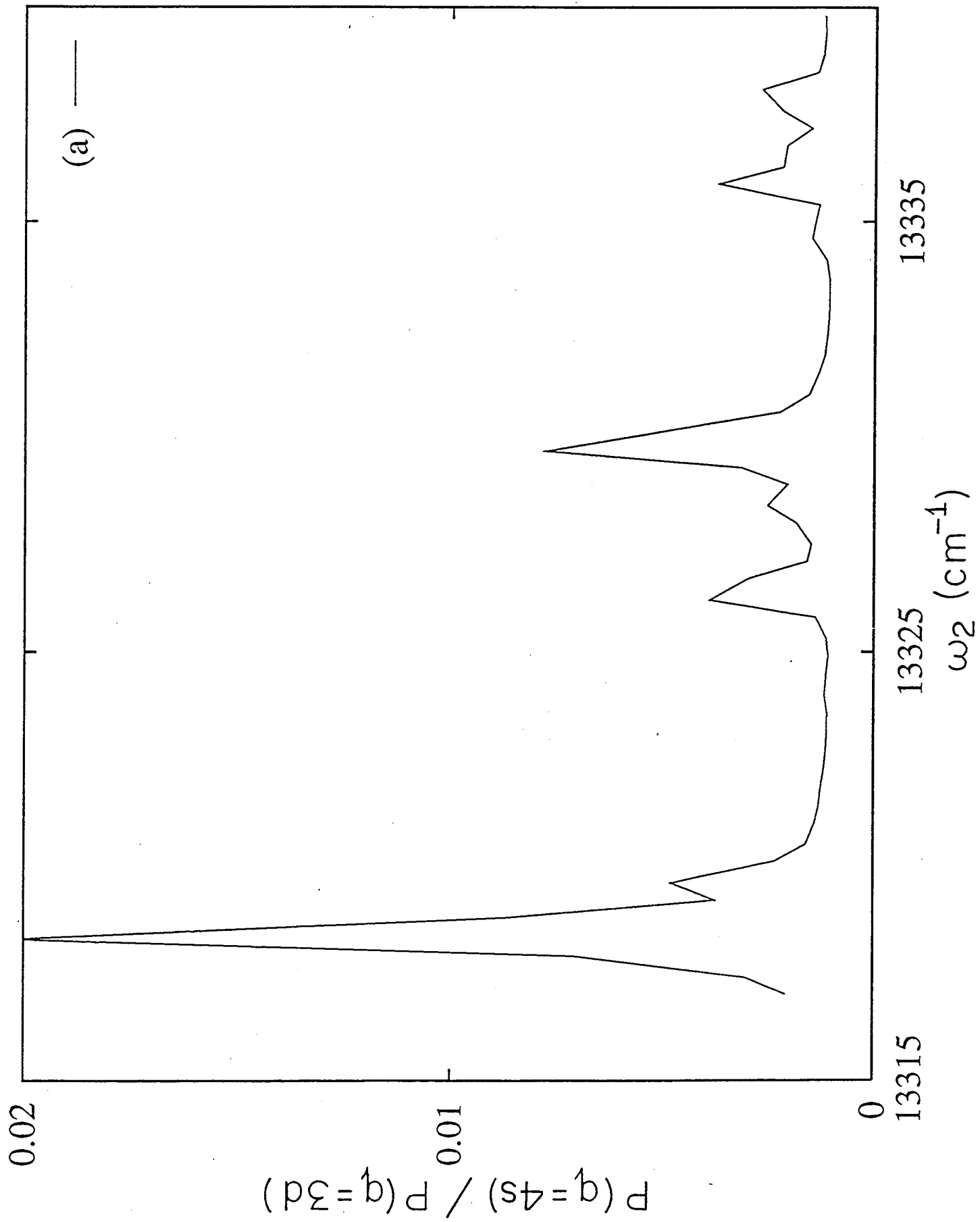
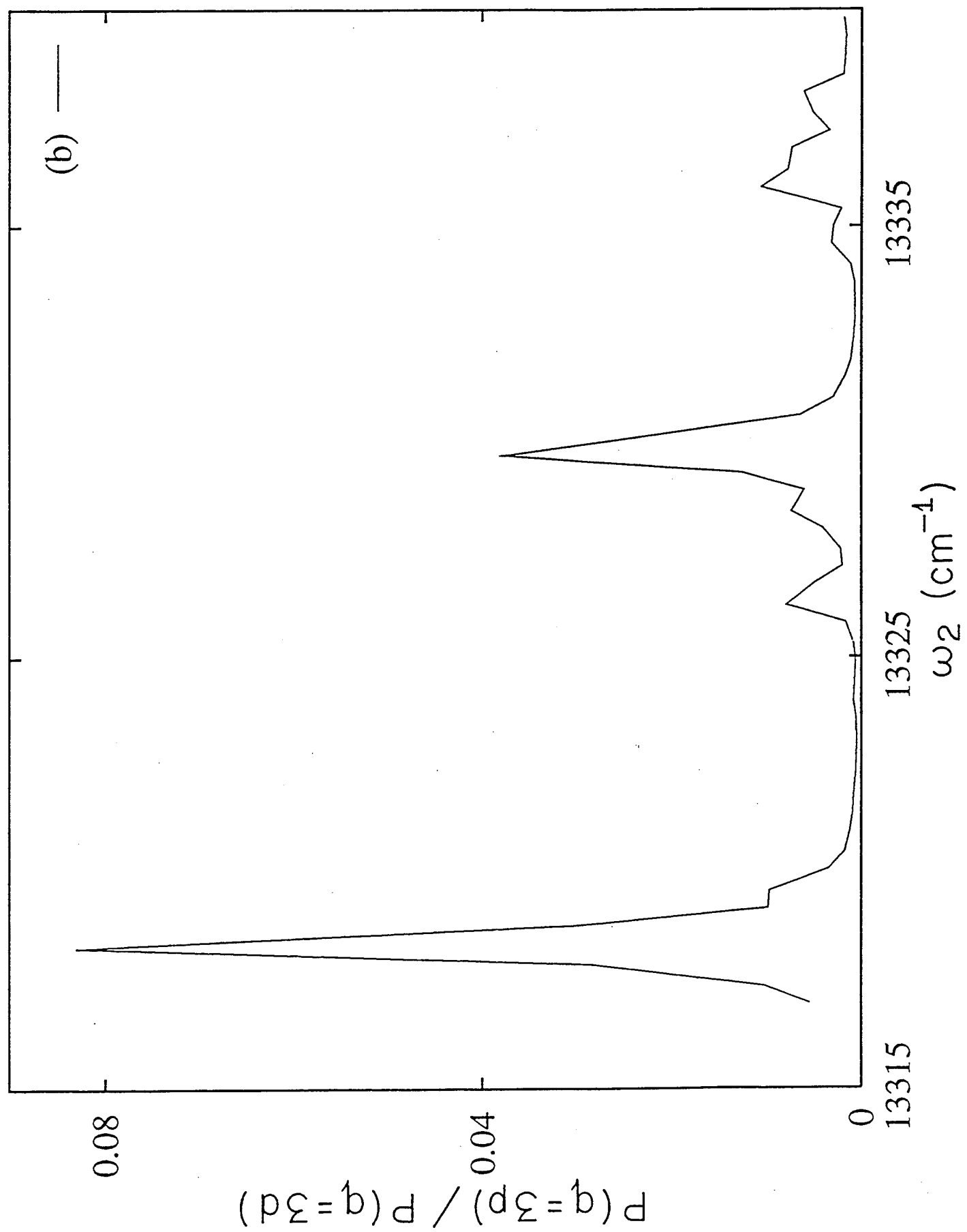


Fig 9

Fig. 10a





Pump-Dump Coherent Control with Partially Coherent Laser Pulses

Xue-Pei Jiang, Moshe Shapiro* and Paul Brumer

Chemical Physics Theory Group, Department of Chemistry

University of Toronto, Toronto, M5S 1A1 Canada

(April 13, 1995)

Abstract

The theory of coherent control of photodissociation with partially coherence laser pulses is developed and applied to the pump-dump control scenario of a collinear model of DH_2 . The coherence characteristics of the pump pulse are shown to be crucial for maintaining control over the product yield, whereas the coherence properties of the dump pulse are only of secondary importance. Control is shown to survive for partially coherent laser pulses, but only for a range of incoherence which precludes control with typical nanosecond laser pulses.

I. INTRODUCTION

Over the past few years, we have formally demonstrated, and computationally verified, that isolated molecular processes can be controlled through excitation with coherent laser sources [1]- [4]. Typically, control is achieved by optically exciting a system in a pure state via more than one coherent excitation route. Interference between these multiple routes, varied through instrumental parameters such as field amplitudes and relative laser phase, results in control over product ratios in molecular processes. Both computational

[1] and experimental studies [5] show that interference effects allow for extensive control over product ratios and probabilities in isolated molecular systems, with near total control possible in some circumstances.

Interference phenomena rely upon the existence of a well defined phase, in this case that of the excited state created by optical excitation. This, in turn, relies both upon coherence characteristics of the molecule prior to excitation, as well as the phases of the optical excitation sources. If both the molecule and laser source are in pure states (e.g. an eigenstate of the molecular Hamiltonian excited with a transform limited pulse) then the excited state is pure and the phases well defined. In many instances, however, either the source or the molecule is a mixed state, introducing partial incoherence effects. We [4] and others [6] have previously discussed the effect of collisional dephasing of the molecular state upon control in an early CW laser control scenario. Here we consider the effect of the partial coherence of the laser source on control in a pump-dump scenario. In the pump-dump scenario [2], control over yield ratios is obtained by varying the tuning characteristics of a pump and dump pulse, as well as the time delay between them. Here we attempt to assess the extent to which control survives laser incoherence.

The structure of this paper is as follows. Section 2 introduces sequential pulse control with partially coherent sources using an approach based on our previous analysis of the two-frequency correlation function describing partially coherent sources [7]. Utilizing a generalized Parseval equality allows us to demonstrate conditions under which the incoherence of the dump pulse is irrelevant to control. Section 3 describes computations on the dissociation of a collinear model of DH_2 to produce $\text{H}+\text{DH}$ and $\text{D}+\text{H}_2$, with a focus on the range of control as the pump laser incoherence increases. Section 4 contains a brief summary.

II. SEQUENTIAL CONTROL WITH PARTIALLY COHERENT PULSES

Control via sequential partially coherent pulses constitutes a straightforward, but significant, extension of the theory for purely coherent pulses [2]. We briefly summarize the

characterization of a partially coherent pulse and then incorporate the description into the control scenario.

A. Partially Coherent Sources

To characterize partially coherent pulses we utilize a model which we have previously applied to intramolecular dynamics induced by partially coherent pulses [7]. Consider a Gaussian laser pulse with time profile $\bar{\epsilon}_x(t)$ and phase $\delta_x(t)$, i.e.

$$\bar{\epsilon}_x(t) = (\epsilon_{x0}/2)e^{-(t-t_x)^2/\tau_x^2}e^{-i(\omega_x t + \delta_x(t))}. \quad (1)$$

Here τ_x is the pulse time width and the pulse is centered about frequency ω_x at time t_x . We adopt a phase diffusion model for the incoherent laser source and assume a Gaussian correlation for the stochastic phases with a decorrelation time scale τ_{xc} . That is, we assume

$$\langle e^{i\delta_x(t_2)}e^{-i\delta_x(t_1)} \rangle = e^{-(t_2-t_1)^2/2\tau_{xc}^2}, \quad (2)$$

where the angle brackets denote an average over the ensemble of laser phases.

Below we require the frequency-frequency correlation function $\langle \epsilon_x(\omega_2)\epsilon_x^*(\omega_1) \rangle$. Here $\epsilon_x(\omega)$ is the Fourier transform of $\bar{\epsilon}(t)$ for $\delta_x(t)$ equal to a constant δ_x , i.e.

$$\epsilon_x(\omega) = 2^{-3/2}\epsilon_{x0}\tau_x e^{-i(\omega_x-\omega)t_x}e^{-\tau_x^2(\omega-\omega_x)^2/4}e^{-i\delta_x} \quad (3)$$

In the phase diffusion model, $\delta_x(t)$ is time dependent, its random variations being incorporated by ensemble averaging over a distribution of δ_x . In particular, assuming Gaussian pulses [Eqs. (1)-(2)], we get [7]

$$\langle \epsilon_x(\omega_2)\epsilon_x^*(\omega_1) \rangle = \frac{\epsilon_{x0}^2\tau_x T_x}{8}e^{i(\omega_2-\omega_1)t_x}e^{-\tau_x^2(\omega_2-\omega_1)^2/8}e^{-T_x^2(\omega_2+\omega_1-2\omega_x)^2/8}, \quad (4)$$

where

$$T_x = \tau_x\tau_{xc}/(\tau_x^2 + \tau_{xc}^2)^{1/2} \quad (5)$$

The pump-dump control scenario, the subject of this paper, involves two lasers. Hence we adopt a similar description for the dump pulse $\bar{\epsilon}_d(t)$, with appropriate change in parameter labels, i.e.

$$\bar{\epsilon}_d(t) = (\epsilon_{d0}/2)e^{-(t-t_d)^2/\tau_d^2}e^{-i(\omega_d t + \delta_d(t))}, \quad (6)$$

$$\langle e^{i\delta_d(t_2)}e^{-i\delta_d(t_1)} \rangle = e^{-(t_2-t_1)^2/2\tau_{dc}^2}, \quad (7)$$

$$\langle \epsilon_d(\omega_2)\epsilon_d^*(\omega_1) \rangle = \frac{\epsilon_{d0}^2\tau_d T_d}{8}e^{i(\omega_2-\omega_1)t_d}e^{-\tau_d^2(\omega_2-\omega_1)^2/8}e^{-T_d^2(\omega_2+\omega_1-2\omega_d)^2/8}, \quad (8)$$

where

$$T_d = \tau_d\tau_{dc}/(\tau_d^2 + \tau_{dc}^2)^{1/2}. \quad (9)$$

Here τ_{xc} and τ_{dc} define the degree of field coherence, the two limiting cases being a coherent source ($\tau_{ic} \rightarrow \infty, i = x, d$) and fully incoherent source ($\tau_{ic} \rightarrow 0, i = x, d$).

The significant parameter to describe characteristics of the laser-molecule interaction is the frequency spectrum of the pulse. For the excitation pulse this is given by

$$I_x(\omega) = \frac{T_x}{\sqrt{2\pi}}e^{-T_x^2(\omega-\omega_x)^2/2} \quad (10)$$

whose full width at half maximum (FWHM) is $2\sqrt{2\ln 2}/T_x$. For the coherent pulse $T_x = \tau_x$ giving a FWHM of the intensity spectrum equal to $\Delta_x/\sqrt{2}$ where $\Delta_x \equiv 4\sqrt{\ln 2}/\tau_x$ is the FWHM of the frequency profile [Eq.(3)] of the pulse. Similar definitions apply to characterize the dump pulse. Further, for consistency we define the partial coherence parameter $\Delta_{xc} = 4\sqrt{\ln 2}/\tau_{xc}$ and similar parameters (Δ_d, Δ_{dc}) for the dump pulse. Note that fitting Eq. (10) to the measured pulse frequency spectrum provides a means of obtaining T_x and ω_x from experimental data [7].

B. Control of Photodissociation

We first summarize the expressions for control using sources with known phases [2], i.e., fully coherent sources. We then average over the ensemble of laser phases characterizing the

partially coherent pulse to give the result for control in the presence of partially coherent sources.

Consider then a molecule with Hamiltonian H_M (with eigenkets and eigenvalues denoted $|E_n\rangle$ and E_n) subjected to an external field comprised of two temporally separated pulses $\bar{\epsilon}(t) = \bar{\epsilon}_x(t) + \bar{\epsilon}_d(t)$. The total Hamiltonian is of the form:

$$H = H_M + V = H_M - \mu[\bar{\epsilon}(t) + \bar{\epsilon}^*(t)] \quad (11)$$

where μ is the dipole operator along the electric field direction. The $\bar{\epsilon}_x(t)$ pulse lifts the system to the excited electronic states with nuclear eigenfunctions $|E_n\rangle$ and $\bar{\epsilon}_d(t)$ subsequently induces a transition to a lower or higher surface where dissociation occurs. The fields are assumed sufficiently weak for perturbation theory to be valid.

If the molecule is initially in state $|E_g\rangle$ then the state prepared after the $\bar{\epsilon}_x(t)$ pulse, whose width is chosen to excite a number of levels $|E_j\rangle$, is given in first order perturbation theory (at times [8] $t > t_x + 2\tau_x$) as:

$$|\phi(t)\rangle = |E_g\rangle e^{-iE_g t/\hbar} + \sum_j c_j |E_j\rangle e^{-iE_j t/\hbar} \quad (12)$$

with

$$c_j = (\sqrt{2\pi}/i\hbar) \langle E_j | \mu | E_g \rangle \epsilon_x(\omega_{jg}) \equiv d_j \epsilon_x(\omega_{jg}) \quad (13)$$

where $\omega_{jg} = (E_j - E_g)/\hbar$ is the excitation frequency from $|E_g\rangle$ to $|E_j\rangle$ and where d_j is defined by the second equality.

Subsequently, the system is subjected to a dump pulse $\bar{\epsilon}_d(t)$. Its wavefunction, expanded in a complete set of continuum eigenstates $|E, n, q^-\rangle$ labeled by energy E , arrangement channel label q and remaining quantum labels n is then:

$$|\psi(t)\rangle = |\phi(t)\rangle + \sum_{n,q} \int dE B(E, n, q|t) |E, n, q^-\rangle e^{-iEt/\hbar} \quad (14)$$

The probability $P(E, q)$ of forming product in arrangement channel q at energy E is given by [2]

$$P(E, q) = (2\pi/\hbar^2) \sum_n \left| \sum_j c_j \langle E, n, q^- | \mu | E_j \rangle \epsilon_d(\omega_{EE_j}) \right|^2 \quad (15)$$

where $\omega_{EE_j} = (E - E_j)/\hbar$ and c_j are given by Eqs. (12) and (13). Note that the sum is over all quantum numbers n , including scattering angles.

Expanding the square allows us to write the probability in a canonical form:

$$\begin{aligned} P(E, q) &= (2\pi/\hbar^2) \sum_{ij} c_i c_j^* \epsilon_d(\omega_{EE_i}) \epsilon_d^*(\omega_{EE_j}) \mu_{i,j}^{(q)}(E) \\ &= (2\pi/\hbar^2) \sum_{ij} d_i d_j^* \epsilon_x(\omega_{ig}) \epsilon_x^*(\omega_{jg}) \epsilon_d(\omega_{EE_i}) \epsilon_d^*(\omega_{EE_j}) \mu_{i,j}^{(q)}(E) \end{aligned} \quad (16)$$

where

$$\mu_{i,j}^{(q)}(E) \equiv |\mu_{i,j}^{(q)}(E)| e^{i\alpha_{i,j}^{(q)}(E)} = \sum_n \langle E, n, q^- | \mu | E_i \rangle \langle E_j | \mu | E, n, q^- \rangle \quad (17)$$

To incorporate effects due to a partially coherent source we average Eq. (16) over the ensemble of phases of the excitation and dump pulses, giving

$$P(E, q) = (2\pi/\hbar^2) \sum_{ij} d_i d_j^* \langle \epsilon_x(\omega_{ig}) \epsilon_x^*(\omega_{jg}) \rangle \langle \epsilon_d(\omega_{EE_i}) \epsilon_d^*(\omega_{EE_j}) \rangle \mu_{i,j}^{(q)}(E) \quad (18)$$

Assuming the phase diffusion model described above, then the frequency-frequency correlation functions is given by Eq. (4). The probability $P(q)$ of forming product in channel q is then obtained by integrating over the pulse width:

$$P(q) = \int dE P(E, q) = (2\pi/\hbar^2) \sum_{i,j} d_i d_j^* \langle \epsilon_x(\omega_{ig}) \epsilon_x^*(\omega_{jg}) \rangle \int dE \langle \epsilon_d(\omega_{EE_i}) \epsilon_d^*(\omega_{EE_j}) \rangle \mu_{i,j}^{(q)}(E) \quad (19)$$

It is often the case that the Franck-Condon factors contained in $\mu_{i,k}^{(q)}(E)$ vary sufficiently slowly over the range of E encompassed by the dump pulse to be regarded as constant [9]. Under these circumstances we can use the following generalized Parseval's equality to show that $P(q)$ is independent of the coherence properties of the dump pulse. Specifically we have

$$\begin{aligned} \int d\omega \langle \epsilon^*(\omega - \omega_1) \epsilon(\omega - \omega_2) \rangle &= \frac{1}{2\pi} \int d\omega \int \int dt_1 dt_2 \langle \epsilon^*(t_1) \epsilon(t_2) \rangle e^{i\omega(t_2 - t_1)} e^{i(\omega_1 t_1 - \omega_2 t_2)} \\ &= \int \int dt_1 dt_2 \langle \epsilon^*(t_1) \epsilon(t_2) \rangle \delta(t_2 - t_1) e^{i(\omega_1 t_1 - \omega_2 t_2)} \\ &= \int dt \langle \epsilon^*(t) \epsilon(t) \rangle e^{i(\omega_1 - \omega_2)t}. \end{aligned} \quad (20)$$

[The conventional Parseval equality $\int d\omega \langle |\epsilon(\omega)|^2 \rangle = \int dt \langle \epsilon^*(t)\epsilon(t) \rangle$ is the special case of $\omega_1 = \omega_2$.] Since the right hand side is independent of the phase of $\epsilon(t)$ then the frequency integrated correlation function is independent of the degree of coherence of the pulse.

Assuming the E independence of $\mu_{i,j}^{(q)}(E)$ over the pulse width allows us to write Eq. (19) as

$$P(q) = (2\pi/\hbar^2) \sum_{ij} d_i d_j^* \langle \epsilon_x(\omega_{ig}) \epsilon_x^*(\omega_{jg}) \rangle F(\omega_{ji}) \mu_{i,j}^{(q)}(E) \quad (21)$$

with

$$F(\omega_{ji}) = \int dt \langle |\bar{\epsilon}_d(t)|^2 \rangle e^{i(E_j - E_i)t/\hbar} \quad (22)$$

For the Gaussian dump pulse [Eq.(6)] we have that

$$F(\omega) = \left(\frac{\epsilon_{d0}}{2}\right)^2 \sqrt{\frac{\pi}{2}} \tau_d e^{-\tau_d^2 \omega^2 / 8} e^{i\omega t_d}. \quad (23)$$

Given Eqs. (4),(17) and (23), Eq. (21) assumes the form

$$P(q) = (2\pi/\hbar^2) \sum_{kj} d_k d_j^* |\langle \epsilon_x(\omega_{kg}) \epsilon_x^*(\omega_{jg}) \rangle F(\omega_{jk}) \mu_{k,j}^{(q)}(E)| e^{[i\omega_{kj}\delta_t + i\alpha_{k,j}^{(q)}(E)]} \quad (24)$$

where $\delta_t = (t_d - t_x)$. Of particular interest is the ability to control the reaction selectivity, i.e. the relative production of product in channel q , given by

$$R(q) = P(q) / \sum_{q'} P(q') \quad (25)$$

The essence of control lies in the interference terms ($i \neq j$) in Eq. (24) which contribute to either constructively enhance, or destructively deplete, a given product arrangement q . These terms are sensitive to the frequency of the lasers and the time delay δ_t , which serve as laboratory control parameters in this scenario. For the simplest case, excitation which encompasses only two levels, $P(q)$ is given by:

$$\begin{aligned} P(q) = & (2\pi/\hbar^2) [|d_1|^2 \langle |\epsilon_x(\omega_{1g})|^2 \rangle \mu_{1,1}^{(q)} F(\omega_{11}) \\ & + |d_2|^2 \langle |\epsilon_x(\omega_{2g})|^2 \rangle \mu_{2,2}^{(q)} F(\omega_{22}) \\ & + 2 |d_1 d_2^* \mu_{1,2}^{(q)} \langle \epsilon_x(\omega_{1g}) \epsilon_x^*(\omega_{2g}) \rangle F(\omega_{21}) | \cos(\omega_{21}\delta_t + \alpha_{1,2}^{(q)} + \beta)], \end{aligned} \quad (26)$$

with $\langle E_1 | \mu | E_g \rangle \langle E_g | \mu | E_2 \rangle \equiv |\langle E_1 | \mu | E_g \rangle \langle E_g | \mu | E_2 \rangle| e^{i\beta}$. Since decoherence affects both the direct terms as well as the cross terms the extent of control is dependent on the laser properties through the relative magnitudes of $|\langle \epsilon_x(\omega_{1g}) \epsilon_x^*(\omega_{2g}) \rangle|$ and $\langle |\epsilon_x(\omega_{ig})|^2 \rangle$, $i = 1, 2$.

The situation is more complicated with the inclusion of more terms under the excitation profile. However, the probability of dissociation into a given channel [Eq. (24)] is seen to be essentially comprised of a sum of two level terms. Control is dependent on the relative size of the $k \neq j$ interference term and the diagonal $k = j$ terms. To expose the dependence on the coherence of the pump field denote the terms $|d_k d_j^* F(\omega_{jk}) \mu_{k,j}^{(q)}(E)|$ by $a_{k,j}^{(q)}$ and consider the ratio of the $k \neq j$ term in Eq.(24) to the associated diagonal terms. That is, consider the contrast ratio:

$$C_{kj} = \frac{a_{k,j}^{(q)} \langle \epsilon_x(\omega_{kg}) \epsilon_x^*(\omega_{jg}) \rangle}{a_{k,k}^{(q)} \langle |\epsilon_x(\omega_{kg})|^2 \rangle + a_{j,j}^{(q)} \langle |\epsilon_x(\omega_{jg})|^2 \rangle} \quad (27)$$

For the Gaussian model of a partially coherent source Eq.(27) assumes the form:

$$C_{kj} = \exp\left[\frac{-\omega_{kj}^2(\tau_x^2 - T_x^2)}{8}\right] \left[\frac{a_{k,j}^{(q)} \exp(-\omega_{jk} T_x^2 \delta_{E_{jk}} / 2\hbar)}{a_{k,k}^{(q)} + a_{j,j}^{(q)} \exp(-\omega_{jk} T_x^2 \delta_{E_{jk}} / \hbar)} \right] \quad (28)$$

Here $\delta_{E_{jk}} \equiv E_x - E_{av} \equiv \hbar\omega_x - (E_k + E_j)/2$. The second term in Eq. (28), in brackets, is a function of $T_x^2 \delta_{E_{jk}}$. If two bound state levels dominate the pump excitation then this term contributes a scaling characteristic to control plots. That is, if we plot contours of constant dissociation probability as a function of δ_t and $\delta_{E_{jk}}$ then, barring the first term, plots with different T_x will appear similar, with a new range scaled by $\delta_{E'} = (T_x/T'_x)^2 \delta_{E_{jk}}$.

The first term in Eq. (28) can be rewritten as

$$\begin{aligned} A_{kj} &= \exp\left[\frac{-\omega_{kj}^2(\tau_x^2 - T_x^2)}{8}\right] \\ &= \exp\left[\frac{-\omega_{kj}^2 \tau_x^2}{8} \left[1 - \frac{1}{(\tau_x/T_{xc})^2 + 1}\right]\right], \end{aligned} \quad (29)$$

which affords additional insight into the dependence of control, achieved by varying δ_t , on coherence characteristics of the pump laser. Note first that Eq. (29) implies that for fixed τ_x control comes predominantly from nearby molecular states, i.e. those with small ω_{kj} . Second, for fixed pulse duration τ_x , control is expected to decrease with decreasing

τ_{xc} , i.e. with decreasing pulse coherence. This is reasonable since decreasing τ_x leads to the preparation of mixed molecular states with increasing degrees of state impurity [10] and hence loss of phase information. Somewhat unexpected, however, is the prediction of improved control with decreasing pulse duration τ_x at fixed (τ_x/τ_{xc}) , embodied in the $\exp(-\omega_{kj}^2\tau_x^2)$ term. This interesting dependence will be shown numerically below.

Below we consider the photodissociation of model DH_2 . In particular we examine control as a function of δ_t and of the central frequency ω_x of the pump pulse. The excitation energy $\hbar\omega_x$ associated with the pulse center is defined relative to two particular energy levels. That is, we consider control as a function of the detuning parameter $\delta_E \equiv E_x - E_{av} \equiv \hbar\omega_x - (E_1 + E_2)/2$, where E_1 and E_2 are two selected neighboring energy levels.

III. NUMERICAL RESULTS

To quantitatively examine the effect of partial coherence on control we consider a collinear triatomic model composed of two electronic states with masses of DH_2 . The pump pulse raises DH_2 from the ground electronic state, preparing a bound state superposition on the excited state surface. A subsequent dump pulse brings the system down to the continuum of the ground electronic state where photodissociation to two products occurs: $\text{D} + \text{H}_2 \leftarrow \text{DH}_2 \rightarrow \text{H} + \text{DH}$. Previously [2] we examined control in this system using purely coherent pulses. In that study an excitation pulse with $\Delta_x = 20 \text{ cm}^{-1}$ was used to prepare an initial superposition of two levels and dissociation was carried out with a dump pulse with $\Delta_d = 80 \text{ cm}^{-1}$. Varying the control parameters δ_t and the detuning δ_E led to substantial control over the relative product yield. In that work two different cases were examined in detail, corresponding to excitation around the levels 32+33 and levels 56+57 (where 32 denotes the 32nd level, etc.) of the excited electronic state. In this paper we examine excitation with δ_E measured with respect to the same level pairs, as well as others, but with varying Δ_{xc} . For small Δ_{xc} only two levels are excited but as Δ_{xc} increases the excitation encompasses a larger number of levels. We present results as a function of the laser parameters Δ_x, Δ_{xc} ,

etc. to allow a direct comparison with the spacing between energy levels. A sampling of these levels is provided in Table I.

Consider first excitation about $E_{av} = (E_{32} + E_{33})/2$. We assume that $\mu_{ij}(E)$ is independent of E , an approximation justified later below. Each panel of Fig. 1 shows a contour plot of the fractional yield of DH [i.e., $P(\text{DH})/(P(\text{DH})+P(\text{H}_2))$] as a function of δ_t and δ_E , for different values of Δ_{xc} . Figure 1a shows, for comparison purposes, the case of a coherent pulse ($\Delta_{xc} = 0$); the range of control is large with the yield ratio varying from 0.19 to 0.92. Thus, for coherent pulses a wide range of product yield is possible as the relative intensity through detuning and time delay between pulses are varied.

Figures 1b to 1e, which show control in the same system but with differing amounts of pump laser incoherence, demonstrates that increasing incoherence is accompanied by a reduction in the range of control. (Note that in each successive figure the ordinate axis scale changes to accomodate both the increasing frequency width of $I_x(\omega)$ associated with increasing Δ_{xc} and the observed shifts in the yield extrema.) For example, with $\Delta_{xc} = 8 \text{ cm}^{-1}$ [Fig. 1b] control is similar to that in Fig. 1a whereas with $\Delta_{xc} = 80 \text{ cm}^{-1}$ control [Fig. 1d] is essentially lost. There appears to be little qualitative change in going to $\Delta_{xc} = 200 \text{ cm}^{-1}$ [Fig. 1e] despite the inclusion, in this width, of many additional bound levels.

In examining Fig. 1e note that the yield depends on δ_E but not on δ_t . This dependence is a consequence of the (generally uninteresting) predisposition of various bound levels of the excited electronic state to preferentially dissociate to particular products. The δ_t dependence of the yield, which is indicative of interference induced yield control, disappears with increasing laser incoherence.

These computations assume that $\mu_{ij}(E)$ is independent of E in order to take advantage of the generalized Parseval equality which implies that the control results are independent of the dump pulse partial coherence, and hence independent of Δ_{dc} . To test this approximation we recomputed the control results shown in Fig. 1a using variable $\mu_{ij}(E)$ and Δ_{dc} ; results are shown in Fig. 2. It is clear that although control diminishes with decreasing Δ_{dc} the effect is weak compared to variations of Δ_{xc} . Further, the gross qualitative structure

of the control plots are seen to be relatively insensitive to the dump pulse incoherence. Other computational studies gave similar results. Thus, throughout this paper we simplify computations by neglecting the Δ_{dc} dependence.

The pattern shown in Fig. 1 and Fig. 2, where the control plot is dominated by a single well defined peak and valley, is characteristic of the excitation of essentially two levels, i.e. two molecular levels under the laser excitation envelope have significant Frank-Condon factors. Slightly more complicated behavior is shown in Fig. 3 with excitation referred to the (22,23) pair of levels, using a faster excitation pulse with $\Delta_x = 200 \text{ cm}^{-1}$. In this case several levels are excited under the pulse and the control picture loses some of its symmetry and simplicity in the neighborhood of $\delta_E = 0$. However, the same observed loss of control with increasing partial laser coherence is evident.

Figure 4 shows results typical of those obtained with the excitation of a large number of levels. In this case the energy spectrum of DH_2 was compressed as shown in Table 2 and excitation was carried out with a $\Delta_{xc} = 200 \text{ cm}^{-1}$ pulse. The resultant dependence of the yield ratio on δ_E and δ_t is far more complex than the behavior seen in previous figures. However, the reduction of control with increasing Δ_{xc} is clearly evident, with control lost by $\Delta_{xc} = 1000 \text{ cm}^{-1}$.

From these and related studies we find that control in the model DH_2 system is lost when $(\Delta_{xc}/\Delta_x) = (\tau_x/\tau_{xc}) \approx 4 - 5$. This precludes the use of typical nanosecond lasers, where $(\Delta_{xc}/\Delta_x) > 10^2$, for pump-dump control.

Finally we examine the implication [see discussion below Eq. (29)] that control improves with increasing Δ_x for fixed Δ_{xc}/Δ_x . Figure 5 shows results of laser excitation with δ_E measured relative to the center of the (32,33) energy level pair. In particular, panels 5a to 5c show typical results for excitation of a pair of levels, with Δ_x varying from 20 cm^{-1} to 80 cm^{-1} , with $\Delta_{xc}/\Delta_x = 2$. There is clearly an improvement in the range of accessible yield with increasing Δ_x . However, this is accompanied by a large scale in the value of δ_E at which the yield extrema occur. Thus, with increasing Δ_x control is found at much larger detunings, where the field strength is substantially reduced. Thus, although the control as a

function of δ_t improves with increasing Δ_x at fixed Δ_{xc}/Δ_x , the absolute yield is substantially reduced. Further, as seen in Fig. 5d, which is similar to Fig. 5c but includes excitation of all bound states under the laser envelope, the increasing width associated with increasing Δ_x will encompass additional levels, causing significant alterations in the control plot.

Finally, Fig. 6a and 6b show, for comparison purposes, excitation with *coherent* pulses of similar Δ_x to those in Fig. 5b and 5c. (See also Fig 1a for the related case with $\Delta_x = 20$ cm^{-1} .) The resultant control plots all appear similar but with a larger scaling with increasing Δ_x . This off-resonance is associated with a reduction in the field strength and hence lower yield. This behavior is consistent with the functional form of Eq. (28). That is, for coherent pulses $T_x = \tau_x$ so that only the bracketed term in Eq.(28) contributes. Hence, as expected, the $T_x^2 \delta_E$ behavior demonstrated by this term is manifest as similar, but δ_E rescaled, contour plots as Δ_x is varied. Finally note also, by comparing Figs. 5 and 6, that the extent of control is always greater with the coherent pulses than with the partially coherent pulses.

IV. CONCLUSION

We have examined the theory of coherent control in the pump-dump scenario for partially coherent pulses. The coherence of the pump pulse has been shown to be of primary importance in maintaining control, whereas the coherence of the dump pulse is of secondary importance. Increasing the incoherence of the pump pulse results in a systematic degradation of control when the time delay between the pulses is varied. Further, we found that control improves, for a fixed Δ_{xc}/Δ_x with increasing Δ_x , but that the yield reduces substantially. Control with varying δ_t was seen to survive for values of Δ_{xc}/Δ_x less than 4, a range which precludes pump-dump control with typical nanosecond lasers.

ACKNOWLEDGMENTS

This work was supported by the U.S. Office of Naval Research under contract number N00014-90-J-1014, by the Ontario Laser and Lightwave Research Centre and by NSF grant

PHY-9206064 to Prof. Robert Gordon (University of Illinois). We thank Dr. Tamar Seideman (NRC, Canada) for providing the overlap matrix elements used to obtain Figure 2.

REFERENCES

* Permanent Address: Chemical Physics Department, The Weizmann Institute of Science, Rehovot, Israel

- [1] For reviews see: P. Brumer and M. Shapiro, *Scientific American* **272**, March 1995, pp. 56; M. Shapiro and P. Brumer, *International Reviews of Physical Chemistry* **13**, 187 (1994);
- [2] T. Seideman, M. Shapiro, and P. Brumer, *J. Chem. Phys.* **90**, 7132 (1989); I. Levy, M. Shapiro and P. Brumer, *J. Chem. Phys.* **93**, 2493 (1990).
- [3] For pump-dump studies from an alternate perspective see D.J. Tannor and S.A. Rice, *J. Chem. Phys.* **83**, 5013 (1985); D.J. Tannor, R. Kosloff, and S.A. Rice, *J. Chem. Phys.* **85**, 5805 (1985); R. Kosloff, S.A. Rice, P. Gaspard, S. Tersigni, and D.J. Tannor, *Chem. Phys.* **139**, 201 (1989).
- [4] M. Shapiro and P. Brumer, *J. Chem. Phys.* **90**, 6179 (1989).
- [5] S.M. Park, S-P. Lu, and R.J. Gordon, *J. Chem. Phys.* **94**, 8622 (1991); S-P. Lu, S.M. Park, Y. Xie, and R.J. Gordon, *J. Chem. Phys.* **96**, 6613 (1992); C. Chen, Y-Y. Yin, and D.S. Elliott, *Phys. Rev. Lett.* **64**, 507 (1990); *ibid* **65**, 1737 (1990).
- [6] P. Gross, D. Neuhauser and H. Rabitz, *J. Chem. Phys.* **94**, 1158 (1991).
- [7] X-P. Jiang and P. Brumer, *J. Chem. Phys.* **94**, 5833 (1991); X-P. Jiang and P. Brumer, *Chem. Phys. Lett.* **180**, 222 (1991);
- [8] R.D. Taylor and P. Brumer, *Disc. Far. Soc.* **75**, 117 (1983).
- [9] M. Shapiro, *J. Chem. Phys.*, **101**, 3849 (1994).
- [10] X-P. Jiang and P. Brumer, *Chem. Phys. Lett.* **208**, 179-186 (1993).

FIGURE CAPTIONS

Figure 1: Contour plots of the fraction of DH yield as a function of the detuning parameter $\delta_E = E_x - E_{av} = \hbar\omega_x - (E_{33} + E_{32})/2$ and delay time δ_t for partially coherent pulsed excitation in the neighborhood of the pair of levels 32 and 33 where $E_{33} - E_{32} = 15.7 \text{ cm}^{-1}$, $\Delta_x = 20 \text{ cm}^{-1}$; (a) $\Delta_{xc} = 0 \text{ cm}^{-1}$, (b) $\Delta_{xc} = 8 \text{ cm}^{-1}$, (c) $\Delta_{xc} = 40 \text{ cm}^{-1}$, (d) $\Delta_{xc} = 80 \text{ cm}^{-1}$, (e) $\Delta_{xc} = 200 \text{ cm}^{-1}$.

Figure 2: As in Figure 1a but with nonconstant $\mu_{ij}(E)$. The pump pulse is transform-limited with $\Delta_x = 20 \text{ cm}^{-1}$, and the dump pulse is of width $\Delta_d = 80 \text{ cm}^{-1}$. Each panel corresponds to a different value of dump pulse partial coherence Δ_{dc} : (a) $\Delta_{dc} = 80 \text{ cm}^{-1}$, (b) $\Delta_{dc} = 120 \text{ cm}^{-1}$, (c) $\Delta_{dc} = 200 \text{ cm}^{-1}$.

Figure 3: Same as Figure 1 but in the neighborhood of the pair of levels 22 and 23 where $E_{23} - E_{22} = 46.4 \text{ cm}^{-1}$, $\Delta_x = 200 \text{ cm}^{-1}$, (a) $\Delta_{xc} = 0 \text{ cm}^{-1}$, (b) $\Delta_{xc} = 200 \text{ cm}^{-1}$, (c) $\Delta_{xc} = 1000 \text{ cm}^{-1}$,

Figure 4: Same as Fig. 3 for compressed levels (see Table II). where $\Delta_x = 200 \text{ cm}^{-1}$, (a) $\Delta_{xc} = 0 \text{ cm}^{-1}$, (b) $\Delta_{xc} = 200 \text{ cm}^{-1}$, (c) $\Delta_{xc} = 800 \text{ cm}^{-1}$.

Figure 5: Excitation of the pair of levels numbered 32 and 33 with $\Delta_x/\Delta_{xc} = 2$ and variable Δ_x . (a) $\Delta_x = 20 \text{ cm}^{-1}$, (b) $\Delta_x = 40 \text{ cm}^{-1}$, (c) $\Delta_x = 80 \text{ cm}^{-1}$.

Figure 6: Excitation of the pair of levels numbered 32 and 33 with a coherent source and variable Δ_x : (a) $\Delta_x = 40 \text{ cm}^{-1}$, (b) $\Delta_x = 80 \text{ cm}^{-1}$. See also Figure 1a for the case of $\Delta_x = 20 \text{ cm}^{-1}$.

TABLE I

State number	Energy in cm^{-1}	State number	Energy in cm^{-1}	State number	Energy in cm^{-1}
37	684	26	728		
36	470	25	582	59	882
35	147	24	426	58	642
34	99.7	23	23.2	57	13.0
33	7.85	22	-23.2	56	-13.0
32	-7.85	21	-146	55	-649
31	-507	20	-559	54	-549
30	-694	19	-560		

TABLE I. Energies of excited states around (32,33), (22,23) and (56,57), where the energy zero is taken as the average energy of the pair.

TABLE II

State Number	Energy in cm^{-1}
34	631
33	539
32	523
31	473
30	286
29	206
28	181
27	128
26	94.0
25	79.4
24	63.5
23	23.2
22	-23.2
21	-146
20	-187
19	-188
18	-212
17	-248
16	-290
15	-322
14	-502
13	-566
12	-572
11	-758

TABLE II. Energies of compressed excited states around (22,23), where the zero is taken as the average energy of the pair.

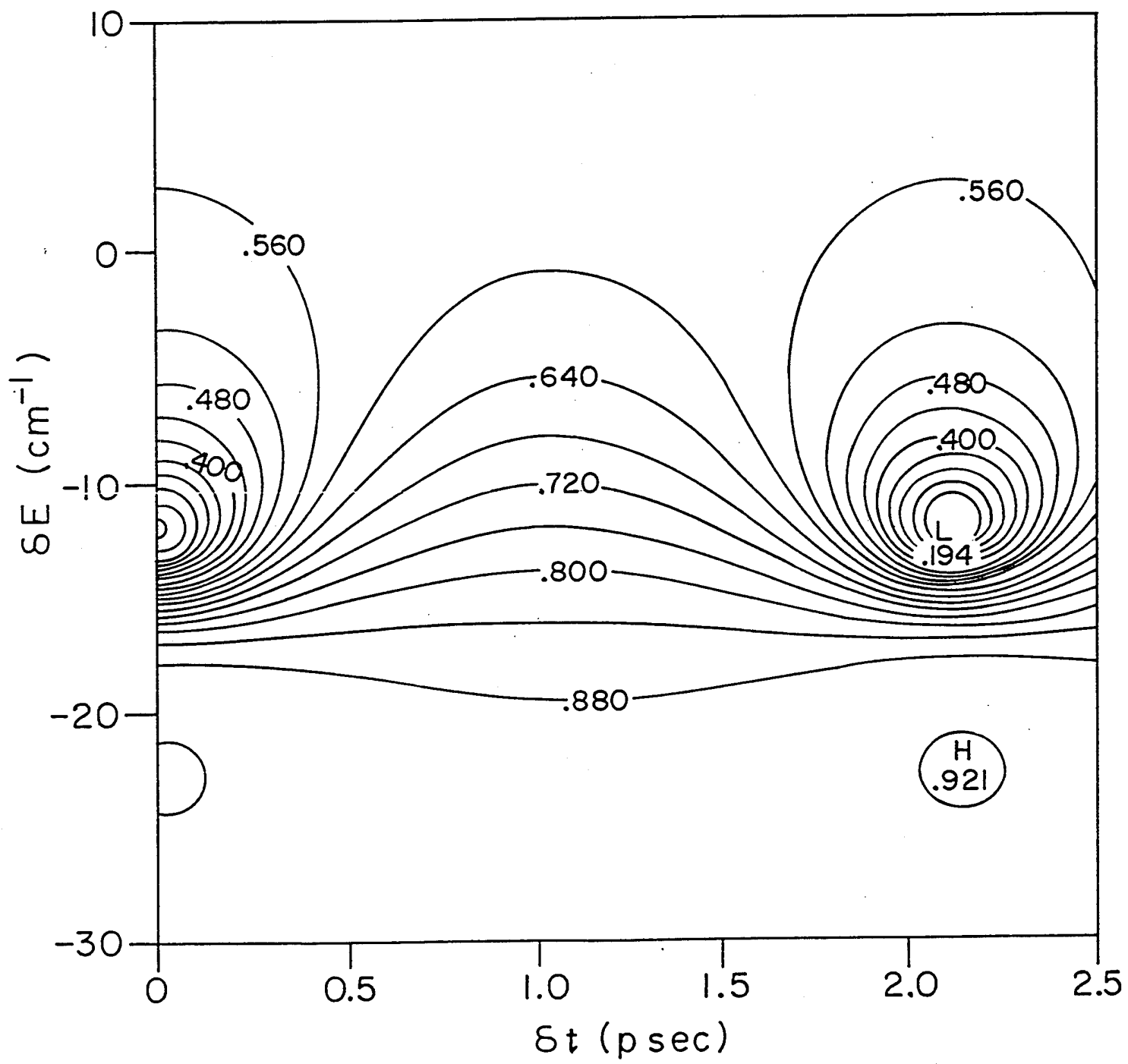


Fig. 1a

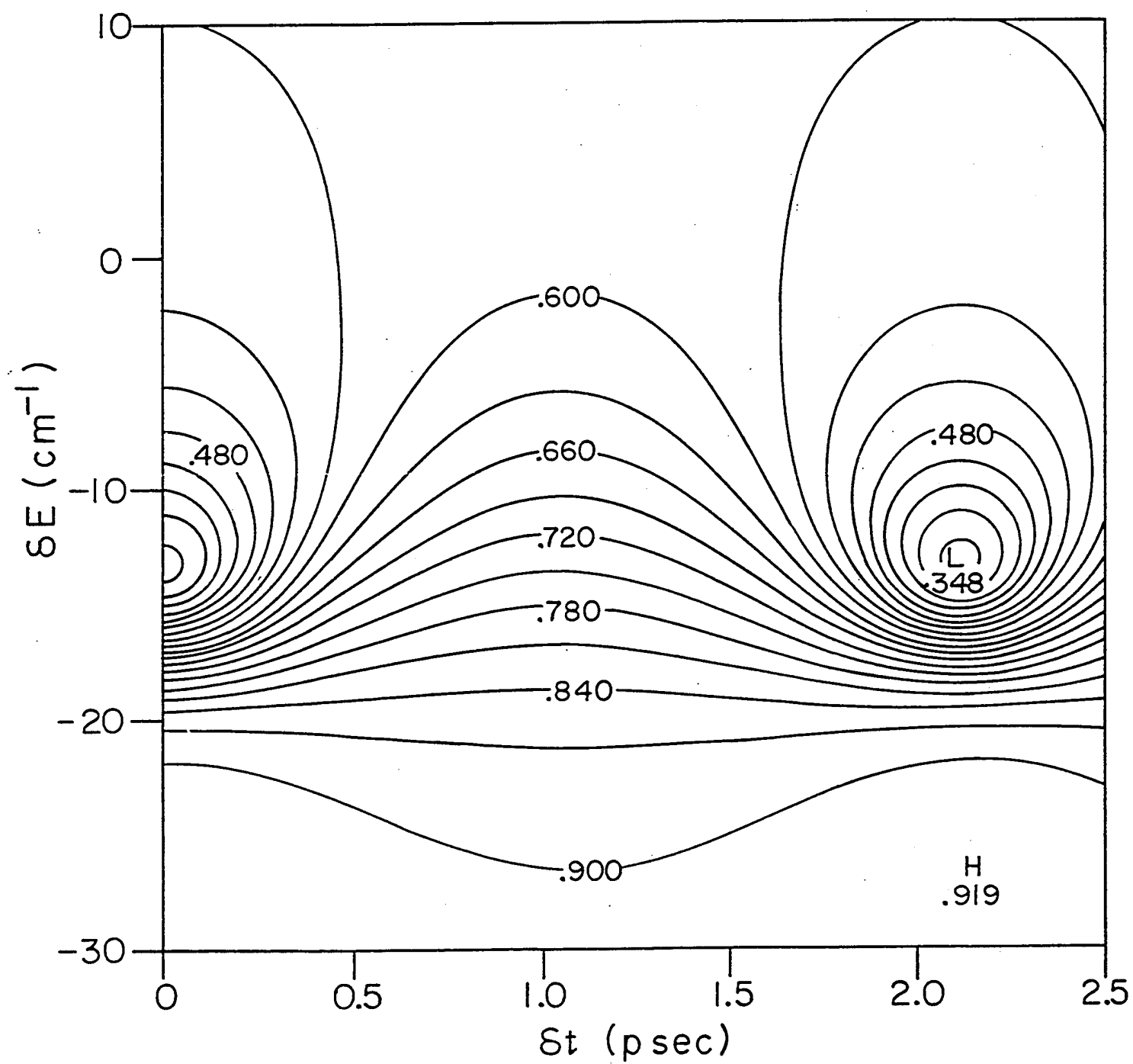


Fig. 1b

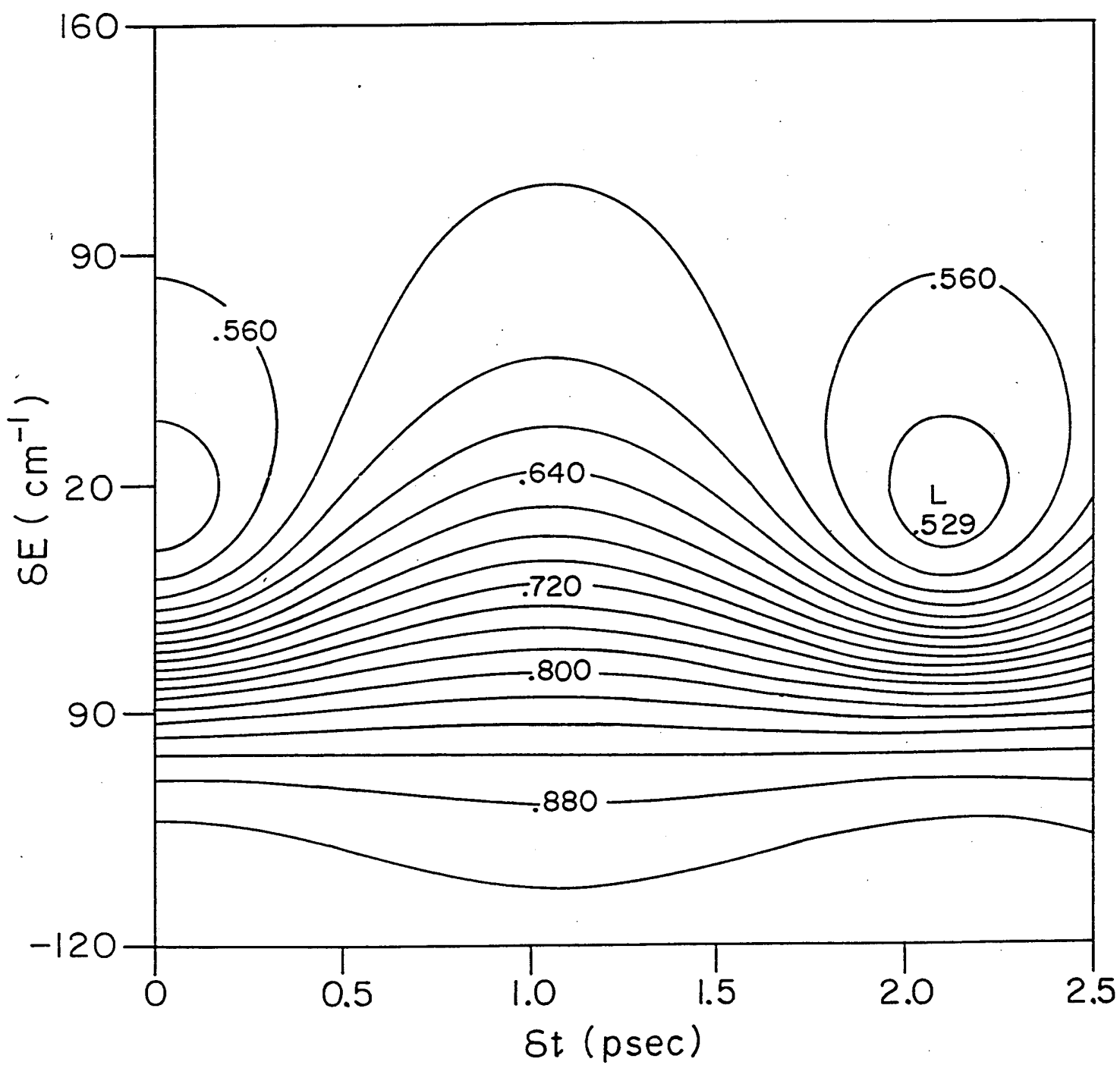


Fig 1c

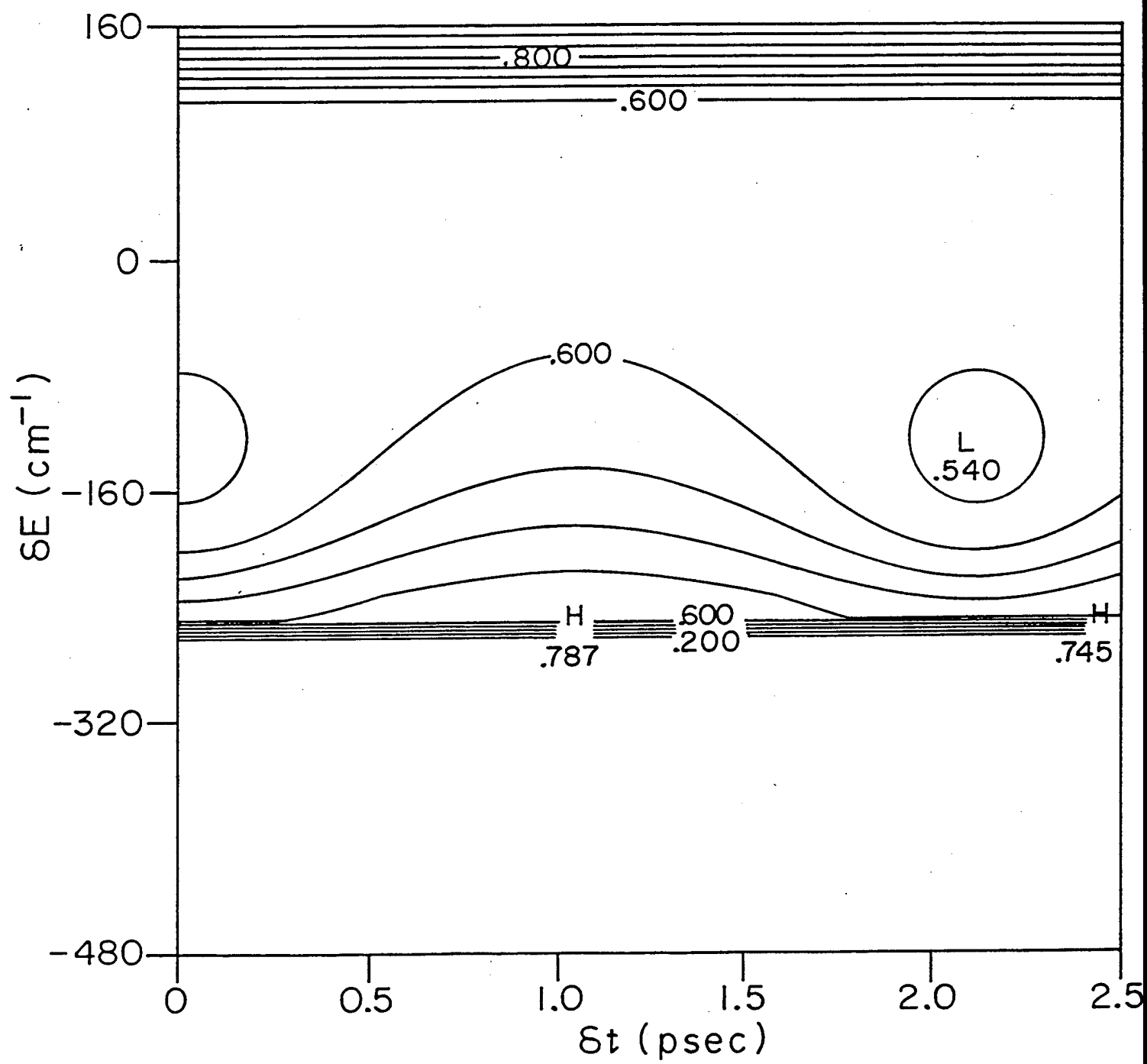


Fig 10

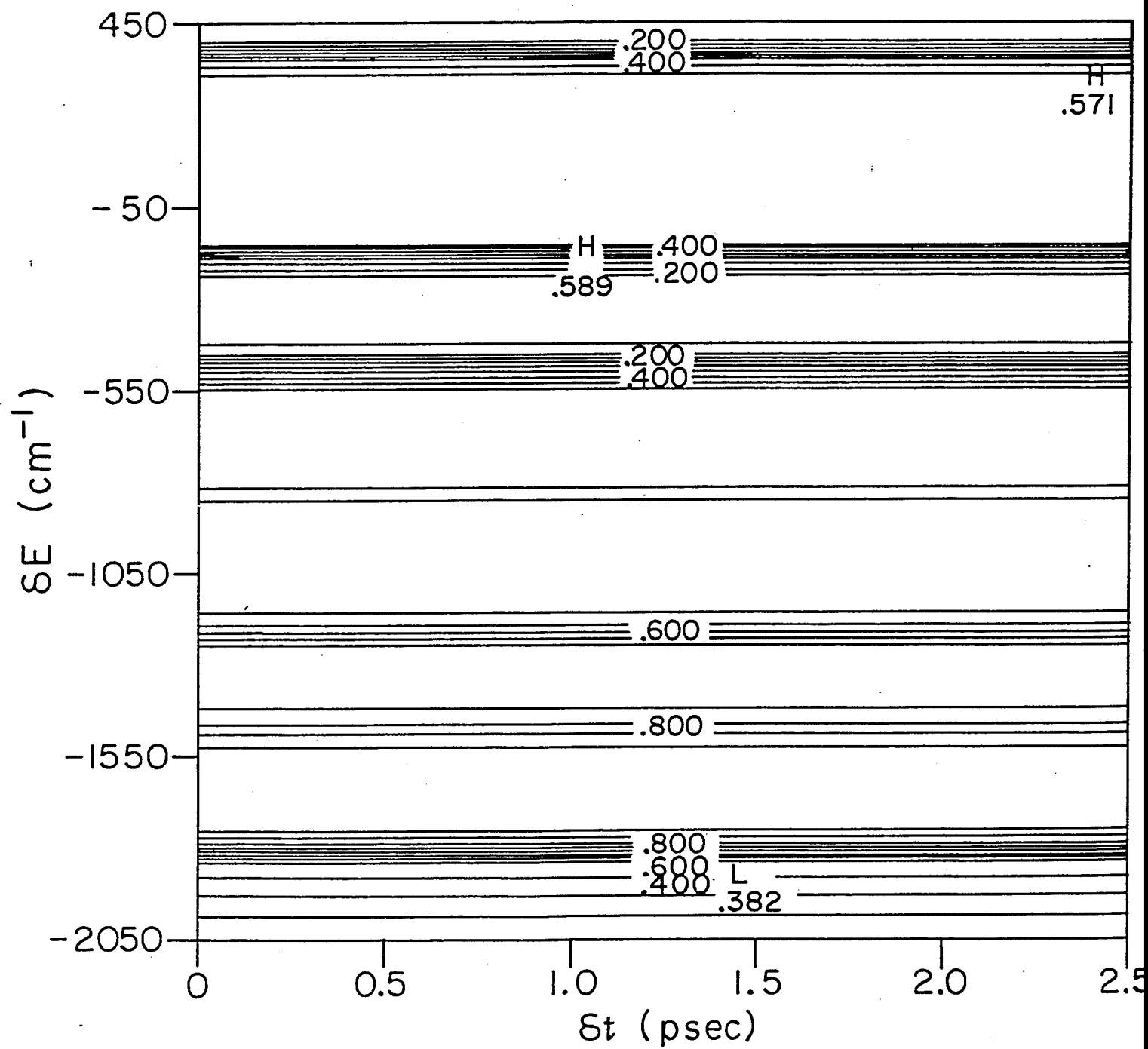


Fig 1E

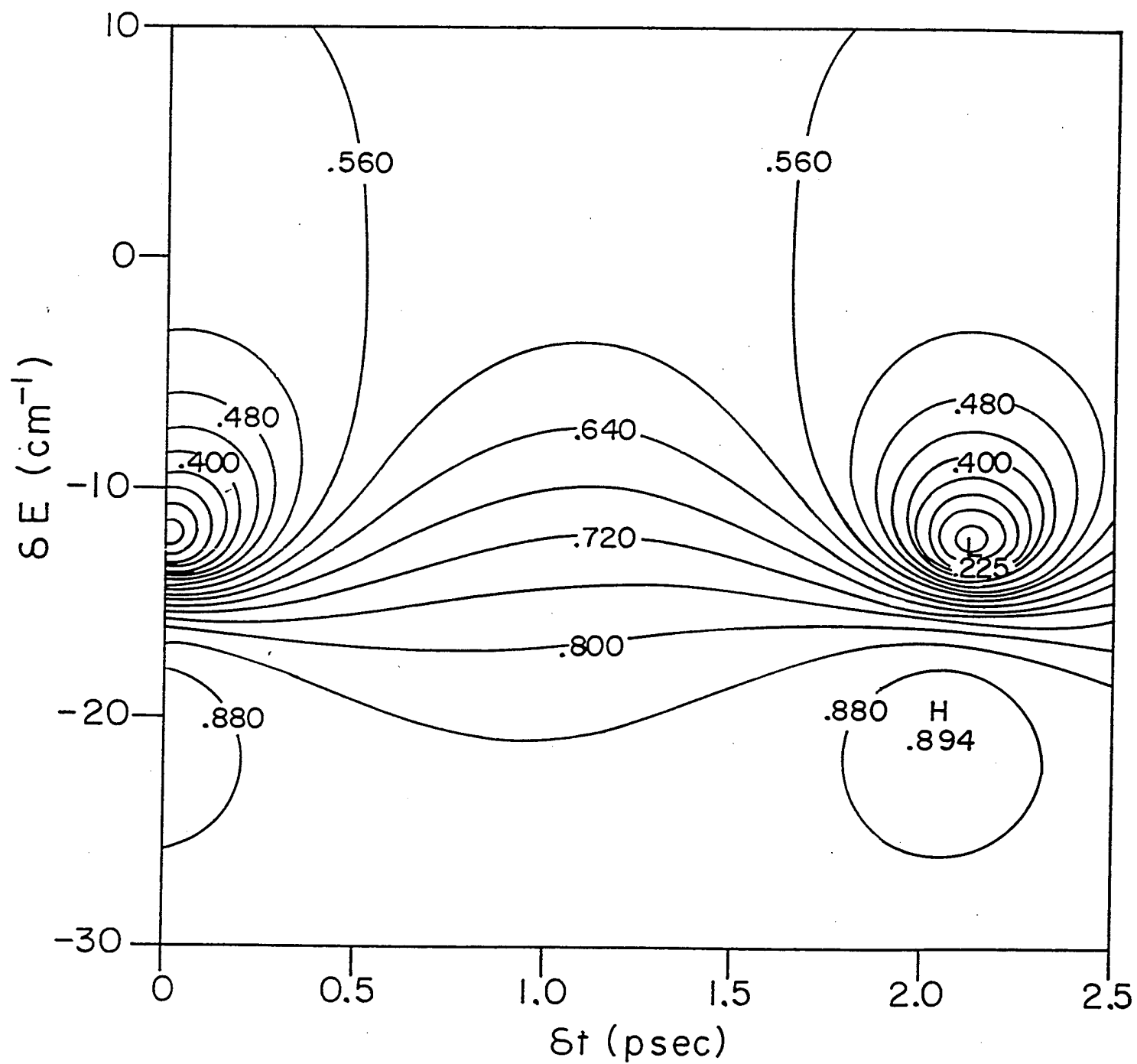


Fig 2A

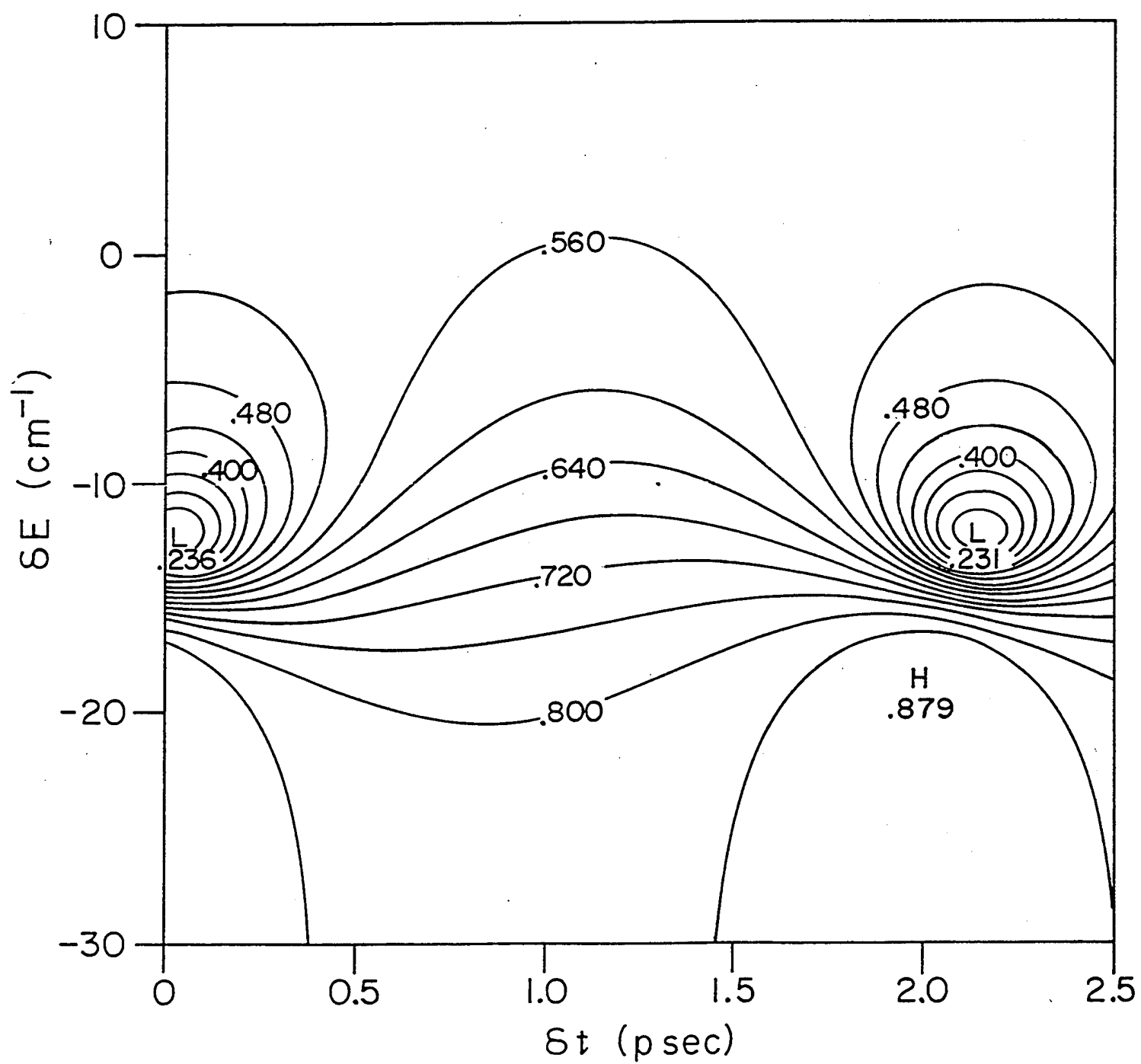


Fig. 2B

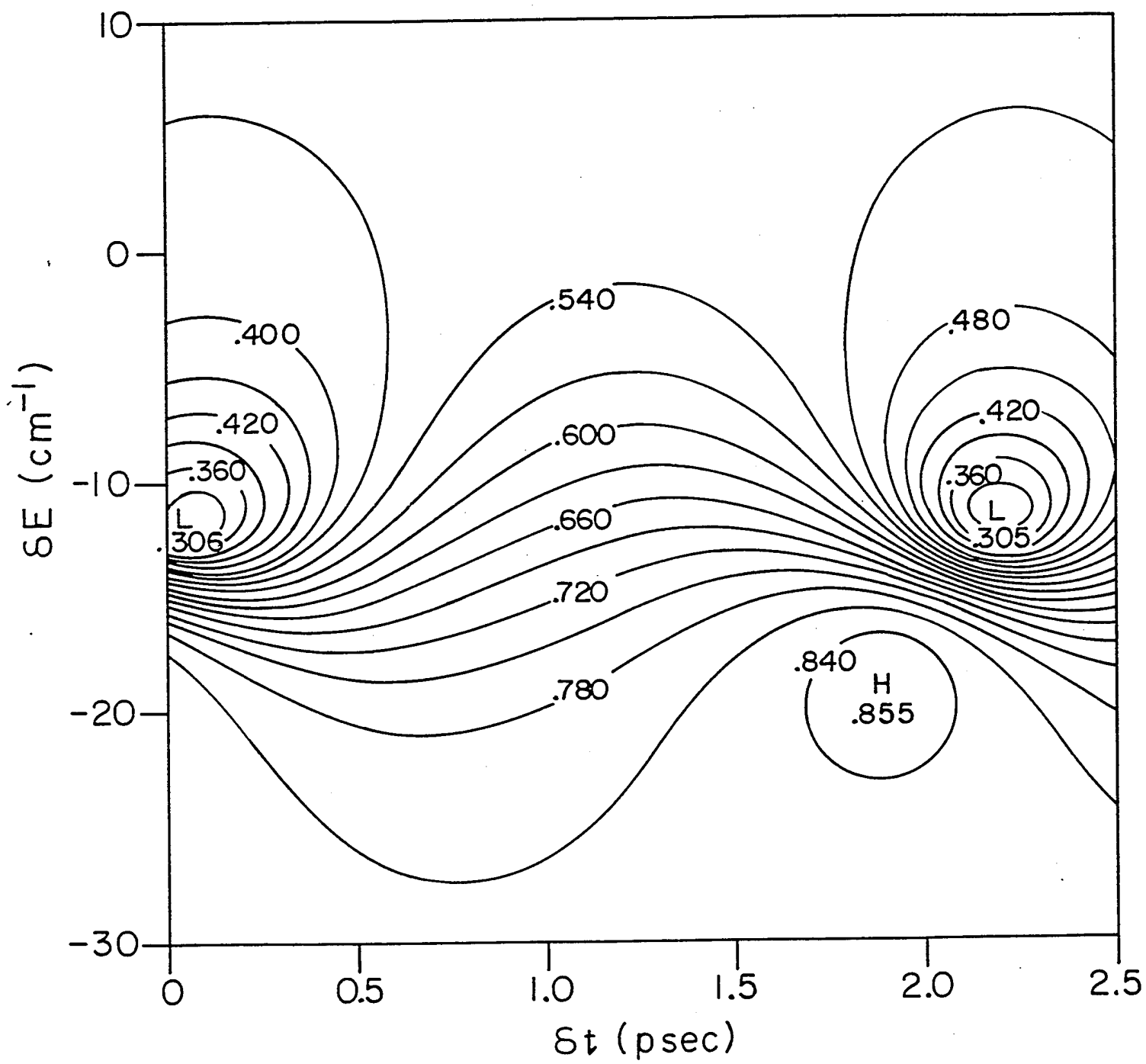


Fig 2C

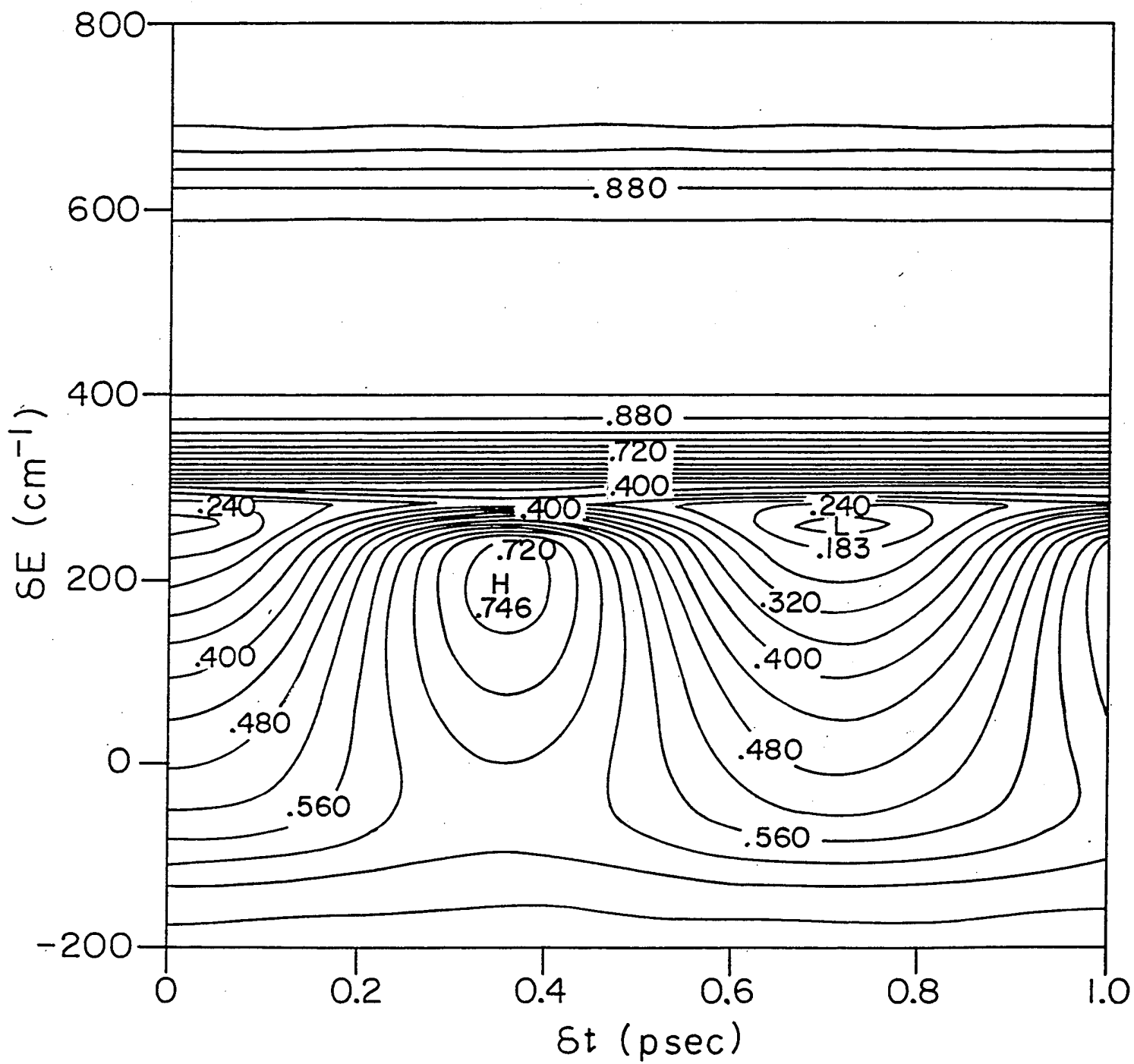


Fig 3A

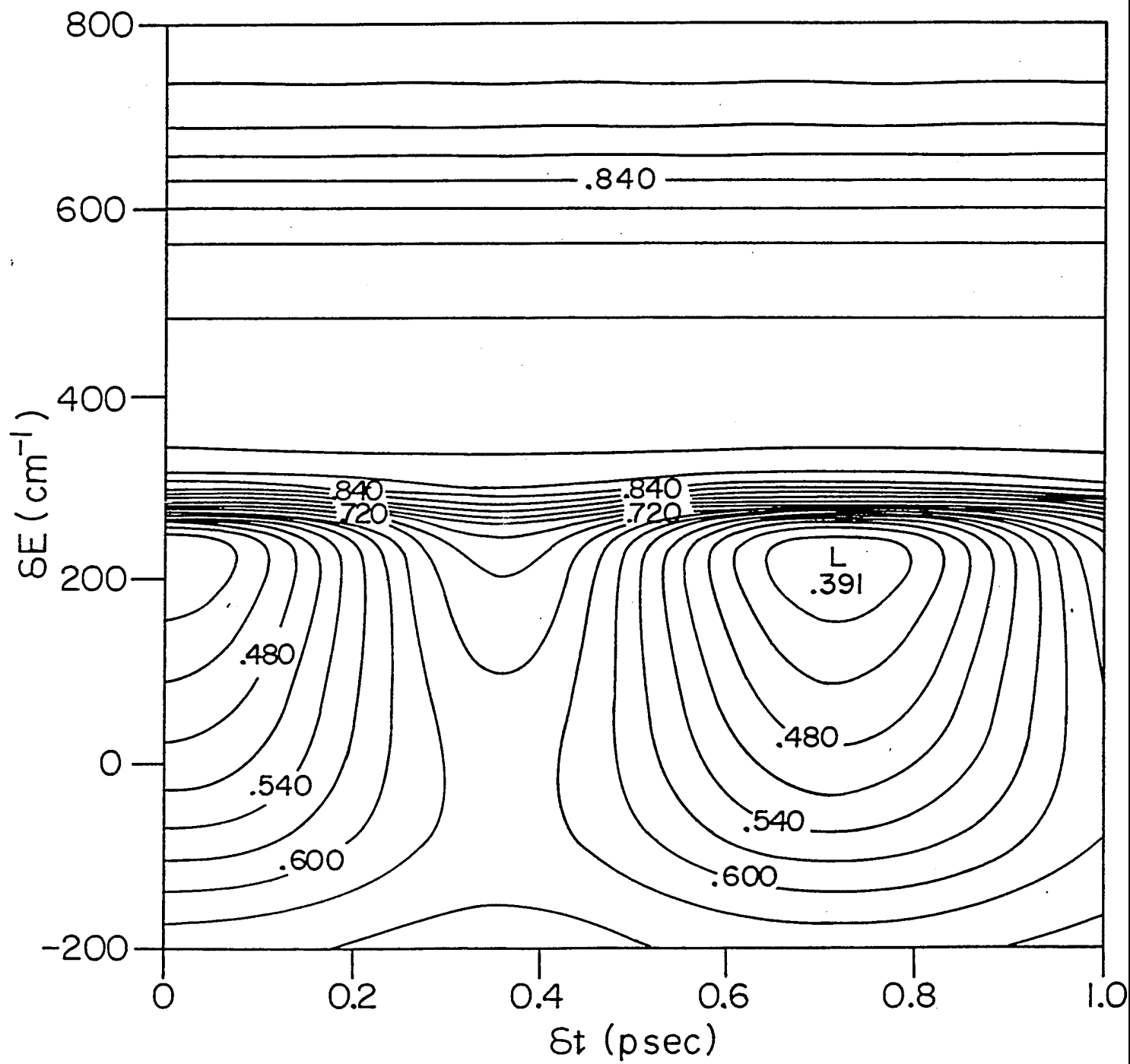


Fig. 3B

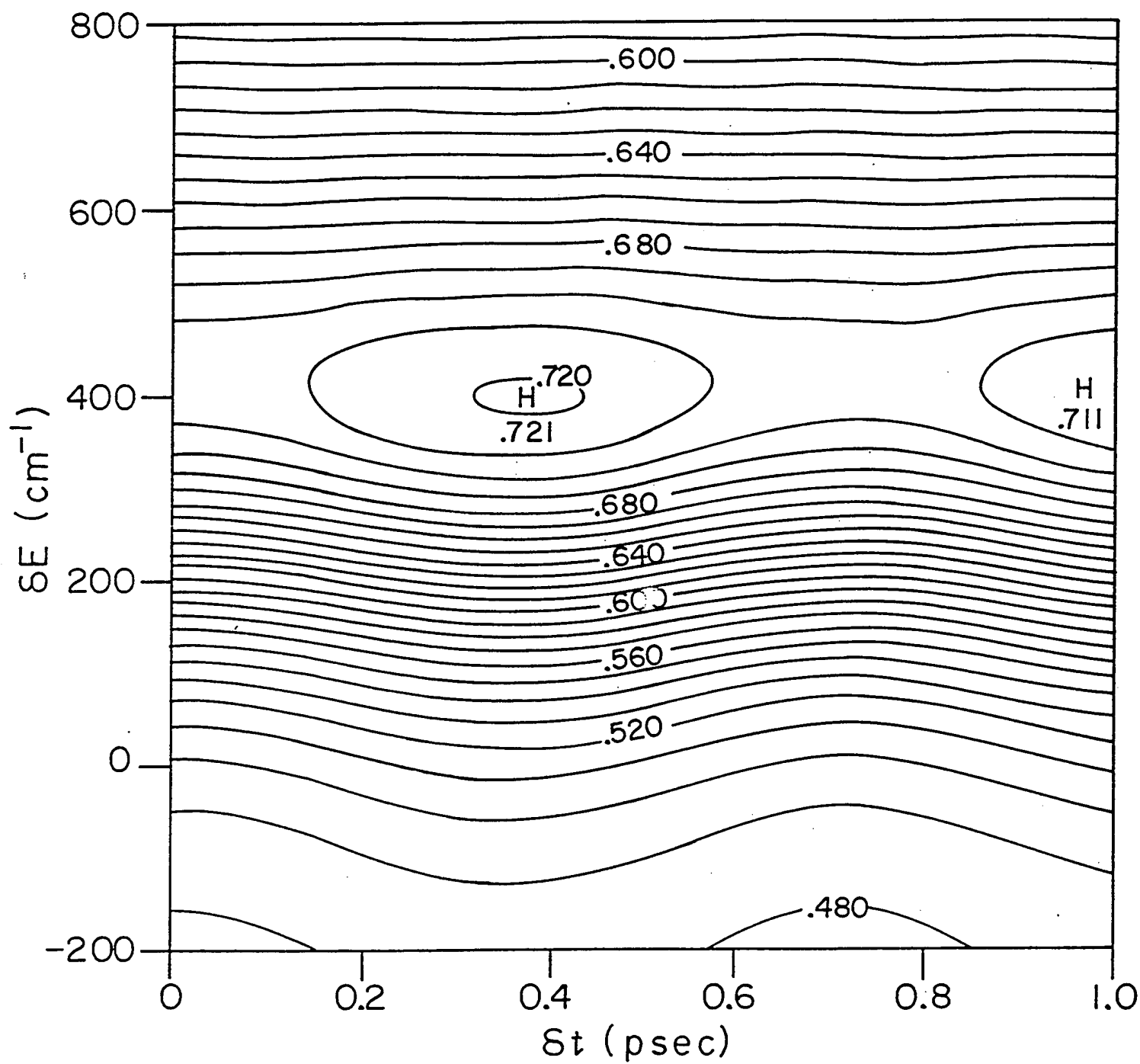


Fig. 3C

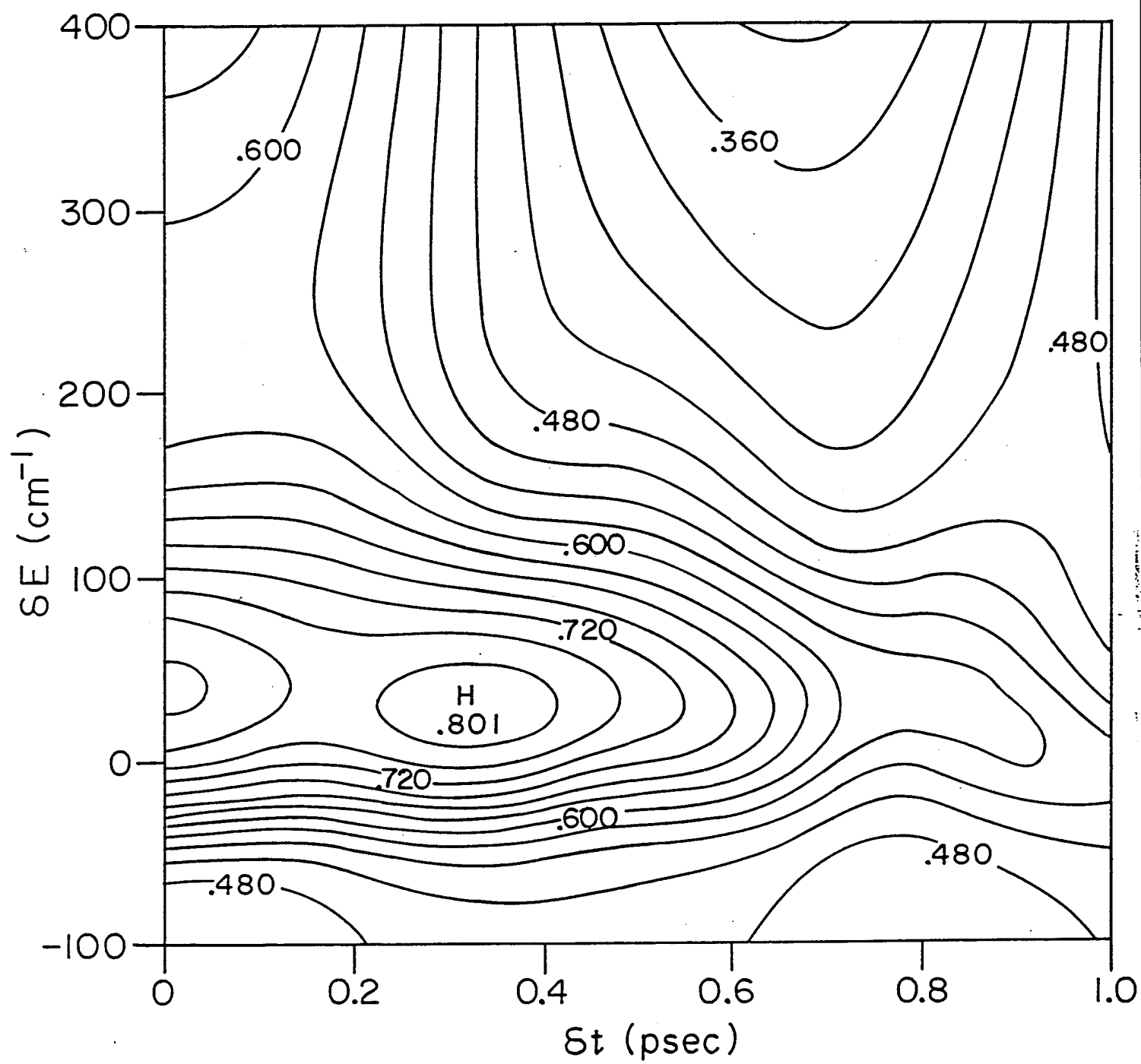


Fig. 4A

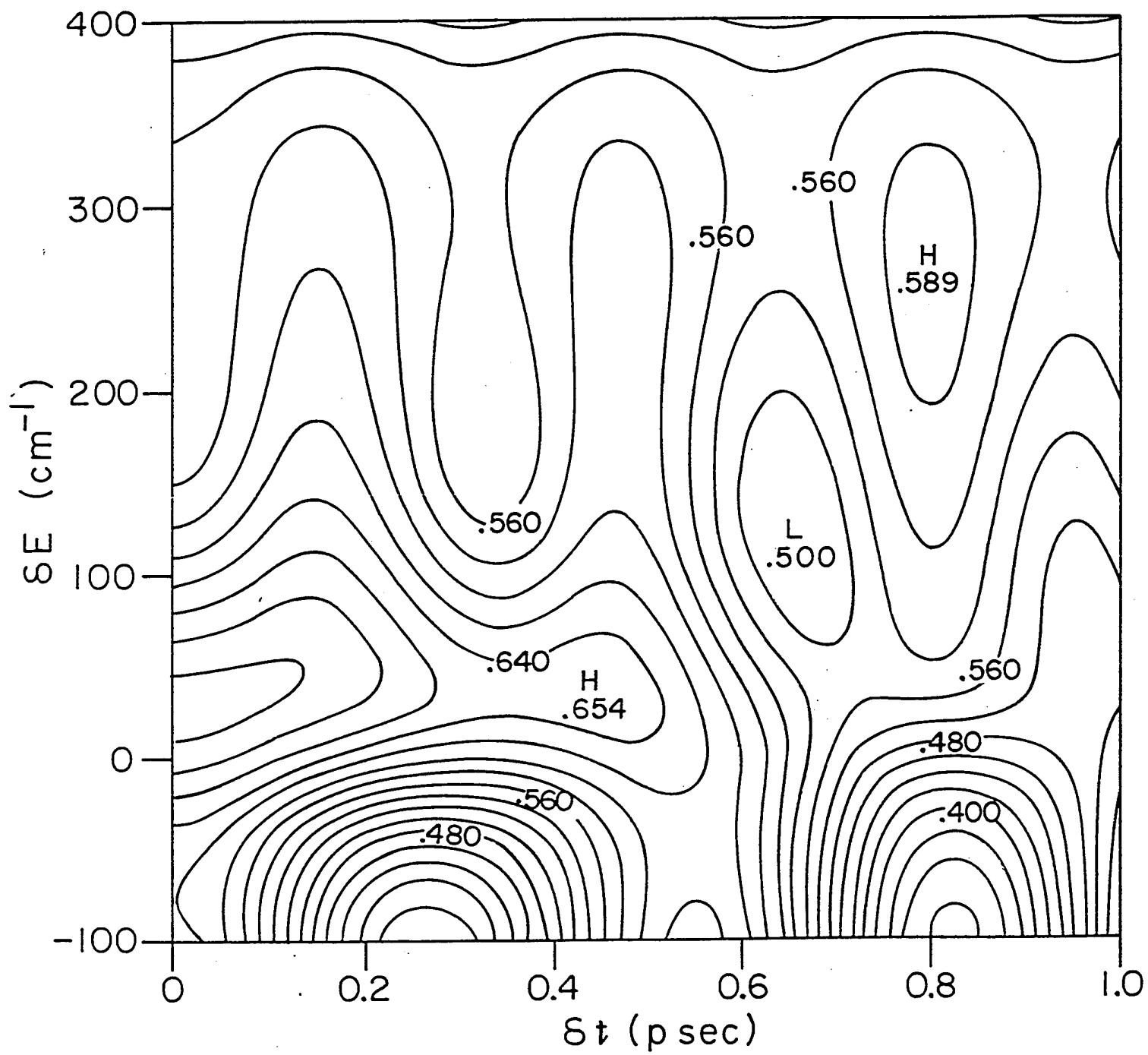


Fig. 4B

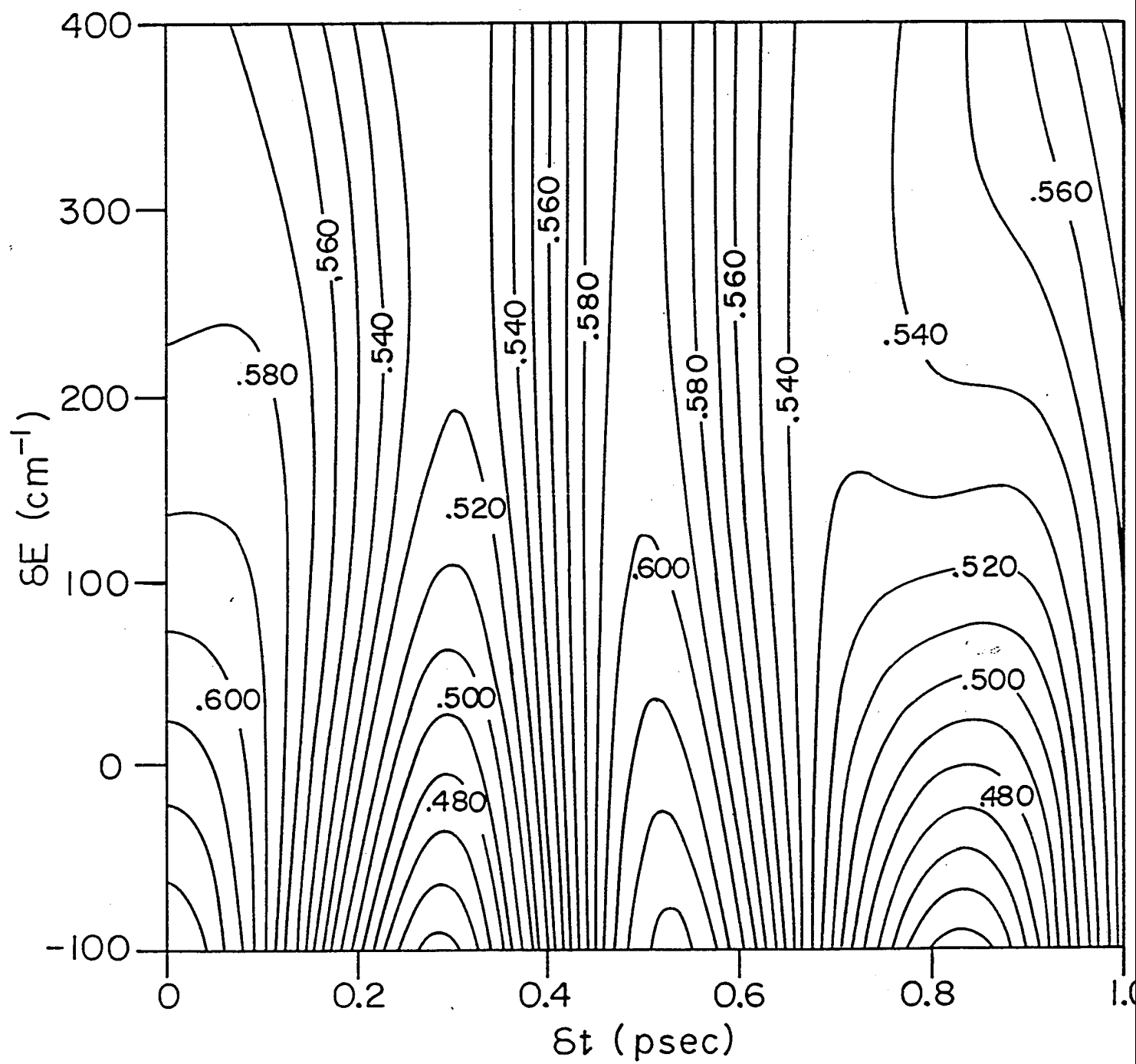


Fig. 4c

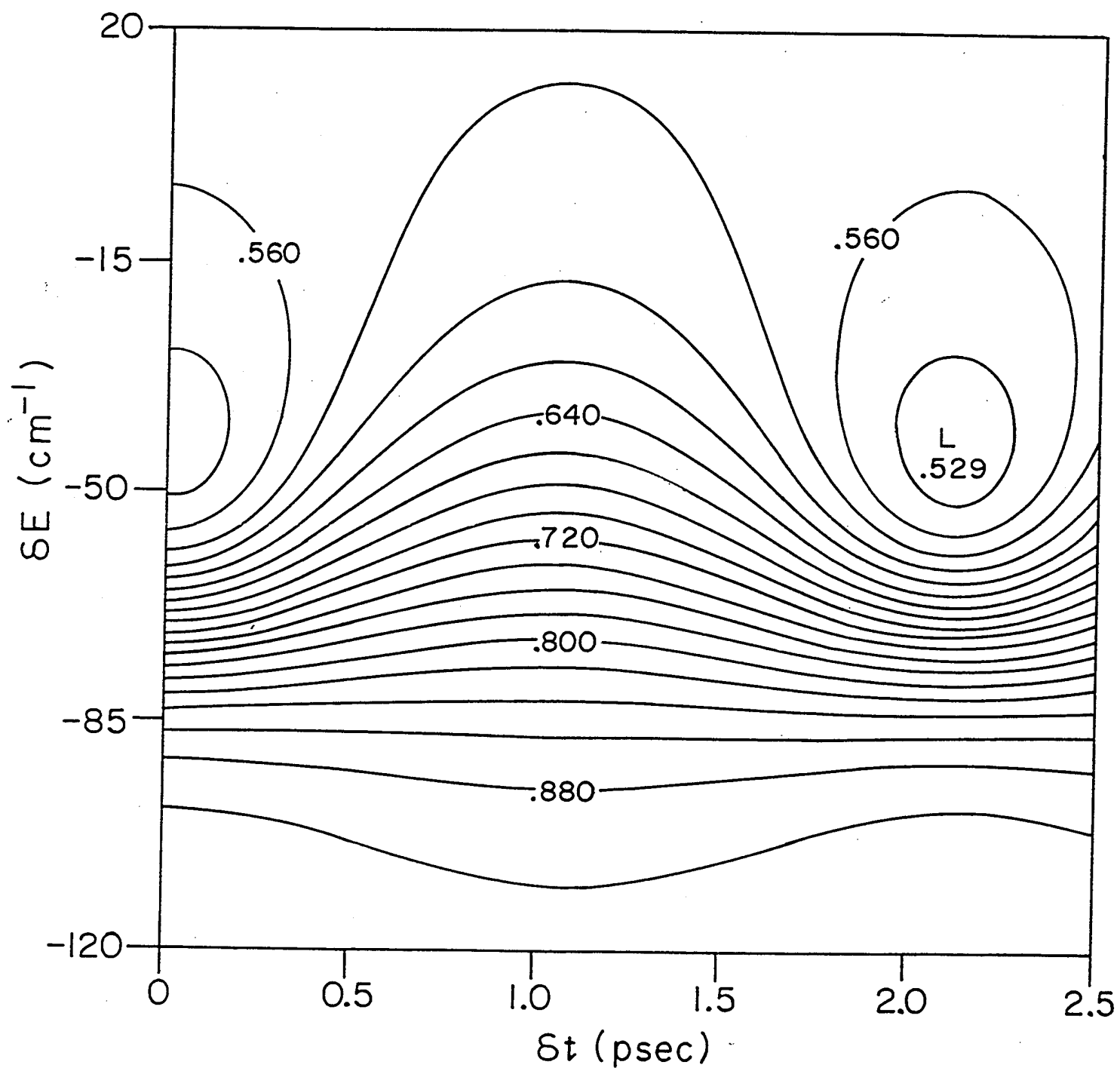


Fig. 5A

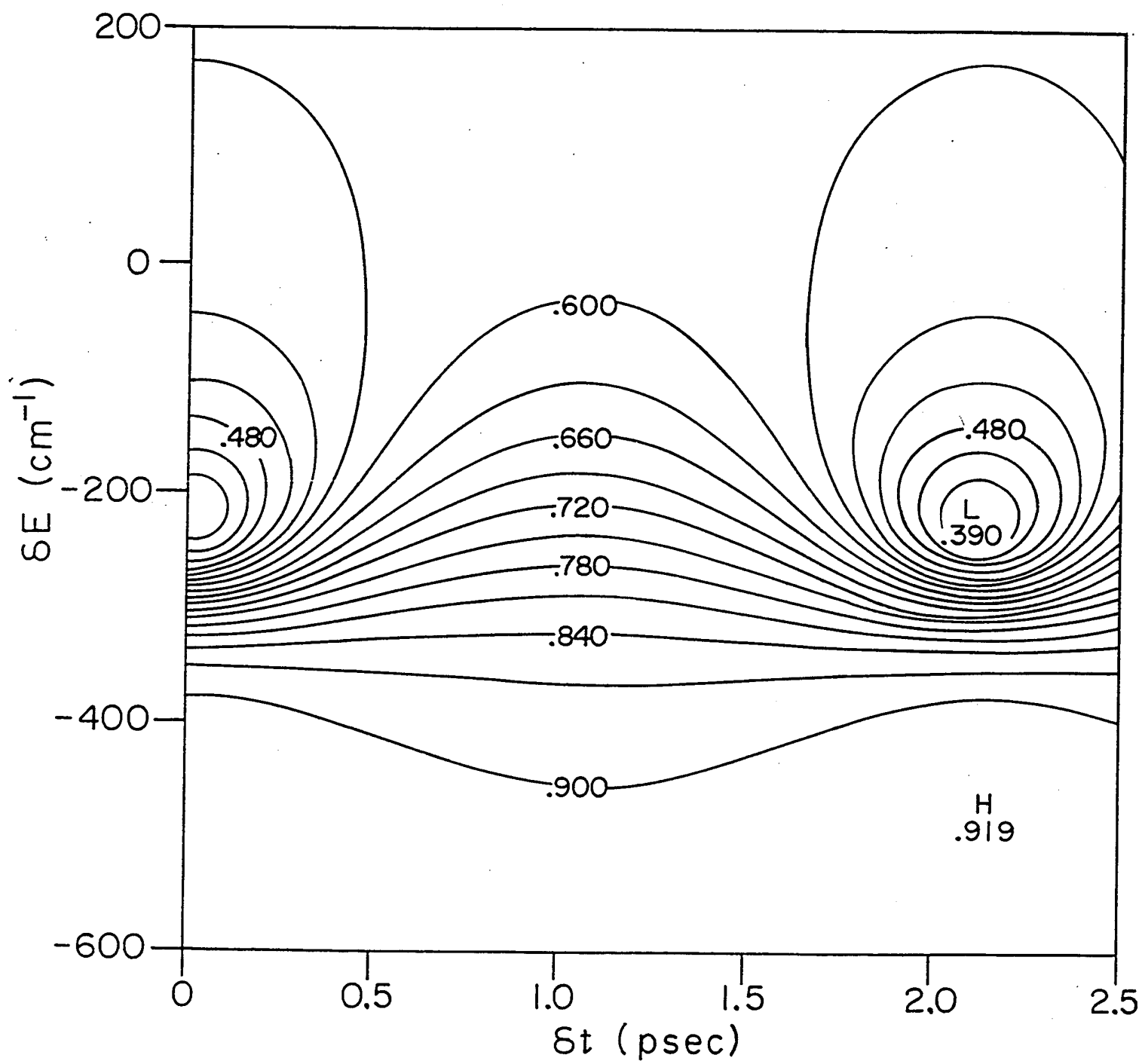


Fig. 5B

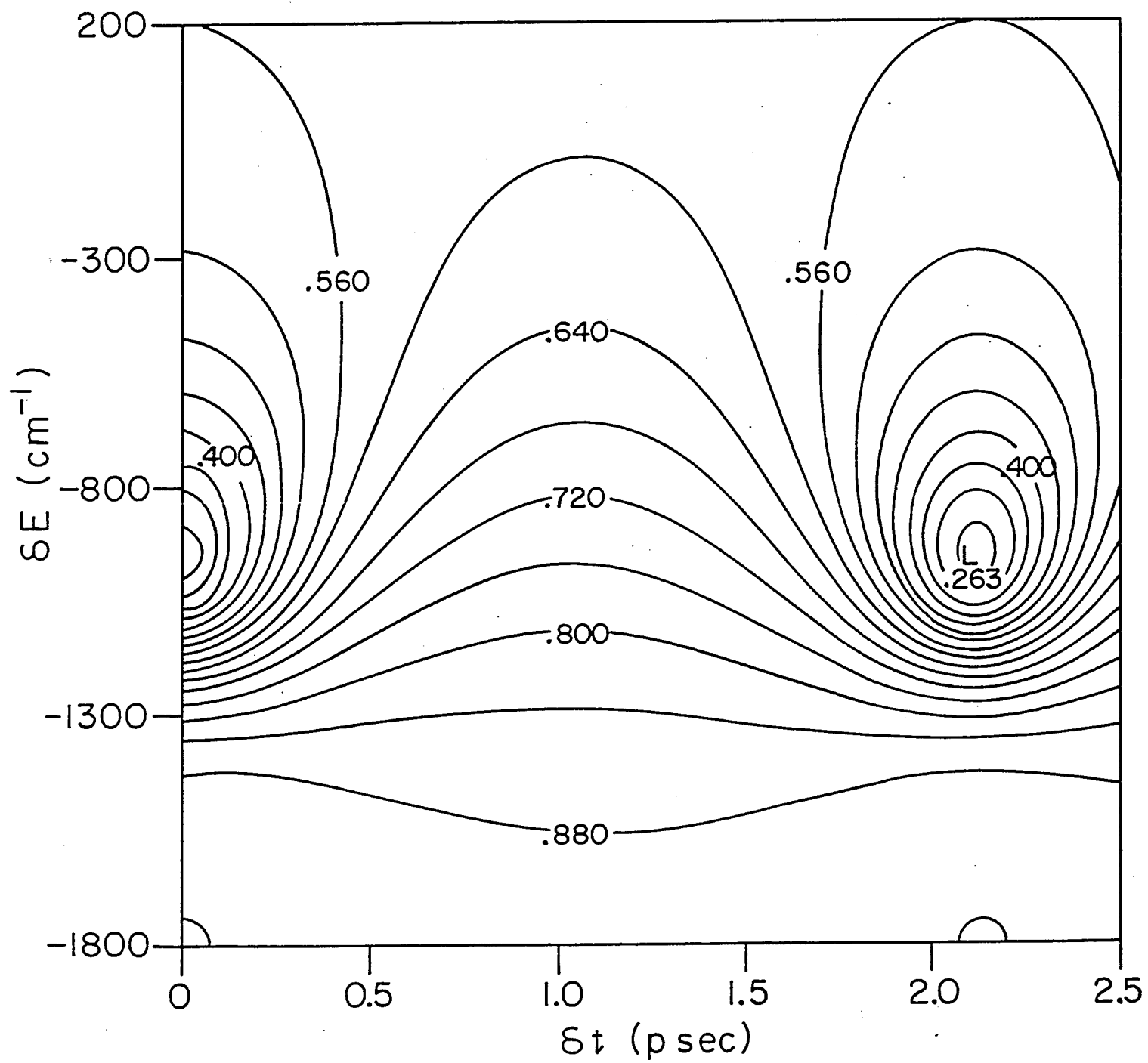


Fig. 5c

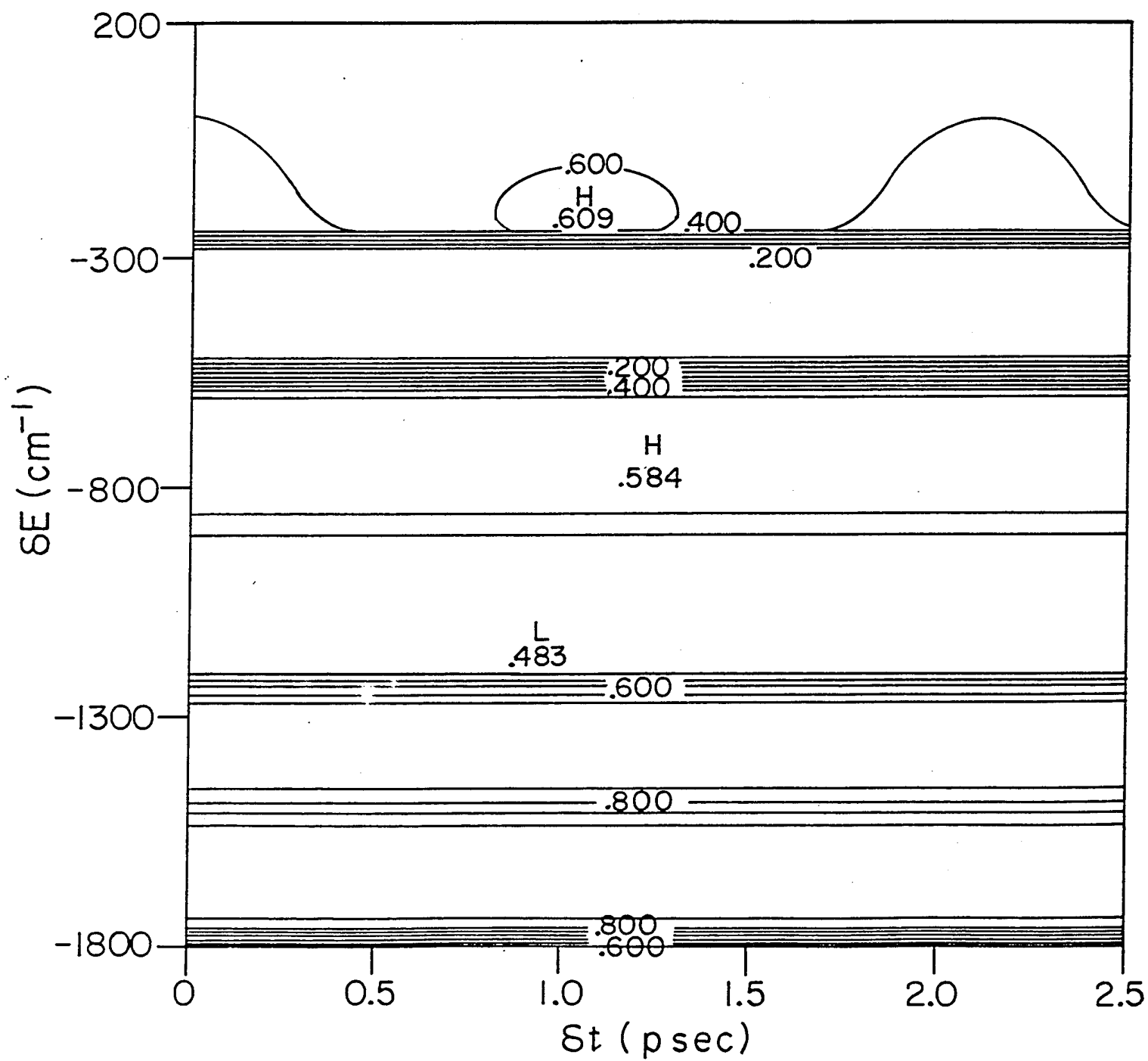


Fig. 5D

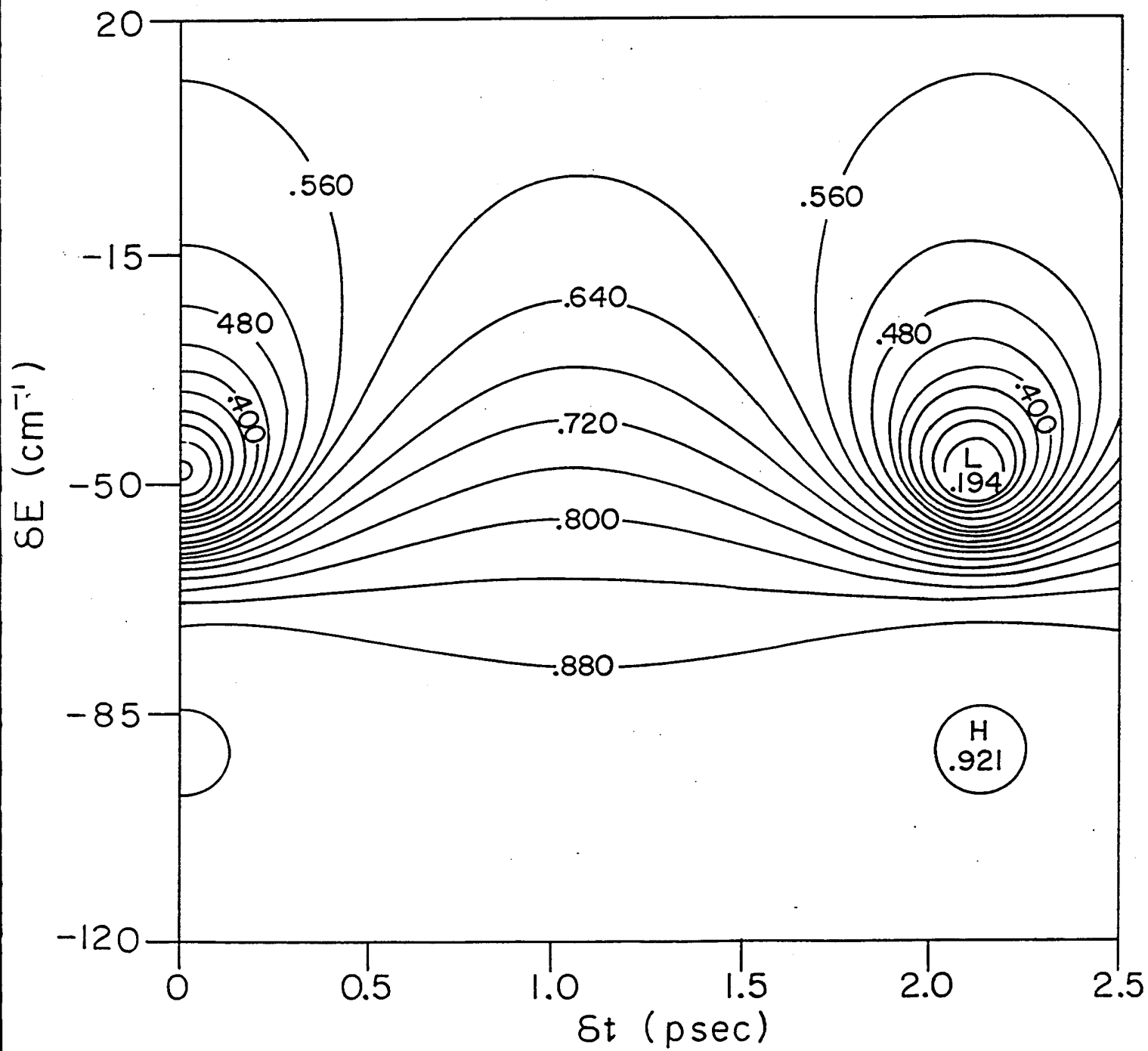


Fig. 6A

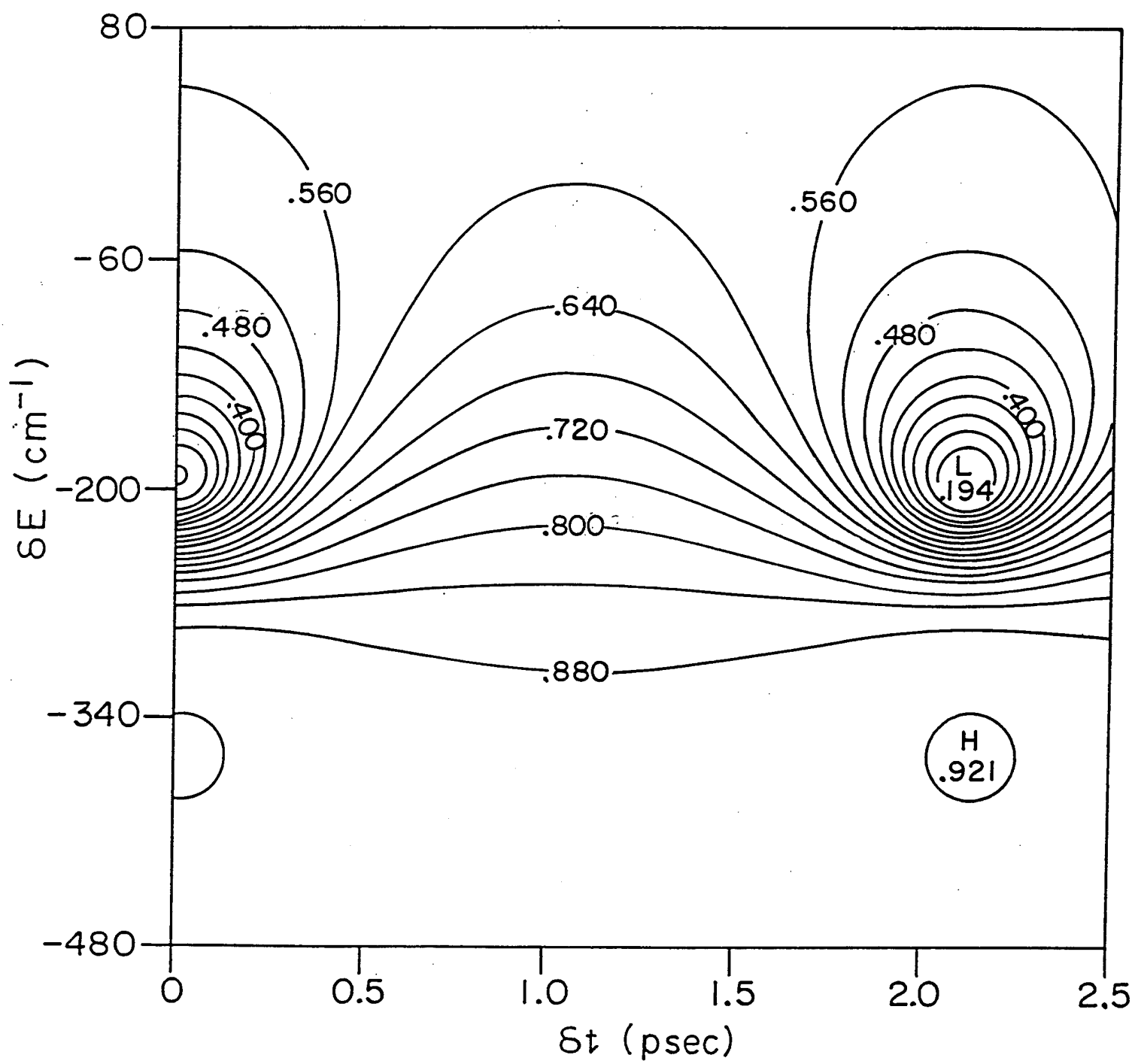


Fig. 6B

Electronic Spectroscopy of Diatomics on a Dynamic Surface:

IBr on MgO(001)

Xue-Pei Jiang, Moshe Shapiro* and Paul Brumer

Chemical Physics Theory Group,

Department of Chemistry

University of Toronto,

Toronto M5S 1A1 Canada

Abstract

A model for computing the absorption spectrum of a diatomic adsorbed on a non-zero temperature surface is developed. In particular, the exact time dependent expression for the absorption spectrum, averaged over the surface variables, is constructed. The required time evolution of the dipole transition density operator is then modeled by a quantum Langevin-type Equation derived by the method of Caldeira and Leggett. The resultant equation is treated numerically and sample spectra are given for IBr on an MgO(001) surface at a temperature of 150° K. The results, parameterized by a diatom-surface coupling constant, illustrate the broadening of the spectrum in the presence of the stochastic thermal substrate motion.

I. INTRODUCTION

Studies of the spectroscopy of molecules on surfaces has yielded much information about molecule-surface interactions. [1] A proper analysis of this data requires a theory which incorporates, within quantum mechanics, the effect of temperature, of the dynamic solid, and of the adsorbate-surface interaction. A complete theory of this kind, particularly for electronic spectroscopy, is well beyond modern computational limitations, necessitating the development of useful models.

In this paper we describe a model, and associated computational method, for the electronic spectroscopy of diatomics adsorbed on a surface. Use of this phenomenological quantum model allows us to go beyond traditional zero-temperature studies to incorporate effects due to non-zero temperature. That is, the model allows for the incorporation of the non-static surface, treated as an external bath at temperature T , with the adsorbate-surface coupling parametrized by a phenomenological friction. Model computations of the electronic absorption spectrum of IBr on MgO(001) demonstrate the broadening effect of the surface on the electronic absorption spectrum.

The paper is organized as follows: Section II contains a description of the theory, including the derivation of the generalization of the Caldeira-Leggett equation to treat two electronic surfaces. Limitations of the technique are also described. A useful numerical technique for propagating this equation, based on the short time split operator plus FFT approach, is described in Section III and the method is applied to IBr on an MgO(001) surface in Section IV. A short summary concludes the paper.

II. THEORY

A. Photoabsorption

The total cross section $\sigma(\omega)$ for photoabsorption from an initial state $|i\rangle$ of the ground electronic state to all vib-rotational states $|f\rangle$ of the electronically excited state with a

photon of frequency ω is given by:

$$\sigma(\omega) = (2\omega/\hbar c\epsilon_0) \sum_f |\langle f|\mu|i\rangle|^2 \delta(\omega_{fi} - \omega) \quad (1)$$

$\omega_{fi} = (E_f - E_i)/\hbar$, where E_f and E_i are the energies of the states $|f\rangle$ and $|i\rangle$. The expression can be rewritten as [2]:

$$\sigma(\omega) = A \int_{-\infty}^{\infty} dt e^{i(\omega+\omega_i)t} \langle i|\mu e^{-iH_e t/\hbar} \mu|i\rangle \quad (2)$$

where $A = 2\omega/(\hbar^2 c\epsilon_0)$, $\omega_i = E_i/\hbar$ and H_e is the Hamiltonian of the excited electronic state. For the case where excitation is out of a thermal ensemble at temperature T Eq. (2) becomes

$$\sigma(\omega) = \frac{2\pi}{\hbar c\epsilon_0} \sum_{if} \frac{e^{-\beta E_i}}{\text{Tr}[e^{-\beta H_g}]} |\langle f|\mu|i\rangle|^2 \delta(\omega_{fi} - \omega) \quad (3)$$

$$= \frac{A}{\text{Tr}[e^{-\beta H_g}]} \int_{-\infty}^{\infty} dt e^{i\omega t} \text{Tr}[e^{-\beta H_g} \mu e^{-iH_e t/\hbar} \mu e^{iH_g t/\hbar}] \quad (4)$$

$$= \frac{A}{\text{Tr}[e^{-\beta H_g}]} \int_{-\infty}^{\infty} dt e^{i\omega t} \text{Tr}[\mu \rho(t)] \quad (5)$$

where

$$\rho(t) = e^{-iH_e t/\hbar} \mu e^{-\beta H_g} e^{iH_g t/\hbar} \quad (6)$$

so that

$$\rho(0) = \mu e^{-\beta H_g} \quad (7)$$

Equation (6) looks similar to the standard propagation of an operator $\mu e^{-\beta H_g}$ except that $H_e \neq H_g$, reflecting a transition between two electronic states.

To generalize this result to include the solid we regard H_e and H_g as the Hamiltonian for the entire system, i.e. the diatomic plus surface. A theory for the absorption cross section then results if we trace over the degrees of freedom of the surface. Denoting this trace by $\langle \rangle$ we have:

$$\langle \sigma(\omega) \rangle = \frac{A}{\text{Tr}[e^{-\beta H_g}]} \int_{-\infty}^{\infty} dt e^{i\omega t} \text{Tr}[\mu \bar{\rho}(t)] \quad (8)$$

where $\bar{\rho}(t) = \langle \rho(t) \rangle$.

The central problem is to compute $\bar{\rho}(t)$, i.e. $\rho(t)$ averaged over the surface degrees of freedom. This task is much simplified by adopting the pseudo-one dimensional model of McCarthy et al [3].

B. Pseudo-One Dimensional Model

Consider a diatomic molecule at fixed tilt angle θ to the surface. Its in-plane motion is described by the vibrational coordinate r and in-plane angle ϕ . McCarthy et al [3] note that the in-plane librational motion in angle ϕ , with frequencies in the range of 3.5 cm^{-1} is far slower than the vibrational motion, with frequencies of $\approx 267 \text{ cm}^{-1}$. As a consequence we adopt an extreme adiabatic picture and assume that ϕ is fixed during the absorption of light.

Under these circumstances, application of this model in the theory above produces $\langle\sigma(\omega; \phi)\rangle$, the averaged absorption cross section which is parametrically dependent on ϕ . As discussed below, at the temperatures of interest there are many occupied librational levels so that we can replace a quantum average over librational levels by a classical average over the angle ϕ .

It remains to establish a method of computing $\bar{\rho}(t)$ for a one degree of freedom system (r with ϕ fixed) in the presence of a bath. A convenient method for modeling this computation is developed below.

C. Generalized Caldeira-Leggett Equation

To perform the average over the surface degrees of freedom requires a specific model for the surface, regarded as a background bath, and for the surface-diatom interaction. We derive a phenomenological model for $\bar{\rho}(t)$ by modifying the approach of Caldeira and Leggett [4] to accommodate the role of two Hamiltonians, H_g and H_e . Caldeira and Leggett adopted the influence functional method of Feynman and Vernon [5] to treat the problem of quantum Brownian motion. The resultant equation of motion for the reduced density matrix

was also independently obtained by Dekker and by Zurek [6], with the result being used to treat the decoherence of quantum systems coupled to an environment. Here we generalize this approach to accommodate the transition character of $\bar{\rho}(t)$, i.e. the appearance of two Hamiltonians in the definition of $\bar{\rho}(t)$. The result is a useful phenomenological equation for the absorption cross section of a system coupled to an external bath.

To avoid rewriting the lengthy derivation of Caldeira and Leggett we indicate below how to rederive their Eqs. (2.14)- (2.16) so as to accommodate the two electronic surfaces which enter our $\rho(t)$. We explicitly adopt their notation to allow the direct comparison with their equations.

Consider the coordinate space expression for the propagated $\bar{\rho}(t)$, i.e.

$$\langle x\mathbf{R}|\rho(t)|y\mathbf{Q}\rangle = \int dx'dy'd\mathbf{R}'d\mathbf{Q}' \langle x\mathbf{R}|e^{-iH_e t/\hbar}|x'\mathbf{R}'\rangle \langle x'\mathbf{R}'|\rho(0)|y'\mathbf{Q}'\rangle \langle y'\mathbf{Q}'|e^{iH_g t/\hbar}|y\mathbf{Q}\rangle \quad (9)$$

where the small letters denote the system variables and the capital letters, bath variables. Consistent with Caldeira and Leggett we assume a one-degree of freedom system; extension to systems with more degrees of freedom can be done. The propagation terms above can be expressed as path integral as:

$$\langle x\mathbf{R}|e^{-iH_e t/\hbar}|x'\mathbf{R}'\rangle = \int \int DxD\mathbf{R} e^{iS_e[x,\mathbf{R}]/\hbar}, \quad (10)$$

$$\langle y'\mathbf{Q}'|e^{iH_g t/\hbar}|y\mathbf{Q}\rangle = \int \int DyD\mathbf{Q} e^{-iS_g[y,\mathbf{Q}]/\hbar}. \quad (11)$$

The actions S_e and S_g are both of the form ($l = e, g$)

$$S_l = S_l^{(s)} + S_l^{(b)} + S_l^{(int)} = \int_0^t L dt' \quad (12)$$

where $S_l^{(s)}$, $S_l^{(b)}$ and $S_l^{(int)}$ are associated with each of the three terms in L :

$$L = L_l^{(s)} + L_l^{(b)} + L_l^{(int)} = \left[\frac{1}{2m} \dot{x}^2 - V_l(x) \right] + \left[\sum_i \frac{1}{2M_i} \dot{\mathbf{R}}_i^2 - \sum_i V_b(\mathbf{R}_i) \right] - \sum_i V_i(x, \mathbf{R}_i). \quad (13)$$

Here, the superscript 's' stands for system, 'b' for the bath, and 'int', for the interaction and $V_l(x)$ differs for S_g and S_e , where it is the ground and excited potentials respectively. M_i are the masses of the atoms in the solid and m is the reduced mass of the adsorbate.

Integration over all the coordinates of environment leads to

$$\bar{\rho}(x, y, t) = \int d\mathbf{R} \langle x\mathbf{R} | \bar{\rho}(t) | y\mathbf{R} \rangle = \int dx' dy' J(x, y, t; x', y', 0) \bar{\rho}(x', y', 0) \quad (14)$$

where

$$J(x, y, t; x', y', 0) = \int \int DxDy e^{iS_g^{(s)}(x)/\hbar} e^{-iS_e^{(s)}(y)/\hbar} \mathcal{F}(x, y) \quad (15)$$

and

$$\mathcal{F}(x, y) = \int d\mathbf{R}' d\mathbf{Q}' d\mathbf{R} \rho_b(\mathbf{R}', \mathbf{Q}', 0) \int \int D\mathbf{R} D\mathbf{Q} e^{(i/\hbar)(S_g^{(int)}[x, \mathbf{R}] - S_e^{(int)}[y, \mathbf{Q}] + S_b[\mathbf{R}] - S_b[\mathbf{Q}])} \quad (16)$$

is the so-called influence functional. The term $\rho_b(\mathbf{R}', \mathbf{Q}', 0)$ is the density matrix of the bath, which arose by factoring $\rho(0)$ [Eq. (7)] into the product of the bath and system terms. Following Leggett et al [4] we assume an harmonic oscillator bath for $V_b(\mathbf{R}_i)$ and a bilinear form for $V_i(x, \mathbf{R}_i)$ to calculate $\mathcal{F}(x, y)$ explicitly. Further, in exact accord with their approach, we assume a thermal equilibrium distribution for $\rho_b(\mathbf{R}')$, in accordance with the adoption of an infinite and passive bath, and take the high temperature limit $k_B T \gg \hbar\omega_b$, and finally obtain the dynamical equation for $\bar{\rho}(t)$:

$$\begin{aligned} \frac{\partial \bar{\rho}}{\partial t} = & \left[-\frac{\hbar}{2mi} \frac{\partial^2 \bar{\rho}}{\partial x^2} + \frac{\hbar}{2mi} \frac{\partial^2 \bar{\rho}}{\partial y^2} + \frac{V_g(x)}{i\hbar} \bar{\rho} - \frac{V_e(y)}{i\hbar} \bar{\rho} \right] \\ & - \gamma \left(x \frac{\partial \bar{\rho}}{\partial x} + y \frac{\partial \bar{\rho}}{\partial y} \right) + \gamma \left(x \frac{\partial \bar{\rho}}{\partial y} + y \frac{\partial \bar{\rho}}{\partial x} \right) - \frac{2m\gamma k_B T}{\hbar^2} (x - y)^2 \bar{\rho}, \end{aligned} \quad (17)$$

where $\gamma = \zeta/m$ and where ζ defines the coupling of the system to the bath. The formalism of Dekker and Zurek [6] would lead to the same equation via a different formulation.

The resultant equation differs from the normal equation of Caldeira and Leggett insofar as it involves two potentials $V_g \neq V_e$. The Caldeira-Leggett result obtains if $V_g = V_e$. Equation (17) has three types of terms. The first term in brackets is the free motion term whereas the others relate to dissipation and fluctuation: the last term in this equation is the white noise fluctuation average contribution, $(x \frac{\partial \bar{\rho}}{\partial x} + y \frac{\partial \bar{\rho}}{\partial y})$ is a friction term which label “type I” whereas $(x \frac{\partial \bar{\rho}}{\partial y} + y \frac{\partial \bar{\rho}}{\partial x})$ is a friction term which we label as type II..

Equation (17) is a generalization of quantum Liouville equation. The kinetic energy and potential terms correspond to the quantum dynamics governed by Schrödinger equation, the last term results from the fluctuating forces which destroys quantum coherence, and the two middle terms describe dissipation associated with friction. It can be easily proved that the trace of $\bar{\rho}(t)$ is preserved during the propagation and that the fluctuating force term which appears in the end of Eq.(17) reduces the off-diagonal term of density matrix. Therefore, this equation depicts the temporal dephasing process caused by the stochastic fluctuating force. There is no population decay or amplitude damping in the equation although we do add a radiative lifetime term in the computation of the time evolution.

D. Propagation

Since the Eq. (17) is linear we can use the short time split operator technique to propagate the dissipative dynamics. Specifically, the split operator technique [7], applied to Eq. (17) gives:

$$\begin{aligned} \rho(x, y, t + \Delta t) = & \exp\left(-\frac{\hbar\Delta t}{2im} \frac{\partial^2}{\partial x^2} + \frac{\hbar\Delta t}{2im} \frac{\partial^2}{\partial y^2}\right) \exp\left(\frac{V_1(x)\Delta t}{i\hbar} - \frac{V_2(y)\Delta t}{i\hbar}\right) \\ & \exp\left(-\gamma\Delta t\left(x\frac{\partial}{\partial x} + y\frac{\partial}{\partial y}\right)\right) \exp\left(\gamma\Delta t\left(x\frac{\partial}{\partial y} + y\frac{\partial}{\partial x}\right)\right) \exp\left(-\frac{2m\gamma k_B T \Delta t}{\hbar^2}(x-y)^2\right) \rho(x, y, t) \end{aligned} \quad (18)$$

A widely applied numerical technique to propagate a wavefunction via $e^{-iH_{et}/\hbar}$ is the fast Fourier transform (FFT) method [8] which transforms back and forth between the q and p representations to facilitate the short time propagation of pure kinetic and pure potential terms. If the propagation involves two potential energy surfaces which are coupled electronically, i.e. surface-crossing, then an extra transformation between diabatic and adiabatic representations is necessary to deal with the propagation of the 2×2 matrix of potentials. This approach was discussed previously [9] and is adopted below to treat the Caldeira-Leggett equation which involves two potentials.

There are a number of issues which make the propagation of Eq. (17) more difficult than the standard application to the wavefunction. First, we are propagating a density matrix

whose dimensionality is twice that of the wavefunction. This makes the computation costly: the cpu time spent on FFT of a one dimensional wavefunction is roughly $N \log_2 N$ where N is the total time steps of the propagation. This increases to $(N \log_2 N)^2$ for the density matrix because involves (x, y) , i.e. twice the number of independent variables. Secondly, the propagation of dissipative dynamics introduces three extra terms over that of pure state propagation: the propagation of the white noise fluctuation average [the last term in Eq. (17)] is straightforward in the coordinate representation while the friction term of type II, containing mixed x and y , can be propagated by a series of one dimensional FFT. For this term, one applies the FFT technique in the form:

$$\exp(\gamma x \frac{\partial}{\partial y} \Delta t) \rho(x, y) = \frac{1}{2\pi} \int dk e^{-iky} e^{-i\gamma \Delta t k x} \int dz e^{ikz} \rho(x, z) \quad (19)$$

The friction term of type I, however, which contains only x or y , requires special treatment. To treat this term we note that $\{x^2, xp + px, p^2\}$ form a Lie algebra, that is,

$$[x^2, p^2] = 2i\hbar(xp + px), \quad (20)$$

$$[xp + px, p^2] = 4i\hbar p^2, \quad (21)$$

$$[x^2, xp + px] = 4i\hbar x^2. \quad (22)$$

Then, the application of Wei-Norman theorem [10] gives

$$e^{H_{harm} t} = e^{\beta_1 p^2} e^{\beta_2 (xp + px)} e^{\beta_3 x^2}, \quad (23)$$

where $H_{harm} = p^2/2\mu + cx^2$ with arbitrary c and the β_i satisfy a set of ordinary differential equations [11]. Equation (23) can then be propagated, from which we can extract $\exp(-\gamma \Delta t (x \frac{\partial}{\partial x})) = \exp(-\gamma \Delta t xp)$

Our numerical computation uses a 256x256 grid which covers the region from 4 a.u. to 10 a.u. An absorbing boundary condition is used to meet the requirement of a vanishing density matrix at the boundary.

III. IBr ON MgO(001)

As an example of this approach we consider IBr adsorbed on an MgO(001) surface. In particular, we extend the previous study of McCarthy et al [3] for a static surface to a diatomic on a dynamic surface at temperature T and consider the effect, on the absorption spectrum, of the diatom-surface coupling, embodied in the parameter γ .

The IBr is assumed fixed at a tilt angle of $\theta = 90^\circ$ to the surface. The total Hamiltonian is of the form:

$$H = \frac{-\hbar^2}{2\mu} \left[\frac{1}{r} \frac{\partial}{\partial r} \left(r \frac{\partial}{\partial r} \right) + \frac{1}{r^2} \frac{\partial^2}{\partial \phi^2} \right] + T_s(\mathbf{R}) + V(\mathbf{R}, r, \phi) \quad (24)$$

Here \mathbf{R} denotes the coordinates of the solid, $T_s(\mathbf{R})$ is the kinetic energy of the solid and the total potential is

$$V(\mathbf{R}, r, \phi) = V_s(\mathbf{R}) + V_a(r, \phi) + V_{as}(\mathbf{R}, r, \phi) \quad (25)$$

The three potential contributions, the potential of the surface $V_s(\mathbf{R})$ of the adsorbate $V_a(r, \phi)$ and their interaction $V_{as}(\mathbf{R}, r, \phi)$ are taken from McCarthy et al. In particular, IBr is described by the ground X ($^1\Sigma^+$) state and three excited states [A ($^3\Pi_1$), B ($^3\Pi_{0+}$) and Y (0^+)] and V_s is modeled by a 4×5 slab of atoms. The B and Y surfaces are coupled by non-Born Oppenheimer coupling terms. The adsorbate-surface interaction V_{as} is taken as a sum of pairwise interactions between the diatom and the surface. Note, as mentioned above, that V_{as} is assumed to be the same for the ground and excited states of IBr, a reasonable assumption since all states are covalent in character, and necessary for the application of Eq. (17).

The four potential curves X, A, B, and Y are shown as dashed curves in Fig. 1. Figure 1 also shows the full potential curves of adsorbed IBr, i.e., the potential including $V_{IBr}(r)$ and $V_{int}(r, \phi)$ where the center of mass, θ , and ϕ are all at the equilibrium positions. Compared to the $V_{IBr}(r)$ of free IBr, shown with dotted lines, adsorption lowers the IBr energy for all r .

Figure 2a shows an energy landscape, with the position of the center of IBr at $x_{cm} = 5.8$ a.u., $y_{cm} = 5.8$ a.u., $z_{cm} = 4.5$ a.u. In order to interpret Fig. 2a, note that the IBr molecule is parallel to the surface and that the origin of the polar coordinate coincides with the center of mass of IBr, which is chosen to be above an Mg^{+2} of the substrate. Note that there is no contour plot for $r < 4$ a.u. since the $V_{IBr}(r)$ becomes increasingly repulsive (its equilibrium position is 4.666 a.u.) and large in value. Around $r = 5.4$ a.u., one sees dashed contours, indicating a valley of negative V . There are several minima in this belt, with the one at $\phi = 270^\circ$ seemingly the most stable. Outside the potential belt the total energies are all positive. Figure 2a is an arbitrary cut of the potential and does not correspond to the global minimum, which is at $x_{cm} = 5.38$ a.u., $y_{cm} = 6.21$ a.u., $z_{cm} = 5.73$ a.u., $\theta = 90^\circ$, $\phi = 264^\circ$, and the bond length $r_{eq} = 4.666$ a.u.. Figure 2b does show a contour plot of the interaction energy on a small scale near the potential minimum.

Dipole moment functions for excitation were obtained from Ref. [3]. Computations were carried out over photon wavelengths ranging from 530 nm to 590 nm. At these energies the static surface computations [3] show structure due to transitions to the bound regions of the $^1\Sigma^+$ and $^3\Pi_0$ states. At higher energies the system undergoes photodissociation by a $^3\Pi_0 \rightarrow YO^+$ transition. We do not focus on features of the absorption spectrum in this region since they are already quite broad in the case of a static surface [3] and are only marginally modified by adsorption to the *dynamic* surface. Further, we do not attempt to produce the structure in the region of $\lambda < 540$ nm, which would require longer propagation times and larger boundaries.

Computations of $\langle \sigma(\omega; \phi) \rangle$, i.e. the excitation cross section at fixed libration angle ϕ were carried out as described above at $T = 150^\circ$ C and for an average over ϕ . Note that at $T = 150^\circ$ C more than 100 librational levels are populated. This, plus the observation that the potential in the r and ϕ motion is essentially separable near the potential minimum (see Fig. 2) suggests replacing the quantum average over the librational states by the classical average over ϕ :

$$\begin{aligned}
\langle \sigma(\omega) \rangle &= \int dp_\phi d\phi \exp[-(p_\phi^2/2m + V(r_e, \phi))/kT] \langle \sigma(\omega; \phi) \rangle \\
&= \sqrt{2m\pi kT} \int d\phi \exp[-V(r_e, \phi)/kT] \langle \sigma(\omega; \phi) \rangle
\end{aligned} \tag{26}$$

where p_ϕ is the momentum conjugate to ϕ and $V(r_e, \phi)$ is the librational potential experienced by the adsorbed diatom at $r = r_e = XX$, the equilibrium internuclear position at the potential minimum. Tests of several sets of angles showed that the angle integral could be done numerically with as few as nine points.

A. Computational Results

Sample computational results are shown in Figure 3 for a surface at $T = 150^\circ$. We focus on the region ($\lambda > 542$ nm) where the spectrum shows considerable structure, i.e in the regime corresponding to absorption to the quasi-bound states of the B and Y potentials. At this temperature only the ground vibrational state of the diatom is significantly populated, reducing the computational effort. Figure 3a shows the absorption spectrum resulting from a computation at a single librational angle at the minimum of the librational potential, $\phi = 264^\circ$ degrees. Here the friction term $\gamma=0$, thus, any observed line broadening is due to dissociation. Figure 3a shows sharp structure with some broadened features in the neighborhood of 560 nm and 570 nm reflecting the nonadiabatic coupling of the B state to the repulsive Y state. Averaging over many angles, with the result shown in Fig. 3b, results in a further loss of peak heights and a loss of structure in the region of 540 to 550 nm.

Note that in doing these computations we assume a dipole transition exclusively to the B state. By doing this, we eliminate the artifact of boundary reflection associated with the FFT technique. This assumption will not affect the spectra in the 400 to 600 nm wavelength range, the Franck-Condon region between surface X and B. It does, however, substantially affect the wavelength range around 300 nm, corresponding to Franck-Condon excitation between the X and Y surfaces.

Figures 3a and 3b may be compared to the previous zero temperature results of McCarthy et al, computed by a time independent method. Doing so shows that our resonant peak

heights are somewhat lower. This is due to the finite propagation time (3.8 ps) and the short range absorbing boundary condition in our calculation. This does not affect the comparison of results of different γ calculations, discussed below.

Figure 3c shows the absorption spectrum at $\gamma = 10^{-7}$, including angle averaging. It clearly demonstrates the heavily broadened peaks resulting from the energy dissipation by the substrate MgO. Nevertheless, the broadening due to the nonadiabaticity can still be recognized around 560 and 570 nm. This broadening becomes increasingly significant as γ increases. This is evident in Figure 3d where the vast majority of structure is now gone.

Clearly the spectrum is very sensitive to the values of γ which models the adsorbate-surface interaction. This allows a direct determination of γ by a fit to experimental data.

IV. SUMMARY

We have introduced a model which allows the computation of the electronic absorption spectrum of a molecule adsorbed to a surface. The dynamic motion of the surface is explicitly included, with the model parametrized by a friction constant and a surface temperature. The strong dependence of the spectral line widths on the friction constant have been explicitly demonstrated in a computation on IBr adhering to an MgO surface.

ACKNOWLEDGMENTS

This work was supported by the U.S. Office of Naval Research under contract number N00014-90-J-1014 and by the Ontario Laser and Lightwave Research Centre. One of us (XPJ) would like to thank Dr. D. Gruner, Dr. G. Campolieti and Dr. Z. Chen for computational assistance and discussions.

REFERENCES

* Permanent Address: Department of Chemical Physics, The Weizmann Institute of Science, Rehovot, Israel.

- [1] See, e.g. *Vibrational Spectroscopy of Molecules on Surfaces*, eds. J.T. Yates, Jr. and T.E. Madey, Plenum, New York (1987).
- [2] E.J. Heller, *J. Chem. Phys.* **68**, 3891 (1978)
- [3] M.I. McCarthy, R.B. Gerber, and M. Shapiro, *J. Chem. Phys.* **92**, 7708 (1990); M.I. McCarthy and R.B. Gerber, *J. Chem. Phys.* **93**, 887 (1990).
- [4] A.O. Caldeira and A.J. Leggett, *Physica* **121A**, 587 (1983); A.O. Caldeira and A.J. Leggett, *Ann. Phys. (N.Y.)* **149**, 374 (1983).
- [5] R.P. Feynman and A.R. Hibbs, *Quantum Mechanics and Path Integrals*, (McGraw-Hill, N.Y.)
- [6] H. Dekker, *Phys. Rep.* **80**, 1(1981); W.H. Zurek, *Physics Today*, October 1991, pp. 36.
- [7] H. Trotter, *Proc. Amer. Math. Soc.* **10**, 545 (1959)
- [8] J.A. Fleck Jr., J.R. Morris, and M.D. Feit, *Appl. Phys.* **10**, 1929 (1976); M.D. Feit, J.A. Fleck, Jr. and A. Steiger, *J. Comput. Phys.* **47**, 412 (1986)
- [9] X-P. Jiang, R. Heather, and H. Metiu, *J. Chem. Phys.* **90**, 2555 (1989)
- [10] Wei-Norman reference
- [11] Xue-Pei Jiang, (unpublished)

FIGURE CAPTIONS

Fig. 1 One dimensional potential curves of IBr on MgO(001). The solid lines are adsorbed IBr and dashed lines refer to free IBr.

Fig. 2 (a) Two dimensional contour plot of the potential $V_{IBr}(r) + V_{int}(r, \phi)$ when $x_{cm} = 5.8$ a.u. , $y_{cm} = 5.8$ a.u., $z_{cm} = 4.5$ a.u. $\theta = 90^\circ$, where the IBr molecule is in the ground electronic state.

(b) Two dimensional contour plot of the interaction potential around the equilibrium position. $\Delta V_{int}(r, \phi) = V_{int}(r, \phi) - V_{int}^{min}(r, \phi)$ when $x_{cm} = 5.38$ a.u., $y_{cm} = 6.21$ a.u., $z_{cm} = 5.73$ a.u. $\theta = 90^\circ$. This interaction is the same for the ground or excited electronic state of IBr.

Fig. 3 Absorption spectra of IBr/MgO(001) at $T = 150K$: (a) $\gamma = 0$ for a single ϕ angle. Results averaged over ϕ for various values of γ are shown in (b) $\gamma = 0$, (c) $\gamma = 10^{-7}$ (d) $\gamma = 5 * 10^{-7}$.

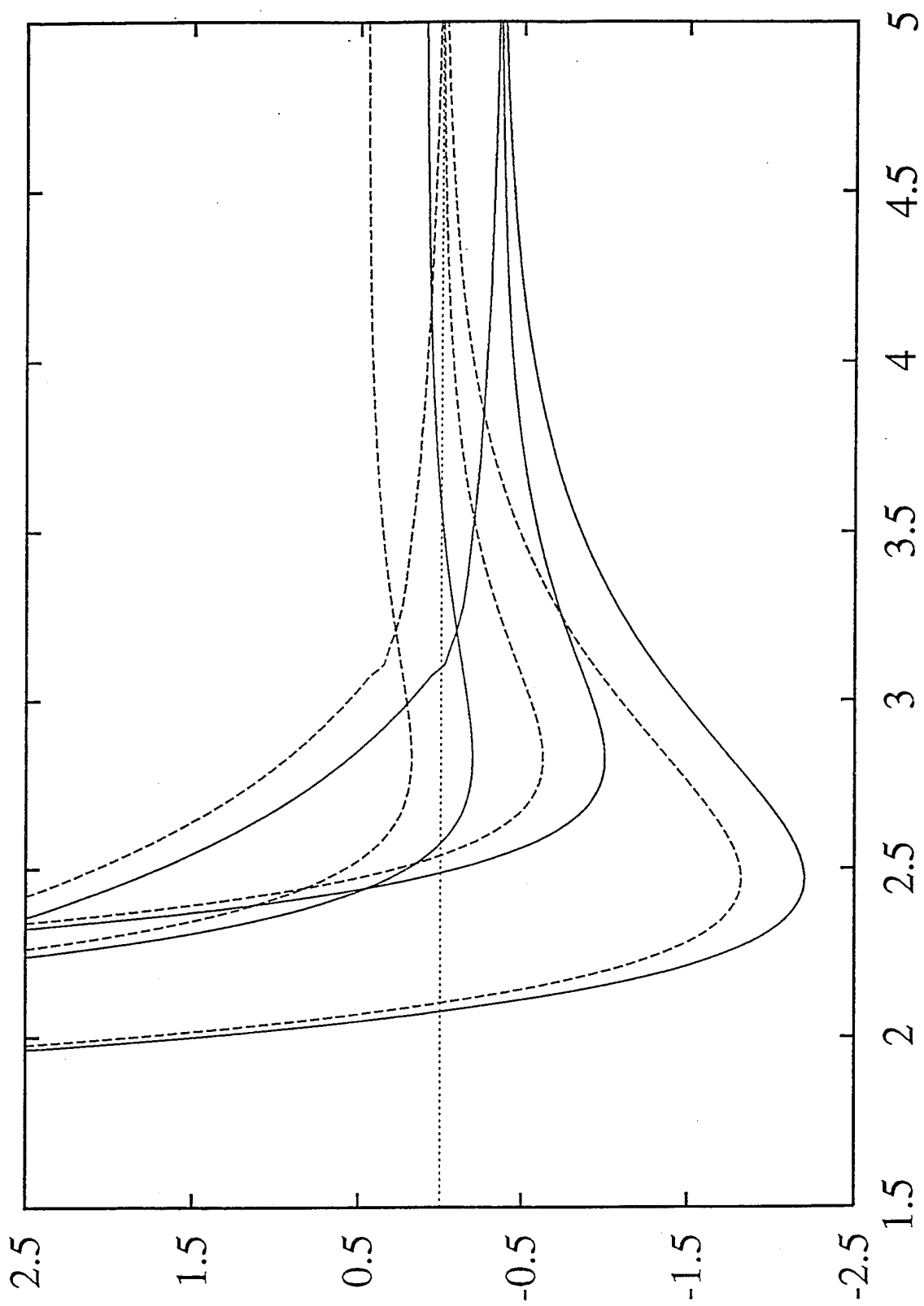
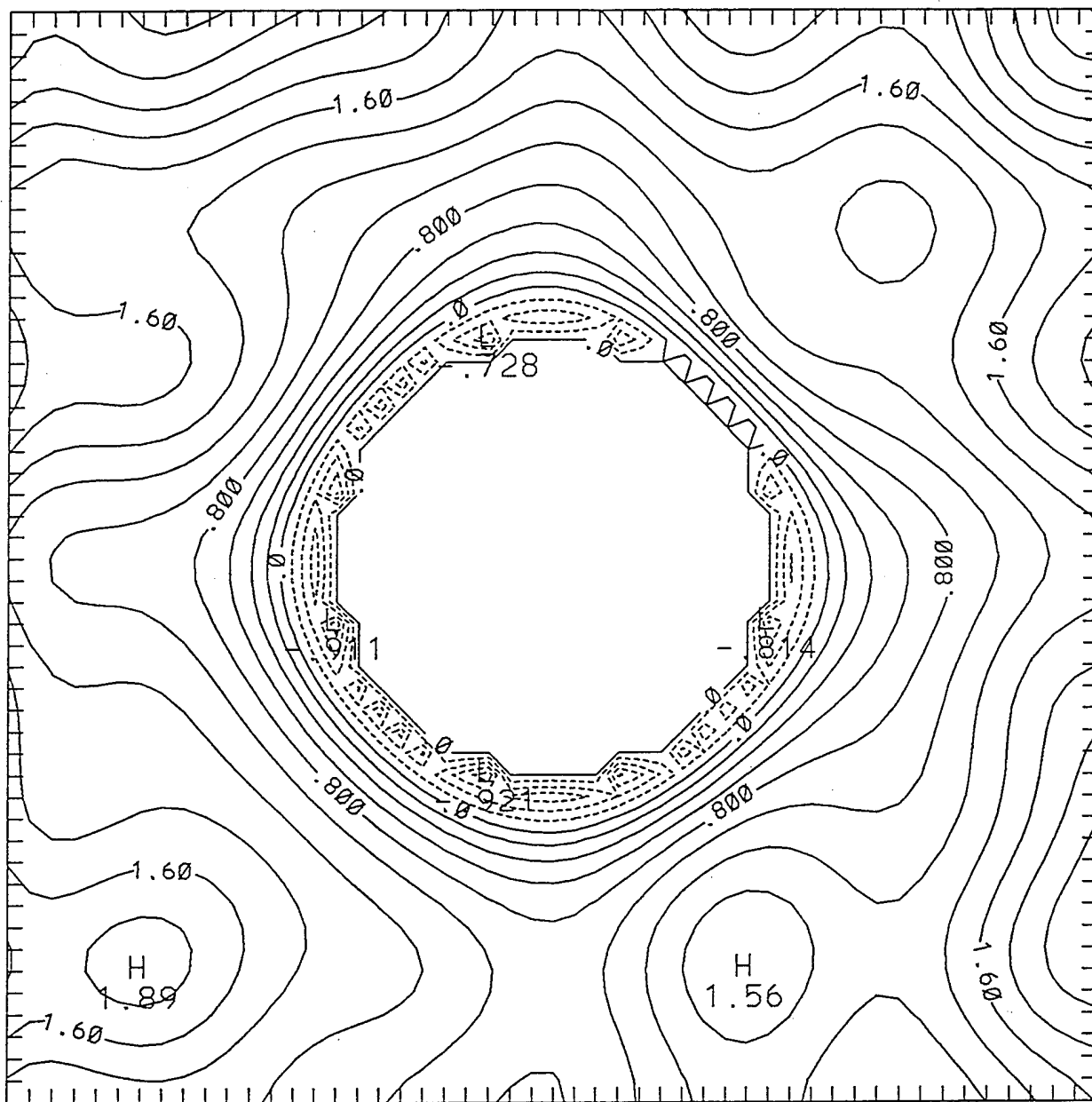
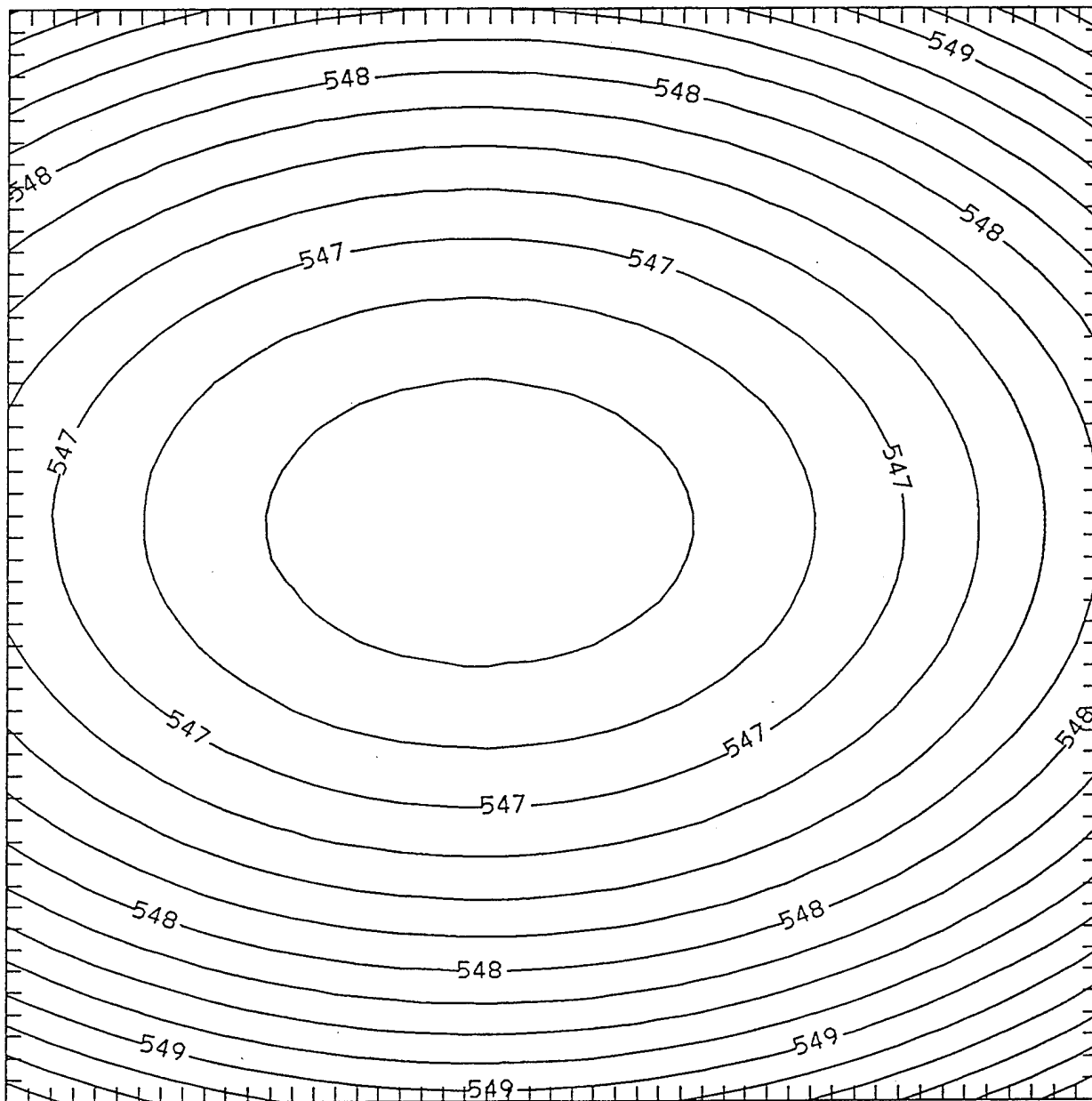


Fig 1



CONTOUR FROM -.80000 TO 2.80000 CONTOUR INTERVAL OF .20000 PT(3,3)= 1.4079

Fig 2a



JR FROM .54570E-03 TO .55050E-03 CONTOUR INTERVAL OF .30000E-06 PT(3,3)= .54946E-03 LABELS SCALED BY .1000

Fig 2b

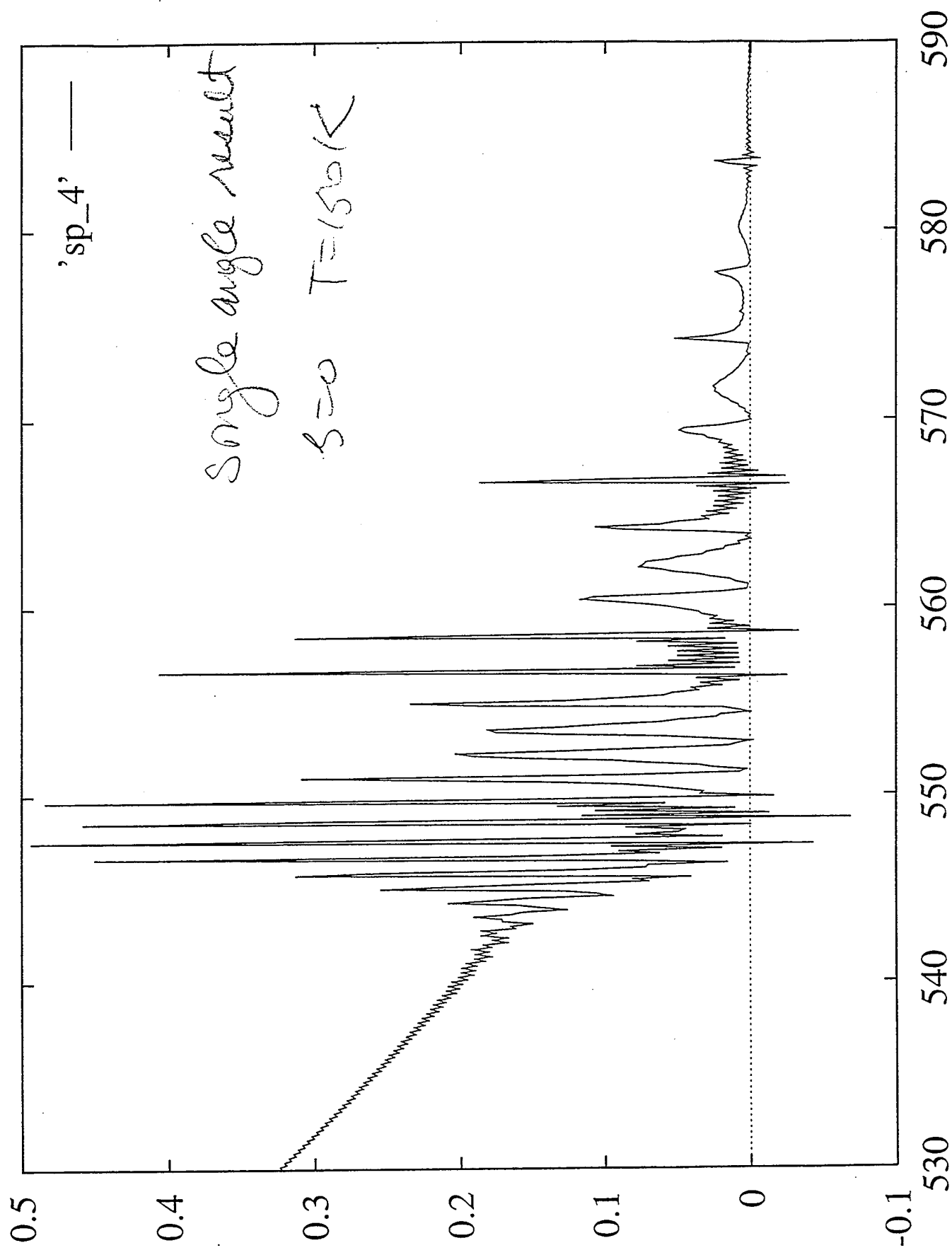


Fig 3a

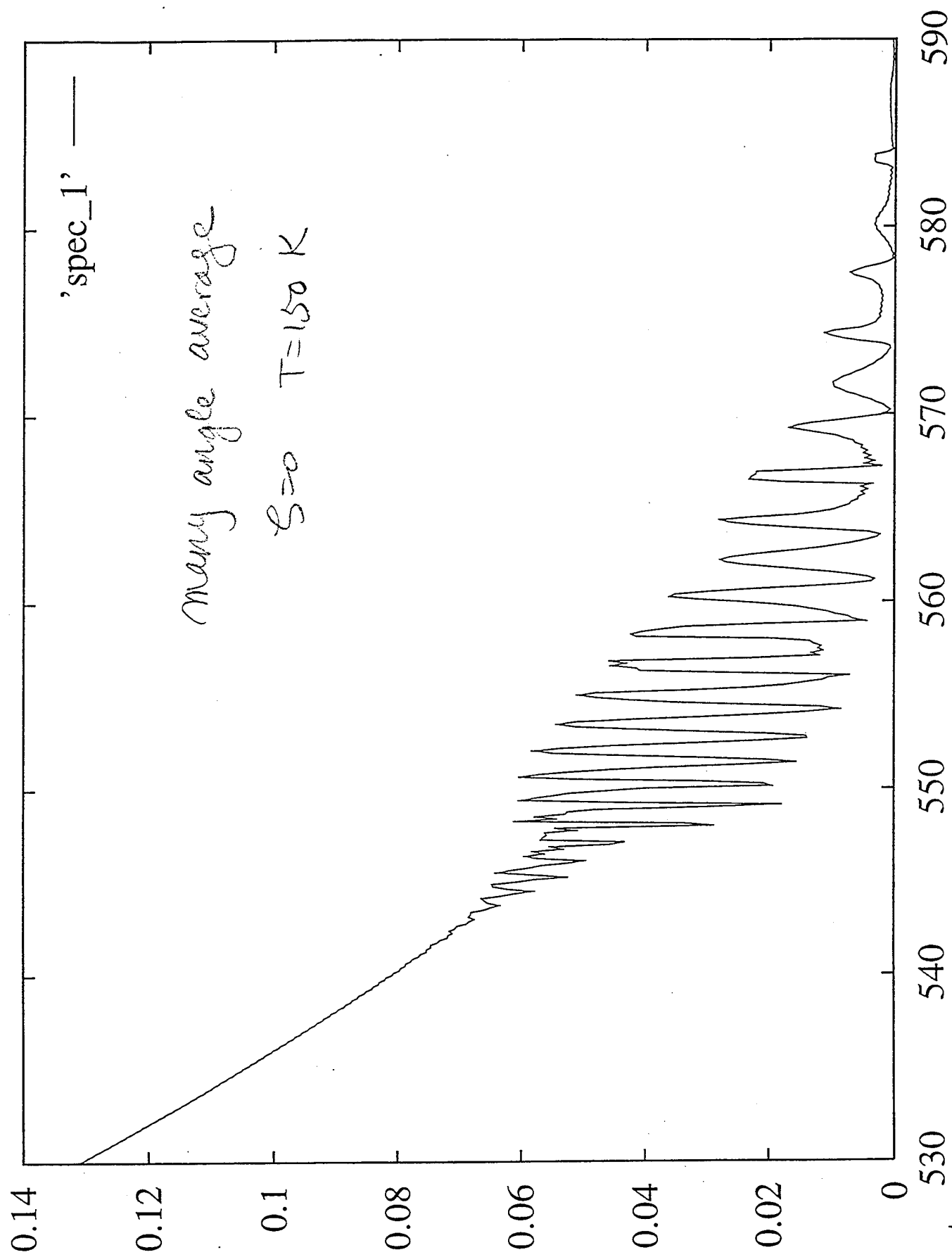


Fig 3b

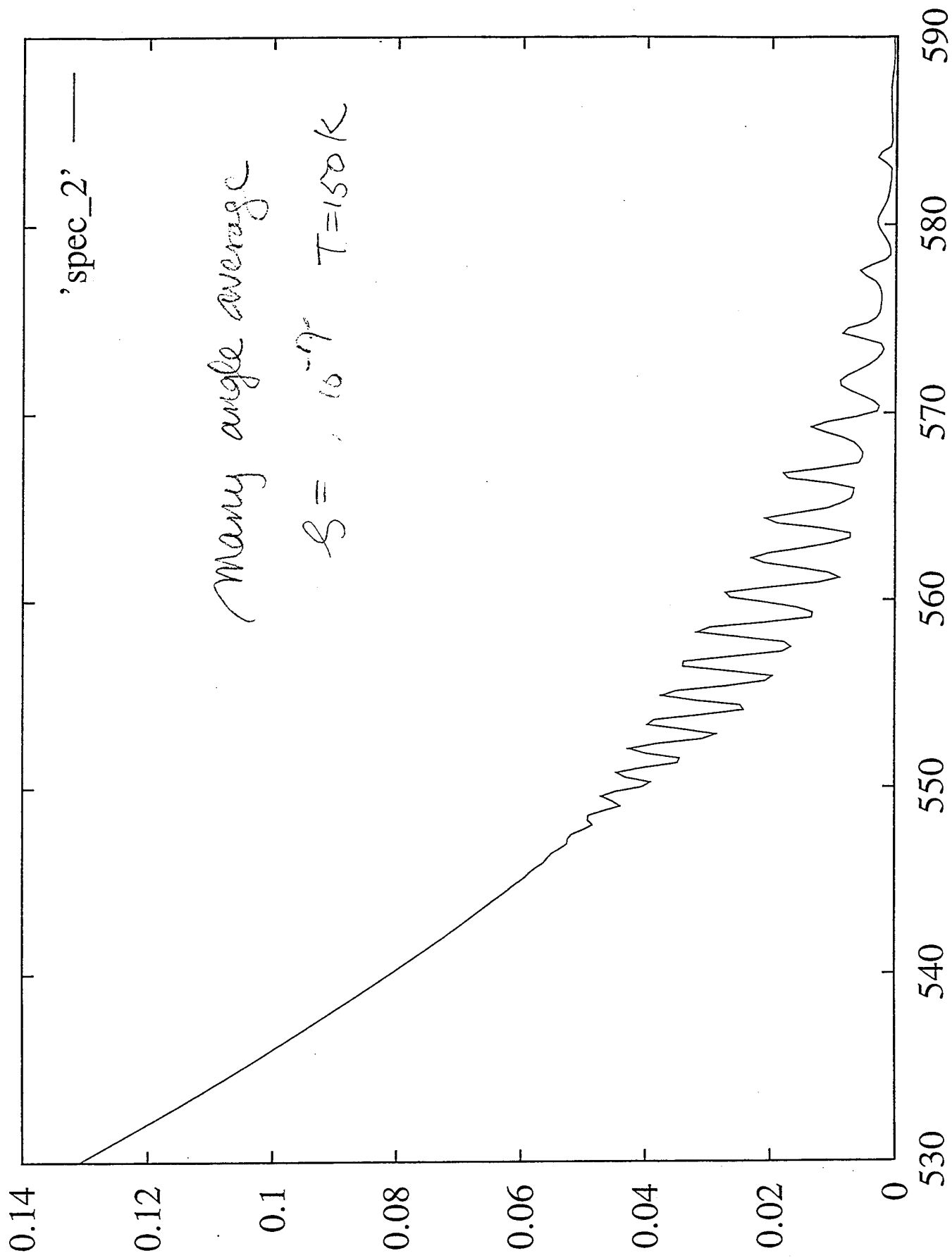


Fig 30

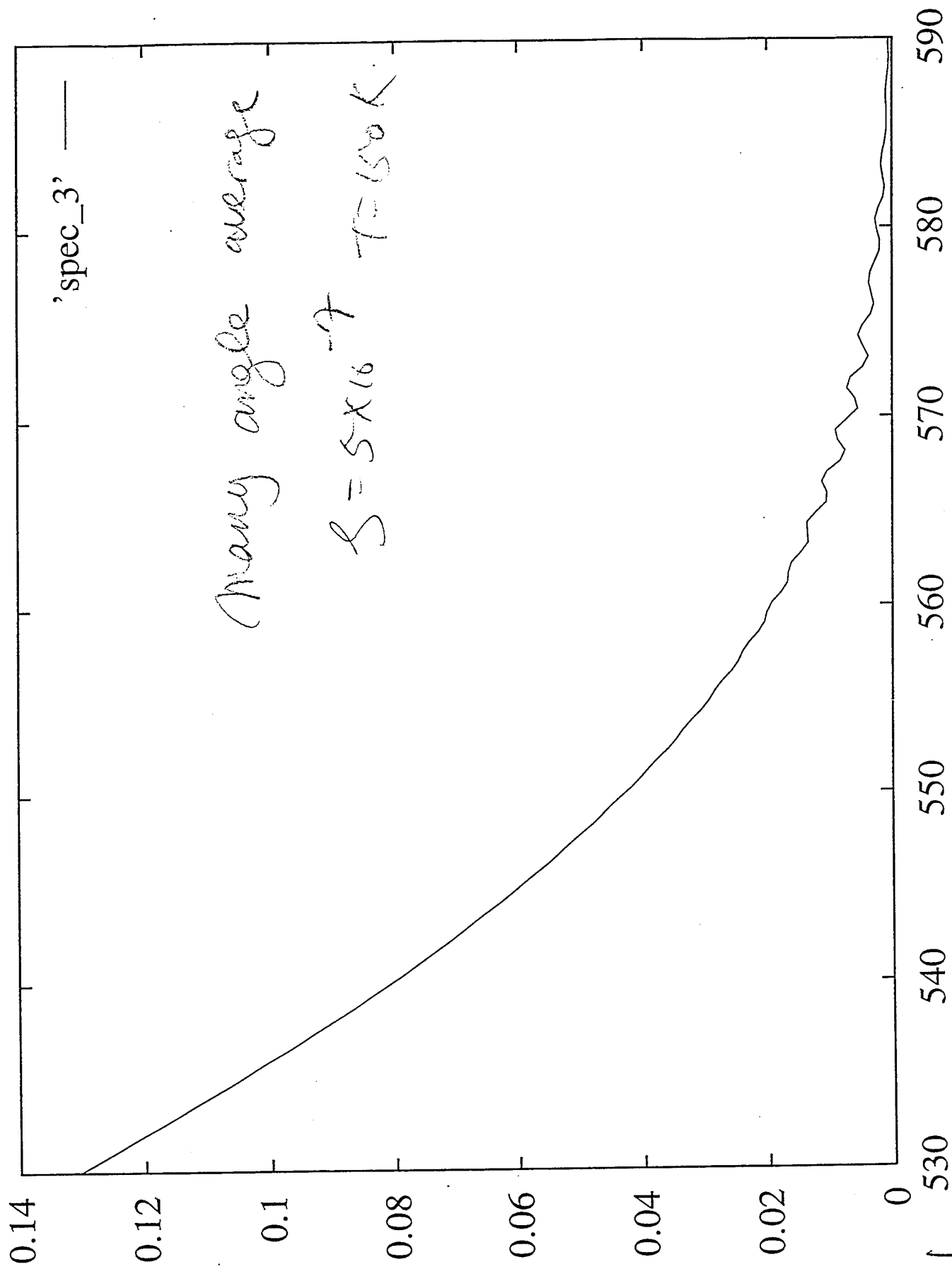


Fig 3d

LASER CONTROL OF MOLECULAR PROCESSES: RESONANT EXCITATION IN A THERMAL ENVIRONMENT

ZHIDANG CHEN, MOSHE SHAPIRO* and PAUL BRUMER

Chemical Physics Theory Group, Department of Chemistry

University of Toronto

Toronto, Ontario M5S 1A1, Canada

ABSTRACT

Coherent radiative control is a quantum-interference based approach to controlling molecular processes by the use of coherent radiation. A method of carrying out such control in the presence of thermal broadening effects and laser jitter is described and applied to the photodissociation of Na_2 .

1. Introduction

Control over molecular dynamics using lasers is an issue at the forefront of modern molecular physics. The theory of coherent radiative control of molecular dynamics, which we have developed over the last seven years¹, affords a direct method for controlling reaction dynamics using coherence properties of weak lasers, with a large range of yield control expected in laboratory scenarios. In addition, the theory of coherent control provides deep insights into the essential features of reaction dynamics, and of quantum interference, which are necessary to achieve control over elementary molecular processes.

As in all interference phenomena the known system phase, both molecular and optical, plays a crucial role. Incoherence effects leading to a mixed initial matter-photon state, such as partial laser coherence or an initially mixed molecular state, degrade control in quantum interference based methods. As a consequence, all but one⁴ of our previous coherent control scenarios were limited to isolated molecules in a pure state, e.g. molecular beam systems. Below we show that it is possible to maintain control in a molecular system in thermal equilibrium by interfering two distinct resonant two-photon routes to photodissociation. The proposed control scenario also provides a method for overcoming destructive interference loss due to jumps in laser phase.

In section 2, we provide a schematic overview of coherent radiative control including an example which emphasizes the general principles, and in section 3, we

describe the new coherent control scenario.

2. Interference and Control: An Example

Consider molecular scattering which, at total energy E produces a number of distinct products. The total Hamiltonian is denoted $H = H_q^0 + V_q$, where H_q^0 is the Hamiltonian of the separated products in the arrangement channel labeled by q , ($q = 1, 2, \dots$) and V_q is the interaction between products in arrangement q . We denote eigenvalues of H_q^0 by $|E, n, q^0\rangle$, where n denotes all quantum numbers other than E ; eigenfunctions of H , which correlate with $|E, n, q^0\rangle$ at large product separation, are labeled $|E, n, q^-\rangle$. By definition of the minus states, a state prepared experimentally as a superposition $|\Psi(t=0)\rangle = \sum_{n,q} c_{n,q} |E, n, q^-\rangle$ has probability $|c_{n,q}|^2$ of forming product in channel q , with quantum numbers n . As a consequence, control over the probability of forming a product in any asymptotic state is equal to the probability of initially forming the appropriate minus state which correlates with the desired product. The essence of control lies, therefore, in forming the desired linear combination at the time of preparation. The essential *modus operandi* of coherent radiative control is to utilize the phase and intensity of laser excitation to alter the coefficients $c_{n,q}$ and in this way to enhance production of the desired product.

Consider, as an example of coherent control, a specific scenario for unimolecular photoexcitation³ where a system, initially in pure state ϕ_g (or $|E_i\rangle$ below), is excited to energy E , by simultaneous application of two CW frequencies ω_3 and ω_1 ($\omega_3 = 3\omega_1$), providing two independent optically driven routes from ϕ_g to $|E, n, q^-\rangle$. Straightforward perturbation theory, valid for the weak fields under consideration, gives the probability $P(E, q; E_i)$ of forming product at energy E in arrangement q as:

$$P(E, q; E_i) = P_3(E, q; E_i) + P_{13}(E, q; E_i) + P_1(E, q; E_i). \quad (1)$$

with P_3 being the probability of one photon absorption:

$$P_3(E, q; E_i) = \left(\frac{\pi}{\hbar}\right)^2 \epsilon_3^2 \sum_n |\langle E, n, q^- | (\hat{\epsilon}_3 \cdot \hat{d})_{e,g} | E_i \rangle|^2. \quad (2)$$

Here \hat{d} is the electric dipole operator, and

$$(\hat{\epsilon}_3 \cdot \hat{d})_{e,g} = \langle e | \hat{\epsilon}_3 \cdot \hat{d} | g \rangle, \quad (3)$$

where $|g\rangle$ and $|e\rangle$ are the ground and excited electronic state wavefunctions, respectively. The term P_1 is the probability of three photon absorption:

$$P_1(E, q; E_i) = \left(\frac{\pi}{\hbar}\right)^2 \epsilon_1^6 \sum_n |\langle E, n, q^- | T | E_i \rangle|^2, \quad (4)$$

with

$$T = (\hat{\epsilon}_1 \cdot \hat{d})_{e,g} (E_i - H_g + 2\hbar\omega_1)^{-1} (\hat{\epsilon}_1 \cdot \hat{d})_{g,e} (E_i - H_e + \hbar\omega_1)^{-1} (\hat{\epsilon}_1 \cdot \hat{d})_{e,g}, \quad (5)$$

and P_{13} is the interference term between the two processes:

$$P_{13}(E, q; E_i) = -2 \left(\frac{\pi}{\hbar}\right)^2 \epsilon_3 \epsilon_1^3 \cos(\theta_3 - 3\theta_1 + \delta_{13}^{(q)}) |F_{13}^{(q)}| \quad (6)$$

The amplitude $|F_{13}^{(q)}|$ and phase $\delta_{13}^{(q)}$ are defined by

$$|F_{13}^{(q)}| \exp(i\delta_{13}^{(q)}) = \sum_n \langle E_i | T | E, n, q^- \rangle \langle E, n, q^- | (\hat{\epsilon}_3 \cdot \hat{d})_{e,g} | E_i \rangle. \quad (7)$$

The branching ratio $R_{qq'}$ for channels q and q' , can then be written as

$$R_{qq'} = \frac{P(E, q; E_i)}{P(E, q'; E_i)} = \frac{\epsilon_3^2 F_3^{(q)} - 2\epsilon_3 \epsilon_1^3 \cos(\theta_3 - 3\theta_1 + \delta_{13}^{(q)}) |F_{13}^{(q)}| + \epsilon_1^6 F_1^{(q)}}{\epsilon_3^2 F_3^{(q')} - 2\epsilon_3 \epsilon_1^3 \cos(\theta_3 - 3\theta_1 + \delta_{13}^{(q')}) |F_{13}^{(q')}| + \epsilon_1^6 F_1^{(q')}}, \quad (8)$$

where

$$F_1^{(q)} = \left(\frac{\hbar}{\pi}\right)^2 \frac{P_1(E, q; E_i)}{\epsilon_1^6}, \quad F_3^{(q)} = \left(\frac{\hbar}{\pi}\right)^2 \frac{P_3(E, q; E_i)}{\epsilon_3^2}, \quad (9)$$

with $F_3^{(q')}$ and $F_1^{(q')}$ defined similarly. Since the interference term is controllable through variation of laboratory parameters (here the relative intensity and relative phase of the two lasers), so too is the product ratio R .

This 3-photon + 1-photon scenario has now been experimentally implemented⁵ in studies of HCl ionization through a resonant bound Rydberg state. A similar phase control experiment has been performed on atoms⁶, in the simultaneous 3-photon + 5-photon ionization of Hg.

The 3-photon plus 1-photon case is but one example of a scenario which embodies the essential principle of coherent control, i.e. that *coherently driving a pure state through multiple optical excitation routes to the same final state allows for the possibility of control*. Given this general principle, numerous scenarios may be proposed to obtain control in the laboratory². Such proposals must, however, properly account for a number of factors which reduce or eliminate control. Amongst these are the need to (a) adhere to selection rule requirements, (b) minimize extraneous and parasitic uncontrolled satellites, (c) insure properly treated laser spatial dependence and phase jitter and (d) allow maintenance of coherence over time scale associated with any relaxation processes, e.g. collisions. A practical method for overcoming several of these difficulties is described below.

3. Coherent Control via Resonant Two-Photon versus Two-Photon Interference

We first discuss resonant two photon photodissociation of diatomic molecules and then apply the results to the control scenario we propose. Our recent analysis⁷ of resonant two photon dissociation yielded the following results, which serve as input to the coherent control scenario discussed later below. Consider a molecule in a state $|E_i, J_i, M_i\rangle$ which is subjected to two laser fields ω_1 and ω_2 . Absorption of the first photon ω_1 lifts the system to a region close to an intermediate bound state $|E_m, J_m, M_m\rangle$, and a second photon ω_2 carries the system to the dissociating states $|E, \hat{k}q^- \rangle$. These continuum states are of energy E and correlate with the product in channel q , in the direction specified by the angles $\hat{k} = (\theta_k, \phi_k)$. Photon states of the incident lasers are described by the coherent states. Specifically if we denote the phases of the coherent states by ϕ_1 and ϕ_2 , the wavevectors by k_1 and k_2 with overall

phases $\theta_i = \mathbf{k}_i \cdot \mathbf{r} + \phi_i$ ($i = 1, 2$) and the electric field amplitudes by ϵ_1 and ϵ_2 , then the probability amplitude for resonant two photon ($\omega_1 + \omega_2$) photodissociation is given⁷ by

$$\begin{aligned}
 T_{\mathbf{k}_q, i}(E, E_i J_i M_i, \omega_2, \omega_1) &= \\
 &= \sum_{E_m, J_m} \frac{\langle E, \mathbf{k}_q^- | d_2 \epsilon_2 | E_m J_m M_i \rangle \langle E_m J_m M_i | d_1 \epsilon_1 | E_i J_i M_i \rangle}{\omega_1 - (E_m + \delta_m - E_i) + i\Gamma_m} \exp[i(\theta_1 + \theta_2)] \\
 &= \frac{\sqrt{2\mu k_q}}{h} \sum_{J, p, \lambda \geq 0} \sum_{E_m, J_m} \begin{pmatrix} J & 1 & J_m \\ -M_i & 0 & M_i \end{pmatrix} \begin{pmatrix} J_m & 1 & J_i \\ -M_i & 0 & M_i \end{pmatrix} \\
 &\times \sqrt{2J+1} D_{\lambda, M_i}^{Jp}(\theta_k, \phi_k, 0) t(E, E_i J_i, \omega_2, \omega_1, q | Jp\lambda, E_m J_m) \exp[i(\theta_1 + \theta_2)] \quad (10)
 \end{aligned}$$

Here d_i is the component of the dipole moment along the electric-field vector of the i th laser mode, $E = E_i + (\omega_1 + \omega_2)$, δ_m and Γ_m are respectively the radiative shift and width of the intermediate state, μ the reduced mass, and k_q is the relative momentum of the dissociated product in q -channel. The D_{λ, M_i}^{Jp} is the parity adapted rotation matrix with λ the magnitude of the projection on the internuclear axis of the electronic angular momentum and $(-1)^J p$ the parity of the rotation matrix. We have set $\hbar \equiv 1$, and assumed for simplicity that the lasers are linearly-polarized and their electric-field vectors are parallel. Note that the T -matrix element in Eq.(10) is a complex quantity, whose phase is the sum of the laser phase $\theta_1 + \theta_2$ and the phase of t .

We now consider a molecule irradiated with three interrelated frequencies, $\omega_0, \omega_+, \omega_-$ such that $2\omega_0 = \omega_+ + \omega_-$. Photodissociation occurs at $E = E_i + 2\omega_0 = E_i + (\omega_+ + \omega_-)$. The frequencies ω_+ and ω_0 are chosen resonant with intermediate bound state levels. The probability of photodissociation at energy E into arrangement channel q is then given by the square of the sum of the T matrix elements from pathway "a" ($\omega_0 + \omega_0$) and pathway "b" ($\omega_+ + \omega_-$):

$$\begin{aligned}
 P_q(E, E_i J_i; \omega_0, \omega_+, \omega_-) &= \\
 &\equiv \frac{1}{2J_i + 1} \sum_{M_i} \int d\mathbf{k} \left| T_{\mathbf{k}_q, i}(E, E_i J_i M_i, \omega_0, \omega_0) + T_{\mathbf{k}_q, i}(E, E_i J_i M_i, \omega_-, \omega_+) \right|^2 \\
 &\equiv P^{(q)}(a) + P^{(q)}(b) + P^{(q)}(ab) \quad (11)
 \end{aligned}$$

Here $P^{(q)}(a)$ and $P^{(q)}(b)$ are the independent photodissociation probabilities associated with routes a and b respectively and $P^{(q)}(ab)$ is the interference term between them, discussed below. Note that the two T matrix elements in Eq.(11) are associated with different lasers and as such contain different laser phases. Specifically, the overall phase of the three laser fields are $\theta_0 = \mathbf{k}_0 \cdot \mathbf{r} + \phi_0, \theta_+ = \mathbf{k}_+ \cdot \mathbf{r} + \phi_+$ and $\theta_- = \mathbf{k}_- \cdot \mathbf{r} + \phi_-$, where ϕ_0, ϕ_+ and ϕ_- are the photon phases, and $\mathbf{k}_0, \mathbf{k}_+$, and \mathbf{k}_- are the wavevectors of the laser modes ω_0, ω_+ and ω_- , whose electric field strengths are $\epsilon_0, \epsilon_+, \epsilon_-$ and intensities I_0, I_+, I_- .

The optical path-path interference term $P^{(q)}(ab)$ is given by

$$P^{(q)}(ab) = 2|F^{(q)}(ab)| \cos(\alpha_a^q - \alpha_b^q) \quad (12)$$

with relative phase

$$\alpha_a^q - \alpha_b^q = (\delta_a^q - \delta_b^q) + (2\theta_0 - \theta_+ - \theta_-). \quad (13)$$

where the amplitude $|F^{(q)}(ab)|$ and the molecular phase difference $(\delta_a^q - \delta_b^q)$ are defined by

$$\begin{aligned} & |F^{(q)}(ab)| \exp[i(\delta_a^q - \delta_b^q)] \\ &= \frac{8\pi\mu k_q}{(2J_i + 1)h^2} \sum_{M_i} \sum_{J_p, \lambda \geq 0} \sum_{E_m, J_m} \sum_{E'_m, J'_m} \begin{pmatrix} J & 1 & J_m \\ -M_i & 0 & M_i \end{pmatrix} \begin{pmatrix} J_m & 1 & J_i \\ -M_i & 0 & M_i \end{pmatrix} \begin{pmatrix} J & 1 & J'_m \\ -M_i & 0 & M_i \end{pmatrix} \\ & \times \begin{pmatrix} J'_m & 1 & J_i \\ -M_i & 0 & M_i \end{pmatrix} t(E, E_i J_i, \omega_0, \omega_0, q | J_p \lambda, E_m J_m) t^*(E, E_i J_i, \omega_-, \omega_+, q | J_p \lambda, E'_m J'_m). \end{aligned} \quad (14)$$

Consider now the quantity of interest, the branching ratio of the product in q -channel to that in q' -channel, denoted by $R_{qq'}$:⁸

$$R_{qq'} = \frac{\mu_{aa}^{(q)} + x^2 \mu_{bb}^{(q)} + 2x |\mu_{ab}^{(q)}| \cos(\alpha_a^q - \alpha_b^q) + (B^{(q)}/\mathcal{E}_0^4)}{\mu_{aa}^{(q')} + x^2 \mu_{bb}^{(q')} + 2x |\mu_{ab}^{(q')}| \cos(\alpha_a^{q'} - \alpha_b^{q'}) + (B^{(q')}/\mathcal{E}_0^4)} \quad (15)$$

where $\mu_{aa}^{(q)} = P^{(q)}(a)/\epsilon_0^4$, $\mu_{bb}^{(q)} = P^{(q)}(b)/(\epsilon_+^2 \epsilon_-^2)$ and $|\mu_{ab}^{(q)}| = |F^{(q)}(ab)|/(\epsilon_0^2 \epsilon_+ \epsilon_-)$ and $x = \epsilon_+ \epsilon_- / \epsilon_0^2 = \sqrt{I_+ I_- / I_0}$. The terms with $B^{(q)}, B^{(q')}$, described below, correspond to resonant photodissociation routes to energies other than $E = E_i + 2\hbar\omega_0$ and hence to terms which do not coherently interfere with the a and b pathways. We discuss the minimization of these terms elsewhere^{8,9}. Here we just emphasize that the product ratio in Eq. (15) depends upon both the laser intensities and relative laser phase. Hence manipulating these laboratory parameters allows for control over the relative cross section between channels.

Because the t -matrix element in Eq.(10) contains a factor $[\omega_1 - (E_m + \delta_m - E_i) + i\Gamma_m]^{-1}$, the probability is greatly enhanced near resonance, i.e. when the detuning $\Delta = \omega_1 - (E_m + \delta_m - E_i)$ is small. This allows us to selectively photodissociate one level from a thermal bath, re-establishing coherence necessary for quantum interference.

The proposed scenario, embodied in Eq. (15), also provides a means by which control can be improved by eliminating effects due to laser phase jumps. Specifically, the term $(2\phi_0 - \phi_+ - \phi_-)$ contained in the relative phase $\alpha_a^q - \alpha_b^q$ can be subject to the phase fluctuations arising from laser instabilities. If such fluctuations are sufficiently large then the interference term in Eq.(15), and hence control, disappears¹⁰. In order to overcome this problem we generate ω_- as $2\omega_0 - \omega_+$ using a nonlinear crystal. This latter beam is assumed generated by second harmonic generation from the laser ω_0 (with phase ϕ_0), and then subtracting ω_+ from it. Under these conditions¹¹ the quantity $2\phi_0 - \phi_+ - \phi_-$ in the phase difference between the $(\omega_0 + \omega_0)$ and $(\omega_+ + \omega_-)$ routes is a constant. That is, fluctuations in ϕ_0 cancel and have no effect on the relative phase $\alpha_a^q - \alpha_b^q$; the 2-photon plus 2-photon scenario is thus insensitive to the laser jitter of the incident laser fields.

Equation (15) is the primary result of this three frequency arrangement. However, the approach is not limited to the specific frequency scheme discussed

above. Essentially all that is required is that the two resonant photodissociation routes lift the molecule to the same energy and lead to interference, and that the cumulative laser phases of the two routes be independent of the laser phase fluctuations. For example, the paths a and b can be composed of totally different photons, $(\omega_+^{(a)} + \omega_-^{(a)})$ and $(\omega_+^{(b)} + \omega_-^{(b)})$, with $\omega_+^{(a)} + \omega_-^{(a)} = \omega_+^{(b)} + \omega_-^{(b)}$ and with $\omega_+^{(a)}$ and $\omega_+^{(b)}$ in resonance with intermediate states. Both these sets of frequencies can be generated, for example, by splitting $2\omega_0$ light into two beams, which are passed through two nonlinear crystals to produce $(\omega_+^{(a)}, \omega_-^{(a)})$ and $(\omega_+^{(b)}, \omega_-^{(b)})$, respectively. In this way, we obtain two excitation pathways whose relative phase is independent of laser phase jumps in the initial $2\omega_0$ source. Given these four frequencies we now have an additional degree of freedom in the choice of excitation photons in order to optimize control via the reduction of the background terms. The analysis of four frequency control is similar to that of the three color case, and is given in details in⁹.

The ratio $R_{qq'}$ depends on a number of laboratory control parameters including the relative laser intensities x , relative laser phase, and the ratio of ϵ_+ and ϵ_- . In addition, the relative cross sections can be altered by modifying the detuning. Numerical examples for the range of control afforded by this scenario have been studied^{8,9} extensively for Na_2 molecule, with both three and four colour arrangements. We cite some of the results here.

Consider first the photodissociation of Na_2 in the regime below the $\text{Na}(3d)$ threshold where dissociation is to two product channels $\text{Na}(3s) + \text{Na}(3p)$ and $\text{Na}(3s) + \text{Na}(4s)$. In a typical example⁸, we chose excitation $\omega_0 = 631.899$ nm and $\omega_+ = 562.833$ nm. The corresponding ω_- is 720.284 nm. The yield of $\text{Na}(3p)$ was found to vary from 30% to 90%, as $\delta\theta$ and x are varied, providing an enormous range of control over the photodissociation products.

With energy E higher than $\text{Na}(3d)$ threshold, the three Na products, $3p$, $4s$ and $3d$, can be observed simultaneously. Three product control using a three frequency arrangement is given in reference⁹ where the contour plots provide the $\text{Na}(3p)$, $\text{Na}(4s)$ and $\text{Na}(3d)$ yields. There we consider an initial state consisting of $v_i = 10$, $J_i = 0$ with path a , comprised of $\omega_0 + \omega_0$, with $\omega_0 = 591.306$ nm, and path b consisting of $\omega_+ = 582.057$ nm and $\omega_- = 600.853$ nm. The results also show wideranging control, with the $\text{Na}(3p)$ product controllable over a range of 11% to 42%, the $\text{Na}(4s)$ over a range of 2.4% to 57%, and $\text{Na}(3d)$ over the range 12% to 72%.

Additional results and detailed discussion are provided in References^{8,9}.

4. Summary

By using two two-photon pathways which are each resonant with a bound intermediate, one can overcome thermal population effects in coherent control. In addition, by using nonlinear optics method for generating the required radiation one can overcome incoherence effects due to laser phase jitter. Finally, the availability of a number of control parameters, including the detuning to the bound states, the field strengths and the relative laser phases, allows one to substantially reduce other

uncontrolled background terms. The result is an effective means of eliminating major incoherence effects in radiative control, allowing quantum interference effects to dominate and allowing for coherent control in a natural environment.

5. Acknowledgements

We acknowledge support from the U.S. Office of Naval Research under contract number N00014-90-J-1014.

6. References

* Permanent Address: Chemical Physics Department, The Weizmann Institute of Science, Rehovot, Israel

1. P. Brumer and M. Shapiro, *Annual Reviews of Physical Chemistry*, **43** (1992) 257.
2. See, e.g., P. Brumer and M. Shapiro, *Chem. Phys. Lett.* **126** (1986) 541; C. Asaro, P. Brumer and M. Shapiro, *Phys. Rev. Lett.* **60** (1988) 1634; T. Seideman, P. Brumer, M. Shapiro, *J. Chem. Phys.* **90** (1989) 7132; I. Levy, M. Shapiro and P. Brumer, *J. Chem. Phys.* **93** (1990) 2493; C. K. Chan, P. Brumer and M. Shapiro, *J. Chem. Phys.* **94** (1991) 4103; G. Kurizki, M. Shapiro, and P. Brumer, *Phys. Rev. B* **39** (1989) 3435; M. Shapiro and P. Brumer, *J. Chem. Phys.* **95** (1991) 8658.
3. M. Shapiro, J.W. Hepburn and P. Brumer, *Chem. Phys. Lett.* **149** (1988) 451.
4. M. Shapiro and P. Brumer, *J. Chem. Phys.* **90** (1989) 6179. This limited method relies on a scheme where a saturating laser field constantly reestablishes coherence against collisional dephasing effects.
5. S.M. Park, S-P. Lu, and R.J. Gordon, *J. Chem. Phys.* **94** (1991) 8622.
6. C. Chen, Y-Y. Yin, and D.S. Elliott, *Phys. Rev. Lett.* **64** (1990) 507; *Phys. Rev. Lett.* **65** (1990) 1737.
7. Z. Chen, M. Shapiro and P. Brumer, *J. Chem. Phys.* **98** (1993) 8647.
8. Z. Chen, P. Brumer, and M. Shapiro, *Chem. Phys. Lett.* **198** (1992) 498.
9. Z. Chen, P. Brumer, and M. Shapiro, *J. Chem. Phys.* **98** (1993) 6843.
10. The effect of laser partial coherence on coherent control is examined in X-P. Jiang, P. Brumer and M. Shapiro (to be submitted).
11. M. Schubert and B. Wilhelmi, *Nonlinear Optics and Quantum Electronics*, (Wiley, New York, 1986).